Advances in Quantum Chemistry

Volume 50

ADVANCES IN

QUANTUM CHEMISTRY

VOLUME 50

ADVANCES IN
QUANTUM CHEMISTRY

RESPONSE THEORY AND MOLECULAR PROPERTIES
A tribute to Jan Linderberg and Poul Jørgensen

EDITORS

JOHN R. SABIN
QUANTUM THEORY PROJECT
UNIVERSITY OF FLORIDA
GAINESVILLE, FLORIDA

ERKKI BRÄNDAS
DEPARTMENT OF QUANTUM CHEMISTRY
UPPSALA UNIVERSITY
UPPSALA, SWEDEN

FOUNDING EDITOR

PER-OLOV LÖWDIN
1916–2000

GUEST EDITOR

HANS JØRGEN Aa. JENSEN
DEPARTMENT OF CHEMISTRY
UNIVERSITY OF SOUTHERN DENMARK
ODENSE M, DENMARK

VOLUME 50

ELSEVIER

AMSTERDAM • BOSTON • HEIDELBERG • LONDON • NEW YORK • OXFORD
PARIS • SAN DIEGO • SAN FRANCISCO • SINGAPORE • SYDNEY • TOKYO

Academic Press is an imprint of Elsevier

ACADEMIC
PRESS

Academic Press is an imprint of Elsevier
84 Theobald's Road, London WC1X 8RR, UK
Radarweg 29, PO Box 211, 1000 AE, Amsterdam, The Netherlands
30 Corporate Drive, Suite 400, Burlington, MA 01803, USA
525 B Street, Suite 1900, San Diego, California 92101-4495, USA

This book is printed on acid-free paper ♾

ISBN-13: 978-0-12-034850-3
ISBN-10: 0-12-034850-0
ISSN: 0065-3276

For information on all Academic Press publications visit our web site at http://books.elsevier.com

Printed and bound in USA

05 06 07 08 09 10 10 9 8 7 6 5 4 3 2 1

Contents

Contributors

Numbers in parentheses indicate the pages where the authors' contributions can be found.

Hans Ågren (1), Department of Theoretical Chemistry, School of Biotechnology, Royal Institute of Technology (KTH), SE-106 91, Sweden, agren@theochem.kth.se

Janet E. Del Bene (23), Department of Chemistry, Youngstown State University, One University Plaza, Youngstown, OH 44555, USA, jedelbene@ysu.edu

Raphael J.F. Berger (235), Department of Chemistry, University of Helsinki, P.O. Box 55 (A.I. Virtanens Plats 1), FIN-00014 University of Helsinki, Finland

Sonia Coriani (143), Dipartimento di Scienze Chimiche, Università degli Studi di Trieste, Via L. Giorgieri 1, I-34127 Trieste, Italy, coriani@univ.trieste.it

Peter Cronstrand (1), Theoretical Chemistry, Royal Institute of Technology, AlbaNova University Center, SE-106 91 Stockholm, Sweden

I.M. Degtyarenko (91), Laboratory of Physics, Helsinki University of Technology, P.O. Box 1100, FIN-02015 Espoo, Finland, imd@fyslab.hut.fi

José Elguero (23), Instituto de Química Médica, CSIC, Juan de la Cierva, 3, E-28006 Madrid, Spain

Allan Gross (125), Meteorological Research Department, Danish Meteorological Institute Lyngbyvej 100, DK-2100 Copenhagen Ø, Denmark, agr@dmi.dk

Frank Harris (61), Quantum Theory Project, University of Florida, PO Box 118435, Gainesville, FL 32611-8435, USA, harris@qtp.ufl.edu

Christof Hättig (37), Forschungszentrum Karlsruhe GmbH, Institute of Nanotechnology, PO Box 3640, 76021 Karlsruhe, Germany, Christof.Haettig@int.fzk.de

Trygve Helgaker (77), Kjemisk institutt, Universitetet i Oslo, Postboks 1033 Blindern, N-0315 Oslo, Norway, t.u.helgaker@kjemi.uio.no

Karl J. Jalkanen (91), Quantum Protein (QuP) Center, Department of Physics, Technical University of Denmark, Building 309, Room 126, DK-2800 Lyngby, Denmark, jalkanen@fysik.dtu.dk

V. Würtz Jürgensen (91), Quantum Protein (QuP) Center, Department of Physics, Technical University of Denmark, Building 309, DK-2800 Lyngby, Denmark, wuertz@fysik.dtu.dk

Vladimír Kellö (249), Department of Physical and Theoretical Chemistry, Faculty of Natural Sciences, Comenius University, Mlynská dolina, 84215 Bratislava, Slovakia, kelloe@fns.uniba.sk

Yi Luo (1), Theoretical Chemistry, Royal Institute of Technology, AlbaNova University Center, SE-106 91 Stockholm, Sweden

Ola B. Lutnæs (77), Department of Chemistry, University of Oslo, P.O. Box 1033 Blindern, N-0315 Oslo, Norway

Kurt V. Mikkelsen (125), Kemisk Institut Københavns Universitet, Universitetsparken 5, 2100 København Ø, Denmark, kmi@theory.ki.ku.dk

Chris E. Mohn (77), Department of Chemistry, University of Oslo, P.O. Box 1033 Blindern, N-0315 Oslo, Norway

Jens Oddershede (xxi), Kemisk Institut, Syddansk Universitet, Campusvej 55, 5230 Odense M, Denmark, jod@adm.sdu.dk

N. Yngve Öhrn (xiii), Quantum Theory Project, University of Florida, Gainesville, FL 32611, USA, ohrn@qtp.ufl.edu

Magdalena Pecul (185), Department of Chemistry, University of Tromsø, N-9037 Tromsø, Norway

Zilvinas Rinkevicius (271), Royal Institute of Technology, Department of Biotechnology, SE-10691 Stockholm, Sweden

Antonio Rizzo (143), Istituto per i Processi Chimico–Fisici, Consiglio Nazionale delle Ricerche, Area della Ricerca di Pisa, Via G. Moruzzi 1, loc. San Cataldo, I-56124 Pisa, Italy, rizzo@ipcf.cnr.it

Kenneth Ruud (77, 185), Institutt for kjemi, Det matematisk-naturvitenskapelige fakultet, Universitetet i Tromsø, 9037 Tromsø, Norway, Kenneth.Ruud@chem.uit.no

Jack Simons (213), Department of Chemistry, University of Utah, Salt Lake City, UT 84112, USA, simons@chemistry.utah.edu

Dage Sundholm (235), P.O. Box 55 (A.I. Virtasen aukio 1), FIN-00014 University of Helsinki, Finland, sundholm@chem.helsinki.fi

Lyudmyla Telyatnyk (271), Royal Institute of Technology, Department of Biotechnology, SE-10691 Stockholm, Sweden

Miroslav Urban (249), Department of Physical and Theoretical Chemistry, Faculty of Natural Sciences, Comenius University, Mlynská dolina, 84215 Bratislava, Slovakia, urban@fns.uniba.sk

Olav Vahtras (271), Department of Theoretical Chemistry, School of Biotechnology, Royal Institute of Technology (KTH), SE-106 91, Sweden, vahtras@theochem.kth.se

Danny Yeager (289), Department of Chemistry, Texas A&M University, PO Box 30012, College Station, TX 77842-3012, USA, Yeager@Mail.Chem.Tamu.Edu

David J.D. Wilson (77), Department of Chemistry, University of Oslo, P.O. Box 1033 Blindern, N-0315 Oslo, Norway

Preface

In the last decades, impressive advances have been made in the use of quantum mechanical methods to calculate molecular properties including response properties. Linear and non-linear response methods have been developed and implemented for most of the approximate wave functions used in quantum chemistry, giving a range of computational methods of varying cost and accuracy. Thus it is presently possible to calculate for example excitation energies, linear and nonlinear optical properties, one- and multi-photon transition rates, and magnetically induced transition moments for a wide range of molecules and target accuracies. These calculations aid in the interpretation of a wide range of spectroscopies including electron spin resonance, nuclear magnetic resonance and magnetic circular dichroism and general laser spectroscopy.

We found it therefore appropriate and timely to arrange an international meeting devoted to these topics and the conference *Response Theory and Molecular Properties* was held in the period May 5–8, 2004, at Sandbjerg Estate, Denmark. The conference also celebrated two of the Danish pioneers in this field, Prof. Jan Linderberg and Prof. Poul Jørgensen, who in 2004 turned 70 and 60 years old, respectively. The conference gathered about 70 participants and included more than 30 lectures by leading experts, covering many aspects of the calculation of molecular properties and the development and use of response theory.

The present proceedings includes papers by a number of the invited lecturers. We hope that the wide range of properties, molecules, and computational methods discussed will provide the reader with a sense of the creativity and activity in the field. The proceedings also includes the lectures given by Prof. Yngve Öhrn, Gainesville and Prof. Jens Oddershede that outline the scientific career and contributions of Jan Linderberg and Poul Jørgensen, respectively.

We would like to thank all the lecturers and participants of the conference for their contributions to an enjoyable and interesting meeting. On a more personal note, we would like to congratulate Jan and Poul with their birthdays and thank them for their contributions to our own scientific developments and careers. We wish them many happy and fruitful years to come.

Jeppe Olsen
Hans Jørgen Aagaard Jensen

This page intentionally left blank

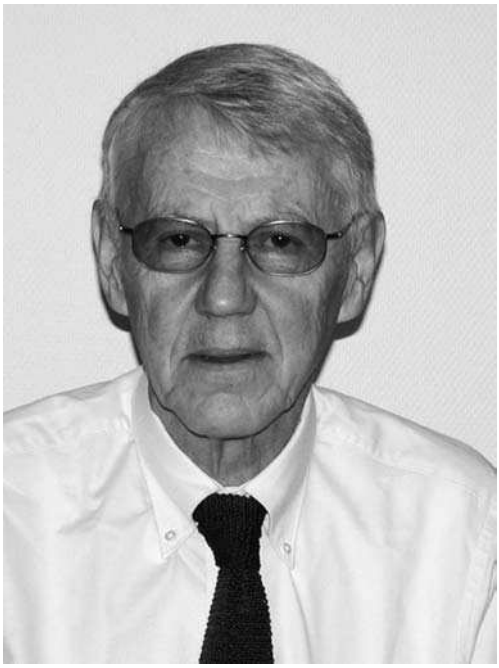

Jan Linderberg, Scientist, Teacher, Friend

Yngve Öhrn

Quantum Theory Project, Departments of Chemistry and Physics, University of Florida, PO Box 118435, Gainesville, FL 32611-8435, USA

Abstract

It is difficult to write an article about a close friend and colleague, and when asked to do so about Jan Erik Linderberg, I hesitated. It would be far less demanding to give a speech about him with a few jokes and reminiscences. Nevertheless, I have tried to present Jan as I know him. I am not trying to list everything that he has done in science and otherwise. That is too difficult a task. I have instead picked a few examples of his published works and glimpses of events in his career and present them as illustrations of Jan the Scientist, the Teacher, and the Friend.

1. INTRODUCTION

I first got to know Jan Linderberg as a fellow graduate student in the Quantum Chemistry Group of Professor Per-Olov Löwdin at Uppsala University. Actually “graduate student” is

a misnomer, since at the time there was no formal graduate program in quantum chemistry at Uppsala, and this fledgeling research group existed with the support of various research grants from Swedish and United States sources. Per-Olov, or Pelle as we all called him, was a master at raising research money and he hired a number of interested young scientists to carry out quantum mechanical calculations on atoms and molecules. I joined the group in the Fall of 1958. Jan was then already a member of this outfit and so were other interesting personalities, such as Anders Fröman, Jean-Louis Calais, Jan Nordling, Einar Lundquist, and Klaus Appel. In addition there were a couple of visiting foreign scientists. I remember the presence of Harrison Shull, from the University of Indiana, and George Hall, from Nottingham University, in the Fall of 1958. In these early days of electronic computing, the group had an in-house Alwac III, which was less powerful than a modern day calculator. This computer was kept running by Klaus Appel, and the rest of us tried to use it by writing machine code, a very slow and cumbersome activity.

We spent our time reading the classical papers in the field and also learning from our seniors in the frequent seminars. The research results were first written up in Technical Reports to be sent to the granting agencies. The advent of a new report required the involvement the entire group. A secretary typed the text on a special wax stencil from a hand written manuscript, leaving spaces for the formulae that were added by hand. The duplication process was done with a hand cranked mimeograph machine that emitted a pungent smell of alcohol and produced a bluish type. The stacks of pages were placed on a long table in the library and we all walked a round the table assembling a report with a green cover and stapled on one edge. This and other activities of the group introduced an informal atmosphere in the interaction among the members, something quite unique in Swedish academic life at the time.

The group had little administrative help from the university and the necessary book keeping of research grants and other funds was put in the hands of Jan Linderberg. He spent some time every week recording debit and credit items in a large ledger. His numbers were then used when auditors from the university and from the granting agencies came to check on our work. Jan's sense of order and penchant for accuracy made him particularly well suited to handle the finances. The university auditor, Mr. Mårdell, once remarked during one of his visits that Jan had the Debit and Credit sides of the ledger opposite to established accounting practice. After some discussion Jan challenged the auditor on his definitions, and Mr. Mårdell had to admit that the only definite criterion was that the Debit side of the ledger should be kept "towards the window".

Jan and I soon became very good friends. We realized that we both greatly enjoyed a mid-morning coffee break away from the office. Most mornings we walked out of the group quarters at the street level of Rundelsgränd to have a cup of java and a piece of cake at Alma Cafe in the central university building. In doing so we had to pass Pelle's window, and he soon let us know that he disapproved of our coffee habit. This did not slow us down one bit. We also learned that we shared many ideas about science and that we simply enjoyed each others company.

Pelle had spent time as a visiting scientist at US universities in the 1950s and he had been approached by some institutions to establish a research program in the emerging field of quantum chemistry and theoretical solid state physics. In 1959 he decided to accept an offer from the University of Florida to do just that, and all of us youngsters suddenly were given the opportunity to spend some time at this university. Rather characteristically, Jan was one of the very first to take advantage of this offer, and he moved, in early 1960

with his wife Gunnel and infant son Johan, to Gainesville, Florida to assume a one-year appointment as Research Associate in Physics. Inspired by Jan's decision and by the news that trickled back to Uppsala from "over there" my family and I chose the same path about a year later and Jan's and my appointments at the University of Florida overlapped for a couple of months in 1961.

2. THE SCIENTIST

Jan's first paper is published in 1959 in Swedish. It appeared in a Conference Proceedings and treats interpolations with the use of exponential functions. He then published a paper with Harrison Shull (*J. Mol. Spectroscopy* **5** (1960) 1) investigating electron correlation in 3- and 4-electron atoms. I think this paper is the first to point out the interesting effect that the $(2s)^2$ and $(2p)^2$ near degeneracy has on electron correlation in Beryllium-like ions.

While at University of Florida (UF) he published a paper on perturbative treatment of the Hartree–Fock equations (*Phys. Rev.* **121** (1961) 816). When the proofs came and the question of page charges had to be settled, Jan took the paperwork from Physical Review to the Assistant Chairman in the Department of Physics, and found out that he had never seen or dealt with such matters. This is a small illustration of where physics at UF was at the time and how much it needed an influx of some industrious Swedes. Fortunately things have changed and science at UF now ranks among the best in the nation.

Starting in 1962 and continuing through early 1964 Jan set a fast pace in his research with an eye on presenting a doctoral dissertation. He focused his efforts on dispersion energy and electron correlation in molecular crystals, and, in particular, rare gas crystals. In the spring semester 1964 he went to the custodian of the central university building to obtain a couple of two-inch nails and to borrow a hammer to literally nail his thesis "Role of correlation in electronic systems" to the main bulletin board for public scrutiny. In May he successfully defended his dissertation in a public forum where Docent Stig Lundqvist, as university appointed opponent and I as Jan's appointed opponent tried to find weaknesses where there were none.

In typical Jan fashion, there was no time for rest, other than a daily coffee break, and he applied for and won a one-year temporary appointment as Professor of Theoretical Physics at Umeå University in northern Sweden. He moved there in July 1964 and theoretical physics got a real boost in Umeå as did the coffee shop business.

Jan and I had started a closer collaboration when we both were back in Uppsala in 1963. This was the beginning of the propagator era in our lives. The physical separation between Umeå and Uppsala did not slow the collaboration. We managed to produce a paper that, I think, we both are very proud of, "Propagators for alternant hydrocarbons" (*Phys. Rev.* **139** (1965) A1063), which was later reprinted in the series "Selected Papers in Physics", by the Physical Society of Japan (*Theory of Molecular Structure* II, 1966 p. 131).

Anyone who has worked with Jan quickly finds out that he is a wizard of mathematics and that his thinking does not always follow straight lines of reasoning. I have many times watched in amazement how he can see patterns of regularity and order in wildly chaotic mathematical expressions. Examples of his unconventional thinking are two small papers he published in 1967 and 1970. "Consistency requirements in the Pariser–Parr–Pople model", *Chem. Phys. Lett.* **1** (1967) 39 presents the idea that parameter values in so-called

semi-empirical Hamiltonians can be obtained via requirements that operator representatives in a very limited basis of such quantities as position and momentum are required to satisfy the commutation relations of quantum mechanics. The other paper I refer to is "Use of contour integral method in molecular orbital theory", *Chem. Phys. Lett.* **5** (1970) 134. In this paper Jan shows how formulae, originally introduced by Coulson and Longuet–Higgins, involving contour integration in the complex energy plane, actually can be used efficiently in numerical work.

The variety of topics covered by Jan's published papers is impressive and a testimony to the way he works. Many of our colleagues in the field of theoretical chemistry do not stray very far from the path they take in their early career and seem satisfied to be doing more of the same. That is obviously not the way to characterize Jan's career. His one hundred plus published papers cover method development such as propagator or Green function theory applied to molecular problems, statistical atomic central field models, hyperspherical coordinates for scattering, isoparametric finite elements, theory of dissociative recombination, differential ionization energy, and many others. Furthermore, Jan never does theory for its own sake. There is always an application and an often novel numerical approach to reach an interesting and meaningful solution. He is the complete quantum chemist, in the sense that he in many cases works out the equations, he codes them for the computer, and he runs the calculations. The applications covered by his published papers include, cohesive energy of solids, band structure of graphite, London forces, spin densities, g-tensors for electron spin resonance, magneto-optical activity, optical activity of organic disulphides, photochemical rearrangement reactions, *etc*. This is not a scientist stuck in one method and one set of problems.

Another trait of Jan as a scientist is a deep knowledge of the literature. He takes great care to give credit where credit is due and it is interesting to note how many of his papers have references to work done decades ago.

3. THE TEACHER

Jan's unconventional way of approaching a problem coupled with his unique facility to perform mathematical operations in his head sometimes makes his lectures hard to follow for the novice. However, for those willing to work hard and not give up there are ample rewards in learning many clever tricks and interesting new ways to look at a problem. I have in my possession several sets of typed notes by Jan relating to a particular course given at Århus, or Utah or wherever he may have enlightened a group of graduate students. He has always been generous to send me these gems of didactic reasoning.

One such undated note called "Symmetry feature of the 3,3,5 polytope" deals with the discretization of the unit sphere and how it relates to Coxeter groups and the approximate treatment of angular momentum in terms of finite rotations. Another entitled "Concerning orthogonal polynomials" relates to optimization procedures, and interpolations in the complex domain. One dated October 1992 is called "Concerning forms, bilinear, sesquilinear, and quadratic" and presents a way to deal with polynomials of several variables. This note also includes three challenging problems for the reader to sharpen his/her understanding of the theory.

During one of his recent stays at the University of Utah Jan gave a series of lectures on Green functions and linear response theory with the use of electron field operators. He

prepared a set of notes for his students and as usual sent me copies. These notes are not copied from some text on the subject, but present a fresh new way to learn about these matters. I always gain some insight from Jan's pamphlets and try to incorporate the ideas in my own teaching.

When Jan became Professor of Theoretical Chemistry at Århus University in 1966 he introduced a new way to teach quantum chemistry. I still have his lecture notes in Swedish from that first year. So not only did his Danish students have to cope with another Scandinavian language but also with an unconventional way to teach theory in a chemistry department. The first chapter deals with Maxwells equations and the quantization of the radiation field. The treatment of electrons starts with the Dirac equation, and the Heisenberg equation of motion gets as prominent a role as does the Schrödinger one. I have heard that the older professors of chemistry at Århus at the time were a bit concerned that this was going to be too difficult for the chemistry students.

There were, however, a number of Danish students, who took the opportunity to learn from the new professor and a small, but soon very influential, group of theoretical chemists gathered at Århus under Jan's leadership. Many of these early students have gone on to prominent careers such as Erik W. Thulstrup, Poul Jørgensen, Jens Oddershede, and others. Soon the group grew with foreign postdoctorals, some of them former graduate students of mine at the University of Florida, such as Joseph Kouba, Rodney J. Bartlett, Nelson H.F. Beebe, and Manoj Mishra, and some from other places such as Mark Ratner, Ian L. Cooper, and others.

I had the good fortune to spend fourteen months in 1970–71 with the Linderberg group at Århus, and on many other occasions I was the Visiting Professor in the group for a couple of months and thoroughly enjoyed the science and the fellowship there. In the early days we often spent the Friday summer afternoons on the soccer field. Sometimes we organized real tournaments against the organic groups or some of the physics groups. These were serious battles with real team uniforms. I have pictures to prove it. It was fun and much of this activity has led to lifelong friendships and lasting international professional contacts.

Another aspect of Jan as teacher is the way he interacts with his chemistry and physics faculty colleagues who may need help or guidance with some theoretical matter. Jan is always approachable for consultation and I have many times seen him provide answers and useful suggestions to an experimental colleague. Some of the questions raised during such sessions have led to collaborations and published papers, such as "ESR spectra of ClO_2 and BrO_2 exchange coupled to molecular oxygen", *Chem. Phys. Lett.* **33** (1975) 612 with J.R. Byberg, and "Electron-transfer fluorescence quenching of radical ions. Experimental work and theoretical calculations", *J. Am. Chem. Soc.* **106** (1984) 5083 with Jens Eriksen, Karl Anker Jørgensen, and Henning Lund.

From very early in his career Jan realized that the teaching of quantum chemistry is an international activity. He has lectured at several international institutes and schools in Scandinavia and elsewhere. Already in 1962 he participated as an instructor in the legendary Coulson Theoretical Chemistry Summer School at Oxford, England. He has been a guest lecturer at universities in Norway, Sweden, Germany, Hungary, Switzerland, Northern Ireland, Canada, Japan, Italy, India, and the United Sates.

4. THE FRIEND AND TRAVEL COMPANION

Jan and Gunnel were born and grew up in Karlskoga, Sweden. They often return there to enjoy the Swedish nature and to relax with their relations. The people Jan used to know when growing up in the home town of Alfred Nobel and close to where the famous Bofors guns are manufactured, I think, in many ways still form a reference frame for him and his view of the world. There is a fundamental, stable coherence in Jan's persona that is always present, and I think, it derives from the sound values and attitudes he experienced from his parents and surroundings in Karlskoga. The inherent value in learning and achievement, in manual as well as intellectual skills, was something both he an I grew up with. This provides a basis for Jan's thoughts and actions. These basic personal values, I think, is the main reason that Jan and I early on felt a special friendship for each other and this is also a principal reason for why we have enjoyed doing science together.

I have had the privilege to be able to visit Jan at Århus University on many occasions for shorter times and, although less frequent, Jan has visited me at the University of Florida. However, we have not really spent that much common time at the same institution and much of our collaboration has been of the long distance kind. Nevertheless, at last count we have managed to co-author about twenty research papers and two editions of a book.

When we are together at the same time-space point we like to write our papers sitting together and working out the formulation of each sentence. We also work best by using the blackboard for derivations while we discuss, and delight in the rare successes and agonize over the many failures.

With such close collaboration it is unavoidable that the families get involved, and our spouses and children have enjoyed each others company over the years.

Jan and I both like physical exercise and try to stay in some reasonable shape. Many times we have run together in the forests around Århus and Jan is quite a determined long distance runner. I don't think I have been able to outrun him on any of our jaunts in the Danish woods. He and Gunnel have, in the last several years, taken up the sport of orienteering. This is an activity, where you attempt, in the shortest time possible, to find a set of stations each marked with a small colorful screen usually in rather severe terrain. You use a detailed map and compass and have to find the stations in order. Jan likes to tell stories about his successful and not so successful starts in such competitive events. Actually, I think that Gunnel has had more prominent results in orienteering than has Jan.

Jan and I have traveled together to scientific meetings around the world. As young graduate students we each gave seminars at the famous Bates group at the University of Belfast, Northern Ireland. There we also had our first experience with oversized steins of Irish stout, but managed not to disgrace ourselves or our hosts. We travelled to Japan in 1976 to a conference on Electronic Structure held on the north island of Hokkaido. Jan flew from Denmark and I from Florida. We met in Tokyo and arrived together a day early to Tomakomai, a small paper mill town on the coast of Hokkaido. We took a walk about town and realized that the locals had no experience with westerners. People in the street laughed at us and stared at us. Jan is a strapping six foot four inches and although I am barely six feet tall, we both towered over the local Japanese. In particular Jan became very popular and when a school class on excursion wanted to have their picture taken with Jan, he kindly obliged. Jan loves to travel and he rarely hesitates to accept an opportunity to cross the Atlantic. I am no different. So, since 1966 there has hardly been a year when we have not

met somewhere. When we meet after some time of little or no communication, we more often than not discover that we have been thinking about similar matters.

With Jan's retirement and my own impending one, we will have less opportunities for professional travel, but on the other hand we will have more time to "do integrals", which are Jan's code words for working out new theoretical and computational schemes. So, maybe more co-authored papers are just around the corner. I would very much like that.

ACKNOWLEDGEMENTS

It is a great pleasure and an honor to be asked to contribute to this volume in recognition of Jan's career. I thank Jeppe Olsen and Hans-Jørgen Jensen for the invitation and for organizing the meeting at Sandbjerg in honor of Jan.

This page intentionally left blank

Poul Jørgensen and His Science

Jens Oddershede

Department of Chemistry, University of Southern Denmark, DK-5230 Odense M, Denmark

Abstract

Having had the privilege of knowing Poul Jørgensen since before he started in science, being one of his first scientific co-workers, and having followed his development from a distance in the later years, it is a special pleasure for me to have this chance to take a closer look at his scientific career and at his contributions to our field. In my opinion his science is characterized by a long series of new and important methodological contributions to the field of electronic structure. I have tried to focus on some of his most important contributions and I have also shown how modern quantum chemistry—including the science of Poul Jørgensen—is never the work of one man. I conclude with some personal remarks about the impact of Poul Jørgensen's science on contemporary electronic structure theory.

1. INTRODUCTION

I met Poul Jørgensen in one of the dormitories on campus at Aarhus University when we were both students in the mid 1960s. He was a chemistry student and I a student of

chemistry and physics. Since he had started at the university one year prior to me, it was not until we both moved in to the dormitory that I got to know him.

He introduced me to Jan Linderberg and got me interesting in doing my degree with Jan in quantum chemistry. As you can see from Yngve Öhrn's contribution in this issue on Jan Linderberg, he had just been appointed professor of Quantum Chemistry at Aarhus University in 1966 and Poul and I became his first students. Exactly who was first is perhaps a little difficult to decide as can be seen from the following.

After Poul had introduced me to Jan and to the field of quantum chemistry, he decided to leave chemistry all together! Poul has always been—and still is—very actively engaged in sports; in his early years it was track and field that had his interest and in later years it has been orienteering. He had decided to make his hobby his living, which meant leaving chemistry and going to Copenhagen University to study sports science. That was the summer of 1967. Thus, when I started as a graduate student in September 1967, Poul had left. Luckily for me—and for quantum chemistry—Poul soon discovered that sports is more fun from a practical than from an academic point of view, and during the fall of 1967 he returned to active service at the Theoretical Chemistry Division at the Chemistry Department in Aarhus. However, by then the first course of quantum chemistry at Aarhus University had started (1 September 1967) with Jan Linderberg as the professor and me as the Teaching Assistant. Poul had to wait a year to achieve this honour—and source of income!

If this gave him the extra time needed to concentrate on his thesis or he just was more determined than I, I do not know. However, whatever the reason was, he graduated first (July 1969)—just about one year before I did (May 1970), so it is fair to say that Poul was indeed Jan's first student.

Being a student in the group of Jan Linderberg in those days was not always so easy. Jan had very high standards, both for himself and for his students. It could at times be difficult for him to comprehend the level of ignorance of the Danish students in those days. We had to work very hard in order to follow what "the master" tried to explain to us. After a session with Jan on a given topic we had to study for days to sort out in our own minds what he had been trying to teach us. Jan was always extremely friendly and was also patiently trying to explain it to us again and again, but we felt that there were some missing links and details in the explanations that we just did not understand—and Jan simply could not comprehend that we did not know them.

Thus, there was no other way out of this predicament than to start all over on our own and to be our own mutual tutors. So we did, and this was the start of a series of long lasting scientific collaborations between former graduate students of Jan Linderberg, including that between Poul and me. I doubt that this was a deliberate act on Jan's part but it was a useful one. We were brought up to stand our own feet and we were also trusted to do so. Very often one sees that thesis advisors want to or need to be part of their students' work, and this makes it difficult for the students to develop their own independent profile and line of work. This was never a problem in Jan Linderberg's group. Both Poul and I have only two papers in common with Jan. This is not an indication of lack of interest from Jan's side. On the contrary, he was always there with good advice and help. However, it was a sign of "no interference" and it gave us both a chance to develop our own scientific careers, careers that are clearly influenced by the guidance and subject pioneered by Jan Linderberg and his co-workers.

The very international atmosphere that Jan created at his new group in Aarhus also influenced both Poul and me. Long term visitors, postdocs, *etc.*, as, *e.g.*, Yngve Öhrn, Mark Ratner, Nelson H.F. Beebe, Rodney J. Bartlett, Pekka Pykkö, Josef Michl, Jack Simons and John R. Sabin, as well as very many lectures and short term visitors taught us early on that quantum chemistry is a truly international science and that the inspiration one receives from scientists with different culture and upbringing is invaluable to the progress of one's own science.

Add to that the social dimension that was created by sports activities, as well as the fact that we also met after working hours in our homes and at outings, and one has a most fruitful environment for the development good and dedicated scientists such as Poul and many others.

2. THE CAREER

After graduation Poul was a postdoc in Aarhus as well as with Yngve Öhrn in Florida (1972–73), in Utah with Jack Simons (1974) and in Pasadena with V. McKoy (1974–75) before being appointed *lektor* (associate professor) at Aarhus University in 1975. In 2000 he became professor. In Denmark becoming professor is not a matter of individual promotion but relies on the availability of a vacant professorship. When the dean at long last decided to create an individual professorship that Poul could apply for, the promotion was long overdue—but most welcomed by Poul and all of us who had followed his scientific achievements.

Poul's first paper on *Time-dependent Hartree–Fock calculations in the Pariser–Parr–Pople model. Application to aniline, azulene and pyridine* appeared in *Int. J. Quantum Chem.* in 1970 (co-authored by Jan Linderberg). Since then he has published nearly 300 papers and other contributions in the international scientific literature. The list of publication also includes three textbooks and together with Jeppe Olsen and Trygve Helgaker he has organized a series of summer schools in *Quantum Chemistry and Molecular Properties* in Denmark since 1990. Both the textbooks and the summer schools have had a considerable influence on the coming generations of quantum chemists.

In the 34 years that have passed since his maiden paper, Poul Jørgensen has made many seminal contributions to the field of electronic structure theory. Typically, for both his scientific legacy and for the field in general, these contributions are the results of collaboration with a long list of colleagues and students. In fact, the list of publication reveals that he has had 98 co-authors during the 34 years. About half of those are co-authors on a single paper. However, Poul Jørgensen's scientific career is characterized by a longstanding collaboration with a few other scientists. Table 1 lists the names of some of them as well as the number of joint publications with Poul.

Two co-authors—Trygve Helgaker and Jeppe Olsen—stand out as long-term co-workers of Poul, and as we shall see later, they have important shares in the many contributions Poul has made to his field.

3. SCIENTIFIC MILESTONES

Trying to determine the most important scientific contributions of a very active and versatile scientist such as Poul Jørgensen is a difficult task—and some may even say a hazardous

Table 1. The top ten co-authors of Poul Jørgensen and their number of joint publications (spring 2004)

1.	Trygve Helgaker	99
2.	Jeppe Olsen	83
3.	Hans Jørgen Aagaard Jensen	48
4.	Henrik Koch	46
5.	Ove Christiansen	40
6.	Christof Hättig	31
7.	Kenneth Ruud	30
8.	Keld Bak	29
9.	Danny L. Yeager	28
10.	Hans Ågren	27

one. The choice will always represent a personal taste. Others—including Poul—may well disagree with the choices made. However, despite all these uncertainties and despite the fact that Poul has only just passed 60 and still is scientifically at the peak of his career I shall risk being proved wrong, and try to pinpoint some of the subfields of electronic structure theory where I find that Poul's fingerprints are especially noticeable. My background for doing so is my experience from the first years of collaborations with him and the role of the interested spectator since I left Aarhus University in 1977.

In looking over more than 30 years of scientific activities I find that it is possible to identify seminal contributions by Poul Jørgensen in at least 8 different fields of quantum chemistry. In my view it is also possible to match these contributions to specific publications. These papers have all, in one way or another, become central sources to consult if one is interested in these subfields. In order to have a measure of the interest, the total number of citations to each paper is also indicated.

3.1. E.S. Nielsen, P. Jørgensen and J. Oddershede: Transition moments and dynamic polarizabilities of a second-order polarization propagator approach, *J. Chem. Phys.* 73 (1980) 6238—130 citations

Poul and I were brought up in a wave function free environment! Jan Linderberg early on made it clear to us that propagators or Green's functions were the future of quantum chemistry. Why calculate individual state energies and subtract them from each other in order to determine their energy difference? Why not use the propagators to obtain the energy differences directly as poles of these functions and then determine the response properties of molecules, as, *e.g.*, dynamic polarizabilities, directly from the functions themselves? We did not question this dogma. Students never do. However, it was obvious to all of us who were involved in this development in the early seventies that unless we were able to develop propagator methods based on *ab initio* methods we would never be able to convince the rest of the world that our belief was the right one. Thus, Poul, Nelson Beebe and I set out to develop *ab initio* based polarization propagator methods. That is, on the methods used to calculate number conserving excitation phenomena as excitation energies and molecular response properties. Other research groups engaged in similar developments for electron

propagator methods for non-number conserving processes such as electron addition and removal.

Poul and I ended up with methods based on perturbative techniques, methods that would ensure that all terms up through a particular order of Møller–Plesset perturbation theory were included in the energy difference and in the response function. The most complete method of the kind was the Second-Order Polarization Propagator Approach (SOPPA)—an acronym suggested by Nelson Beebe—and the reference given in the heading gives the most complete account of this method. The method is still used and it has survived the test of time as a useful and rather accurate way of calculating, for example, the magnetic properties of molecules.

3.2. E. Dalgaard and P. Jørgensen: Optimization of orbitals for multiconfigurational reference states, *J. Chem. Phys.* 69 (1978) 3833—154 citations

Poul Jørgensen did not remain completely faithful to the gospel of Jan Linderberg staying away from wave function-based methods! He and another one of Jan's students, Esper Dalgaard, together with many other scientists in our field at about the same time (late seventies) got interested in ways of developing and improving the rather widely used multiconfigurational self-consistent (MCSCF) methods. The main new idea in their paper was the use of an exponential ansatz for the form of the MCSCF wave function, an idea that Poul also has pursued in many of his later developments. Both the orbital and the configurational variation parameters were cast into the form of exponents and it thus become easier to treat them at a balanced level of approximation. A second-order MCSCF method was derived. The ansatz also made it possible to formulate a MCSCF-based time-dependent Hartree–Fock method as demonstrated in a paper by Danny Yeager and Poul Jørgensen (*Chem. Phys. Lett.* **65** (1979) 77). The method of Esper and Poul represents one of the most elegant ways of understanding the connection between orbital and configurational variation parameters in MCSCF-based methods. It paved the way for a series of papers in which Poul and his co-workers, using Newton–Raphson update techniques, demonstrated how to obtain guaranteed convergence in ground state MCSCF calculations.

3.3. P. Jørgensen and J. Simons: *Ab initio* analytical gradients and Hessians, *J. Chem. Phys.* 79 (1983) 334—106 citations

The analytical parameterization of the MCSCF state made it natural for Poul Jørgensen and Jack Simons, a friend and co-worker ever since Poul was a visiting professor in Utah in 1977, to look into the possibility of evaluating analytic gradients and Hessians for SCF and MCSCF wave functions. The paper cited above represents the first reference to this work, even though it may not be the most well known of their papers on this subject. Based on citation counts it appears that the one they wrote together with two of Jack's students, Hugh Taylor and Judy Ozmont, on how to combine these ideas with update techniques to "walk on potential energy surfaces" (*J. Chem. Phys.* **87** (1983) 2745) is more popular.

Analytic derivative techniques were developed in many different research groups in the early to mid eighties. Poul and Jack made significant contributions to this development. It

was thus very appropriate that the two of them together arranged a workshop on "Geometrical derivatives of energy surfaces and molecular properties" at Sandbjerg—the same place we have this meeting—in August 1985, the proceedings of which has become a standard reference in analytical derivative techniques.

3.4. J. Olsen and P. Jørgensen: Linear and non-linear response functions for an exact state and for a MCSCF state, *J. Chem. Phys.* 82 (1985) 3225—295 citations

After his excursions into wave function methods, Poul returned to his "childhood learning" in this his next seminal contribution to electronic structure theory. Together with Jeppe Olsen he wrote what has become the standard reference in response theory. Poul and Jeppe had decided that the term polarization propagator created too many negative reactions in the electronic structure community so they suggested to use the term response functions for these functions instead—a phrase that has been widely used ever since.

Using the time-dependent Ehrenfest equation, they derived the form of the response functions for both an exact and an approximate (MCSCF) reference function. Here again, the exponential ansatz for the wave function was crucial for the development.

The main achievement of their work was that this paper for the first time devised a general way of calculating higher order response functions, that is, including non-linear response functions. This lead to the first *ab initio* implementation of quadratic response functions for an MCSCF wave function by H. Hettema, H.J. Aagaard Jensen, P. Jørgensen and J. Olsen in *J. Chem. Phys.* **97** (1992) 1174. In later years, even higher order response functions have been programmed and many of the most interesting contemporary response calculations make use of these non-linear response functions.

Most of the later theoretical developments of response methods is based on the work of Olsen and Jørgensen from 1985, so this is clearly one of Poul's most influential contributions to the field of electronic structure theory.

3.5. H. Koch and P. Jørgensen: Coupled cluster response functions, *J. Chem. Phys.* 93 (1990) 3333—211 citations

In recent years Poul Jørgensen and Henrik Koch's work on coupled cluster-based response function is probably the single development in the Aarhus group that has caught the most attention from the outside electronic structure community. Based on the general ideas in the 1985 work of Olsen and Jørgensen, Koch and Jørgensen formulated a response function for a coupled cluster reference state. Here again, it came in handy that the formulation of response functions was developed in terms of exponential wave functions. However, what made this piece of work particularly useful was the fact that Poul and his co-workers derived a series of perturbative approximation to the full coupled cluster response theory. The second-order method (CC2) is described in a paper by O. Christiansen, H. Koch and P. Jørgensen, *Chem. Phys. Lett.* **243** (1995) 409 and the CC3 method is derived in a paper by H. Koch, O. Christiansen, P. Jørgensen, A.S. de Meras and T. Helgaker in *J. Chem. Phys.* **106** (1997) 1808.

The perturbative approximations are useful in that they allow an hierarchical study of the importance of including electron correlation in the calculation of excitation energies

and of other response properties up to and including third order. This is one order higher that is possible to perform with the SOPPA-like methods that have never been formulated consistently beyond second order in terms of perturbation theory.

3.6. T. Helgaker and P. Jørgensen: An electronic Hamiltonian for origin independent calculation of magnetic properties, *J. Chem. Phys.* 95 (1991) 2595—66 citations

Even though Poul's main interest has been the development of new electronic structure methods, as is apparent from the previous subsections, he has also had a keen interest in proving that these methods can indeed produce accurate results for properties that may be difficult to compute with other methods.

Magnetic properties of molecules represent one such class of properties. However, the gauge-origin dependence of calculated magnetic properties is an added difficulty as soon as one enters this field. The use of London orbitals represents a standard way of circumventing the problem. Using second-quantization, Trygve and Poul have shown how to include the effect of London orbitals not in the wave function, but as extra terms in the electronic Hamiltonian, thus making a calculation of magnetic properties in a gauge-invariant fashion a straightforward task using response methods as well.

This methodological development has spurred a long series of response calculations of magnetic properties by authors such as Kenneth Ruud and co-workers.

3.7. J. Olsen, O. Christiansen, H. Koch and P. Jørgensen: Surprising cases of divergent behaviour in Møller–Plesset perturbation theory, *J. Chem. Phys.* 105 (1996) 5082—66 citations

To me—and I guess to many of us in the electronic structure community—it came as surprise when the paper listed above proved that total energy calculations using the widely applied Møller–Plesset perturbation theory (MBPT) diverged in higher orders for "well-behaved, normal closed shell systems" such as Ne and HF. Later calculations on other systems have substantiated the initial results and proved that this is a rather general feature of MBPT.

Depending on your preference, you may either conclude from these findings that there is problem with MBPT or that it is advisable to stick to the lower order of MBPT, for which the calculations seem to behave nicely and reasonably! However, knowing that MBPT is a general tool in many black-box electronic structure codes used by non-experts in electronic structure methods, the findings of Jørgensen and co-workers concerning the convergence difficulties of MBPT-calculations ought to be more widely communicated to the chemistry and biochemistry circles.

3.8. A. Halkier, H. Koch, P. Jørgensen, O. Christiansen, I.B. Nielsen and T. Helgaker: A systematic *ab initio* study of the water dimer in hierarchies of basis sets and correlation models, *Theor. Chim. Acta* 97 (1997) 150—78 citations

The last development that I shall draw the reader's attention to is Poul and co-workers' recent series of papers in which they determine the normal distribution of the error in com-

puted quantities. Using hierarchical electronic structure methods—such as the perturbative approximations to the coupled cluster response method—and hierarchical basis sets, they are able to estimate error bars on calculated electronic structure properties. This is a common practise in experimental papers, but is rarely seen done in a systematic fashion in theoretical papers.

Clearly this line of work makes the theoretical results more reliable and thus more useful for those who wish to use our numbers.

4. CONCLUDING REMARKS

Poul Jørgensen's scientific contributions are, of course, not limited to the few examples I have chosen to highlight very briefly in the preceding section, nor has he at an age of 60 stopped contributing to the field of electronic structure theory. He is still going strong, and I expect many more important contributions from him—and the test of time may prove me wrong in some of the choices I have made in order to illustrate his scientific achievements.

The focus of Poul's science has been on method developments using *ab initio* methods. This is his primary interest; this is where he has made his major contributions to our field. Application of his methods has often been left in the hands of his many co-workers. Applications have held his interest but primarily as a tool to show that his latest method is the best!

It is characteristic of Poul's science that he does not stick to the same method for very long. In his earlier career, he was promoting perturbative propagator methods. However, when he became interested in MCSCF and MCSCF-based response methods he lost interest in the perturbative propagator methods at the same time. Currently, he is a staunch advocate of coupled cluster-based response methods, and MCSCF-based response methods are out!

It is of course quite natural and reasonable to be of the opinion that your latest theoretical development is the best. However, this attitude also may have the effect that you do not allow yourself the benefit of discovering that different methods works in different situations and that the truth is not always one-dimensional.

However, Poul is the kind of person that focuses his strengths in one direction, and he has a tendency to have a black-and-white outlook at the world. He has had his disagreements with his colleagues in the scientific community and he has never followed "main streams". Perhaps for these reasons he has not gotten the full international recognition that his scientific contributions warrant. Surely, he is well-known in our circles and he is also invited to very many conferences and events in quantum chemistry. However, he is not a "science entrepreneur"; he does not sell the same method for years and he does not even try to please those in power and of influence.

Poul is the way he is. We—his friends—enjoy that and enjoy his friendship. He makes us proud of our field and we are looking forward to seeing many more scientific advances from his hand.

My best wishes to you, Poul, on your 60th birthday. All the best for you and your science in the many more active years to come!

ACKNOWLEDGEMENTS

I would like to thank Poul Jørgensen for more than 30 years of personal and scientific friendship. He has always been—and will always be—one of the scientists that I admire most.

I would also like to take this opportunity to thank my master and teacher, Jan Linderberg, for introducing me to quantum chemistry and for his continuing support and interest in my career in the many years since my graduation.

Thanks also to Jeppe Olsen and Hans Jørgen Aagaard Jensen for bringing us all together at Sandbjerg again (the first propagator workshop was arranged by Jan Linderberg and held at Sandbjeg in 1976). This gave us a chance to honour the two persons that have meant most in the development of propagator and response methods.

This page intentionally left blank

Multi-Photon Absorption of Molecules

Peter Cronstrand, Yi Luo and Hans Ågren

Theoretical Chemistry, Royal Institute of Technology, AlbaNova University Center, SE-106 91 Stockholm, Sweden

Abstract

Recent applications of response theory formulations of Olsen and Jørgensen on multi-photon absorption of molecules have been briefly reviewed. The connection between the calculated microscopic and experimentally measured macroscopic properties is derived. The performance of various computational approaches ranging from Hartree–Fock and Coupled Cluster to Density Functional theory for these spectral properties is analyzed. Using analytic response theory results as reference, the validity of the commonly applied few-states models for two- and three-photon absorption of molecules have been examined. A design strategy for three-dimensional charge-transfer multi-photon absorption systems is presented.

Contents

1. INTRODUCTION

The field of multi-photon absorption (MPA) can on a superficial level be described as having experienced three phases of activity, each separated with periods of about 30 years; initially a theoretical discovery, a phase of experimental confirmation and applications, and the present phase characterized by a dynamic interplay between experiment and theory. The pioneering prediction by Göppert-Mayer [1] already in 1930 pointed out a truly unique feature; the ability of matter to absorb more than one single photon at a time. In these early days the phenomenon was far from having a chance of being experimentally confirmed and remained therefore as a rather exotic, albeit interesting, aspect of light-matter interaction. The birth of the laser in 1960 released a floodgate of research in particular within the

ADVANCES IN QUANTUM CHEMISTRY, VOLUME 50
ISSN: 0065-3276 DOI: 10.1016/S0065-3276(05)50001-7

evolving discipline of non-linear optics (NLO). So the phenomena of two-photon absorption (TPA) [2] and three-photon absorption (3PA) [3] could soon thereafter be confirmed, in 1961, respectively, 1963.

On the theoretical side we consider the formulation of response theory of Olsen and Jørgensen in 1985 [4] as a large step towards and implementation of a practical scheme for large scale molecular calculations of multi-photon absorption (MPA). Traditionally, the physical origin of all MPA processes has been traced to various orders of the non-linear susceptibilities, $\chi^{(1)}, \chi^{(3)}, \chi^{(5)}, \ldots$. However, much more efficient computational schemes can be obtained by examining the resonance conditions in the sum-over-states (SOS) representation and by identifying products of first, second, third order of transition moments. A decisive simplification is therefore given by an evaluation the multi-photon transition moments as residues of (hyper)polarizabilities or, as encoded in response methodology, as residues of linear, quadratic or cubic response functions. These considerations enabled the MPA cross-sections to be extracted at the same order as the corresponding (hyper)polarizability; *i.e.*, σ^{TPA} from β and σ^{3PA} from γ. This is a considerable simplification from, for example, evaluating the 3PA cross-section from the fifth order polarizability. Other advantages of response theory for general molecular property calculations are well known, and will probably be reviewed in other contributions to this volume.

Calculations using response theory was greatly promoted in the late 90s by the discovery of organic systems with large cross sections along with a growing attention motivated by a new generation of novel photonic technologies [5–15]. Although theoretical modelling has been available at an *ab initio* level since quite long time, it has not until recently reached a stage where it can match the increasing pool of experimental results. The original response theory work on Hartree–Fock and multi-configurational quadratic response functions have been extended to cubic response functions and a wider selection of wavefunctions, in particular to the coupled cluster hierarchies of electron correlated wave functions, and lately also to density functional theory (DFT). The present implementation of response theory in the program DALTON thus provides a flexible and powerful toolbox for theoretical modelling of multi-photon absorption of which only some aspects will be covered in this review.

We start by deriving some basic relations in MPA which later is connected to computational schemes viable for direct response calculations. In the following section we recast the attained expressions into modified sum-over-states (SOS) expressions suitable for truncation into so called few-states models. Henceforth we review a sample of applications starting with examining the validity of the few-states models, followed by some results for explicit three-dimensional systems. Finally, we demonstrate the applicability of DFT by comparing with CC results and present DFT calculations of three-photon absorption for a set of chromophores.

2. MULTI-PHOTON CROSS-SECTIONS

2.1. Macroscopic approach

On a macroscopic scale, the MPA processes can be elucidated by considering the rate of absorbed energy per volume unit when subjected to an external electric field, $\boldsymbol{E}$

$$\left\langle \frac{\mathrm{d}}{\mathrm{d}t}\left(\frac{\text{absorbed energy}}{\text{volume}}\right)\right\rangle_{\text{time}} = \langle \mathbf{j}\cdot\mathbf{E}\rangle. \tag{1}$$

The current density, $\boldsymbol{j}$, induced in a non-magnetic medium with no free charge carriers, can be expanded as

$$\mathbf{j} = \frac{\partial \mathbf{P}}{\partial t} + c\nabla \times \mathbf{M} - \frac{\partial}{\partial t}\nabla \times \mathbf{Q} + \cdots \tag{2}$$

where the terms represent the electric dipole, magnetic dipole and electric quadrupole polarization. In the field of nonlinear optics the latter terms are neglected in general and the electric dipole term is expanded as

$$\mathbf{P} = \mathbf{P}^{(1)} + \mathbf{P}^{(2)} + \mathbf{P}^{(3)} + \mathbf{P}^{(4)} + \mathbf{P}^{(5)} + \cdots \tag{3}$$

where it is sufficient to consider terms of odd order and the highlighted terms because of the time averaging procedure [16]

$$P_i^{(1)} = \chi_{ij}^{(1)}(-\omega;\omega)E_j \mathrm{e}^{-\mathrm{i}\omega t} + c.c. + \cdots, \tag{4}$$

$$P_i^{(3)} = 3\chi_{ijkl}^{(3)}(-\omega;\omega,-\omega,\omega)E_j \mathrm{e}^{-\mathrm{i}\omega t} E_k^* \mathrm{e}^{\mathrm{i}\omega t} E_l \mathrm{e}^{-\mathrm{i}\omega t} + c.c. + \cdots, \tag{5}$$

$$\begin{aligned} P_i^{(5)} = {} & 10\chi_{ijklmn}^{(5)}(-\omega;\omega,-\omega,\omega,-\omega,\omega)E_j \mathrm{e}^{-\mathrm{i}\omega t} E_k^* \mathrm{e}^{\mathrm{i}\omega t} \\ & \times E_l \mathrm{e}^{-\mathrm{i}\omega t} E_m^* \mathrm{e}^{\mathrm{i}\omega t} E_n \mathrm{e}^{-\mathrm{i}\omega t} + c.c. + \cdots. \end{aligned} \tag{6}$$

In the expansion of the rate of absorbed energy we can determine the first order contribution of the rate of absorbed energy as

$$\left\langle \frac{\partial \mathbf{P}^{(1)}}{\partial t} \cdot \mathbf{E} \right\rangle = 2\omega \,\mathrm{Im}\big[\chi_{ij}^{(1)}(-\omega;\omega)\big] E_i E_j^*. \tag{7}$$

This corresponds to one-photon transitions and the remaining terms can be ascertained as

$$\left\langle \frac{\partial \mathbf{P}^{(3)}}{\partial t} \cdot \mathbf{E} \right\rangle = 6\omega \,\mathrm{Im}\big[\chi_{ijkl}^{(3)}(-\omega;\omega,-\omega,\omega)\big] E_i E_j^* E_k E_l^*, \tag{8}$$

$$\left\langle \frac{\partial \mathbf{P}^{(5)}}{\partial t} \cdot \mathbf{E} \right\rangle = 20\omega \,\mathrm{Im}\big[\chi_{ijklmn}^{(5)}(-\omega;\omega,-\omega,\omega,-\omega,\omega)\big] E_i E_j^* E_k E_l^* E_m E_n^* \tag{9}$$

which correspond to two- and three-photon absorption. The expressions can be abbreviated further by introducing the intensity, I, as $I = \frac{nc}{2\pi} E^2$ (in cgs units) [17] and identifying the one-, two- and three-photon absorption coefficients, α, β and γ, as

$$\alpha = \frac{2\pi\hbar\omega}{nc} \,\mathrm{Im}\big[\chi_{ij}^{(1)}(-\omega;\omega)\big], \tag{10}$$

$$\beta = \frac{24\pi^2\hbar^2\omega}{n^2c^2} \,\mathrm{Im}\big[\chi_{ijkl}^{(3)}(-\omega;\omega,-\omega,\omega)\big], \tag{11}$$

$$\gamma = \frac{160\pi^3\hbar^3\omega}{n^3c^3} \,\mathrm{Im}\big[\chi_{ijklmn}^{(5)}(-\omega;\omega,-\omega,\omega,\omega,-\omega)\big] \tag{12}$$

which can be related to the phenomenological equations describing the attenuation of a light beam experiencing OPA, TPA and 3PA as

$$\frac{\mathrm{d}I}{\mathrm{d}z} = -\alpha I - \beta I^2 - \gamma I^3. \tag{13}$$

Trough the relations

$$\sigma^{\mathrm{TPA}} = \frac{\hbar\omega\beta}{N} \tag{14}$$

and

$$\sigma^{\mathrm{3PA}} = \frac{\hbar^2\omega^2\gamma}{N} \tag{15}$$

one can finally define the OPA, TPA and 3PA cross-sections, σ^{OPA}, σ^{TPA} and σ^{3PA}.

2.2. Microscopic approach

At a microscopic level, the susceptibilities correspond to (hyper)polarizabilities which in principle are attainable by quantum chemistry methods, but less feasible for larger systems. Instead of evaluating the imaginary part of (hyper)polarizabilities as such we can achieve a considerable downshift of the order of the property by only considering the resonant terms for $\gamma(-\omega;\omega,-\omega,\omega)$ with $\omega = \frac{1}{2}\omega_f$ where ω_f is the excitation energy to the final two-photon state $|f\rangle$. Under these conditions it is possible to rewrite γ as

$$\begin{aligned}
\gamma_{\alpha\beta\gamma\delta}(-\omega;\omega,-\omega,\omega) &= \hbar^{-3}\sum\mathcal{P}_{1,3} \\
&\times \sum_{km}\left[\frac{\langle 0|\mu_\alpha|k\rangle\langle k|\mu_\gamma|f\rangle\langle f|\mu_\beta|m\rangle\langle m|\mu_\delta|0\rangle}{(\omega_k-\omega)(-\mathrm{i}\Gamma_f/2)(\omega_m-\omega)}\right. \\
&\left.+\frac{\langle 0|\mu_\gamma|k\rangle\langle k|\mu_\alpha|f\rangle\langle f|\mu_\beta|m\rangle\langle m|\mu_\delta|0\rangle}{(\omega_k-\omega)(-\mathrm{i}\Gamma_f/2)(\omega_m-\omega)}\right] \\
&= \mathrm{i}\frac{2\hbar^{-3}}{\Gamma_f}\sum\mathcal{P}_{-\sigma,2}\sum_k\frac{\langle 0|\mu_\alpha|k\rangle\langle k|\mu_\gamma|f\rangle}{(\omega_k-\omega)}\sum\mathcal{P}_{1,3}\sum_m\frac{\langle f|\mu_\beta|m\rangle\langle m|\mu_\delta|0\rangle}{(\omega_m-\omega)} \\
&= \mathrm{i}\frac{2\hbar^{-1}}{\Gamma_f}S_{\alpha\gamma}S^*_{\delta\beta}.
\end{aligned} \tag{16}$$

Hence, in the vicinity of two-photon resonance it is sufficient to evaluate the two-photon transition matrix elements $S_{\alpha\beta}$ defined as

$$S_{\alpha\beta} = \hbar^{-1}\sum_k\left[\frac{\langle 0|\mu_\alpha|k\rangle\langle k|\mu_\beta|f\rangle}{\omega_k-\omega}+\frac{\langle 0|\mu_\beta|k\rangle\langle k|\mu_\alpha|f\rangle}{\omega_k-\omega}\right]. \tag{17}$$

Due to the slow convergence of these so called sum-over-states (SOS) expressions an explicit summation does not form a viable option for *ab initio* methods, except when they can be truncated to a few leading terms. These truncations have traditionally been considered legitimate for so-called charge transfer (CT) systems, where the excitation scheme is completely dominated by a few major excitation channels. In addition, they may also serve as a valuable tool for interpretation purposes because of their ability to display the relation of the TPA probability, δ^{TPA}, to other somewhat more intuitive quantities. A more computationally efficient approach is offered by residue analysis of the (hyper)polarizabilities. The

single residue of the first order hyper-polarizability can be written as

$$\begin{aligned}
&\lim_{\omega_2 \to -\omega_f} (\omega_2 - \omega_f)\beta_{ijk}(-\omega_\sigma; \omega_1, \omega_2) \\
&\quad = \frac{1}{\hbar} \sum_n \left[\frac{\langle 0|\mu_i|n\rangle\langle n|\mu_j|f\rangle\langle f|\mu_k|0\rangle}{(\omega_n - \omega_1 - \omega_f)} + \frac{\langle 0|\mu_j|n\rangle\langle n|\mu_i|f\rangle\langle f|\mu_k|0\rangle}{(\omega_n + \omega_1)} \right] \\
&\quad = \frac{1}{\hbar} \sum_n \left[\frac{\langle 0|\mu_i|n\rangle\langle n|\mu_j|f\rangle}{(\omega_{nf} - \omega_1)} + \frac{\langle 0|\mu_j|n\rangle\langle n|\mu_i|f\rangle}{(\omega_{n0} + \omega_1)} \right] \langle f|\mu_k|0\rangle. \qquad (18)
\end{aligned}$$

It is clear that the term inside the brackets is connected to the two-photon absorption matrix element given by equation (17), when evaluated for $\omega_1 = -\omega_{f0}/2$.

The final step in order to relate the microscopic origin to the macroscopic detection consists in relating the two coordinate systems; that of the laboratory and that of the molecules. Specifically we need to be able to relate the quantity that defines the macroscopic coordinates in the microscopic realm, that is the polarization of light, with the transition dipole moments evaluated at the quantum level. Since experiments rarely are made on single molecules, but an ensemble of molecules which for gases or liquids has no preferred direction, the relation must include a full orientation averaging. Thus, we want to establish a relation such as

$$\left\langle \left| S^{0f}(\lambda, \nu) \right|^2 \right\rangle = \left\langle (\lambda_A \nu_B \lambda_C^* \nu_D^*)(l_{Aa} l_{Bb} l_{Cc} l_{Dd}) \left(S_{AB}^{0f} \left(S_{DE}^{0f} \right)^* \right) \right\rangle. \qquad (19)$$

In the beginning of 1970s, Monson and McClain [18,19] derived the following relations for accomplishing this task

$$\delta^{\mathrm{TPA}} = F\delta_F + G\delta_G + H\delta_H \qquad (20)$$

where F, G and H are defined as

$$F = -|\boldsymbol{\lambda} \cdot \boldsymbol{\nu}^*|^2 + 4|\boldsymbol{\lambda} \cdot \boldsymbol{\nu}|^2 - 1, \qquad (21)$$

$$G = -|\boldsymbol{\lambda} \cdot \boldsymbol{\nu}^*|^2 - |\boldsymbol{\lambda} \cdot \boldsymbol{\nu}|^2 + 4, \qquad (22)$$

$$H = 4|\boldsymbol{\lambda} \cdot \boldsymbol{\nu}^*|^2 - |\boldsymbol{\lambda} \cdot \boldsymbol{\nu}|^2 - 1 \qquad (23)$$

and

$$\delta_F = \sum_{a,b} S_{aa} S_{bb}^*, \qquad \delta_G = \sum_{a,b} S_{ab} S_{ab}^*, \qquad \delta_H = \sum_{a,b} S_{ab} S_{ba}^*. \qquad (24)$$

For linearly polarized light this implies that $F = G = H = 2$.

The microscopically determined two-photon probability, δ^{TPA}, is subsequently related to the macroscopic cross-section, σ^{TPA}, as

$$\sigma^{\mathrm{TPA}} = \frac{24\pi^2\hbar\omega^2}{c^2} \mathrm{Im}\left[\chi^{(3)}\right] = \frac{4\pi^2\hbar\omega^2}{c^2} \mathrm{e}^4 a_0^4 E_h^{-3} \delta^{\mathrm{TPA}} = \frac{4\pi^2\alpha a_0^5\omega^2}{c} \delta^{\mathrm{TPA}}. \qquad (25)$$

Provided the Bohr radius, a_0 and the speed of light are given in cgs units and the frequency, ω and the TPA probability, δ^{TPA} in atomic units the resulting unit will be $\mathrm{cm}^4\,\mathrm{s\,photon}^{-1}$. The result can be generalized further by introducing the finite lifetime broadening as

$$\sigma^{\mathrm{TPA}} = \frac{4\pi^3\alpha a_0^5\omega^2}{c} \delta^{\mathrm{TPA}} \Delta(\omega_f - 2\omega, \Gamma_f) \qquad (26)$$

through the normalized Lorentzian

$$\Delta(\omega_f - 2\omega, \Gamma_f) = \frac{1}{\pi} \frac{\Gamma_f}{(\omega_f - 2\omega)^2 + \Gamma_f^2}. \tag{27}$$

2.3. Three-photon absorption

In complete analogy with TPA, 3PA cross-sections determined by third order transition moments which in turn can be evaluated through a single residue of the second order hyperpolarizability. Again, orientational averaging is required in order to relate the intrinsic coordinates of a single molecule to the ensemble of freely moving particles as measured in the laboratory coordinate system. As for TPA one therefore seeks to evaluate:

$$\delta^{\mathrm{3PA}} = \left|T^{0f}(\lambda, \nu, \xi)\right|^2 = \left(\lambda_A \nu_B \xi_C T^{0f}_{ABC}\right)\left(\lambda_D \nu_E \xi_F T^{0f}_{DEF}\right)^*. \tag{28}$$

According to McClain [20,21] the orientation averaged values for the 3PA probability δ_{3PA} for linearly (L) and circularly (C) polarized light can be written as:

$$\delta^{\mathrm{3PA}}_L = \frac{1}{35}(2\delta_G + 3\delta_F), \tag{29}$$

$$\delta^{\mathrm{3PA}}_C = \frac{1}{35}(5\delta_G - 3\delta_F), \tag{30}$$

where

$$\delta_F = \sum_{i,j,k} T_{ij} T_{kkj}, \tag{31}$$

$$\delta_G = \sum_{i,j,k} T_{ijk} T_{ijk}. \tag{32}$$

Similar to TPA, we can finally relate the orientationally averaged three-photon absorption probabilities, δ_{3P}, to the three-photon cross-section, σ^{3PA}, as

$$\sigma^{\mathrm{3PA}} = \frac{4\pi^4 a_0^8 \alpha}{3c} \frac{\omega^3 \delta^{\mathrm{3PA}} \Delta(\omega_f - 3\omega, \Gamma_f)(\omega)}{\Gamma_f}. \tag{33}$$

With the same convention concerning the units as for TPA the final cross-sections will be obtained in units of $\mathrm{cm}^6\,\mathrm{s}^2\,\mathrm{photon}^{-1}$.

3. RESPONSE FUNCTIONS

To some extent response theory [4,22] can be seen as an elaborate scheme of time-dependent perturbation theory. By means of this theory we can avoid the explicit summation of the expressions attained in the previous section by solving algebraic equations. Secondly, the formalism is *analytically transferable*, *i.e.*, the same technique may subsequently be applied to retrieve properties from a wave function irrespective of the actual parameterization of the wave function.

For exact states these can be given in their spectral representation with

$$-\langle\langle A;\, B\rangle\rangle_{\omega_1} = \sum \mathcal{P} \sum_p \frac{\langle 0|A|p\rangle\langle p|B|0\rangle}{\omega_p - \omega_1} \tag{34}$$

as the linear response function and

$$-\langle\langle A;\, B,\, C\rangle\rangle_{\omega_1,\omega_2} = \sum \mathcal{P} \sum_{p,q\neq 0} \frac{\langle 0|A|p\rangle\langle p|\bar{B}|q\rangle\langle q|C|0\rangle}{(\omega_p + \omega_0)(\omega_q - \omega_2)} \tag{35}$$

as the quadratic response function, where $\langle p|\bar{B}|q\rangle = \langle p|B - \langle 0|B|0\rangle|q\rangle$ and $-\omega_0 = \omega_1 + \omega_2 + \cdots$. $\mathcal{P}$ is the permutation operator. If the chosen operator is the dipole operator, μ, the response functions, $\langle\langle \mu_i;\, \mu_j, \mu_k, \ldots\rangle\rangle_{\omega_1,\omega_2,\ldots}$ will correspond to the (hyper)polarizabilities α, β and γ.

The response functions contain inherently information about the excited states. The poles determine the location of the excitation energies and further information can be retrieved by examining resonance conditions through a residue analysis. From the expression for the linear response function for an exact wave function, where the unperturbed Hamiltonian is diagonal, we can easily evaluate transition dipole moments between the ground state, $|0\rangle$, and an excited state, $|f\rangle$ as

$$\lim_{\omega_1\to-\omega_f}(\omega_1 - \omega_f)\langle\langle \mu_i;\, \mu_j\rangle\rangle_{\omega_1} = \langle 0|\mu_i|f\rangle\langle f|\mu_j|0\rangle. \tag{36}$$

The single residue of the quadratic response function provides information on the two-photon transition matrix elements

$$\begin{aligned}
&\lim_{\omega_2\to-\omega_f}(\omega_2 - \omega_f)\langle\langle \mu_i;\, \mu_j, \mu_k\rangle\rangle_{-\omega_1,\omega_2} \\
&\quad = -\sum_n \Bigg[\frac{\langle 0|\mu_i|n\rangle\langle n|(\mu_j - \langle 0|\mu_j|0\rangle)|f\rangle}{\omega_n - \omega_2} \\
&\qquad + \frac{\langle 0|\mu_j|n\rangle\langle n|(\mu_i - \langle 0|\mu_i|0\rangle)|f\rangle}{\omega_n - \omega_1} \Bigg] \langle f|\mu_k|0\rangle
\end{aligned} \tag{37}$$

where $\omega_1 + \omega_2 = \omega_m$. From the double residue of the same response function one can deduce the transition dipole moments between excited states

$$\begin{aligned}
&\lim_{\omega_1\to\omega_f}(\omega_1 - \omega_f)\Big[\lim_{\omega_2\to-\omega_m}(\omega_2 - \omega_m)\langle\langle \mu_i;\, \mu_j, \mu_k\rangle\rangle_{-\omega_1,\omega_2}\Big] \\
&\quad = -\langle 0|\mu_i|f\rangle\langle f|\big(\mu_i - \langle 0|\mu_i|0\rangle\big)|i\rangle\langle i|\mu_k|0\rangle.
\end{aligned} \tag{38}$$

We emphasize that this is done from the reference state, $|0\rangle$, preferably the ground state, with no further reference to any excited state.

For approximate wavefunctions the two-photon transition matrix element, $S_{\alpha\beta}$, can within the response terminology be evaluated directly as [4]

$$\begin{aligned}
S_{AB} = &-N_j^A(\omega_f/2)B_{jk}^{[2]}N_k^F(\omega_f) - N_j^B(-\omega_f/2)A_{(jk)}^{[2]}N_k^F(\omega_f) \\
&- N_j^A(\omega_f/2)\left(E_{j(kl)}^{[3]} + \frac{1}{2}\omega_f S_{jlk}^{[3]} - \omega_f S_{jkl}^{[3]}\right)N_j^B(-\omega_f/2)N_k^F(\omega_f).
\end{aligned} \tag{39}$$

In analog, the three-photon tensor elements are evaluated as

$$\begin{aligned}
T_{abc} = {} & N_j^A(\omega_f/3)T_{jklm}^{[4]}(\omega_f/3,\omega_f/3,\omega_f/3)N_k^B(-\omega_f/3)N_l^C(-\omega_f/3)N_m^F(\omega_f) \\
& - N_j^A(\omega_f/3)\big[T_{jkl}^{[3]}(-\omega_f/3,\omega_f/3-\omega_f/3)N_k^B(\omega_f/3)N_l^{CF}(-\omega_f/3,\omega_f/3) \\
& + T_{jkl}^{[3]}(-\omega_f/3,2\omega_f/3)N_k^C(-\omega_f/3)N_l^B(\omega_f/3) \\
& + T_{jkl}^{[3]}(\omega_f,-2\omega_f/3)N_k^F(\omega_f)N_l^{BC}(\omega_f/3,-\omega_f/3)\big] \\
& - N_j^A(\omega_f/3)\big[B_{jkl}^{[3]}N_k^C(-\omega_f/3)N_l^F(\omega_f) + C_{jkl}^{[3]}N_k^B(-\omega_f/3,\omega_f)\big] \\
& + N_j^A(\omega_f/3)\big[B_{jk}^{[2]}N_k^{CF}(-\omega_f/3,\omega_f) + C_{jk}^{[2]}N_k^{BF}(-\omega_f/3,\omega_f)\big] \\
& + A_{jk}^{[2]}\big[N_j^B(-\omega_f/3)N_k^{CF}(-\omega_f/3,\omega_f) + N_j^C(-\omega_f/3)N_k^{BF}(-\omega_f/3,\omega_f) \\
& + N_j^F(\omega_f)N_k^{BC}(-\omega_f/3,-\omega_f/3) - A_{jkl}^{[3]}N_j^B(\omega_f/3)N_k^C(-\omega_f/3)N_l^F(\omega_f)\big]
\end{aligned} \tag{40}$$

where

$$N_j^X(\omega_a) = \big(E^{[2]} - \omega_a S^{[2]}\big)_{jk}^{-1} X_k^{[1]}, \quad X \in \{A, B, C\}, \tag{41}$$

$$\big(E^{[2]} - \omega_a S^{[2]}\big)_{jk} N_k^F(\omega_f) = 0 \tag{42}$$

and

$$\begin{aligned}
\big(E^{[2]} - (\omega_1+\omega_2)S^{[2]}\big)N_j^{BC}(\omega_1,\omega_2) &= T_{klm}^{[3]}(\omega_1,\omega_2)N_l^B(\omega_1)N_m^C(\omega_2) \\
&\quad - C_{kl}^{[2]}N_l^B(\omega_1) - B_{kl}^{[2]}N_l^C(\omega_2), \\
\big(E^{[2]} - (\omega_f-\omega_a)S^{[2]}\big)N_j^{XF}(\omega_a,\omega_f) &= T_{klm}^{[3]}(-\omega_a,\omega_f)N_l^X(-\omega_a)N_l^F(\omega_f) \\
&\quad - X_{kl}^{[2]}N_l^F(\omega_f), \\
X \in \{B, C\}.
\end{aligned} \tag{43}$$

The terms $T_{jkl}^{[3]}$ and $T_{jklm}^{[4]}$, which are *separate* from the three-photon transition matrix elements, are short-hand notation for

$$T_{jkl}^{[3]}(\omega_1,\omega_2) = \big(E_{j(kl)}^{[3]} - \omega_1 S_{jkl}^{[3]} - \omega_2 S_{jkl}^{[3]}\big), \tag{44}$$

$$T_{jklm}^{[4]}(\omega_1,\omega_2,\omega_3) = \big(E_{j(klm)}^{[4]} - \omega_1 S_{jk(lm)}^{[4]} - \omega_2 S_{jl(km)}^{[4]} - \omega_3 S_{jm(kl)}^{[4]}\big). \tag{45}$$

The many parameters not defined here can be found in the paper of Olsen and Jørgensen [4]. Again it is noteworthy that the same approach can be applied for a wide selection of wavefunctions, from low scaling methods as Hartree–Fock (HF) and density functional theory (DFT) to highly correlated schemes as coupled cluster (CC).

Response theory at the self-consistent field (SCF) level has often been applied for the calculations of multi-photon absorption of large organic molecules. Considering the size of these systems and computational tractability the method of choice for incorporating electron correlation is DFT. Recently, response theory up to the fourth property order has been implemented in the framework of DFT, which enables improvements of the predictions with a high degree of correlation.

4. FEW-STATES MODELS

4.1. Two-photon absorption

The explicit formulas for the transition matrix and tensor elements are normally given as sum-over-states (SOS) expressions. An option is therefore to enforce a truncation of the SOS-expression and only include a few dominating states and excitation channels. This may be motivated by the increasing energy term in the denominator or the assumption that only a few excitation paths actually will contribute in a full summation. The convergence rates with respect to the inclusion of states in the summation are known to be slow, except for charge-transfer (CT) systems which fortunately—but not surprisingly—coincides with a class of systems proposed for TPA and 3PA applications. These so-called few-states models where only a limited set of excited states and accompanying transition moments are addressed to represent the full excitation scheme is clearly inferior to response theory as a methodology, but the decomposition into simple properties such as excitation energies and transition dipole moments can enable valuable interpretation and promote an enhanced intuitive understanding through so-called structure-to-property relations.

Following the orientationally averaging procedure devised by Monson and McClain [18], but rearranging the terms in a slightly more intuitive fashion we can rewrite the two-photon probability for linear polarized light δ_L^{TPA}, and circular polarized light, δ_C^{TPA}, as

$$\delta_L^{\mathrm{TPA}} = 24\delta_1 + 8\delta_2 - 16\delta_3, \tag{46}$$

$$\delta_C^{\mathrm{TPA}} = 16\delta_1 + 12\delta_2 - 24\delta_3 \tag{47}$$

where

$$\delta_1 = \sum_{ij} \frac{(\boldsymbol{\mu}^{0i} \cdot \boldsymbol{\mu}^{if})(\boldsymbol{\mu}^{0j} \cdot \boldsymbol{\mu}^{jf})}{\omega_i \omega_j}, \tag{48}$$

$$\delta_2 = \sum_{ij} \frac{(\boldsymbol{\mu}^{0i} \times \boldsymbol{\mu}^{if}) \cdot (\boldsymbol{\mu}^{0j} \times \boldsymbol{\mu}^{jf})}{\omega_i \omega_j}, \tag{49}$$

$$\delta_3 = \sum_{ij} \frac{(\boldsymbol{\mu}^{0i} \times \boldsymbol{\mu}^{0j}) \cdot (\boldsymbol{\mu}^{if} \times \boldsymbol{\mu}^{jf})}{\omega_i \omega_j}. \tag{50}$$

This reformulation emphasizes the vector nature of the transition dipole moments. The terms δ_1 and δ_2 thus describe the alignments—or absence of alignments—of the channels leading to the actual two-photon state, *i.e.*, indirectly the symmetry of the excited state. Obviously, a perfect alignment is preferable, however not possible in each molecular point group. Far more intriguing is the task of controlling the interference term, δ_3. In order to avoid negative contributions, the summation would ultimately consist of terms entangled in arrangements such as $\boldsymbol{\mu}^{00}$, $\boldsymbol{\mu}^{11} \perp \boldsymbol{\mu}^{01}$ and where $\boldsymbol{\mu}^{00}$ is directed in the opposite direction to $\boldsymbol{\mu}^{11}$. These conditions can easily be fulfilled by arbitrary vectors, but are not likely to occur for transition dipole moments for a real system. From inspection it is also clear that the D_{2h} molecular point group is less appropriate, since all excitation paths unavoidably will be orthogonal. The distribution between the different terms δ_1, δ_2 and δ_3 thus defines a

clarifying signature of the processes underlying a particular TPA cross-section. Apparently, it is useful to distinguish between states where the dominating contributions are from parallel (P) or orthogonal (O) sub-paths. This may be especially relevant for non-symmetrical species where the character of the two-photon state cannot be determined directly by referring to symmetry rules.

Few-states models are obtained by truncating the summation in equation (17) to include a finite number of excited states. For instance, by truncating equation (46) to three states and restrict to two dimensions one obtains

$$\delta^{\mathrm{TPA}} = 8\frac{(\mu^{0i}\mu^{if})^2(2\cos^2(\theta_{0i}^{if})+1)}{(\omega_i)^2}. \tag{51}$$

The angle, θ_{01}^{1f} between the relevant transition dipole moments, $\boldsymbol{\mu}^{01}$ and $\boldsymbol{\mu}^{1f}$, is unknown from an experimentally point a view and have to be assumed to be zero, which may be motivated for purely one-dimensional systems. Including yet a state will yield a four state model and the possibility of constructive or destructive interference between the excitation channels.

4.2. Three-photon absorption

The monochromatic three-photon transition tensor element T_{abc} is defined as

$$T_{abc} = \sum \mathcal{P}_{a,b,c} \sum_{n,m} \frac{\langle 0|\mu_a|m\rangle\langle m|\mu_b|n\rangle\langle n|\mu_c|f\rangle}{(\omega_m - 2\omega_f/3)(\omega_n - \omega_f/3)}. \tag{52}$$

Confining to two states this can be rewritten as

$$T_{zzz} = 27 \times \frac{2\mu_z^{0f}(\mu_z^{00}-\mu_z^{ff})^2 - (\mu_z^{0f})^3}{2\omega_f^2} = 27 \times \frac{\mu_z^{0f}[2(\Delta\mu_z)^2 - (\mu_z^{0f})^2]}{2\omega_f^2} \tag{53}$$

and, for a one-dimensional system, the total three-photon absorption probability δ^{3PA} for linearly polarized light will become

$$\delta_L^{\mathrm{3PA}} = \frac{(T_{zzz})^2}{7}. \tag{54}$$

5. VALIDITY OF FEW-STATES MODELS

The matrix equations describing multi-photon excitations given in the response section are indeed not very illuminating, but by inspecting the **E** and **S** terms under certain conditions we can identify a connection with the conventional SOS expressions. If $H_0 O_n|0\rangle = E_n|n\rangle$, as for instance is the case for FCI, the second-order Hessians and overlap matrices, will be diagonal and the third-order matrices will vanish, with the final consequence that the equation for the TP transition moment [equation (39)] will equal the SOS expression in equation (17). Thus, when approaching FCI we can expect a convergence for the absorption cross-sections between the two formalisms. At other levels of theory, the two approaches will be different even when performing a complete summation of the excited states.

For a small diatomic such as LiH and a small basis set (here we confine to STO-3G) we can include *all* excited states in the SOS summations, both at the Hartree–Fock, and the full-configuration interaction (FCI) level. In Table 1 we present the results for two- and three-photon transition matrix elements between the ground state $X^1\Sigma^+$ and the two lowest singlet excited states of Σ^+ symmetry. At the FCI level, the SOS and response approaches agree on the final property values, whereas, at the SCF level, this is no longer

Table 1. Two-photon S_{zz} and three-photon matrix elements T_{zzz} for LiH at the SCF and FCI levels with the STO-3G basis set

Property	State	SCF		FCI	
		SOS[a]	Response	SOS[a]	Response
S_{zz}	$1^1\Sigma^+$	42.417	42.406	76.490	76.490
	$2^1\Sigma^+$	10.680	10.344	−8.2558	−8.2558
T_{zzz}	$1^1\Sigma^+$	5939.8	5857.6	13355.1	13355.1
	$2^1\Sigma^+$	−663.65	−1134.7	−39.695	−39.695

All quantities are given in a.u. Taken from [15].

[a] The SOS calculations include all states in the given representation.

Table 2. A comparison of truncated sum-over-states values with response results for two-photon S_{zz} and three-photon T_{zzz} matrix elements

States	S_{zz}	T_{zzz}
1	−62.867	−1767.6
2	−62.836	−1763.8
3	−62.774	−1746.3
4	−61.970	−1596.7
5	−80.226	−3210.7
6	−75.316	−2214.0
7	−71.047	−3032.2
8	−70.996	−3017.9
9	−71.030	−3012.1
10	−71.165	−3021.9
11	−70.458	−2942.4
12	−70.416	−2954.8
13	−70.946	−3106.7
14	−70.548	−3236.4
15	−70.528	−3236.6
Response	−70.142	−5442.7

Results are obtained for the 2^1A_1 charge-transfer state of pNA at the SCF/6-31G level. All quantities are given in a.u. Taken from [15].

so due to the contributions from the third-order Hessian matrix. The discrepancy is more pronounced for the higher order property T_{zzz}.

We also note a rapid convergence for all properties with respect to the number of states included in the SOS summations at the FCI level. Already with inclusion of five of the total 29 excited states, the properties are converged to within 1%. At the SCF level, on the other hand, the values predicted by SOS (all states included) and response agree to within a few percent for S_{zz} and for T_{zzz} of the first excited state. For the second excited state, however, the results predicted with the two methods differ by a factor of two. This shows that the quality of truncated SOS models depends not only on the property at hand but that it is also state specific.

A similar observation can be made for para-nitro-aniline (pNA) as shown in Table 2. For TPA we note a mutual convergence between SOS and direct response after inclusion of 7

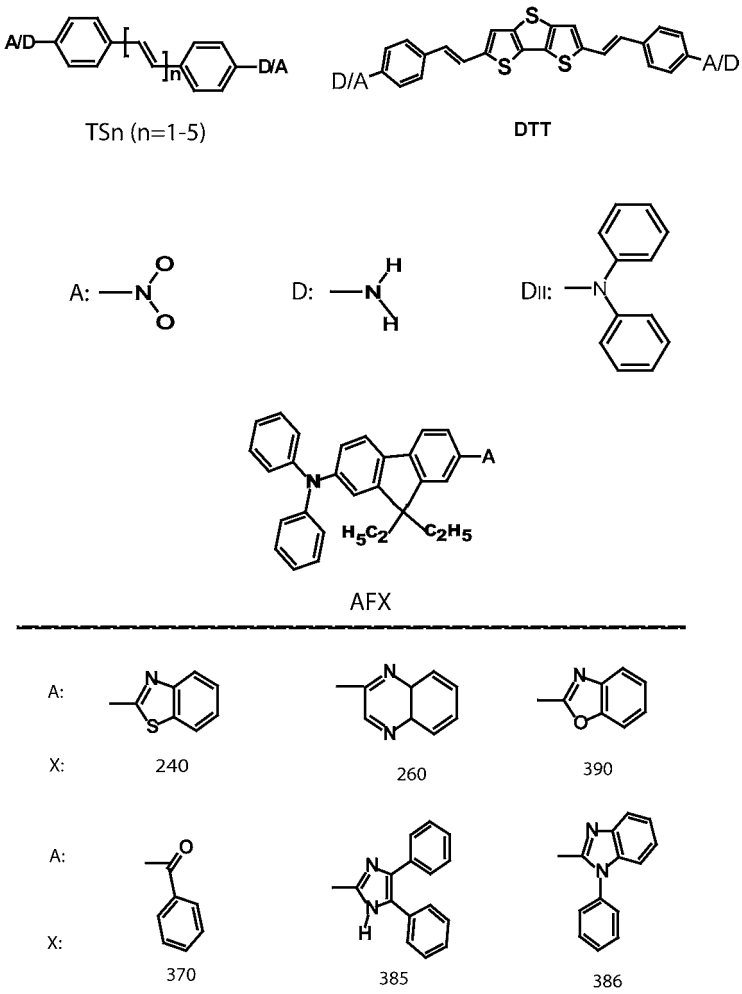

Fig. 1. Molecular structures.

Table 3. A comparison of truncated sum-over-states values with response results for two-photon S_{zz} (a.u.) and three-photon T_{zzz} ($\times 10^4$ a.u.) matrix elements

Molecule	ω[a]	Osc. str.	S_{zz}		T_{zzz}	
			SOS[b]	Response	SOS[b]	Response
AF-240	4.08	1.328	129.2	129.4	2.31	4.05
AF-260	4.11	1.222	156.4	148.2	1.61	4.30
AF-370	4.30	0.365	79.5	81.9	0.22	1.65
AF-385	4.13	1.477	15.7	14.0	3.20	3.78
AF-386	4.27	1.159	65.0	60.9	1.84	2.61
AF-390	4.16	1.430	123.2	118.2	2.36	3.86
DTT	3.17 (4.34)	1.886	99.0	94.0	11.54	7.48
DTT-DD(101)	3.10 (4.19)	2.153	107.3	190.2	15.15	9.78
DTT-AD(102)	2.97	2.219	436.4	430.0	13.51	18.31
DTT-DD(103)	3.04 (4.07)	2.545	206.5	256.5	22.06	14.68
DTT-AD(104)	2.97	2.390	424.9	416.7	17.44	20.15
DTT-AA	3.01 (4.04)	2.275	622.0	674.4	18.79	13.35

Results are obtained for a series of chromophores at the SCF/6-31G level. The excitation energies ω are given in eV. Taken from [15].

[a] The state with strongest TPA is given in parenthesis for symmetrical molecules.

[b] A two-state model is employed for all AF compounds except AF-370 where a three-states model was used. A two-state model is employed for all DTT compounds except symmetrical DTT where a three-states model is used for S_{zz}.

states, whereas for 3PA it appears as if the value is converged, while still deviating from the direct response value by more than 50%.

The majority of systems proposed for TPA applications are various types of π-conjugated structures modified by the attachments of electron accepting (A) and donating (D) groups, as for instance those shown in Fig. 1.

As depicted in Table 3 and Fig. 2, the agreement between the few-states models (FSM) and response methods for S_{zz} is striking for all compounds. The deviation for TPA is occasionally 10%, but mostly below 5% if DTT-DD is disregarded. This is in sharp contrast to the performance of FSMs for T_{zzz} which show substantial discrepancies when compared against response results. The mean value of deviation is close to 40%, and the error can occasionally exceed 200%. Perhaps even more crucial is the fact that few-states models fail to predict the same ordering of the compounds as the response values with respect to the strength of T_{zzz}.

6. THREE-DIMENSIONAL SYSTEMS

The two principal strategies for optimizing multi-photon cross sections have been to either propose new types of π-conjugated structures or to modify structures by attaching electron accepting and/or electron donating groups at certain locations. Introducing electron accepting (A) and electron donating (D) groups to conjugated systems has the well

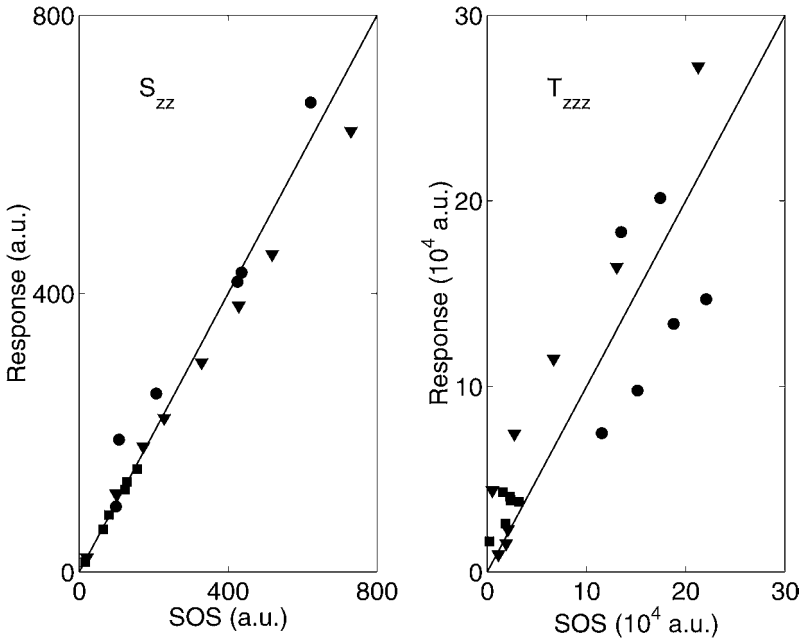

Fig. 2. Correlation between results obtained with few-states models and the response method for two-photon S_{zz} and three-photon T_{zzz} matrix elements. The systems included are derivatives of stilbene (triangle), AF (square), and DTT (ring).

known effect of localizing the otherwise de-localized highest occupied and lowest unoccupied orbitals (HOMO-LUMO) and thereby establishing an effective charge-transfer path across the molecule. Due to the increase of transition dipole moment guiding this transition and an overall alignment involving all transition dipole moments, this technique leads to enhancements of several orders of magnitude for TPA [10,11]. However, the attachment of various functional groups also affect the symmetry of the molecule, which, as seen from the generalized few-states model formula, may have a significant influence by imposing restrictions among the excitation paths leading to the final multi-photon absorption state. Para-cyclophane (PCP), see Fig. 3, constitutes an interesting example in this context since it is explicitly three-dimensional and also offers the possibility of through-space delocalization as a means of gaining contributions to the cross-sections. From the agreements between the direct response and the few-states models results for TPA, displayed in Table 4 or Fig. 4, it is evident that it is sufficient to consider three states in order to incorporate the major sources to the cross sections for all PCP compounds.

The distributions among the terms, δ_1^{TPA}, δ_2^{TPA} and δ_3^{TPA}, are displayed in the histograms in Fig. 5 for compounds PCP0, PCP1, PCP2 and PCP8. In general the first excited state can be classified as having a clear P-character and it is also far more intense than the second state. The dipolar structures, PCP0 and PCP1, show similar features. Both are, as expected, completely dominated by the δ_1^{TPA} term, which indicates an alignment between the relevant transition dipole moments and a pronounced P-character. PCP2 and PCP8 belong to the D_2 point group, which is not fortunate in terms of the TPA probability, because of the restrictions of the transition dipole operators impelled by symmetry rules. A typical path to

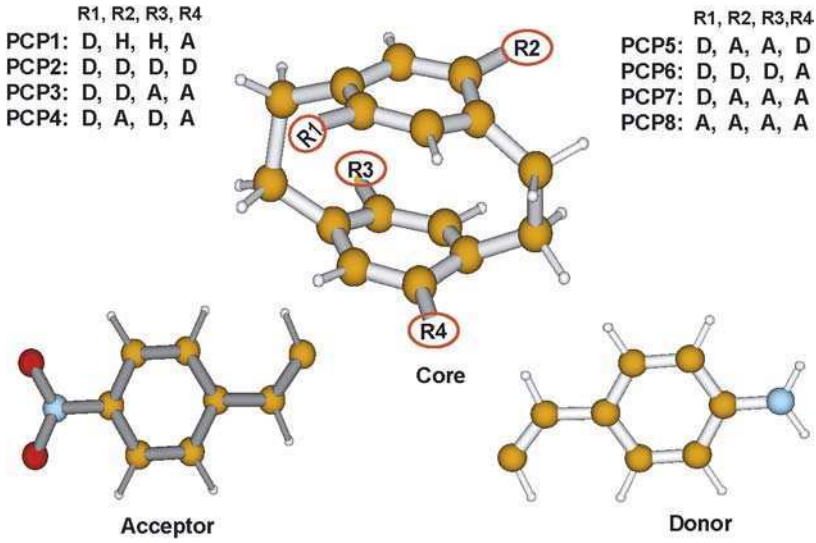

Fig. 3. Molecular structures.

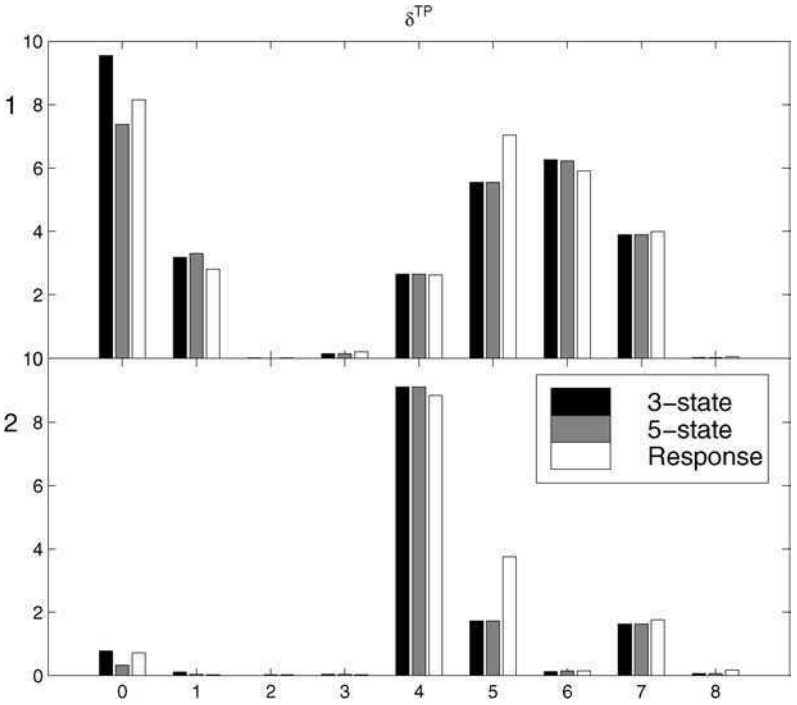

Fig. 4. The two-photon probability, δ^{TP}, in 10^5 a.u. as determined from response and few-states models for the first (1) and second (2) excited state for the systems PCP0-PCP8.

Table 4. The two-photon probability, δ^{TP}, in a.u. as calculated by the 3-states model, the 5-states model and by response theory at the SCF level with the 6-31G basis set

Molecule	ω_{exp}	ω_{theo}	$\delta_{\mathrm{TPA}}^{\mathrm{3state}}$	$\delta_{\mathrm{TPA}}^{\mathrm{5state}}$	$\delta_{\mathrm{TPA}}^{\mathrm{response}}$
0	416	345	9.549e+05	7.383e+05	8.15E+05
0		270	7.748e+04	3.376e+04	7.24E+04
1	–	306	3.183e+05	3.299e+05	2.81E+05
1	–	297	1.086e+04	3.707e+03	3.15E+03
2	446	341	3.059e+02	3.524e+01	7.38E+02
2		337	9.588e+02	2.751e+03	2.44E+03
3	433	361	1.366e+04	1.368e+04	2.00E+04
3		344	4.232e+03	4.229e+03	3.61E+03
4	479	363	2.647e+05	2.647e+05	2.63E+05
4		360	9.117e+05	9.117e+05	8.84E+05
5	491	361	5.552e+05	5.552e+05	7.04E+05
5		358	1.734e+05	1.734e+05	3.76E+05
6	441	363	6.258e+05	6.222e+05	5.91E+05
6		342	1.323e+04	1.451e+04	1.50E+04
7	444	361	3.894e+05	3.894e+05	3.99E+05
7		356	1.633e+05	1.633e+05	1.76E+05
8	–	355	1.504e+03	1.504e+03	3.75E+03
8	–	352	6.447e+03	6.447e+03	1.80E+04

the final excited state will include orthogonal dipole operators which will not only reduce δ_1^{TP} at the cost of δ_2^{TPA}, but most likely also lead to destructive interference by adding a substantial negative contribution from the δ_3^{TPA} term. It is noteworthy that the distinction between P- and O-character still applies even when the system has an undefined symmetry.

As demonstrated by Fig. 5 and as indicated by equation (48) an explicit dipolar structure seems to be preferable because other configurations will then inevitably introduce non-parallel sub-paths in the excitation scheme with destructive interference as a consequence. Thus, the supposed flexibility when going from 1D to higher dimensions appears to be somewhat fictitious in the sense that an unambiguous dipolar structure still will be the most efficient TPA property of this system.

7. COMPARISON BETWEEN DFT AND *AB INITIO* RESULTS

Quantum chemical modelling of non-linear absorption has until the implementation of density functional response theory been limited to Hartree–Fock or semi-empirical methods for extensive systems. DFT improves the description offered by HF, by supplying fractions of correlation energy obtained at a moderate computational cost. Because of the possibility within the response framework to go through the CC hierarchy and so apply a convergence scheme in the n-electron space for any available property, the low-scaling methods HF and DFT can be thoroughly benchmarked. The convergence and accuracy of results is well documented for energies [23–26], excited state energies, transition dipole moments, from

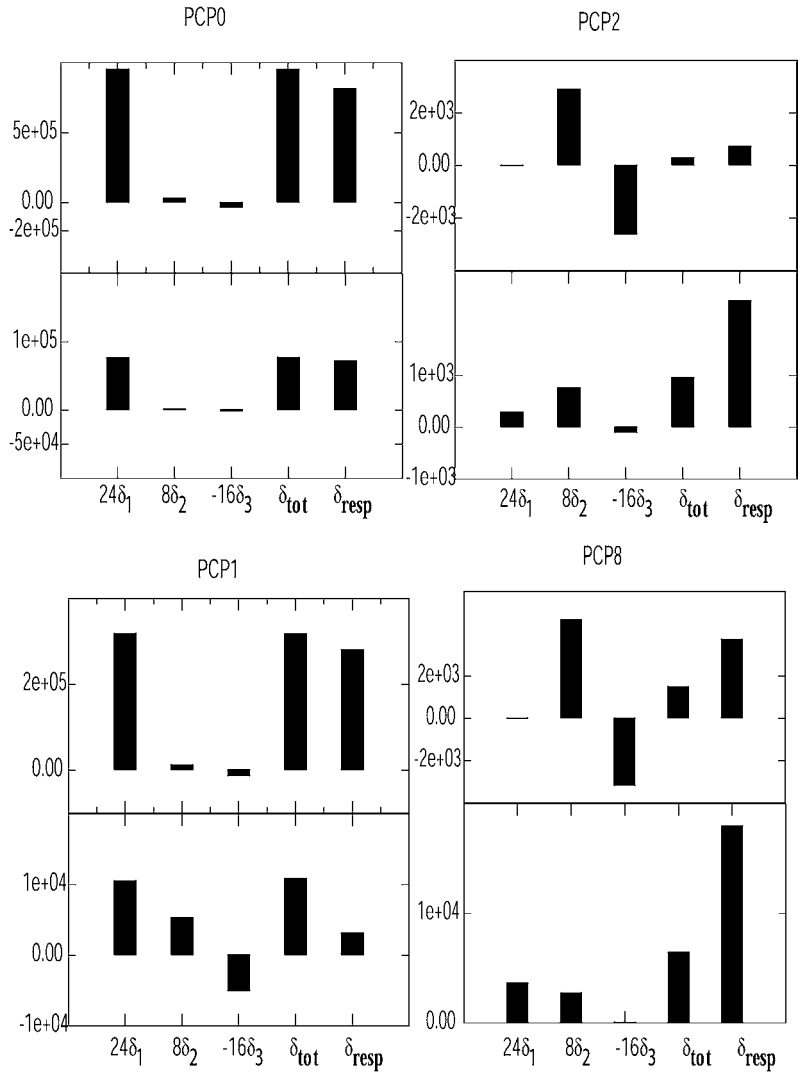

Fig. 5. The distribution between δ_1^{TP}, δ_2^{TP} and δ_3^{TP} in a.u. as calculated by the three-states model compared with the total value $\delta_{\mathrm{tot}}^{\mathrm{TP}}$ and $\delta_{\mathrm{resp}}^{\mathrm{TP}}$ from response.

ground-to-excited-state as well as excited-to-excited-state and (hyper)polarizabilities. The general trend is that the initial CCS-value, which is of similar quality as HF, is somewhat over-corrected by the CC2-method, and stabilized by CCSD somewhere in between the predictions of CCS and CC2. The refinement when moving to CC3 is often modest, which reflects that the most important contribution relates to the inclusion of singles and doubles. This roughly sketched oscillatory pattern for the sequence HF–CC2–CCSD is reproduced for excitation energies, δ^{TPA} and δ^{3PA} as depicted in Table 5. The moderate contributions from triples, as estimated from the insignificant differences between excitation energies

Table 5. H_2O. Excitation energies ω (in eV), two-photon probabilities, δ^{TPA} (in 10^3 a.u.) and three-photon probabilities, δ^{3PA} (in 10^4 a.u.) for linear polarized light as calculated by response theory at the CC, DFT and HF levels

State	$1B_2$			$1B_1$		
	ω	δ^{TPA}	δ^{3PA}	ω	δ^{TPA}	δ^{3PA}
HF	8.60	0.07	3.46	10.27	0.64	0.49
CC2	7.20	0.24	13.96	8.86	2.72	3.72
CCSD	7.57	0.16	8.35	9.33	1.64	2.06
CC3	7.58	–	–	9.35	–	–
B3LYP	6.87	0.18	11.9	8.28	1.93	2.96
BLYP	6.24	0.25	26.1	7.50	2.82	5.51
LDA	6.54	0.24	19.5	7.87	2.63	4.72
State	$2A_1$			$2B_2$		
	ω	δ^{TPA}	δ^{3PA}	ω	δ^{TPA}	δ^{3PA}
HF	10.87	0.24	2.98	11.75	0.72	3.45
CC2	9.53	0.48	8.56	10.35	2.46	54.66
CCSD	9.91	0.33	5.26	10.79	1.83	26.69
CC3	9.91	–	–	10.82	–	–
B3LYP	9.01	0.39	6.60	9.80	1.91	17.9
BLYP	8.35	0.49	8.82	8.98	2.94	39.8
LDA	8.61	0.49	10.6	9.31	2.70	26.5

The aug-cc-pVTZ basis set was employed for ω and δ^{3PA}, whereas δ^{TPA} was obtained by the Sadlej basis set.

predicted by CCSD and CC3, strengthen the predictive credibility of the δ^{TPA} and δ^{3PA} values obtained at the CCSD level.

While the excitation energies predicted by CCSD neatly is bracketed between the HF and B3LYP results, the orderings between the estimates for δ^{TPA} and δ^{3PA}. are more irregular. The HF results are uniformly the lowest, but CCSD and B3LYP interchangeably predict the largest value. The overall mutual agreement between CCSD and B3LYP seems to support the use of B3LYP for exploring the δ^{TPA} and δ^{3PA} for larger structures. Optionally in conjunction with another low-scaling method as HF, in order to attain a balanced description. We should note that performance of B3LYP for larger structures are hampered by "overpolarization", due to incorrect asymptotic behaviour of the functional. This might lead to overestimation of the cross-sections.

In Table 6 and in Fig. 6 we display the three-photon absorption probabilities, δ^{3PA}, for the first excited state for the series of modified *trans*-stilbene and DTT molecules, see Fig. 1. As seen in Fig. 6 the qualitative agreement concerning trends between HF and DFT is comforting, though the enhancement when attaching substituents is in general predicted to be more dramatic with DFT than for HF. A homologous (AA or DD) substitution will raise δ^{3PA} approximately by a factor between 2 and 18. Indisputably, AD substituted compounds give the largest responses and supersedes the non-substituted systems with at least one

Table 6. Excitation energies in eV, three-photon probabilities, δ^{3PA}, for linear polarized light in 10^6 a.u. and three-photon cross sections, σ^{3PA} in 10^{-82} $cm^6\,s^2$ as calculated by response at the HF and DFT levels with 6-31G basis set

Molecule	Exp.	HF			DFT		
	ω	ω	δ^{3PA}	σ^{3PA}	ω	δ^{3PA}	σ^{3PA}
TS	≈ 4.0[a]	4.59	12.3	0.121	4.08	76.6	0.533
TS-DD	3.32[b]	4.35	32.9	0.277	3.67	261	1.32
TS-AA		4.22	77.8	0.598	3.34	138	0.525
TS-AD	3.06[c]	4.05	289	1.96	2.78	5990	13.1
DTT		3.17	806.08	2.63	2.66	11574	22.2
DTT-DD(101)	2.88[d] 2.67[e]	3.10	1382.17	4.20	2.50	31842.6	50.8
DTT-AA	2.92[e]	3.01	2590.45	7.25	2.25	114951	134
DTT-AD(102)	2.85[d]	2.97	4808.37	12.9	1.92	649761	472

[a] From Refs. [27,28]. [b] From Ref. [29]. [c] From Ref. [30]. [d] From Ref. [31]. [e] From Ref. [32].

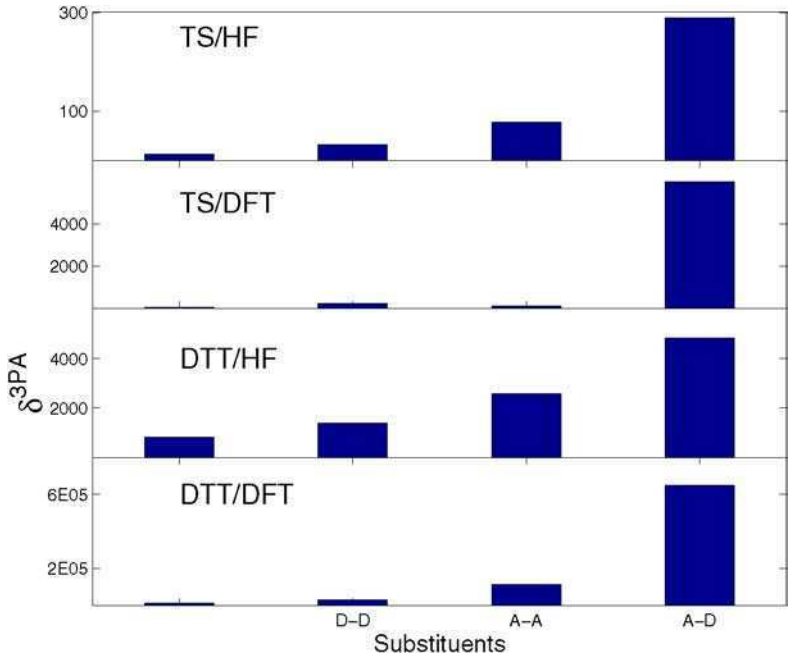

Fig. 6. Comparison between HF and B3LYP results obtained for TS and DTT.

order of magnitude and often close to two. As demonstrated by the substantial difference between TS- and DTT-based systems, the electron richness of the basic building block, interpreted as the strength of the π-center, also strongly influences the σ^{3PA}.

8. CONCLUSION

Different computational approaches for calculations of multi-photon absorption cross sections of molecules have been discussed. It is clearly shown that the response theory formulation of Olsen and Jørgensen [4] has great advantages. For instance, using the residue of response functions, one can calculate the MPA cross-sections at the same order as the corresponding (hyper)polarizability, which is a significant simplification compared to computing the MPA cross section from the $(2M - 1)$th order polarizability. The importance of response theory is further illustrated by the fact that the 3PA cross section of molecules converges very slowly with respect to the number of states included. Over the years, response theory has been implemented at different computational levels, such as Hartree–Fock, MCSCF, Coupled Cluster and Density Functional Theory. We believe that the recent development of response theory at the DFT level opens new opportunities for a variety of applications.

ACKNOWLEDGEMENTS

This work was supported by the Swedish Research Council (VR), the Carl Trygger Foundation (CTS) and by a grant from the photonics project run jointly by the Swedish Materiel Administration (FMV) and the Swedish Defense Research Establishment (FOI). The computing time provided by National Supercomputer Center in Linköping (NSC) is gratefully acknowledged.

REFERENCES

[1] M. Göppert-Mayer, *Ann. Phys.* **9** (1930) 273.
[2] W. Kaiser, C.G. Garret, *Phys. Rev. Lett.* **7** (1961) 229.
[3] S. Singh, L.T. Bradley, *Phys. Rev. Lett.* **12** (1964) 612.
[4] J. Olsen, P. Jørgensen, *J. Chem. Phys.* **82** (1985) 3235.
[5] M. Albota, D. Beljonne, J.L. Brédas, J.E. Ehrlich, J. Fu, A.A. Heikal, S.E. Hess, T. Kogej, M.D. Levin, S.R. Marder, D. McCord-Maughon, J.W. Perry, H. Röckel, M. Rumi, G. Subramaniam, W.W. Webb, X. Wu, C. Xu, *Science* **281** (1998) 1653.
[6] B.A. Reinhardt, L.L. Brott, S.J. Clarson, A.G. Dillard, J.C. Bhatt, R. Kannan, L. Yuan, G.S. He, P.N. Prasad, *Chem. Mater.* **10** (1998) 1863.
[7] G.S. He, P.P. Markowicz, T. Lin, P.N. Prasad, *Nature* **415** (2002) 767.
[8] P. Norman, Y. Luo, H. Ågren, *Chem Phys. Lett.* **286** (1998) 8.
[9] C.-K. Wang, O. Macak, Y. Luo, H. Ågren, *J. Chem. Phys.* **114** (2001) 9813.
[10] P. Norman, Y. Luo, H. Ågren, *J. Chem. Phys.* **111** (1999) 7759.
[11] P. Cronstrand, Y. Luo, H. Ågren, *J. Chem. Phys.* **117** (2002) 11102.
[12] P. Macak, Y. Luo, P. Norman, H. Ågren, *J. Chem. Phys.* **113** (2002) 7055.
[13] P. Macak, Y. Luo, H. Ågren, *Chem. Phys. Lett.* **330** (2000) 447.
[14] Y. Luo, P. Norman, P. Macak, H. Ågren, *J. Phys. Chem. A* **104** (2000) 4718.
[15] P. Cronstrand, P. Norman, Y. Luo, H. Ågren, *J. Chem. Phys.* **121** (2004) 2020.
[16] H. Mahr, in: H. Rabin, C.L. Tang (Eds.), *Quantum Electronics, vol. IA*, Academic Press, New York, 1975, p. 225.
[17] R.W. Boyd, *Nonlinear Optics*, Academic Press, London, 2003.
[18] P.R. Monson, W.M. McClain, *J. Chem. Phys.* **53** (1970) 29.
[19] W.M. McClain, *J. Chem. Phys.* **55** (1971) 2789.
[20] W.M. McClain, *J. Chem. Phys.* **58** (1973) 324.

[21] W.M. McClain, *J. Chem. Phys.* **57** (1972) 2264.
[22] O. Christiansen, P. Jørgensen, C. Hättig, *Int. J. Quantum Chem.* **68** (1998) 1.
[23] O. Christiansen, A. Halkier, H. Koch, P. Jørgensen, T. Helgaker, *J. Chem. Phys.* **108** (1998) 2801.
[24] O. Christiansen, H. Koch, P. Jørgensen, *J. Chem. Phys.* **103** (1995) 7429.
[25] P. Cronstrand, O. Christiansen, P. Norman, H. Ågren, *Phys. Chem. Chem. Phys.* **3** (2001) 2567.
[26] P. Cronstrand, O. Christiansen, P. Norman, H. Ågren, *Phys. Chem. Chem. Phys.* **2** (2000) 5357.
[27] G. Hohlneicher, B. Dick, *J. Photochem.* **27** (1984) 215.
[28] M.S. Gudipati, M. Mauds, J. Daverkausen, G. Hohlneicher, *Chem. Phys.* **192** (1995) 37.
[29] J.W. Robinson, *Handbook of Spectroscopy, vol. II*, CRC Press, Florida, 1974.
[30] M. Rumi, J.E. Ehrlich, A.A. Heikal, J.W. Perry, S. Barlow, Z. Hu, D. McCord-Maughon, T.C. Parker, H. Röckel, S. Thayumanavan, S.R. Marder, D. Beljonne, J.L. Brédas, *J. Am. Soc.* **122** (2000) 9500.
[31] O.-K. Kim, K.-S. Lee, H.Y. Woo, K.-S. Kim, G.S. He, J. Swiatkiewicz, P.N. Prasad, *Chem. Mater.* **12** (2000) 284.
[32] L. Ventelon, L. Moreaux, J. Mertz, M. Blanchard-Desce, *Chem. Commun. (London)* **1999** (1999) 2055.

This page intentionally left blank

Two-Bond Spin–Spin Coupling Constants ($^{2h}J_{X-Y}$) Across X–H–Y Hydrogen Bonds: Some Fundamental Questions

Janet E. Del Bene[1] and José Elguero[2]

[1]*Department of Chemistry, Youngstown State University, Youngstown, OH 44555, USA*
[2]*Instituto de Química Médica, CSIC, Juan de la Cierva, 3, E-28006 Madrid, Spain*

Dedicated to Jan Linderberg and Poul Jørgensen

Abstract

Investigations of spin–spin coupling constants ($^{2h}J_{X-Y}$) across X–H–Y hydrogen bonds constitute a relatively new and exciting area of theoretical and experimental research. Despite the tremendous progress that has been made in a short period of time, there remain many fundamental questions that need to be addressed. Among these are the following:

(1) Is it possible to predict the signs of two-bond spin–spin coupling constants ($^{2h}J_{X-Y}$) across X–H–Y hydrogen bonds?
(2) What determines the sign of $^{2h}J_{X-Y}$?
(3) Does the measurement of a two-bond coupling constant prove that the hydrogen bond is covalent?
(4) What role does the proton play in coupling across hydrogen bonds?

Systematic studies of two-bond coupling constants for series of complexes stabilized by C–H–N, N–H–N, O–H–N, F–H–N, C–H–O, N–H–O, O–H–O, and F–H–O hydrogen bonds have been carried out using the *ab initio* equation-of-motion coupled cluster singles and doubles (EOM–CCSD) method. The results of these studies are used to provide some answers to these questions.

Contents

1. INTRODUCTION

A new and important area of both experimental and theoretical research is the investigation of NMR two-bond spin–spin coupling constants across hydrogen bonds [1–43]. Research

ADVANCES IN QUANTUM CHEMISTRY, VOLUME 50
ISSN: 0065-3276 DOI: 10.1016/S0065-3276(05)50002-9

efforts of many investigators have been directed toward extracting structural information from NMR spectral data, interpreting the NMR results, and understanding the factors that are important in determining the signs and magnitudes of coupling constants. Despite the tremendous progress that has been made in a relatively short time, there are still some very fundamental questions that remain. In this paper, the results of recent work carried out in this laboratory will be used to address the following questions.

1. Is it possible to predict the signs of two-bond spin–spin coupling constants ($^{2h}J_{X-Y}$) across X–H–Y hydrogen bonds?
2. What determines the sign of $^{2h}J_{X-Y}$?
3. Does the measurement of a two-bond coupling constant prove that the hydrogen bond is covalent?
4. What role does the proton play in coupling across hydrogen bonds?

2. METHODS

The optimized structures of hydrogen-bonded complexes have been obtained at second-order Møller-Plesset perturbation theory (MP2) [44–47] with the 6-31 + G(d,p) basis set [48–51], using the Gaussian 98 suite of programs [52]. Coupling constants for the optimized complexes and other related complexes were computed using the *ab initio* equation-of-motion coupled cluster singles and doubles (EOM–CCSD) method in the CI-like approximation [53–56], with the Ahlrichs [57] qzp basis set on C, N, O, and F atoms, qz2p on the hydrogen-bonded hydrogen, and Dunning's cc-pVDZ basis [58,59] on all other hydrogens. In nonrelativistic theory, the total spin–spin coupling constant has four components: the paramagnetic spin-orbit (PSO), diamagnetic spin-orbit (DSO), Fermi-contact (FC), and spin-dipole (SD) terms. All terms have been evaluated using the ACES II program[1]. All calculations were done on the Cray SV1 or the Itanium cluster at the Ohio Supercomputer Center.

3. RESULTS AND DISCUSSION

A systematic investigation of X–Y coupling constants across X–H–Y hydrogen bonds has been completed for eight series of complexes stabilized by hydrogen bonds formed from the second-period elements ^{13}C, ^{15}N, ^{17}O, and ^{19}F. Specifically, these include C–H–N, N–H–N, O–H–N, F–H–N, C–H–O, N–H–O, O–H–O, and F–H–O hydrogen bonds. These studies have established that for all complexes in these series, $^{2h}J_{X-Y}$ is determined by the Fermi-contact (FC) term. The dominance of the FC term is not due to a cancellation of other terms, but arises because the FC term is usually more than an order of magnitude greater than any other term.

It has also been demonstrated that the FC term, and therefore $^{2h}J_{X-Y}$, are dependent on the X–Y distance, as illustrated for the FH:NCLi complex in Fig. 1. Because the FC

[1] ACES II is a program product of the Quantum Theory Project, University of Florida. Authors: J.F. Stanton, J. Gauss, J.D. Watts, M. Nooijen, N. Oliphant, S.A. Perera, P.G. Szalay, W.J. Lauderdale, S.R. Gwaltney, S. Beck, A. Balkova, D.E. Bernholdt, K.-K. Baeck, P. Tozyczko, H. Sekino, C. Huber, and R.J. Bartlett. Integral packages included are VMOL (J. Almlof, and P.R. Taylor); VPROPS (P.R. Taylor); ABACUS (T. Helgaker, H.J.Aa. Jensen, P. Jørgensen, J. Olsen, and P.R. Taylor). Brillouin–Wigner perturbation theory was implement by J. Pittner.

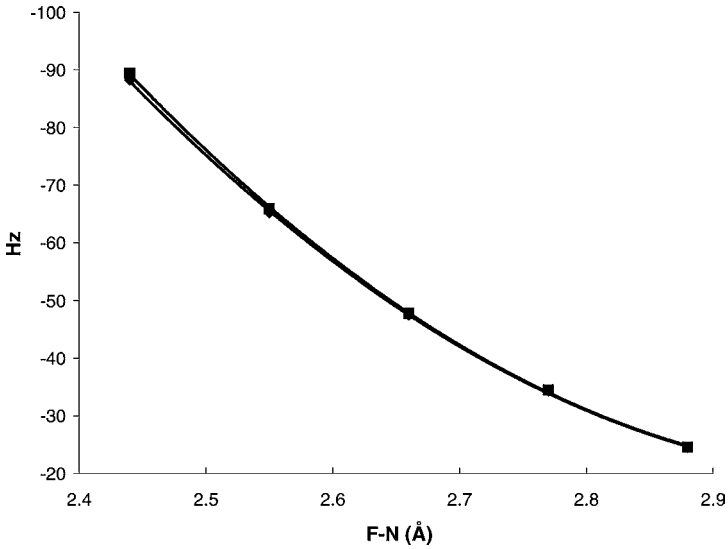

Fig. 1. $^{2h}J_{F-N}$ and the Fermi-contact term versus the F–N distance for FH:NCLi. Solid squares: $^{2h}J_{F-N}$; Solid diamonds: Fermi-contact term.

term is a good approximation to $^{2h}J_{X-Y}$, FC and $^{2h}J_{X-Y}$ will be used interchangeably in this paper. Notably absent from the above list of hydrogen bonds is F–H–F, since terms other than the FC term make significant contributions to $^{2h}J_{F-F}$. F–F coupling in FHF^- and $(HF)_2$ clusters has been discussed in detail in previous papers [26,60].

3.1. Prediction of the signs of two-bond spin–spin coupling constants ($^{2h}J_{X-Y}$) across hydrogen bonds

Of the four questions presented in the Introduction, the first asks whether or not it is possible to predict the signs of two-bond spin–spin coupling constants across *X*–H–*Y* hydrogen bonds. Figure 2 presents a plot of two-bond N–N coupling constants for a set of neutral complexes (with CNH as the proton donor to NCH, NCLi, pyridine, and NH_3; and pyrrole:NCH) and cationic complexes (with pyridinium and diazinium as proton donors to NCH and NCLi; and NH_4^+ as the proton donor to NCH, NCLi, N_2 and NH_3) stabilized by N–H–N or N–H^+–N hydrogen bonds [30]. One notable feature of this graph is that all N–N coupling constants are positive.

Figure 3 presents a plot of the values of $^{2h}J_{C-N}$ versus the C–N distance for a set of neutral and charged complexes stabilized by C–H–N hydrogen bonds [43]. The neutral complexes include those with sp-hybridized carbons (HCCH, FCCH, ClCCH, and NCH) as proton donors to nitrogen bases with the nitrogen sp (NCH and NCLi) or sp^3 (NH_3) hybridized, as well as one complex (NCH:pyridine) with an sp^2 hybridized nitrogen as the proton acceptor. Complexes with an sp^2 hybridized carbon [F(O)CH] as the proton donor to NCH and NH_3, and with an sp^3 hybridized carbon (F_3CH) as the proton donor to NCH and NH_3, have also been included. The cationic complexes include $HNCH^+$:NCH, pyridinium:CNH, and H_3NH^+:CNH, while the anionic complexes include the set having

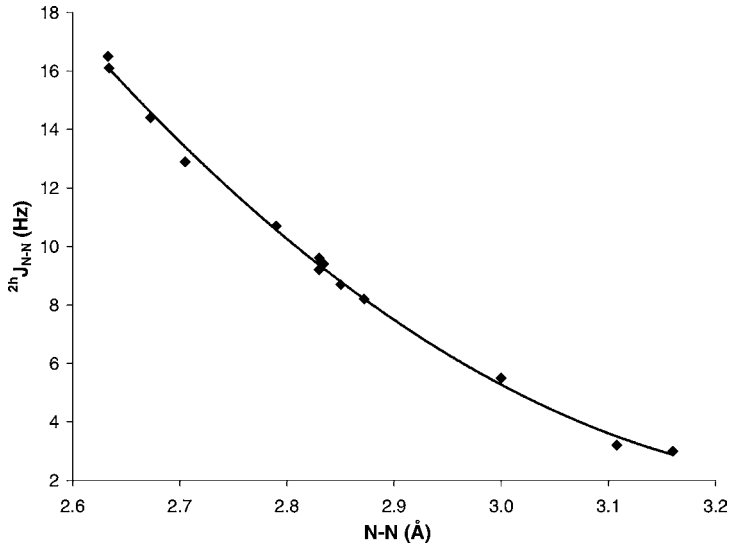

Fig. 2. $^{2h}J_{N-N}$ versus the N–N distance for the equilibrium structures of neutral and cationic complexes with N–H–N hydrogen bonds.

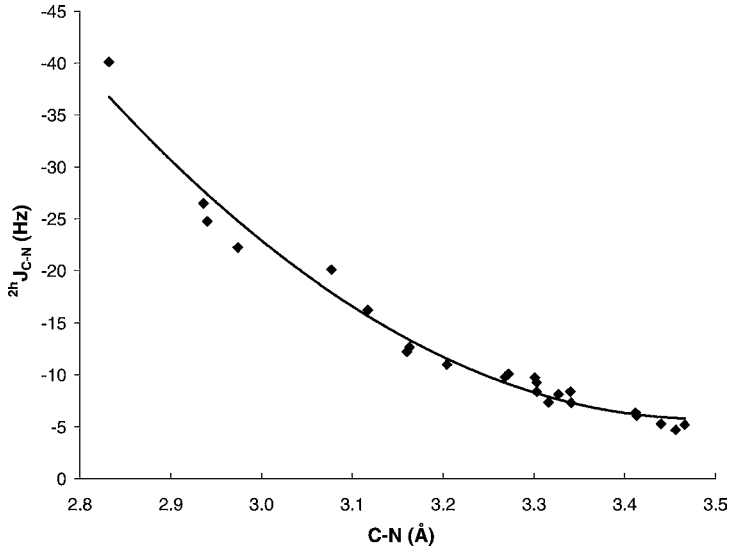

Fig. 3. $^{2h}J_{C-N}$ versus the C–N distance for the equilibrium structures of neutral and charged complexes stabilized by C–H–N hydrogen bonds.

HCCH, FCCH, and NCH as proton donors to NC^-. Figure 3 shows that irrespective of the charge on the complex or whether the hydrogen bond has C–H as the proton donor to N, or N–H as the proton donor to C, all C–N coupling constants are negative.

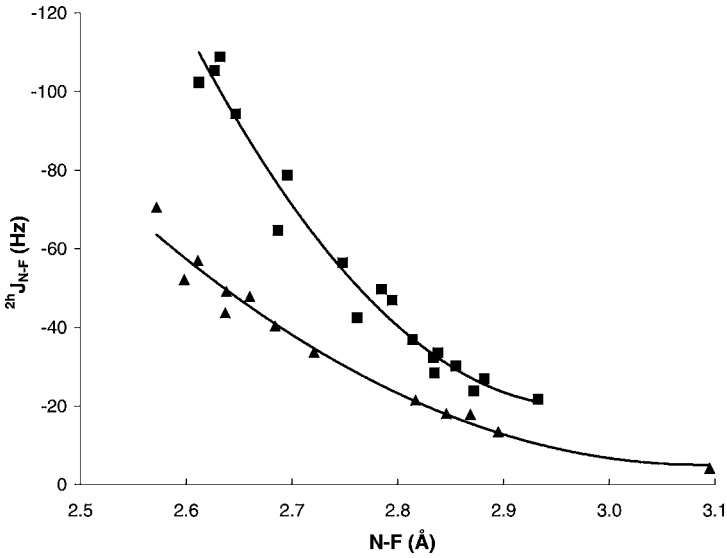

Fig. 4. $^{2h}J_{F-N}$ versus the F–N distance for the optimized structures of neutral and cationic complexes stabilized by F–H–N hydrogen bonds. Solid squares: cations; Solid triangles: neutrals.

Figure 4 shows two plots, one for neutral complexes with F–H···N hydrogen bonds [41], and one for cationic complexes with $N–H^+\cdots F$ hydrogen bonds [42]. The neutral complexes have FH as the proton donor to sp (HCN, LiCN, FCN, and NCCN), sp^2 (pyridine, 4-Li-pyridine, 1,4-diazine, and 1,3,5-triazine) and sp^3 [NH_3, NFH_2, NF_2H, NF_3, and $NH_2(CH_3)$] hybridized nitrogens. The cationic complexes are stabilized by hydrogen bonds in which sp, sp^2, and sp^3 hybridized nitrogens are the $N–H^+$ donors to FH. The proton donors include protonated sp bases derived from HCN (HCN, LiCN, CH_3CN, FCN, and NCCN), protonated sp^2 aromatic (pyridine, 4-Li-pyridine, 1,4-diazine, 1,3,5-triazine, and 1,2,4,6-tetrazinium) and imine ($H_2C{=}NH$, F(H)C=NH, and $H_2C{=}NF$) bases, and protonated sp^3 bases derived from NH_3 [NH_3, NFH_2, NF_2H, NF_3, and $NH_2(CH_3)$]. From Fig. 4 it is apparent that cationic complexes have larger coupling constants than neutral complexes at the same F–N distance, a consequence of the increased proton-shared character of the cationic hydrogen bonds. However, for purposes of this paper, it is important to note that the equilibrium values of $^{2h}J_{F-N}$ in Fig. 4 are always negative.

Table 1 reports values of $^{2h}J_{X-Y}$ for five series of complexes stabilized by N–H–O, C–H–O, O–H–O, F–H–O, and C–H–F hydrogen bonds. The examples listed are representative of various types of hydrogen bonds involving the same two elements *X* and *Y*. For example, the complexes with O–H–O hydrogen bonds are $(H_2O)_2$ with a traditional hydrogen bond, and the protonated and deprotonated water dimer, $O_2H_5^+$ and $O_2H_3^-$, charged complexes with symmetric, proton-shared hydrogen bonds. Complexes with F–H–O hydrogen bonds include those with HF as the proton donor ($FH{:}OH_2$ and $FH{:}OCH_2$) and those with HF as the proton acceptor ($H_2COH^+{:}FH$ and $H_2OH^+{:}FH$). From Table 1 it can be seen that all complexes with N–H–O, O–H–O, and C–H–F hydrogen bonds have positive coupling constants, while those with C–H–O and F–H–O hydrogen bonds have negative coupling constants.

Table 1. $^{2h}J_{X-Y}$ (Hz) for representative complexes with N–H–O, C–H–O, O–H–O, F–H–O, and C–H–F hydrogen bonds

N–H–O hydrogen bonds	
Complex	$^{2h}J_{X-Y}$
HOH:NCH	1.1
H_2OH^+:NCH	34.1
HOH:NC^-	6.6
$HCNH^+$:OC	11.3

C–H–O hydrogen bonds	
Complex	$^{2h}J_{X-Y}$
F_2HCH:OCH_2	−1.6
F_2HCH:OH_2	−5.5
NCH:OC	−2.7
$HNCH^+$:OC	−14.0

O–H–O hydrogen bonds	
Complex	$^{2h}J_{X-Y}$
$O_2H_5^+$	39.5
$O_2H_3^-$	16.3
$(H_2O)_2$	1.5
$(H_2CO)_2H^+$	21.0

F–H–O hydrogen bonds	
Complex	$^{2h}J_{X-Y}$
FH:OH_2	−18.4
FH:OCH_2	−12.2
H_2COH^+:FH	−33.3
H_2OH^+:FH	−71.0

C–H–F hydrogen bonds	
Complex	$^{2h}J_{X-Y}$
NCH:FH	32.0
$HNCH^+$:FH	141.5
OCH^+:FH	228.3
FH:CO	33.7

When coupling constants involving different atoms are compared, it is the reduced coupling constant, $^{2h}K_{X-Y}$, that should be used [61]. Thus,

$$^{2h}K_{X-Y} \propto {}^{2h}J_{X-Y}/(\gamma_X)(\gamma_Y)$$

where γ_X and γ_Y are the magnetogyric ratios of atoms X and Y. The second-row nuclei investigated in this work include two that have positive magnetogyric ratios (^{13}C and ^{19}F) and two that have negative magnetogyric ratios (^{15}N and ^{17}O). The signs of $^{2h}J_{X-Y}$ and $^{2h}K_{X-Y}$ for C–H–N, N–H–N, O–H–N, F–H–N, C–H–O, N–H–O, O–H–O, and F–H–O hydrogen bonds are summarized in Table 2. It is apparent that the signs of the reduced two-bond spin–spin coupling constants are positive in all cases [62]. Thus, it is possible to predict the signs of two-bond X–Y coupling constants across X–H–Y hydrogen bonds. If neither or both X and Y have negative magnetogyric ratios, $^{2h}J_{X-Y}$ is positive. If either X or Y has a negative magnetogyric ratio, then $^{2h}J_{X-Y}$ is negative. Unfortunately, there is little experimental data to test this prediction, but the available data are consistent. The N–N coupling constants across the N–H–N hydrogen bonds in the AU and GC pairs are positive [6,7,39,63], as is an N–N coupling constant across an intramolecular N–H–N hydrogen bond [29]. The F–N coupling constant for the FH:collidine (FH:2,4,6-trimethylpyridine) complex is negative [28].

3.2. Factors that determine the signs of reduced two-bond coupling constants

Having established that the signs of reduced two-bond spin–spin coupling constants are positive, it is appropriate to seek some insight into what determines these signs. The Dirac Vector Model [64], which is based on considerations of ground-state bonding, states that all one-bond coupling constants are positive, two-bond are negative, three-bond positive, etc. However, it is known that this model is often violated, even in relatively simple molecules [65]. Moreover, since X–Y coupling across an X–H–Y hydrogen bond is a two-bond coupling, the Dirac Vector Model predicts that $^{2h}K_{X-Y}$ should be negative. Thus, this model cannot explain the signs given in Table 2.

Since the Fermi-contact term is an excellent approximation to $^{2h}J_{X-Y}$, an appropriate question to ask is what determines the sign of the reduced Fermi-contact term. Some insight into the answer to this question can be gained by considering the recently-proposed Nuclear Magnetic Resonance Triplet Wavefunction Model (NMRTWM) [66]. This model arose from consideration of the equation relating $^{2h}J_{X-Y}$ to the second-derivative of the energy (E) with respect to the nuclear magnetic moments (μ_X and μ_Y),

$$J_{X-Y} = \partial^2 E / \partial \mu_X \cdot \partial \mu_Y$$

and from the sum-over-states expression for computing the Fermi-contact term, which arises from the coupling of excited triplet states to the ground state through the Fermi-contact operator [67]. The excited triplet states must be σ-type states so that there is s-electron density at nuclei X and Y, and must be of the appropriate symmetry. NMRTWM states that the alignment of nuclear magnetic moments responds to the phases of excited triplet state wavefunctions. The Model is illustrated for a symmetric X–H–X hydrogen bond in Fig. 5, which shows nodal patterns of wavefunctions for lower-energy excited triplet states. If the nuclear magnetic moment is arbitrarily assigned as "up" when the phase of the wavefunction is positive, then the nuclear magnetic moments of the two X atoms are parallel if the wavefunction has either no nodes or two nodes intersecting the axis between the two X atoms, as shown in Fig. 5 "a" and "c". These patterns gives rise to a negative reduced coupling constant. However, if the wavefunction has one (or an odd number of nodes) between the two X atoms, then one node must pass through the H atom, as shown in Fig. 5 "b". In this case, the nuclear magnetic moments of the two X atoms have

Table 2. Signs of $^{2h}J_{X-Y}$ and $^{2h}K_{X-Y}$ for complexes with X–H–Y hydrogen bonds

X–H–Y	Sign of $^{2h}J_{X-Y}$	Sign of $^{2h}K_{X-Y}$
C–H–N	−	+
N–H–N	+	+
O–H–N	+	+
F–H–N	−	+
C–H–O	−	+
O–H–O	+	+
F–H–O	−	+
C–H–F	+	+

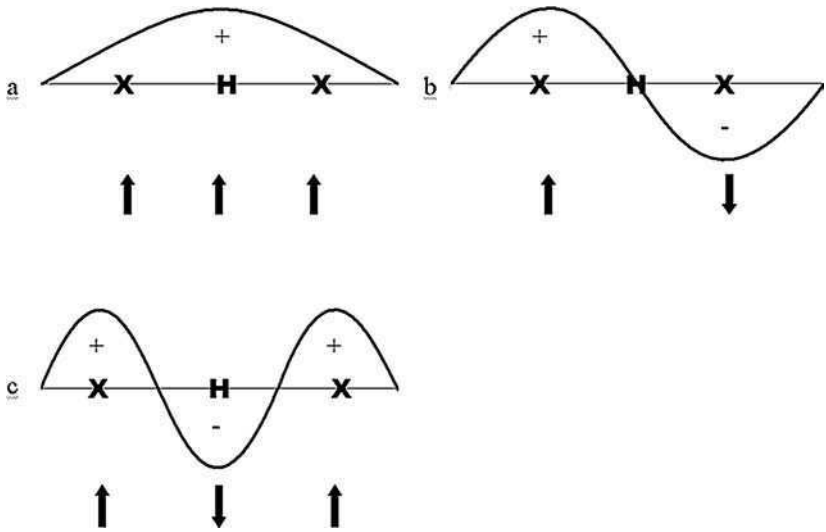

Fig. 5. Nodal patterns and nuclear magnetic moment alignments for a symmetric X–H–X hydrogen bond.

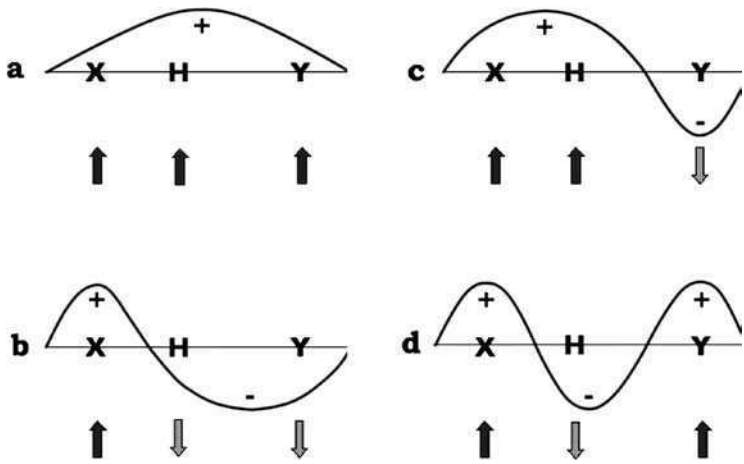

Fig. 6. Nodal patterns and nuclear magnetic moment alignments for an asymmetric X–H–Y hydrogen bond.

an antiparallel alignment, and the signs of the reduced Fermi-contact term and $^{2h}K_{X-X}$ are positive. This suggests that triplet states that have one node dominate and determine the signs of reduced spin–spin coupling constants, $^{2h}K_{X-X}$.

Figure 6 shows the nodal patterns of wavefunctions and nuclear magnetic moment alignments for triplet states having zero, one, or two nodes intersecting the X–H–Y hydrogen-bonding axis. For this example, the hydrogen bond is a traditional hydrogen bond, and the assumption is made that none of the nodes accidentally pass through a nucleus. Nodal

patterns "a" and "d" with zero and two nodes, respectively, give rise to parallel alignments of the magnetic moments of X and Y, thus making the reduced Fermi-contact term negative. Patterns "b" and "c" have only one node, intersecting the X–H covalent bond or the H–Y hydrogen bond. In both cases, the magnetic moments of X and Y have an antiparallel alignment. Since an antiparallel alignment leads to a positive value of the FC term, it is triplet states of types "b" and "c" that dominate. Which is the more important cannot be determined since a complete sum-over-states calculation is not feasible [67,68].

3.3. Two-bond coupling constants and hydrogen bond covalency

The third question posed in the Introduction asks whether or not the experimental measurement of a spin–spin coupling constant across an hydrogen bond proves that the hydrogen bond is covalent. Statements that this is the case have been made by several investigators, but these claims have been disputed by others [6,12,69–71]. Those who did not support this claim noted that through-space couplings can occur between atoms in a repulsive orientation, an example being ^{19}F–^{19}F coupling in cis-1,2-difluoroethene. There is, however, a way in which this question can be addressed more directly [72,73]. Table 3 reports X–Y coupling constants for selected equilibrium structures of complexes stabilized by X–H–Y hydrogen bonds, and structures related to these by the removal of the hydrogen-bonded proton. The first complex is the protonated water dimer, $O_2H_5^+$. The O–O coupling constant of this complex is 39.9 Hz at the equilibrium O–O distance of 2.386 Å. For comparison, coupling constants for two H_2O molecules at the same O–O distance and with the same orientation of the two H_2O molecules are also given. For the first comparative structure, H^+ has been removed, but its basis functions kept. The O–O coupling constant

Table 3. Two-bond spin–spin coupling constants ($^{2h}J_{X-Y}$, Hz) and X–Y distances (Å) for hydrogen-bonded complexes and related structures

Complex	R_{X-Y}	$^{2h}J_{X-Y}$	Related structure	R_{X-Y}	J_{X-Y}
$O_2H_5^+$ (C_2)	2.386	39.9	O_2H_4 (C_2)[a]	2.386	25.6
			O_2H_4 (C_2)[b]	2.386	25.0
$N_2H_7^+$ (D_{3d})	2.598	17.2	N_2H_6 (D_{3d})	2.598	13.5
FH:NH_3	2.637	−45.2	F^-:NH_3	2.637	−51.7
HOH:OH_2 (C_s)	2.914	1.5	H_2O:OH_2 (D_{2h})[c]	2.914	5.8
$C_3H_4O_2$ (C_s)[d]	2.600	3.5	$C_3H_4O_2$ (C_s)[e]	2.600	5.1

[a] The two H_2O molecules have the same orientation as in the equilibrium protonated dimer $O_2H_5^+$ with the hydrogen-bonded proton removed, but with the basis functions on this proton remaining.

[b] The two H_2O molecules have the same orientation as in the equilibrium protonated dimer $O_2H_5^+$ with the hydrogen-bonded proton and its basis functions removed.

[c] A planar arrangement of two optimized H_2O molecules with D_{2h} symmetry and no hydrogen bond. The two O atoms are adjacent, and the H atoms are on the outside of the two oxygens.

[d] The optimized equilibrium structure of malonaldehyde with an asymmetric O–H–O hydrogen bond.

[e] A conformer of malonaldehyde derived from the optimized structure by rotating the O–H bond of the C–O–H group by 180° about the C–O bond, thereby destroying the O–H–O hydrogen bond.

decreases to 25.6 Hz. For the second comparison, both H^+ and its basis functions have been removed. The O–O coupling constant decreases further, but by only 0.6 Hz. Since the coupling constant decreases when H^+ is removed, the presence of the H atom must influence the magnitude of the O–O coupling constant. However, since coupling between the two O atoms remains despite the fact that there is no hydrogen bond suggests that the measurement of a two-bond coupling constant across a hydrogen bond is not a proof that the hydrogen bond is covalent. That $J_{O–O}$ changes so little whether or not the H atom basis functions are present suggests that there is no significant basis set superposition effect on $J_{O–O}$. The second example in Table 3 is similar to the first, in this case it is the protonated ammonia dimer, $N_2H_7^+$, and its deprotonated structure N_2H_6 that are compared. The two NH_3 molecules in N_2H_6 have the same orientation as they do in $N_2H_7^+$. The coupling constant between the two N atoms decreases from 17.2 to 13.5 Hz when the proton is removed, but the two N atoms still couple despite the fact that there is no hydrogen bond, and the interaction between the two molecules is repulsive.

In the next example a neutral complex, $FH:NH_3$, is compared with its deprotonated analogue, $F^-:NH_3$. $^{2h}J_{F–N}$ is -45.2 Hz at the equilibrium F–N distance of 2.637 Å in $FH:NH_3$. $J_{F–N}$ increases (in an absolute sense) to -51.7 Hz in the structure $F^-:NH_3$ which has the same F–N distance, despite the fact that there is no hydrogen bond.

The first three examples involve the removal of H^+, so that the charge on the complex changes from $+1$ to 0, or from 0 to -1. In the next example, the charge is unchanged when the O–O coupling constant in the water dimer $(H_2O)_2$ is compared with the O–O coupling constant between two H_2O molecules in a nonhydrogen-bonded orientation. At the equilibrium O–O distance of 2.914 Å in the water dimer, $^{2h}J_{O–O}$ is quite small at 1.5 Hz. By contrast, the O–O coupling constant between two H_2O molecules in a repulsive orientation of D_{2h} symmetry in which the two O atoms are adjacent is 5.8 Hz at the same O–O distance.

The final example is malonaldehyde, which has an equilibrium structure of C_s symmetry and is stabilized by an asymmetric intramolecular O–H–O hydrogen bond. The equilibrium structure has an O–O distance of 2.600 Å, and $^{2h}J_{O–O}$ is 3.5 Hz. If the hydrogen-bonded O–H is rotated by 180° about the C–O bond, the hydrogen bond is broken, but all other coordinates remain the same. In this non-hydrogen-bonded conformation, $J_{O–O}$ increases to 5.1 Hz. These data demonstrate that even in the absence of an X–H–Y hydrogen bond, X and Y can couple. The coupling constant for the nonhydrogen-bonded structure may be greater or less than that of the corresponding hydrogen-bonded structure, depending on the nature of the complex. Thus, the measurement of a two-bond coupling constant across an X–H–Y hydrogen bond cannot be interpreted as proof that the hydrogen bond is covalent.

3.4. Role of the proton in coupling across hydrogen bonds

It is therefore appropriate to ask just what role does the proton play in X–Y coupling across a hydrogen bond. The proton is essential for hydrogen bond formation, which brings the atoms X and Y close enough to couple. Through the hydrogen bond, a stable complex is formed which can be probed experimentally. Another important role for the proton is to influence the magnitude of coupling constants. Hydrogen bond formation alters the electron densities of atoms X and Y in both ground and excited triplet states. Changing the s-electron densities of these atoms changes $^{2h}J_{X–Y}$. However, the proton is not directly involved in the mechanism of X–Y coupling.

4. CONCLUSIONS

Four questions concerning two-bond X–Y spin–spin coupling across X–H–Y hydrogen bonds were raised in the Introduction, and discussed in this paper. The following statements summarize the answers given to these questions. The answers to questions 1 and 2 apply to all hydrogen-bonded complexes formed from the second-period elements C, N, O, and F except those with F–H–F hydrogen bonds.

1. The signs of all two-bond reduced spin–spin coupling constants ($^{2h}K_{X-Y}$) for X–H–Y hydrogen bonds formed from the elements ^{13}C, ^{15}N, ^{17}O, and ^{19}F are positive. Thus, it is possible to predict the signs of the experimentally measured coupling constants ($^{2h}J_{X-Y}$) taking into account the magnetogyric ratios of X and Y.
2. $^{2h}J_{X-Y}$ is determined solely by the Fermi-contact term. The nuclear magnetic resonance triplet wavefunction model (NMRTWM) applies specifically to the reduced FC term, and suggests that the alignment of nuclear magnetic moments and therefore the sign of $^{2h}K_{X-Y}$ are sensitive to the nodal patterns of wavefunctions for excited triplet states.
3. The measurement of a two-bond X–Y coupling constant across an X–H–Y hydrogen bond does not constitute proof that the hydrogen bond is covalent.
4. Although the proton is not involved in the mechanism of X–Y coupling, the proton is necessary for the formation of an X–H–Y hydrogen bond. This leads to a stable complex in which the atoms X and Y are close enough to couple. The proton influences the magnitudes of X–Y coupling constants by altering the s-electron densities of X and Y in ground and excited triplet states.

ACKNOWLEDGEMENTS

It is a pleasure to thank the National Science Foundation (grant CHE-9873815), the Spanish DGI/MCyT (project no. BQU-2000-0906), and the Ohio Supercomputer Center for support of this work.

REFERENCES

[1] J. Laynez, M. Menéndez, J.L.S. Velasco, A.L. Llamas-Saiz, C. Foces-Foces, J. Elguero, P. Molina, M. Alajarín, *J. Chem. Soc. Perkin Trans.* **2** (1993) 709.
[2] N.S. Golubev, G.S. Denisov, S.N. Smirnov, D.N. Shehepkin, H.-H. Limbach, *Z. Phys. Chem.* **196** (1996) 73.
[3] S.N. Smirnov, N.S. Golubev, G.S. Denisov, H. Benedict, P. Schah-Mohammedi, H.-H. Limbach, *J. Am. Chem. Soc.* **118** (1996) 4094.
[4] I.G. Shenderovich, S.N. Smirnov, G.S. Denisov, V.A. Gindin, N.S. Golubev, A. Dunger, R. Reibke, S. Kirpekar, O.L. Malkina, H.-H. Limbach, *Ber. Bunsen. Phys. Chem.* **102** (1998) 422.
[5] H. Benedict, H.-H. Limbach, M. Wehlan, W.-P. Fehlhammer, N.S. Golubev, R. Janoschek, *J. Am. Chem. Soc.* **120** (1998) 2939.
[6] A.G. Dingley, S. Grzesiek, *J. Am. Chem. Soc.* **120** (1998) 8293.
[7] A.J. Dingley, J.E. Masse, R.D. Peterson, M. Barfield, J. Feigon, S. Grzesiek, *J. Am. Chem. Soc.* **121** (1999) 6019.
[8] C. Scheurer, R. Brüschweiler, *J. Am. Chem. Soc.* **121** (1999) 8661.
[9] N.S. Golubev, I.G. Shenderovich, S.N. Smirnov, G.S. Denisov, H.-H. Limbach, *Chem. Eur. J.* **5** (1999) 492.
[10] S.N. Smirnov, H. Benedict, N.S. Golubev, G.S. Denisov, M.M. Kreevoy, R.L. Schowen, H.-H. Limbach, *Can. J. Chem.* **77** (1999) 943.

[11] S.A. Perera, R.J. Bartlett, *J. Am. Chem. Soc.* **122** (2000) 1231.
[12] H. Benedict, I.G. Shenderovich, O.L. Malkina, V.G. Malkin, G.S. Denisov, N.S. Golubev, H.-H Limbach, *J. Am. Chem. Soc.* **122** (2000) 1979.
[13] J.E. Del Bene, S.A. Perera, R.J. Bartlett, *J. Am. Chem. Soc.* **122** (2000) 3560.
[14] J.E. Del Bene, M.J.T. Jordan, *J. Am. Chem. Soc.* **122** (2000) 4794.
[15] J.E. Del Bene, R.J. Bartlett, *J. Am. Chem. Soc.* **122** (2000) 10480.
[16] P. Schah-Mohammedi, I.G. Shenderovich, C. Detering, H.-H. Limbach, P.M. Tolstoy, S.N. Smirnov, G.S. Denisov, N.S. Golubev, *J. Am. Chem. Soc.* **122** (2000) 12878.
[17] M. Pecul, J. Leszczynski, J. Sadlej, *J. Phys. Chem. A* **104** (2000) 8105.
[18] M. Fierman, A. Nelson, S.I. Khan, M. Barfield, D.J. O'Leary, *Org. Lett.* **2** (2000) 2077.
[19] M. Barfield, A.J. Dingley, J. Feigon, S. Grzesiek, *J. Am. Chem. Soc.* **123** (2001) 4014.
[20] J. Czernek, R. Brüschweiler, *J. Am. Chem. Soc.* **123** (2001) 11079.
[21] M. Pecul, M.J. Sadlej, J. Leszczynski, *J. Chem. Phys.* **115** (2001) 5498.
[22] M.J.T. Jordan, J.S.-S. Toh, J.E. Del Bene, *Chem. Phys. Lett.* **346** (2001) 288.
[23] J.E. Del Bene, M.J.T. Jordan, *Mol. Struct. (Theochem)* **346** (2001) 288.
[24] J.E. Del Bene, S.A. Perera, R.J. Bartlett, *J. Phys. Chem. A* **105** (2001) 930.
[25] K. Chapman, D. Crittenden, J. Bevitt, M.J.T. Jordan, J.E. Del Bene, *J. Chem. Phys. A* **105** (2001) 5442.
[26] J.E. Del Bene, M.J.T. Jordan, S.A. Perera, R.J. Bartlett, *J. Phys. Chem. A* **105** (2001) 8399.
[27] J. Toh, M.J.T. Jordan, B.C. Husowitz, J.E. Del Bene, *J. Phys. Chem. A* **105** (2001) 10906.
[28] I.G. Shenderovich, A.P. Burtsev, G.S. Denisov, N.S. Golubev, H.-H. Limbach, *Magn. Reson. Chem.* **39** (2001) S99.
[29] M. Pietrzak, H.-H. Limbach, M. Perez-Torralba, D. Sanz, R.M. Claramunt, J. Elguero, *Magn. Reson. Chem.* **39** (2001) S100.
[30] J.E. Del Bene, S.A. Perera, R.J. Bartlett, *Magn. Reson. Chem.* **39** (2001) S109.
[31] D.L. Bryce, R.E. Wasylischen, *J. Biomol. NMR* **19** (2001) 371.
[32] I.G. Shenderovich, H.-H. Limbach, S.N. Smirnov, P.M. Tolstoy, G.S. Denisov, N.S. Golubev, *Phys. Chem. Chem. Phys.* **4** (2002) 5488.
[33] J.E. Del Bene, M.J.T. Jordan, *J. Phys. Chem. A* **106** (2002) 5385.
[34] J.E. Del Bene, R.J. Bartlett, J. Elguero, *Magn. Reson. Chem.* **40** (2002) 767.
[35] D.L. Bryce, R.E. Wasylischen, *J. Mol. Struct.* **602–603** (2002) 463.
[36] J. Vaara, J. Jokisaari, R.E. Wasylischen, D.L. Bryce, *Prog. NMR Spectrosc.* **41** (2002) 233.
[37] S.P. Brown, M. Perez-Torralba, D. Sanz, R.M. Claramunt, L. Emsley, *Chem. Commun.* (2002) 1852.
[38] S.P. Brown, M. Perez-Torralba, D. Sanz, R.M. Claramunt, L. Emsley, *J. Am. Chem. Soc.* **124** (2002) 1152.
[39] J. Elguero, I. Alkorta, *Int. J. Mol. Sci.* **4** (2003) 64.
[40] S. Grzesiek, F. Cordier, A.J. Dingley, *Biol. Magn. Reson.* **20** (2003) 255.
[41] J.E. Del Bene, S.A. Perera, R.J. Bartlett, M. Yáñez, O. Mó, J. Elguero, I. Alkorta, *J. Phys. Chem. A* **107** (2003) 3121.
[42] J.E. Del Bene, S.A. Perera, R.J. Bartlett, M. Yáñez, O. Mó, J. Elguero, I. Alkorta, *J. Phys. Chem. A* **107** (2003) 3126.
[43] J.E. Del Bene, S.A. Perera, R.J. Bartlett, O. Mó, M. Yáñez, J. Elguero, I. Alkorta, *J. Phys. Chem. A* **107** (2003) 3222.
[44] J.A. Pople, J.S. Binkley, R. Seeger, *Int. J. Quantum Chem. Quantum Chem. Symp.* **10** (1976) 1.
[45] R. Krishnan, J.A. Pople, *Int. J. Quantum Chem.* **14** (1978) 91.
[46] R.J. Bartlett, D.M. Silver, *J. Chem. Phys.* **62** (1975) 3258.
[47] R.J. Bartlett, G.D. Purvis, *Int. J. Quantum Chem.* **14** (1978) 561.
[48] W.J. Hehre, R. Ditchfield, J.A. Pople, *J. Chem. Phys.* **56** (1982) 2257.
[49] P.C. Hariharan, J.A. Pople, *Theor. Chim. Acta.* **238** (1973) 213.
[50] G.W. Spitznagel, T. Clark, J. Chandrasekhar, P.V.R. Schleyer, *J. Comput. Chem.* **3** (1982) 3633.
[51] T. Clark, J. Chandrasekhar, G.W. Spitznagel, P.V.R. Schleyer, *J. Comput. Chem.* **4** (1983) 294.
[52] M.J. Frisch, G.W. Trucks, H.B. Schlegel, G.E. Scuseria, M.A. Robb, J.R. Cheeseman, V.G. Zakrzewski, J.A. Montgomery Jr., R.E. Stratmann, J.C. Burant, S. Dapprich, J.M. Millam, A.D. Daniels, K.N. Kudin, M.C. Strain, O. Farkas, J. Tomasi, V. Barone, M. Cossi, R. Cammi, B. Mennucci, C. Pomelli, C. Adamo, S. Clifford, J. Ochterski, G.A. Petersson, P.Y. Ayala, Q. Cui, K. Morokuma, D.K. Malick, A.D. Rabuck, K. Raghavachari, J.B. Foresman, J. Cioslowski, J.V. Ortiz, A.G. Baboul, B.B. Stefanov, G. Liu, A. Liashenko, P. Piskorz, I. Komaromi, R. Gomperts, R.L. Martin, D.J. Fox, T. Keith, M.A. Al-Laham, C.Y. Peng, A. Nanayakkara, C. Gonzalez, M. Challacombe, P.M.W. Gill, B. Johnson, W. Chen, M.W. Wong, J.L. Andres, C. Gonzalez, M. Head-Gordon, E.S. Replogle, J.A. Pople, *Gaussian 98, Rev A. 9*, Gaussian, Inc., Pittsburgh, PA, 1998.

[53] S.A. Perera, H. Sekino, R.J. Bartlett, *Chem. Phys.* **101** (1994) 2186.
[54] S.A. Perera, M. Nooijen, R.J. Bartlett, *J. Chem. Phys.* **104** (1996) 3290.
[55] S.A. Perera, R.J. Bartlett, *J. Am. Chem. Soc.* **117** (1995) 8476.
[56] S.A. Perera, R.J. Bartlett, *J. Am. Chem. Soc.* **118** (1996) 7849.
[57] A. Schäfer, H. Horn, R. Ahlrichs, *J. Chem. Phys.* **97** (1992) 2571.
[58] T.H. Dunning Jr., *J. Chem. Phys.* **90** (1989) 1007.
[59] D.E. Woon, T.H. Dunning Jr., *J. Chem. Phys.* **103** (1995) 4572.
[60] J.E. Del Bene, J. Elguero, I. Alkorta, M. Yáñez, O. Mó, *J. Chem. Phys.* **120** (2004) 3237.
[61] W.T. Raynes, *Magn. Reson. Chem.* **30** (1992) 686.
[62] J.E. Del Bene, J. Elguero, *Magn. Reson. Chem.* **42** (2004) 421.
[63] S.H.M. Søntjens, M.H.P. Genderen, R.P. Sijbesma, *J. Org. Chem.* **68** (2003) 9070.
[64] R.M. Lynden-Bell, R.K. Harris, *Nuclear Magnetic Resonance Spectroscopy*, Appleton Century Crofts, New York, 1969.
[65] J.E. Del Bene, J. Elguero, I. Alkorta, *J. Phys. Chem. A* **108** (2004) 3662.
[66] J.E. Del Bene, J. Elguero, *Chem. Phys. Lett.* **382** (2003) 100.
[67] S. Kirpekar, H. Jørgen Aa Jensen, J. Oddershede, *Chem. Phys.* **188** (1994) 171.
[68] H. Sekino, R.J. Bartlett, in: S. Karna (Ed.), *Nonlinear Optical Materials*, American Chemical Society, Washington, DC, 1994.
[69] S. Grzesiek, F. Cordier, A.J. Dingley, *Methods in Enzymology*, vol. 338, Academic Press, London, 2001.
[70] W.D. Arnold, E. Oldfield, *J. Am. Chem. Soc.* **122** (2000) 12835.
[71] W.D. Arnold, J. Mao, H. Sun, E. Oldfield, *J. Am. Chem. Soc.* **122** (2000) 12164.
[72] R.J. Bartlett, J.E. Del Bene, S.A. Perera, in: G.R. Eaton, D.C. Wiley, O. Jardetzky (Eds.), *Structures and Mechanisms: From Ashes to Enzymes*, in: *ACS Symposium Series*, vol. 827, Oxford Univ. Press, 2002, pp. 150–164.
[73] J.E. Del Bene, *J. Phys. Chem. A* **108** (2004) 6820.

This page intentionally left blank

Structure Optimizations for Excited States with Correlated Second-Order Methods: CC2 and ADC(2)

Christof Hättig

Forschungszentrum Karlsruhe, Institute of Nanotechnology, P.O. Box 3640, D-76021 Karlsruhe, Germany
E-mail: christof.haettig@int.fzk.de

Abstract

The performance of the second-order methods for excitation energies CC2 and ADC(2) is investigated and compared with the more approximate CIS and CIS(D) methods as well as with the coupled-cluster models CCSD, CCSDR(3) and CC3. As a by-product of this investigation the first implementation of analytic excited state gradients for ADC(2) and CIS(D_∞) is reported.

It is found that for equilibrium structures and vibrational frequencies the second-order models CIS(D), ADC(2) and CC2 give often results close to those obtained with CCSD. The main advantage of CCSD lies in its robustness with respect to strong correlation effects. For adiabatic excitation energies CC2 is found to give from all second-order methods for excitation energies (including CCSD) the smallest mean absolute errors. ADC(2) and CIS(D_∞) are found to give almost identical results.

An advantage of ADC(2) compared to CC2 is that the excitation energies are obtained as eigenvalues of a Hermitian secular matrix, while in coupled-cluster response the excitation energies are obtained as eigenvalues of a non-Hermitian Jacobi matrix. It is shown that, as a consequence of the lack of Hermitian symmetry, the latter methods will in general not give a physically correct description of conical intersections between states of the same symmetry. This problem does not appear in ADC(2).

Contents

1. INTRODUCTION

Since the early days of response theory [1–4] the description of electronic excitations, including ionization and electron attachment, has been a central subject of this branch of

ADVANCES IN QUANTUM CHEMISTRY, VOLUME 50
ISSN: 0065-3276 DOI: 10.1016/S0065-3276(05)50003-0

theoretical chemistry. Its main idea, the direct calculation of molecular properties as, *e.g.*, excitation and ionization energies, transition strengths, frequency-dependent properties, *etc.*, provides a viable alternative to state specific approaches. For frequency-dependent properties the response function approach, *i.e.*, the evaluation of (higher-order) polarization propagators, is today the most successful and efficient route to calculate such quantities. For excitation and ionization energies it bypasses through the evaluation of these quantities as poles of the polarization propagator some subtle balance problems encountered in state specific approaches. But at least as important for the response function or propagator approach to molecular properties has been that it offers a route for the description of electronic excitations with single reference wavefunction models since it does not require (non-linear) optimizations for excited states. This ansatz is the basis for such successful and widely applied approaches as time-dependent density functional theory (TDDFT) and coupled-cluster response theory.

Partially because of the success of the latter two methods and their availability in several quantum chemistry packages, the interest in earlier ansätze for approximate calculations of polarization propagators or response functions as, *e.g.*, the polarization propagator approaches (SOPPA [5–7], TOPPA [5], *etc.*) or the algebraic diagrammatic construction [6] has in recent years been relatively limited. These approaches aimed at a direct expansion of the response functions in orders of the electron fluctuation potential without reference to a specific wavefunction model for the ground state. Giving up the reference to a certain model for the ground state energy, introduces additional freedom which allows, *e.g.*, to enforce some properties of the exact response function, which else are often lost. On the other hand, if total energies are needed—for example for the determination of equilibrium structures of excited or ionized states—the reference to a specific model for the ground-state energy or wavefunction is unavoidable.

Excitation energies may be taken as an example to demonstrate what is meant above: Given a ground-state model for the energy, a general approach to derive the expressions for the response functions is through the construction of a time-dependent quasi-energy Lagrangian. The latter is made up of the expectation value for the energy $\langle H \rangle$ and some constraints $f_k[H]$ for the (wavefunction) parameters λ_k, both generalized for the time-dependent case by replacing the time-independent Hamiltonian with the Schrödinger operator $H(t) - \mathrm{i}\frac{\partial}{\partial t}$:

$$L(\bar{\lambda}_k, \lambda_k, t) = \left\langle H(t) - \mathrm{i}\frac{\partial}{\partial t} \right\rangle + \sum_k \bar{\lambda}_k f_k \left[H(t) - \mathrm{i}\frac{\partial}{\partial t} \right] (\lambda_{k'}, t). \tag{1}$$

The expressions for the response functions are then obtained by taking the derivatives of $L(\bar{\lambda}_k, \lambda_k, t)$ with respect to strengths parameters of harmonic time-dependent perturbations with the sum of all frequencies restricted to zero [7–9]. The poles of the response functions occur at the eigenvalues of the stability matrix of the Lagrangian, *i.e.*, for variational methods (SCF, DFT, MCSCF, CI, *etc.*) at the eigenvalues of the electronic Hessian

$$(\mathbf{E} - \omega_k \mathbf{S})\vec{c}^{(k)} = 0, \quad E_{ij} = \left(\frac{\mathrm{d}^2 \langle H \rangle}{\mathrm{d}\lambda_i \, \mathrm{d}\lambda_j} \right)_0, \tag{2}$$

and for non-variational methods, as the coupled-cluster methods are, at the eigenvalues of the electronic Jacobian

$$(\mathbf{A} - \omega_k \mathbf{S})\vec{c}^{(k)} = 0, \quad A_{ij} = \left(\frac{\mathrm{d}^2 L}{\mathrm{d}\bar{\lambda}_i \, \mathrm{d}\lambda_j} \right)_0. \tag{3}$$

For response methods derived from an approximation for the ground-state energy or wavefunction, the expressions for the stability matrix, and thus its structure, properties, and symmetries are determined by the approximations used for the ground-state. In particular, the stability matrix will in general be non-symmetric for any non-variational method. A well-known example for this is the non-symmetric coupled-cluster eigenvalue problem [10,11]. The loss of Hermitian symmetry leads to different left and right eigenvectors, which increases somewhat the computational costs if both vectors are needed, but else does not give rise to major problems. But a potentially more severe consequence is that eigenvalues may become complex and then can no longer be used to obtain a qualitatively correct and quantitatively accurate description of the corresponding excited states. In propagator type methods which avoid such a connection to a ground-state model these problems can be bypassed by imposing Hermitian symmetry of the stability or secular matrix by construction, as it is done, *e.g.*, in SOPPA and in the ADC methods.

In the present article some of the above mentioned problems will be studied at the example of three iterative second-order methods, namely the approximate coupled-cluster singles-and-doubles model [12] CC2, the iterative variant of the doubles correction to configuration interaction singles [13] CIS(D_∞) and the algebraic diagrammatic construction through second order [6,14] ADC(2). As shown in the next section these three methods are closely related to each other and thus are an interesting example to discuss some aspects of response theory. In Section 3 the problems that may arise from non-Hermitian secular matrices will be discussed in connection with conical intersections between two excited states. The remaining sections will be concerned with the implementation of analytic derivatives for CIS(D_∞) and ADC(2), which are a prerequisite for an efficient determination of stationary points on the (excited state) potential energy surfaces, and a comparison of the performance of the three methods CC2, CIS(D_∞) and ADC(2) for equilibrium structures and vibrational frequencies.

2. RELATION BETWEEN CC2 AND THE CIS(D_∞) AND ADC(2) MODELS

For the CC2 model, which has been designed such that for single replacement dominated transitions the excitation energies are correct through second-order in the fluctuation potential, the Jacobian becomes

$$\mathbf{A}^{\mathrm{CC2}} = \left(\begin{array}{c|c} \langle {}^{a}_{i} | [(\widehat{H} + [\widehat{H}, T_2]), \tau^{c}_{k}] | \mathrm{HF} \rangle & \langle {}^{a}_{i} | [\widehat{H}, \tau^{cd}_{kl}] | \mathrm{HF} \rangle \\ \hline \langle {}^{ab}_{ij} | [\widehat{H}, \tau^{c}_{k}] | \mathrm{HF} \rangle & \langle {}^{ab}_{ij} | [F, \tau^{cd}_{kl}] | \mathrm{HF} \rangle \end{array} \right) \tag{4}$$

where F is the usual Fock operator and $\widehat{H} = \exp(-T_1) H \exp(T_1)$, *i.e.*, a Hamiltonian similarity transformed with the exponential function of the single replacement part of the cluster operator $T = T_1 + T_2$. Here and in the following indices $i, j, k, \ldots$ are used for orbitals which are occupied in the reference determinant $|\mathrm{HF}\rangle$ and indices $a, b, c, \ldots$ are used for virtual orbitals. τ^{c}_{k} and τ^{cd}_{kl} denote, respectively, single and double replacement operators.

As by-product of its construction as derivative of the residual of ground-state cluster equations, the CC2 Jacobian contains some contributions which would not be needed to obtain excitation energies correct through second-order: the terms introduced via the

similarity transformation with $\exp(-T_1)$ contribute only in third and higher orders to the excitation energies of single replacement dominated transitions. The "minimal" Jacobian which gives excitation energies correct through second order is obtained by replacing in $\mathbf{A}^{\mathrm{CC2}}$ the CC2 ground-state cluster amplitudes by the amplitudes from first-order perturbation theory—which implies that the singles replacement part of the cluster operator T_1 vanishes, if the Brillouin condition is fulfilled. The resulting Jacobian is that of the CIS(D_∞) model, an iterative variant of CIS(D) introduced by Head-Gordon *et al.* [15]:

$$\mathbf{A}^{\mathrm{CIS}(D_\infty)} = \left(\begin{array}{c|c} \langle {}^{a}_{i}|[(H+[H,T_2^{(1)}]),\tau_k^c]|\mathrm{HF}\rangle & \langle {}^{a}_{i}|[H,\tau_{kl}^{cd}]|\mathrm{HF}\rangle \\ \hline \langle {}^{ab}_{ij}|[H,\tau_k^c]|\mathrm{HF}\rangle & \langle {}^{ab}_{ij}|[F,\tau_{kl}^{cd}]|\mathrm{HF}\rangle \end{array}\right). \tag{5}$$

Similar as the CIS(D) perturbative second-order correction to CIS excitation energies, also the CIS(D_∞) excitation energies cannot directly be derived from the response function of a known (ground-state) wavefunction model. A characteristic it has in common with propagator methods. Indeed, the secular matrix for CIS(D_∞) differs only in a small (but important) detail from a propagator method proposed about two decades ago by Schirmer [6]: the algebraic diagrammatic construction through second order ADC(2). The secular matrix used in ADC(2) is just the symmetric or, in the complex case, the Hermitian part of that for the CIS(D_∞) model:

$$\mathbf{A}^{\mathrm{ADC}(2)} = \frac{1}{2}\left(\mathbf{A}^{\mathrm{CIS}(D_\infty)} + \left(\mathbf{A}^{\mathrm{CIS}(D_\infty)}\right)^{\dagger}\right). \tag{6}$$

Provided that the Hartree–Fock reference determinant fulfills the Brillouin condition $\langle {}^{a}_{i}|H|\mathrm{HF}\rangle = 0$, *i.e.*, for a closed-shell or an unrestricted open-shell case, the CIS(D_∞) Jacobian can be rewritten as:

$$\mathbf{A}^{\mathrm{CIS}(D_\infty)} = \left(\begin{array}{c|c} \langle {}^{a}_{i}|H-E_{\mathrm{HF}}|{}^{c}_{k}\rangle + \langle {}^{a}_{i}|[[H,T_2^{(1)}],\tau_k^c]|\mathrm{HF}\rangle & \langle {}^{a}_{i}|H|{}^{cd}_{kl}\rangle \\ \hline \langle {}^{ab}_{ij}|H|{}^{c}_{k}\rangle & \langle {}^{ab}_{ij}|F-E_0|{}^{cd}_{kl}\rangle \end{array}\right) \tag{7}$$

with $E_{\mathrm{HF}} = \langle \mathrm{HF}|H|\mathrm{HF}\rangle$ and $E_0 = \langle \mathrm{HF}|F|\mathrm{HF}\rangle$. Thus, in these cases the symmetrization in equation (6) affects only the second-order contribution to the singles-singles block, *i.e.*, the terms proportional to the ground-state doubles $T_2^{(1)}$. All other contributions are already Hermitian.

The above relations between CC2, CIS(D_∞), and ADC(2) provide a simple recipe to implement the latter two methods in an existing CC2 program:

- For CIS(D_∞) the only modification required is that the converged CC2 ground-state amplitudes are replaced by those from first-order perturbation theory.
- For ADC(2) in addition the contributions of $[H, T_2^{(1)}]$ to the singles-singles block have to be symmetrized. This can be achieved with a few additional operations at costs of $\mathcal{O}(n^2N^2)$.

3. INTERSECTIONS OF EXCITED STATES IN COUPLED-CLUSTER RESPONSE THEORY

As pointed out in the introduction, the coupled-cluster response or equation-of-motion methods lead to Jacobi or secular matrices which in general are not symmetric. While this usually does not cause any problems in single-point calculations for vertical excitation

spectra or in the optimization of excited state equilibrium structures, it has serious consequences for the topology of the potential surfaces at intersections between excited states.

If one assumes that the Jacobi matrix has been block diagonalized by applying a (non-unitary) transformation

$$\tilde{\mathbf{A}} = \mathbf{LAR} \quad \text{with } \mathbf{LR} = \mathbf{1}, \tag{8}$$

such that for a pair of nearly degenerate states (i, j) one is left with a 2×2-problem which has been decoupled from all other eigenvalues:

$$\tilde{\mathbf{A}} = \begin{pmatrix} \ddots & 0 & 0 & 0 \\ 0 & A_{ii} & A_{ij} & 0 \\ 0 & A_{ji} & A_{jj} & 0 \\ 0 & 0 & 0 & \ddots \end{pmatrix}. \tag{9}$$

The 2×2 block for this effective two-state problem can in general be written in the form

$$\tilde{\mathbf{A}}^{2\times 2} = \begin{pmatrix} \bar{E} - \Delta & S - A \\ S + A & \bar{E} + \Delta \end{pmatrix}. \tag{10}$$

which gives the eigenvalues $E_{1,2} = \bar{E} \pm \sqrt{\Delta^2 + S^2 - A^2}$. For a symmetric matrix, *i.e.*, when $A = 0$ for all values of the coordinates, the two states will be degenerate if both parameters Δ and S become zero. This leads to the well-known result [16,17] that (ignoring spin-orbit effects) states of the same symmetry may have a seam of intersection with the dimension $N^{\text{int}} - 2$, where N^{int} is the number of internal degrees of freedom (nuclear coordinates). For states of different symmetry S vanishes for symmetry reasons and the intersection seam may have the dimension $N^{\text{int}} - 1$.

For a non-symmetric Jacobi matrix, as in general obtained for the iterative coupled-cluster response or equation-of-motion coupled-cluster methods, a number of different cases can be distinguished, depending on the magnitude of the antisymmetric contribution to the coupling A:

1. $A^2 < \Delta^2 + S^2$, which is the situation usually encountered in single-point calculations for vertical excitation energies and in the optimization of equilibrium structures for excited states: One obtains two real eigenvalues $E_{1,2} = \bar{E} \pm \sqrt{\Delta^2 + S^2 - A^2}$.
2. $A^2 > \Delta^2 + S^2$: this leads to a conjugated pair of degenerate roots with eigenvalues $E_{1,2} = \bar{E} \pm \mathrm{i}\sqrt{A^2 - \Delta^2 - S^2}$.
3. $A^2 = \Delta^2 + S^2$, a condition, which for states of the same symmetry in general will be fulfilled in $N^{\text{int}} - 1$ dimensions. In this case one obtains an unphysical apparent degeneracy. It can be considered as a kind of instability along a path which connects the two previous cases.
4. Only for $A = \Delta = S = 0$ a true intersection of the states is found. For states of the same symmetry this condition will only be fulfilled in $N^{\text{int}} - 3$ dimension, *i.e.*, in a manifold which compared to the intersection seam of a symmetric matrix is reduced by one dimension.

Methods with a non-symmetric secular matrix will thus in general not be able to describe conical intersections between states of the same symmetry qualitatively correct. Figure 1 shows a typical two-dimensional cut through potential energy surfaces in a plane where the two states intersect. While a symmetric secular matrix leads to a conical intersection,

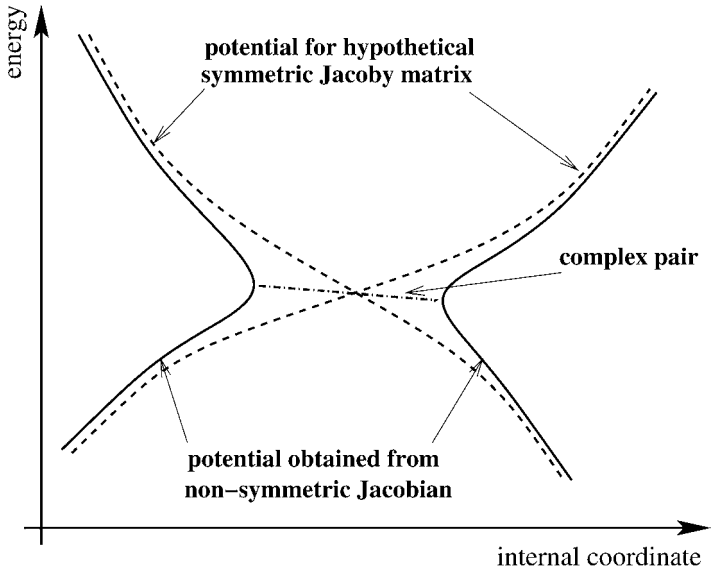

Fig. 1. Intersection of two states of the same symmetry as described by a symmetric and a non-symmetric secular matrix. The potential curves obtained with a symmetric secular matrix are shown as broken lines. The full lines are the potential curves for a non-symmetric secular matrix in the region where both eigenvalues are real, while for the region where the eigenvalues are complex only the real part is shown as a dashed and dotted line.

the potential energy curves obtained with a non-symmetric secular matrix pass—as the intersection is approached—through a point with an (apparent) degeneracy of the two states before a region is entered in which the eigenvalues are complex. This region encloses the intersection seam obtained with a symmetric matrix. At the points with apparent degeneracies the derivatives of the potential energy curves with respect to the coordinate Q become singular.

Figure 2 shows a three-dimensional plot of a similar situation, but now the energy axis has been skipped and instead the points where the two eigenvalues are degenerate are shown in a space spanned by the tuning coordinates of the conical intersection and one coordinate along the intersection seam. In this subspace, the points at which the two states become degenerate with a non-symmetric Jacobian ($A^2 = \Delta^2 + S^2$) form a tube or cone around the intersection seam obtained with a symmetric secular matrix. If the antisymmetric contribution to the off-diagonal matrix element A is a parameter independent of the symmetric contribution S, a true intersection of the two states is only found in a subspace with a dimensionality which—compared to the dimensionality of intersection seam obtained with a symmetric secular matrix—is reduced by one.

The standard coupled-cluster response and equation-of-motion coupled-cluster methods (CC2, CCSD, ...) will thus in general not give a qualitatively correct description of potential energies surfaces (for excited states) at or close to conical intersections. Only if, *e.g.*, because of symmetry reasons, the antisymmetric and the symmetric contribution to the coupling matrix element vanish simultaneously a true intersection will be found. To obtain a qualitatively correct description of intersections between states of the same sym-

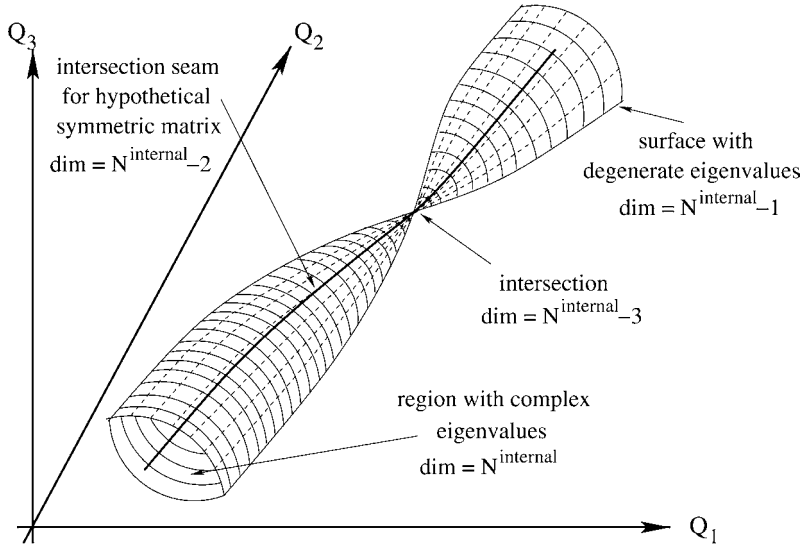

Fig. 2. Intersection of two states shown in a space spanned by the two tuning coordinates of the conical intersection and one coordinate along the intersection seam. The thick line is the intersection seam obtained with a symmetric secular matrix. For the non-symmetric matrix the surface on which the two eigenvalues are degenerate is plotted.

metry requires a symmetric secular matrix. For such problems the algebraic diagrammatic construction methods could be a useful alternative. But in order to make them applicable to intersections in molecules with more than a few atoms, efficient techniques for the localization of stationary points on (excited state) potential energy surfaces are needed [16]. Analytic gradients for excitation energies and total energies of excited states are one important prerequisite for this.

4. IMPLEMENTATION OF ANALYTIC EXCITED STATE GRADIENTS FOR ADC(2) AND CIS(D_∞)

4.1. The relaxed excited state Lagrange function

Since in contrast to the CC2 model, ADC(2) and CIS(D_∞) are not derived from the response function of a ground state method, there is no unique definition of total energies. One could combine the excitation energies provided by these methods with ground state energies of any suitable method. However, both for consistency to which order in the fluctuation potential correlation effects are accounted for and for computational convenience second-order Møller–Plesset perturbation theory appears to be the most natural choice. With this definition of the total energies, the implementation of analytic gradients for excited states becomes a relatively simple task. Indeed, all the expressions can be obtained as simplifications of those for the CC2 model [18]. In particular, one can define a variational Lagrange function for the total energy of an excited state f as [18,7,19]:

$$L^f = \langle \mathrm{HF}|H + [H, T_2]|\mathrm{HF}\rangle + \sum_{i,j=1}^{2} \sum_{\mu_i \nu_j} \bar{E}^f_{\mu_i} A_{\mu_i \nu_j} E^f_{\nu_j}$$
$$+ \omega^f \left(1 - \sum_{i=1}^{2} \sum_{\mu_i} \bar{E}^f_{\mu_i} E^f_{\mu_i}\right) + \bar{t}^f_{\mu_2} \Omega_{\mu_2} + \sum_{\mu_0} \bar{\kappa}^f_{\mu_0} F_{\mu_0}. \tag{11}$$

The first term on the right hand side gives the MP2 ground state energy, with $|\mathrm{HF}\rangle$ the Hartree–Fock reference wave functions and $T_2 = \sum_{\mu_2} t_{\mu_2} \tau_{\mu_2}$ the cluster operator for the first-order doubles. (In the following μ_1 or ν_1 will be used to enumerate single replacements and μ_2 or ν_2 for double replacements.)

The second term in equation (11) represents the excitation energy and the subsequent term ensures the (bi-)orthonormality of the eigenvectors $\bar{E}^f$ and E^f. To cover both the ADC(2) and the CIS(D_∞) model, different left ($\bar{E}^f$) and right (E^f) eigenvectors are allowed in the above equation. Requiring stationarity of the Lagrangian with respect to E^f and $\bar{E}^f$ leads to the left and right eigenvalue problems for the Jacobian **A**, which determine $\bar{E}^f$, E^f and ω^f. Since for ADC(2) the Jacobian **A** is Hermitian, for this model left and right eigenvectors will be equivalent.

The last two terms of the Lagrangian in equation (11) resemble terms in the Lagrange function for the MP2 ground state energy. The first one determines the Lagrange multipliers $\bar{t}_{\mu_2}$ for the ground states doubles equations,

$$\Omega_{\mu_2} = \langle \mu_2|H + [F, T_2]|\mathrm{HF}\rangle = 0 \tag{12}$$

where F is the Fock operator (for the definition of the projection manifold $\langle \mu_2|$ see, *e.g.*, Ref. [20]), and the other determines the Lagrange multipliers $\bar{\kappa}_{\mu_0}$ for the Hartree–Fock equations, *i.e.*, it implements the constraint that the subspace μ_0 of the Fock matrix elements is zero. Depending on the choice for the manifold μ_0 one obtains either the Brillouin condition ($F_{ia} = 0$) or the canonical condition (diagonal Fock matrix) or an intermediate semi-canonical condition. The Hartree–Fock state is for the following parameterized as

$$|\mathrm{HF}\rangle = \sum \exp_{\mu_0}\left(\kappa_{\mu_0}(\tau_{\mu_0} - \tau^\dagger_{\mu_0})\right)|\mathrm{HF}_0\rangle \tag{13}$$

where $|\mathrm{HF}_0\rangle$ is either the unperturbed state, or if the orbital basis depends on the perturbation—as it does in the case of geometric derivatives and also for magnetic fields if GIAOs are used—a determinant build from the orthonormalized molecular orbital (OMO) basis for the distorted system [21].

Similar as MP2 and CC2, also the ADC(2) and CIS(D_∞) models can be implemented very efficiently using the resolution-of-the-identity (RI) approximation which allows for a fast AO to MO transformation

$$B^Q_{ai} = \sum_P \left(\sum_\alpha C_{\alpha a} \sum_\beta C_{\beta i} (\alpha\beta|P)\right) V^{-1/2}_{PQ} \tag{14}$$

and a subsequent fast formation of four-index integrals in the MO basis

$$(ai|bj) \approx (ai|bj)^{\mathrm{RI}} = \sum_Q B^Q_{ai} B^Q_{bj}. \tag{15}$$

In the latter equations $V_{PQ} = (P|Q)$ and $(\alpha\beta|P)$ are, respectively, two- and three-index electron repulsion integrals (ERIs) and P, Q denote orbitals from an auxiliary basis used

to resolve the identity. Since only N^3-scaling intermediates are needed on disk, the I/O requirements are reduced drastically compared to a conventional four-index transformation. For further details about the RI approximation, *e.g.*, the choice of auxiliary basis sets and the accuracies obtained for ground and excited state energies and properties, the reader is referred to Refs. [18,22,23].

4.2. The effective orbital-relaxed one- and two-particle density matrices

In the present implementation the Hartree–Fock equations are still solved using conventional four-index integrals. Therefore, one needs to distinguish between contributions to the Lagrangian which arise from the reference state and the Fock operator and those which are calculated using the RI approximation. However, this is anyway advantageous since it leads to simple expressions to account for a frozen core approximation. For this purpose, the Lagrange function, equation (11), is rewritten as

$$\begin{aligned} L = {} & \langle \mathrm{HF}|H|\mathrm{HF}\rangle + \sum_{\mu_0} \bar{\kappa}_{\mu_0} F_{\mu_0} + \sum_{pq} \big(D_{pq}^{F,\xi}(\bar{t}) + D_{pq}^{F,A}(\bar{E},E)\big) F_{pq} \\ & + \bar{\omega}\Bigg(1 - \sum_{i=1,2}\sum_{\mu} \bar{E}_{\mu} E_{\mu}\Bigg) \\ & + \frac{1}{2}\sum_{pqrs} \big(d_{pqrs}^{\mathrm{nsep},\xi}(\bar{t}) + d_{pqrs}^{\mathrm{nsep},A}(\bar{E},E)\big)(pq|rs)^{\mathrm{RI}}, \end{aligned} \tag{16}$$

where the superscript f is from now on omitted for brevity. Above, the one-particle densities

$$D_{pq}^{F,\xi}(\bar{t}) = \sum_{\mu_2} \bar{t}_{\mu_2} \langle \mu_2|[E_{pq}, T_2]|\mathrm{HF}\rangle \tag{17}$$

and

$$\begin{aligned} D_{pq}^{F,A}(\bar{E},E) = {} & \sum_{i=1,2}\sum_{\mu_1\nu_i} \bar{E}_{\mu_1} \langle \mu_1|[E_{pq}, \tau_{\nu_i}]|\mathrm{HF}\rangle E_{\nu_i} \\ & + \sum_{\mu_2\nu_2} \bar{E}_{\mu_2} \langle \mu_2|[E_{pq}, \tau_{\nu_2}]|\mathrm{HF}\rangle E_{\nu_2} \end{aligned} \tag{18}$$

have been introduced. These densities contain only contributions from the correlation and excitation treatment. The two contributions to the non-separable two-electron density read:

$$d_{pqrs}^{\mathrm{nsep},\xi}(\bar{t}) = \langle \mathrm{HF}|[e_{pqrs}, T_2]|\mathrm{HF}\rangle + \sum_{\mu_2} \bar{t}_{\mu_2} \langle \mu_2|e_{pqrs}|\mathrm{HF}\rangle \tag{19}$$

and

$$\begin{aligned} d_{pqrs}^{\mathrm{nsep},A}(\bar{E},E) = {} & \sum_{\mu_1\nu_1} \bar{E}_{\mu_1} \langle \mu_1|[e_{pqrs}, \tau_{\nu_1}] + \big[[e_{pqrs}, \tau_{\nu_1}], T_2\big]|\mathrm{HF}\rangle E_{\nu_1} \\ & + \sum_{\mu_1\nu_2} \bar{E}_{\mu_1} \langle \mu_1|[e_{pqrs}, \tau_{\nu_2}]|\mathrm{HF}\rangle E_{\nu_2} \\ & + \sum_{\mu_2\nu_1} \bar{E}_{\mu_2} \langle \mu_2|[e_{pqrs}, \tau_{\nu_1}]|\mathrm{HF}\rangle E_{\nu_1}. \end{aligned} \tag{20}$$

Explicit expressions for the densities are given in Tables 1 and 2 for a closed-shell RHF reference determinant and an excited singlet state. For the modifications needed for excited triplet states or for an UHF reference determinant see Refs. [24,18]. Note that the elements of D^F and d^{nsep} are non-zero only if all indices refer to active orbitals. $D^{F,\xi}_{pq}$ and $d^{\mathrm{nsep},\xi}$ are related to the unrelaxed correlation contributions to the MP2 one- and two-electron densities, which are recovered as $D^{F,\xi}_{pq}(\bar{t}^{\mathrm{MP1}})$ and $d^{\mathrm{nsep},\xi}_{pqrs}(\bar{t}^{\mathrm{MP1}})$ where $\bar{t}^{\mathrm{MP1}}$ are the Lagrangian multipliers from first-order Møller–Plesset perturbation theory. $D^{F,A}$ and $d^{\mathrm{nsep},A}$ contain the contributions from the eigenvectors, which do not have counterparts in the expressions for the MP2 ground state densities.

The equations determining the Lagrangian multipliers $\bar{t}_{\nu_2}$ for the ground state doubles equations are obtained as

$$\sum_{\mu_2} \bar{t}_{\mu_2} \langle \mu_2 | [F, \tau_{\nu_2}] | \mathrm{HF} \rangle = -\langle \mathrm{HF} | [H, \tau_{\nu_2}] | \mathrm{HF} \rangle - \sum_{\mu_1 \gamma_1} \bar{E}_{\mu_1} \langle \mu_1 | \big[[H, \tau_{\gamma_1}], \tau_{\nu_2} \big] | \mathrm{HF} \rangle E_{\gamma_1}. \tag{21}$$

They reduce to the calculation of MP1-like doubles amplitudes with modified two-electron integrals [23,25,26] and can in the canonical orbital basis directly be inverted. Similar the

Table 1. Explicit expressions for the one-particle densities $D^{F,\xi}(\bar{t})$ and $D^{F,A}(\bar{E}, E)$ defined in equations (17) and (18)

	$D^{F,\xi}(\bar{t})$	$D^{F,A}(\bar{E}, E)$
D_{ij}	$-\sum_{abk} \bar{t}^{ab}_{jk} t^{ab}_{ik}$	$-\sum_a \bar{E}_{aj} E_{ai} - \sum_{abk} \bar{E}^{ab}_{jk} E^{ab}_{ik}$
D_{ia}	0	$\sum_{jb} \bar{E}_{bj} (2E^{ab}_{ij} - E^{ba}_{ij})$
D_{ab}	$\sum_{ijc} \bar{t}^{ac}_{ij} t^{bc}_{ij}$	$\sum_i \bar{E}_{ai} E_{bi} + \sum_{ijc} \bar{E}^{ac}_{ij} E^{bc}_{ij}$

Table 2. Explicit expressions for the non-separable two-particle density matrices $d^{F,\xi}(\bar{t})$ and $d^{F,A}(\bar{E}, E)$ defined in equations (19) and (20)

	$d^{\xi}(\bar{t})$	$d^{A}(\bar{E}, E)$
d_{ijka}	0	$-\sum_b \bar{E}_{bj} (2E^{ba}_{ik} - E^{ab}_{ik}) - \sum_b \bar{E}^{ba}_{jk} E_{bi}$
d_{ijab}	0	$-\bar{E}_{aj} E_{bi}$
d_{iajb}	$4t^{ab}_{ij} - 2t^{ba}_{ij} + \bar{t}^{ab}_{ij}$	$\mathcal{S}^{ab}_{ij} \{ 2C_{ai} E_{bj} - C_{bi} E_{aj} - \sum_k (\sum_c \bar{E}_{ck} E_{cj})(2t^{ba}_{ki} - t^{ab}_{ki}) - \sum_c (\sum_k \bar{E}_{ck} E_{bk})(2t^{ca}_{ji} - t^{ac}_{ji}) \} + 2\bar{E}_{bj} E_{ai}$
d_{iabc}	0	$\sum_j \bar{E}_{bj} (2E^{ac}_{ij} - E^{ba}_{ij}) + \sum_j \bar{E}^{ab}_{ij} E_{cj}$

The intermediate C used for the formulation of $d^{F,A}(\bar{E}, E)$ is defined as $C_{ai} = \sum_{jb} \bar{E}_{bj} (2t^{ab}_{ij} - t^{ba}_{ij})$; for the definition of the Lagrangian multipliers $\bar{t}^{ab}_{ij}$ and the symmetrization operator $\mathcal{S}$ see text.

double replacement parts of the eigenvectors E and $\bar{E}$ are obtained as:

$$\sum_{\nu_2}\left(\langle\mu_2|[F,\tau_{\nu_2}]|\mathrm{HF}\rangle - \omega\delta_{\mu_2\nu_2}\right)E_{\nu_2} = -\sum_{\nu_1}\langle\mu_2|[H,\tau_{\nu_1}]|\mathrm{HF}\rangle E_{\nu_1}, \tag{22}$$

and

$$\sum_{\mu_2}\bar{E}_{\mu_2}\left(\langle\mu_2|[F,\tau_{\nu_2}]|\mathrm{HF}\rangle - \omega\delta_{\mu_2\nu_2}\right) = -\sum_{\mu_1}\bar{E}_{\mu_1}\langle\mu_1|[H,\tau_{\nu_2}]|\mathrm{HF}\rangle. \tag{23}$$

The Lagrangian multipliers for the Hartree–Fock equations $\bar{\kappa}$ are determined as usual from a set of CPHF or Z-vector equations:

$$\sum_{AI}\bar{\kappa}_{AI}(A_{AIBJ} - \delta_{AB}\varepsilon_A - \delta_{IJ}\varepsilon_I) = -\eta^{\kappa}_{BJ} \tag{24}$$

where the indices I, J and A, B denote, respectively, general (*i.e.*, active and frozen) occupied and virtual orbitals and ε_p are the SCF orbital energies. The CPHF matrix A_{pqrs} is defined as $A_{pqrs} = 4(pq|rs) - (pr|qs) - (ps|rq)$ with conventional four-index ERIs. The evaluation of the right-hand side vector η^{κ} from one- and two-electron density intermediates is done in the same way as described for CC2 in Ref. [18].

The first derivative of the excited state energy with respect to an external perturbation x can now be evaluated from an expression which is analogous to that for RI-CC2 [25,18]:

$$\begin{aligned}\left(\frac{\mathrm{d}L}{\mathrm{d}x}\right)_{x=0} = &\sum_{\alpha\beta} D^{\mathrm{eff,ao}}_{\alpha\beta}h^{[x]}_{\alpha\beta} + \frac{1}{2}\sum_{\alpha\beta\gamma\delta} d^{\mathrm{sep,ao}}_{\alpha\beta\gamma\delta}(\alpha\beta|\gamma\delta)^{[x]} - \sum_{\alpha\beta} F^{\mathrm{eff,ao}}_{\alpha\beta}S^{[x]}_{\alpha\beta}\\ &+ \sum_{\alpha\beta P}\Delta^{\mathrm{ao},P}_{\alpha\beta}(\alpha\beta|P)^{[x]} - \sum_{PQ}\gamma_{PQ}V^{[x]}_{PQ},\end{aligned} \tag{25}$$

where $h^{[x]}$, $S^{[x]}$, $(\alpha\beta|\gamma\delta)^{[x]}$, $(\alpha\beta|P)^{[x]}$ and $V^{[x]}_{PQ}$ are the derivatives of, respectively, the one-electron Hamiltonian, the overlap and the four-, three- and two-index coulomb integrals in the AO basis. $D^{\mathrm{eff,ao}}_{\alpha\beta}$ is the relaxed one-particle density in the atomic orbital basis and $d^{\mathrm{sep,ao}}_{\alpha\beta\gamma\delta}$ the separable part of the two-electron density which is easily constructed on-the-fly:

$$d^{\mathrm{sep,ao}}_{\alpha\beta\gamma\delta} = \mathcal{S}^{\alpha\beta}_{\gamma\delta}\left(1 - \frac{1}{2}\mathcal{P}_{\beta\delta}\right)\left(D^{\mathrm{eff,ao}}_{\alpha\beta} - \frac{1}{2}D^{\mathrm{SCF,ao}}_{\alpha\beta}\right)D^{\mathrm{SCF,ao}}_{\gamma\delta}. \tag{26}$$

Here, $\mathcal{S}^{\alpha\beta}_{\gamma\delta}$ symmetrizes a function according to $\mathcal{S}^{\alpha\beta}_{\gamma\delta}f^{\alpha\beta}_{\gamma\delta} = f^{\alpha\beta}_{\gamma\delta} + f^{\beta\alpha}_{\delta\gamma}$ and $\mathcal{P}_{\alpha\beta}$ denotes a permutation operator which interchanges two indices. $F^{\mathrm{eff,ao}}_{\alpha\beta}$ is the usual effective Fock matrix that appears in expressions for gradients of correlated methods and the densities $\Delta^{\mathrm{ao},P}_{\alpha\beta}$ and γ_{PQ} are defined as:

$$\Delta^{\mathrm{ao},P}_{\alpha\beta} = \sum_{pq} C_{\alpha p}C_{\beta q}\sum_{rsQ} d^{\mathrm{nsep,ex}}_{pqrs}(rs|Q)V^{-1}_{PQ}, \tag{27}$$

and

$$\gamma_{PQ} = \sum_{\alpha\beta R}(\alpha\beta|R)\Delta^{\mathrm{ao},P}_{\alpha\beta}V^{-1}_{RQ}. \tag{28}$$

For ADC(2) and CIS(D_∞) the course of a gradient calculation after the solution of the eigenvalue problem (which for CIS(D_∞) implies the determination of both the right and the left eigenvectors) can be sketched as follows:

- First the eigenvectors are normalized as $\sum_{i=1,2} \sum_{\mu_i} \bar{E}_{\mu_i} E_{\mu_i} = 1$.
- Then the unrelaxed one-electron densities $D^{F,\xi}$ and $D^{F,A}$ and intermediates for the two-electron densities are computed.
- The right-hand side η^κ for the CPHF equations and the effective Fock matrix F^{eff} are set up and the CPHF equations are solved.
- Finally the contributions to the gradient are evaluated by contracting the derivative integrals with the respective densities.

Note, that in contrast to CC2 for ADC(2) and CIS(D_∞) after the solution of the eigenvalue problem no other equations with $\mathcal{O}(N^5)$ scaling costs must be solved iteratively.

5. PERFORMANCE OF CORRELATED SECOND-ORDER METHODS FOR EXCITED STATE STRUCTURES AND VIBRATIONAL FREQUENCIES

From the discussion in Sections 2 and 3 it follows that for well-isolated states, *i.e.*, far from same-symmetry intersections, the non-Hermitian contribution to the Jacobian in which ADC(2) and CIS(D_∞) differ should have only a small effect on the eigenvalues and vectors. Test calculations on a few diatomic molecules and CH_2O and C_2H_2 show (see Table 3) that indeed ADC(2) and CIS(D_∞) give not only vertical excitation energies, but also adiabatic excitation energies, bond lengths and vibrational frequencies, which are almost identical. The differences are close to or fall even below the convergence threshold used for the calculations. Since ADC(2) has both conceptual and computational advantages over CIS(D_∞), the latter model will in the following not be considered further.

In the next two subsections the results of two sets of test calculations are presented. The first test is a comparison of a hierarchy of single-reference methods for excited states up to approximated coupled-cluster singles, doubles and triples methods in large basis sets but restricted to diatomic molecules. In the second part only ADC(2) and CC2 are compared for a set of small and medium sized polyatomic molecules for which excited state geometries and frequencies are experimentally well-known.

5.1. Benchmark study on the four diatomic molecules N_2, CO, BH, and BF

For the comparison of the second-order methods for excitation energies with highly correlated methods which account also for the effects of connected triples, four molecules N_2, CO, BH, and BF have been selected since for these several excited states are experimentally well known and have minima at not too far stretched internuclear distances and accurate basis sets are available. The test set consists of 11 singlet and 19 triplet states:

N_2: $A^3\Sigma_g^+$, $B^3\Pi_g$, $B'^3\Sigma_u^-$, $a'^1\Sigma_u^-$, $a^1\Pi_g$, $w^1\Delta_u$, $C^3\Pi_u$,
CO: $a^3\Pi$, $A^1\Pi$, $B^1\Sigma^+$, $C^1\Sigma^+$,
BF: $a^3\Pi$, $A^1\Pi$, $B^1\Sigma^+$, $C^1\Sigma^+$, $b^3\Sigma^+$, $d^3\Pi$,
BH: $A^1\Pi$, $B^1\Sigma^+$

Table 3. Comparison of ADC(2) and CIS(D_∞) for excitation energies and structures of excited states

Molecule	State	Property	CIS(D_∞)	ADC(2)	CC2	Exp.
N_2	$w^1\Delta_u$	T_{vert}	10.629 eV	10.628 eV	10.584 eV	
		T_e	9.36 eV	9.36 eV	9.37 eV	8.94 eV
		R_e	128.1 pm	128.1 pm	129.3 pm	126.8 pm
		ω_e	1449 cm^{-1}	1449 cm^{-1}	1360 cm^{-1}	1559 cm^{-1}
BF	$A^1\Pi$	T_{vert}	6.424 eV	6.424 eV		
		T_e	6.36 eV	6.37 eV	6.36 eV	6.34 eV
		R_e	131.2 pm	131.2 pm	131.4 pm	130.4 pm
		ω_e	1214 cm^{-1}	1214 cm^{-1}	1213 cm^{-1}	1265 cm^{-1}
CH_2O	$1^1A''$	T_{vert}	3.930 eV	3.930 eV	4.025 eV	
		T_0	3.30 eV	3.30 eV	3.52 eV	3.49 eV
		d(CO)	138.2 pm	138.2 pm	135.5 pm	132.3 pm
		ϕ^{d}	14.6 deg	14.6 deg	25.7 deg	34.0 deg
		$\nu_2(a')$	1344 cm^{-1}	1344 cm^{-1}	1321 cm^{-1}	1293 cm^{-1}
CH_2O	$1^3A''$	T_{vert}	3.477 eV	3.476 eV	3.556 eV	
		T_0	2.91 eV	2.91 eV	3.05 eV	3.12 eV
		d(CO)	134.5 pm	134.5 pm	133.6 pm	132.3 pm
		ϕ^{d}	33.4 deg	33.5 deg	38.1 deg	41.1 deg
		$\nu_2(a')$	1323 cm^{-1}	1320 cm^{-1}	1298 cm^{-1}	1283 cm^{-1}
C_2H_2	1^1A_u	T_{vert}	7.224 eV	7.224 eV	7.199 eV	
		T_0	5.38 eV	5.38 eV	5.33 eV	5.23 eV
		d(CC)	137.3 pm	137.3 pm	138.1 pm	137.5 pm
		$\nu_2(a_g)$	1426 cm^{-1}	1426 cm^{-1}	1368 cm^{-1}	1385 cm^{-1}

The calculations on N_2 and BF where carried out in the aug-cc-pwCVQZ basis sets and all electrons have been active, while for CH_2O and C_2H_2 the aug-cc-pVQZ basis and a frozen core approximation was used. Experimental values taken from Refs. [27–29].

and the following methods have been included in the comparison:

- configuration interaction singles (CIS), which is equivalent to coupled-cluster singles (CCS)—provided that the Hartree–Fock reference wavefunction fulfills the Brillouin condition;
- CIS(D), a perturbative doubles correction to CIS;
- the algebraic diagrammatic construction through second order ADC(2);
- the approximate coupled-cluster singles and doubles model CC2;
- coupled-cluster singles and doubles (CCSD);
- CCSDR(3), a perturbative triples correction to CCSD—since for this method no implementation for triplet excited states is available, the results for CCSDR(3) include only the 11 singlet states of the test set;
- the approximate coupled-cluster singles, doubles, and triples model CC3.

For single excitation dominated transitions, as the investigated states are, CIS is correct through first order in the fluctuation potential, the methods CIS(D), ADC(2), CC2 and CCSD are correct through second order, and CCSDR(3) [30] and CC3 [31,32] are correct through third order. As in Section 4 the total energies for CIS(D) and ADC(2) were defined as the sum of the excitation energies obtained with these models and the MP2 ground state energy, the CCSDR(3) excitation energies were combined with the ground state energies from the CC(3) perturbative triples correction [30] to CCSD. The CCSD, CCSDR(3), CC(3), and CC3 calculations have been carried out with the Dalton quantum chemistry package [33]; for all other calculations a development version of Turbomole was used.

To avoid any bias of the results due to core correlation effects all electrons have been correlated and the aug-cc-pwCVQZ basis [34–37] has been used. This basis set should even for the triples methods CCSDR(3) and CC3 give results close to the basis set limit. Detailed results for the bond lengths, the harmonic vibrational frequencies and the adiabatic excitation energies are given in Appendix A; a summary of the results is shown in Figs. 3–5.

For none of the three investigated quantities (bond lengths, vibrational frequencies and adiabatic excitation energies) the convergence within the coupled-cluster hierarchy is as smooth as it is usually found for vertical excitation energies. In particular for the bond lengths and the vibrational frequencies the results indicate some oscillations within the CC model hierarchy, similar to that found for ground state bond length and vibrational frequencies [20]: CIS gives, similar as SCF for the ground state, much too short bond lengths—for the 19 states included in this test set R_e is on the average underestimated by about 3 pm. CC2 overestimates the correlation contribution and thus the bond lengths and their change upon excitation, while CCSD gives again too short bond lengths, even though CCSD is much more robust with respect to strong correlation effects, as encountered in N_2 and CO if the bond is stretched upon excitation from a bounding into an anti-bonding orbital. After inclusion of the effects of connected triples at the CCSDR(3) and the CC3 level the results are very accurate.

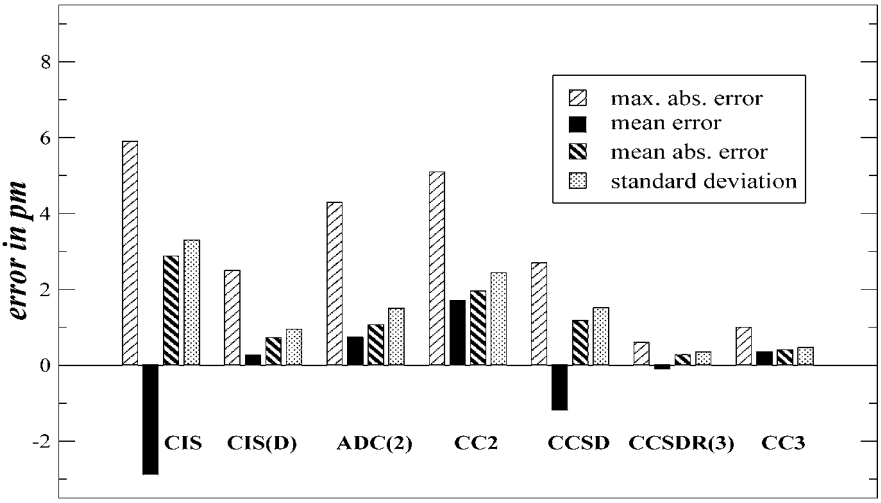

Fig. 3. Errors in calculated bond lengths for 19 excited states. Experimental data from Ref. [28]; for technical details of the calculations see text.

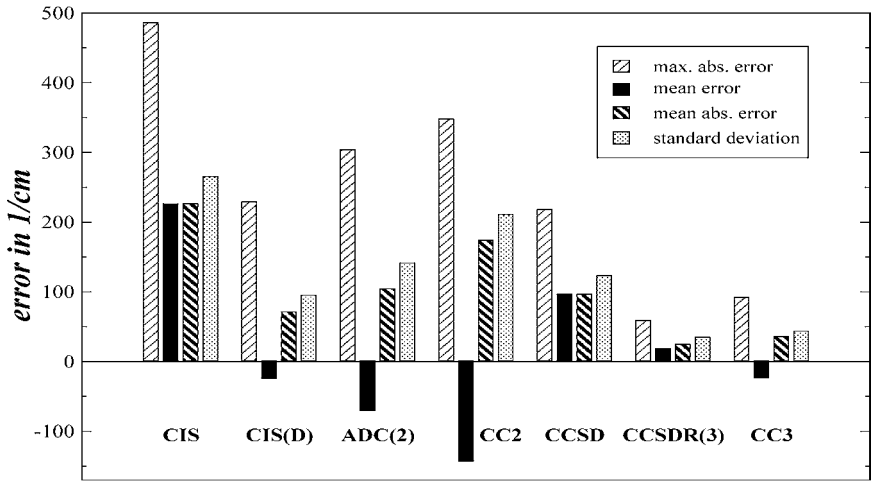

Fig. 4. Errors in calculated harmonic frequencies for 19 excited states in N_2, CO, BH, and BF. Experimental reference data taken from Ref. [28]; for technical details of the calculations see text.

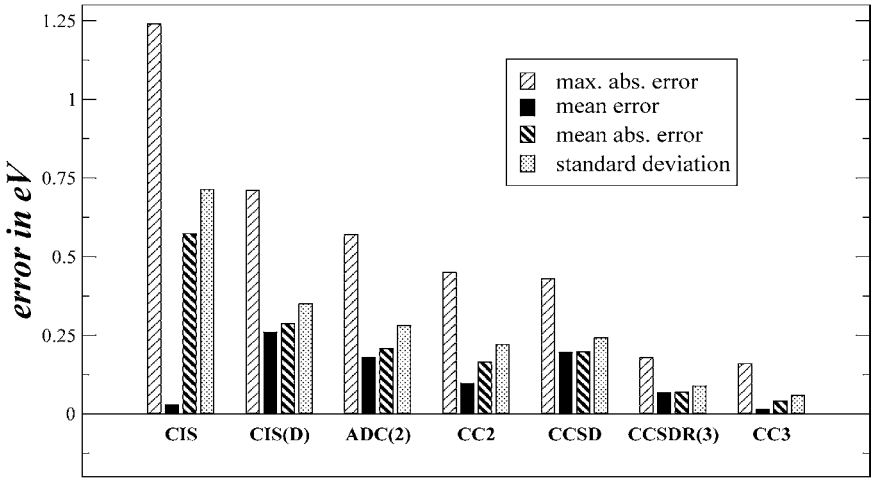

Fig. 5. Errors in adiabatic excitation energies for 19 excited states in N_2, CO, BH, and BF. Experimental reference data taken from Ref. [28]; for technical details of the calculations see text.

Compared to CC2 the ADC(2) model profits from the somewhat better stability of the underlying MP2 for the ground state, while the results for the perturbative doubles correction CIS(D) are intermediate between the results for CIS and ADC(2). However, two of the example molecules, N_2 and CO, are difficult cases for single-reference methods and in particular for CC2. Taking this into account, one can, based on the above trends, expect that for single replacement dominated excited states CC2 and CC3 for larger molecules with polyatomic chromophores give equilibrium geometries of similar accuracy as

obtained with these methods for the ground state, *i.e.*, close to the accuracy obtained with, respectively MP2 and CCSD(T). Similar, CCSD cannot be expected to give for excited states geometries which are more accurate than those for ground states. Its main advantage lies in its robustness.

The results for harmonic frequencies corroborate the above observations. For almost all excited states it is found that the vibrational frequencies are overestimated (underestimated) the more the bond lengths are underestimated (overestimated). Thus, CIS and, to a lesser extend, CCSD give too high vibrational frequencies, while CC2 usually yields to low vibrational frequencies. Again, after inclusion of approximate triples in the methods CCSDR(3) and CC3 the results are close to the experimental values.

In contrast to the smooth convergence of vertical excitation energies in the hierarchy CCS–CC2–CCSD–CC3, the adiabatic excitation energies change more irregular: no improvement is obtained when going from CC2 to CCSD. The CCSD results have about the same accuracy as those obtained with ADC(2). The errors obtained with the perturbative doubles correction CIS(D) are slightly larger. First after the inclusion of connected triples at the CCSDR(3) and CC3 level a systematic and significant improvement upon CC2 is obtained.

5.2. Comparison of ADC(2) and CC2 for polyatomic molecules

The benchmark results from the previous subsection include only states in four diatomic molecules. It will of cause require further studies, in particular for polyatomic molecules to see how general these findings are. But, for polyatomic molecules excitations are usually delocalized over chromophores which comprise several atoms and, as a consequence, the changes in the bond lengths upon excitation will be more moderate than they are in small molecules.

This means that the results will be much more dominated by the performance of the underlying ground state method. Though, one would expect for polyatomic molecules—in particular if the differences between the bond lengths in the ground and the excited states are not large—that the approximate doubles methods ADC(2) and CC2 give results of almost the same accuracy as obtained for ground state geometries with MP2 and CC2. However, for small molecules like CH_2O, C_2H_2, where the excitation process is essentially localized at one bond, similar difficulties as found above for the diatomic molecules have to be expected.

In Tables 4–6 some results are listed for 0–0 transition energies, equilibrium bond lengths and angles and vibrational frequencies for 13 excited states of small polyatomic molecules, where accurate experimental results are available. The CC2 results, which have been taken from Ref. [18], and the ADC(2) results, which are from the present work, have been obtained in the aug-cc-pVQZ basis sets (aug-cc-pV($Q + d$)Z for the atoms Si–Cl) [34–36,39]. The frozen core approximations has been used throughout, with the 1s orbitals frozen for the atoms B–F and 1s2s2p frozen for Si–Cl.

In contrast to the diatomic molecules investigated in Section 5.1, where from the experimental data values for T_e, R_e and ω_e could be extracted, for the excited states in these molecules experimental data is only available for T_0, R_0 and fundamental frequencies. This limits somewhat the comparability with the calculated values, which have been obtained within the harmonic approximation. This impairs in particular the results for C–H

Table 4. 0–0 transition energies (in eV) in the harmonic approximation

Molecule	State	CC2	ADC(2)	Exp.
SO_2	1^3B_1	2.92	2.94	3.19[a]
SiF_2	1^1B_1	5.49	5.44	5.34[b]
CCl_2	1^1B_1	2.11	2.00	2.14[b]
CS_2	1^3A_2	3.29	3.18	3.25[a]
HCN	$1^1A''$	6.72	6.82	6.48[a]
HCP	$1^1A''$	4.48	4.51	4.31[a]
C_2H_2	1^1A_u	5.33	5.38	5.23[a]
CH_2O	$1^1A''$	3.52	3.30	3.49[c]
	$1^3A''$	3.05	2.91	3.12[c]
CH_2S	1^1A_2	2.15	2.03	2.03[c]
	$1^3A''$	1.79	1.69	1.80[c]
CHOCHO	1^1A_u	2.70	2.63	2.72[a]
HC_2CHO	$1^1A''$	3.17	2.90	3.24[a]

[a] From Ref. [28]. [b] From Ref. [38]. [c] From Ref. [29].

bond lengths and the corresponding stretchings modes, for which anharmonic effects are sizable.

The results listed in Tables 4–6 indicate that the above anticipated trends are indeed found for polyatomic molecules. In the 0–0 transition energies f.ex. the mean absolute error (MAE) is for CC2 0.1 eV, only for SO_2 and HCN the errors are larger than 0.2 eV. Also for ADC(2) the MAE of 0.17 eV for these polyatomic molecules is considerable smaller than for the diatomic molecules studied in Section 5.1. Interestingly, the difference in mean absolute errors for CC2 and ADC(2) is almost the same for the excited states in the polyatomic molecules listed in Table 4 and for the excited states in the diatomic molecules (Table A.3) studied in the previous subsection.

For bond lengths and angles and for vibrational frequencies the performance of the two methods is—at least for the present test set—on the average very similar. ADC(2) improves upon CC2 in several cases where multiple bonds are weakened upon excitation, *e.g.*, for HCN, HCP, C_2H_2 or the difficult case of SO_2. On the other hand, ADC(2) performs inferior for $n \rightarrow \pi^*$ transitions as in CH_2O, CH_2S and HC_2CHO, where it gives by far too long C–O distances and too low frequencies for the modes involving these bonds. However, one has to keep in mind that the calculated CC2 and ADC(2) results are not strictly comparable to the experimental reference data, since in the calculations anharmonic effects have been neglected. Even though this is not expected, it cannot, without further investigations, be excluded that corrections from the anharmonicities will change the conclusions about the performance of CC2 and ADC(2) for excited state equilibrium structures.

6. SUMMARY AND CONCLUSIONS

The coupled-cluster methods CCS (CIS), CIS(D), CC2, CCSD, CCSDR(3), and CC3 form today a relatively well-established hierarchy of black-box methods for excited states. The

Table 5. Excited state structure parameters (bond lengths in pm and angles in degrees) calculated with CC2 and ADC(2)

Molecule	State	Parameter	CC2	ADC(2)	Exp.
SO_2	1^3B_1	d(SO)	155.4	151.8	149.4
		∠(OSO)	128.8	126.5	126.1
SiF_2[a]	1^1B_1	d(SiF)	162.8	162.3	160.1
		∠(FSiF)	115.9	116.0	115.9
CCl_2[a]	1^1B_1	d(CCl)	164.8	164.7	165.2
		∠(ClCCl)	132.0	131.6	131.4
CS_2	1^3A_2	d(CS)	164.9	163.7	164.0
		∠(SCS)	135.7	136.7	135.8
HCN	$1^1A''$	d(CH)	111.5	111.3	114.0
		d(CN)	132.1	129.3	129.7
		∠(HCN)	122.3	127.6	125.0
HCP	$1^1A''$	d(CP)	171.6	168.2	169.0
		∠(HCP)	128.4	137.1	128.0
C_2H_2[b]	1^1A_u	d(CC)	138.1	137.3	137.5
		d(CH)	109.2	109.1	110.5
		∠(HCC)	122.0	122.2	121.4
CH_2O[c]	$1^1A''$	d(CH)	108.7	108.4	109.8
		d(CO)	135.5	138.2	132.3
		∠(HCH)	121.6	124.1	118.4
		ϕ[d]	25.7	14.6	34.0
CH_2O[c]	$1^3A''$	d(CH)	109.2	108.9	108.4
		d(CO)	133.6	134.5	130.7
		∠(HCH)	118.0	119.8	117.9
		ϕ[d]	38.1	33.5	41.1
CH_2S[c]	1^1A_2	d(CH)	108.3	108.3	107.7
		d(CS)	170.6	171.9	168.2
		∠(HCH)	121.2	121.2	120.7
CH_2S[c]	$1^3A''$	d(CH)	108.2	108.2	108.2
		d(CS)	168.9	169.3	168.3
		∠(HCH)	120.5	121.3	119.3
		ϕ[d]	15.0	4.3	11.9
trans-$(CHO)_2$[e]	1^1A_u	d(CC)	147.9	147.7	146.0
		d(CH)	109.5	109.4	112.0
		d(CO)	125.4	125.0	125.0
		∠(HCC)	114.5	114.9	114.0
		∠(OCC)	123.9	123.6	124.0

(*Continued*)

performance of these methods for vertical excitation energies has been investigated in several benchmark studies [44] and are well understood. With the implementation of analytic gradients [18,45,46] it is for some of these methods now possible to obtain equilibrium

Table 5. (*Continued*)

Molecule	State	Parameter	CC2	ADC(2)	Exp.
HC_2CHO	$1^1A''$	$d(C_1C_2)$	123.8	122.9	123.8
		$d(C_1H)$	106.3	106.3	107.5
		$d(C_2C_3)$	136.0	135.8	136.4
		$d(C_3H)$	108.5	108.3	109.1
		$d(C_3O)$	140.6	144.9	132.5

Unless otherwise stated the experimental data was taken from Refs. [28,27].

[a] Experimental values from [38]. [b] Experimental values from [40]. [c] Experimental values from [29]. [d] Out-of-plane angle of the oxygen or sulfur atom, respectively. [e] Experimental values from Ref. [41].

Table 6. Harmonic vibrational frequencies (cm^{-1}) calculated with CC2 and ADC(2)

Molecule	State	Parameter	CC2	ADC(2)	Exp.
SO_2	1^3B_1	$\nu_1(a_1)$	673	852	906
		$\nu_2(a_1)$	285	337	360
SiF_2	1^1B_1	$\nu_1(a_1)$	705	714	598
		$\nu_2(a_1)$	235	236	342
CCl_2[a]	1^1B_1	$\nu_1(a_1)$	641	643	634
		$\nu_2(a_1)$	308	310	303
CS_2	1^3A_2	$\nu_1(a_1)$	682	727	692
		$\nu_2(a_1)$	243	311	311
HCN	$1^1A''$	$\nu_2(a')$	1345	1661	1496
		$\nu_3(a')$	963	973	941
HCP	$1^1A''$	$\nu_2(a')$	888	1061	951
		$\nu_3(a')$	636	647	567
C_2H_2	1^1A_u	$\nu_2(a_g)$	1368	1426	1385
		$\nu_3(a_g)$	1086	1088	1048
CH_2O[b]	$1^1A''$	$\nu_1(a')$	3064	3107	2846
		$\nu_2(a')$	1321	1344	1293
		$\nu_3(a')$	1015	859	1183
		$\nu_5(a'')$	3202	3255	2968
		$\nu_6(a'')$	873	867	904
	$1^3A''$	$\nu_2(a')$	1298	1320	1283
CH_2S[b]	1^1A_2	$\nu_1(a_1)$	3127	3124	3034
		$\nu_2(a_1)$	1343	1346	1320
		$\nu_3(a_1)$	799	751	859
		$\nu_4(b_1)$	3253	3254	3081
		$\nu_5(b_1)$	769	772	799
		$\nu_2(a')$	1337	1342	1320
		$\nu_3(a')$	846	826	859

(*Continued*)

Table 6. (*Continued*)

Molecule	State	Parameter	CC2	ADC(2)	Exp.
trans-$(CHO)_2$[c]	1^1A_u	$\nu_1(a_g)$	3052	3070	2809
		$\nu_2(a_g)$	1369	1410	1391
		$\nu_3(a_g)$	1233	1252	1195
		$\nu_4(a_g)$	995	1019	952
		$\nu_5(a_g)$	494	504	509
		$\nu_6(a_u)$	754	760	720
		$\nu_7(a_u)$	219	221	233
		$\nu_8(b_g)$	763	782	735
		$\nu_{10}(b_u)$	1248	1219	1281
		$\nu_{11}(b_u)$	1176	1096	1172
		$\nu_{12}(b_u)$	372	372	379
HC_2CHO[d]	$1^1A''$	$\nu_2(a')$	3170	3200	2953
		$\nu_3(a')$	1898	1970	1946
		$\nu_4(a')$	1218	1205	1304
		$\nu_5(a')$	1074	1090	1120
		$\nu_6(a')$	780	695	952
		$\nu_7(a')$	642	655	650
		$\nu_8(a')$	471	477	507
		$\nu_9(a')$	171	172	189
		$\nu_{10}(a'')$	550	593	507
		$\nu_{11}(a'')$	416	449	390
		$\nu_{12}(a'')$	324	340	346

Unless stated otherwise, the experimental values are taken from Refs. [28,27].

[a] Experimental values from Ref. [38]. [b] Experimental values from Ref. [29]. [c] Experimental values from Ref. [42]. [d] Experimental values from Ref. [43].

structures for electronically excited states of small and medium sized molecules in an almost routine manner.

The benchmark study in Section 5.1, which compares the performance these methods, indicates, in agreement with previous results in the literature [46–49], that the accuracies obtained for equilibrium structures and harmonic frequencies of single excitation dominated excited states are almost comparable to those obtained for the ground state. It is found that CCSD, even though much more robust with respect to strong correlation effects than the approximate singles-and-doubles methods CIS(D), ADC(2), and CC2, is in general for equilibrium structures not systematically more accurate than these methods. As a consequence CCSD is also not able to improve for adiabatic excitation energies upon the results obtained at the CC2 level.

A drawback of the standard CC response or equation-of-motion CC methods is the lack of Hermitian symmetry of the Jacobi or secular matrix. While this will usually not affect their performance for equilibrium structures, it leads to qualitative wrong results for the potential energy surfaces of excited states in the vicinity of intersec-

tions between states of the same symmetry: instead of a conical intersection seam these methods will give a region with a conjugated pair of complex eigenvalues. Propagator type methods, as the algebraic diagrammatic construction (ADC) models, which have a Hermitian secular matrix could for such situations be a valuable alternative.

In Section 4 the equations for orbital-relaxed one- and two-particle densities and analytic gradients of excited states have been derived for the ADC(2) and the CIS(D_∞) model. These have been implemented in the RICC2 module [50] of the Turbomole package [51] and were used to investigate the performance of ADC(2) for excited state potential energy surfaces. The results presented in Sections 5.1 and 5.2 show, that ADC(2) gives equilibrium structures and harmonic frequencies with an accuracy comparable to that of CC2. In some cases, as for example N_2 and CO, ADC(2) is due to the underlying MP2 ground state more robust than CC2. Only for excitation energies ADC(2) gives somewhat larger errors than CC2.

ACKNOWLEDGEMENTS

This work is dedicated to Prof. Jan Linderberg and Prof. Poul Jørgensen on the occasion of their, respectively, 70th and 60th birthdays. I am grateful to Poul Jørgensen for having given me the opportunity to join the Theoretical Chemistry group at the Århus university as a postdoc from 1996–1999. I wish to thank both Poul and Jan for their hospitality during these years and all my later visits in Århus. I am looking forward to many more of them.

I thank Jochen Schirmer and Andreas Köhn for a number of useful discussions about ADC(2) and CC2.

APPENDIX A

In Tables A.1–A.3 the data underlying Figs. 3–5 is collected.

Table A.1. Bond lengths R_e (pm) of diatomic molecules

Molecule	State	CIS	CIS(D)	ADC(2)	CC2	CCSD	CCSDR(3)	CC3	Exp.
N_2	$A^3\Sigma_u^+$	122.8	129.0	129.4	131.5	126.8	–	129.3	128.7
	$B^3\Pi_g$	117.6	122.2	123.1	124.9	119.5	–	121.4	121.3
	$B'^3\Sigma_u^-$	123.3	128.6	129.2	130.7	125.2	–	128.3	127.8
	$a'^1\Sigma_u^-$	123.3	128.5	129.0	130.4	124.8	126.9	128.0	127.5
	$a^1\Pi_g$	119.0	123.0	124.5	126.5	120.1	121.5	122.2	122.0
	$w^1\Delta_u$	122.8	127.6	128.1	129.3	124.2	126.3	127.4	126.8
	$C^3\Pi_u$	110.1	114.3	115.4	116.3	113.1	–	114.6	114.9

(*Continued*)

Table A.1. (*Continued*)

Molecule	State	CIS	CIS(D)	ADC(2)	CC2	CCSD	CCSDR(3)	CC3	Exp.
CO	$a^3\Pi$	117.5	121.0	121.4	122.7	119.4	–	121.1	120.6
	$A^1\Pi$	121.0	126.0	127.8	128.6	122.2	123.3	124.5	123.5
	$B^1\Sigma^+$	108.5	112.3	112.6	113.8	110.9	112.1	112.5	112.0
	$C^1\Sigma^+$	108.2	111.7	112.0	113.5	110.8	112.0	112.4	112.2
BF	$a^3\Pi$	129.8	131.5	131.6	131.9	130.6	–	131.1	130.8
	$A^1\Pi$	128.4	131.1	131.2	131.4	130.1	130.5	130.7	130.4
	$b^3\Sigma^+$	120.0	121.3	121.4	121.9	121.1	–	121.9	121.5
	$B^1\Sigma^+$	119.3	120.4	120.5	121.0	120.2	120.9	121.0	120.7
	$C^1\Sigma^+$	120.8	122.1	122.2	122.7	121.8	122.4	122.5	122.0
	$d^3\Pi$	119.9	121.0	121.0	121.5	120.7	–	121.5	121.0
BH	$A^1\Pi$	120.3	120.6	120.5	120.6	121.9	122.1	122.2	121.9
	$B^1\Sigma^+$	119.9	120.2	120.4	120.5	121.4	121.5	121.5	121.6

For the technical details see Section 5.1; experimental values from Ref. [28].

Table A.2. Harmonic vibrational frequencies ω_e (cm^{-1}) of diatomic molecules

Molecule	State	CIS	CIS(D)	ADC(2)	CC2	CCSD	CCSDR(3)	CC3	Exp.
N_2	$A^3\Sigma_u^+$	1873	1407	1379	1223	1582	–	1420	1461
	$B^3\Pi_g$	2008	1653	1576	1432	1884	–	1728	1733
	$B'^3\Sigma_u^-$	1841	1440	1402	1290	1701	–	1480	1517
	$a'^1\Sigma_u^-$	1841	1447	1412	1303	1732	1582	1491	1530
	$a^1\Pi_g$	1904	1616	1505	1353	1858	1753	1685	1694
	$w^1\Delta_u$	1859	1483	1449	1360	1752	1604	1509	1559
	$C^3\Pi_u$	2533	2133	1994	1885	2265	–	2113	2047
CO	$a^3\Pi$	1965	1686	1645	1542	1830	–	1688	1743
	$A^1\Pi$	1646	1326	1214	1170	1594	1536	1426	1518
	$B^1\Sigma^+$	2480	1982	1830	1815	2233	2120	2064	2113
	$C^1\Sigma^+$	2488	2154	2111	1945	2287	2174	2124	2176
BF	$a^3\Pi$	1379	1298	1291	1277	1334	9999	1314	1324
	$A^1\Pi$	1365	1238	1214	1213	1279	1259	1251	1265
	$b^3\Sigma^+$	1744	1638	1631	1592	1652	9999	1599	1629
	$B^1\Sigma^+$	1784	1711	1699	1666	1724	1689	1670	1694
	$C^1\Sigma^+$	1703	1612	1607	1577	1631	1601	1587	1613
	$d^3\Pi$	1774	1704	1697	1663	1725	9999	1679	1697
BH	$A^1\Pi$	2550	2480	2480	2473	2335	2309	2305	2251
	$B^1\Sigma^+$	2528	2498	2484	2476	2398	2390	2389	2400

For the technical details see Section 5.1; experimental values from Ref. [28].

Table A.3. Adiabatic excitation energies T_e (eV) of diatomic molecules

Molecule	State	CIS	CIS(D)	ADC(2)	CC2	CCSD	CCSDR(3)	CC3	Exp.
N_2	$A^3\Sigma_u^+$	5.30	6.70	6.62	6.54	6.33	–	6.13	6.22
	$B^3\Pi_g$	7.71	7.64	7.44	7.31	7.59	–	7.38	7.39
	$B'^3\Sigma_u^-$	7.52	8.79	8.70	8.67	8.62	–	8.19	8.22
	$a'^1\Sigma_u^-$	7.52	8.82	8.73	8.72	8.82	8.54	8.43	8.45
	$a^1\Pi_g$	9.60	8.86	8.56	8.39	8.85	8.67	8.61	8.59
	$w^1\Delta_u$	8.13	9.46	9.36	9.37	9.34	9.04	8.90	8.94
	$C^3\Pi_u$	11.82	11.51	11.29	11.24	11.23	–	11.11	11.05
CO	$a^3\Pi$	5.78	6.26	6.18	6.08	6.17	–	6.02	6.04
	$A^1\Pi$	8.82	8.24	8.07	7.97	8.26	8.11	8.04	8.07
	$B^1\Sigma^+$	12.02	11.49	11.35	11.11	11.21	10.96	10.94	10.78
	$C^1\Sigma^+$	12.57	11.79	11.88	11.64	11.75	11.51	11.50	11.40
BF	$a^3\Pi$	2.73	3.44	3.42	3.43	3.59	–	3.60	3.61
	$A^1\Pi$	6.56	6.39	6.37	6.36	6.40	6.34	6.34	6.34
	$b^3\Sigma^+$	7.24	7.73	7.67	7.57	7.69	–	7.57	7.57
	$B^1\Sigma^+$	8.33	8.35	8.33	8.22	8.29	8.16	8.15	8.10
	$C^1\Sigma^+$	8.51	8.74	8.72	8.64	8.71	8.62	8.63	8.56
	$d^3\Pi$	8.58	8.87	8.85	8.77	8.87	–	8.76	8.77
BH	$A^1\Pi$	2.85	2.79	2.80	2.80	2.90	2.86	2.88	2.87
	$B^1\Sigma^+$	6.41	6.54	6.48	6.48	6.57	6.52	6.54	6.49

For the technical details see Section 5.1; experimental values from Ref. [28].

REFERENCES

[1] D.N. Zubarev, *Usp. Fiz. Nauk* **71** (1960);
D.N. Zubarev, *Soviet Phys. Uspekhi* **3** (1960) 320.
[2] J. Linderberg, Y. Öhrn, *Proc. Roy. Soc. (London) A* **285** (1965) 445.
[3] Y. Öhrn, J. Linderberg, *Phys. Rev. A* **139** (1965) 1063.
[4] J. Linderberg, Y. Öhrn, *Propagators in Quantum Chemistry*, Academic Press, London, 1973.
[5] J. Oddershede, *Adv. Quantum Chem.* **11** (1978) 275.
[6] J. Schirmer, *Phys. Rev. A* **26** (1981) 2395.
[7] O. Christiansen, P. Jørgensen, C. Hättig, *Int. J. Quantum Chem.* **68** (1998) 1.
[8] C. Hättig, O. Christiansen, P. Jørgensen, *J. Chem. Phys.* **108** (1998) 8331.
[9] T.B. Pedersen, H. Koch, *J. Chem. Phys.* **108** (1998) 5194.
[10] H. Koch, H.J.A. Jensen, P. Jørgensen, T. Helgaker, *J. Chem. Phys.* **93** (1990) 3345.
[11] J.F. Stanton, R.J. Bartlett, *J. Chem. Phys.* **98** (1993) 7029.
[12] O. Christiansen, H. Koch, P. Jørgensen, *Chem. Phys. Lett.* **243** (1995) 409.
[13] M. Head-Gordon, R.J. Rico, M. Oumi, T.J. Lee, *Chem. Phys. Lett.* **219** (1994) 21.
[14] A.B. Trofimov, J. Schirmer, *J. Phys. B* **28** (1995) 2299.
[15] M. Head-Gordon, M. Oumi, D. Maurice, *Mol. Phys.* **96** (1999) 593.
[16] D.R. Yarkony, *J. Phys. Chem. A* **105** (2001) 6277.
[17] J. von Neumann, E. Wigner, *Zeit. F. Phys.* **30** (1929) 467.
[18] A. Köhn, C. Hättig, *J. Chem. Phys.* **119** (2003) 5021.
[19] C. Hättig, P. Jørgensen, *J. Chem. Phys.* **109** (1998) 9219.
[20] T. Helgaker, P. Jørgensen, J. Olsen, *Molecular Electronic-Structure Theory*, John Wiley & Sons, New York, 2000.

[21] T. Helgaker, P. Jørgensen, *Adv. Quant. Chem.* **19** (1988) 183.
[22] F. Weigend, A. Köhn, C. Hättig, *J. Chem. Phys.* **116** (2002) 3175.
[23] C. Hättig, A. Köhn, *J. Chem. Phys.* **117** (2002) 6939.
[24] C. Hättig, K. Hald, *Phys. Chem. Chem. Phys.* **4** (2002) 2111.
[25] C. Hättig, *J. Chem. Phys.* **118** (2003) 7751.
[26] C. Hättig, A. Köhn, K. Hald, *J. Chem. Phys.* **116** (2002) 5401.
[27] K.P. Huber, G. Herzbergm, *Molecular Spectra and Molecular Structure: III. Electronic Spectra and Electronic Structure of Polyatomic Molecules*, Van Nostrand Reinhold, New York, 1966.
[28] K.P. Huber, G. Herzberg, *Molecular Spectra and Molecular Structure: IV. Constants of Diatomic Molecules*, Van Nostrand, New York, 1979.
[29] D.J. Clouthier, D.A. Ramsay, *Ann. Rev. Phys. Chem.* **34** (1983) 31.
[30] O. Christiansen, H. Koch, P. Jørgensen, *J. Chem. Phys.* **105** (1996) 1451.
[31] H. Koch, O. Christiansen, P. Jørgensen, A. Sánchez de Merás, T. Helgaker, *J. Chem. Phys.* **106** (1997) 1808.
[32] O. Christiansen, H. Koch, P. Jørgensen, *J. Chem. Phys.* **103** (1995) 7429.
[33] T. Helgaker, H.J.Å. Jensen, P. Jørgensen, J. Olsen, K. Ruud, H. Ågren, A.A. Auer, K.L. Bak, V. Bakken, O. Christiansen, S. Coriani, P. Dahle, E.K. Dalskov, T. Enevoldsen, B. Fernandez, C. Hättig, K. Hald, A. Halkier, H. Heiberg, H. Hettema, D. Jonsson, S. Kirpekar, R. Kobayashi, H. Koch, K.V. Mikkelsen, P. Norman, M.J. Packer, T.B. Pedersen, T.A. Ruden, A. Sanchez, T. Saue, S.P.A. Sauer, B. Schimmelpfennig, K.O. Sylvester-Hvid, P.R. Taylor, O. Vahtras, Dalton—an electronic structure program, release 1.2, 2001.
[34] T.H. Dunning, *J. Chem. Phys.* **90** (1989) 1007.
[35] D.E. Woon, T.H. Dunning, *J. Chem. Phys.* **98** (1993) 1358.
[36] D.E. Woon, T.H. Dunning, *J. Chem. Phys.* **100** (1994) 2975.
[37] K.A. Peterson, T.H. Dunning, *J. Chem. Phys.* **117** (2002) 10548.
[38] D.J. Clouthier, J. Karolczak, *J. Chem. Phys.* **94** (1991) 1.
[39] T.H. Dunning, K.A. Peterson, A.K. Wilson, *J. Chem. Phys.* **114** (2001) 9244.
[40] T.R. Huet, M. Godefroid, M. Herman, *J. Mol. Spectrosc.* **114** (1990) 32.
[41] J.M. Hollas, Molecular structure from rotational and vibrational transitions in electronic spectra, in: R. Fausto (Ed.), *Recent Experimental and Computational Advances in Molecular Spectroscopy*, Kluwer, Dordrecht, 1993, pp. 32–61.
[42] R.Y. Dong, R. Nanes, D.A. Ramsay, *Can. J. Chem.* **71** (1993) 1595.
[43] J.C.D. Brand, J.H. Calloman, J.K.G. Watson, *Discussions of the Faraday Society* **35** (1963) 175.
[44] H. Koch, O. Christiansen, P. Jørgensen, J. Olsen, *Chem. Phys. Lett.* **244** (1995) 75;
O. Christiansen, H. Koch, P. Jørgensen, J. Olsen, *Chem. Phys. Lett.* **256** (1996) 185;
O. Christiansen, K.L. Bak, H. Koch, S.P.A. Sauer, *Chem. Phys. Lett.* **284** (1998) 47;
A.B. Trofimov, G. Stelter, J. Schirmer, *J. Chem. Phys.* **117** (2002) 6402.
[45] J.B. Foresman, M. Head-Gordon, J.A. Pople, M.J. Frisch, *J. Phys. Chem.* **96** (1992) 135;
J.F. Stanton, *J. Chem. Phys.* **99** (1993) 8840.
[46] J.F. Stanton, J. Gauss, *J. Chem. Phys.* **100** (1994) 4695.
[47] J.F. Stanton, J. Gauss, N. Ishikawa, M. Head-Gordon, *J. Chem. Phys.* **103** (1995) 4160.
[48] K.W. Sattelmeyer, J.F. Stanton, J. Olsen, J. Gauss, *Chem. Phys. Lett.* **347** (2001) 499.
[49] H. Larsen, J. Olsen, P. Jørgensen, O. Christiansen, *J. Chem. Phys.* **113** (2000) 6077;
H. Larsen, J. Olsen, P. Jørgensen, O. Christiansen, *J. Chem. Phys.* **114** (2001) 10985 (Erratum).
[50] C. Hättig, F. Weigend, *J. Chem. Phys.* **113** (2000) 5154.
[51] R. Ahlrichs, M. Bär, M. Häser, H. Horn, C. Kölmel, *Chem. Phys. Lett.* **162** (1989) 165.

Angular Symmetry and Hylleraas Coordinates in Four-Body Problems

Frank E. Harris

Department of Physics, University of Utah, Salt Lake City, UT 84112, USA
and
Quantum Theory Project, P.O. Box 118435, University of Florida, Gainesville, FL 32611, USA

Abstract

The most accurate studies of few-body Coulomb systems have used wavefunctions of forms that are simple in Hylleraas coordinates (those that explicitly include all the interparticle distances). In most studies the wavefunction has been constructed from Slater-type orbitals about a single center (relative to which the other particles are at positions $\mathbf{r}_i$) by adjoining to each orbital product a polynomial in the other interparticle distances r_{ij}. Matrix elements have then usually been evaluated by expanding the r_{ij} in terms of the $\mathbf{r}_i$. This type of wavefunction is not ideal for "nonadiabatic" systems in which all the particles are of comparable (finite) mass; a preferable alternative is to use a wavefunction constructed from exponentials in all the Hylleraas coordinates. It is not practical to use the usual expansion methods for Hylleraas exponential wavefunctions, and this paper considers issues arising when four-body systems are treated directly in the Hylleraas coordinates for states of general angular symmetry. The two problems treated here are (1) convenient and compact expression of the kinetic energy for angular eigenstates, and (2) angular integrations in matrix elements. Both these problems differ from their well-known counterparts in orbital formulations, in part because the r_{ij} are not orthogonal coordinates, and in part because the angles of the $\mathbf{r}_i$ are not all independent variables.

Contents

1. INTRODUCTION

The mathematics that arises when angular momentum eigenfunctions are expressed in a coordinate system that includes all the interparticle distances is of a kind that would interest Jan Linderberg, as evidenced by the nice paper entitled "Hyperspherical coordinates in four particle systems" published by Öhrn and Linderberg [1] in 1983. It thus seems fitting that the present topic be included in the proceedings of a meeting at which he was a principal honoree. The autumn of 2003 marked the fortieth anniversary of my first meeting with Jan

ADVANCES IN QUANTUM CHEMISTRY, VOLUME 50
ISSN: 0065-3276 DOI: 10.1016/S0065-3276(05)50004-2

(when I came for an extended visit to Uppsala), and already at that time I was struck by both the breadth and the depth of his mathematical knowledge and skill. The unfolding of his career reinforced my first impressions, and I have enjoyed being his colleague and friend for more than four decades.

The search for optimum sets of coordinates in few-body problems has a long history, extending at least as far back as the work of Jacobi and of Radau in the nineteenth century. In addition to considering hyperspherical coordinates, a number of recent authors have investigated more general internal (*shape*) coordinates in few-body systems. A glimpse into the current state of such efforts is provided by the work of Littlejohn and Reinsch [2] and the many citations included therein. It is apparent from these works that the coordinates most directly reflecting shape symmetry are functions of the various interparticle distances and are too complicated to be easy starting points for matrix evaluation. An alternative is to use the individual interparticle distances as coordinates, appending the angular dependence to a shape function. The first treatment of angular eigenstates in this way was probably due to Breit [3], who considered three-particle P states. Other studies along similar lines included those of Bhatia and Temkin [4] and Schwartz [5], the latter of which we will find to be a useful take-off point for the present study.

The use of the interparticle distances in wavefunctions dates back to the early work of Hylleraas [6], who found that inclusion of the interelectron distance as an explicit coordinate (often referred to as a "Hylleraas coordinate") could lead to surprisingly good results for the ground-state energy of the He atom. For two-electron atoms, use of the nuclear-electron distances (r_1 and r_2) and the Hylleraas coordinate r_{12} proved computationally convenient, in part because the volume element for the internal coordinates was of the form $r_1 r_2 r_{12}\, dr_1\, dr_2\, dr_{12}$. This simplicity did not extend to systems with more than three particles, but nevertheless the systematic use of Hylleraas coordinates has seen considerable use in recent years, most frequently as adjuncts to a Slater-type orbital basis. Most workers have expanded expressions containing powers of the interparticle distances in terms of the orbital coordinates, using formulas first reported by Sack [7]; the present state of this approach is nicely summarized in recent review articles by Drake [8] and King [9]; these papers examine both three and four-body problems (*e.g.*, the Li atom).

A smaller number of studies, the earliest of which were by Delves and Kalotas [10] and by Thakkar and Smith [11], have used exponentials in all the Hylleraas coordinates for three-body systems. This type of wavefunction is of particular value when all the particles have comparable, finite masses. Such systems, often termed "nonadiabatic", require a description in which the correlations of all particle pairs are placed on an equal footing. Extension to Hylleraas exponential wavefunctions for four-body systems only became practical when closed formulas for the radial integrals became available [12–14]. When these exponentials are used in a four-body problem, it is not advisable to attempt to expand in terms of the orbital coordinates, and it is best to continue with the explicit use of the Hylleraas coordinates.

If the r_{ij} are expanded in the orbital coordinates, the construction of angular-momentum eigenfunctions and the evaluation of the kinetic energy proceed exactly as in a totally orbital formulation. However, if it is chosen to evaluate matrix elements directly in the Hylleraas basis, new considerations arise. For three-body systems, the use of Hylleraas functions (in that case, r_{12}) was addressed by Bhatia and Temkin [4] and Schwartz [5], and a rather compact formulation of the kinetic energy operator for general angular states was recently given by this author [15] (see also Frolov and Smith [16]). For spherically

symmetric (S) states of four-body problems, a Hylleraas-coordinate representation of the kinetic-energy operator is straightforward and has been exhibited by a number of authors (see, for example, Rebane [17]). However, for application to states of general angular dependence, the situation is considerably more complicated. An analysis has been provided by Yan and Drake [18], but their partitioning into radial and angular parts has led to formulas which seem more unwieldy than necessary. Accordingly, there still remains a need for a Hylleraas-coordinate formulation of the kinetic energy for general angular dependence that is compact and compatible with the analytical methods for evaluation of the resulting radial integrals. Such a formulation and its use in matrix element evaluation are the issues addressed in the present communication.

2. WAVEFUNCTIONS

We consider four-body systems with spatial wavefunctions depending on the space-fixed coordinates $\mathbf{r}_1$, $\mathbf{r}_2$, $\mathbf{r}_3$, $\mathbf{r}_4$; it is convenient to transform to the coordinate $\mathbf{R}$ of the system's center of mass and to relative coordinates $\mathbf{r}_{14}$, $\mathbf{r}_{24}$, $\mathbf{r}_{34}$, where $\mathbf{r}_{ij}$ stands for $\mathbf{r}_i - \mathbf{r}_j$; we also define $r_{ij} = |\mathbf{r}_{ij}|$ and $\hat{\mathbf{r}}_{ij} = \mathbf{r}_{ij}/r_{ij}$. After separation of the center of mass, the nine remaining coordinates can be chosen to be the three Euler angles describing overall rotation of the wavefunction and the six internal coordinates r_{12}, r_{13}, r_{14}, r_{23}, r_{24}, and r_{34}, together with a discrete two-valued inversion index. The ranges of the r_{ij} consist of all values permitting the formation of a tetrahedron with edges of lengths r_{ij}. A given set of r_{ij} defines two tetrahedra which are mirror images of each other; the inversion index enables specification of each.

Wavefunctions of general angular dependence can be written in terms of a basis whose members have the generic form

$$\Psi(\mathbf{r}_{14}, \mathbf{r}_{24}, \mathbf{r}_{34}) = \mathcal{Y}_{LM}^{l_1 l_2 (l') l_3}(\mathbf{r}_{14}, \mathbf{r}_{24}, \mathbf{r}_{34}) g(r_{12}, r_{13}, r_{14}, r_{23}, r_{24}, r_{34}). \tag{1}$$

Here $\mathcal{Y}_{LM}^{l_1, l_2 (l') l_3}$ is an angular momentum eigenfunction built from individual spherical harmonics of respective quantum numbers l_1, l_2, and l_3, combined in such a way that the angular momenta described by l_1 and l_2 couple to a resultant of quantum number l', which in turn is coupled with the l_3 angular momentum to a final resultant of quantum numbers L, M. The well-known formula describing the angular-momentum coupling is given for reference in Appendix A, and the expression we use for $\mathcal{Y}$ is

$$\begin{aligned}\mathcal{Y}_{LM}^{l_1 l_2 (l') l_3}(\mathbf{r}_{14}, \mathbf{r}_{24}, \mathbf{r}_{34}) = {} & (-1)^{-l_1+l_2+l_3-l'} r_{14}^{l_1} r_{24}^{l_2} r_{34}^{l_3} \\ & \times \sqrt{(2l'+1)(2L+1)} \sum_{(m)} (-1)^{-m_1'-M} \begin{pmatrix} l_1 & l_2 & l' \\ m_1 & m_2 & -m' \end{pmatrix} \\ & \times \begin{pmatrix} l' & l_3 & L \\ m' & m_3 & -M \end{pmatrix} Y_{l_1 m_1}(\hat{\mathbf{r}}_{14}) Y_{l_2 m_2}(\hat{\mathbf{r}}_{24}) Y_{l_3 m_3}(\hat{\mathbf{r}}_{34}). \end{aligned} \tag{2}$$

The quantities of form $\left(\begin{smallmatrix} a & b & c \\ d & e & f \end{smallmatrix}\right)$ are Wigner 3-j symbols [19], and the notation (m) indicates that the summation is to be over all values of m_1, m_2, m_3, and m' for which the 3-j symbols do not vanish.

Extending an analysis given by Schwartz for the three-body problem [5], we now note that the multiplication of an angular function $\mathcal{Y}_{LM}^{l_1 l_2 (l') l_3}$ by a quantity of the form $\mathbf{r}_{i4} \cdot \mathbf{r}_{j4}$

converts a function $\mathcal{Y}$ into linear combinations of various $\mathcal{Y}$ in which L and M remain unchanged but l_i and l_j become $l_i \pm 1$ and $l_j \pm 1$ (in all combinations that do not cause $l_i < 0$, $l_j < 0$, or $l_1 + l_2 + l_3 < L$). We note also that these linear combinations of $\mathcal{Y}$ preserve the parity of $l_1+l_2+l_3$. These observations mean that there exist linear recurrence relations of types illustrated by the following (for $i, j = 1, 2$):

$$\mathcal{Y}_{LM}^{l_1 l_2 (l') l_3} = C_1 \mathcal{Y}_{LM}^{l_1-1, l_2-1 (l') l_3} + C_2 \mathcal{Y}_{LM}^{l_1-2, l_2 (l') l_3} + C_3 \mathcal{Y}_{LM}^{l_1, l_2-2 (l') l_3} + C_4 \mathcal{Y}_{LM}^{l_1-2, l_2-2 (l') l_3}. \tag{3}$$

Here C_1 will include the scalar product $\mathbf{r}_{14} \cdot \mathbf{r}_{24}$. Similar relations hold for other pairs i, j, but with additional terms in which l' changes. Those coefficients C_j that correspond to illegal combinations of the various l will, of course, vanish.

The recurrence relations illustrated in equation (3) will enable any $\mathcal{Y}_{LM}^{l_1 l_2 (l') l_3}$ to be reduced to a linear combination of similar functions either all having $l_1 + l_2 + l_3 = L$ or all having $l_1 + l_2 + l_3 = L + 1$, with coefficients that may be polynomials in the scalar products $\mathbf{r}_{i4} \cdot \mathbf{r}_{j4}$. Since these scalar products are "radial functions" that depend only on the r_{ij}, with the specific form

$$\mathbf{r}_{i4} \cdot \mathbf{r}_{j4} = \frac{1}{2}\left(r_{i4}^2 + r_{j4}^2 - r_{ij}^2\right), \tag{4}$$

the coefficients C_j can be incorporated into the radial function g of equation (1), and it therefore can be seen that the most general four-body wavefunction is expressible in the basis given at equation (1) with $l_1 + l_2 + l_3$ restricted to the values L and $L + 1$.

In the present exposition we restrict consideration to situations not involving external fields, so the matrix elements we compute will be independent of M. For simplicity we continue the analysis for $M = L$. The restrictions on the possible values of the l_i then enable important simplifications to equation (1). If $l_1+l_2+l_3 = L$, the only possible value of l' is $l_1 + l_2$, and the corresponding $\mathcal{Y}$ reduces to the following form to which we assign the shorthand Φ_0:

$$\Phi_0^{l_1, l_2, l_3} = \mathcal{Y}_{LL}^{l_1 l_2 (l_1+l_2) l_3}(\mathbf{r}_{14}, \mathbf{r}_{24}, \mathbf{r}_{34}) = r_{14}^{l_1} r_{24}^{l_2} r_{34}^{l_3} Y_{l_1 l_1}(\hat{\mathbf{r}}_{14}) Y_{l_2 l_2}(\hat{\mathbf{r}}_{24}) Y_{l_3 l_3}(\hat{\mathbf{r}}_{34}). \tag{5}$$

Notice that in writing Φ_0 the values of L, M, and the $\hat{\mathbf{r}}_{i4}$ have been suppressed but are assumed to be those consistent with the final member of equation (5), *i.e.*, $L = l_1 + l_2 + l_3$, $M = L$. The center member of equation (5) is useful for matrix element evaluations (*vide infra*), while the final member is a good starting point for the application of various operators arising from the kinetic energy.

The case $l_1 + l_2 + l_3 = L + 1$ is a bit more complicated. If all three l_i are nonzero there will be two basis functions, one with $l' = l_1 + l_2$ and another with $l' = l_1 + l_2 - 1$; if two l_i are nonzero the basis function is unique; and the case of one nonzero l_i is not consistent with $l_1 + l_2 + l_3 = L + 1$. It turns out to be convenient to span the basis space by the functions

$$\begin{aligned}
\Phi_2^{l_1 l_2 l_3} &= \mathcal{Y}_{LL}^{l_1 l_2 (l_1+l_2-1) l_3}(\mathbf{r}_{14}, \mathbf{r}_{24}, \mathbf{r}_{34}) \\
&= r_{14}^{l_1} r_{24}^{l_2} r_{34}^{l_3} \Bigg[\left(\frac{l_1}{l_1+l_2}\right)^{1/2} Y_{l_1 l_1}(\hat{\mathbf{r}}_{14}) Y_{l_2, l_2-1}(\hat{\mathbf{r}}_{24}) \\
&\quad - \left(\frac{l_2}{l_1+l_2}\right)^{1/2} Y_{l_1, l_1-1}(\hat{\mathbf{r}}_{14}) Y_{l_2 l_2}(\hat{\mathbf{r}}_{24}) \Bigg] Y_{l_3 l_3}(\hat{\mathbf{r}}_{34}),
\end{aligned} \tag{6}$$

$$\begin{aligned}\Phi_3^{l_1 l_2 l_3} &= \mathcal{Y}_{LL}^{l_1 l_3 (l_1+l_3-1) l_2}(\mathbf{r}_{14}, \mathbf{r}_{34}, \mathbf{r}_{24}) \\ &= r_{14}^{l_1} r_{34}^{l_3} r_{24}^{l_2} \Bigg[\left(\frac{l_1}{l_1+l_3} \right)^{1/2} Y_{l_1 l_1}(\hat{\mathbf{r}}_{14}) Y_{l_3, l_3-1}(\hat{\mathbf{r}}_{34}) \\ &\quad - \left(\frac{l_3}{l_1+l_3} \right)^{1/2} Y_{l_1, l_1-1}(\hat{\mathbf{r}}_{14}) Y_{l_3 l_3}(\hat{\mathbf{r}}_{34}) \Bigg] Y_{l_2 l_2}(\hat{\mathbf{r}}_{24}). \end{aligned} \tag{7}$$

We note that Φ_3 can be obtained from Φ_2 by exchange of the indices 2 and 3 in both the l_i and the $\mathbf{r}_{i4}$. Again, it is assumed that $l_1 + l_2 + l_3 = L + 1$. Just as for Φ_0, the central member of these equations will be advantageous for matrix element evaluations, while the final member will be useful for the application of operators. In cases where there is only one basis function for the given l_i, either Φ_2 and Φ_3 will become linearly dependent or one will vanish.

The use of Φ_2 and Φ_3 instead of a pair of functions such as $\mathcal{Y}_{LM}^{l_1 l_2 (l_1+l_2) l_3}(\mathbf{r}_{14}, \mathbf{r}_{24}, \mathbf{r}_{34})$ and $\mathcal{Y}_{LM}^{l_1 l_2 (l_1+l_2-1) l_3}(\mathbf{r}_{14}, \mathbf{r}_{24}, \mathbf{r}_{34})$ has significant computational advantages, one of which is the simplification resultant from the symmetry relationship between Φ_2 and Φ_3. Another advantage stems from the fact that a $\mathcal{Y}$ with $l' = l_1 + l_2$ would be a sum of Y products containing three terms, and with more complicated coefficients than appear in equation (7).

3. KINETIC ENERGY

For nonrelativistic Coulomb systems, the potential energy consists of terms proportional to r_{ij}^{-1} and it is obvious how to incorporate these contributions into matrix elements. However, the kinetic energy is much more problematic, as the basis functions contain nonorthogonal coordinates (the r_{ij}) and exhibit redundancy between the r_{ij} and the coordinates occurring in the angular factors. If computations are restricted to spherically symmetric (S) states, this problem is minimal; for states of general angular symmetry, it is not.

A starting point for our present discussion of the kinetic energy operator T is its form in the space-fixed coordinates $\mathbf{r}_1, \mathbf{r}_2, \mathbf{r}_3, \mathbf{r}_4$, which we write in a system of units in which $\hbar = 1$, with the particle at $\mathbf{r}_i$ having mass m_i:

$$\mathsf{T} = -\frac{1}{2m_1}\nabla_1^2 - \frac{1}{2m_2}\nabla_2^2 - \frac{1}{2m_3}\nabla_3^2 - \frac{1}{2m_4}\nabla_4^2. \tag{8}$$

We consider the application of T to functions which formally depend upon the overcomplete set of relative coordinates $\mathbf{r}_{12}, \mathbf{r}_{13}, \mathbf{r}_{14}, \mathbf{r}_{23}, \mathbf{r}_{24}, \mathbf{r}_{34}$, with the result that we may write ∇_i as

$$\nabla_i = \sum_{j, j\neq i} \nabla_{ij}. \tag{9}$$

Here we have used the fact that $\nabla_{ji} = -\nabla_{ij}$, and have kept in mind that the $\mathbf{r}_{ij}$ on which the ∇_{ij} act are treated as formally independent, so that, for example, $\nabla_{ij} f(\mathbf{r}_{ik}) = 0$. We can then form each ∇_i^2 and bring T to the form

$$\mathsf{T} = -\frac{1}{2} \sum_{ij,\ i<j} \frac{1}{\mu_{ij}} \nabla_{ij}^2 - \sum_i \frac{1}{m_i} \sum_{jk\neq i,\ j<k} \nabla_{ij} \cdot \nabla_{ik}, \tag{10}$$

where $\mu_{ij}^{-1} = m_i^{-1} + m_j^{-1}$.

Now we apply T to wavefunctions of the form

$$\Psi = \Phi_n^{l_1 l_2 l_3} g(r_{12}, r_{13}, r_{14}, r_{23}, r_{24}, r_{34}), \tag{11}$$

where $n = 0,\ 2$, or 3, and Φ_n is given by equation (5), (6), or (7). Recognizing that Ψ consists of an angular factor Φ and a "radial" factor g, we apply equation (10) in a more extended form, suppressing for clarity the arguments of g:

$$\begin{aligned} \mathsf{T}\Psi = &- \sum_{ij,\ i<j} \frac{1}{2\mu_{ij}} \left[\nabla_{ij}^2 \Phi_n + 2(\nabla_{ij}\Phi_n)\cdot\nabla_{ij} + \Phi_n \nabla_{ij}^2\right] g \\ &- \sum_i \frac{1}{m_i} \sum_{jk\neq i,\ j<k} \left[(\nabla_{ij}\cdot\nabla_{ik}\Phi_n) + (\nabla_{ij}\Phi_n)\cdot\nabla_{ik} + (\nabla_{ik}\Phi_n)\cdot\nabla_{ij} \right. \\ &\qquad \left. + \Phi_n \nabla_{ij}\cdot\nabla_{ik}\right] g. \end{aligned} \tag{12}$$

We next call attention to the relations

$$\nabla_{ij}^2 \Phi_n = 0, \tag{13}$$

$$\nabla_{ij}\Phi_n = 0 \quad (i \neq 4 \text{ and } j \neq 4), \tag{14}$$

$$\nabla_{ij}\cdot\nabla_{ik}\Phi_n = 0, \tag{15}$$

$$\nabla_{ij} g = \mathbf{r}_{ij} \frac{1}{r_{ij}} \frac{\partial g}{\partial r_{ij}}, \tag{16}$$

$$\nabla_{ij}^2 g = \frac{\partial^2 g}{\partial r_{ij}^2} + \frac{2}{r_{ij}} \frac{\partial g}{\partial r_{ij}}, \tag{17}$$

$$\nabla_{ij}\cdot\nabla_{ik} g = (\hat{\mathbf{r}}_{ij}\cdot\hat{\mathbf{r}}_{ik}) \frac{\partial^2 g}{\partial r_{ij}\partial r_{ik}}, \tag{18}$$

where equation (13) expresses the fact that $r^l Y_{lm}$ is a solution of the Laplace equation, equation (14) holds because Φ_n depends explicitly only on $\mathbf{r}_{14}$, $\mathbf{r}_{24}$, $\mathbf{r}_{34}$, and equations (16)–(18) are valid because g is a function of only the distances r_{ij}. Equation (15) is automatically satisfied unless $i = 4$ or $j = k = 4$; for $i = 4$ and for $j = k = 4$ it is valid because of the limitation to $L \geqslant l_1 + l_2 + l_3 - 1$; for a proof of this statement the reader is referred to Ref. [15].

We now use equations (13)–(18) to simplify equation (12), obtaining after some manipulation the result

$$\begin{aligned} \mathsf{T}\Psi = &-\Phi_n \left[\sum_{ij,\ i<j} \frac{1}{2\mu_{ij}} \left(\frac{\partial^2 g}{\partial r_{ij}^2} + \frac{2}{r_{ij}} \frac{\partial g}{\partial r_{ij}} \right) + \sum_{i=1}^{4} \frac{1}{m_i} \sum_{jk\neq i,\ j<k} (\hat{\mathbf{r}}_{ij}\cdot\hat{\mathbf{r}}_{ik}) \frac{\partial^2 g}{\partial r_{ij}\partial r_{ik}} \right] \\ &- \frac{1}{m_4} \sum_{jk\neq 4} (\mathbf{r}_{j4}\cdot\nabla_{k4}\Phi_n) \frac{1}{r_{j4}} \frac{\partial g}{\partial r_{j4}} - \sum_{i=1}^{3} \frac{1}{m_i} \sum_{j\neq i} (\mathbf{r}_{ij}\cdot\nabla_{i4}\Phi_n) \frac{1}{r_{ij}} \frac{\partial g}{\partial r_{ij}}. \end{aligned} \tag{19}$$

The quantities $\hat{\mathbf{r}}_{ij}\cdot\hat{\mathbf{r}}_{ik}$ reduce to radial functions by a trivial extension of equation (4):

$$\hat{\mathbf{r}}_{ij}\cdot\hat{\mathbf{r}}_{ik} = \frac{r_{ij}^2 + r_{ik}^2 - r_{jk}^2}{2 r_{ij} r_{ik}}, \tag{20}$$

so we see that the dependence of the kinetic energy on the angular part of the wavefunction is localized in the quantities $(\mathbf{r}\cdot\nabla\Phi)$ in the second line of equation (19). The first line of equation (19) is the form for S states given by Rebane [17] and others.

It is interesting to compare equation (19) with the corresponding equation of Yan and Drake [18]. Both are exact in the nonrelativistic limit, taking full account of the finite masses of all four particles. However, our formulation has included a factor r^l with each spherical harmonic, thereby forming solid harmonics which are solutions to the Laplace equation, while Yan and Drake have not chosen to do so. Our choice has improved the separation of the radial and angular contributions and causes equation (19) to be significantly simpler than its Yan/Drake counterpart. The simplification extends also to the evaluation of the $(\mathbf{r}\cdot\nabla\Phi)$; our formulas (shown below) are more compact than they would be if, following Yan and Drake, we had restricted ∇ to its angular components. The other major departure of the present work from that of Yan and Drake is in our intention to evaluate the radial integrals directly in the Hylleraas coordinates, while Yan and Drake proceed by introduction of the Sack expansion [7].

To complete the analysis of the kinetic energy we must reduce the $(\mathbf{r}\cdot\nabla\Phi)$ to calculable quantities. The evaluation proceeds by methods similar to those discussed in Appendix B of Ref. [15]. That approach (summarized in Appendix A hereto) leads to the following formulas which can serve as a starting point for the relationships we require:

$$(\mathbf{r}_{j4}\cdot\nabla_{j4})\, r_{j4}^{l} Y_{lm}(\hat{\mathbf{r}}_{j4}) = l r_{j4}^{l} Y_{lm}(\hat{\mathbf{r}}_{j4}), \tag{21}$$

$$\begin{aligned}(\mathbf{r}_{j4}\cdot\nabla_{k4})\, & r_{j4}^{l_j} r_{k4}^{l_k} Y_{l_j l_j}(\hat{\mathbf{r}}_{j4}) Y_{l_k l_k}(\hat{\mathbf{r}}_{k4}) \\ &= \left[\frac{l_k(l_j+1)(2l_k+1)}{2l_j+3}\right]^{1/2} r_{j4}^{l_j+1} r_{k4}^{l_k-1} Y_{l_j+1,l_j+1}(\hat{\mathbf{r}}_{j4}) Y_{l_k-1,l_k-1}(\hat{\mathbf{r}}_{k4}),\end{aligned} \tag{22}$$

$$\begin{aligned}(\mathbf{r}_{j4}\cdot\nabla_{k4})\, & r_{j4}^{l_j} r_{k4}^{l_k} Y_{l_j l_j}(\hat{\mathbf{r}}_{j4}) Y_{l_k l_k-1}(\hat{\mathbf{r}}_{k4}) \\ &= \left[\frac{2l_k+1}{2l_j+3}\right]^{1/2} r_{j4}^{l_j+1} r_{k4}^{l_k-1} Y_{l_j+1,l_j}(\hat{\mathbf{r}}_{j4}) Y_{l_k-1,l_k-1}(\hat{\mathbf{r}}_{k4}) \\ &\quad + \left[\frac{(l_k-1)(l_j+1)(2l_k+1)}{2l_j+3}\right]^{1/2} r_{j4}^{l_j+1} r_{k4}^{l_k-1} Y_{l_j+1,l_j+1}(\hat{\mathbf{r}}_{j4}) Y_{l_k-1,l_k-2}(\hat{\mathbf{r}}_{k4}),\end{aligned} \tag{23}$$

$$\begin{aligned}(\mathbf{r}_{j4}\cdot\nabla_{k4}) & r_{j4}^{l_j} r_{k4}^{l_k} Y_{l_j,l_j-1}(\hat{\mathbf{r}}_{j4}) Y_{l_k l_k}(\hat{\mathbf{r}}_{k4}) \\ &= \left[\frac{l_j l_k(2l_k+1)}{2l_j+3}\right]^{1/2} r_{j4}^{l_j+1} r_{k4}^{l_k-1} Y_{l_j+1,l_j}(\hat{\mathbf{r}}_{j4}) Y_{l_k-1,l_k-1}(\hat{\mathbf{r}}_{k4}).\end{aligned} \tag{24}$$

It is also obvious that

$$\mathbf{r}_{ij}\cdot\nabla_{i4} = \mathbf{r}_{i4}\cdot\nabla_{i4} - \mathbf{r}_{j4}\cdot\nabla_{i4}, \tag{25}$$

so the above equations suffice for the reduction of all the $(\mathbf{r}\cdot\nabla\Phi)$ appearing in equation (19). It is perhaps worth remarking that the fact that the operators $\mathbf{r}\cdot\nabla$ connect contiguous index values l_j is a reflection of the fact that $r^l Y_{lm}$ is a hyperspherical harmonic (in four-dimensional space) [20], providing yet another connection to the work of Öhrn and Linderberg [1].

It is now straightforward, albeit tedious, to combine the relationships in equations (21)–(25) with the definitions of the Φ_n given in equations (5)–(7) to complete the evaluation of the $(\mathbf{r}\cdot\nabla\Phi)$. It is convenient to introduce some notation permitting a more succinct representation of the results. Accordingly, we define an operator L_j^i with the effect that it

will replace l_i and l_j in $\Phi_n^{l_1 l_2 l_3}$ by respectively $l_i + 1$ and $l_j - 1$ (*i.e.*, it will *raise* l_i and *lower* l_j so that, *e.g.*, $\llcorner_2^1 \Phi_n^{l_1 l_2 l_3} = \Phi_n^{l_1+1, l_2-1, l_3}$). We find

$$\mathbf{r}_{i4} \cdot \nabla_{i4} \Phi_n = l_i \Phi_n, \tag{26}$$

$$\mathbf{r}_{i4} \cdot \nabla_{j4} \Phi_0 = \left[\frac{l_j (l_i - 1)(2l_j + 1)}{2l_i + 3} \right]^{1/2} \llcorner_j^i \Phi_0 \quad (i, j = 1, 2, 3;\ j \neq i), \tag{27}$$

$$\mathbf{r}_{14} \cdot \nabla_{j4} \Phi_j = B(l_1, l_j) \llcorner_j^1 \Phi_j \quad (j = 2, 3), \tag{28}$$

$$\mathbf{r}_{14} \cdot \nabla_{j4} \Phi_k = C(l_1, l_j, l_k) \llcorner_j^1 \Phi_k \quad (j = 2, k = 3 \text{ or } j = 3, k = 2), \tag{29}$$

$$\mathbf{r}_{j4} \cdot \nabla_{14} \Phi_j = B(l_j, l_1) \llcorner_1^j \Phi_j \quad (j = 2, 3), \tag{30}$$

$$\mathbf{r}_{j4} \cdot \nabla_{k4} \Phi_j = C(l_j, l_k, l_1) \llcorner_k^j \Phi_j \quad (j, k = 2, 3;\ k \neq j), \tag{31}$$

$$\mathbf{r}_{j4} \cdot \nabla_{14} \Phi_k = F_k \llcorner_1^j \Phi_k + F_j \llcorner_1^j \Phi_j \quad (j = 2, k = 3 \text{ or } j = 3, k = 2), \tag{32}$$

$$\mathbf{r}_{j4} \cdot \nabla_{k4} \Phi_k = G_k \llcorner_k^j \Phi_k + G_j \llcorner_k^j \Phi_j \quad (j = 2, k = 3 \text{ or } j = 3, k = 2), \tag{33}$$

$$\mathbf{r}_{ij} \cdot \nabla_{i4} \Phi_n = l_i \Phi_n - \mathbf{r}_{j4} \cdot \nabla_{i4} \Phi_n \quad (i, j = 1, 2, 3;\ j \neq i). \tag{34}$$

In these equations,

$$B(l, l') = \left[\frac{l(l' - 1)(2l' + 1)}{2l + 3} \right]^{1/2}, \tag{35}$$

$$C(l, l', l'') = \left[\frac{l\, l'(2l' + 1)(l + l'' + 1)}{(2l + 3)(l + l'')} \right]^{1/2}, \tag{36}$$

$$F_k = l_1 \left[\frac{(2l_1 + 1)(l_j + 1)(l_1 + l_k - 1)}{(l_1 - 1)(2l_j + 3)(l_1 + l_k)} \right]^{1/2}, \tag{37}$$

$$F_j = -\left[\frac{l_k (2l_1 + 1)(l_1 + l_j)}{(l_1 - 1)(2l_j + 3)(l_1 + l_k)} \right]^{1/2}, \tag{38}$$

$$G_k = \left[\frac{(l_j + 1)(l_k - 1)(2l_k + 1)(l_1 + l_k - 1)}{(2l_j + 3)(l_1 + l_3)} \right]^{1/2}, \tag{39}$$

$$G_j = \left[\frac{(2l_k + 1)(l_1 + l_j + 1)}{(2l_j + 3)(l_1 + l_3)} \right]^{1/2}. \tag{40}$$

Summarizing, we see that the angular dependence of $\mathsf{T}\Psi$ can be written entirely in terms of the angular-momentum eigenfunctions introduced at equations (5)–(7). This means that the angular contributions to kinetic-energy matrix elements will reduce to forms similar to those encountered for overlap integrals. This point will be examined in more detail in Section 4.

4. ANGULAR MATRIX ELEMENTS

We now consider the evaluation of matrix elements involving wavefunctions of the type specified in equation (1). The details of the formulation will depend upon the extent to

which the particles are identical as well as their possible spin states and permutational symmetry. Since the wavefunctions under study are of particular value for nonadiabatic systems and may involve exotic species such as mesons or antiparticles, there is no single set of symmetry operations applicable to all four-body problems. For this reason we do not attempt a detailed discussion of spin or permutation symmetry. Rather, we limit our analysis to the primitive spatial-coordinate matrix elements that will arise irrespective of the symmetry.

We start with the observation that a particle permutation on Φ_0 results in an instance of Φ_0 with its l indices permuted, while a particle permutation on Φ_2 (or Φ_3) can only produce linear combinations of Φ_2 and Φ_3, possibly with permuted l indices. We also note that

(1) The kinetic-energy operator T converts a function Φ_0 into a linear combination of itself and other instances of Φ_0;
(2) The set of functions Φ_2, Φ_3 is closed under the operation of T; and
(3) Φ_3 can be reached from an instance of Φ_2 by a coordinate and index permutation.

Finally, we observe that the operators for the Coulombic energy, proportional to $1/r_{ij}$, do not affect the angular part of the wavefunction. Based on the above, we see that all the spatial matrix elements required for nonrelativistic energy computations in four-body Coulomb systems correspond to one of the two generic forms

$$I_0 = \int \mathrm{d}\tau_R \, \mathrm{d}\tau_\Omega \left[\Phi_n^{l_1 l_2 l_3}(\mathbf{r}_{14}, \mathbf{r}_{24}, \mathbf{r}_{34})\right]^* \Phi_n^{\lambda_1 \lambda_2 \lambda_3}(\mathbf{r}_{14}, \mathbf{r}_{24}, \mathbf{r}_{34}) f_R, \tag{41}$$

$$I_p = \int \mathrm{d}\tau_R \, \mathrm{d}\tau_\Omega \left[\Phi_n^{l_1 l_2 l_3}(\mathbf{r}_{14}, \mathbf{r}_{24}, \mathbf{r}_{34})\right]^* \Phi_n^{\lambda_1 \lambda_2 \lambda_3}(\mathbf{r}_{14}, \mathbf{r}_{34}, \mathbf{r}_{24}) f_R, \tag{42}$$

where n can without restriction be limited to the values 0 and 2. Here f_R indicates a function of only the interparticle distances; it may include contributions from an operator in the Hamiltonian as well as the radial parts of a pair of wavefunctions. The symbol $\mathrm{d}\tau_\Omega$ refers to an integration over the orientations of the four-body system with fixed values of the r_{ij} and a sum over the two values of the inversion index; the symbol $\mathrm{d}\tau_R$ refers to integration over the interparticle distances. The orientation integral has a straightforward description in terms of Euler angles, which we denote α, β, γ, with volume element $\mathrm{d}\alpha \, \sin\beta \, \mathrm{d}\beta \, \mathrm{d}\gamma$, where α and γ have the range $(0, 2\pi)$ and β has the range $(0, \pi)$. The volume element $\mathrm{d}\tau_R$ is complicated and will not be discussed now.

In previous work [21] we have shown that the evaluation of equations (41) and (42) best proceeds by first performing the angular integration, the result of which will be polynomials in the r_{ij}. The radial integrations are then of a type that can be handled by the method described first by Fromm and Hill [12] (with improvements we have reported in more recent work [13,14]).

The angular integration differs from that usually encountered in atomic problems because it is carried out at fixed values of all the interparticle distances, as is evident from the fact that there are now only three independent angular variables (the Euler angles) rather than the six coordinates associated with the respective orientations of $\hat{\mathbf{r}}_{14}$, $\hat{\mathbf{r}}_{24}$, and $\hat{\mathbf{r}}_{34}$. The evaluation proceeds by combining the spherical harmonics, using equation (A.2) in Appendix A, to write $Y^*_{l_j m_j}(\hat{\mathbf{r}}_{j4}) Y_{\lambda_j \mu_j}(\hat{\mathbf{r}}_{j4})$ as a sum (over Λ_j, and formally also over t_j)

of $Y_{\Lambda_j t_j}(\hat{\mathbf{r}}_{j4})$, for $j = 1, 2, 3$. For the matrix element I_0, we get the cumbersome expression

$$I_0 = (-1)^{l'+\lambda'} \frac{2L+1}{(4\pi)^{3/2}} \sum_{(\Lambda)} (l_1, l_2, l', l_3, \lambda_1, \lambda_2, \lambda', \lambda_3, \Lambda_1, \Lambda_2, \Lambda_3)^{1/2} \times \begin{pmatrix} l_1 & \lambda_1 & \Lambda_1 \\ 0 & 0 & 0 \end{pmatrix} \begin{pmatrix} l_2 & \lambda_2 & \Lambda_2 \\ 0 & 0 & 0 \end{pmatrix} \begin{pmatrix} l_3 & \lambda_3 & \Lambda_3 \\ 0 & 0 & 0 \end{pmatrix} J_0, \tag{43}$$

where $(a, b, \ldots, z) \equiv (2a+1)(2b+1)\cdots(2z+1)$ and the sign factor has been simplified recognizing that both wavefunctions have the same parity. Here

$$J_0 = \sum_{(m)(\mu)(t)} (-1)^{\mu_1+\mu_2+m_3} \begin{pmatrix} l_1 & \lambda_1 & \Lambda_1 \\ -m_1 & \mu_1 & -t_1 \end{pmatrix} \begin{pmatrix} l_2 & \lambda_2 & \Lambda_2 \\ -m_2 & \mu_2 & -t_2 \end{pmatrix} \times \begin{pmatrix} l_3 & \lambda_3 & \Lambda_3 \\ -m_3 & \mu_3 & -t_3 \end{pmatrix} \begin{pmatrix} l_1 & l_2 & l' \\ m_1 & m_2 & -m' \end{pmatrix} \begin{pmatrix} l' & l_3 & L \\ m' & m_3 & -L \end{pmatrix} \times \begin{pmatrix} \lambda_1 & \lambda_2 & \lambda' \\ \mu_1 & \mu_2 & -\mu' \end{pmatrix} \begin{pmatrix} \lambda' & \lambda_3 & L \\ \mu' & \mu_3 & -L \end{pmatrix} \int \mathrm{d}\tau_R \, r_{14}^{l_1+\lambda_1} r_{24}^{l_2+\lambda_2} r_{34}^{l_3+\lambda_3} f_R K, \tag{44}$$

and K is the angular integral

$$K = \int \mathrm{d}\tau_\Omega \, Y_{\Lambda_1 t_1}(\hat{\mathbf{r}}_{14}) Y_{\Lambda_2 t_2}(\hat{\mathbf{r}}_{24}) Y_{\Lambda_3 t_3}(\hat{\mathbf{r}}_{34}). \tag{45}$$

Because the integration includes a sum over the inversion index, the integral in equation (45) will vanish unless $\Lambda_1 + \Lambda_2 + \Lambda_3$ is even, while in that case the inversion index summation will have the effect of multiplying the orientation integral by two.

A convenient way to perform the integration in equation (45) is to take its integrand for some fixed orientation, then reaching other orientations by applying the same rotational transformation to each of the spherical harmonics. Thus, if in some initial orientation the values of the angular variables are $\hat{\mathbf{r}}_{j4}$, their values after the entire four-body system has been subjected to a rotation R would become $\mathsf{R}\hat{\mathbf{r}}_{j4}$, with the spherical harmonics transforming according to

$$Y_{lm}(\mathsf{R}\,\hat{\mathbf{r}}) = \sum_\sigma D^l_{\sigma m}(\mathsf{R}) Y_{l\sigma}(\hat{\mathbf{r}}). \tag{46}$$

The coefficients D have well-known properties (see, for example, Edmonds [19]). Using equation (46) for each of the spherical harmonics in equation (45), we can replace the integration over the orientations of the $\hat{\mathbf{r}}_{ij}$ by one over the Euler angles of the rotational transformation R, where the quantity now to be integrated is the product of the D coefficients, and the Y themselves are to be evaluated at an arbitrary initial orientation. Carrying out this prescription, we have

$$K = \sum_{(\sigma)} Y_{\Lambda_1\sigma_1}(\hat{\mathbf{r}}_{14}) Y_{\Lambda_2\sigma_2}(\hat{\mathbf{r}}_{24}) Y_{\Lambda_3\sigma_3}(\hat{\mathbf{r}}_{34}) \int \mathrm{d}\tau_\Omega \, D^{\Lambda_1}_{\sigma_1 t_1}(\mathsf{R}) D^{\Lambda_2}_{\sigma_2 t_2}(\mathsf{R}) D^{\Lambda_3}_{\sigma_3 t_3}(\mathsf{R})$$

$$= \begin{cases} 16\pi^2 \begin{pmatrix} \Lambda_1 & \Lambda_2 & \Lambda_3 \\ t_1 & t_2 & t_3 \end{pmatrix} \sum_{(\sigma)} \begin{pmatrix} \Lambda_1 & \Lambda_2 & \Lambda_3 \\ \sigma_1 & \sigma_2 & \sigma_3 \end{pmatrix} \\ \quad \times Y_{\Lambda_1\sigma_1}(\hat{\mathbf{r}}_{14}) Y_{\Lambda_2\sigma_2}(\hat{\mathbf{r}}_{24}) Y_{\Lambda_3\sigma_3}(\hat{\mathbf{r}}_{34}) \quad (\Lambda_1 + \Lambda_2 + \Lambda_3 \text{ even}), \\ 0 \quad \text{otherwise.} \end{cases} \tag{47}$$

The second line of equation (47) is reached using the known formula for the integral of a product of three D coefficients, given for reference as equation (A.3) in Appendix A. The value of that integral has been multiplied by two in equation (47) to take account of the inversion index sum, and the resulting condition on the Λ has been explicitly noted.

It is important to understand that equation (47) ultimately depends only on the relations between $\mathbf{r}_{14}$, $\mathbf{r}_{24}$, and $\mathbf{r}_{34}$, and not on their values at any particular orientation. This observation in turn means that the (σ) summation in that equation must in fact produce a result that is independent of the arbitrary orientation chosen for its evaluation. Expressions of this type, referred to as *rotational invariants*, have been discussed in the literature [22], and can be classified by their values of Λ_1, Λ_2, and Λ_3. To emphasize the role of the rotational invariants and to introduce a notation consistent with their appearance in other work by this author, we rewrite equation (47) as

$$K = \begin{cases} 16\pi^2 \dfrac{(\Lambda_1, \Lambda_2, \Lambda_3)^{1/2}}{(4\pi)^{3/2}} \begin{pmatrix} \Lambda_1 & \Lambda_2 & \Lambda_3 \\ t_1 & t_2 & t_3 \end{pmatrix} \widehat{K}_{\Lambda_1\Lambda_2\Lambda_3} & (\Lambda_1 + \Lambda_2 + \Lambda_3 \text{ even}), \\ 0 \quad \text{otherwise}, \end{cases} \tag{48}$$

with $\widehat{K}_{\Lambda_1,\Lambda_2,\Lambda_3}$ defined as

$$\widehat{K}_{\Lambda_1\Lambda_2\Lambda_3} = \frac{(4\pi)^{3/2}}{(\Lambda_1, \Lambda_2, \Lambda_3)^{1/2}} \times \sum_{(\sigma)} \begin{pmatrix} \Lambda_1 & \Lambda_2 & \Lambda_3 \\ \sigma_1 & \sigma_2 & \sigma_3 \end{pmatrix} Y_{\Lambda_1\sigma_1}(\hat{\mathbf{r}}_{14}) Y_{\Lambda_2\sigma_2}(\hat{\mathbf{r}}_{24}) Y_{\Lambda_3\sigma_3}(\hat{\mathbf{r}}_{34}). \tag{49}$$

We are now ready to insert equation (48) into equation (44). As explained elsewhere [21], the (m), (μ), and (t) summations can be performed, leading after some manipulation to the following final result for I_0:

$$\begin{aligned} I_0 = \frac{(-1)^{L+l_1+l_2+l'}}{4\pi} \sum_{(\Lambda)} (\Lambda_1, \Lambda_2, \Lambda_3)(l_1, l_2, l', l_3, \lambda_1, \lambda_2, \lambda', \lambda_3)^{1/2} \begin{pmatrix} l_1 & \lambda_1 & \Lambda_1 \\ 0 & 0 & 0 \end{pmatrix} \\ \times \begin{pmatrix} l_2 & \lambda_2 & \Lambda_2 \\ 0 & 0 & 0 \end{pmatrix} \begin{pmatrix} l_3 & \lambda_3 & \Lambda_3 \\ 0 & 0 & 0 \end{pmatrix} \begin{Bmatrix} l_3 & \lambda_3 & \Lambda_3 \\ \lambda' & l' & L \end{Bmatrix} \begin{Bmatrix} \lambda_1 & \lambda_2 & \lambda' \\ l_1 & l_2 & l' \\ \Lambda_1 & \Lambda_2 & \Lambda_3 \end{Bmatrix} \\ \times \int \mathrm{d}\tau_R \, r_{14}^{l_1+\lambda_1} r_{24}^{l_2+\lambda_2} r_{34}^{l_3+\lambda_3} \widehat{K}_{\Lambda_1\Lambda_2\Lambda_3} f_R. \end{aligned} \tag{50}$$

Here the quantities $\{\ldots\}$ containing six elements are 6-j symbols; those with nine elements are 9-j symbols. For definition and evaluation methods for these symbols see, for example, Edmonds [19].

Although equation (50) contains a triple summation, the number of terms that contribute to the sum is severely limited by the conditions under which the n-j symbols are nonzero. The quantities in the upper row of each 3-j symbol, and those in each row or column of the 9-j symbol, must satisfy a *triangle condition*, meaning that each of the three symbols of the row or column must be no larger than the sum of the other two symbols. Moreover, if the lower row of a 3-j symbol contains only zeros, the sum of the symbols in the upper row must be even. In addition, we have the requirement that $\Lambda_1 + \Lambda_2 + \Lambda_3$ be even.

Considerations similar to those used for I_0 can be applied to I_p. However, because the variables $\mathbf{r}_{j4}$ occur in different orders in the two wavefunctions, the angular momentum

coupling is less symmetric than for I_0. For this reason the locations of the various indices in the equations analogous to equations (43) and (44) is not the same as in those equations, with result that the index summations yield a different result. We find

$$I_p = \frac{(-1)^{L+\lambda_1+\lambda_2+\lambda'}}{4\pi} \sum_{(\Lambda)} (\Lambda_1, \Lambda_2, \Lambda_3)(l_1, l_2, l', l_3, \lambda_1, \lambda_2, \lambda', \lambda_3)^{1/2} \begin{pmatrix} l_1 & \lambda_1 & \Lambda_1 \\ 0 & 0 & 0 \end{pmatrix} \times \begin{pmatrix} l_2 & \lambda_3 & \Lambda_2 \\ 0 & 0 & 0 \end{pmatrix} \begin{pmatrix} l_3 & \lambda_2 & \Lambda_3 \\ 0 & 0 & 0 \end{pmatrix} \sum_{\tau} (2\tau+1) \begin{Bmatrix} l_3 & l' & L \\ \tau & \lambda_2 & \Lambda_3 \end{Bmatrix} \begin{Bmatrix} \lambda_1 & \lambda_2 & \lambda' \\ L & \lambda_3 & \tau \end{Bmatrix} \times \begin{Bmatrix} \lambda_3 & \lambda_1 & \tau \\ l_2 & l_1 & l' \\ \Lambda_2 & \Lambda_1 & \Lambda_3 \end{Bmatrix} \int \mathrm{d}\tau_R \, r_{14}^{l_1+\lambda_1} r_{24}^{l_2+\lambda_3} r_{34}^{l_3+\lambda_2} \widehat{K}_{\Lambda\Lambda'\Lambda''} f_R. \tag{51}$$

Although equation (51) contains a fourfold summation, the number of terms contributing to the sum will again be modest.

5. ROTATIONAL INVARIANTS

It can be shown that $\widehat{K}_{\Lambda_1\Lambda_2\Lambda_3}$ can be written entirely in terms of the scalar products $\hat{\mathbf{r}}_{i4}\cdot\hat{\mathbf{r}}_{j4}$, and therefore, by virtue of equation (20), is a function only of the quantities r_{ij}. That fact is hardly surprising if it is recognized that these distances determine (except for inversion) the relative geometry, but it is fortunate and very useful that the $\widehat{K}$ are polynomials in the scalar products.

The $\widehat{K}_{\Lambda_1\Lambda_2\Lambda_3}$ can be seen from equation (49) to be symmetric under index permutation because the 3-j symbols with even $\Lambda_1 + \Lambda_2 + \Lambda_3$ have symmetry under column interchange. The presence of the Λ_j in a 3-j symbol also indicates that they must satisfy a triangle condition. These conditions, along with the restrictions already noted for equations (50) and (51), all combine to cause a very modest number of $\widehat{K}_{\Lambda_1\Lambda_2\Lambda_3}$ to suffice for the description of states of most L values of interest.

Since the $\widehat{K}$ are independent of the orientation chosen for the $\hat{\mathbf{r}}_{ij}$, it is prudent to undertake the evaluation of $\widehat{K}_{\Lambda_1\Lambda_2\Lambda_3}$ in an orientation in which one of the $\hat{\mathbf{r}}_{i4}$ is aligned with the polar axis. Proceeding from such a starting point, we have reported elsewhere [21] all the independent $\widehat{K}_{\Lambda_1\Lambda_2\Lambda_3}$ with $\Lambda_1+\Lambda_2+\Lambda_3 \leqslant 8$, a range permitting the study of arbitrary S, P, D, and F states. We include here in Table 1 a subset of those data. In the table the scalar products are identified as cosines of the angles between the unit vectors:

$$\cos\theta_{ijk} = \hat{\mathbf{r}}_{ij} \cdot \hat{\mathbf{r}}_{ik}. \tag{52}$$

6. RADIAL INTEGRATION

It is not the purpose of this communication to treat the radial integrations that are parts of equations (50) and (51). We do note that the radial integrals in those equations are of the form

$$I_R = \int \mathrm{d}\tau_R \, r_{14}^{n_1} r_{24}^{n_2} r_{34}^{n_3} \widehat{K}_{\Lambda_1\Lambda_2\Lambda_3} f_R, \tag{53}$$

Table 1. Rotational invariants $\widehat{K}_{\Lambda\Lambda'\Lambda''}$, expressed in terms of the quantities $\cos\theta_{ijk}$ defined in equation (52)

Λ	Λ'	Λ''	$\widehat{K}_{\Lambda\Lambda'\Lambda''}$
0	0	0	1
1	1	0	$-\cos\theta_{123}/\sqrt{3}$
2	2	0	$(3\cos^2\theta_{123}-1)/2\sqrt{5}$
2	2	2	$(3\cos^2\theta_{123}+3\cos^2\theta_{124}+3\cos^2\theta_{134}-9\cos\theta_{123}\cos\theta_{124}\cos\theta_{134}-2)/5\sqrt{70}$
3	3	0	$-(5\cos^3\theta_{123}-3\cos\theta_{123})/2\sqrt{7}$
3	3	2	$-[25\cos^3\theta_{123}+\cos\theta_{123}(30\cos^2\theta_{124}+30\cos^2\theta_{124}-21)$ $+\cos\theta_{124}\cos\theta_{134}(3-75\cos^2\theta_{123})]/4\sqrt{105}$
3	2	1	$(5\cos^2\theta_{123}\cos\theta_{124}-2\cos\theta_{123}\cos\theta_{134}-\cos\theta_{124})\sqrt{105}/70$

and because of the presence of the powers of r_{j4} and the form of $\widehat{K}_{\Lambda_1\Lambda_2\Lambda_3}$, their integrands will reduce to polynomials in the r_{ij} multiplied by the wavefunction product f_R. If f_R consists of exponentials in the r_{ij}, the radial integrals will be of types whose analytical evaluation has been reported [12–14].

7. CONCLUSION

The essence of this paper is the development of a formula for the kinetic energy of a four-body system of general angular symmetry, in a form which is simpler and more compact than those previously reported. The use of this formula makes clear that matrix elements of the nonrelativistic Hamiltonian for four-body Coulomb systems can be written as a linear combination of basic radial integrals, each with a coefficient characteristic of the angular symmetry. The integrands of the radial integrals consist of a product of two radial wavefunctions, multiplied by a polynomial in the r_{ij}. This observation, in turn, means that the Hamiltonian and overlap matrices can be constructed from the same set of basic integrals.

ACKNOWLEDGEMENTS

The author acknowledges stimulating discussions with Professor Vedene Smith and Dr. Alexei Frolov of Queen's University, Kingston, Ontario, Canada. It is also a pleasure to thank Professor Jan Linderberg for encouragement and advice. Presentation of this work was supported by Aarhus University. The research reported here was carried out with support from the U. S. National Science Foundation, Grant PHY-0303412.

APPENDIX A: ANGULAR MOMENTUM FORMULAS

Two spherical harmonics $Y_{lm}(\hat{\mathbf{r}})$ and $Y_{l'm'}(\hat{\mathbf{r}}')$ couple as follows to form a resultant angular momentum eigenfunction of quantum numbers L, M:

$$Y_{LM}(\hat{\mathbf{r}},\hat{\mathbf{r}}') = (-1)^{l'-l-M}\sqrt{2L+1}\sum_m \begin{pmatrix} l & l' & L \\ m & M-m & -M \end{pmatrix} Y_{lm}(\hat{\mathbf{r}})Y_{l',M-m}(\hat{\mathbf{r}}'). \tag{A.1}$$

The 3-j symbols evaluate to real numbers, so equation (A.1) is still satisfied if each Y is replaced by the corresponding Y^*.

The product of two spherical harmonics of the same argument can be written as a linear combination of harmonics according to the equation

$$Y^*_{lm}(\hat{\mathbf{r}})Y_{l'm'}(\hat{\mathbf{r}}) = \sum_{\Lambda t}(-1)^{m'}\left[\frac{(2l+1)(2l'+1)(2\Lambda+1)}{4\pi}\right]^{1/2} \times \begin{pmatrix} l & l' & \Lambda \\ 0 & 0 & 0 \end{pmatrix}\begin{pmatrix} l & l' & \Lambda \\ -m & m' & -t \end{pmatrix} Y_{\Lambda t}(\hat{\mathbf{r}}). \tag{A.2}$$

Rotation matrices $D^l_{\sigma m}(\mathsf{R})$ were defined as quantities satisfying equation (46). If R corresponds to a rotation described by Euler angles (α, β, γ), we may write $D^l_{\sigma m}(\mathsf{R})$ as $D^l_{\sigma m}(\alpha, \beta, \gamma)$. The coefficients $D^l_{\sigma m}$ satisfy the following integral relationship, given as equation (4.6.2) of Ref. [19]:

$$\int_0^{2\pi} \mathrm{d}\alpha \int_0^{\pi} \sin\beta\, \mathrm{d}\beta \int_0^{2\pi} \mathrm{d}\gamma\, D^l_{\sigma m}(\alpha,\beta,\gamma) D^{l'}_{\sigma' m'}(\alpha,\beta,\gamma) D^{l''}_{\sigma'' m''}(\alpha,\beta,\gamma) = 8\pi^2 \begin{pmatrix} l & l' & l'' \\ \sigma & \sigma' & \sigma'' \end{pmatrix}\begin{pmatrix} l & l' & l'' \\ m & m' & m'' \end{pmatrix}. \tag{A.3}$$

Equations (21)–(24) give evaluations for differential forms of the type $(\mathbf{r}\cdot\nabla\Phi)$. One can invoke the machinery of irreducible tensor operators for this purpose, as was done for the three-body problem by Éfros [23]. However, it is simple and straightforward just to write the solid harmonics in Cartesian coordinates and carry out the evaluation in that system.

In particular, we have

$$r^l Y_{ll}(\hat{\mathbf{r}}) = (-1)^l \left(\frac{(2l+1)!!}{4\pi(2l)!!}\right)^{1/2} (x+\mathrm{i}y)^l, \tag{A.4}$$

$$r^l Y_{l,l-1}(\hat{\mathbf{r}}) = (-1)^{l-1} \left(\frac{(2l+1)!!}{4\pi(2l-2)!!}\right)^{1/2} (x+\mathrm{i}y)^{l-1} z. \tag{A.5}$$

Then, for example, the application of $\mathbf{r}_{j4}\cdot\nabla_{k4}$ becomes that of $x_{j4}(\partial/\partial x_{k4}) + y_{j4}(\partial/\partial y_{k4}) + z_{j4}(\partial/\partial z_{k4})$. More details are in Appendix B of Ref. [15].

REFERENCES

[1] Y. Öhrn, J. Linderberg, *Mol. Phys.* **49** (1983) 53.
[2] R.G. Littlejohn, M. Reinsch, *Phys. Rev. A* **52** (1995) 2035.
[3] G. Breit, *Phys. Rev.* **35** (1930) 569.
[4] A.K. Bhatia, A. Temkin, *Rev. Mod. Phys.* **36** (1964) 1050.
[5] C.L. Schwartz, *Phys. Rev.* **123** (1961) 1700.
[6] E.A. Hylleraas, *Z. Phys.* **54** (1929) 347.
[7] R.A. Sack, *J. Math. Phys.* **5** (1964) 245.
[8] G.W.F. Drake, *Phys. Scr.* **T83** (1999) 83.
[9] F.W. King, *J. Mol. Struct. (Theochem)* **400** (1997) 7.
[10] L.M. Delves, T. Kalotas, *Aust. J. Phys.* **21** (1968) 431.
[11] A.J. Thakkar, V.H. Smith Jr., *Phys. Rev. A* **15** (1977) 1.

[12] D.M. Fromm, R.N. Hill, *Phys. Rev. A* **36** (1987) 1013.
[13] F.E. Harris, *Phys. Rev. A* **55** (1997) 1820.
[14] F.E. Harris, A.M. Frolov, V.H. Smith Jr., *J. Chem. Phys.* **119** (2003) 8833.
[15] F.E. Harris, *Adv. Quantum Chem.* **47** (2004) 129.
[16] A.M. Frolov, V.H. Smith Jr., *Phys. Rev. A* **53** (1996) 3853.
[17] T.K. Rebane, *Opt. Spektrosc.* **75** (1993) 945;
T.K. Rebane, *Opt. Spektrosc.* **75** (1993) 557.
[18] Z.-C. Yan, G.W.F. Drake, *J. Phys. B* **30** (1997) 4723.
[19] A.R. Edmonds, *Angular Momentum in Quantum Mechanics*, Princeton Univ. Press, Princeton, NJ, 1960.
[20] J. Avery, *Hyperspherical Harmonics: Applications in Quantum Theory*, Kluwer, Dordrecht, 1989.
[21] F.E. Harris, in: E.J. Brändas, E.S. Kryachko (Eds.), *Fundamental World of Quantum Chemistry*, vol. 3, Kluwer, Dordrecht, 2004, pp. 115–127.
[22] L.C. Biedenharn, J.D. Louck, *Angular Momentum in Quantum Physics: Theory and Application*, Addison–Wesley, Reading MA, 1981.
[23] V.D. Éfros, *Zh. Eksp. Teor. Fiz.* **90** (1986) 10;
V.D. Éfros, *Sov. Phys. JETP* **63** (1986) 5.

This page intentionally left blank

The Rotational *g* Tensor as a Benchmark for *Ab Initio* Molecular Property Calculations

Chris E. Mohn[1], David J.D. Wilson[1,*], Ola B. Lutnæs[1], Trygve Helgaker[1] and Kenneth Ruud[2]

[1]*Department of Chemistry, University of Oslo, P.O. Box 1033 Blindern, N-0315 Oslo, Norway*
[2]*Department of Chemistry, University of Tromsø, N-9037 Tromsø, Norway*

Abstract

Ab initio calculations using large multiconfigurational self-consistent field wave functions and density functional theory are presented for the rotational g tensors of HOF, H_2O, H_2S and O_3. Rapid convergence toward the basis-set limit is ensured using rotational London atomic orbitals. The effect of zero-point vibrational corrections and the choice of molecular geometries are analyzed and the results are compared to highly accurate experimental results obtained by microwave Zeeman spectroscopy and by various molecular beam techniques. Electron-correlation corrections and zero-point vibrational corrections are found to be equally important and both must be taken into account when comparing with highly accurate experimental data.

Contents

1. INTRODUCTION

Calculations of the rotational g tensor are a challenge to *ab initio* theory. The errors introduced due to truncations in the one- and N-electron spaces (basis set and electron correlation treatment, respectively) are often much larger than the experimental standard deviations obtained in highly accurate molecular beam (MB) [1] and microwave (MW) Zeeman experiments [2]. Theoretical studies of the rotational g tensor have been presented at various levels of theory, including Hartree–Fock [3–5], second-order Møller–Plesset perturbation theory (MP2) [6–8], the linearized coupled-cluster doubles (L-CCD)

* Present address: Department of Chemistry, La Trobe University, Bundoora 3083, Victoria, Australia.

ADVANCES IN QUANTUM CHEMISTRY, VOLUME 50
ISSN: 0065-3276 DOI: 10.1016/S0065-3276(05)50005-4

method [8], second-order polarization propagator approximation (SOPPA) [9–11], multiconfigurational self-consistent-field (MCSCF) theory [12–14] and even full configuration-interaction (FCI) [15,16] for diatomic and small polyatomic molecules. The results presented in these studies are in qualitative agreement with experiment but often differ by more than ten experimental standard deviations from experimental measurements, especially at lower levels of theory.

In a few cases it is possible, by systematically improving the quality of the basis sets and the N-electron treatment, to extrapolate the results achieved at different levels of theory so as to allow for a critical comparison with experimental observations. In a detailed study of the water molecule, Ruud *et al.* [14] showed that large restricted active space self-consistent field (RASSCF) wave functions, including up to 40 active orbitals, were necessary for a critical comparison with experiment. However, a discrepancy with respect to experiment remained, suggesting that molecular vibrations could also give substantial contributions to the rotational g tensor. Indeed, rovibrational effects were found to be as important as electron correlation effects and thus non-negligible when a quantitative agreement with experiment is needed. The importance of including molecular vibrations in calculations of rotational g tensors has also be demonstrated by Cybulski and Bishop for diatomic molecules calculated at the MP2 and L-CCD levels of theory [8] and Sauer *et al.* [9] for small polyatomic molecules in SOPPA calculations.

In recent years, density-functional theory (DFT) has emerged as one of the most commonly used quantum-mechanical methods for studying a wide range of molecular properties. Both local density approximation (LDA) and generalized gradient approximation (GGA) functionals have been developed. In particular, GGA functionals such as the Becke–Lee–Yang–Parr functional (BLYP) and the hybrid Becke-3-parameter-Lee–Yang–Parr functional (B3LYP) often describe electron correlation effects of molecular properties with an accuracy comparable to that of MP2 and CCSD theories. Thus, it is of considerable interest to compare the results of g tensor calculations using DFT methods with those obtained using large MCSCF wave functions and with accurate experimental data. There have been few reported DFT studies of rotational g tensors [17], and none that include rotational London (gauge-origin independent) atomic orbitals [4].

The availability of highly accurate g tensor data from experiment, typically with small error bars, serves as a severe test on the performance of modern electronic structure theory. As a result, although contributions from electron correlation and molecular vibrations to the rotational g tensor are typically small in magnitude, they usually cannot be neglected in comparing with experimental data [9,14,18].

In this work, we carry out calculations of the rotational g tensor of four small diamagnetic molecules (HOF, H_2O, H_2S and O_3). Differing in the importance and relative magnitudes of static and dynamic electron correlation, these molecules constitute a suitable set for testing the accuracy of various computational approaches in the calculation of g tensors. Large MCSCF wave functions have been constructed by systematically increasing the size of the active space, using rotational London atomic orbitals to ensure origin-independent results and fast basis-set convergence. The zero-point vibrational corrections to the rotational g tensors are calculated by expanding the property surface about a variationally determined geometry [18,19]. The effect of electron correlation on the vibrational contribution to the rotational g tensor is discussed using modest-sized multiconfigurational wave functions. We pay particular attention to the possible errors in the calculated g tensors

arising from errors in the molecular geometries. Our MCSCF results are also compared to those obtained from DFT theory.

The paper is organized as follows. In Section 2, we outline the theory of g-tensor calculations, whereas computational details are given in Section 3. In Section 4, the results from the calculations are presented and compared with other theoretical investigations and experimental data. Some concluding remarks are given in Section 5.

2. THEORY

Consider a rotating diamagnetic molecule in an external static magnetic field. In the Born–Oppenheimer approximation, the electrons adjust instantaneously to the rotating nuclear framework. Consequently, in this approximation, the molecule possesses no magnetic moment due to the rotational movement. The observed small magnetic moment of a rotating molecule therefore arises from a breakdown in the separability of electronic and rotational degrees of freedom, causing a first-order Zeeman splitting in the rotational spectrum. This energy shift is related to the rotational g tensor (atomic units):

$$\Delta E = -\mu_{\mathrm{N}} \mathbf{B}^{\mathrm{T}} \mathbf{g} \mathbf{J}. \tag{1}$$

Here **B** is the static external magnetic induction, **J** the total angular momentum, **g** is the rotational g tensor and μ_{N} is the nuclear magneton. The electronic contribution to **g** can be identified as a second-order, time-independent property obtained by differentiating the electronic energy ε with respect to the magnetic induction and the total rotational angular momentum:

$$\mathbf{g}_{\mathrm{e}} = -\mu_{\mathrm{N}} \left. \frac{\mathrm{d}^2 \varepsilon(\mathbf{B}^{\mathrm{T}}, \mathbf{J})}{\mathrm{d}\mathbf{B}\, \mathrm{d}\mathbf{J}} \right|_{\mathbf{B},\mathbf{J}=\mathbf{0}}. \tag{2}$$

Let H_{e}^0 be the spin-free non-relativistic electronic Hamiltonian of a non-rotating diamagnetic molecule in the absence of an external magnetic field. For a rotating molecule in an external magnetic field, we can write down the electronic Hamiltonian in the center-of-mass (CM) system in the following manner

$$H_{\mathrm{e}} = H_{\mathrm{e}}^0 - \mathbf{J}^{\mathrm{T}} \mathbf{I}_{\mathrm{nuc}}^{-1} \mathbf{L}_{\mathrm{CM}} + \frac{1}{2}(\mathbf{B} \cdot \mathbf{L}_O) + \frac{1}{2} \mathbf{B}^{\mathrm{T}} \left[(\mathbf{r}^{\mathrm{T}} \cdot \mathbf{R}_O) - \mathbf{r} \mathbf{R}_O^{\mathrm{T}} \right] \mathbf{I}_{\mathrm{nuc}}^{-1} \mathbf{J}. \tag{3}$$

The nuclear Hamiltonian of interest is given as

$$H_{\mathrm{nuc}} = \frac{1}{2} \sum_K Z_K \mathbf{B}^{\mathrm{T}} \left[\mathbf{R}_K^{\mathrm{T}} \cdot \mathbf{R}_K \mathbf{1} - \mathbf{R}_K \mathbf{R}_K^{\mathrm{T}} \right] \mathbf{I}_{\mathrm{nuc}}^{-1} \mathbf{J}. \tag{4}$$

The position of the electrons and the nuclei are given by **r** and **R**, respectively; Z_K is the nuclear charge, $\mathbf{I}_{\mathrm{nuc}}^{-1}$ is the inverse diagonal moment-of-inertia tensor, and **L** is the electronic angular momentum. The subscript O refers to an arbitrary gauge origin; all other quantities are given with respect to the molecular CM, about which the molecule rotates.

The use of gauge-including rotational London orbitals [4] ensures rigorous gauge-origin independent results and accelerates the convergence toward the basis-set limit (compared with conventional field-independent orbitals). The rotational London atomic orbitals are defined as

$$\omega_\mu(\mathbf{B}, \mathbf{J}) = \exp\left[-\mathrm{i} \left(\mathbf{A}_\mu^{\mathbf{B}} + \mathbf{A}_\mu^{\mathbf{J}} \right) \cdot \mathbf{r} \right] \chi_\mu, \tag{5}$$

with

$$\mathbf{A}_\mu^{\mathbf{J}} = -\mathbf{I}_{\text{nuc}}^{-1}\mathbf{J} \times \mathbf{R}_\mu, \tag{6}$$

$$\mathbf{A}_\mu^{\mathbf{B}} = \frac{1}{2}\mathbf{B} \times (\mathbf{R}_\mu - \mathbf{R}_O), \tag{7}$$

where $\mathbf{R}_\mu$ is the position of the conventional atomic orbital χ_μ.

From the Hamiltonian equation (3) and the rotational London orbitals equation (5), one can derive the expressions for the rotational g tensor using the machinery of time-independent response-theory described elsewhere [20]. We note the close relationship between the rotational g tensor and the magnetizability tensor. Indeed, the rotational g tensor can be obtained from the magnetizability tensor as [4]

$$\mathbf{g} = -4M_{\text{p}}\big(\boldsymbol{\xi}^{\text{LAO}} - \boldsymbol{\xi}^{\text{dia}}(\text{CM})\big)\mathbf{I}_{\text{nuc}}^{-1} + \mathbf{g}^{\text{nuc}}, \tag{8}$$

where M_{p} is the proton mass, $\boldsymbol{\xi}^{\text{LAO}}$ is the magnetizability calculated with London atomic orbitals and $\boldsymbol{\xi}^{\text{dia}}(\text{CM})$ is the diamagnetic contribution to the magnetizability tensor, calculated using conventional atomic orbitals with a gauge origin at the molecular CM. Finally, $\mathbf{g}^{\text{nuc}}$ is given by

$$\mathbf{g}^{\text{nuc}} = \frac{M_{\text{p}}}{2\mu_{\text{N}}}\sum_K Z_K\big[\big(\mathbf{R}_K^{\text{T}} \cdot \mathbf{R}_K\big)\mathbf{1} - \mathbf{R}_K\mathbf{R}_K^{\text{T}}\big]\mathbf{I}_{\text{nuc}}^{-1} \tag{9}$$

and represents the contribution to $\mathbf{g}$ from the rotating nuclear framework.

2.1. Zero-point vibrational corrections

The zero-point vibrational corrections (ZPVC) to the rotational g tensor are here calculated by expanding the property surface about an *effective* geometry $\mathbf{r}_{\text{eff}}$, chosen to minimize the energy functional [19]

$$\widetilde{E}^{(0)} = V_{\text{exp}}^{(0)} + \big\langle \widetilde{\Psi}^{(0)} \big| H_{\text{vib}}^{(0)} \big| \widetilde{\Psi}^{(0)} \big\rangle, \tag{10}$$

where $H_{\text{vib}}^{(0)}$ is the harmonic-oscillator Hamiltonian and the trial function $\widetilde{\Psi}^{(0)}$ is a simple product of harmonic-oscillator eigenfunctions of different vibrational modes; $V_{\text{exp}}^{(0)}$ is the zeroth-order term in the expansion of the potential with respect to an arbitrary expansion point $\mathbf{r}_{\text{exp}}$. The vibrational average of the rotational g tensor is given as [18]

$$\langle \mathbf{g} \rangle = \frac{\langle \Psi | \mathbf{g} | \Psi \rangle}{\langle \Psi | \Psi \rangle}. \tag{11}$$

Expanding the vibrational wave function about the effective geometry using Rayleigh–Schrödinger perturbation theory, the leading first-order term vanishes and the following simple expression for the leading-order ZPVC to the rotational g tensor is obtained:

$$\langle \mathbf{g} \rangle = \big(\langle \mathbf{g}_0^{(0)} \rangle_{\text{eff}} - \langle \mathbf{g}_0^{(0)} \rangle_{\text{e}}\big) + \langle \mathbf{g}_2^{(0)} \rangle_{\text{eff}}. \tag{12}$$

Here $\langle \mathbf{g}_0^{(0)} \rangle_{\text{eff}}$ is $\mathbf{g}$ calculated at the effective geometry, $\langle \mathbf{g}_0^{(0)} \rangle_{\text{e}}$ is $\mathbf{g}$ calculated at the optimized equilibrium geometry, and $\langle \mathbf{g}_2^{(0)} \rangle_{\text{eff}}$ is the second-order contribution to $\mathbf{g}$ calculated from the zeroth-order vibrational wave function. Hence, a large proportion of the ZPVC is

recovered from the zeroth-order trial function alone, provided the vibrational wave function is expanded about an effective geometry [18].

The calculation of vibrational corrections involves two steps. First, we determine the effective geometry by the calculation of one Hessian and $6K-11$ gradients along the normal coordinates (K is the number of atoms). Next, at this effective geometry, the second-derivative of the rotational g tensor, $\langle \mathbf{g}_2^{(0)} \rangle_{\text{eff}}$ is calculated, requiring one Hessian evaluation and $6K-11$ property evaluations.

3. COMPUTATIONAL DETAILS

A detailed basis-set analysis was carried out at the Hartree–Fock level of theory, using Dunning's correlation-consistent basis sets [21,22] and the atomic natural orbitals (ANO) developed by Widmark *et al.* [23]. Diffuse functions proved to be important for calculating the rotational g tensor, as observed previously [4,12]. For H_2S, we also tested the core–valence correlation-consistent sets [24,25], in which additional tight functions are included in the basis set.

At the MCSCF level, the effect of electron correlation was examined using complete-active-space (CAS) and restricted-active-space (RAS) self-consistent field (SCF) wave functions [26–30]. We use the notation $^{\text{inactive}}\text{CAS}^{\text{active}}$ where inactive denotes the number of orbitals in the inactive space (doubly occupied) and active the number of orbitals in the active space (where any occupation number between 0 and 2 is allowed). RASSCF wave functions are likewise denoted as $^{\text{inactive}}_{\text{RAS1}}\text{RAS}^{\text{RAS2}}_{\text{RAS3}}$ [28,30], where RAS2 corresponds to the active space of the CASSCF wave function, and where only single and double excitations are allowed into RAS3 and out of RAS1. The number of orbitals in each space is given according to the number of orbitals in each irrep of the molecular point group. For H_2O, H_2S, and O_3, the irreps are A_1, B_1, B_2, and A_2, and for HOF A' and A''. The chosen occupations in the different orbital spaces were based on an analysis of the MP2 natural orbital occupation numbers [31].

Our starting point in all cases was an appropriately large RAS2 space with an empty RAS3 space. We then considered the effects of moving orbitals from the RAS2 to the RAS3 space so as to minimize the size of the RAS2 space (and computational expense) without any significant loss of accuracy in comparison with experiment. The effects of dynamical electron correlation were examined by systematically increasing the size of the RAS3 space. Excitations out of the RAS1 space were only considered whenever the MP2 natural occupation numbers indicated this to be necessary, which was only the case for the H_2S molecule.

DFT calculations were carried out using the LDA, BLYP and hybrid B3LYP functionals. The ZPVC calculations were carried out at both the Hartree–Fock and MCSCF levels of theory. In all calculations, the molecules are oriented in the principal axis system of the moment of inertia tensor such that $I_{xx} < I_{yy} < I_{zz}$. The molecular geometries used in this work are collected in Table 1. The Hartree–Fock and MCSCF calculations were carried out with Dalton 1.0; the DFT calculations were carried out with a local development version of Dalton [32].

Table 1. Geometries used in this work

Molecule	Method	Geometry parameter	Value	Reference
H_2O	CCSD(T)	r_{OH}	95.70 pm	[33]
		$\angle$(HOH)	104.20°	
H_2S	Experiment	r_{SH}	133.56 pm	[34]
		$\angle$(HSH)	92.12°	
HOF	Experiment	r_{OF}	143.50 pm	[35]
		r_{OH}	96.57 pm	
		$\angle$(HOF)	97.54°	
O_3	Experiment	r_{OO}	127.17 pm	[36]
		$\angle$(OOO)	116.78°	

4. RESULTS

4.1. H_2O

The rotational Zeeman properties of the water molecule have been extensively studied in the literature—see, for instance, Refs. [7,8,12,14]. In particular, Ruud *et al.* [14] have shown that the set of ${}^{1000}\mathrm{RAS}^{4221}_{\mathrm{RAS3}}$ wave functions provides a balanced description of the electronic structure. They also examined the convergence of ${}^{1000}\mathrm{RAS}^{4221}_{\mathrm{RAS3}}$ wave functions with respect to the RAS3 space by systematically increasing the RAS3 space. Although their largest MCSCF expansion includes 32 RAS3 orbitals, further improvements in the description were desirable. We have here extended their expansion, including up to 48 orbitals in the RAS3 space. A further RAS3 extension is not expected to produce significant changes in the rotational g tensor without simultaneously extending the RAS2 space and moreover including the core electrons in the active space. Thus, our largest MCSCF expansion (${}^{1000}\mathrm{RAS}^{4221}_{17;11;11;9}$) appears to be sufficiently converged with respect to the RAS2 space and the inactive space.

The sensitivity of the rotational g tensor to changes in the molecular geometry was investigated by calculating the tensor at 55 discrete points using a modest-size ${}^{1000}\mathrm{RAS}^{4221}_{2111}$ wave function in the aug-cc-pVTZ basis. The resulting property surface can be obtained from the authors upon request; here, we only comment on some findings from these calculations. The $\mathbf{g}_{xx}$ component is sensitive to changes in the bond distance r_{OH}—for example, when the bond distance increases by 1.0 pm, g_{xx} decreases by 0.010 (*i.e.*, ten experimental (MW) standard-deviations). In contrast, the rotational g tensor of water is quite insensitive to changes in the bond angle.

The sensitivity to changes in the geometry (in particular bond lengths), suggests that highly accurate equilibrium geometries should be used for g-tensor calculations. We therefore used geometries obtained from CCSD(T)/cc-pCVQZ calculations [33] rather than those obtained from MCSCF calculations (as used by Ruud *et al.* [14]), noting that the CCSD(T) geometry is in better agreement with the highly accurate experimental equilibrium geometries [37–39]. The ZPVCs were calculated at the Hartree–Fock and ${}^{1000}\mathrm{RAS}^{4221}_{4220}$ levels of theory, in the aug-cc-pVTZ basis.

Table 2. Rotational g tensors for H_2O, with and without corrections for zero-point vibrations

Method	g_{xx}	g_{yy}	g_{zz}
HF	0.6827	0.7338	0.6641
DFT/LDA	0.6565	0.7169	0.6407
DFT/BLYP	0.6734	0.7356	0.6606
DFT/B3LYP	0.6430	0.7071	0.6289
$^{1000}\mathrm{RAS}^{4220}_{17;11;11;9}$	0.6686	0.7292	0.6528
MP2[a]	0.6822	0.7453	0.6670
MP3[a]	0.6735	0.7330	0.6561
L-CCD[a]	0.6682	0.7288	0.6507
$^{1000}\mathrm{RAS}^{4220}_{17;11;11;9}$ + ZPVC(HF)[b]	0.6477	0.7189	0.6475
$^{1000}\mathrm{RAS}^{4220}_{17;11;11;9}$ + ZPVC(MC)[c]	0.6372	0.7089	0.6409
$^{1000}\mathrm{RAS}^{4220}_{6332}$ + ZPVC[d]	0.640(3)	0.709(3)	0.637(1)
MW[e]	0.657(1)	0.718(7)	0.645(6)
MB[f]	0.6650(20)	0.7145(20)	0.6465(20)

[a] Without London atomic orbitals [6–8]. [b] Hartree–Fock calculated ZPVC. [c] $^{1000}\mathrm{RAS}^{4220}_{4221}$ calculated ZPVC. [d] $^{1000}\mathrm{RAS}^{4220}_{6332}$ calculated ZPVC [14]. [e] Microwave (MW) experiment [40]. [f] Molecular Beam (MB) experiment [41].

Our results are collected in Table 2, together with experimental data and results from previous theoretical investigations. We begin by considering the results obtained in the absence of rovibrational corrections, and subsequently consider the ZVPCs.

Although in qualitatively good agreement with the experimental data, the Hartree–Fock values overshoot our best RASSCF results by roughly ten experimental standard deviations. Relative to the $^{1000}\mathrm{RAS}^{4221}_{17;11;11;9}$ description, none of the DFT methods considered improves on the Hartree–Fock values for *all* three components. However, in comparison with experiment, there is surprising agreement for the LDA functional results, although this agreement disappears once ZPVCs are considered. Of the GGA functionals considered, BLYP is in closest agreement with the $^{1000}\mathrm{RAS}^{4221}_{17;11;11;9}$ results, differing by less than four experimental standard deviations for all components of the g tensor. Moreover, the BLYP result is in very good agreement with those from MP2 and MP3. In comparison, the B3LYP results differ by more than ten experimental standard deviations from the RAS results.

In spite of the relatively good agreement of DFT methods with the $^{1000}\mathrm{RAS}^{4221}_{17;11;11;9}$ results, the differences between both the BLYP and B3LYP results and the $^{1000}\mathrm{RAS}^{4221}_{17;11;11;9}$ results are still too great for a critical evaluation of the experimental data from DFT methods.

We also note that the results obtained using our best RASSCF wave function ($^{1000}\mathrm{RAS}^{4221}_{17;11;11;9}$) are in excellent agreement with those obtained using the L-CCD approach [8] (which therefore appear to be superior to the MP2 and MP3 results reported in the same article).

The ZPVCs were calculated at both the Hartree–Fock and RAS levels of theory. It is clear that the effect of electron correlation on the vibrationally corrected value is significant—for instance, g_{xx} decreases by about five experimental standard deviations (MB experiment) when electron correlation is included (see Table 2). The inclusion of the ZPVCs shows that the good agreement with experimental data obtained with our largest RASSCF wave function is fortuitous, illustrating the importance of including ZPVCs for a critical comparison with experiment. All three components decrease in magnitude upon the inclusion of ZPVCs. Comparing our vibrationally corrected results with those obtained at a fixed geometry, we find that the ZPVCs are as important as electron-correlation corrections.

Finally, when comparing our results with those of MW spectroscopy and MB, we confirm the findings of Ruud *et al*. [14]. That is, the experimentally derived rotational g tensor of water, which is calculated using a commonly-used relation between the rotational g tensors of different isotopomers, is not valid for a vibrating molecule. This discrepancy is most pronounced for the g_{xx} component, which is consistent with the observation that this component is the most sensitive to geometrical distortions.

4.2. H_2S

The experimental data for the rotational g tensor of H_2S have not been investigated since the late 1950s [42]. The relatively large standard deviations for this molecule and the lack of absolute signs call for a theoretical investigation of the rotational g tensor.

A basis-set analysis was carried out using Dunning's correlation-consistent basis sets (aug-cc-pVXZ where $X \in \{D, T, Q\}$) [21,22] and ANO [23] basis sets, revealing a slow aug-cc-pVXZ convergence. The aug-cc-pVXZ basis sets are designed for valence-electron correlation. To recover correlation in the outer-core region, the corresponding core-valence correlation-consistent basis-sets aug-cc-pCVXZ [24,25] must be used. The ANO basis sets do not suffer from this inadequacy, converging smoothly and rapidly toward the basis-set limit. For MCSCF calculations of the rotational g tensor in H_2S, we chose a contracted ANO basis set with 7s6p4d3f and 5s4p3d contracted basis functions for sulphur and hydrogen, respectively. The aug-cc-pCVTZ basis set was used in the DFT calculations.

We examined two sets of MCSCF expansions for H_2S. First, we kept the 1s, 2s, and 2p sulphur orbitals in the inactive space, distributing ten electrons among nine orbitals in RAS2 and up to twenty orbitals in RAS3. However, since the MP2 natural orbital occupation numbers suggested that excitations out of the 2s and 2p shells are important, we constructed a second set of RASSCF wave functions by also including the core electrons in the active space. Since the MP2 natural orbital occupation numbers of H_2S indicated that the 2s orbital on sulphur is more strongly occupied than the 2p orbitals, the 1s and 2s sulphur orbitals were therefore kept frozen, whereas the 2p orbitals were included in RAS1. Unfortunately, the inclusion of six additional electrons in the active space severely restricts the RAS3 expansion, making it impossible to include more than six orbitals in RAS3. A comparison of the two expansions clearly indicates that excitations out of the 2p sulphur orbitals are important. However, in trying to describe dynamic correlation, we are forced to freeze the 2p shell. Thus, neither of these expansions can be considered entirely satisfactory.

In Table 3, we compare the Hartree–Fock, DFT (LDA, BLYP and B3LYP) and RASSCF results for the rotational g tensor of H_2S with the experimental MW spectroscopy data

Table 3. Rotational g tensors of H_2S, with and without corrections for zero-point vibrational corrections

Method	g_{xx}	g_{yy}	g_{zz}
HF	0.3854	0.1289	0.1941
DFT/LDA	0.4254	0.2342	0.2695
DFT/BLYP	0.3691	0.1418	0.2028
DFT/B3LYP	0.3807	0.1516	0.2101
${}^{2000}_{1110}\mathrm{RAS}^{4221}_{3210}$	0.4089	0.1672	0.2458
${}^{3110}\mathrm{RAS}^{4221}_{8552}$	0.3969	0.1841	0.2289
${}^{2000}_{1110}\mathrm{RAS}^{4221}_{3210} + \mathrm{ZPVC}$[a]	0.3914	0.1520	0.2495
${}^{3110}\mathrm{RAS}^{4221}_{8552} + \mathrm{ZPVC}$[a]	0.3794	0.1679	0.2326
MW[b]	|0.355(8)|	|0.195(8)|	|0.209(8)|

[a] Hartree–Fock/ANO calculated ZPVC. [b] Microwave (MW) spectroscopy [42].

reported in Ref. [42]. Whereas the measurements give only the absolute values of the rotational g tensor, the calculations show all components to be positive. The Hartree–Fock values for g_{xx} and g_{zz} are in good agreement with experiment, but g_{yy} is significantly underestimated relative to experiment. The RAS results indicate that this underestimation arises from an incomplete treatment of electron correlation. The RAS expansions overshoot g_{xx} and g_{zz}, taking the results further away from experiment (compared to Hartree–Fock results). However, excitations out of the 2p shell have only a minor influence on the out-of-plane component g_{zz}, suggesting that the experimental result is too low. Including the Hartree–Fock ZPVCs improves the agreement with experiment for g_{xx} but has the opposite effect for the g_{yy} and g_{zz} components.

Of the DFT functionals, the LDA results are too large for all components. The BLYP and B3LYP results show an overall improvement over Hartree–Fock and LDA results compared to experiment and the RAS results, with the BLYP result being closest in agreement with the RAS results.

4.3. HOF

The HOF molecule is known to exhibit strong electron correlation effects [33]. A Hartree–Fock basis-set analysis suggested that the aug-cc-pVTZ basis is appropriate for MCSCF wave functions, which were constructed by freezing the core electrons on oxygen and fluorine. The 16 valence electrons were then distributed among a maximum of 25 active orbitals—10 in RAS2 and up to 15 in RAS3. However, further improvement in the description of the electronic structure is desirable since test calculations indicated that g_{xx} and g_{yy} were not fully converged with respect to the RAS3 expansion, although g_{zz} appears to be sufficiently converged.

In all calculations we used the equilibrium geometry of Halonen *et al.* [35], which is in good agreement with the geometry of Thiel *et al.* [43] and a recently published

Table 4. Rotational g tensors of HOF, with and without corrections for zero-point vibrational corrections

Method	g_{xx}	g_{yy}	g_{zz}
HF	0.7022	−0.0954	−0.0441
DFT/LDA	0.6854	−0.1275	−0.0728
DFT/BLYP	0.6553	−0.1298	−0.0767
DFT/B3LYP	0.6703	−0.1201	−0.0667
$^{20}\mathrm{RAS}^{73}_{10;5}$	0.6848	−0.1038	−0.0556
$^{20}\mathrm{RAS}^{73}_{10;5}$ + ZPVC(HF)[a]	0.6599	−0.1050	−0.0571
$^{20}\mathrm{RAS}^{73}_{10;5}$ + ZPVC(MC)[b]	0.6540	−0.1063	−0.0567
MW[c]	0.642(1)	−0.119(1)	−0.061(1)

[a] Hartree–Fock calculated ZPVC. [b] $^{20}\mathrm{RAS}^{62}_{42}$ calculated ZPVC. [c] Microwave (MW) spectroscopy [45].

CCSD(T)/cc-pCVQZ optimized structure [33,44]. The ZPVC calculations were carried out at the Hartree–Fock and $^{20}\mathrm{RAS}^{62}_{42}$ levels of theory.

The Hartree–Fock and DFT results in Table 4 are in reasonably good agreement with experiment. The uncorrelated Hartree–Fock values are too positive, while the DFT results are generally too negative compared to the $^{20}\mathrm{RAS}^{73}_{10;5}$ correlation correction (without rovibrational corrections). In contrast to results obtained for H_2S, the B3LYP functional performs better than the BLYP functional with respect to reproducing the RAS data. Although electron correlation improves the agreement with experiment somewhat, it is still not entirely satisfactory.

Addition of ZPVCs to the $^{20}\mathrm{RAS}^{73}_{10;5}$ results for HOF improves the agreement with experiment for all three components. The ZPVC to g_{xx}, in particular, is substantial—nearly twice as large as the correlation correction. By contrast, vibrations have only a minor influence on g_{yy} and g_{zz}. We would also like to stress the importance of electron correlation for the ZPVC itself: g_{xx} was found to decrease by approximately six experimental standard deviations when calculated at the MCSCF rather than Hartree–Fock level of theory.

Overall, the vibrationally corrected MCSCF results for the rotational g tensor of HOF are in very good agreement with experiment. The out-of-plane component g_{zz} is only four experimental standard deviations away from the experimental value, which is entirely satisfactory bearing in mind the very small error bars for this molecule. The discrepancies between experiment and our vibrationally corrected RASSCF values for g_{xx} and g_{yy} probably arise from a slow convergence with respect to the size of the active space. Clearly, further improvements in the description of the electronic structure is required for full agreement with experiment.

4.4. O_3

Ozone is a prime example of a molecule with large static and dynamic correlation effects, for which a multiconfigurational treatment is needed for an accurate description of

the electronic structure. Test calculations indicated that, for this molecule, the correlation-consistent basis sets are better suited to g-tensor calculations than are the ANO sets. The MCSCF wave functions were constructed with the 1s orbitals inactive and by distributing the remaining 18 electrons among 12 RAS2 orbitals and 13 RAS3 orbitals. The resulting wave function contains more than four million determinants. Again, the small RAS2 space tends to exaggerate correlation effects, whereas the RAS3 space is not sufficiently large to describe dynamic correlation accurately. The electronic structure for ozone is complicated and larger active spaces would be desirable. Although g_{yy} and in particular g_{xx} are not sufficiently converged, the out-of-plane component g_{zz} appears to be converged with respect to the size of the active space.

The rotational g tensor for ozone is very sensitive to changes in the geometry. Calculations at the experimental equilibrium geometry of Tanaka *et al.* [36] and at the CCSD(T)/cc-pCVQZ optimized geometry [33] were carried out using a $^{2100}\mathrm{CAS}^{5421}$ wave function in the aug-cc-pVTZ basis. Although the differences between the results at the two geometries are small in magnitude, for g_{xx} it amounts to about one hundred experimental standard deviations. The more trustworthy experimental equilibrium geometries should therefore be used for a satisfactory comparison with the experimental data. The effects of vibrations were examined using the modest-size $^{2100}\mathrm{CAS}^{5421}$/aug-cc-pVTZ wave function, which has been be shown to give a qualitatively good description of the electronic structure of ozone [12].

We have collected our results in Table 5, together with other theoretical calculations and available experimental data. The Hartree–Fock results are qualitatively incorrect, differing from experiment by a factor two for g_{xx} and g_{yy}. The DFT methods improve the agreement with experiment, although the g_{xx} is still poorly described. By contrast, even a small MCSCF wave function gives results in good agreement with experimental data [46,47]. Systematic expansion of the RAS3 space indicated that dynamical correlation effects on the g tensor made it successively more negative. The MCSCF results listed in Table 5 are

Table 5. Rotational g tensors of O_3, with and without corrections for zero-point vibrational corrections

Method	g_{xx}	g_{yy}	g_{zz}
HF	−5.7514	−0.3992	−0.0675
DFT/LDA	−3.4004	−0.2455	−0.0806
DFT/BLYP	−3.2679	−0.2444	−0.0823
DFT/B3LYP	−3.6380	−0.2658	−0.0784
$^{2100}\mathrm{RAS}^{5421}_{5332}$	−2.8732	−0.2277	−0.0730
$^{2100}\mathrm{RAS}^{5421}_{5332}$ + ZPVC[a]	−2.9440	−0.2295	−0.0744
MW[b]	−2.960(8)	−0.227(5)	−0.086(5)
MW[c]	−2.968(35)	−0.228(7)	−0.081(6)
MB[d]	−2.9877(9)	−0.2295(3)	−0.0760(3)

[a] $^{2100}\mathrm{CAS}^{5421}$ calculated ZPVC. [b] Microwave (MW) spectroscopy; Burrus [42]. [c] Microwave (MW) spectroscopy; Pochan *et al.* [46]. [d] Molecular beam (MB) experiment; Meerts *et al.* [47].

too positive for all components of the g tensor. Addition of ZPVCs (which are negative for all components of the g tensor) further improves the agreement with experiment.

The vibrationally corrected ${}^{2100}\mathrm{RAS}^{5421}_{5332}$ results are in excellent agreement with the experimental MW and MB data. Both g_{xx} and g_{yy} are within the experimental error bars reported by Pochan *et al.* [46], while g_{zz} is just outside. Compared to the MB results, our estimate of g_{xx} is well outside the extremely small standard deviation reported. The out-of-plane component g_{zz} is comparable to the MB value and close to the experimental value of Meerts *et al.* [47]. The very good agreement between our results and the results of Meerts *et al.* for g_{zz} suggests that the value reported by Burrus *et al.* may be too negative.

5. CONCLUSIONS

We have calculated the rotational g tensor of four small polyatomic molecules, using large MCSCF wave functions. For comparison, Hartree–Fock and DFT calculations have also been carried out. Vibrational corrections were included and the sensitivity to small changes in the geometry was analyzed. Although small, the effects of electron correlation and vibrations must both be taken into account for critical comparison with experiment. Indeed, in systems with little static correlation, the ZPVCs are as large as the correlation corrections and in some cases larger—for the g_{xx} component of the rotational g tensor of HOF, the ZPVC is nearly twice as large as the correlation correction. The effect of correlation on the ZPVCs themselves is also non-negligible.

Of the DFT functionals considered, it was clear that GGA functionals performed better than the LDA functional. However, no general trend was observed. The molecules considered in this work represent extreme examples of differing electronic environments, hence to evaluate the reliability of DFT methods in the calculation of rotational g tensors and magnetizabilities, a more representative sample of organic compounds would need to be considered.

For the water molecule, we confirm the findings of Ruud *et al.* [14] that the experimental results obtained from MW spectroscopy and MB techniques are hampered by errors due to the breakdown of a commonly used relationship between the dipole moment and the rotational g tensor for different isotopomers. We emphasize that large MCSCF wave functions and the inclusion of ZPVCs were both necessary to identify this difficulty in analyzing experimental data.

For H_2S, a careful investigation of the correlation contributions revealed the importance of an accurate description of the outer-core region. Hence, core–valence optimized basis sets should be used, as well as core-correlated wave functions. Unfortunately, these demands prevent a sufficiently large expansion of the RAS3 space to properly describe the effects of dynamic correlation. Nevertheless, the B3LYP results are in good agreement with the MCSCF results. Further experimental and theoretical investigation of the g tensor of H_2S may be warranted.

Our results for HOF are in good agreement with the data reported from MW spectroscopy. Although our vibrationally corrected results overshoot the experimental results by about ten experimental standard deviations for g_{xx} and g_{yy}, the results reported for g_{zz} differ by only four experimental standard deviations, which is satisfactory bearing in mind the very small standard deviations reported for this molecule. Still, larger MCSCF expansions are needed to examine the convergence pattern of the in-plane components.

Moreover, the effect of electron correlation on the ZPVCs themselves was found to be important. The MCSCF calculated ZPVC to g_{xx} decreases by about six experimental standard deviations relative to the Hartree–Fock description.

The complicated electronic structure of ozone is a challenge to *ab initio* theory. Nevertheless, our vibrationally corrected RASSCF results agree remarkably well with the experimental results for this molecule. In particular, all the components of the rotational g tensor are within the experimental error bars from MW experiments reported in Ref. [47], suggesting that the g_{zz} value in Ref. [46] is slightly too low. Again, the ZPVC were found to be important in order to approach the very accurate MB data.

ACKNOWLEDGEMENTS

This work has received support from the Norwegian Research Council through a Strategic University Program in Quantum Chemistry (Grant No. 154011/420). DJDW has been supported by the Norwegian Research Council through a postdoctoral fellowship (Grant No. 155137/432). We also acknowledge a grant of computer time from the Norwegian Supercomputing Program.

REFERENCES

[1] N.F. Ramsey, *Molecular Beams*, Clarendon, Oxford, 2000.
[2] W.H. Flygare, *Chem. Rev.* **74** (1974) 653.
[3] H.M. Kelly, P.W. Fowler, *Chem. Phys. Lett.* **206** (1993) 568.
[4] J. Gauss, K. Ruud, T. Helgaker, *J. Chem. Phys.* **105** (1996) 2804.
[5] K. Ruud, T. Helgaker, *Chem. Phys. Lett.* **264** (1997) 17.
[6] D.M. Bishop, S.M. Cybulski, *J. Chem. Phys.* **98** (1993) 8057.
[7] S.M. Cybulski, D.M. Bishop, *J. Chem. Phys.* **100** (1994) 2019.
[8] S.M. Cybulski, D.M. Bishop, *J. Chem. Phys.* **106** (1996) 4082.
[9] S.P.A. Sauer, V. Špirko, J. Oddershede, *Chem. Phys.* **153** (1991) 189.
[10] S.P.A. Sauer, *Chem. Phys. Lett.* **297** (1998) 475.
[11] J.F. Ogilvie, J. Oddershede, S.P.A. Sauer, *Adv. Chem. Phys.* **111** (1998) 475.
[12] K. Ruud, T. Helgaker, P. Jørgensen, *J. Chem. Phys.* **107** (1997) 10599.
[13] P.-O. Åstrand, K.V. Mikkelsen, K. Ruud, T. Helgaker, *J. Phys. Chem.* **100** (1996) 19771.
[14] K. Ruud, J. Vaara, J. Lounila, T. Helgaker, *Chem. Phys. Lett.* **297** (1998) 467.
[15] K. Ruud, P.-O. Åstrand, T. Helgaker, K.V. Mikkelsen, *J. Mol. Struct. (Theochem)* **388** (1996) 231.
[16] P.-O. Åstrand, K. Ruud, K.V. Mikkelsen, T. Helgaker, *Chem. Phys. Lett.* **271** (1997) 163.
[17] P.J. Wilson, R.D. Amos, N.C. Handy, *J. Mol. Struct. (Theochem)* **506** (2000) 335.
[18] K. Ruud, P.-O. Åstrand, P.R. Taylor, *J. Chem. Phys.* **112** (2000) 2668.
[19] P.-O. Åstrand, K. Ruud, P.R. Taylor, *J. Chem. Phys.* **112** (2000) 2655.
[20] J. Olsen, P. Jørgensen, *J. Chem. Phys.* **82** (1985) 3235.
[21] T.H. Dunning Jr, *J. Chem. Phys.* **90** (1989) 1007.
[22] R.A. Kendall, T.H. Dunning Jr, R.J. Harrison, *J. Chem. Phys.* **96** (1992) 6796.
[23] P.-O. Widmark, P.-Å. Malmqvist, B.O. Roos, *Theor. Chim. Acta* **77** (1990) 291.
[24] D.E. Woon, T.H. Dunning Jr, *J. Chem. Phys.* **98** (1993) 1358.
[25] K.A. Peterson, T.H. Dunning Jr, *J. Chem. Phys.* **117** (2002) 10548.
[26] B.O. Roos, P.R. Taylor, P.E.M. Siegbahn, *Chem. Phys.* **48** (1980) 157.
[27] B.O. Roos, *Adv. Chem. Phys.* **69** (1987) 399.
[28] J. Olsen, B.O. Roos, P. Jørgensen, H.J.Aa. Jensen, *J. Chem. Phys.* **89** (1988) 2185.
[29] H.J.Aa. Jensen, P. Jørgensen, T. Helgaker, J. Olsen, *Chem. Phys. Lett.* **162** (1989) 333.
[30] P.-Å. Malmqvist, A. Rendell, B.O. Roos, *J. Phys. Chem.* **94** (1990) 5477.

[31] H.J.Aa. Jensen, P. Jørgensen, H. Ågren, J. Olsen, *J. Chem. Phys.* **88** (1988) 3834.
[32] T. Helgaker, H.J. Aa. Jensen, P. Jørgensen, J. Olsen, K. Ruud, H. Ågren, T. Andersen, K.L. Bak, V. Bakken, O. Christiansen, P. Dahle, E.K. Dalskov, T. Enevoldsen, B. Fernandez, H. Heiberg, H. Hettema, D. Jonsson, S. Kirpekar, R. Kobayashi, H. Koch, K.V. Mikkelsen, P. Norman, M.J. Packer, T. Saue, P.R. Taylor, O. Vahtras, DALTON release 1.0, an *ab initio* electronic structure program, 1997.
[33] T. Helgaker, P. Jørgensen, J. Olsen, *Molecular Electronic-Structure Theory*, John Wiley & Sons, Ltd, New York, 2000.
[34] T.H. Edwards, N.K. Moncur, L.E. Snyder, *J. Chem. Phys.* **46** (1967) 2139.
[35] L. Halonen, T.-K. Ha, *J. Chem. Phys.* **89** (1988) 4885.
[36] T. Tanaka, Y. Marino, *J. Mol. Spectrosc.* **33** (1970) 538.
[37] W.S. Benedict, N. Gailar, E.K. Plyler, *J. Chem. Phys.* **24** (1956) 1139.
[38] A.R. Hoy, P.R. Bunker, *J. Mol. Spectrosc.* **74** (1979) 1265.
[39] S. Carter, I.M. Mills, J.N. Murrell, *J. Mol. Spectrosc.* **81** (1980) 110.
[40] S.G. Kukolich, *J. Chem. Phys.* **50** (1969) 3751.
[41] J. Verhoeven, A. Dymanus, *J. Chem. Phys.* **52** (1970) 3222.
[42] C.A. Burrus, *J. Chem. Phys.* **30** (1959) 976.
[43] W. Thiel, G. Scuseria, H.F. Schaefer III, W.D. Allen, *J. Chem. Phys.* **89** (1988) 4965.
[44] J. Breidung, W. Thiel, J. Gauss, J.F. Stanton, *J. Chem. Phys.* **110** (1999) 3687.
[45] S.L. Rock, E.F. Pearson, E.H. Appleman, C.L. Norris, W.H. Flygare, *J. Chem. Phys.* **59** (1973) 3940.
[46] J.M. Pochan, R.G. Stone, W.H. Flygare, *J. Chem. Phys.* **51** (1969) 4278.
[47] W.L. Meerts, S. Stolte, A. Dymanus, *Chem. Phys.* **19** (1977) 467.

Linear Response Properties Required to Simulate Vibrational Spectra of Biomolecules in Various Media: (R)-Phenyloxirane (A Comparative Theoretical and Spectroscopic Vibrational Study)

K.J. Jalkanen[1], V. Würtz Jürgensen[1] and I.M. Degtyarenko[2]

[1]*Quantum Protein (QuP) Center, Department of Physics, Technical University of Denmark, Building 309, DK-2800 Lyngby, Denmark*
E-mails: jalkanen@fysik.dtu.dk, wuertz@fysik.dtu.dk
[2]*Laboratory of Physics, Helsinki University of Technology, P.O. Box 1100, FIN-02015 Espoo, Finland*
E-mail: imd@fyslab.hut.fi

Abstract

We here present a combined VA, VCD, Raman and ROA vibrational study of phenyloxirane. We have simulated the vibrational absorption (VA), also called IR, vibrational circular dichroism (VCD), Raman scattering and Raman optical activity (ROA) intensities utilizing the density functional theory (DFT) B3LYP hybrid exchange correlation functional and other exchange-correlation functionals (PBE, PW91, PBE1) with the 6-31G(d,p), 6-31++G(d,p), cc-pVDZ, aug-cc-pVDZ, cc-pVTZ and augmented correlation consistent polarized valence triple zeta (aug-cc-pVTZ) basis sets. Previously authors have focused on either the VA and VCD spectra or the Raman and ROA spectra of molecules, since the experimental and theoretical instruments and methods for calculating these quantities are quite distinct. Here we show that the combined analysis gives more information, especially with respect to the electric dipole, magnetic dipole, electric dipole – electric dipole polarizability, electric dipole – electric quadrupole polarizability and electric dipole – magnetic dipole polarizability changes during the various induced transitions. The coupling of vibrational and electronic excitations may be used to aid in understanding the photo induced chemical reactivity observed in many systems. This work is a continuation of our goal to interpret the results of experimental studies on the basis of theoretical results, which can help to understand the structure and function of proteins, other biomolecules and ligands in their native environments. As the physical tools used to observe and study biological processes have evolved, so have the theoretical methods and models to interpret, understand and completely utilize the results of these new measurements. The work on developing methods for modeling amino acids, peptides, proteins and ligands in both the non aqueous (lipid) and aqueous environments has involved, of course, many groups. A review of our contributions to this field has recently been presented. In addition to interpreting existing and new experimental results, we will discuss structural, energetic, conformational, and vibrational studies on a variety of systems that have been used to test and validate levels of theory, and in addition to suggest modifications to existing levels of theory, which can make them even more useful than they currently are.

Contents

ADVANCES IN QUANTUM CHEMISTRY, VOLUME 50
ISSN: 0065-3276 DOI: 10.1016/S0065-3276(05)50006-6

1. INTRODUCTION

Ashvar and coworkers have recently presented the vibrational absorption (VA) and vibrational circular dichroism (VCD) spectra for a variety of rigid ring systems and compared their density functional theory (DFT) calculations with their experimental measurements [10,12,11,9]. The currently implemented methods to calculate the atomic polar and atomic axial tensors seem to be able to reproduce the VA and VCD intensities quite well. Previously both Stephens and coworkers and Suhai and coworkers have shown that an accurate geometry and Hessian are the most critical parameters. Without a good experimental or theoretical geometry and an accurate representation of the normal modes as derived from the Hessian, one is not able to accurately predict either the absolute VA and VCD intensities or even the relative intensities [72,76,83,132,27,52,51,73]. Hence the question of finding and developing methods that can accurately predict and find the experimental structure are very important also in the field of modeling and studying small to medium sized pharmaceutical molecules, as they are in protein and ligand modeling. In the protein modeling field people have used the known NMR and X-ray structures in the Worldwide Protein Data Bank (wwPDB) to try to predict and(or) find the structures of closely related sequences of proteins [26]. Here the two main methods are the so called homology method and the neural network method [99]. Extensive reviews of both methods have occurred and hence there is no need to elaborate or go into detail.

The use of other experimental data has also been used to try to shine some light on the structure determination problem. For example, electronic circular dichroism (ECD), VA, and Raman spectroscopy have been used to try to determine the amount of secondary structural elements in a given new protein, where the X-ray or NMR structures are not yet available [104,136,138,98]. In addition to these three methods, two relatively new methods have recently been able to make contributions, VCD and ROA [85,84,22]. Even through these two methods were both experimentally developed and the first spectra measured in the 1970s [69,68,18,20], only recently has the interpretation of the VA and VCD intensities in strongly perturbing environments been shown to be feasible [60,137,52,74,75]. Previously the theory of VCD has been put on a firm basis [35,130,131,28] similar to that for VA [114,161]. In addition, to the rigorous theoretical basis for the VA and VCD intensities, the implementation at the restricted Hartree–Fock (RHF), multi configuration self consistent field (MCSCF) and DFT levels utilizing finite difference techniques, coupled Hartree–Fock and the random phase approximation have been reported [2,134,4,5,79,62, 15,16,14,30,29]. The theory of Raman scattering has been also put on a rigorous theoretical basis [57,97]. The EDEDP and their derivatives with respect to nuclear displacements that are necessary to simulate the Raman scattering spectra have been implemented at the RHF and DFT levels [89,3,81].

In addition, a rigorous theory of Raman optical activity has been derived by Barron and Buckingham [19] and been implemented by finite difference techniques utilizing Amos's implementation of the electric dipole – magnetic dipole polarizabilities (EDMDP) and

electric dipole – electric quadrupole polarizabilities (EDEQP) in the Cambridge Analytical Derivatives Package (CADPAC) [1] by Polavarapu and Jalkanen [116,21,159,38,60,74], subsequently implemented in the Dalton program by Helgaker, Bak, Ruud, Jørgensen and Olsen [67,119] and in latest release of Gaussian [54]. Here we look at the combination of VA, VCD, Raman scattering and ROA spectroscopies to explore the properties of phenyloxirane.

2. METHODS AND MATERIALS

In this work we have optimized the geometry of phenyloxirane at the B3LYP/6-31++G(d,p) level of theory with Gaussian 03 [54]. At this same level of theory we have additionally calculated the Hessian, the atomic polar tensors (APT), the atomic axial tensors (AAT), and the electric dipole – electric dipole polarizability derivatives (EDEDPD), which allows us to simulate the VA, VCD and Raman spectra. In addition we have calculated the EDMDP and EDEQP at the optimized geometry and at the displaced geometries that has allowed us to calculate the EDMDP and EDEQP derivatives, EDMDPD and EDEQPD, respectively. We have used the two point finite difference to calculate the derivatives with respect to the nuclear Cartesian coordinates. By having these quantities and the EDEDPD, we can additionally simulate the ROA spectra. The EDMDP and EDEQP were all calculated at the RHF/6-31G(d,p) level with the Cambridge Analytical Derivatives Package (CADPAC), version 5.2 provided to us by Nick Handy and Roger Amos [6,1]. In addition, we have calculated the EDEDPD, EDMDPD and the EDEQPD at the B3LYP level of theory with the 6-31G(d,p) and aug-cc-pVDZ basis sets, which allows us to also simulate the ROA spectra at this level of theory. We have utilized the finite difference methods and the gauge invariant atomic orbitals (GIAO) method to calculate the EDMDP at the displaced geometries as implemented in Gaussian 03 RevC.02 [54]. This is similar to the implementation for the calculation of the ROA spectra available in the Dalton program [67,119].

In addition, we have calculated the VA, VCD, and Raman spectra at the PBE, PW91 and PBE1 levels of theory with the correlation consistent polarized valence triple zeta (aug-cc-pVTZ) basis set. Furthermore we have investigated the basis set dependence of the VA, VCD and Raman spectra at the B3LYP level of theory; the basis sets being compared are the 6-31G(d,p), 6-31++G(d,p), cc-pVDZ, aug-cc-pVDZ, cc-pVTZ and aug-cc-pVTZ [86,43,53,33,66]. Note that the cc-pVTZ and aug-cc-pVTZ are relatively large basis sets and are used to benchmark the lower basis set level calculations, as these large basis sets are not feasible for doing complete potential energy surfaces scans including the VA, VCD, Raman and ROA spectra at all points. Hence it is important to compare the quality for both the 6-31G(d,p) [split valence plus polarization functions] and 6-31++G(d,p) [split valence plus diffuse functions plus polarization functions] basis sets, the level of agreement with both the larger basis sets and the experimental spectra being the measures. The cc-pVXZ, X = D and T, are the correlation consistent polarized valence double (D)and triple (T) zeta basis sets developed in the group of Dunning [43]. In addition, they have extended these basis sets to treat anions, electron affinities and weakly bonded systems (H-bonding and dispersion energies) by adding additional diffuse functions to generate the aug-cc-pVXZ, X = D and T [86]. For the helium dimer, it has been shown that aug-cc-pVTZ basis sets or larger are necessary to get qualitative results that can be used to extrapolate to the CBS limit for the binding energy (well depth), equilibrium bond length and the harmonic frequency.

The helium dimer is a very rigorous test for both the *ab initio* or DFT levels of theory. It has been shown that Møller Plesset perturbation theory to fourth order (MP4) or coupled cluster that includes all single and double excitations and a posteriori perturbative correction for connected triple excitations [CCSD(T)] level *ab initio* levels of theory are necessary. The MP2, MP3 and CCSD levels of theory are inadequate in order to get quantitative results for these properties [142]. Hence the need to find and document DFT exchange correlation functionals that are of equivalent accuracy to the MP4 and CCSD(T) or better are required, since MP4 and CCSD(T) *ab initio* levels of theory are computationally very demanding. The results, however, at these levels of theory can be used to benchmark many properties. In addition, they have been used to benchmark linear response properties as well, *e.g.*, the calculation of polarizabilities and hyperpolarizabilities, and reaction barrier heights where it was shown that aug-cc-pVXZ basis sets must be used to get quantitative accuracy [115,151].

Therefore, in addition, we have also determined the optimized structure of phenyloxirane with the B1B95 exchange correlation functional and the TPSS meta-GGA exchange correlation functional as implemented in Gaussian 03 with the aug-cc-pVTZ basis set [129, 24]. This basis set or a higher level correlation consistent basis set should be used to check the accuracy of the new DFT GGA, meta GGA, hybrid and meta hybrid functionals [160, 36,148,115].

Finally utilizing the SIESTA (Spanish Initiative for Electronic Simulations with Thousands of Atoms) program we have at the PBE level of theory with the DZP basis set optimized the structure of phenyloxirane. Details of SIESTA relaxation (geometry optimizations) are as follows. In order to determine the equilibrium structure, we relax all the atomic coordinates (that is, reduce the size of the forces (gradients) on each atom) with a conjugate gradient algorithm, reaching a tolerance in the forces of 0.04 eV Å^{-1}. We use the fully self-consistent density functional method implemented in the SIESTA program [105, 127]. The electronic energy is obtained within general gradient approximation (GGA) as parametrized by Perdew, Burke and Ernzerhof [109,110]. Core electrons were replaced by nonlocal Troullier–Martins [139] norm-conserving pseudopotentials, whereas valence electrons are described in terms of linear combination of numerical pseudoatomic orbitals of the Sankey type [123,124]. In these calculations we used the double-ζ plus polarization basis set, it provides a sufficiently accurate description of the system that we intend to study. Real space integrations were performed on a regular grid with an equivalent cutoff of 150 Ry.

We assume here that the basis set dependence for the various exchange correlation GGA functionals and hybrid methods, mega hybrid methods, double hybrid methods and double meta hybrid methods will be approximately the same [160], but these remain to be thoroughly investigated. Clearly the state of the art of DFT simulations for molecular properties, which include the effects due to the solvent and protein environment where hydrogen bonding and dispersion forces are important, is in a state of high activity and fluctuation. We do not here investigate all of the recent developments with respect to both the development of exchange-correlation functionals and the developments of methods to treat response properties, but rather take the pragmatic approach of showing that current methods do now exist in three programs, which allow one to calculate the VA, VCD, Raman and ROA spectra to a high degree of accuracy, being CADPAC, Gaussian 03 or Dalton.

As new DFT GGA and hybrid exchange correlation functionals are developed, of course the best ones need to be implemented and tested for all of the pieces needed to simulate these spectra, that is, the geometries, relative energies, gradients, Hessians, the electric dipole moments, the magnetic dipole moments, the EDEDP, the EDMDP and the EDEQP and their derivatives with respect to nuclear displacement. In addition, how all of these quantities change with changes in the environment needs to be taken into account, both implicitly and explicitly and probably both. Finally the effects due to temperature and the frequency of the radiation also need to be taken into account, possibly with time dependent DFT and its various implementations, be it Car Parinello molecular dynamics (CPMD) or Born Oppenheimer quantum molecular dynamics (BOQMD). In this work, however, we do not take these parameters into account. Since the Raman and ROA spectra are not resonance enhanced, that is, the radiation used for the Raman and ROA measurements was not close to an electronic transition, this approximation is OK. But clearly, if one wishes to simulate the resonance Raman and resonance ROA spectra, the frequency of the incoming radiation must be treated theoretically via time dependent DFT. Here the exchange correlation functionals must satisfy the additional constraint that they also treat excited states correctly. This is an even more serious problem for many of the currently used exchange correlation functionals and their modifications and their combinations with exact exchange. A detailed discussion of this problem is also beyond the scope of this work.

3. RESULTS

3.1. Structure

In Table 1 we present the geometrical parameters for the B3LYP optimized structures of phenyloxirane with the 6-31G(d,p), 6-31++G(d,p), cc-pVDZ, aug-cc-pVDZ, cc-pVTZ and aug-cc-pVTZ basis sets [95,23]. In addition, we present the geometrical parameters presented by Ashvar and coworkers [10]. The atom numbering in Table 1 is shown in Fig. 1. In addition, we present the optimized structure of phenyloxirane calculated at the PBE level of theory with the Dunning double zeta polarized basis set. Finally, we also present the optimized structures of phenyloxirane at the PBE, PBE1, PW91, B1B95 and TPSS levels of theory with the aug-cc-pVTZ basis set [109,110,112,108,24,129]. Here we investigate the effect of changing the exchange correlation functional on the geometrical properties.

As one can see by comparing our calculated geometrical parameters at the B3LYP level of theory with the various basis sets with those presented recently by Ashvar and coworkers [10], the structures are very similar. The effect of the diffuse functions seems to be to make the bond lengths in the benzene ring a bit longer (6-31++G(d,p)). In addition, we have investigated the effects of changing the DFT exchange correlation functional at the aug-cc-pVTZ basis set level, the largest differences being between the results for PBE1 and B1B95 exchange correlation functional and with those for the B3LYP hybrid exchange correlation functional. For example, the C1–O3 (C2–O3) bonds in the oxirane ring are shorter by 0.012 (0.13) and 0.013 (0.09) Å, while the C1–C2 bond is only shorter by 0.006 and 0.006 Å, for the PBE and B1B95 methods with respect to the B3LYP method with the aug-cc-pVTZ basis set, respectively. The C2–C10 bond from the oxirane ring to the benzene ring is

Table 1. Structural parameters for (R)-phenyloxirane for various basis sets for B3LYP level of theory and additionally for the PBE, PBE1, PW91, B1B95 and TPSS levels of theory with the aug-cc-pVTZ basis set

	B3LYP [10] TZ2P [10]	PBE DZP	B3LYP G(d,p)	B3LYP ppG(d,p)	B3LYP ccpVDZ	B3LYP AccpVDZ	B3LYP ccpVTZ	B3LYP AccpVTZ	PBE AccpVTZ	PBE1 AccpVTZ	PW91 AccpVTZ	B1B95 AccpVTZ	TPSS AccpVTZ
$r_{1,3}$	1.430	1.453	1.430	1.429	1.431	1.436	1.427	1.427	1.434	1.415	1.434	1.414	1.437
$r_{2,3}$	1.433	1.460	1.435	1.433	1.433	1.441	1.431	1.433	1.444	1.420	1.444	1.422	1.448
$r_{1,2}$	1.474	1.498	1.478	1.476	1.480	1.479	1.472	1.472	1.479	1.466	1.478	1.466	1.477
$r_{2,10}$	1.488	1.506	1.492	1.490	1.494	1.493	1.488	1.486	1.488	1.482	1.486	1.480	1.489
$r_{9,10}$	1.395	1.422	1.400	1.398	1.402	1.402	1.395	1.395	1.401	1.391	1.400	1.388	1.400
$r_{8,9}$	1.390	1.416	1.395	1.393	1.397	1.398	1.389	1.390	1.396	1.387	1.395	1.385	1.395
$r_{7,8}$	1.390	1.417	1.396	1.394	1.398	1.398	1.390	1.390	1.396	1.387	1.395	1.385	1.395
$r_{7,12}$	1.391	1.418	1.397	1.394	1.399	1.400	1.391	1.391	1.398	1.388	1.397	1.387	1.397
$r_{11,12}$	1.389	1.416	1.394	1.392	1.397	1.397	1.389	1.389	1.395	1.386	1.393	1.383	1.393
$r_{10,11}$	1.395	1.421	1.400	1.398	1.402	1.403	1.395	1.395	1.402	1.391	1.401	1.389	1.401
$\theta_{1,3,2}$	62.0	61.9	62.1	62.1	62.2	61.9	62.0	61.9	61.8	62.3	61.8	61.8	61.6
$\theta_{3,1,2}$	59.1	59.3	59.1	58.8	59.0	59.2	59.1	59.2	59.4	59.0	59.4	59.6	59.6
$\theta_{3,2,1}$	58.9	58.8	58.8	59.1	58.8	58.9	58.9	58.8	58.8	58.7	58.8	58.6	58.9
$\theta_{3,2,10}$	117.8	117.8	117.6	117.6	117.5	117.7	117.9	117.9	117.8	117.7	117.6	117.2	117.4
$\theta_{1,2,10}$	122.5	121.9	122.2	122.2	122.0	122.6	122.5	122.7	122.4	122.1	122.4	121.6	122.5
$\theta_{2,10,9}$	119.5	119.5	119.8	119.7	120.0	119.5	119.6	119.5	119.6	119.7	119.6	120.2	119.7
$\theta_{2,10,11}$	121.3	121.2	120.9	121.1	120.8	121.4	121.3	121.4	121.3	121.1	121.3	120.5	121.2
$\theta_{8,9,10}$	120.6	120.5	120.5	120.5	120.5	120.6	120.6	120.6	120.6	120.5	120.6	120.4	120.5
$\theta_{7,8,9}$	120.1	120.1	120.1	120.1	120.1	120.1	120.1	120.1	120.1	120.1	120.1	120.1	120.1
$\theta_{8,7,12}$	119.6	119.7	119.7	119.7	119.7	119.6	119.6	119.6	119.7	119.7	119.7	119.7	119.7
$\theta_{7,12,11}$	120.3	120.3	120.3	120.3	120.3	120.4	120.3	120.3	120.3	120.3	120.3	120.2	120.3
$\theta_{10,11,12}$	120.3	120.2	120.3	120.3	120.3	120.3	120.3	120.3	120.3	120.3	120.3	120.3	120.3
$\theta_{9,10,11}$	119.1	119.3	119.2	119.2	119.2	119.1	119.1	119.1	119.1	119.2	119.1	119.3	119.1
$\tau_{3,1,2,10}$	105.2	−105.3	−104.9	−105.1	−104.9	−104.9	−105.3	−105.1	−105.1	−105.1	−105.1	−104.5	−104.7
$\tau_{3,2,10,9}$	163.9	164.3	165.2	168.0	169.0	160.9	161.7	161.7	159.1	162.5	159.0	157.2	158.0
$\tau_{3,2,10,11}$	16.4	−16.3	−15.4	−12.6	−11.2	−19.4	−18.7	−18.7	−21.3	−18.0	−21.4	−23.4	−22.4
$\tau_{1,2,10,9}$	126.9	−126.9	−126.1	−123.1	−122.4	−130.1	−129.1	−129.1	−132.0	−128.9	−132.1	−134.6	−133.1

(*continued on next page*)

Table 1. (*Continued*)

	B3LYP [10] TZ2P [10]	PBE DZP	B3LYP G(d,p)	B3LYP ppG(d,p)	B3LYP ccpVDZ	B3LYP AccpVDZ	B3LYP ccpVTZ	B3LYP AccpVTZ	PBE AccpVTZ	PBE1 AccpVTZ	PW91 AccpVTZ	B1B95 AccpVTZ	TPSS AccpVTZ
$\tau_{1,2,10,11}$	52.7	52.5	59.3	56.3	57.5	49.7	50.5	50.5	47.7	50.7	47.6	44.8	46.5
$\tau_{8,9,10,2}$	178.7	178.8	178.6	178.5	178.9	178.8	178.8	178.8	178.7	178.7	178.7	178.6	178.7
$\tau_{2,10,11,12}$	178.9	−179.1	−178.7	−178.8	−179.0	−179.1	−179.1	−179.0	−179.0	−178.9	−179.0	−178.8	−179.0
$\tau_{7,8,9,10}$	0.6	0.5	0.5	0.5	0.5	0.6	0.5	0.5	0.5	0.5	0.5	0.4	0.5
$\tau_{12,7,8,9}$	0.2	−0.1	0.2	0.1	0.2	0.1	0.1	0.1	0.2	0.2	0.2	0.1	0.2
$\tau_{8,7,12,11}$	0.4	−0.2	−0.4	−0.4	−0.4	−0.4	−0.4	−0.4	−0.4	−0.4	−0.4	−0.3	−0.4
$\tau_{10,11,12,7}$	0.0	0.1	−0.1	0.0	−0.1	0.0	0.0	0.0	0.0	0.0	0.0	−0.0	−0.0
$\tau_{9,10,11,12}$	0.7	0.3	0.7	0.6	0.8	0.7	0.7	0.6	0.7	0.7	0.7	0.6	0.7
$\tau_{8,9,10,11}$	0.9	−0.6	−0.9	−0.9	−1.1	−1.0	−0.9	−0.9	−0.9	−0.9	−0.9	−0.8	−0.9
$\tau_{6,2,10,9}$	25.6	25.0	26.4	29.4	29.9	22.9	23.5	23.5	20.6	23.6	20.6	18.4	20.2

The B3LYP/TZ2P results are taken from Ref. [10]. The PBE/DZP results are from the SIESTA program. All other results are from the Gaussian 03.

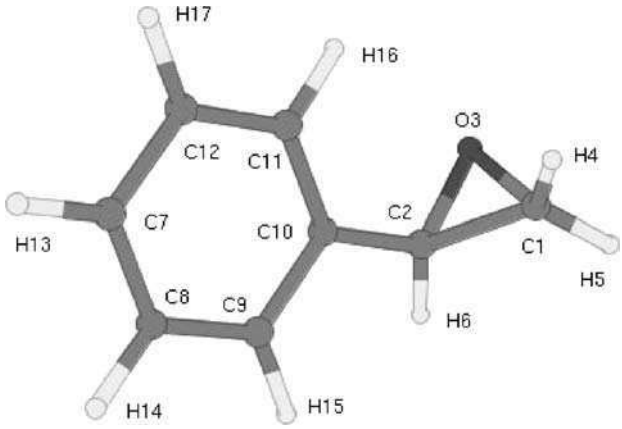

Fig. 1. (R)-Phenyloxirane structure, atom numbering for Table 1.

shorter by 0.004 and 0.006 Å for the PBE and B1B95 levels of theory with respect to the B3LYP level of theory. In the benzene ring, the C–C bond lengths are approximately all 0.003–0.004 Å shorter for PBE1, but a bit shorter for B1B96, being 0.003–0.006 Å, with respect to the B3LYP level of theory.

In contrast, the C1–O3 (C2–O3) bond lengths in the oxirane ring are calculated to be longer with the PBE, PW91, and TPSS levels (of theory), now being 0.007 (0.011), 0.007 (0.011) and 0.010 (0.015) Å for the PBE, the PW91, and the TPSS levels with respect to the B3LYP level, respectively. The C1–C2 bond length in the oxirane ring is also longer, 0.007, 0.006 and 0.005 Å with respect to the PBE, the PW91, and the TPSS levels, respectively. The C2–C10 bond from the oxirane ring to the benzene ring is 0.002, 0.000 and 0.003 Å longer for the PBE, the PW91, and the TPSS levels with respect to the B3LYP level, respectively. In the benzene ring, the CC bond lengths are longer by 0.006–0.007 Å for PBE, 0.005–0.006 Å for PW91 and 0.005–0.006 Å for TPSS. Note that the PBE, PW91 and TPSS levels give very similar results, as do the PBE1 and B1B95 levels, with the B3LYP level giving results in between these two extremes. With respect to the benzene ring CC bond lengths, the PBE, PW91 and TPSS levels give very similar bond lengths, with the PBE1 and B1B95 giving shorter values, and B3LYP giving intermediate lengths. The valence angles are all very similar at all the levels. The largest differences are seen in the SIESTA PBE results. Here the bond lengths in the oxirane ring are more than 0.1 Å longer than those calculated with the PBE level with the larger basis set, aug-cc-pVTZ. Note that in the SIESTA calculations, we use pseudopotentials, whereas in the Gaussian calculations we do not.

With respect to the basis set effect at the B3LYP level, the largest effect is seen with augmenting (addition of diffuse functions) the cc-pVDZ basis, with the two C–O ring bond lengths increasing by 0.005 and 0.007 Å, respectively. By contrast, the ring CC bond decreases by only 0.001 Å. We have optimized the geometry of the (R)-phenyloxirane, while Ashvar and coworkers have the (S)-enantiomer, as seen by, *e.g.*, $\tau_{3,1,2,10}$, being −105.1 for us (B3LYP/6-31++G(d,p)), and 105.2 by them. This will of course give us the opposite sign for all of the VCD and ROA intensities. Similarly the other dihedral angles, $\tau_{3,2,10,11}$ and $\tau_{3,2,10,9}$ are of opposite sign, again reflecting the opposite enantiomer. $\tau_{3,2,10,11}$ has

values ranging from −11.2 for the cc-pVDZ basis set to −19.4 with the aug-cc-pVDZ basis, reflecting the large effect of adding the diffuse functions to the cc-pVDZ basis set at the B3LYP level. Note the value of this angle has not changed with the addition of the diffuse functions to the cc-pVTZ basis set, the value being −18.7 in both cases. At the other DFT levels of theory (exchange correlation functionals) the value of this torsion angle varies from −18.0 at the PBE1 level to −23.4 with the B1B95 level, while the PBE, PW91 and TPSS levels give −21.3, −21.4 and −22.4, respectively, again all with the aug-cc-pVTZ basis set.

In the next four subsection, we discuss our simulated VA, VCD, Raman scattering, and ROA spectra and compare them to recent calculations and measurements of the VA and VCD spectra of Ashvar and coworkers [10] and Raman and ROA measurements by Hecht and Barron [64,63]. In addition, we shall try to see how the changes in geometry that we see with the different DFT exchange correlation functional are reflected in these spectra, and ultimately which structural parameters are reflected in the various vibrational spectra.

3.2. Vibrational absorption

In Fig. 2 we present our simulated B3LYP VA spectra for phenyloxirane with various basis sets. Our simulated spectra are very similar to the simulated VA spectra of Ashvar and coworkers, which were also calculated at the B3LYP level of theory but with a different basis set, the so called TZ/2P basis set developed by Amos and Handy and a part

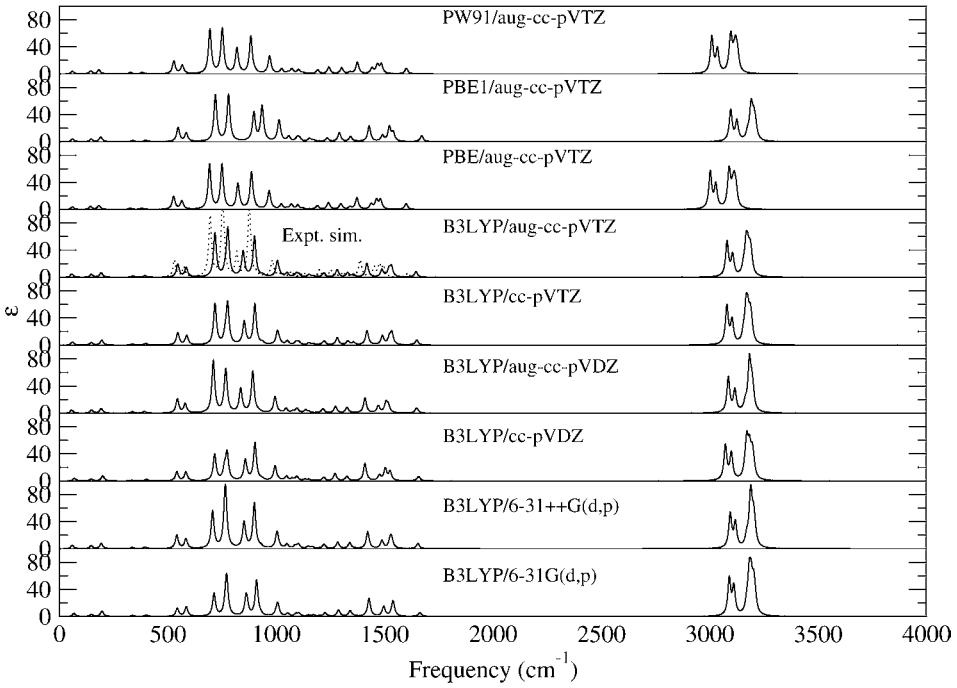

Fig. 2. Phenyloxirane VA spectra for various DFT methods.

of the CADPAC basis set library [133,6]. In addition, we present the simulated VA spectra calculated at the PBE, PBE1 and PW91 levels (of theory) with the largest basis set, aug-cc-pVTZ. We also use the reported experimental frequencies and dipole strengths to simulate the experimental spectra of Ashvar. Here we use a line width of 8 cm^{-1} for our Expt. sim. also reported in Fig. 2. All of the spectra calculated at the B3LYP level are very similar, as we have performed calculations only with polarized spit valence quality of basis set (6-31G(d,p), that is, the so called polarization d functions on carbon and oxygen and polarization p functions on hydrogen) or better. Of course, increasing the quality of the basis set has led to an improvement in the quality of the calculation and representation of the experimental spectra, but the main features of the spectra are well represented already with the 6-31G(d,p) basis set at the B3LYP level. This is consistent with previous works performed in Stephens' group where they showed that the main effect is adding the polarization functions to the split valence basis sets, the effects of further increases are much smaller. Previously Pulay and workers have recommended the use of only split valence basis sets for geometry optimizations and frequency calculations, but the split valence basis sets are not of sufficient accuracy for the VA intensities, that is, for the calculation of the APT [114].

Hence the geometry and Hessian calculated with the 6-31G(d,p) basis set and an appropriate *ab initio* or DFT level of theory are accurate and can be used to also predict the VCD, Raman and ROA intensities, given that the required tensors are calculated (which normally require a larger basis set, that is, the APT, AAT, EDEDPD, EDMDPD and EDEQPD). The VA intensities are more sensitive to the changes in the coupling in the off diagonal elements of the vibrational coordinate force constants than the vibrational frequencies [76]. This is due to mixing of the internal coordinates. The VA intensities have been shown to be very sensitive to the accuracy of the force field, especially the off diagonal force constants [132,76,72]. The VA intensities require the calculation of the APT in addition to the Hessian [114]. This is a real test of the accuracy of the force field, much better than just the root mean square (RMS) deviation of the calculated harmonic and experimental frequencies. Note also that the experimental frequencies are anharmonic and the calculated frequencies are harmonic.

The bands that were most affected by changing the basis set from 6-31++G(d,p) to aug-cc-pVTZ were those calculated at 1361 and 1357 cm^{-1} where the intensity changes from 0.7 to 6.7 (experimental 1329 cm^{-1} with intensity being 3.6), the pair at 1006/1002 cm^{-1} and 1018/1006 cm^{-1} where the intensities are 47.4/10.9 and 1.9/54.2 (only one band being found in the experiment at 983 cm^{-1} with intensity 56.5), 763 and 765 cm^{-1} but with intensities 54.8 and 18.7 (experimental 752 cm^{-1} with intensity 96.3). Hence in some cases the smaller basis set gave better agreement than the larger basis set. With respect to the change in the exchange correlation functional at the highest basis set level, the PBE and PW91 frequencies and intensities are very similar, while the B3LYP and PBE1 are very similar. The relative order of the CH stretch modes are different comparing the two sets, reflecting small changes in the force constants, both diagonal and off-diagonal elements. In the mid IR the PBE and PW91 mode calculated at 1600 and 1602 cm^{-1}, respectively, are closer to the experimental value at 1608 cm^{-1}, than the B3LYP and PBE1 values of 1646 and 1672 cm^{-1}, respectively. But since the experimental values are anharmonic and all of our calculated values are harmonic, this better agreement for this one mode may not reflect an overall better accuracy. The vibrational frequencies can be correlated with

the geometries, and the similarities in the spectra with respect to the different functionals appear to also reflect the aforementioned differences in the geometries.

In Table 2 we present the calculated vibrational frequencies and dipole strengths (used to simulate the VA intensities) at the B3LYP level using the 6-31++G(d,p) and aug-cc-pVTZ basis sets. In addition we present the simulated VA spectra calculated also at the B3LYP level, but with the 6-31G(d,p), cc-pVDZ, aug-cc-pVDZ and cc-pVTZ basis sets in Fig. 2. These simulations show that the simulations of the VA spectra with these basis sets (that is, cc-pVDZ, aug-cc-pVDZ and cc-pVTZ) are not greatly different than the two presented in Table 2 (that is, 6-31++G(d,p) and aug-cc-pVTZ). The fine features of the spectra change, the major features are very similar. In addition, we also present the calculated vibrational frequencies and dipole strengths at the PBE, PBE1 and PW91 levels at the highest basis set level we used in this study, that is, the aug-cc-pVTZ, in Table 2. The spectral simulations for these other DFT levels of theory are also given in Fig. 2. Here we can see that the changes in the spectra with respect to changing the exchange correlation functional (levels of theory) are larger than the changes with respect to basis set for the B3LYP level of theory.

3.3. Vibrational circular dichroism

In Fig. 3 we present our simulated VCD spectra for (R)-phenyloxirane with various basis sets at the B3LYP DFT level along with the corresponding experimentally simulated spectra for (S)-phenyloxirane (Expt. sim.). Here we use the frequencies and rotational strengths extracted from the experimental spectra by Ashvar and coworkers for our experimental simulated spectra and spectra line width of 8 cm^{-1}. Note that the experimental spectra is not complete, as the experimental setup does not allow a complete VCD spectra to be measured. There is good agreement between our simulated VA and VCD spectra and that of Ashvar and coworkers [10] as shown in Figs. 3 and 8 (discussed later). The agreement between the calculated and measured VCD intensities is a further confirmation of a good geometry and Hessian as can be seen comparing our simulated spectra in Figs. 3 and 8 with the experimental spectra presented in Figs. 4, 5, 7 and 8 of Ref. [10] and our experimental simulated spectra presented also in Figs. 3 and 8. In addition, we present our predicted VCD spectra calculated with the aug-cc-vPTZ basis set at the PBE, PBE1 and PW91 levels of theory. The main features of the VCD spectra are all well produced with the high quality aug-cc-pVTZ basis set and these four DFT levels of theory. The VCD intensities, like the VA intensities are very sensitive to the force field and it has been shown that the most sensitive part of the VA and VCD intensity calculations is having an accurate geometry and Hessian [132,72]. The nature of the normal modes are tested by their ability to accurately simulate the VA and VCD intensities, given accurate APT and AAT [130,134,4,77,131,28,78,5,79,62,15,16,14,30].

In Table 3 we present the calculated vibrational frequencies and rotational strengths (used to simulate the VCD intensities) with the B3LYP hybrid DFT method using the 6-31++G(d,p) and aug-cc-pVTZ basis sets. In addition we present the simulated VCD spectra calculated also with the B3LYP hybrid DFT method but with the 6-31G(d,p), cc-pVDZ, aug-cc-pVDZ and cc-pVTZ basis sets in Fig. 3. These simulations also show that the simulations of the VCD spectra with these basis sets (*i.e.*, cc-pVDZ, aug-cc-pVDZ and cc-pVTZ) are not very different than the two simulations for which the rotational strengths

Table 2. Comparison of vibrational frequencies and VA intensities for phenyloxirane

	$\bar{\nu}$ (cm^{-1}) B3LYP ppGdp	($\bar{\nu}$ (cm^{-1})) exp [10]	D_i B3LYP ppGdp	(D_i) exp [10]	$\bar{\nu}$ (cm^{-1}) B3LYP AccpVTZ	D_i	$\bar{\nu}$ (cm^{-1}) PBE AccpVTZ	D_i	$\bar{\nu}$ (cm^{-1}) PBE1 AccpVTZ	D_i	$\bar{\nu}$ (cm^{-1}) PW91 AccpVTZ	D_i
r_1	3209.		12.0		3193.	12.8	3122.	17.3	3212.	13.2	3129.	17.3
r_2	3203.		23.9		3186.	20.0	3113.	24.4	3204.	17.1	3120.	24.3
r_3	3192.		26.6		3176.	19.5	3105.	11.4	3195.	12.6	3112.	10.8
r_4	3188.		32.8		3169.	30.7	3096.	0.2	3191.	26.6	3103.	0.2
r_5	3181.		0.6		3166.	0.2	3091.	35.0	3185.	0.2	3098.	34.1
r_6	3171.		9.8		3157.	8.3	3086.	7.5	3176.	7.2	3093.	7.8
r_7	3119.		26.8		3106.	22.9	3029.	26.2	3126.	21.3	3036.	25.7
r_8	3095.		37.1		3081.	38.1	3003.	41.4	3098.	33.7	3011.	40.8
r_9	1655.	(1608.)	10.4	(7.5)	1646.	11.2	1600.	11.9	1672.	11.8	1602.	11.8
		(1601.)		(1.3)								
r_{10}	1633.	(1586.)	0.3	(0.1)	1625.	0.4	1581.	0.2	1651.	0.3	1582.	0.2
r_{11}	1534.	(1496.)	17.3	(3.1)	1533.	21.2	1482.	20.8	1541.	18.7	1486.	21.1
r_{12}	1527.	(1477.)	19.1	(26.9)	1521.	16.9	1464.	21.3	1523.	31.5	1468.	20.1
r_{13}	1489.	(1452.)	17.9	(22.2)	1489.	16.3	1439.	12.0	1491.	13.3	1443.	12.5
r_{14}	1423.	(1389.)	40.1	(35.9)	1419.	33.1	1373.	28.5	1430.	37.1	1375.	28.6
		(1383.)		(9.7)								
r_{15}	1361.	(1329.)	0.7	(3.6)	1357.	6.7	1342.	5.4	1370.	0.8	1342.	4.0
		(1311.)		(9.7)								
r_{16}	1340.	(1295.)	14.6	(4.9)	1330.	10.7	1299.	14.2	1344.	12.0	1303.	15.4
		(1288.)		(0.8)								
r_{17}	1285.	(1252.)	16.6	(18.3)	1282.	19.9	1242.	18.1	1292.	23.2	1245.	18.0
r_{18}	1222.	(1201.)	11.4	(19.6)	1221.	11.7	1191.	10.2	1236.	9.3	1194.	10.7
r_{19}	1201.	(1177.)	0.9	(2.0)	1200.	0.9	1160.	1.2	1196.	1.3	1163.	1.2
r_{20}	1184.	(1157.)	0.3	(1.8)	1182.	0.3	1144.	0.3	1177.	0.2	1148.	0.3
r_{21}	1168.	(1144.)	5.0	(8.1)	1171.	3.3	1123.	2.9	1171.	3.8	1126.	2.8
r_{22}	1147.	(1126.)	5.7	(11.1)	1152.	7.7	1100.	12.2	1154.	8.8	1104.	12.0
		(1106.)		(0.6)								
r_{23}	1103.	(1077.)	12.9	(6.3)	1104.	8.2	1071.	15.2	1108.	9.6	1073.	15.1

(*continued on next page*)

Table 2. (*Continued*)

	$\bar{\nu}$ (cm^{-1}) B3LYP ppGdp	($\bar{\nu}$ (cm^{-1})) exp [10]	D_i B3LYP ppGdp	(D_i) exp [10]	$\bar{\nu}$ (cm^{-1}) B3LYP AccpVTZ	D_i	$\bar{\nu}$ (cm^{-1}) PBE AccpVTZ	D_i	$\bar{\nu}$ (cm^{-1}) PBE1 AccpVTZ	D_i	$\bar{\nu}$ (cm^{-1}) PW91 AccpVTZ	D_i
r_{24}	1089.	(1069.)	8.5	(12.1)	1093.	10.3	1051.	3.4	1098.	12.0	1054.	3.4
r_{25}	1050.	(1026.)	13.4	(12.5)	1051.	12.6	1024.	15.9	1059.	15.3	1026.	15.8
r_{26}	1014.	(1002.)	1.2	(2.6)	1021.	1.5	990.	0.2	1023.	0.2	993.	0.2
r_{27}	1006.	(983.)	47.4	(56.5)	1018.	1.9	974.	3.4	1020.	5.5	977.	2.7
r_{28}	1002.		10.9		1006.	54.2	968.	61.1	1014.	67.4	970.	59.0
r_{29}	986.	(966.)	0.1	(0.2)	999.	0.1	955.	0.3	1002.	0.0	958.	0.3
r_{30}	929.	(909.)	5.9	(9.9)	939.	6.2	900.	3.1	941.	11.1	902.	3.2
r_{31}	900.	(877.)	169.7	(275.5)	901.	152.3	887.	140.4	935.	119.2	885.	141.9
r_{32}	862.		5.4		867.	0.8	833.	5.9	898.	108.0	834.	1.6
r_{33}	852.	(819.)	100.8	(96.1)	848.	100.2	824.	101.5	869.	1.3	820.	105.5
r_{34}	767.	(755.)	237.6	(270.5)	778.	209.5	751.	199.0	781.	202.3	752.	202.8
r_{35}	763.	(752.)	54.8	(96.3)	765.	18.7	744.	1.4	772.	2.4	746.	0.9
r_{36}	708.	(696.)	176.3	(295.3)	718.	205.8	693.	218.8	720.	219.0	695.	217.1
		(673.)		(2.3)								
		(664.)		(0.4)								
		(655.)		(0.7)								
r_{37}	631.	(619.)	0.1	(0.1)	634.	0.1	610.	0.2	629.	0.2	613.	0.2
r_{38}	584.	(575.)	55.7	(57.3)	586.	52.9	566.	49.3	586.	47.9	567.	50.0
r_{39}	542.	(531.)	83.4	(109.3)	547.	79.9	527.	82.7	548.	86.3	529.	81.4
r_{49}	416.		1.6		418.	1.4	400.	1.9	416.	1.3	401.	1.9
r_{41}	396.		14.9		395.	14.7	381.	12.0	398.	12.8	382.	12.4
r_{42}	337.		12.7		339.	13.3	328.	14.3	338.	12.3	329.	14.7
r_{43}	194.		90.3		193.	78.3	183.	72.1	191.	81.7	183.	72.4
r_{44}	147.		69.5		148.	66.5	144.	69.0	147.	59.4	145.	70.7
r_{45}	59.		200.8		57.	191.5	60.	146.2	60.	162.9	60.	148.0

Table 3. Comparison of vibrational frequencies and VCD intensities for (R)-phenyloxirane, experimental data was for (S)-phenyloxirane

	$\bar{\nu}$ (cm^{-1}) B3LYP ppGdp	($\bar{\nu}$ (cm^{-1})) exp [10]	R_i B3LYP ppGdp	(R_i) exp [10]	$\bar{\nu}$ (cm^{-1}) B3LYP AccpVTZ	R_i	$\bar{\nu}$ (cm^{-1}) PBE AccpVTZ	R_i	$\bar{\nu}$ (cm^{-1}) PBE1 AccpVTZ	R_i	$\bar{\nu}$ (cm^{-1}) PW91 AccpVTZ	R_i
r_1	3209.		−1.7		3193.	−2.2	3122.	−1.9	3212.	−1.7	3129.	−1.9
r_2	3203.		0.4		3186.	0.6	3113.	0.6	3204.	0.8	3120.	0.5
r_3	3192.		−0.1		3176.	1.1	3105.	1.6	3195.	0.8	3112.	1.6
r_4	3188.		4.5		3169.	3.6	3096.	0.5	3191.	3.1	3103.	0.5
r_5	3181.		0.2		3166.	−0.1	3091.	3.0	3185.	0.3	3098.	3.0
r_6	3171.		0.4		3157.	0.7	3086.	1.0	3176.	0.6	3093.	1.0
r_7	3119.		4.4		3106.	3.3	3029.	3.1	3126.	3.3	3036.	2.9
r_8	3095.		0.9		3081.	1.5	3003.	1.3	3098.	−0.2	3011.	1.7
r_9	1655.	(1608.) (1601.)	0.7		1646.	0.6	1600.	0.7	1672.	0.6	1602.	0.7
r_{10}	1633.	(1586.)	−0.1		1625.	−0.3	1581.	−0.1	1651.	−0.2	1582.	−0.1
r_{11}	1534.	(1496.)	1.4	(−1.6)	1533.	0.6	1482.	0.4	1541.	1.8	1486.	0.4
r_{12}	1527.	(1477.)	13.3	(−7.5)	1521.	12.4	1464.	15.4	1523.	15.7	1468.	14.7
r_{13}	1489.	(1452.)	2.2	(−9.7)	1489.	3.2	1439.	0.9	1491.	1.9	1443.	1.2
r_{14}	1423.	(1389.) (1383.)	6.2	(−8.6) (3.8)	1419.	5.0	1373.	7.1	1430.	1.1	1375.	6.9
r_{15}	1361.	(1329.) (1311.)	−0.1	(−4.2) (−2.2)	1357.	4.4	1342.	−8.8	1370.	−5.1	1342.	−7.7
r_{16}	1340.	(1295.) (1288.)	−4.0	(8.3) (0.8)	1330.	−9.4	1299.	2.1	1344.	2.2	1303.	1.6
r_{17}	1285.	(1252.)	−17.8	(26.0)	1282.	−19.3	1242.	−25.4	1292.	−25.6	1245.	−25.2
r_{18}	1222.	(1201.)	7.9	(−16.2)	1221.	9.2	1191.	9.4	1236.	9.9	1194.	9.4
r_{19}	1201.	(1177.)	−0.8	(0.4)	1200.	−0.6	1160.	−0.8	1196.	−0.7	1163.	−0.8
r_{20}	1184.	(1157.)	−0.1	(−0.1)	1182.	−0.1	1144.	−0.1	1177.	−0.1	1148.	−0.1
r_{21}	1168.	(1144.)	0.6	(2.6)	1171.	−0.1	1123.	0.9	1171.	−1.9	1126.	0.9
r_{22}	1147.	(1126.) (1106.)	5.2	(−19.4)	1152.	8.5	1100.	13.6	1154.	10.8	1104.	13.4
r_{23}	1103.	(1077.)	1.5	(−2.8)	1104.	1.4	1071.	0.6	1108.	1.5	1073.	0.7

(*continued on next page*)

Table 3. (*Continued*)

	$\bar{\nu}$ (cm^{-1}) B3LYP ppGdp	($\bar{\nu}$ (cm^{-1})) exp [10]	R_i B3LYP ppGdp	(R_i) exp [10]	$\bar{\nu}$ (cm^{-1}) B3LYP AccpVTZ	R_i	$\bar{\nu}$ (cm^{-1}) PBE AccpVTZ	R_i	$\bar{\nu}$ (cm^{-1}) PBE1 AccpVTZ	R_i	$\bar{\nu}$ (cm^{-1}) PW91 AccpVTZ	R_i
r_{24}	1089.	(1069.)	−0.3	(−0.4)	1093.	−0.5	1051.	−1.0	1098.	0.3	1054.	−1.0
r_{25}	1050.	(1026.)	0.6	(−1.2)	1051.	0.3	1024.	0.2	1059.	0.2	1026.	0.2
r_{26}	1014.	(1002.)	−0.5	(0.7)	1021.	−0.7	990.	−0.1	1023.	0.1	993.	−0.1
r_{27}	1006.	(983.)	47.4	(14.4)	1018.	0.04	974.	−0.3	1020.	−0.4	977.	−0.2
r_{28}	1002.		−2.7		1006.	−11.0	968.	−15.5	1014.	−14.0	970.	−14.9
r_{29}	986.	(966.)	0.0		999.	0.1	955.	0.04	1002.	0.1	958.	0.0
r_{30}	929.	(909.)	1.1		939.	0.8	900.	2.0	941.	−0.4	902.	1.7
r_{31}	900.	(877.)	−8.0		901.	−6.9	887.	−7.0	935.	−4.3	885.	−7.1
r_{32}	862.		−8.2		867.	−3.8	833.	−8.3	898.	2.8	834.	−4.8
r_{33}	852.	(819.)	16.0		848.	15.2	824.	17.9	869.	3.0	820.	15.6
r_{34}	767.	(755.)	−12.0		778.	−22.7	751.	−27.3	781.	−21.6	752.	−28.4
r_{35}	763.	(752.)	−21.5		765.	−12.1	744.	1.3	772.	−3.7	746.	0.5
r_{36}	708.	(696.) (673.) (664.) (655.)	3.6		718.	1.5	693.	−0.5	720.	0.2	695.	−0.6
r_{37}	631.	(619.)	0.2		634.	0.1	610.	0.1	629.	0.2	613.	0.1
r_{38}	584.	(575.)	−14.9		586.	−13.8	566.	−9.6	586.	−11.2	567.	−10.0
r_{39}	542.	(531.)	0.6		547.	−1.1	527.	−4.9	548.	−3.5	529.	−4.7
r_{49}	416.		−0.1		418.	−0.03	400.	−0.04	416.	−0.02	401.	−0.03
r_{41}	396.		−4.1		395.	−4.3	381.	−4.1	398.	−4.7	382.	−4.0
r_{42}	337.		−7.1		339.	−6.6	328.	−6.6	338.	−6.3	329.	−6.7
r_{43}	194.		7.5		193.	6.1	183.	5.7	191.	8.8	183.	5.5
r_{44}	147.		−3.6		148.	−3.6	144.	−3.0	147.	−3.9	145.	−2.8
r_{45}	59.		26.3		57.	27.3	60.	26.9	60.	25.5	60.	27.1

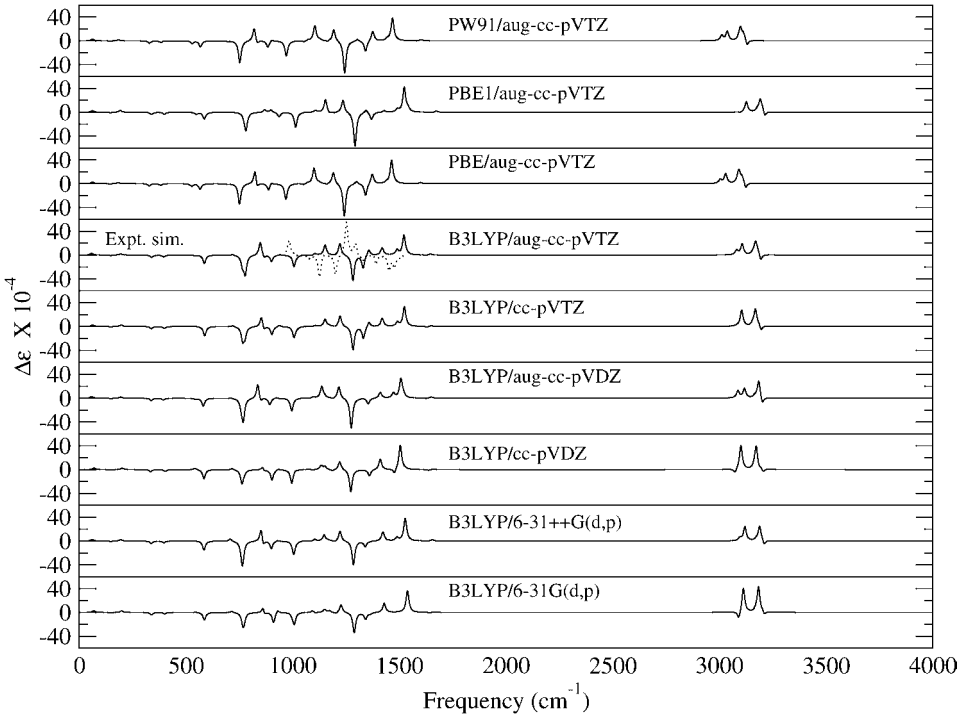

Fig. 3. (R)-Phenyloxirane VCD spectra for various DFT methods.

are presented in Table 3, though there are some regions of the spectra where there are differences. For example, with the 6-31++G(d,p), aug-cc-pVDZ and aug-cc-pVTZ basis sets the lower frequency band in the CH stretch region are both positive, whereas with the basis sets without the diffuse functions, they are of opposite sign. In addition, we also present the calculated vibrational frequencies and rotational strengths at the PBE, PBE1 and PW91 levels of theory with the aug-cc-pVTZ basis set. The spectral simulations for these other DFT methods are also given in Fig. 3. Again we can see the changes with respect to changing the functional are larger than the changes with respect to the basis set at the B3LYP level of theory, but the differences are not that distinct. With the PBE and PW91 functional we also see the positive signed feature in the lower region of the CH stretch region with the aug-cc-pVTZ basis set, similar to what we saw with the basis sets that included the diffuse functions at the B3LYP level.

Hence it appears in order to get the fine features in the VCD spectra, one requires the addition of diffuse functions in addition to the polarization functions, which previously have been shown to be important [72]. Here the basis set dependence clearly affects the VCD intensities more than it has the VA intensities. It appears that larger basis sets are required for calculating VCD intensities at the same level of accuracy as the VA intensities. Therefore, it may be that one might want to increase the quality of the basis set for the calculation if one focuses on VCD intensities in addition to the VA intensities. In many cases, researchers have only focused on the VA intensities of the amide I modes in their determination of the secondary structure content. Keiderling's and Suhai's groups have

shown that the VCD intensities are also very sensitive to secondary structure and can be used in addition to the VA intensities, especially in cases where the VA intensities do not give enough information [80,60,84]. This is not inconsistent with other biomolecular modeling studies where the question one asks or the quantity one wishes to calculate and the accuracy with which one is satisfied determines the method to use (or here basis set for a given method), and not vice versa. In many cases, a method or basis set for a given method will give good results for some quantities, but for other quantities, much larger basis sets for a given method, may be required. A case in point are the dispersion or van der Waals forces of the He_2 dimer, where the binding energy is approximately 11.0 K or 7.65 cm^{-1} experimentally and calculated to be 33.5 μ-Hartrees at the CCSD(T)t-aug-cc-pV6Z counterpoise corrected level of theory [142].

The good agreement between the calculated VA and VCD spectra with the experimental spectra of Ashvar and coworkers [10] leads us to believe that the Raman and ROA spectra will be accurately predicted, given that we have accurate EDEDPD, EDMDPD and EDEQPD. We give these additional new tests and confirmatory evidence for the accuracy of the geometry and Hessian determined at the DFT level of theory, beyond those reported by Ashvar and coworkers, the predicted Raman scattering and ROA intensities, covered in the next two subsections. Here will also document the accuracy of the B3LYP level of theory with the 6-31G(d,p) and aug-cc-pVDZ basis sets. In addition, we document the accuracy of the RHF level of theory with the 6-31G(d,p) basis set.

3.4. Raman scattering

In Fig. 4 we present our simulated Raman scattering spectra for phenyloxirane. The Raman scattering spectra for phenyloxirane have been reported by Hecht and Barron [64,63]. The Raman intensities monitor changes in the EDEDP as the atoms vibrate. In many cases modes, which are not seen or a very low intensity in the IR or VA spectra, are seen in Raman spectra. For example, the CH stretch mode at 3181 cm^{-1}, that has very little intensity in the VA spectra, has a large intensity in the Raman. Hence the Raman spectral measurements are required to validate the accuracy of this mode, both with respect to the frequency and to its nature in reproducing the Raman intensity, when coupled with the EDEDPD. In addition, the band calculated at 862 cm^{-1} with weak intensity in the VA spectra of Ashvar and coworkers is not observed. The Raman intensity of this band is also calculated to be weak in intensity in our Raman simulations. Hence this band would be hard to see also in the Raman spectra. Surprisingly this band has a calculated strong ROA intensity, so if one could get enough molecules in the path of the laser, then the ROA spectra should be evident, though you might not look for it based the Raman measurements alone.

The agreement between the calculated and measured Raman intensities further gives us a measure of the accuracy of DFT to be able to calculate the EDEDPD. This is important if one wishes to be able to simulate accurately the Raman intensities of the aromatic amino acids, phenylalanine, tryptophan and tyrosine. We have utilized the aug-cc-pVDZ and aug-cc-pVTZ basis sets for our Raman simulations, in addition to the cc-pVDZ and cc-pVTZ basis sets and the 6-31++G(d,p) and the 6-31G(d,p) basis sets. Here we can see that the polarization functions seem to have the largest effects on the Raman spectra, and the additional diffuse functions are not that important as they have been shown to be for van der

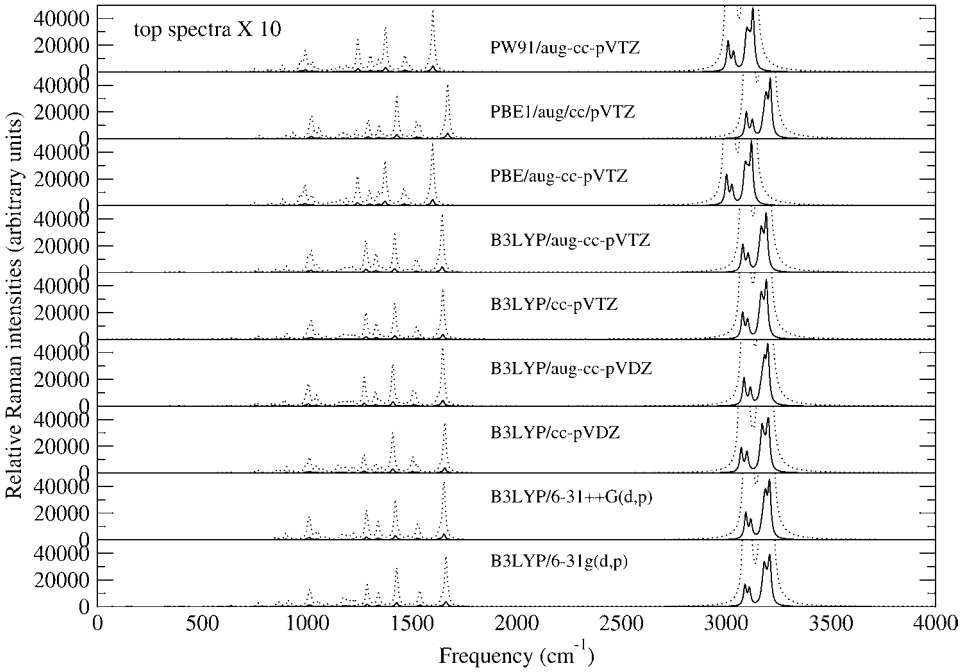

Fig. 4. Phenyloxirane Raman scattering spectra for various DFT methods.

Waals complexes. But to investigate this more thoroughly, we will look to the ROA intensities, discussed in the next subsection. In addition, we have simulated the Raman spectra with the aug-cc-pVTZ basis set at the PBE, PBE1 and PW91 levels. The relative intensities appear to be very similar, but there are some shifts in the frequencies. This is not surprising, given the differences observed in the bond lengths in the oxirane and benzene rings as a function of the DFT functional (method) used. Since the two parent rings, oxirane and benzene, are very symmetrical, the intensities can be to a large extent determined by symmetry and the interactions appear to be such that they are not largely disturbed. In a future work we shall more carefully compare the benzene and oxirane vibrational modes with those found here in phenyloxirane. Since the chirality is reflected in the ROA spectra, it should reveal more information than the simple Raman spectra.

Goddard's group has recently derived new functionals, the XLYP and X3LYP functionals that better treat dispersion than the BLYP and B3LYP functionals [156,155]. These functionals are expected therefore to treat the EDEDP better than the BLYP and B3LYP functionals, but this remains to be shown. The XLYP functional uses the Slater [126], Becke 88 [23] and Perdew 91 [108,111,112] exchange functionals and the Lee, Yang and Parr (LYP) correlation functional [95]. The X3LYP hybrid functional, in addition uses the Hartree–Fock exchange and a bit of the Vosko, Wilk and Nusair (VWN) correlation functional [146]. The testing of these functional for properties, in addition to their testing for geometries and interactions energies remains to be done. In addition, new nonempirical functionals have also recently been developed and implemented in commercial codes [129], which go beyond the GGA approximation and correct some of the deficiencies of the older functionals, for example, the exchange potential's divergence at the nuclei.

In Table 4 we present the calculated vibrational frequencies and Raman scattering intensities (used to simulate the Raman scattering spectra) with the B3LYP hybrid DFT method using the 6-31++G(d,p) and aug-cc-pVTZ basis sets. In addition we present in Fig. 4 the simulated Raman scattering spectra calculated also with the B3LYP hybrid DFT method but with the 6-31G(d,p), cc-pVDZ, aug-cc-pVDZ and cc-pVTZ basis sets. These simulations show that the simulations of the Raman scattering spectra with these basis sets are not drastically different from the two presented here, though the differences are larger visually than those seen at first glance in the VA and VCD spectra. In addition, again we also present the calculated vibrational frequencies and Raman scattering intensities with the PBE, PBE1 and PW91 DFT methods at the highest basis set level we used in this study, that is, the aug-cc-pVTZ. The spectral simulations for these other DFT methods are also given in Fig. 4 and Table 4. Here one sees changes in the peak heights and frequencies that reflect some of the changes in the geometrical parameters (bond lengths and valence angles), which resulted due to changing the DFT exchange correlation functional.

3.5. Raman optical activity

At the B3LYP/6-31++G(d,p) optimized structure we have calculated the Hessian and EDEDPD that allowed us to simulate the Raman scattering spectra. Additionally, we have calculated the RHF/6-31G(d,p) EDMDPD and EDEQPD, which when combined with the B3LYP/6-31++G(d,p) Hessian and EDEDPD allow us to simulate the ROA spectra. In Fig. 5 we present our DCP and ICP ROA spectra for (R)-phenyloxirane. Comparing our simulated ICP and DCP ROA spectra presented in Fig. 5 with those measured by Hecht and Barron in their works and presented in Figs. 3, 4 and 5 of Ref. [63] and Fig. 4 of Ref. [64], one can see that the main features of the ICP and DCP Raman spectra are reproduced by using the B3LYP/6-31++G** EDEDPD, combined with the RHF/6-31G(d,p) EDMDPD and the EDEQPD.

As one can see in Fig. 4 and in Fig. 5 of Ref. [63] and Fig. 4 of Ref. [64], the low frequency ROA spectra from 0 to 400 cm^{-1} gives additional information about the chirality and stereoisomer of phenyloxirane in a region that is not currently available in VCD measurements. Here we reproduce the $-/+/-/+/-$ sign pattern in the experimental ROA spectra [63]. Hence the ROA and VCD are really complementary in that the low frequency modes are readily measurable in the ROA with currently available ROA instrumentation, while they not with currently available VCD instrumentation.

The low frequency modes are largely collective modes and involve the backbone and side chain modes in proteins. Hence information gained from the Raman and ROA modes will give information about these collective modes. For protein functionality, these modes are very important as in many cases the path the ligand takes to its binding pocket is not obvious from the X-ray structures. Hence information about these collective modes may help to understand the mechanism for protein binding where the binding pockets are buried in crevices, only accessible via collective breathing modes, just those, which are amenable to probing via Raman and ROA spectroscopy.

In addition to the low frequency Raman and ROA spectra of phenyloxirane reported in Ref. [63], the polarized and depolarized Raman and ROA spectra are also reported in the 400 to 1600 cm^{-1} region [64,63]. Here we have information in the same region as we have

Table 4. Comparison of vibrational frequencies and Raman intensities for phenyloxirane

	$\bar{\nu}$ (cm^{-1}) B3LYP ppGdp	($\bar{\nu}$ (cm^{-1})) exp [10]	Ram_i B3LYP ppGdp	$\bar{\nu}$ (cm^{-1}) B3LYP AccpVTZ	Ram_i	$\bar{\nu}$ (cm^{-1}) PBE AccpVTZ	Ram_i	$\bar{\nu}$ (cm^{-1}) PBE1 AccpVTZ	Ram_i	$\bar{\nu}$ (cm^{-1}) PW91 AccpVTZ	Ram_i
r_1	3209.		264.5	3193.	292.9	3122.	338.1	3212.	306.6	3129.	335.6
r_2	3203.		70.4	3186.	31.0	3113.	18.4	3204.	13.5	3120.	18.9
r_3	3192.		87.4	3176.	84.2	3105.	107.4	3195.	89.7	3112.	107.0
r_4	3188.		103.1	3169.	95.4	3096.	83.4	3191.	94.8	3103.	81.4
r_5	3181.		103.2	3166.	92.5	3091.	115.3	3185.	83.3	3098.	114.2
r_6	3171.		50.2	3157.	46.1	3086.	48.0	3176.	45.2	3093.	48.9
r_7	3119.		103.9	3106.	95.8	3029.	108.6	3126.	99.4	3036.	106.3
r_8	3095.		151.2	3081.	158.4	3003.	182.6	3098.	151.8	3011.	181.1
r_9	1655.	(1608.) (1601.)	66.0	1646.	63.3	1600	70.0	1672.	60.9	1602.	70.2
r_{10}	1633.	(1586.)	6.8	1625.	6.5	1581.	5.0	1651.	5.7	1582.	5.1
r_{11}	1534.	(1496.)	7.5	1533.	4.2	1482.	7.3	1541.	11.4	1486.	6.5
r_{12}	1527.	(1477.)	13.7	1521.	14.5	1464.	20.7	1523.	18.4	1468.	19.6
r_{13}	1489.	(1452.)	3.5	1489.	2.7	1439.	2.4	1491.	1.6	1443.	2.3
r_{14}	1423.	(1389.) (1383.)	52.5	1419.	49.8	1373.	59.7	1430.	54.1	1375.	60.3
r_{15}	1361.	(1329.) (1311.)	1.1	1357.	4.4	1342.	15.9	1370.	4.3	1342.	12.7
r_{16}	1340.	(1295.) (1288.)	24.2	1330.	24.8	1299.	20.3	1344.	15.9	1303.	22.1
r_{17}	1285.	(1252.)	42.9	1282.	46.3	1242.	43.8	1292.	26.6	1244.	47.4
r_{18}	1222.	(1201.)	8.0	1221.	6.8	1191.	10.0	1236.	11.6	1194.	9.0
r_{19}	1201.	(1177.)	5.1	1200.	5.2	1160.	6.4	1196.	5.2	1163.	6.4
r_{20}	1184.	(1157.)	4.3	1182.	4.1	1144.	4.6	1177.	4.1	1148.	4.6
r_{21}	1168.	(1144.)	6.5	1171.	3.7	1123.	4.4	1171.	4.0	1126.	4.2
r_{22}	1147.	(1126.) (1106.)	4.3	1152.	2.4	1100.	2.4	1154.	4.1	1104.	2.3
r_{23}	1103.	(1077.)	1.0	1104.	0.9	1071.	0.8	1108.	0.9	1073.	0.8

(*continued on next page*)

Table 4. (*Continued*)

	$\bar{\nu}$ (cm^{-1}) B3LYP ppGdp	($\bar{\nu}$ (cm^{-1})) exp [10]	Ram_i B3LYP ppGdp	$\bar{\nu}$ (cm^{-1}) B3LYP AccpVTZ	Ram_i	$\bar{\nu}$ (cm^{-1}) PBE AccpVTZ	Ram_i	$\bar{\nu}$ (cm^{-1}) PBE1 AccpVTZ	Ram_i	$\bar{\nu}$ (cm^{-1}) PW91 AccpVTZ	Ram_i
r_{24}	1089.	(1069.)	3.3	1093.	2.4	1051.	3.8	1098.	3.1	1054.	3.5
r_{25}	1050.	(1026.)	13.5	1051.	11.3	1024.	17.0	1059.	17.7	1026.	16.2
r_{26}	1014.	(1002.)	35.3	1021.	34.7	990.	37.5	1023.	34.8	993.	37.8
r_{27}	1006.	(983.)	12.0	1018.	0.2	974.	0.5	1020.	1.5	977.	0.4
r_{28}	1002.		5.0	1006.	21.4	968.	16.4	1014.	11.7	970.	17.0
r_{29}	986.	(966.)	0.1	999.	0.2	955.	0.07	1002.	0.1	958.	0.10
r_{30}	929.	(909.)	1.4	939.	2.1	900.	1.7	941.	2.0	902.	1.7
r_{31}	900.	(877.)	14.0	901.	13.2	887.	13.4	935.	10.7	884.	13.8
r_{32}	862.		0.8	867.	0.9	833.	0.9	898.	5.6	834.	0.6
r_{33}	852.	(819.)	5.9	848.	6.5	824.	6.4	869.	0.6	820.	6.9
r_{34}	767.	(755.)	0.4	778.	0.8	751.	2.7	781.	1.6	752.	2.6
r_{35}	763.	(752.)	9.0	765.	9.0	744.	5.8	772.	7.4	746.	6.1
r_{36}	708.	(696.)	0.0	718.	0.07	693.	0.1	720.	0.1	695.	0.1
		(673.)									
		(664.)									
		(655.)									
r_{37}	631.	(619.)	5.0	634.	3.9	610.	3.7	629.	3.7	613.	3.7
r_{38}	584.	(575.)	1.2	586.	0.9	566.	0.8	586.	0.8	567.	0.8
r_{39}	542.	(531.)	0.5	547.	0.4	527.	0.4	548.	0.3	529.	0.4
r_{49}	416.		0.1	418.	0.1	400.	0.08	416.	0.1	401.	0.1
r_{41}	396.		2.9	395.	3.5	381.	3.9	398.	3.1	382.	3.9
r_{42}	337.		3.0	339.	2.6	328.	2.3	338.	2.2	329.	2.3
r_{43}	194.		0.4	193.	0.6	183.	0.7	191.	0.5	183.	0.7
r_{44}	147.		3.7	148.	3.3	144.	3.3	147.	3.2	145.	3.3
r_{45}	59.		3.2	57.	2.8	60.	3.0	60.	2.8	60.	3.0

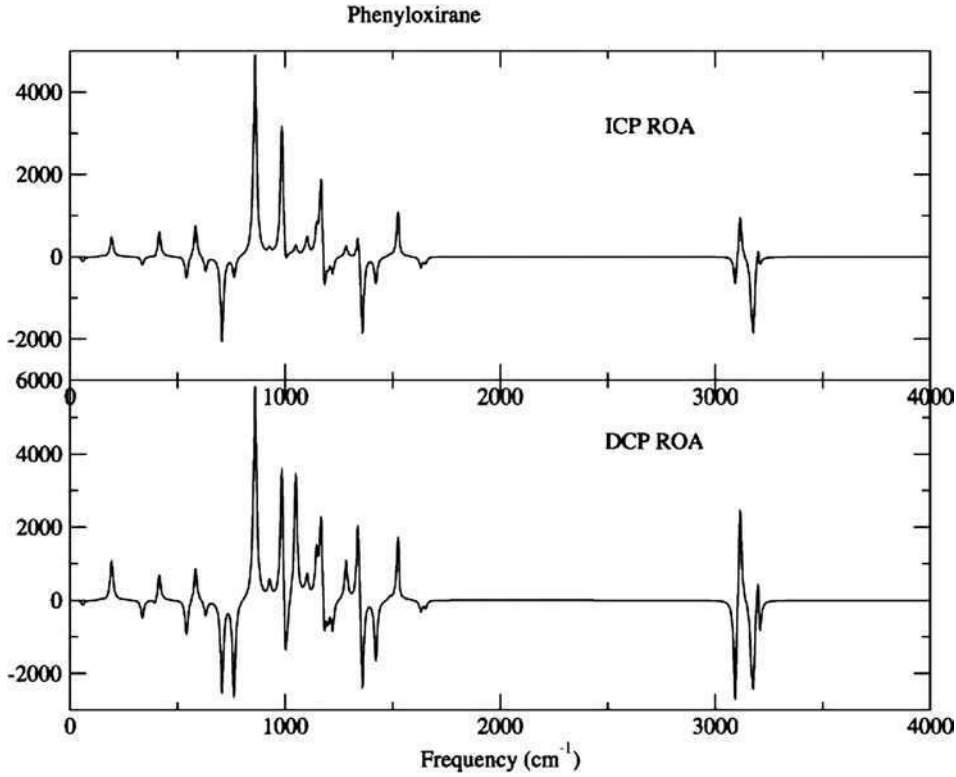

Fig. 5. (R)-Phenyloxirane DCP and ICP Raman optical activity (ROA) spectra calculated with mixed theory (B3LYP/6-31++G(d,p) Hessian and EDEDPD (Gaussian) and RHF/6-31G(d,p) EDMDPD and EDEQPD with CADPAC.

for the VCD. In Figs. 5 and 6 and in Figs. 3 and 4 in Ref. [63] we can compare our predicted with the experimental spectra. In Table 5 we present results utilizing the 6-31G(d,p) basis set, which was used frequently for the early vibrational frequency, Raman scattering, ROA1 (CID1), ROA2 (CID2), ROA3 (CID3), ROA/DCP and ROA/ICP intensity calculations [116,38,60]. Hence we want to document the accuracy of this level of theory also for phenyloxirane. In a future work we will also compare our calculated frequencies, Raman and ROA intensities with the corresponding experimentally measured intensities, which we obtained from trying to integrate the bands in the experimental spectra [37]. It would be nice if the Raman and ROA spectroscopists could report the experimental frequencies, line widths and deconvoluted integrated absolute and relative intensities, similar to the corresponding experimental data reported by the Stephens group for VA and VCD spectra. This makes qualitative comparisons between experiment and theory much easier.

The ROA spectra calculated with the hybrid method (Hessian and EDEDPD at the B3LYP/6-31++G(d,p) level and the EDEQPD and EDMDPD at the RHF/6-31G(d,p) level) are presented in Fig. 5. For large biomolecular structures, the aug-cc-pVDZ basis set might be a comprise between high accuracy and computational cost. A test of this hypothesis can be seen in Fig. 6. In Fig. 6 we present the complete set of spectra (VA, VCD, Raman,

Table 5. Vibrational frequencies, Raman, ROA1 (CID1), ROA2 (CID2), ROA3 (CID3), ROA/DCP and ROA/ICP intensities for (R)-phenyloxirane

	$\bar{\nu}$ (cm^{-1}) B3LYP Gdp	$\bar{\nu}$ (cm^{-1}) B3LYP AcDZ	Ram_i B3LYP Gdp	Ram_i B3LYP AcDZ	$CID1_i$ B3LYP Gdp	CID_i B3LYP AcDZ	$CID2_i$ B3LYP Gdp	$CID2_i$ B3LYP AcDZ	$CID3_i$ B3LYP Gdp	$CID3_i$ B3LYP AcDZ	$\bar{\nu}$ (cm^{-1}) B3LYP ppGdp	Ram_i B3LYP ppGdp	DCP RHF Gdp	ICP RHF Gdp
r_1	3211.	3201.	214.56	286.26	−0.44	−0.14	−0.30	0.09	−2.22	−0.75	3209.	264.5	−11.4	−2.5
r_2	3204.	3195.	94.19	49.26	0.10	0.04	−0.83	−1.06	0.37	0.11	3203.	70.4	11.8	4.3
r_3	3192.	3184.	82.22	114.35	0.20	−0.69	−0.04	−0.52	0.24	−0.80	3192.	87.4	−1.5	−1.2
r_4	3183.	3184.	85.29	68.90	−6.10	−5.14	−2.40	−2.34	−7.99	−8.02	3188.	103.1	4.0	3.0
r_5	3182.	3174.	100.65	97.43	2.25	0.63	0.76	0.28	2.85	0.82	3181.	103.2	−16.9	−13.0
r_6	3172.	3165.	45.07	47.21	1.85	1.10	0.91	0.68	2.70	1.68	3171.	50.4	−10.4	−7.2
r_7	3112.	3117.	97.93	96.60	−1.44	−0.24	−1.62	−0.27	−3.77	−0.66	3119.	103.9	22.5	8.5
r_8	3091.	3087.	120.20	163.23	−0.77	−0.46	−2.82	−2.22	−2.95	−2.18	3095.	151.2	−23.7	−5.9
r_9	1664.	1649.	56.60	66.18	0.95	0.66	0.40	0.34	1.35	0.93	1655.	66.0	−3.1	−2.2
r_{10}	1642.	1626.	5.33	6.24	−0.59	−0.16	−0.46	−0.20	−0.70	−0.19	1633.	6.8	−4.7	−4.0
r_{11}	1542.	1518.	8.16	11.06	3.57	2.88	3.84	3.28	7.45	6.42	1534.	7.5	−9.9	−4.8
r_{12}	1538.	1508.	11.97	14.83	−1.67	0.72	−1.61	0.54	−2.37	1.39	1527.	13.7	33.7	20.7
r_{13}	1497.	1472.	3.48	3.45	26.90	25.56	29.57	27.45	46.49	43.55	1489.	3.5	1.3	0.7
r_{14}	1429.	1411.	50.75	55.64	−0.36	0.11	−1.26	−0.75	−0.85	0.30	1423.	52.5	−28.9	−11.1
r_{15}	1363.	1354.	1.35	4.47	−5.27	−3.73	−1.16	−2.12	−7.58	−8.56	1361.	1.1	−48.9	−35.5
r_{16}	1342.	1328.	17.67	19.35	−4.65	−3.31	−7.20	−6.40	−14.57	−12.45	1340.	24.2	43.9	12.5
r_{17}	1289.	1275.	31.07	41.69	−0.74	0.04	−0.76	0.53	−2.36	0.17	1285.	42.9	20.8	5.4
r_{18}	1227.	1216.	10.39	8.20	−1.33	−4.54	−0.51	−4.75	−1.97	−11.03	1222.	8.0	−16.9	−8.3
r_{19}	1203.	1190.	7.02	5.26	0.96	−0.99	0.51	−0.52	1.53	−2.07	1201.	5.1	−11.5	−5.1
r_{20}	1187.	1171.	6.42	4.33	0.12	0.06	0.10	0.07	0.14	0.07	1184.	4.3	−25.6	−21.8
r_{21}	1172.	1151.	11.22	3.98	1.46	6.88	0.38	2.94	1.73	8.06	1168.	6.5	50.6	43.4
r_{22}	1149.	1136.	1.74	1.98	−9.88	14.40	−11.80	6.99	−14.93	19.91	1147.	1.9	26.4	13.5
r_{23}	1107.	1097.	1.49	0.79	−12.15	−0.98	−3.07	0.73	−14.39	−1.57	1103.	1.0	13.0	9.7
r_{24}	1093.	1077.	4.22	2.61	12.88	7.67	6.50	3.79	18.62	10.52	1089.	3.3	1.9	1.4
r_{25}	1055.	1046.	9.22	17.77	−0.13	−0.09	−0.22	−0.60	−0.65	−1.28	1050.	13.5	81.8	5.4
r_{26}	1016.	1008.	25.44	38.11	−0.02	0.15	0.31	0.78	−0.10	1.63	1014.	35.3	−10.2	−0.9

(*continued on next page*)

Table 5. (*Continued*)

	$\bar{\nu}$ (cm^{-1}) B3LYP Gdp	$\bar{\nu}$ (cm^{-1}) B3LYP AcDZ	Ram_i B3LYP Gdp	Ram_i B3LYP AcDZ	$CID1_i$ B3LYP Gdp	CID_i B3LYP AcDZ	$CID2_i$ B3LYP Gdp	$CID2_i$ B3LYP AcDZ	$CID3_i$ B3LYP Gdp	$CID3_i$ B3LYP AcDZ	$\bar{\nu}$ (cm^{-1}) B3LYP ppGdp	Ram_i B3LYP ppGdp	DCP RHF Gdp	ICP RHF Gdp
r_{27}	1008.	1001.	10.64	0.42	−1.73	9.02	−2.40	9.45	−2.73	12.77	1006.	12.0	−13.2	−4.9
r_{28}	1000.	995.	2.23	11.19	−4.99	−3.94	−7.50	−7.03	−11.36	−10.72	1002.	5.0	−38.2	−8.8
r_{29}	977.	980.	0.13	0.09	45.78	−81.53	43.19	−62.01	166.65	−109.63	986.	0.1	97.9	82.7
r_{30}	929.	921.	2.82	1.74	−5.36	1.87	−0.41	3.69	−7.57	6.13	929.	1.4	11.9	3.3
r_{31}	910.	893.	12.93	12.75	−5.35	−3.58	1.04	0.34	−6.24	−4.33	900.	14.0	−0.2	−0.1
r_{32}	867.	850.	3.73	0.99	−33.79	25.77	−10.60	11.43	−39.61	30.47	862.	0.8	164.1	137.7
r_{33}	862.	837.	7.67	6.65	23.64	7.55	8.31	5.21	27.75	8.81	852.	5.9	15.3	13.1
r_{34}	772.	768.	2.56	1.13	−1.06	4.55	−1.52	10.37	−1.31	16.51	767.	0.4	−7.6	−4.9
r_{35}	766.	760.	7.37	8.72	10.52	6.25	14.55	12.46	44.55	39.64	763.	9.0	−79.4	−12.0
r_{36}	714.	711.	0.58	0.12	−3.27	13.87	−1.38	21.24	−3.96	39.31	708.	0.0	−88.5	−73.2
r_{37}	633.	628.	5.05	4.13	−0.71	−1.06	−0.55	−0.61	−0.84	−1.25	631.	5.0	−16.5	−14.0
r_{38}	586.	581.	1.57	0.91	8.35	1.71	3.97	0.56	9.87	1.99	584.	1.2	39.2	33.5
r_{39}	544.	545.	0.69	0.44	22.51	2.28	15.90	8.33	36.80	5.31	542.	0.5	−44.4	−25.0
r_{40}	418.	415.	0.14	0.07	−129.80	−124.60	−62.21	−98.28	−181.99	−231.09	416.	0.1	43.5	37.1
r_{41}	399.	393.	2.45	3.76	−3.95	−0.92	−2.52	−1.08	−8.98	−2.73	396.	2.9	−10.1	−3.7
r_{42}	338.	337.	3.00	2.56	12.47	7.57	10.38	10.10	23.87	20.84	337.	3.1	−36.6	−15.2
r_{43}	197.	194.	0.29	0.62	−28.36	−9.37	−21.82	−7.17	−63.98	−23.07	194.	0.4	138.6	62.6
r_{44}	148.	149.	5.45	3.40	5.60	5.57	3.35	3.52	6.65	6.65	147.	3.7	3.6	3.0
r_{45}	67.	57.	5.57	2.87	−26.86	−25.99	−11.51	−12.61	−31.49	−30.72	59.	3.2	−58.6	−49.9

Gdp is the 6-31G(d,p) basis set, ppGdp is the 6-31++G(d,p) basis set and AcDZ is the aug-cc-pVDZ basis set.

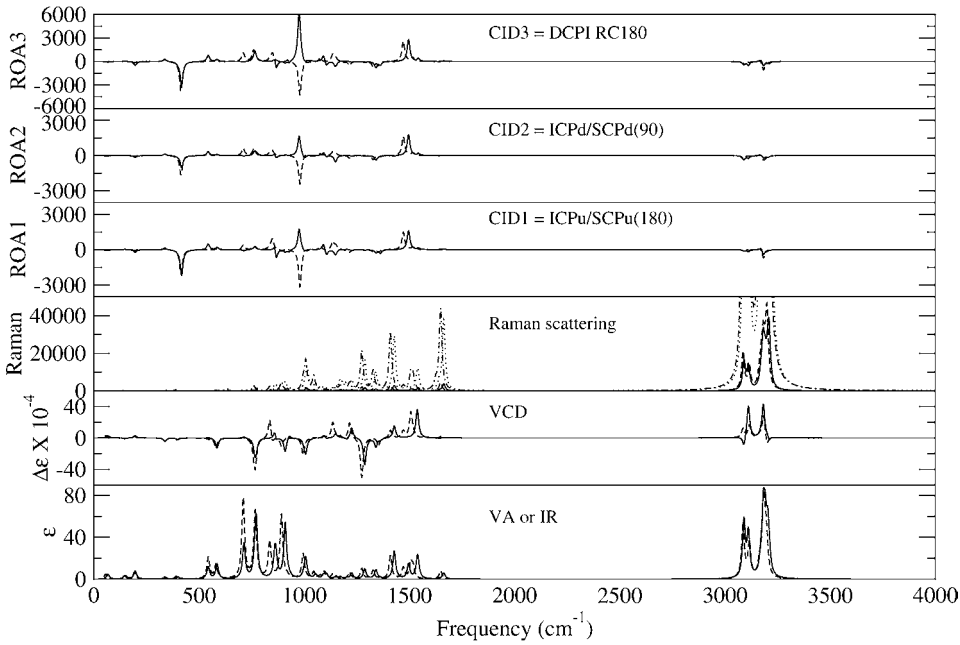

Fig. 6. (R)-Phenyloxirane VA, VCD, Raman, ROA1 (CID1), ROA2 (CID2) and ROA3 (CID3). The solid line spectra calculated at the B3LYP/6-31G(d,p) level (the dotted line is the B3LYP spectra multiplied by 10 for the Raman) and the dashed line at the B3LYP/aug-cc-pVDZ level (the dashed dotted line is the B3LYP/aug-cc-pVDZ spectra multiplied by 10 for the Raman).

ROA1, ROA2 and ROA3) calculated at the B3LYP level of theory with both the 6-31G(d,p) and aug-cc-pVDZ basis sets. Here we see the ROA intensity of the major bands around 980 and 860 cm^{-1} even change in sign when one increases the basis set from 6-31G(d,p) to aug-cc-pVDZ. Here the aug-cc-pVDZ basis set performs much better. This is not unexpected, but shows that the basis set requirements to predict quantitative ROA intensities are higher than those for the Raman intensities. This is similar to the requirement of utilizing a higher quality basis set for VCD spectral intensity calculations than for VA spectral intensity calculations. Hence one is faced with the choice of which basis set one wishes or is required to use for a given spectroscopic property one is interested in, be it just the harmonic frequencies for zero point energy corrections and thermodynamics studies or the VA, VCD, Raman and ROA intensities. If one wishes to have all of these spectra at a relatively high level of accuracy, one is left with the choice of either of the aug-cc-pVDZ or aug-cc-pVTZ basis sets of Dunning. These basis sets appear to the optimal for the combined VA, VCD, Raman and ROA studies.

In Fig. 7 we compare our best combined Raman and ROA spectra, those calculated at the B3LYP/aug-cc-pVDZ level with the experimental Raman and ROA spectra presented by Hecht and Barron [63]. The 6-31G(d,p) basis set is not optimal for calculating the VA, VCD, Raman and ROA spectra. It is a relatively small basis set compared to the complete basis set (CBS) limit, and indeed many people may criticize this basis set as being lacking, but it has been shown to give an adequate accuracy to answer questions in physical

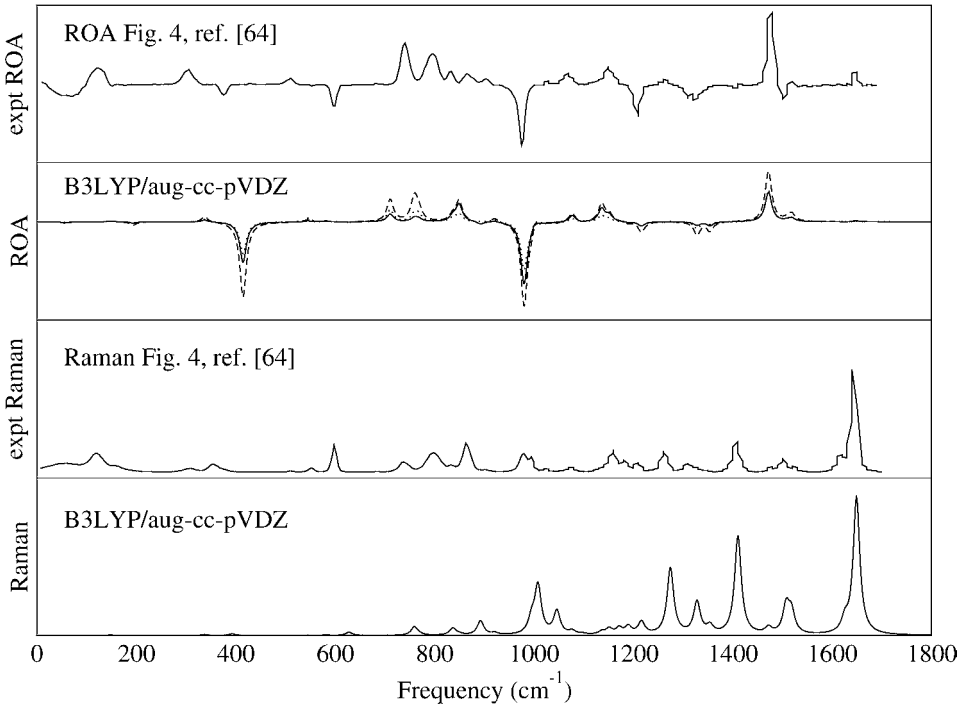

Fig. 7. (R)-Phenyloxirane: Raman spectra for B3LYP/aug-cc-pVDZ; experimental Raman spectra from Hecht *et al.* [64]; ROA1 (CID1), ROA2 (CID2) and ROA3 (CID3) spectra for B3LYP/aug-cc-pVDZ; and experimental ROA spectra from Hecht *et al.* [64].

chemistry, chemical physics, biophysical chemistry and now biophysics by the groups of Polavarapu and Suhai. Hence it is worthwhile to document its accuracy, both quantitatively and visually in comparison to larger basis sets, for example, the aug-cc-pVDZ basis set, which give more accurate values, both for DFT and *ab initio* methods.

The agreement with the experimental data, as extracted from the spectra as anharmonic vibrational frequencies, dipole strengths, rotational strengths and relative integrated peaks in the Raman and ROA experiments is very good with the aug-cc-pVDZ basis set. It increases, however, when one goes to the aug-cc-pVTZ basis set that is seen in Fig. 7 where we compare the Raman and ROA spectra with the experimental Raman and ROA spectra [64] and in Fig. 8 where we compare the VA and VCD spectra with the experimental VA and VCD spectra [10]. The 6-31G(d,p) gives qualitative good results, but can be improved significantly by going to either the aug-cc-pVDZ or aug-cc-pVTZ basis sets. We have only documented the aug-cc-pVTZ basis set for the VA, VCD and Raman spectra. In the future we will also present the ROA spectra for phenyloxirane with the aug-cc-pVTZ basis set and hence document this basis set for reproducing the experimental ROA spectra. But the agreement to date with the aug-cc-pVDZ basis set is excellent, so it should only get better and give us semi-quantitative accuracy of the intensities. To date only the general features in the ROA spectra have been reproduced, which has allowed for stereoisomerical and conformational studies to be undertaken. With higher accuracy calculations and interpre-

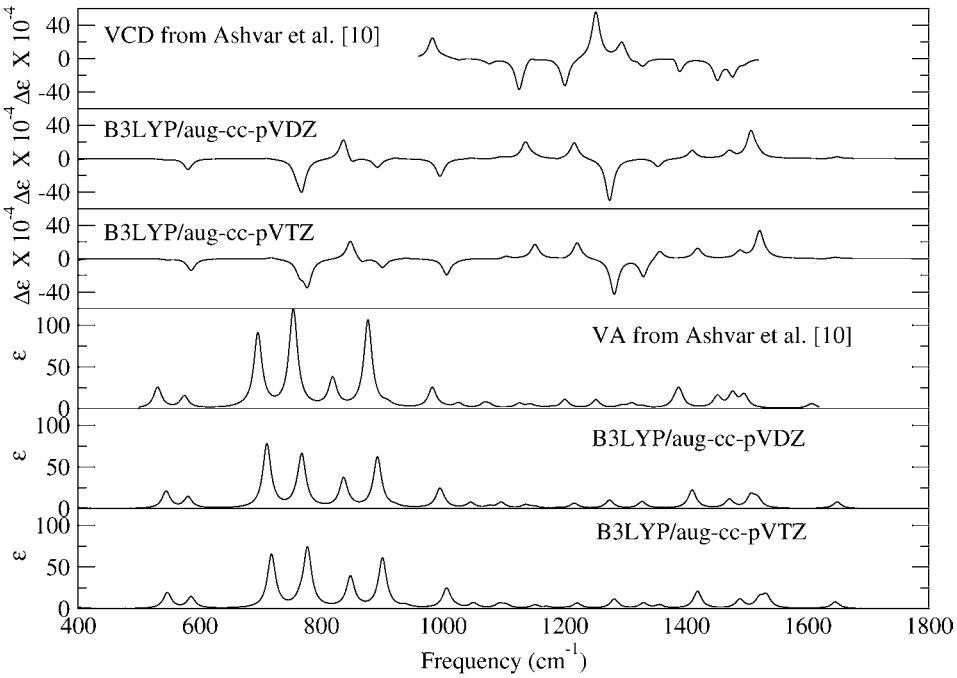

Fig. 8. (R)-Phenyloxirane (RPO): VA spectra for RPO at B3LYP/aug-cc-pVTZ level; VA spectra for RPO at B3LYP/aug-cc-pVDZ level; experimental VA spectra for (S)-Phenyloxirane (SPO) from Ashvar *et al.* [10]; VCD spectra for RPO at B3LYP/aug-cc-pVTZ level; VCD spectra for RPO at B3LYP/aug-cc-pVDZ level; and experimental VCD spectra for SPO from Ashvar *et al.* [10].

tations of Raman and ROA spectra now feasible, more quantitative and detailed questions can hopefully be answered.

Finally in Fig. 7 we compare our B3LYP/aug-cc-pVDZ Raman and ROA simulations with the experimental Raman and ROA spectra extracted from Fig. 4 in Hecht *et al.* [64]. The agreement between the calculated and measured spectra is excellent and the best that we have reported to date. Here we have used the B3LYP level of theory, which Stephens has used and found to give good agreement with the VA and VCD spectra, though with a slightly different basis set.

The aug-cc-pVDZ basis set appears to be able to well reproduce the Raman and ROA spectra, much better than the smaller 6-31G(d,p) that we and other groups have previously used. Finally in Fig. 8 we compare our VA and VCD spectra calculated at the B3LYP/aug-cc-pVXZ, X = D and T, levels with the experimental VA and VCD spectra [10]. Again we see remarkable agreement. These combinations appear to be the best to date and we look forward to further documenting their performance for systems where there has been shown to be strong interactions between the solvent and solute. Previously we did not get optimal agreement in such systems and this may have been due to our use of the relatively small 6-31G(d,p) basis set and the RHF EDMDPD and EDEQPD [60,74,75]. We look forward to reexamining these systems now with the more accurate EDMDPD and EDEQPD. Ad-

ditionally we should look at the effects due to temperature and frequency of the laser used in the Raman and ROA experiments.

The EDMDPD and EDEQPD have not yet been implemented at the XLYP and X3LYP levels of theory, though Stephens and coworkers and recently implemented the EDMDP at the BLYP and B3LYP levels in a development version of Gaussian. These new features are now available in Gaussian 2003 RevC.02, which we have used for our new DFT ROA simulations. In addition, Ruud and Helgaker have recently implemented these tensors at the DFT level in a development version of the Dalton program [119]. We are also in the progress of implementing these tensors using an alternative formulation in a development version of CADPAC. In addition, the XLYP and X3LYP functionals are being implemented as they appear to be the best available functionals for modeling biomolecules, where both H-bonding and dispersion forces are important. In addition, other new functionals must continually be added, especially those which treat van der Waals (dispersion) forces more accurately, charge transfer effects and finally excited electronic states [39,32,128,120,90, 91,55,82,141,107,17,140,45,56,143,96,113,88,147,100,7,8,102]. There has been some recent discussion on how to adequately treat all of these effects self consistently, but to date there is no general consensus in the different communities [101,58,158,157,144,152,25, 153,135,121,42,70,154,41,31,49,40,71,118].

The EDMDP tensors have also been used to calculate the optical rotation spectra [29,13,59]. In addition, recently solvent effects have also been taken into effect via a continuum model [103]. Hence this is a good start in the continuum solvent approach to optical rotation spectra, which can also be applied to ROA simulations.

Alternative formulation of the EDMDP tensors utilizing current density functional theory [93,34,94,92,145] as an alternative to the recently implemented formulation by Stephens, Frisch and Cheeseman [29] and Bak, Rudd, Jørgensen, Olsen and Helgaker [67,119] would be similar to the alternative formulations of the AAT. In addition, the newly derived functionals that treat dispersion and H-bonding better than the BLYP and B3LYP are also expected to better Raman and ROA intensities. In addition, the dynamic polarizabilities, which can be calculated by TD-DFT should also improve the accuracy, especially as one approaches an electronic transition, where the static limit should no longer be valid. It is surprising how good the agreement has been using the simple static limit for the EDEDPD, EDMDPD and EDEQPD. We are presently investigating the frequency dependence of the ROA spectra as a function of the exciting laser wavelength, both far from resonance with electronic transitions, then near resonance and finally resonance ROA. This has applications for the near or resonance enhanced Raman and ROA for aromatic amino acids, phenylalanine, tryptophan and tyrosine. It would be nice to take into account the interaction with surfaces, as the phenomenon of surface enhanced Raman scattering and the analogous phenomenon surfaced enhanced Raman optical activity are areas of interest in our group. Here modeling studies could greatly add to the physical understanding of these phenomenon. To date, the interpretation of the spectra and spectral changes have limited the application of these phenomenon.

These four vibrational spectroscopies, VA, VCD, Raman and ROA, have now reached the stage experimentally and theoretically where they can all be measured routinely in the spectroscopy laboratory and simulated in the quantum theory laboratory. These spectroscopies now can be used along with NMR and X-ray crystallography to answer questions and pose new experiments that should greatly add to our understanding.

4. DISCUSSION

To make measurements on individual molecules requires specialized experimental techniques able to measure the response of either individual or small numbers of molecules. The microwave, infrared or vibrational absorption, and Raman spectra of molecules in the gas phase are the two most common techniques to get structural and functional group information. Another technique is to isolate the molecules in an inert low temperature matrix, for example, Ar or N_2, to perform VA, VCD, Raman, ROA, UV-Vis, ECD, and EPR spectra [125]. Here one is interested in understanding the properties of the individual molecules and also the forces responsible for the stabilization of the low energy conformers. Such data are invaluable to theoreticians who want to benchmark their levels of theory. The bond lengths, valence angles, torsional angles and dipole moments can be determined from microwave studies. From the VA, VCD, Raman and ROA spectra one can get the vibrational frequencies and information about how the electric dipole, magnetic dipole, the EDEDP, the EDMDP, and the EDEQP change with changes in nuclear coordinates. The problem is that normally one does not have enough experimental data to completely determine these quantities. Hence theoretical models are needed to even interpret the experimental data measured, hence the real synergistic relationship between theory and experiment.

From the ECD, VCD and ROA spectra we can get information on the chirality of a molecule [65]. For a molecule with conformational flexibility, one can get conformational data. In addition to gas phase and low temperature matrix measurements, one can in many cases also make measurements on molecules in nonpolar solvents or embedded in micelles. If one can overcome the problem of solubility one can also make measurements of the VA, VCD, Raman, ROA, NMR, EPR, UV-Vis and ECD spectra of molecules. The information is the same for the gas phase as for a low temperature matrix, but the line widths of the spectral features can broaden, so one has in many cases an assignment and deconvolution problem. Here one is aided by theoretical calculations of the spectra for these molecules. In all of the above cases the spectral simulations are relatively straightforward as one must not in general treat the environment explicitly. The assumption is that the nonpolar environment or inert matrix does not greatly perturb the molecule and therefore its properties, or at least one assumes that it does not.

5. CONCLUSIONS AND FUTURE PERSPECTIVES

In this work we have attempted to use the current developments in quantum chemistry to interpret the Raman and ROA spectra of phenyloxirane, one of the first measurements made with right-angle scattering ROA. At the time of these measurement in 1994, the size of the molecule did not allow for a complete high level density functional analysis. With the recent developments in quantum chemistry by the groups developing CADPAC (R.D. Amos, J. Rice, D.J. Tozer and N. Handy), Gaussian (Michael Frisch and J.R. Cheeseman) and Dalton (K. Bak, P. Jørgensen, T. Helgaker, J. Olson and K. Rudd), the interpretation of the VA, VCD, Raman and ROA spectra can now be routinely calculated. With the availability of FTIR VCD instruments by Thermo Electron, Bruker and Bomen and Raman and ROA by Biotools, these spectroscopies can now be used to routinely answer structural and functional groups questions on systems where X-ray crystallography and NMR have not been

able to. In addition, the fast time scale for these spectroscopies allows us to make measurements that are the superposition of the components and not the average. The possible applications for these spectroscopies lie only within the imaginations of the groups working in the field. Future developments that are required are the analytical implementation of the EDMDPD and EDEQPD at the DFT level with a linear scaling algorithm, similar to the currently implemented methods by the SIESTA and SCC-DFTB developed in Barcelona and Heidelberg/Paderborn/Georgia [117,150,149,46,47,61,27,48,44,50,122,106].

In addition, the treatment of the solvent has recently been shown to be very important in stabilizing the zwitterionic species of L-alanine [137] and L-alanyl-alanine [87] and in also producing a conformer for NALANMA that is not found in the gas phase (isolated state) or by using continuum models [80,38,60]. Hence the treatment of explicit solvent water molecules that are directly H-bonded with the polar groups of proteins and, which stabilize the charge via solvation on charged species must be taken into account. Therefore, the determination of the structure and at the optimized structure of the complex, the Hessian is a more difficult problem than originally thought.

The treatment of the second hydration shell and bulk water can probably be treated with the continuum models, so this work was and is by no means not important and unnecessary. On the contrary it is very important and hybrid solvent models may become the best way to treat the solvent effects as do the hybrid exchange correlations functional seem to be the best way at present to treat dispersion effects, H-bonding and the hydrophobic effects (other weak interactions) that have not been adequately treated.

In addition, charge transfer effects may also be important and the recently developed CAM-LYP and CAM-3LYP density functional may be they way we treat these charge transfer effects until more refined methods are developed [158]. In addition, if one wishes to take temperature into account, the QM/MM-MD method can be used. Here as the linear scaling methods are extended so that all of the properties can be calculated at each step of the MD run, then one can foresee being able to simulate the VA, VCD, Raman and ROA spectra by doing the required time to frequency transformations. One will automatically get the required anharmonic effects, which are currently missing in addition to the effects of temperature. It is very important to treat the solvent in an accurate way, which means simple charge models for the first solvation shell waters will not be accurate enough as they will miss the directionality present in H-bonding as shown by the group of Buckingham. The lone pairs have been shown to be very important to get the tetrahedral H-bonding structure. So the present state of quantum chemistry is undergoing a revival with respect to explicit solvent treatment. Here the simple basis set superposition error (BSSE) treatment of dimers and trimers will be exacerbated by having to treat many more water molecules in the molecular complexes. Here there is also plenty of room for new methods and new ways to accurately calculate binding energies, solvation energies and free energies, the hydrophobic effect and even the dynamic structures that are present in the various experiments, be they vibrational, NMR, EPR or X-ray or neutron or electron diffraction measurements. The need for quantum chemists to be able to help interpret the wealth of new and interesting experimental data was never so needed and so fruitful.

ACKNOWLEDGEMENTS

KJJ would like to thank the Danish National Research Foundation and the Quantum Protein (QuP) Center for his salary as an associate professor (lector) at QuP during the 5 year

funding period of QuP (2001–2006). In addition, we would like to thank Prof. Nick Handy and Roger D. Amos for providing a copy of CADPAC, which allows one to calculate the required tensors to simulate the ROA spectra. VWJ would like to thank the Danish National Research Foundation and QuP for her PhD scholarship. Finally we would like to thank the kind referee of the first version of this manuscript for his/her many thoughtful and critical comments, which have helped us make this a much nicer manuscript.

REFERENCES

[1] R.D. Amos, *Chem. Phys. Lett.* **87** (1982) 23.
[2] R.D. Amos, *Chem. Phys. Lett.* **108** (1984) 185.
[3] R.D. Amos, *Chem. Phys. Lett.* **124** (1986) 376.
[4] R.D. Amos, N.C. Handy, K.J. Jalkanen, P.J. Stephens, *Chem. Phys. Lett.* **133** (1987) 21.
[5] R.D. Amos, K.J. Jalkanen, P.J. Stephens, *J. Phys. Chem.* **92** (1988) 5571.
[6] R.D. Amos, J.E. Rice, *Cambridge Analytical Derivatives Package (CADPAC)*, 5.2 edition, Cambridge Univ. Press, Cambridge, UK, 1994.
[7] Y. Andersson, E. Hult, P. Apell, D.C. Langreth, B.I. Lundqvist, *Solid State Comm.* **106** (1998) 235.
[8] Y. Andersson, D.C. Langreth, B.I. Lundqvist, *Phys. Rev. Lett.* **76** (1996) 102.
[9] C.S. Ashvar, F.J. Devlin, K.L. Bak, P.R. Taylor, P.J. Stephens, *J. Phys. Chem.* **100** (1996) 9262.
[10] C.S. Ashvar, F.J. Devlin, P.J. Stephens, *J. Am. Chem. Soc.* **121** (1999) 2836.
[11] C.S. Ashvar, F.J. Devlin, P.J. Stephens, K.L. Bak, T. Eggimann, H. Wieser, *J. Phys. Chem. A* **102** (1998) 6842.
[12] C.S. Ashvar, P.J. Stephens, T. Eggimann, H. Wieser, *Tetrahedron: Asymmetry* **9** (1998) 1107.
[13] J. Autschbach, S. Patchkovskii, T. Ziegler, S.J.A. van Gisbergen, E.J. Baerends, *J. Chem. Phys.* **117** (2002) 581.
[14] K.L. Bak, F.J. Devlin, C.S. Ashvar, P.R. Taylor, M.J. Frisch, P.J. Stephens, *J. Phys. Chem.* **99** (1995) 14918.
[15] K.L. Bak, P. Jørgensen, T. Helgaker, K. Ruud, H.J.Aa. Jensen, *J. Chem. Phys.* **98** (1993) 8873.
[16] K.L. Bak, P. Jørgensen, T. Helgaker, K. Ruud, H.J.Aa. Jensen, *J. Chem. Phys.* **100** (1994) 6621.
[17] A. Banerjee, M.K. Karbola, *J. Chem. Phys.* **117** (2002) 7845.
[18] L.D. Barron, M.P. Bogaard, A.D. Buckingham, *J. Am. Chem. Soc.* **95** (1973) 603.
[19] L.D. Barron, A.D. Buckingham, *Mol. Phys.* **20** (1971) 1111.
[20] L.D. Barron, A.D. Buckingham, *Annu. Rev. Phys. Chem.* **26** (1975) 381.
[21] L.D. Barron, A.R. Gargaro, L. Hecht, P.L. Polavarapu, *Spectrochim Acta A* **47** (1991) 1001.
[22] L.D. Barron, L. Hecht, E.W. Blanch, A.F. Bell, *Progr. Biophys. Molecular Biol.* **117** (2000) 1.
[23] A.D. Becke, *Phys. Rev. A* **38** (1988) 3098.
[24] A.D. Becke, *J. Chem. Phys.* **104** (1996) 1040.
[25] A.D. Becke, *J. Chem. Phys.* **119** (2003) 2972.
[26] H. Berman, K. Henrick, H. Nakamura, *Nature Structural Biol.* **10** (2003) 980.
[27] H.G. Bohr, K.J. Jalkanen, K. Frimand, M. Elstner, S. Suhai, *Chem. Phys.* **246** (1999) 13.
[28] A.D. Buckingham, P.W. Fowler, P.A. Galwas, *Chem. Phys.* **112** (1987) 1.
[29] J.R. Cheeseman, M.J. Frisch, F.J. Devlin, P.J. Stephens, *J. Phys. Chem. A* **104** (2000) 1039.
[30] J.R. Cheeseman, M.J. Frisch, F.J. Devlin, P.J. Stephens, *Chem. Phys. Lett.* **252** (1996) 211.
[31] T.C. Choy, *Phys. Rev. A* **62** (2000) 012506.
[32] X. Chu, A. Dalgarno, *J. Chem. Phys.* **121** (2004) 4083.
[33] T. Clark, J. Chandrasekhar, G.W. Spitznagel, P.v.R. Schleyer, *J. Comp. Chem.* **4** (1983) 294.
[34] S.M. Colwell, N.C. Handy, A.M. Lee, *Phys. Rev. A* **53** (1996) 1316.
[35] D.P. Craig, T. Thirunamachandran, *Mol. Phys.* **35** (1978) 825.
[36] M.P. de Lara-Castells, R.V. Krems, A.A. Buchachenko, G. Delgado-Barrio, P. Villarreal, *J. Chem. Phys.* **115** (2001) 10438.
[37] I.M. Degtyarenko, PhD thesis, Helsinki University of Technology, 2006 expected.
[38] Z. Deng, P.L. Polavarapu, S.J. Ford, L. Hecht, L.D. Barron, C.S. Ewig, K.J. Jalkanen, *J. Phys. Chem.* **100** (1996) 2025.
[39] M. Dion, H. Rydberg, E. Schroeder, D.C. Langreth, B.I. Lundqvist, *Phys. Rev. L* **92** (2004) 246401.

[40] J.F. Dobson, J. Wang, *Phys. Rev. Lett.* **82** (1999) 2123.
[41] J.F. Dobson, J. Wang, *Phys. Rev. B* **62** (2000) 10038.
[42] J.F. Dobson, J. Wang, T. Gould, *Phys. Rev. B* **66** (2002) 081108.
[43] T.H. Dunning Jr., *J. Chem. Phys.* **90** (1989) 1007.
[44] M. Elstner, Weiterentwichlung quantenmechanischer Rechenverfahren fuer organische Molekuele und Polymere, Ph.D. thesis, Universitaet-Gesamthochschule Paderborn, Paderborn, Deutschland, April 1998.
[45] M. Elstner, P. Hobza, S. Suhai, E. Kaxiras, *J. Chem. Phys.* **114** (2001) 5149.
[46] M. Elstner, K.J. Jalkanen, M. Knapp-Mohammady, Th. Frauenheim, S. Suhai, *Chem. Phys.* **263** (2001) 203.
[47] M. Elstner, K.J. Jalkanen, M. Knapp-Mohammady, Th. Frauenheim, S. Suhai, *Chem. Phys.* **256** (2000) 15.
[48] M. Elstner, D. Porezag, G. Jungnickel, J. Elsner, M. Haugk, Th. Frauenheim, S. Suhai, G. Seifert, *Phys. Rev. B* **58** (1998) 7260.
[49] E. Engel, A. Höck, R.M. Dreizler, *Phys. Rev. A* **61** (2000) 032502.
[50] M.V. Fernandex-Serra, J. Junquera, C. Jelsch, E. Artacho, *Solid State Comm.* **16** (2000) 395.
[51] K. Frimand, K.J. Jalkanen, *Chem. Phys.* **279** (2002) 161.
[52] K. Frimand, K.J. Jalkanen, H.G. Bohr, S. Suhai, *Chem. Phys.* **255** (2000) 165.
[53] M.J. Frisch, J.A. Pople, J.S. Binkley, *J. Chem. Phys.* **80** (1984) 3265.
[54] M.J. Frisch, G.W. Trucks, H.B. Schlegel, G.E. Scuseria, M.A. Robb, J.R. Cheeseman, J.A. Pople, *Gaussian 03, Revision C.02*, Gaussian Inc., Pittsburg, PA 15106, 2003.
[55] M. Fuchs, X. Gonze, *Phys. Rev. B* **65** (2002) 235109.
[56] A. Goerling, H.H. Heinze, M. Levy, *J. Mol. Struct. (Theochem)* **501–502** (2000) 271.
[57] L.A. Gribov, W.J. Orville-Thomas, Theory of intensities in the Raman spectra of polyatomic molecules, in: *Theory and Methods of Calculation of Molecular Spectra*, John Wiley and Sons, New York, 1988, pp. 563–595.
[58] S. Grimme, *J. Comput. Chem.* **25** (2004) 1463.
[59] S. Grimme, F. Furche, R. Ahlrichs, *Chem. Phys. Lett.* **361** (2002) 321.
[60] W.-G. Han, K.J. Jalkanen, M. Elstner, S. Suhai, *J. Phys. Chem. B* **102** (1998) 2587.
[61] W.-G. Han, M. Elstner, K.J. Jalkanen, Th. Frauenheim, S. Suhai, *Int. J. Quantum Chem.* **78** (2000) 459.
[62] A.E. Hansen, P.J. Stephens, T.D. Bouman, *J. Phys. Chem.* **95** (1991) 4255.
[63] L. Hecht, L.D. Barron, J. Raman, *Spectrosc.* **25** (1994) 443.
[64] L. Hecht, L.D. Barron, *J. Mol. Struct.* **347** (1995) 449.
[65] L. Hecht, A.L. Phillips, L.D. Barron, *J. Raman Spectrosc.* **26** (1995) 727.
[66] W.J. Hehre, R. Ditchfield, J.A. Pople, *J. Chem. Phys.* **56** (1972) 2257.
[67] T. Helgaker, K. Ruud, K.L. Bak, P. Jørgensen, J. Olsen, *Faraday Discuss.* **99** (1994) 165.
[68] G. Holzwarth, E.C. Hsu, H.S. Mosher, T.R. Faulkner, A. Moscowitz, *J. Am. Chem. Soc.* **96** (1974) 251.
[69] E.C. Hsu, G. Holzwarth, *J. Chem. Phys.* **59** (1973) 4678.
[70] E. Hult, P. Hyldgaard, J. Rossmeisl, B.I. Lundqvist, *Phys. Rev. B* **64** (2001) 195414.
[71] E. Hult, H. Rydberg, B.I. Lundqvist, *Phys. Rev. B* **59** (1999) 4708.
[72] K.J. Jalkanen, Vibrational absorption, vibrational circular dichroism and magnetic susceptibilities, Ph.D. thesis, University of Southern California, Los Angeles, CA, USA, 1989.
[73] K.J. Jalkanen, M. Elstner, S. Suhai, *J. Mol. Struct. (Theochem)* **675** (2004) 61.
[74] K.J. Jalkanen, R.M. Nieminen, K. Frimand, J. Bohr, H.G. Bohr, R.C. Wade, E. Tajkhorshid, S. Suhai, *Chem. Phys.* **265** (2001) 125.
[75] K.J. Jalkanen, R.M. Nieminen, M. Knapp-Mohammady, S. Suhai, *Int. J. Quantum Chem.* **92** (2003) 239.
[76] K.J. Jalkanen, P.J. Stephens, *J. Phys. Chem.* **95** (1991) 5446.
[77] K.J. Jalkanen, P.J. Stephens, R.D. Amos, N.C. Handy, *Chem. Phys. Lett.* **142** (1987) 153.
[78] K.J. Jalkanen, P.J. Stephens, R.D. Amos, N.C. Handy, *J. Phys. Chem.* **92** (1988) 1781.
[79] K.J. Jalkanen, P.J. Stephens, P. Lazzeretti, R. Zanasi, *J. Chem. Phys.* **90** (1988) 3204.
[80] K.J. Jalkanen, S. Suhai, *Chem. Phys.* **208** (1996) 81.
[81] B.G. Johnson, J. Florian, *Chem. Phys. Lett.* **247** (1995) 120.
[82] M. Kamiya, T. Tsuneda, K. Hirao, *J. Chem. Phys.* **117** (2002) 6010.
[83] R.W. Kawiecki, F.J. Devlin, P.J. Stephens, R.D. Amos, *J. Phys. Chem.* **95** (1991) 9817.
[84] T.A. Keiderling, Protein structural studies using vibrational circular dichroism spectroscopy, in: *Spectroscopic Methods For Determining Protein Structure in Solution*, VCH Publishers Inc., 69451 Weinheim, Germany, 1996, pp. 163–189.
[85] T.A. Keiderling, *Curr. Opin. Chem. Biol.* **6** (2002) 682.

[86] R.A. Kendall, T.H. Dunning Jr., R.J. Harrison, *J. Chem. Phys.* **96** (1992) 6796.
[87] M. Knapp-Mohammady, K.J. Jalkanen, F. Nardi, R.C. Wade, S. Suhai, *Chem. Phys.* **240** (1999) 63.
[88] W. Kohn, Y. Meir, D.E. Makarov, *Phys. Rev. Lett.* **80** (1998) 4153.
[89] A. Komornicki, J.W. McIver, *J. Chem. Phys.* **70** (1979) 2014.
[90] N. Kurita, H. Inoue, H. Sekino, *Chem. Phys. Lett.* **370** (2003) 161.
[91] N. Kurita, H. Sekino, *Int. J. Quantum Chem.* **91** (2003) 355.
[92] A.M. Lee, S.M. Colwell, N.C. Handy, *Chem. Phys. Lett.* **229** (1994) 225.
[93] A.M. Lee, N.C. Handy, *Phys. Rev. A* **59** (1999) 209.
[94] A.M. Lee, N.C. Handy, S.M. Colwell, *J. Chem. Phys.* **103** (1995) 10095.
[95] C. Lee, W. Yang, R.G. Parr, *Phys. Rev. B* **37** (1988) 785.
[96] M. Lein, J.F. Dobson, E.K.U. Gross, *J. Comp. Chem.* **20** (1999) 12.
[97] D.A. Long, *Raman Spectroscopy*, McGraw-Hill, New York, 1977.
[98] R.C. Lord, *Appl. Spectrosc.* **31** (1977) 187.
[99] O. Lund, K. Frimand, J. Gorodkin, H.G. Bohr, J. Bohr, J. Hansen, S. Brunak, *Protein Eng.* **10** (1997) 1241.
[100] B.I. Lundqvist, E. Hult, H. Rydberg, A. Bogicevic, J. Strömquist, D.C. Langreth, *Progr. Surf. Sci.* **59** (1998) 149.
[101] R.J. Magyar, A. Fleszar, E.K.U. Gross, *Phys. Rev. B* **69** (2004) 045111.
[102] F. Mele, T. Mineva, N. Russo, M. Toscano, *Theor. Chim Acta* **91** (1995) 169.
[103] R. Mennucci, J. Tomasi, R. Cammi, J.R. Cheeseman, M.J. Frisch, F.J. Devlin, S. Gabriel, P.J. Stephens, *J. Phys. Chem. A* **106** (2002) 6102.
[104] M.G. Mulkerrin, Protein structure analysis using circular dichroism, in: *Spectroscopic Methods for Proteins in Solution*, VCH Publishers Inc., 69451 Weinheim, Germany, 1996, pp. 5–27.
[105] P. Ordejon, E. Artacho, J.M. Soler, *Phys. Rev. B (Rapid Comm.)* **53** (1996) R10441.
[106] P. Ordejon, E. Artacho, J.M. Soler, The SIESTA method for linear scaling *ab initio* simulations, *PHI-K Newsletter* **53** (1996) 134.
[107] M.D. Patey, C.E.H. Dessent, *J. Phys. Chem. A* **106** (2002) 4623.
[108] J.P. Perdew, *Electronic Structure Theory of Solids*, Akademie Verlag, Berlin, 1991, p. 11.
[109] J.P. Perdew, K. Burke, M. Ernyerhoh, *Phys. Rev. Lett.* **77** (1996) 3865.
[110] J.P. Perdew, K. Burke, M. Ernyerhoh, *Phys. Rev. Lett.* **78** (1997) 1396.
[111] J.P. Perdew, J.A. Chevary, S.H. Vosko, K.A. Jackson, M.R. Pederson, D.J. Singh, C. Fiolhais, *Phys. Rev. B* **46** (1992) 6671.
[112] J.P. Perdew, J.A. Chevary, S.H. Vosko, K.A. Jackson, M.R. Pederson, D.J. Singh, C. Fiolhais, *Phys. Rev. B* **48** (1993) 4978.
[113] J.M. Perez-Jorda, E. San-Fabian, A.J. Perez-Jimenez, *J. Chem. Phys.* **110** (1999) 1916.
[114] W. Person, G. Zerbi, *Vibrational Intensities in Infrared and Raman Spectroscopy*, Elsevier, Amsterdam, 1982.
[115] K.A. Peterson, D.W. Woon, T.H. Dunning Jr., *J. Chem. Phys.* **100** (1994) 7410.
[116] P.L. Polavarapu, *J. Phys. Chem.* **94** (1990) 8106.
[117] J. Pu, J. Gao, D.G. Truhlar, *J. Phys. Chem. A* **108** (2004) 5454.
[118] E. Runge, E.K.U. Gross, *Phys. Rev. Lett.* **52** (1984) 997.
[119] K. Ruud, T. Helgaker, P. Bour, *J. Phys. Chem. A* **106** (2002) 7448.
[120] H. Rydberg, M. Dion, N. Jacobson, E. Schroeder, P. Hyldgaard, S.I. Simak, D.C. Langreth, B.I. Lundqvist, *Phys. Rev. Lett.* **91** (2003) 126402.
[121] P. Salek, O. Vahtras, T. Helgaker, H. Ågren, *J. Chem. Phys.* **117** (2002) 9630.
[122] D. Sanchez-Portal, P. Ordejon, E. Artacho, J.M. Soler, *Int. J. Quantum Chem.* **65** (1997) 453.
[123] O.F. Sankey, D.J. Niklewski, *Phys. Rev. B* **40** (1989) 3979.
[124] O.F. Sankey, D.J. Niklewski, D.A. Drabold, J.D. Dow, *Phys. Rev. B* **41** (1990) 12750.
[125] D.W. Schlosser, F.J. Devlin, K.J. Jalkanen, P.J. Stephens, *Chem. Phys. Lett.* **88** (1982) 286.
[126] J.C. Slater, *Phys. Rev.* **81** (1951) 385.
[127] J.M. Soler, E. Artacho, J.D. Gale, A. Garcia, J. Junquera, P. Ordejon, D. Sanchez-Portal, *J. Phys.: Condens. Matter* **14** (2002) 2745.
[128] F. Sottile, V. Olevano, L. Reining, *Phys. Rev. Lett.* **91** (2003) 056402.
[129] V.N. Staroverov, G.E. Scuseria, J. Tao, J.P. Perdew, *J. Chem. Phys.* **1190** (2003) 12129.
[130] P.J. Stephens, *J. Phys. Chem.* **89** (1985) 748.
[131] P.J. Stephens, *J. Phys. Chem.* **91** (1987) 1712.
[132] P.J. Stephens, C. Chabalowski, F.J. Devlin, K.J. Jalkanen, *Chem. Phys. Lett.* **225** (1994) 247.

[133] P.J. Stephens, K.J. Jalkanen, R.D. Amos, P. Lazzeretti, R. Zanasi, *J. Phys. Chem.* **94** (1990) 1811.
[134] P.J. Stephens, M.A. Lowe, *Annu. Rev. Phys. Chem.* **36** (1985) 213.
[135] V. Subramanian, D. Sivanesan, J. Padmanabhan, N. Lakshiminarayanan, T. Ramasami, *Proc. Indian Acad. Sci. (Chem. Sci.)* **111** (1999) 369.
[136] W.K. Surewicz, H.M. Mantsch, Infrared absorption methods for examining protein structure, in: *Spectroscopic Methods for Proteins in Solution*, VCH Publishers Inc., 69451 Weinheim, Germany, 1996, pp. 135–162.
[137] E. Tajkhorshid, K.J. Jalkanen, S. Suhai, *J. Phys. Chem. B* **102** (1998) 5899.
[138] L.G. Tensyeyer, E.W. Kauffman III, Protein structure as revealed by nonresonance Raman spectroscopy, in: *Spectroscopic Methods for Proteins in Solution*, VCH Publishers Inc., 69451 Weinheim, Germany, 1996, pp. 69–95.
[139] N. Troullier, J.L. Martins, *Phys. Rev. B* **43** (1991) 1993.
[140] S. Tsuzuki, H.P. Lüthi, *J. Chem. Phys.* **114** (2001) 3949.
[141] T. van Mourik, R.J. Gdanitz, *J. Chem. Phys.* **116** (2002) 9620.
[142] T. van Mourik, A.K. Wilson, T.H. Dunning Jr., *Mol. Phys.* **96** (1999) 529.
[143] P. van Remoortere, J.E. Mertz, L.E. Scriven, H.T. Davis, *J. Chem. Phys.* **110** (1999) 2621.
[144] I. Vasiliev, R.M. Martin, *Phys. Rev. A* **69** (2004) 052508.
[145] G. Vignale, M. Rasolt, D.J.W. Geldart, *Adv. Quantum Chem.* **21** (1990) 235.
[146] S.H. Vosko, L. Wilk, M. Nusair, *Cand. J. Phys.* **58** (1980) 1200.
[147] T.A. Wesolowski, Y. Ellinger, J. Weber, *J. Chem. Phys.* **108** (1998) 6078.
[148] A.K. Wilson, T. van Mourik, T.H. Dunning Jr., *J. Mol. Struct. (Theochem)* **288** (1996) 339.
[149] H.A. Witek, S. Irle, K. Morokuma, *J. Chem. Phys.* **121** (2004) 5163.
[150] H.A. Witek, K. Morokuma, *J. Comp. Chem.* **25** (2004) 1858.
[151] D.E. Woon, T.H. Dunning Jr., *J. Chem. Phys.* **100** (1994) 2975.
[152] Q. Wu, P.W. Ayers, W. Yang, *J. Chem. Phys.* **119** (2003) 2978.
[153] Q. Wu, W. Yang, *J. Chem. Phys.* **116** (2002) 515.
[154] X. Wu, M.C. Vargas, S. Nayak, V. Lotrich, G. Scoles, *J. Chem. Phys.* **115** (2001) 8748.
[155] X. Xu, W.A. Goddard III, *J. Phys. Chem. A* **108** (2004) 2305.
[156] X. Xu, W.A. Goddard III, *Proc. Natl. Acad. Sci.* **101** (2004) 2673.
[157] T. Yanai, D.P. Tew, N.C. Handy, *Chem. Phys. Lett.* **393** (2004) 51.
[158] T. Yanai, D.P. Tew, N.C. Handy, A new hydrid exchange-functional using the Coulomb-Attenuating Method (CAM-B3LYP). Response theory and molecular properties, Sønderborg, Denmark, May 2004.
[159] G.-S. Yu, T.B. Freedman, L.A. Nafie, T. Deng, P.L. Polavarapu, *J. Phys. Chem.* **99** (1995) 835.
[160] Y. Zhao, D.G. Truhlar, *J. Phys. Chem. A* **108** (2004) 6908.
[161] B.A. Zilles, W.B. Person, *J. Chem. Phys.* **79** (1983) 65.

A Theoretical Model to Calculate Fundamental Physical Parameters for Molecule–Particle Interactions

Allan Gross[1] and Kurt V. Mikkelsen[2]

[1]*Meteorological Research Division, Danish Meteorological Institute, Lyngbyvej 100, DK-2100 Copenhagen Ø, Denmark*
E-mail: agr@dmi.dk
[2]*Department of Chemistry, H.C. Ørsted Institute, University of Copenhagen, DK-2100 Copenhagen Ø, Denmark*
E-mail: kmi@theory.ki.ku.dk

Contents

1. INTRODUCTION

Aerosol particles have an important influence on the atmospheric radiation balance, cloud formation etc. To model mass and heat transfer to and from atmospheric particles it is essential to know what happens to a gas molecule when it encounters the surface of a particle [1]. On a macroscopic level the so-called sticking probabilities/mass accommodation coefficients are used to model evaporation, condensation and heterogeneous chemistry in the atmosphere.

The sticking probability has proven to be an important parameter for prediction of climate parameters such as the concentration of cloud condensation nuclei. For example Pandis *et al.* [2] showed that changing the accommodation coefficient for sulphuric acid from 0.02 to 0.05 in their nucleation and growth model for aerosols in the marine boundary layer reduced the calculated concentration of cloud condensation nuclei by 45%.

ADVANCES IN QUANTUM CHEMISTRY, VOLUME 50
ISSN: 0065-3276 DOI: 10.1016/S0065-3276(05)50007-8

Clement *et al*. [3] have analyzed experimental data and proposed a simple model that describes the interaction as a two-body collision in which energy and momentum are exchanged. This model generally predicts sticking probabilities close to one. In accordance with this work along with the work by Kulmala and Wagner [4] the following suggestion have been made: use sticking probabilities of one if no other experimentally verified information is available.

The problems associated with the understanding and estimation of the probability of adsorption and condensation of a molecule approaching an aerosol particle have been clearly demonstrated in the work presented in Refs. [2,3,5–11]. The theoretical approaches range from total phenomenological approaches to microscopic molecular models [2,3,5–11]. The phenomenological approaches utilize thermodynamic arguments for evaluating the energy terms that enter the macroscopic expression for the transition state theory rate constant of the uptake process [5,6]. Another view within the phenomenological methods is the one based on purely statistical models for the nucleation of aerosols. Generally, it is clear that these models do not utilize or provide a molecular understanding of the considered processes. A fair number of models exists for describing the interactions of a spherical and classical particle scattering off a plane, isotropic, homogeneous surface. These models do not include any molecular detail and will never be able to differentiate among different molecules, except on a basis of size and mass [3]. On the other hand, the microscopic models cover methods where a small number of molecules interact with the approaching molecule. These models enable a molecular understanding of the changes in the structures and properties of the approaching molecule. Unfortunately, the very small number of molecules included in the models renders these approaches insufficient with respect to an appropriate description of the bulk properties of the aerosol particle [8–10]. The number of models that utilize a bulk description of the aerosol particle and a quantum mechanical method for the approaching molecule is limited.

The above considerations suggest that there is a need for microscopic models to provide an understanding of the interactions between gas molecules and atmospheric particles on the molecular level.

Atmospheric gas-phase species can nucleate to form aerosol particles, influence the growth of aerosol particles and the chemical composition of aerosol particles. Therefore, in order to model heterogeneous chemistry/aerosol dynamics it is important to known

1. absorption rate constants,
2. desorption rate constants,
3. sticking coefficients, and
4. surface reaction coefficients (if the gas-phase molecule is able to react on the surface of the aerosol)

of the molecule impinging on the aerosol particle. In Section 1.1 a general description of the interactions between a molecule or atom and an Aerosol Particle/surface (AP) is given, and the general equations describing these quantities are derived. Even though it is rather simple to setup these general equations it is not trivial to estimate the sticking coefficient. This paper will describe how the absorption, desorption and surface reaction rate constants can be calculated using statistical mechanics, and a new model to calculate sticking coefficients will be presented. This model is a QuantuM-STatistical (QM-ST) model based on statistical mechanics and phase-space theory. The QM-ST model can also be used to calcu-

late the same parameters for N-Atomic Molecules (NAMs) colliding with cloud droplets and with small modifications for an NAM interacting with a surface.

A theoretical description of an atomic or molecular system colliding with an aerosol particle involves the following six cases: an atom, a di-atomic molecule, a linear tri-atomic molecule, a spherical top molecule, a symmetric top molecule or an asymmetric top molecule colliding with an Aerosol Particle (AP). For simplicity we will in this paper only describe the case where the symmetry of the colliding NAM is asymmetric since it is relatively easy to revise the equations for the asymmetric case to cases where the N-atomic molecule belongs to a symmetry point group of higher symmetry. In Section 2 the new model to calculate sticking coefficients is reviewed. The new model is tested on three NAM–AP systems:

1. H_2/Pd(100) (Section 3.1),
2. CO/Cu(111) (Section 3.2), and
3. CH_3OH/H_2O_l (Section 3.3).

In Sections 3 and 4 the results for these three NAM–AP systems are presented and discussed.

1.1. Interaction between an N-atomic molecule and an aerosol particle

The interaction between a molecule or atom and a liquid or solid AP can be treated almost similar to the interaction between a NAM and a surface. Therefore a NAM–AP interaction can usually be divided into the following elementary steps:

1. diffusion of the molecule to the AP,
2. adsorption of the molecule at the AP,
3. chemical reaction on the AP,
4. desorption of products from the AP, and
5. diffusion of products away from the AP.

In general, steps one and five are rapid. The rate determining steps are two, three and four. An N-atomic molecule can be attached to aerosols by physisorption and chemisorption. In physisorption the molecule is kept on the aerosol by van der Waals interactions and electrostatic interactions. In chemisorption the molecules stick to the aerosol by forming a chemical bond. The adsorption of the molecule at the aerosol can be divided into three cases:

1. As the NAM approaches the AP, its energy drops and it becomes physisorbed, *i.e.*, a non-reactive gas (A_g) is adsorbed on the AP:

$$A_g \underset{k_{des}}{\overset{k_{ads}}{\rightleftharpoons}} A_{AP} \tag{1}$$

   k_{ads} and k_{des} are the adsorption and desorption constants, respectively.
2. As the NAM approaches the AP, its energy drops as it becomes physisorbed followed by chemisorption as the NAM forms chemical bonds with the surface of the AP (usually taking place by bond breaking in the molecule or reacting with an adsorbed species at the aerosol). The process from physisorption to chemisorption occurs over an energy barrier (E_a) and this leads to the last two cases:

(a) E_a might be so low that it does not rise above the energy of the system (E_{sys}) when the molecule is located at an infinite distance from the aerosol, *i.e.*,

$$A_{\text{g}} \underset{k_{\text{des}}}{\overset{k_{\text{abs}}}{\rightleftharpoons}} A_{\text{AP}} \overset{k_{\text{reac}}}{\rightarrow} B_{\text{AP}} \underset{k'_{\text{abs}}}{\overset{k'_{\text{des}}}{\rightleftharpoons}} B_{\text{g}} \tag{2}$$

where k_{reac} is the rate constant of A if it reacts with the aerosol or a specie absorbed on the aerosol, and k'_{abs} and k'_{des} are the adsorption and desorption constants for the second process, respectively.

(b) E_a is above the energy of the system when the molecule is situated at infinite separation from the aerosol. If quantum effects are ignored we have

$$A_{\text{g}} \underset{k_{\text{des}}}{\overset{k_{\text{abs}}}{\rightleftharpoons}} \begin{cases} A_{\text{AP}} & \text{if } E_{\text{sys}} < E_a, \\ A_{\text{AP}} \overset{k_{\text{reac}}}{\rightarrow} B_{\text{AP}} \underset{k'_{\text{abs}}}{\overset{k'_{\text{des}}}{\rightleftharpoons}} B_{\text{g}} & \text{if } E_{\text{sys}} \geqslant E_a. \end{cases} \tag{3}$$

This means that for case 2(a) the chemisorption is not an activated process, while case 2(b) has an activation energy barrier (E_a). Therefore, if quantum effects such as tunneling are not considered then the NAM needs energy higher than E_a in order to be chemically adsorbed on the AP. The maximum observed energies for physisorption are in the range from 20 to 90 kJ/mol whereas the energies of chemisorption are in the range from 150 to more than 400 kJ/mol.

The ability of A to be adsorb when it hits the AP depends on the extent the solid aerosol is covered or the liquid aerosol is saturated, and if the reaction path for the NAM–AP system has an energy barrier or not for chemical adsorption. If we assume the same physical behaviors as done for the derivation of the Langmuir isotherm [12]:

1. adsorption cannot proceed beyond the mono-layer coverage,
2. all sites are equivalent and the aerosol is uniform (*i.e.*, perfectly flat), and
3. the ability of a molecule to adsorb at a given site is independent of the occupation of the neighbor site.

Let p_{cl} (*i.e.*, the accommodation coefficient) denote the probability of A to be adsorbed on a clean aerosol particle. From a physical-chemical point of view when a molecule approaches a surface, *e.g.*, an AP, it most deliver energy to the phonon-bath on the AP in order to be physisorbed on it. Thus, the sizes of the kinetic, rotational and vibrational energies of the incoming NAM are of fundamental significance in order to determine the probability whether or not the molecule will be physisorbed on the AP. On the other hand, since the size of the AP (or surface) is much larger than the NAM, it is reasonable to assume that:

1. $m_A \ll m_{\text{AP}} \Longrightarrow \mu \approx m_A$ (μ is the reduced mass between A_{g} and the AP and m_A is the mass of A_{g}),
2. the rotational and vibrational energies (states) of the AP do not change after a molecule has collided with it (*i.e.*, $\Delta E^{\text{AP}}_{\text{vib}} = E^{\text{AP}}_{\text{vib},f} - E^{\text{AP}}_{\text{vib},i} \approx 0$), and
3. the AP (or surface) is fixed in space and only A_{g} is able to move.

Thereby, we obtain the state to state adsorption rate of A on an AP (or surface) from

classical collision theory as [13]:

$$
\begin{aligned}
v_{A_g}^{\text{ads}} &= \frac{[A_g]}{4} S \sqrt{\frac{8k_bT}{\pi\, m}} \int_0^{\infty} \mathrm{d}(E_{\text{trans}}/k_bT)\exp(-E_{\text{trans}}/k_bT)E_{\text{trans}}/k_bTa \\
&\quad \times (1-\theta)p_{\text{cl}}\big(E_{\text{trans}}, \bar{v}^{\text{i}}, \bar{j}^{\text{i}}, \bar{v}^{\text{f}}, \bar{j}^{\text{f}}\big)a \\
&= \frac{[A_g]}{4} S \sqrt{\frac{8\, k_b\, T}{\pi\, m}} (1-\theta)\left\langle p_{\text{cl}}\big(T, \bar{v}^{\text{i}}, \bar{j}^{\text{i}}, \bar{v}^{\text{f}}, \bar{j}^{\text{f}}\big)\right\rangle a \\
&= [A_g] k_{\text{abs}}\big(T, \bar{v}^{\text{i}}, \bar{j}^{\text{i}}, \bar{v}^{\text{f}}, \bar{j}^{\text{f}}\big)a
\end{aligned} \tag{4}
$$

where $[A_g]$ is the gas-phase concentration of A_g, S is the symmetry factor for the reaction describing the adsorption process on the AP, E_{trans} is the kinetic energy of the relative translational motion between the center of masses of A_g and the aerosol particle, k_b is Boltzmann constant, T is the temperature, θ is the fraction of the aerosol that is covered by A_g, $\bar{v}^x$ is the vibrational quantum numbers of the molecule A_g, and $\bar{j}^x$ is the rotational quantum number of the molecule A_g (x = i = initial, or f = final). The last quantity a is equal to the surface-area concentration (square centimeters of surface per cubic centimeter of air) of all particles on which reactions occur.

We observe that k_{abs} in equation (4) depends on an initial specific chosen ro-vibrational state and E_{trans}, and the final ro-vibrational state of A_g. This rate of absorption can be summed by different methods utilizing either complete or simplified distributions. For example, by assuming a Boltzmann distribution over the initial ro-vibrational state and then summing up over the initial and final ro-vibrational quantum numbers we can write the total rate of absorption including the symmetry factor as:

$$
k_{\text{abs}}(T) = S\frac{1}{4}\sqrt{\frac{8k_bT}{\pi m}}(1-\theta)\big\langle p_{\text{cl}}(T)\big\rangle a \tag{5}
$$

This equation is identical to the one generally used in atmospheric chemical-aerosol modeling, see, *e.g.*, Jacobson [14].

It is reasonable to assume that the desorption of A_g from the aerosol is proportional to the amount of A_g adsorbed on the aerosol. Therefore, we can write:

$$
v_{A_g}^{\text{des}} = k_{\text{des}}[A_{\text{AP}}] = k_{\text{des}}a\theta \tag{6}
$$

and the differential equation system for the general case is:

$$
\begin{aligned}
\frac{\mathrm{d}[A_g]}{\mathrm{d}t} &= -k_{\text{abs}}[A_g] + k_{\text{des}}[A_{\text{AP}}], \\
\frac{\mathrm{d}[A_{\text{AP}}]}{\mathrm{d}t} &= k_{\text{abs}}[A_g] - k_{\text{des}}[A_{\text{AP}}] - k_{\text{reac}}[A_{\text{AP}}].
\end{aligned} \tag{7}
$$

At equilibrium the net change of $[A_{\text{AP}}]$ and θ are zero, that means $\mathrm{d}[A_{\text{AP}}]/\mathrm{d}t = 0$. Using that on equation (7) we get

$$
k_{\text{des}} + k_{\text{reac}} = S\frac{1}{4}\sqrt{\frac{8k_bT}{\pi m}}\langle p_{\text{cl}}\rangle[A_g]\frac{1-\theta_{\text{eq}}}{\theta_{\text{eq}}}. \tag{8}
$$

From statistical mechanism the equilibrium constant, K_{eq}, for a gas-phase molecule A_g colliding with an unit surface is given as

$$K_{eq} = \frac{k^1_{abs,eq}}{k_{des} + k_{reac}} \tag{9}$$

where

$$k^1_{abs,eq} = k_{abs,eq}/a. \tag{10}$$

From equation (7) it is observed that

$$K_{eq} = \frac{k^1_{abs,eq}}{k_{des} + k_{reac}} = \frac{[A_{AP}]_{eq}}{[A_g]} = \frac{\theta_{eq}}{[A_g]} \tag{11}$$

which gives

$$\theta_{eq} = K_{eq}[A_g]. \tag{12}$$

This shows that the fraction of the surface that is covered by A_g at equilibrium depends on the rate of which A_g is impinging at the surface. If equation (12) is inserted in equation (8) we obtain a quantity which can be used to calculate $k_{des} + k_{reac}$ or k_{des} if either $k_{reac} = 0$ or k_{reac} is known.

2. STICKING COEFFICIENT MODEL

We have presented a QM-ST method based on phase-space theory [15] that can be used to calculate rate constants for gas-phase reactions [16,17]. However, it was concluded from this work that the QM-ST method always overestimate the rate constants for gas-phase reactions. Since the interactions between an NAM and AP are expected to be described more appropriately using this QM-ST approach we find that the rate constants calculated for these systems are more reliable.

The sticking coefficient is a property which only is related to the absorption process on an aerosol or surface. In order to calculate this physical quantity we shall only consider the forward process of reaction (1). Therefore, we consider the situation where an NAM is colliding with an AP:

$$A_g \rightarrow [A_g \cdots AP]^\dagger \rightarrow A_{AP}. \tag{13}$$

Opposite to gas-phase reactions [16,17] the process described by reaction (13) can only take place through a channel that describes the interaction from reactants to the complex formation $[A_g \cdots AP]^\dagger$ (we will denote this channel i), and a channel from $[A_g \cdots AP]^\dagger$ to the product A_{AP} (we will denote this channel f).

The NAM and the aerosol particle have the option of being in the different states and ending up as various products. The states of such systems are specified by the molecules' vibrational quantum numbers, $\bar{v}_x$, rotational quantum numbers, $(\bar{j}^x, \bar{j}^x_z)$, the relative translation energy (E^x_{trans}), and finally the orbital angular momentum quantum numbers (l^x, l^x_z). The motion of the center of mass of A relative to AP does not affect the statistics, therefore it is ignored.

The theory of phase-space methods can be derived in several ways; here a derivation based upon quantum mechanics is given. Phase-space methods are based on three assumptions:

- conservation rules and detailed balance (Assumption 1),
- formation (Assumption 2) of the collision complex ($[A_g \cdots AP]^\dagger$), and
- decomposition (Assumption 3) of $[A_g \cdots AP]^\dagger$.

ASSUMPTION 1. The conservation laws and detailed balancing must be obeyed. Thus, energy, total angular momentum and its projection on one axis, and linear momentum must be conserved. The total energy of the reactants in reaction (13) is

$$E_{\text{tot}} = E_{\text{trans}} + E_{\text{vib}} + E_{\text{vib}}^{\text{AP}} + E_{\text{rot}} + E_{\text{rot}}^{\text{AP}} + V. \tag{14}$$

The first term is the kinetic energy of A relative to AP. The second and third terms are the vibrational energies of A and AP, respectively. The fourth and fifth terms are the rotational energies of A and AP, respectively. For an asymmetric top molecule expressions for the ro-vibrational energy can be found in Fig. 1. For molecules with another kind of symmetry expressions of the ro-vibrational energy can be found in Refs. [16,17].

The last term in equation (14) is the potential energy of the system. Additionally, we assume that $E_{\text{vib}}^{\text{AP}}$ and $E_{\text{rot}}^{\text{AP}}$ do not change after a collision with NAM has occurred, and we

$$E_{\text{vib}} = \sum_i^s \left(v_i + \frac{1}{2}\right)\hbar\omega_i = \sum_i^s E_i$$

where ω_i is the vibrational frequencies for the $s = 3n - 6$ oscillators and $v_i = 0, 1, 2, \ldots$

$$\begin{aligned} E_{\text{rot}} &= C_1 j(j+1) + C_2 k^2 \\ &\quad + C_2\left(k^2 \sum_{n=2}^{\infty} \varepsilon_{0n} C_3^n + j(j+1) \sum_{n=1}^{\infty} \varepsilon_{1n} C_3^n + j^2(j+1)^2 \sum_{n=2}^{\infty} \varepsilon_{2n} C_3^n + \cdots\right) \\ &= E_{\text{rot}_j}^1 + E_{\text{rot}_k}^1 + E_{\text{rot}_k}^2 + E_{\text{rot}_j}^2 + E_{\text{rot}_j}^3 + \cdots \end{aligned}$$

where $I_c > I_b > I_a$, $a = \frac{\hbar^2}{2I_a}$, $b = \frac{\hbar^2}{2I_b}$, and $c = \frac{\hbar^2}{2I_c}$.

The ε constants are given in Ref. [18].

For the near-prolate case ($b \approx c$) $C_1 = (b + c)/2$, $C_2 = a - (b + c)/2$, and $C_3 = \frac{b-c}{2(2a-b-c)}$.

For the near-oblate case ($a \approx b$) $C_1 = (a + b)/2$, $C_2 = c - (a + b)/2$, and $C_3 = \frac{a-b}{2(a+b-2c)}$.

$k_c = j$ when $k = 0$, $k_c = j - k$ when lower and $k_c = j - k + 1$ when upper.

a, b and c describe the three mutually perpendicular principal axes.

Fig. 1. Expressions for the quantum mechanical vibrational energy using the harmonic oscillator approximation and rotational energy using the rigid rotor approximation [18] for an asymmetric top molecule. $\hbar$ is Planck's constant divided by 2π.

have that

$$E'_{\text{tot}} = E_{\text{trans}} + E_{\text{vib}} + E_{\text{rot}} + V \tag{15}$$

also must be conserved.

The total angular momentum ($\bar{J}$) is a summation of the orbital angular momentum ($\bar{l}$) and the rotational angular momenta for the reactants ($\bar{j}$, $\bar{j}^{\text{AP}}$) in reaction (13):

$$\bar{J} = \bar{l} + \bar{j} + \bar{j}^{\text{AP}} \approx \bar{l} + \bar{j}. \tag{16}$$

ASSUMPTION 2. Two conditions must be fulfilled for a $[A_g \cdots \text{AP}]^\dagger$ to be formed: the total energy of A colliding with the aerosol particle exceeds the barrier of the effective potential energy (*i.e.*, the sum of the inter-molecular potential and centrifugal energy) and if the kinetic energy of the NAM–AP system is sufficient to cross the barrier, a maximum value of L^i, L^i_{max}, for which scattering occurs will exist. Based upon these assumptions, the probability of forming $[A_g \cdots \text{AP}]^\dagger$ from every channel is one if the energy of reacting molecules exceed the barrier of the effective potential energy and l^i is less than or equal to l^i_{max}. Otherwise it is zero.

ASSUMPTION 3. Decomposition of $[A_g \cdots \text{AP}]^\dagger$ is uncorrelated with the modes of the reactants except through conservation laws and detailed balancing. Hence, there is an equal probability to decompose $[A_g \cdots \text{AP}]^\dagger$ into the different channels.

The validity of these three assumptions are discussed in Refs. [16,17]. Assumption 3 is reasonable for reactions where the lifetime of a $[A_g \cdots \text{AP}]^\dagger$ is long, since then there is an equal probability of the $[A_g \cdots \text{AP}]^\dagger$ decomposing into the available manifolds of the different reaction channels. On the other hand, if the reaction is very fast our method will overestimate the rate constant. This has been shown to be a problem for some gas-phase reactions with fast decomposition rates. Furthermore, when the phase-space method is used to estimate sticking coefficients for NAM–AP systems, the NAM exchanges energy with the phonon bath of the aerosol.

As assumed in equation (15), small changes of E_{tot} will not change the phase-space of AP (N_{AP}) only the phase-space of NAM (N). Based on this assumption and following the methodology described in Ref. [16] the state to state reaction probability (p_{cl}) of reaction (13) becomes

$$p_{\text{cl}}\left(E_{\text{trans}}, \bar{vr}^{\text{i}}, \bar{vr}^{\text{f}}, J\right) = \left(\frac{N(\bar{vr}^{\text{f}}, E_{\text{trans}}, J)}{N(\bar{vr}^{\text{i}}, E_{\text{trans}}, J) + N(\bar{vr}^{\text{f}}, E_{\text{trans}}, J)}\right) \tag{17}$$

where the compact form $\bar{vr}^x$ is used to describe the total number of rotational and vibrational quantum numbers of the NAM and AP. The reaction probability given here depends on a specific chosen initial and final relative velocity between NAM and AP and their ro-vibrational state. Less complete distributions can be obtained by assuming a Boltzmann distribution over the initial ro-vibrational states and then summing over the initial and final ro-vibrational quantum numbers as described in Ref. [16] and in equation (5).

However, in equation (17) p_{cl} depends on J compared with equations (4) and (5). Two different methods have been used to sum over J:

$$\left\langle p_{\mathrm{cl}}^{\mathrm{ph,av}}\left(E_{\mathrm{trans}}, \bar{vr}^{\mathrm{i}}, \bar{vr}^{\mathrm{f}}\right)\right\rangle = \sum_{J=0}^{J_{\max}}\left(\frac{\sum_{\bar{vr}^{\mathrm{f}}} N(\bar{vr}^{\mathrm{f}}, E'_{\mathrm{tot}}, J)}{\sum_{\bar{vr}^{\mathrm{i}}} N(\bar{vr}^{\mathrm{i}}, E'_{\mathrm{tot}}, J) + \sum_{\bar{vr}^{\mathrm{f}}} N(\bar{vr}^{\mathrm{f}}, E'_{\mathrm{tot}}, J)}\right) \times J_{\max}^{-1} \tag{18}$$

and

$$\left\langle p_{\mathrm{cl}}^{\mathrm{ph,wg}}\left(E_{\mathrm{trans}}, \bar{vr}^{\mathrm{i}}, \bar{vr}^{\mathrm{f}}\right)\right\rangle = \sum_{J=0}^{J_{\max}}(2J+1)\left(\frac{\sum_{\bar{vr}^{\mathrm{f}}} N(\bar{vr}^{\mathrm{f}}, E'_{\mathrm{tot}}, J)}{\sum_{\bar{vr}^{\mathrm{i}}} N(\bar{vr}^{\mathrm{i}}, E'_{\mathrm{tot}}, J) + \sum_{\bar{vr}^{\mathrm{f}}} N(\bar{vr}^{\mathrm{f}}, E'_{\mathrm{tot}}, J)}\right) \times \left(\sum_{J=0}^{J_{\max}}(2J+1)\right)^{-1}. \tag{19}$$

In the last equation we have assumed that $p_{\mathrm{cl}} \times \sigma(p_{\mathrm{cl}} = 1) = \sigma(p_{\mathrm{cl}})$, $\sigma(p_{\mathrm{cl}})$ is the reaction cross-section of reaction (13).

2.1. Calculation of $N(E_{\mathrm{tot}}, J)$

In this section we describe how the total number of states, $\sum_{\bar{vr}^x} N(\bar{vr}^x, E_{\mathrm{tot}}, J) = N(E_{\mathrm{tot}}, J)$ can be calculated. However, we will not derive the equation for all six NAM cases colliding with an AP, instead we will present the equations for the case where A is an asymmetric top molecule. It is relative easy to revise the equations for the other five simpler systems. Furthermore, we use the following notation: $v_{\max}$ = largest allowed vibrational quantum number, $j_{\max}$ = largest allowed rotational quantum number (see Fig. 2, similar expressions for the other types of molecular symmetric point groups can be found in Refs. [16,17]), and $l_{\max}$ = largest allowed orbital angular momentum quantum number for the molecule, see Section 2.2.

From equation (15) we define the available energy as

$$E_{\mathrm{avab}} = E'_{\mathrm{tot}} - E_{\mathrm{vib}} - V. \tag{20}$$

The first step in the evaluation of $N(E'_{\mathrm{tot}}, J)$ is to calculate the number of accessible states related to the rotational motion when the vibrational motion of the molecule is constant $N(\bar{v}, E'_{\mathrm{tot}}, J)$.

An asymmetric top molecule [18] has three rotational quantum numbers j, k and k_c. When $k = 0$, $k_c = j$, otherwise k_c is equal to $j - k$ or $j - k + 1$. Let $\biguplus_{k_c}$ describe the summation over k_c as described above, then the number of accessible states when A is an asymmetric top molecule is given by

$$N(\bar{v}, E_{\mathrm{avab}}, J) = \sum_{j=0}^{j_{\max}} \sum_{k=-j}^{j} \biguplus_{k_c} \sum_{\substack{l=|J-j| \\ l \leqslant l_{\max}}}^{J+j} 1 \tag{21}$$

$$v_{\max_1} = \frac{E_{\text{tot}} - V}{\hbar\omega_1} - \frac{1}{2}$$

$$v_{\max_2} = \frac{E_{\text{tot}} - V - E_1}{\hbar\omega_2} - \frac{1}{2}$$

$$\vdots$$

$$v_{\max_{s-1}} = \frac{E_{\text{tot}} - V - \sum_{i=1}^{s-2} E_i}{\hbar\omega_{s-1}} - \frac{1}{2}$$

$$v_{\max_s} = \frac{E_{\text{tot}} - V - \sum_{i=1}^{s-1} E_i}{\hbar\omega_s} - \frac{1}{2}$$

where ω_s is the vibrational frequencies for the s oscillators.
E_i is defined in Fig. 1.

$j_{\max}(j_{\max}+1) = f(E_a) =$ the inverse of the expression for the energy of the asymmetric top molecule at $k = 0$

$$k^2_{\max} = \frac{E_a - C_1 j(j+1) - C_2 j(j+1)\sum_{n=1}^{\infty} \varepsilon_{1n} C_3^n - C_2 j^2 (j+1)^2 \sum_{n=2}^{\infty} \varepsilon_{2n} (C_3)^n + \cdots}{(C_2 + C_2 \sum_{n=2}^{\infty} \varepsilon_{0n} (C_3)^n)^{-1}}$$

Fig. 2. Expressions describing how to select the maximum vibrational ($v_{\max}$) and rotational ($j_{\max}$ and $k_{\max}$) quantum numbers for an asymmetric top molecule taking part in a NAM–AP collision. E_{tot} and V are the total energy and the potential energy, respectively, for the system under investigation. E_a is the available energy for the vibrational degrees of freedom. The C and ε constants are defined in Fig. 1. $\hbar$ is Planck's constant divided by 2π.

where $l_{\max}$ is given in Section 2.2. The next step is to perform the summation over the vibrational motion for the asymmetric molecule. If we define the following term:

$$S_s^{\text{Asy}} = \prod_{l=1}^{s} \left(\sum_{v_l^{\text{Asy}}=0}^{v_{\max_l}^{\text{Asy}}} 1 \right), \tag{22}$$

the total number of states is:

$$N(E_{\text{tot}}, J) = S_s^{\text{Asy}} \times N(\bar{v}, E_{\text{avab}}, J). \tag{23}$$

2.2. Assignment of maximum orbital angular momentum

The most critical part of the theory lies in the choice of the requirements for the collision complex. The collision complex is formed when the kinetic energy of the NAM–AP system exceeds the barrier of the effective potential, and the orbital angular momentum is less than or equal to the maximum orbital angular momentum. Since a non-activated adsorption

process does not have a potential energy barrier, it can be handled in the same manner as reactions without potential energy barriers as described by Gross *et al.* [16]. For these reactions there exists a distance r^* where the complex NAM–AP is strongly coupled, and it is reasonable to believe that r^* is approximately independent of the two species' internal energy, relative translational energy between them, and their rotational angular momenta. We assume that the maximum of the effective potential occurs in that attractive region of the potential energy surface, and therefore the short-range part of the potential can be neglected. Effectively, the potential between the molecules in the channels is

$$V_{\text{eff}} = V_{\text{LR}} + \frac{l(l+1)\hbar^2}{2m_A} R^{-2} \tag{24}$$

where V_{LR} is the long-range potential. From this potential we can evaluate at which R the effective potential has its maximum value. The maximum angular momentum, $l_{\max}(l_{\max}+1)\hbar^2$ ($\hbar = h/2\pi$ where $\hbar$ is Planck's constant), is then given by

$$l_{\max}(l_{\max}+1)\hbar^2 = n_{\text{LR}} m_A \Gamma^{2/n_{\text{LR}}} \left(2E_{\text{trans}}/(n_{\text{LR}}-2)\right)^{1-2/n_{\text{LR}}} \tag{25}$$

where the magnitude of Γ corresponds to the long-range term (n_{LR}) in the (n_{SR}, n_{LR})-Lennard–Jones potential. This equation is most applicable to low energy conditions, but at higher energies the maximum impact parameter, $b_{\max}$, given by this equation can be lower than r^*. This should not be allowed, therefore it is more reasonable to let $b_{\max}$ be the maximum of these two values. The result, expressed in maximum orbital angular momentum, is

$$l_{\max}(l_{\max}+1)\hbar^2 = \max \begin{cases} nm\Gamma^{2/n}(2E_{\text{trans}}/(n-2))^{1-2/n}, \\ 2mE_{\text{trans}}(n\Gamma - 2\Gamma)^{2/n}(2E_{\text{trans}})^{2/n}. \end{cases} \tag{26}$$

These equations show that we need to obtain information about the long-range potential in order to apply the QM-ST model.

3. TESTS OF THE QUANTUM-STATISTICAL MODEL

Experimental and theoretical estimations of accommodation coefficients on liquid aerosols are very difficult to obtain, such calculations have therefore been performed for very few systems. Therefore we have developed a new simple theoretical method to calculate accommodation coefficients for molecules impinging on aerosols or surfaces with the purpose of estimating this quantity for the interaction between molecules and atmospheric aerosols. The simplicity of the model is related to the fact that the QM-ST model only requires spectroscopic data of NAM and the potential energy difference between the reaction and product channel of reaction (13).

Due to very sparse calculations of accommodation coefficients of molecules colliding on atmospheric aerosols the first tests of the new model have been the following two heterogeneous catalytic molecule metal surface reactions: the non-activated adsorption reaction

$$H_2 + \text{Pd}(100) \rightarrow H_{2\,Pd(100)} \tag{27}$$

and the physisorption reaction

$$\text{CO} + \text{Cu}(111) \rightarrow \text{CO}_{Cu(111)}. \tag{28}$$

Finally, the method has been used to calculate accommodation coefficient for the atmospheric relevant system:

$$CH_3CHO + H_2O_l \rightarrow CH_3CHO_{H_2O_l}. \tag{29}$$

3.1. $H_2 + Pd(100) \rightarrow H_{2\,Pd(100)}$

In order to apply the QM-ST model we have used the spectroscopic data for H_2 from Herzberg [19] and potential information from Gross [20] to calculate the total accommodation coefficient for the system. The results are compared with results from a 6D quantum dynamics calculation [20], and molecular beam adsorption experiments by Rendulic *et al.* [21] and Rettner and Auerbach [22]. The results from these four studies are shown in Fig. 3.

3.2. $CO + Cu(111) \rightarrow CO_{Cu(111)}$

The spectroscopic data for CO and potential information of the CO + Cu(111) reaction used to calculate the accommodation coefficient for the CO/Cu(111) system were taken from Herzberg [19] and Ge *et al.* [23], respectively. In Table 1 the results from the QM-ST model as a function of E_{trans} and the rotational quantum number are shown together with a quantum-classical study from Ge *et al.*

3.3. $CH_3OH + H_2O_l \rightarrow CH_3OH_{H_2O_l}$

For calculation of the accommodation coefficient for the CH_3OH/H_2O_l system we have used the parameters from Clementi *et al.* [24] to estimate the reaction part for methanol

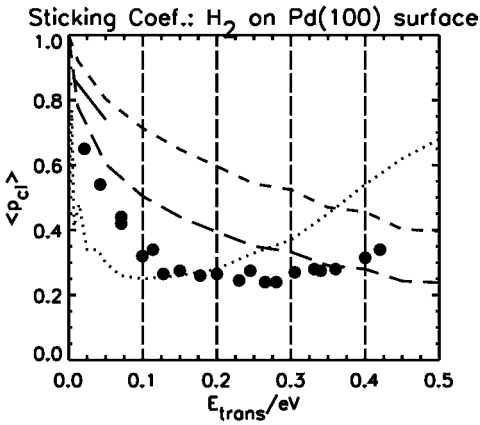

Fig. 3. Accommodation coefficient as a function of E_{trans} for H_2 colliding with a Pd(100) surface. Dotted line: 6D quantum dynamics, beam simulation [20]. Solid line: H_2 molecular beam experiment under normal incidence [21]. Big dots: H_2 effusive beam scattering experiment with an incidence angle of 15° [22]. Dashed line: $\langle p_{\text{cl}}^{\text{ph,wg}} \rangle$, this work. Long-dashed line: $\langle p_{\text{cl}}^{\text{ph,av}} \rangle$, this work.

Table 1. Accommodation coefficient for CO colliding with a Cu(111) surface at different initial translation energies ($E_{\text{trans}}^{\text{CO}}$) and rotational quantum numbers

E_{trans}/eV	j_{CO}	$\langle p_{\text{cl}}^{\text{qm,cl}} \rangle$	$\langle p_{\text{cl}}^{\text{ph,av}} \rangle$	$\langle p_{\text{cl}}^{\text{ph,wg}} \rangle$
0.446	0	0.49	0.49	0.59
1.00	0	0.40	0.35	0.48
5.16	0	0.38	0.042	0.058
8.00	0	0.42	0.090	0.15
1.00	0	0.40	0.35	0.48
1.00	10	0.33	0.35	0.48
1.00	12	0.25	0.27	0.37

For all the calculations $E_{\text{vib}}^{\text{CO}} = 0.134$. $p_{\text{cl}}^{\text{qm,cl}}$ is a quantum-classical simulation from Ge *et al.* [23]. $\langle p_{\text{cl}}^{\text{ph,av}} \rangle$ and $\langle p_{\text{cl}}^{\text{ph,wg}} \rangle$ are from this work.

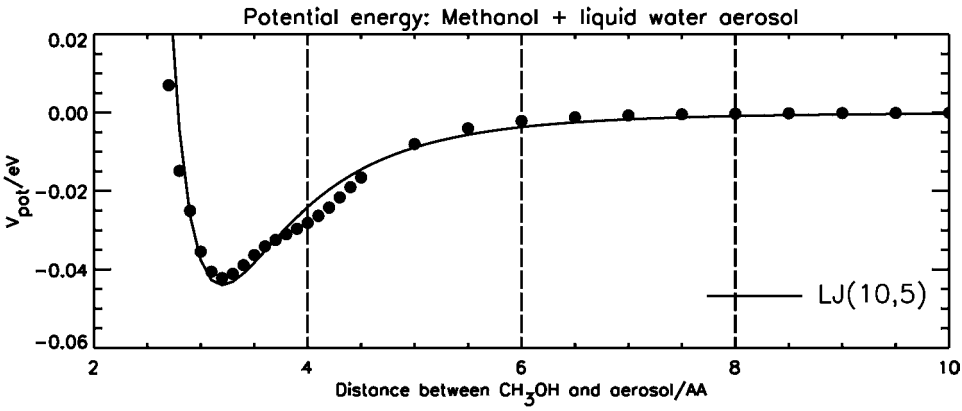

Fig. 4. Potential energy as a function of the reaction path between the center of mass distance between CH_3OH and the liquid water aerosol calculated from the atom-atom potential given in Clementi *et al.* [24]. Big dots: estimated potential energies from Clementi *et al.* Solid line: fit of the estimated potential energies with a (10,5)-Lennard–Jones potential.

approaching a liquid water aerosol. The result from this calculation is shown in Fig. 4. We observe that the potential behave as a (10,5)-Lennard–Jones potential, and it has the typical feature of a physisorption of a molecule on an aerosol; *i.e.*, a reaction without a potential energy barrier. The spectroscopic data of methanol was obtained using Gaussian 98 [25]. The results from this calculation are presented in Table 2.

Opposite to the case where a molecule sticks to a solid aerosol or surface it is possible for the molecule to have rotational energy when it is captured by a liquid aerosol. However, the rotational motion is not as free as in the gas-phase. Therefore, in this study we have calculated the accommodation coefficient for the case where CH_3OH is able or is not able to

Table 2. Table of vibrational frequencies and momentum of inertia of CH_3OH from the *ab initio* calculations performed using Gaussian 94

Vibrational frequencies / cm^{-1}				
346.4323	1088.9005	1114.7048	1196.9140	1403.6295
1517.6718	1518.0882	1537.4890	3045.0206	3109.5960
3183.1410	3924.3900			
Momentum of inertia / amu a_0^2				
14.11657	72.46625	75.14391		

The electronic structure calculation theory used is MP2 and the basis set is 6-31G*.

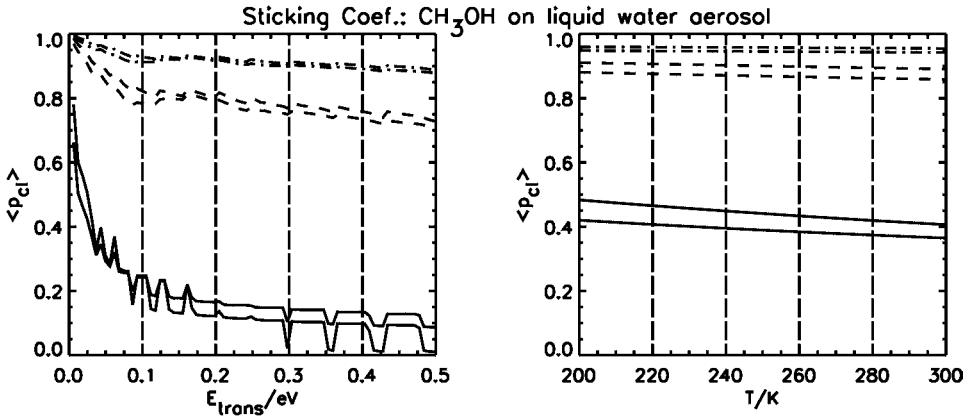

Fig. 5. Accommodation coefficient as a function of E_{trans} and temperature for CH_3OH colliding with a liquid water aerosol. Solid line: accommodation coefficient estimated based on the assumptions that CH_3OH cannot rotate after it has been physisorbed on the aerosol and three equal probable reaction channels exists. Dashed line: accommodation coefficient estimated based on the assumptions that CH_3OH can rotate after it has been physisorbed on the aerosol and only one probable reaction channel exist. Dotted-dashed line: accommodation coefficient estimated based on the assumptions that CH_3OH can rotate after it has been physisorbed on the aerosol and three equal probable reaction channels exists.

rotate. Furthermore, we have also assumed for some of the calculations that the degeneracy of the reaction channel shown in Fig. 4 is three. This degeneracy correspond to the possible number of hydrogen bonds which can be formed between CH_3OH and H_2O. Thus, in Fig. 5 we have plotted the following results: $\langle p_{\text{cl}}^{\text{qm,av}} \rangle$ and $\langle p_{\text{cl}}^{\text{qm,wg}} \rangle$ as a function of E_{trans} (left-hand side figure) and the temperature (right-hand side figure) for the three cases. The three case are: methanol does not rotate after it has been physisorbed on H_2O_l and the degeneracy of the reaction channel is three (the two lowest plots in Fig. 5), methanol is able to rotate after it has been physisorbed on H_2O_l and the degeneracy of the reaction channel is one (the third and fourth lowest plots in Fig. 5), and methanol can rotate after it has been

physisorbed on H_2O_l and the degeneracy of the reaction channel is three (the two highest plots in Fig. 5).

4. DISCUSSION OF THE RESULTS

4.1. $H_2 + Pd(100) \rightarrow H_{2\,Pd(100)}$

While the H_2/Cu system serves as benchmark system for activated adsorption [26–31], then the H_2/Pd has been used as a standard system for studying non-activated adsorption [20, 21,32–40]. Opposite to the majority of NAM–AP systems the interaction between H_2 and Pd(100) does not have a potential energy barrier for the reaction paths towards dissociative adsorption. However, based on the theoretical concept in the QM-ST model introduced in the paper it can be used to calculate sticking coefficients for this type of reactions too, since it does not have a potential energy barrier along its reaction path.

The agreement between our model and the experiments is satisfactory. Especially $\langle p_{cl}^{ph,wg} \rangle$ is in a good agreement with the experiments from Rendulic *et al.* [21] and $\langle p_{cl}^{ph,av} \rangle$ is in a good agreement with the experiments from Rettner and Auerbach [22]. The 6D quantum dynamics calculation decreases much faster at low E_{trans} than the experiments and the QM-ST calculation. Moreover, from 0.1 to 0.5 eV the accommodation coefficient increases for the 6D quantum dynamics calculation while for the QM-ST calculation p_{cl} decrease from 0.0 to 0.5 eV. Rendulic et al. have only estimated p_{cl} for E_{trans} from 0.0 to 0.07 eV while the results from Rettner and Auerbach [22] ranges from 0.0 to 0.425 eV. The latter experiment has almost a constant accommodation coefficient from 0.1 to 0.425 eV, however a small increase from 0.4 to 0.425 eV can be observed. It is difficult to conclude if this is a significant increase of p_{cl} since it is only observed over this very small energy interval. From Fig. 3 we observe that $\langle p_{cl}^{ph,wg} \rangle$ is in better agreement with the experiments from Rendulic *et al.* [21] than the 6D quantum dynamics calculations, and $\langle p_{cl}^{ph,av} \rangle$ is in better agreement with the experiments from Rettner and Auerbach [22] than the 6D quantum dynamics calculations.

4.2. $CO + Cu(111) \rightarrow CO_{Cu(111)}$

The CO/Cu interaction has been much less studied than the H_2/Pd interaction. However, Ge *et al.* [23] have modeled the physisorption of CO on Cu(111). This process does not have a potential energy barrier [23]. Moreover, we have also tested the usefulness of the QM-ST model to estimate the dependence of the accommodation coefficient on different initial rotational energies.

A comparison of the results from the QM-ST study with that of the quantum-classical study shows remarkable good agreement at $E_{trans} = 0.446$ and 1.00 eV while at the very high energies, $E_{trans} = 5.16$ and 8.00 eV the QM-ST method estimated too low sticking coefficients. Even for the study of the rotational energy dependence the agreement between the dynamical and statistical method is very good.

4.3. $CH_3OH + H_2O_l \rightarrow CH_3OH_{H_2O_l}$

The purpose for developing the QM-ST model was to develop a simple method to calculate accommodation coefficients for systems observed in the atmosphere. Therefore, we have

tested the new method on an atmospheric relevant system: the collision of the simplest alcohol on liquid water. The chemistry of alcohols in the atmosphere is interesting since it is used as alternate fuels, including blends with gasoline. The concentration of methanol in the atmosphere is in the range from 1 to 20 ppbV [41] and ethanol from 0.1 to 1 ppbV [41].

We observe that a rotational effect of CH_3OH on H_2O_l has a very large impact on the sticking coefficient. The sticking coefficient increases by a factor of four to five from $E_{\text{trans}} \approx 0.1$ to 0.5 eV and by a factor of approximately two for $\langle p_{\text{cl}}^{\text{qm,av}}(T)\rangle$ and $\langle p_{\text{cl}}^{\text{qm,wg}}(T)\rangle$ between 200 and 300 K.

The temperature dependence of the sticking coefficient calculated in Fig. 5 has never been estimated experimentally or theoretically, however Jayne *et al.* [5] have assumed that $\langle p_{\text{cl}}(T)\rangle = 1$ during the evaluation of their experiment. We observe, if this assumption is correct then CH_3OH most have a rotational degree of freedom when it is physisorbed on the liquid water aerosol.

4.4. Summary

For NAM–AP systems without a potential energy barrier along the reaction path the presented QM-ST model will always give a sticking coefficient which approaches one as E_{trans} approaches zero, and approach zero as E_{trans} approaches infinity. These features are observed for all three systems we have tested the model on, see Figs. 3, 4, and Table 1. However, the experimental results displayed in Fig. 3, and the dynamical calculations displayed in Fig. 3 and Table 1 demonstrate that this is not always a correct picture. The H_2/Pd(100) and CO/Cu(111) systems have a horizontal asymptote as E_{trans} increases. However, the QM-ST model is developed with the purpose of calculating accommodation coefficient for atmospheric relevant systems, and this means for $E_{\text{trans}} \in [0.0\text{ eV}; 0.3\text{ eV}]$ and $T \in [200\text{ K}; 300\text{ K}]$. Within these intervals the QM-ST model seems to be very successful.

5. CONCLUSION

This paper presents the first results of a new QM-ST model which can be used to calculate total sticking coefficients for molecules/atoms impinging on an aerosol/surface. The advantage (usefulness) of the model is that very limited number of parameters are needed to calculate the accommodation coefficient. Spectroscopic data for the molecule impinging on the aerosol and the potential energy difference between the reaction and product channels. All these parameters can with good accuracy be calculated using electronic structure theory. However, if it is possible to use full reaction dynamics to calculate the sticking coefficient for a molecular/aerosol system then this method will, of course, be preferable. Unfortunately, reaction dynamics need full potential energy information and this is only known for very few NAM–AP systems.

Even though the model cannot be used to get a molecular understanding for the NAM–AP problem it can be used to calculate total accommodation coefficient values, and this was also the main purpose of developing the model, since we want to use the results from the QM-ST model in macroscopic atmospheric chemical models.

A comparison of the results, of the systems we have tested the model on in this paper, show that the QM-ST model gives results which are very similar to those obtained using experimental or dynamical methods.

In conclusion, we predict that the QM-ST model presented in this paper is valuable tool to estimate accommodation coefficients for molecules impinging on aerosols. However, further test on other systems are needed.

ACKNOWLEDGEMENTS

This research was supported by the Danish Center for Scientific Computing [A.G., K.V.M.], Statens Naturvidenskabelige Forskningsråd [K.V.M.], Statens Teknisk Videnskabelige Forskningsråd [K.V.M.], and EU network MOLPROP+NANOQUANT +THEONETII [K.V.M.].

REFERENCES

[1] J.H. Seinfeld, S.N. Pandis, *Atmospheric Chemistry and Physics. From Air Pollution to Climate Change*, John Wiley & Sons, New York, 1997.
[2] S.N. Pandis, L.M. Russel, J.H. Seinfeld, *J. Geophys. Res.* **99** (1994) 16945.
[3] C.F. Clement, M. Kulmale, T. Vesala, *J. Aerosol Sci.* **27** (1996) 869.
[4] M. Kulmala, P.E. Wagner, *J. Aerosol Sci.* **32** (2001) 833.
[5] J.T. Jayne, S.X. Duan, P. Davidovits, D.R. Worsnop, M.S. Zahniser, C.E. Kolb, *J. Phys. Chem.* **95** (1991) 6329.
[6] P. Davidovits, J.T. Jayne, S.X. Duan, D.R. Worsnop, M.S. Zahniser, C.E. Kolb, *J. Phys. Chem.* **95** (1991) 6337.
[7] R. Van Dingenen, F. Raes, *Aerosol Sci. Technol.* **15** (1991) 93.
[8] H. Arstila, K. Laaksonen, A. Laaksonen, *J. Chem. Phys.* **108** (1998) 1031.
[9] A.R. Bandy, J.C. Ianni, *J. Phys. Chem. A* **102** (1998) 6533.
[10] J.C. Ianni, A.R. Bandy, *J. Mol. Struct. (Theochem)* **497** (2000) 19.
[11] A. Gross, A. Baklanov, *Int. J. Environ. Pollution*, in press.
[12] P. Atkins, J. de Paula, *Physical Chemistry*, seventh ed., Oxford Univ. Press, London, 2002.
[13] G.D. Billing, K.V. Mikkelsen, *Introduction to Molecular Dynamics and Chemical Kinetics*, John Wiley & Sons, New York, 1996.
[14] M.Z. Jacobson, *Fundamentals of Atmospheric Modeling*, Cambridge Univ. Press, Cambridge, UK, 1999.
[15] G.D. Billing, K.V. Mikkelsen, *Advanced Molecular Dynamics and Chemical Kinetics*, John Wiley & Sons, New York, 1997.
[16] A. Gross, K.V. Mikkelsen, W.R. Stockwell, *Int. J. Quantum Chem.* **84** (2001) 479.
[17] A. Gross, K.V. Mikkelsen, W.R. Stockwell, *Int. J. Quantum Chem.* **84** (2001) 493.
[18] S.R. Polo, *Can. J. Phys.* **36** (1957) 880.
[19] G. Herzberg, *Molecular Spectra and Molecular Structure—I. Spectra of Diatomic Molecules*, second ed., D. van Norstrand Company, Inc., Princeton, NJ, 1959.
[20] A. Gross, *Surf. Sci. Rep.* **32** (1998) 291.
[21] K.D. Reddulic, G. Anger, A. Winkler, *Surf. Sci.* **208** (1989) 404.
[22] C.T. Rettner, D.J. Auerbach, *Chem. Phys. Lett.* **253** (1996) 236.
[23] Q. Ge, L. Wang, G.D. Billing, *Surf. Sci.* **277** (1992) 237.
[24] E. Clementi, F. Cavallone, R. Scordamaglia, *J. Am. Chem. Soc.* **99** (1977) 5531.
[25] M.J. Frisch, G.W. Trucks, H.B. Schlegel, G.E. Scuseria, M.A. Robb, J.R. Cheeseman, V.G. Zakrzewski, J.A. Montgomery, R.E. Stratmann, J.C. Burant, S. Dapprich, J.M. Millam, A.D. Daniels, K.N. Kudin, M.C. Strain, O. Farkas, J. Tomasi, V. Barone, M. Cossi, R. Cammi, B. Mennucci, C. Pomelli, C. Adamo, S. Clifford, J. Ochterski, G.A. Petersson, P.Y. Ayala, Q. Cui, K. Morokuma, D.K. Malick, A.D. Rabuck, K. Raghavachari, J.B. Foresman, J. Cioslowski, J.V. Ortiz, B.B. Stefanov, G. Liu, A. Liashenko, P. Piskorz,

I. Komaromi, R. Gomperts, R.L. Martin, D.J. Fox, T. Keith, M.A. Al-Laham, C.Y. Peng, A. Namayakkara, C. Gonzalez, M. Challacombe, P.M.W. Gill, B.G. Johnson, W. Chen, M.W. Wong, J.L. Andres, M. Head-Gordon, E.S. Replogle, J.A. Pople, *Gaussian 98 (Revision A.6 and A.7)*, Gaussian Inc., Pittsburgh, PA, 1998.
[26] H.A. Mechelsen, D.J. Auerbach, *J. Chem. Phys.* **94** (1991) 7502.
[27] A. Hodgson, D.J. Auerbach, H.A. Michelsen, *Phys. Rev. Lett.* **68** (1992) 1164.
[28] H. Hou, S.J. Gulding, C.T. Rettner, A.M. Wodtke, D.L. Auerbach, *Science* **277** (1997) 80.
[29] A. Gross, B. Hammer, M. Scheffler, W. Brenig, *Phys. Rev. Lett.* **73** (1994) 3121.
[30] G.-J. Kroes, E.J. Baerends, R.C. Mowrey, *Phys. Rev. Lett.* **78** (1997) 3583.
[31] D.A. McCormack, G.-J. Kroes, *Phys. Chem. Chem. Phys.* **1** (1999) 1359.
[32] D. Wetzig, R. Dopheide, M. Rutkowski, R. David, H. Zacharias, *Phys. Rev. Lett.* **76** (1996) 463.
[33] D. Wetzig, M. Rutkowski, H. Zacharias, A. Gross, *Phys. Rev. B* **63** (2001) 205412.
[34] M. Beutl, M. Riedler, K.D. Rendulic, *Chem. Phys. Lett.* **256** (1996) 33.
[35] M. Golstein, G.O. Sitz, *J. Chem. Phys.* **106** (1997) 7378.
[36] A. Gross, S. Wilke, M. Seheffler, *Phys. Rev. Lett.* **75** (1995) 2718.
[37] A. Eichler, J. Hafner, A. Gross, M. Scheffler, *Chem. Phys. Lett.* **311** (1999) 1.
[38] H.F. Busnengo, W. Dong, A. Salin, *Chem. Phys. Lett.* **320** (2000) 328.
[39] A. Dianat, A. Gross, *Phys. Chem. Chem. Phys.* **4** (2002) 4126.
[40] A. Dianat, A. Gross, *J. Chem. Phys.* **120** (2004) 5339.
[41] B.J. Finlayson-Pitts, J.N. Pitts Jr., *Chemistry of the Upper and Lower Atmosphere (Theory, Experiments, and Applications)*, Academic Press, San Diego, CA, 2000.

Birefringences: A Challenge for Both Theory and Experiment

Antonio Rizzo[1] and Sonia Coriani[2]

[1]*Istituto per i Processi Chimico Fisici, Consiglio Nazionale delle Ricerche, Area della Ricerca, Via Moruzzi 1, loc. S. Cataldo, I-56124 Pisa, Italy*
[2]*Dipartimento di Scienze Chimiche, Università degli Studi di Trieste, Via L. Giorgieri 1, I-34127 Trieste, Italy*

Abstract

The phenomenon of birefringence, the anisotropy of the refractive index induced in light when it impinges on matter subject to generally spatially inhomogeneous, electric and/or magnetic induction fields, is discussed. It is shown how the subject presents challenges for theory, computation and experiment. Examples are given for the Cotton–Mouton and Buckingham effects, and for magnetochiral, Jones and magneto-electric birefringences.

Contents

ADVANCES IN QUANTUM CHEMISTRY, VOLUME 50
ISSN: 0065-3276 DOI: 10.1016/S0065-3276(05)50008-X

1. INTRODUCTION

Optical anisotropies, or birefringences [1–3], may occur when radiation impinges on matter in the presence of external electromagnetic fields. Several types of birefringence can be observed depending on the status of polarization of light, geometrical setup, symmetry of the sample subject to radiation and type of external field. Typical and most common examples, known since more than a century, are the linear birefringence observed when polarized light interacts with a sample in the presence of an external electric field with a component perpendicular to the direction of propagation (Kerr effect) [4–6], or the circular birefringence occurring when again linearly polarized light impinges either on a chiral sample (natural optical activity) or on any sample traversed by a static magnetic induction field with a component parallel to the direction of propagation of the beam (Faraday effect) [7,8,2].

Birefringences can be linear, circular or axial. A "linear" birefringence leads to the insurgence of an ellipticity, due to the anisotropy of the components of the refractive index parallel and perpendicular, respectively, to the applied external field. "Circular" birefringence results into a rotation of the plane of polarization due to an anisotropy arising between the right and left circular components of linearly polarized radiation. An "axial" birefringence is observed, for instance, in non-polarized light traversing an assembly of chiral molecules in the same conditions as for the regular Faraday effect (magnetochiral birefringence, see below). It leads to a phase difference between beams traversing in opposite direction through the sample, which in turn yields a measurable difference of intensity in the two counterpropagating beams.

In the last decade there has been a lot of activity in the field of theoretical and computational analysis of birefringences. Here we review some of the recent *ab initio* work, mostly involving the authors, on some optical anisotropies, *i.e.*, the linear birefringences induced by an externally applied magnetic induction field (Cotton–Mouton effect, CME) [9,10], an electric field gradient (Buckingham effect) [11,12] or mixed electric and magnetic induction fields (Jones and magneto-electric birefringences) [13–16] and the axial magnetochiral birefringence [17,18,3,19,20]. The emphasis will be in presenting and discussing the challenging aspects of these processes, in particular with reference to the comparison between theory and experiment. Strengths and weaknesses of the current computational strategies will be outlined, and it will be shown how theory and experiment can be complementary, one coming "to the rescue" of the other in some instances, and how in this interaction both approaches—the computational and the experimental—find ample chances to yield improvements, ultimately leading to advances both on the theoretical understanding of molecular properties and interaction of matter and radiation and on the technology and design of efficient optical apparata. Birefringences provide, in our opinion, an ideal test bed for theory, computation and experiment.

The CME [9,10] has been widely studied in our group, and several aspects of interest for this review have been analyzed in detail. Computational tools permit extremely accurate estimates of the effect in atoms and spherical molecules, where this birefringence, as are those induced by an electric field or an electric field gradient, is entirely determined by high order polarizabilities describing the rearrangement of electrons under the influence of fields and radiation [21]. The same response functions yield also a non negligible contribution to the CME of non spherical systems, a contribution that can be singled out experimentally by a delicate and often very difficult extrapolation of measurements taken

at different temperatures. Examples will be given of the amount of information a computational study can provide on the subject [22]. On the other hand, achieving an accuracy comparable to that of experiment is still very often the ultimate goal for *ab initio* studies of the other, lower order, properties involved in the effect, in particular the molecular magnetizability anisotropy. In the following we will discuss these aspects by making recourse to the experience gathered on several systems and exploiting different computational models and techniques. The success of the close collaboration with the experimentalists working on the field will also be highlighted.

The electric-field-gradient induced linear birefringence (Buckingham effect) [11] is another typical example of a process which requires extra accuracy, both from the point of view of the experiment and of computational science. Also, the theory of the effect has been until very recently the subject of open discussion [12,23–27]. This birefringence is at the basis of one of the most successful techniques for the experimental determination of molecular quadrupole moments [11]. The status of the art of the field will be briefly discussed, with special emphasis on some very recent studies which have brought to attention a remarkable disagreement of the literature on the molecular theory of the effect, and also led to a revision of some of the experimentally derived values of the molecular quadrupole of molecules, for example of N_2 [28], CO [29] and Cl_2 [30].

When unpolarized light passes through a sample of chiral molecules in the presence of an external magnetic induction field parallel to the direction of propagation of the radiation an axial birefringence is observed [17,18,3,19,20]. Two groups measured the resulting phase difference and they disagree quite noticeably on the magnitude of the effect for systems such as proline, limonene and carvone [31–33]. We analyzed this process [34] and, in spite of the approximations made, and of the strong dependence of the response of these floppy molecules to the combination of radiation and external magnetic induction field—which makes even the study of natural optical activity rather challenging [35]—we predict anisotropies much smaller than observed, up to three to four order of magnitude weaker than seen in some instances. This casts, in our view, a shadow on the interpretation which has been made of the results of experiment.

Jones and magneto-electric birefringences [14,16] arise when polarized light goes through atoms or molecules in a direction perpendicular to that of externally applied static electric and magnetic induction fields, arranged parallel (Jones) or perpendicular (magneto-electric) to each other. The resulting linear birefringence (bilinear in the two fields) is currently being investigated experimentally [36,37]. We discuss the results of our *ab initio* analysis carried out on inert gases (He, Ne, Ar, Kr), in centrosymmetric molecules (H_2, N_2, C_2H_2, C_6H_6 and C_6F_6) and in a polar molecule (CO) [38,39]. The emphasis is on the comparison between the strength of these two relatively new birefringences and that of the two traditional linear birefringences to which they superimpose (Kerr, Cotton–Mouton) or of the Buckingham effect.

2. DEFINITIONS AND GENERAL ASPECTS

The termbirefringence defines the difference between refractive indices for two “directions” of light propagation and/or polarization. An isolated isotropic medium without external field does not exhibit birefringence apart from the circular birefringence observed in samples of chiral molecules, in what is known as natural optical activity (NOA) [2,7].

2.1. Linear, circular and axial birefringences

A *linear* birefringence is induced by applying a static electric E or magnetic B field or an electric field gradient ∇E with a component perpendicular to the direction of propagation of a probe beam. Then

$$\Delta n = n_{\parallel} - n_{\perp}, \tag{1}$$

and the real counterpart of the complex refractive index $\tilde{n} = n + \mathrm{i}n'$ for linear polarized monochromatic light with polarization vector parallel ($n_{\parallel}$) and perpendicular ($n_{\perp}$) to the direction of the external field (or field gradient) differ. The processes observed in the various cases are

$\boldsymbol{E} \implies$ Kerr effect,

$\boldsymbol{B} \implies$ Cotton–Mouton effect,

$\boldsymbol{\nabla E} \implies$ Buckingham birefringence

and they are schematically represented in Fig. 1. There, as in the other schemes of this section, the externally applied field is rendered as a bold arrow, whose direction in this specific case forms an angle θ with that of polarization of the light beam. In the following figures we will consider $\theta = 0°$ for sake of simplicity. The two directions which define $n_{\parallel}$ and $n_{\perp}$ are indicated.

A linear birefringence is also induced when the electric and magnetic induction fields are both present along the path of the beam traversing the sample. If static $\boldsymbol{E}$ and $\boldsymbol{B}$ fields are applied perpendicular to each other and to the path of radiation, magneto-electric birefringence is observed, see Fig. 2. When they are applied parallel to each other and still with components perpendicular to the beam, Jones birefringence occurs, see Fig. 3. Jones and magneto-electric birefringences superimpose to the two more conventional linear birefringences (Kerr and Cotton–Mouton). Their optical axes (that is, the perpendicular axes to which the birefringence refers) are different. In magneto-electric birefringence, they coincide with those of the Kerr and Cotton–Mouton birefringences, and they are defined by the parallel and perpendicular direction with respect to the external fields (see Fig. 2). Jones birefringence has optical axes bisecting those of the other birefringences, lying thus at $+45°$ and $-45°$ with respect to the direction of the external fields, see Fig. 3. Thus in

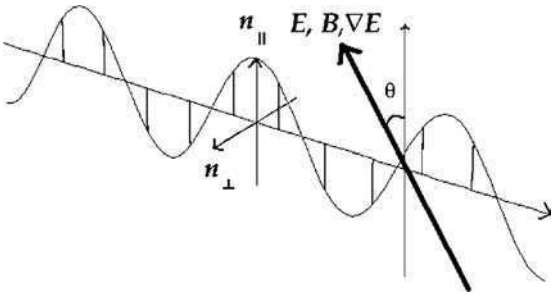

Fig. 1. Kerr, Cotton–Mouton or Buckingham *linear* birefringences. The result is an *ellipticity*.

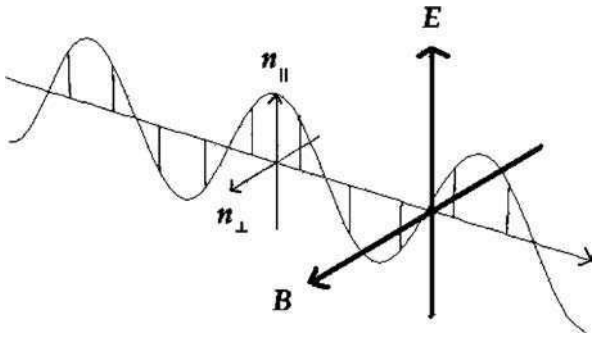

Fig. 2. Magneto electric *linear* birefringence.

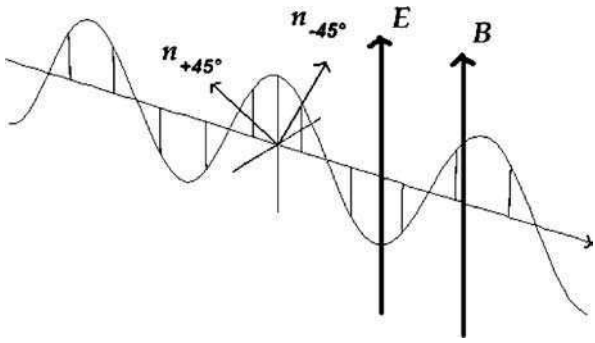

Fig. 3. Jones *linear* birefringence.

this case

$$\Delta n = n_{+45^\circ} - n_{-45^\circ}. \tag{2}$$

The role of the external field can also be taken by a linearly polarized pump beam which propagates parallel or antiparallel to the probe beam. The linear birefringence induced in this way is known as optical Kerr effect, and its implications have been discussed for example by Buckingham [40].

Linear birefringences are usually estimated by measuring the *ellipticity* acquired by the polarized beam traversing the sample. The anisotropy of the refractive index induces a phase difference ϕ, also known as retardation or retardance, between the two perpendicular components of the polarization vector, whose tip in turn starts moving along an ellipse. The ellipse is characterized by a ratio of the two axes (ellipticity) which, for small effects, is roughly proportional to half of the retardance of the beam. For an optical path l and wavelength λ

$$\phi = 2\pi \frac{l}{\lambda} \Delta n \sin 2\theta \tag{3}$$

where θ is the angle seen in Fig. 1.

Circular birefringence is behind the well known phenomenon of optical rotation in NOA [2,7,41]. The anisotropy results in this case from a differential interaction of a chiral sample

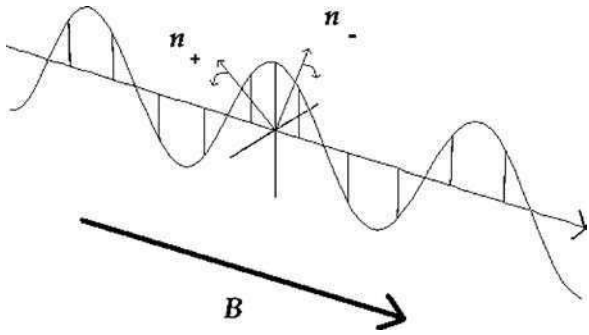

Fig. 4. Faraday *circular* birefringence. The result is an *optical rotation*.

with the left and right circularly polarized components of the linearly polarized probe light. Circular birefringence, however, can also be induced in any medium by the application of a static magnetic field aligned parallel to the probe beam. In this case the effect goes under the name of magneto-optical activity or Faraday effect [42,43,7,8], see Fig. 4. In both cases the anisotropy is written as

$$\Delta n = n_- - n_+, \tag{4}$$

the difference between refractive indices for left (n_-) and right (n_+) circularly polarized components of the linearly polarized probe light. In transparent regions of the sample, the resulting effect is the *rotation* α of the plane of polarization (optical or magneto-optical rotation)

$$\alpha = \frac{\pi l}{\lambda}\Delta n. \tag{5}$$

Circular birefringence can moreover be induced by static orthogonal electric and magnetic induction fields in optically active fluids, in the same arrangement as seen for magneto-electric birefringence [44,45], or by circularly polarized light instead of a static magnetic field (Optical Faraday effect) [46].

An *axial* birefringence, defined as the difference

$$\Delta n = n^{\uparrow\uparrow} - n^{\uparrow\downarrow} \tag{6}$$

between refractive indices for unpolarized probe light propagating parallel ($n^{\uparrow\uparrow}$) and antiparallel ($n^{\uparrow\downarrow}$) to a reference direction, can be induced by a static magnetic induction field B in an isotropic sample of chiral molecules. The effect is known as magnetochiral birefringence [17,18,3,19,20], see Fig. 5. This birefringence coexists with those due to natural optical activity and to the magnetic field induced (Faraday) one, and the corresponding phase difference, measured on beams travelling in opposite directions through the sample, is measured through the determination of their intensity after the beams are brought to interference [32].

Changes in the absorption index n'—the imaginary counterpart $\tilde{n}$—give rise to dichroisms, essentially the absorptive analogs of birefringences. For example, in regions of absorption the light beam emerging from a chiral sample or from any sample subject to a magnetic induction field aligned with the direction of propagation of the beam becomes elliptically polarized (electric or magnetic circular dichroism) [2,7,8].

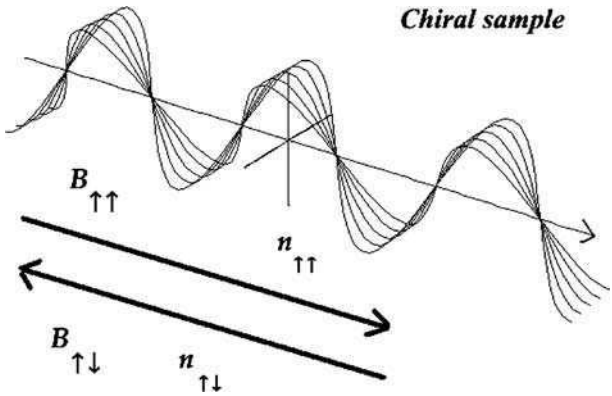

Fig. 5. Magnetochiral *axial* birefringence. What is measured is the difference in intensity for counterpropagating light beams.

When the field inducing the anisotropy is time-dependent, the birefringence is said to be "optically induced". Optically induced birefringences yield in general different information on the electronic structure of the sample with respect to those induced by static fields. See the work by Woźniak [47] for interesting discussions on the subject.

2.2. Field and temperature dependence

In general terms we can write the field dependence of a given birefringence as

$$\Delta n = w \times F_1^{n_1} F_2^{n_2} \times {}_mW(\lambda, T) \tag{7}$$

where F_1, F_2 identify the field strengths and n_1 and n_2 the corresponding power. The quantity w is a combination of fundamental constants, depending on the specific process, as does the molar quantity ${}_mW$. ${}_mW$ is usually identified as the "constant" for that birefringence (the Kerr, Cotton–Mouton, Buckingham, Jones, Verdet constant, for instance, the last one defined in studies of Faraday rotation). The specific dependence on the fields for some birefringences is summarized in Table 1.

At a fixed pressure the general form of an optical anisotropy is

$$\Delta n \propto A_0 + \frac{A_1}{T} + \frac{A_2}{T^2} + \cdots. \tag{8}$$

In the above equation A_0 includes all molecular contributions due to the *reorganization* of the electrons as a result of the action of the external field(s). $A_1, A_2, \ldots$ are connected to different mechanisms of *reorientation* of the molecules, involving the interaction of the field(s) with permanent electric or magnetic multipole moments. The terms exhibiting a more than inverse linear dependence on the temperature are usually connected to the presence of permanent magnetic dipole moments or higher order processes involving more complicated interactions between fields and multipoles. The temperature dependence is vanishing for systems of spherical symmetry.

Table 1. The field dependence for some birefringences

Kerr (electro-optical)	E^2
Cotton–Mouton	B^2
Jones (magneto-electric)	EB
Buckingham	∇E
Faraday	B
Magnetochiral	B

2.3. Connection to molecular response properties

$A_0, A_1, A_2, \ldots$ involve isotropic averages of molecular, generally frequency dependent, tensor properties, as permanent multipole moments, polarizabilities and hyperpolarizabilities. The connection between the macroscopic observables and the molecular properties for the various effects, and hence the explicit expressions for the A_i quantities, is usually established from a semiclassical description of the interaction of light with molecules: the molecules are treated as quantum mechanical objects perturbed by classical electromagnetic fields. So classical electrodynamic and quantum mechanical perturbation theories are at the basis of the formulation.

Charge distributions are written in terms of multipole electric moments and current distributions in magnetic multipole moments. The (complex) induced molecular moments are first expanded in the (radiation) electromagnetic fields of the probe light. Following the scheme and the notation of Barron [2] (see also [48]), where complex quantities (as for the refractive index above) are denoted by a wide tilde superscript, the components of the induced electric dipole ($\tilde{\boldsymbol{\mu}}$), electric quadrupole ($\widetilde{\boldsymbol{\Theta}}$) and magnetic dipole ($\widetilde{\boldsymbol{m}}$) can be written as

$$\tilde{\mu}_\alpha = \tilde{\alpha}_{\alpha\beta}\widetilde{E}_\beta + \frac{1}{3}\tilde{A}_{\alpha,\beta\gamma}\widetilde{\nabla_\beta E_\gamma} + \widetilde{G}_{\alpha\beta}\widetilde{B}_\beta + \cdots, \tag{9}$$

$$\widetilde{\Theta}_{\alpha\beta} = \tilde{A}^*_{\gamma,\alpha\beta}\widetilde{E}_\gamma + \widetilde{D}^*_{\gamma,\alpha\beta}\widetilde{B_\gamma} + \widetilde{C}_{\alpha\beta,\gamma\delta}\widetilde{\nabla_\gamma E_\delta} + \cdots, \tag{10}$$

$$\widetilde{m}_\alpha = \tilde{\xi}_{\alpha\beta}\widetilde{B}_\beta + \widetilde{G}^*_{\beta,\alpha}\widetilde{E_\beta} + \frac{1}{3}\widetilde{D}_{\alpha,\beta\gamma}\widetilde{\nabla_\beta E_\gamma} + \cdots \tag{11}$$

with Einstein's convention for summation over repeated indices assumed here and throughout. The above equations involve complex fields and complex frequency dependent tensors. The real and imaginary components play a role in either the transparent or absorptive regions of the sample. So, for instance,

$$\tilde{\alpha}_{\alpha\beta} = \alpha_{\alpha\beta} - \mathrm{i}\alpha'_{\alpha\beta} = \tilde{\alpha}^*_{\beta\alpha}, \tag{12}$$

$$\tilde{A}_{\alpha,\beta\gamma} = A_{\alpha,\beta\gamma} - \mathrm{i}A'_{\alpha,\beta\gamma} = \tilde{A}_{\alpha,\gamma\beta}, \tag{13}$$

$$\widetilde{G}_{\alpha,\beta} = G_{\alpha,\beta} - \mathrm{i}G'_{\alpha,\beta}, \tag{14}$$

$$\tilde{\xi}_{\alpha\beta} = \xi_{\alpha\beta} - \mathrm{i}\xi'_{\alpha\beta} = \tilde{\xi}^*_{\beta\alpha} \tag{15}$$

for the complex electric dipole polarizability $\tilde{\boldsymbol{\alpha}}$, the electric dipole-electric quadrupole $\tilde{\boldsymbol{A}}$ and electric dipole – magnetic dipole $\widetilde{\boldsymbol{G}}$ polarizabilities and the magnetizability $\tilde{\boldsymbol{\xi}}$, respec-

tively. Conventional sum-over-states quantum expressions of the tensors can be recovered via a perturbative expansion of the moments in terms of the unperturbed wave functions [2,48],

$$\alpha_{\alpha\beta} = \frac{2}{\hbar}\sum_{j\neq n}\frac{\omega_{jn}}{\omega_{jn}^2-\omega^2}\Re\{\langle n|\mu_\alpha|j\rangle\langle j|\mu_\beta|n\rangle\} = \alpha_{\beta\alpha}, \tag{16}$$

$$\alpha'_{\alpha\beta} = -\frac{2}{\hbar}\sum_{j\neq n}\frac{\omega}{\omega_{jn}^2-\omega^2}\Im(\langle n|\mu_\alpha|j\rangle\langle j|\mu_\beta|n\rangle) = -\alpha'_{\beta\alpha}, \tag{17}$$

$$A_{\alpha,\beta\gamma} = \frac{2}{\hbar}\sum_{j\neq n}\frac{\omega_{jn}}{\omega_{jn}^2-\omega^2}\Re\{\langle n|\mu_\alpha|j\rangle\langle j|\Theta_{\beta\gamma}|n\rangle\}, \tag{18}$$

$$A'_{\alpha,\beta\gamma} = -\frac{2}{\hbar}\sum_{j\neq n}\frac{\omega}{\omega_{jn}^2-\omega^2}\Im(\langle n|\mu_\alpha|j\rangle\langle j|\Theta_{\beta\gamma}|n\rangle), \tag{19}$$

$$G_{\alpha,\beta} = \frac{2}{\hbar}\sum_{j\neq n}\frac{\omega_{jn}}{\omega_{jn}^2-\omega^2}\Re(\langle n|\mu_\alpha|j\rangle\langle j|m_\beta|n\rangle) = G_{\beta,\alpha}, \tag{20}$$

$$G'_{\alpha,\beta} = -\frac{2}{\hbar}\sum_{j\neq n}\frac{\omega}{\omega_{jn}^2-\omega^2}\Im(\langle n|\mu_\alpha|j\rangle\langle j|m_\beta|n\rangle) = -G'_{\beta,\alpha}, \tag{21}$$

$$\xi_{\alpha\beta} = \frac{2}{\hbar}\sum_{j\neq n}\frac{\omega_{jn}}{\omega_{jn}^2-\omega^2}\Re(\langle n|m_\alpha|j\rangle\langle j|m_\beta|n\rangle) + \langle n|\xi^{\mathrm{dia}}_{\alpha\beta}|n\rangle = \xi_{\beta\alpha}. \tag{22}$$

Above, ω is the frequency of radiation, $|n\rangle$ and $|j\rangle$ indicate the reference state and an excited state, respectively, and $\hbar\omega_{jn} = E_j - E_n$ is the corresponding excitation energy. The operators involved in the definitions are:

$$\mu_\alpha = \sum_i q_i r_{i\alpha}, \tag{23}$$

$$m_\alpha = \sum_i \frac{q_i}{2m_i}\varepsilon_{\alpha\beta\gamma}r_{i\beta}p_{i\gamma} = \sum_i \frac{q_i}{2m_i}l_{i\alpha}, \tag{24}$$

$$\Theta_{\alpha\beta} = \frac{1}{2}\sum_i q_i(3r_{i\alpha}r_{i\beta} - r_{i\gamma}r_{i\gamma}\delta_{\alpha\beta}), \tag{25}$$

$$\xi^{\mathrm{dia}}_{\beta\gamma} = \frac{1}{4}\sum_i \frac{q_i^2}{m_i}(r_{i\beta}r_{i\gamma} - r_{i\delta}r_{i\delta}\delta_{\beta\gamma}) \tag{26}$$

with the sum running over the particles of charge q_i, mass m_i, and components of the position $r_{i\alpha}$, linear momentum $p_{i\alpha}$, angular momentum $l_{i\alpha}$. $\varepsilon_{\alpha\beta\gamma}$ is the alternating Levi-Civita tensor. Operators which we define here, although they will be introduced later in this work, are the traced quadrupole moment operator

$$q_{\alpha\beta} = \sum_i q_i r_{i\alpha}r_{i\beta} \tag{27}$$

and the linear momentum

$$\mu^p_\alpha = \sum_i \frac{q_i}{m_i}p_{i\alpha}. \tag{28}$$

The presence of additional static fields is often accounted for through a second expansion of the dynamic molecular property tensors (lower order terms) in powers of the external (static) fields. For example, in the presence of mixed electric and magnetic induction fields, the real part of the tensor component $\widetilde{G}_{\alpha,\beta}$, equation (20) above, can be expanded as

$$G_{\alpha,\beta}(\boldsymbol{E},\boldsymbol{B}) = G_{\alpha,\beta} + G_{\alpha,\beta\gamma}B_\gamma + G_{\alpha,\beta\gamma,\delta}B_\gamma E_\delta + \cdots. \tag{29}$$

For the resulting higher order polarizabilities quantum mechanical sum-over-states expressions are found by using perturbed wavefunctions and energies in the sum-over-states expressions for the lower order tensors. Thus starting from equation (20), and with the following substitutions arising from the presence of an external magnetic induction field B [18,38]

$$\omega_{jn} \to \omega_{jn} - \frac{B_\gamma}{\hbar}(m_\gamma^{jj} - m_\gamma^{nn}) = \omega_{jn} - \frac{B_\gamma}{\hbar}\Delta m_\gamma^{jn}, \tag{30}$$

$$|j\rangle \to |j\rangle - \frac{B_\gamma}{\hbar}\sum_{k\neq j}\frac{1}{\omega_{jk}}\langle k|m_\gamma|j\rangle = |j\rangle - \frac{B_\gamma}{\hbar}\sum_{k\neq j}\frac{m_\gamma^{kj}}{\omega_{jk}}, \tag{31}$$

$$\frac{1}{\omega_{jn}^2-\omega^2} \to \approx \frac{1}{\omega_{jn}^2-\omega^2}\left[1 + \frac{2\omega_{jn}\Delta m_\gamma^{jn}B_\gamma}{\hbar(\omega_{jn}^2-\omega^2)}\right] \tag{32}$$

$$m_\beta \to m_\beta + \xi_{\beta\gamma}^{\text{dia}}B_\gamma \tag{33}$$

where $m_\alpha^{nn} = \langle n|m_\alpha|n\rangle$ and $m_\alpha^{jj} = \langle j|m_\alpha|j\rangle$, after some algebra one obtains

$$G_{\alpha,\beta\gamma} = G_{\alpha,\beta\gamma}^{\text{dia}} + G_{\alpha,\beta\gamma}^{\text{para}}, \tag{34}$$

$$G_{\alpha,\beta\gamma}^{\text{dia}} = \frac{2}{\hbar}\sum_{j\neq n}\frac{\omega_{jn}}{\omega_{jn}^2-\omega^2}\Re\left\{\langle n|\mu_\alpha|j\rangle\langle j|\xi_{\beta\gamma}^{\text{dia}}|n\rangle\right\}, \tag{35}$$

$$\begin{aligned} G_{\alpha,\beta\gamma}^{\text{para}} = \frac{2}{\hbar^2}\sum_{j\neq n}\Bigg\{ & \frac{\omega_{jn}^2+\omega^2}{(\omega_{jn}^2-\omega^2)^2}(m_\gamma^{jj}-m_\gamma^{nn})\Re\big(\langle n|\mu_\alpha|j\rangle\langle j|m_\beta|n\rangle\big) \\ & + \sum_{k\neq n}\frac{\omega_{jn}}{\omega_{kn}(\omega_{jn}^2-\omega^2)}\Re\big[\langle k|m_\gamma|n\rangle\big(\langle n|\mu_\alpha|j\rangle\langle j|m_\beta|k\rangle \\ & + \langle n|m_\beta|j\rangle\langle j|\mu_\alpha|k\rangle\big)\big] + \sum_{k\neq j}\frac{\omega_{jn}}{\omega_{kj}(\omega_{jn}^2-\omega^2)} \\ & \times \Re\big[\langle j|m_\gamma|k\rangle\big(\langle n|\mu_\alpha|j\rangle\langle k|m_\beta|n\rangle + \langle n|m_\beta|j\rangle\langle k|\mu_\alpha|n\rangle\big)\big]\Bigg\}. \end{aligned} \tag{36}$$

An alternative, more compact formulation of the tensor properties, which is at the basis of their computational evaluation, is in terms of response functions [49]. All second-order properties are expressed as a linear response, which, in the notation of Ref. [50], we indicate as

$$\alpha_{\alpha\beta}(-\omega;\omega) = -\Re\langle\langle\mu_\alpha;\mu_\beta\rangle\rangle_\omega = -\langle\langle\mu_\alpha;\mu_\beta\rangle\rangle_\omega, \tag{37}$$

$$\alpha'_{\alpha\beta}(-\omega;\omega) = +\Im\langle\langle\mu_\alpha;\mu_\beta\rangle\rangle_\omega = 0, \tag{38}$$

$$G_{\alpha,\beta}(-\omega;\omega) = -\Re\langle\langle\mu_\alpha;m_\beta\rangle\rangle_\omega = 0, \tag{39}$$

$$G'_{\alpha,\beta}(-\omega;\omega) = +\Im\langle\langle \mu_\alpha; m_\beta \rangle\rangle_\omega = -\mathrm{i}\langle\langle \mu_\alpha; m_\beta \rangle\rangle_\omega, \tag{40}$$

$$A_{\alpha,\beta\gamma}(-\omega;\omega) = -\Re\langle\langle \mu_\alpha; \Theta_{\beta\gamma} \rangle\rangle_\omega = -\langle\langle \mu_\alpha; \Theta_{\beta\gamma} \rangle\rangle_\omega, \tag{41}$$

$$A'_{\alpha,\beta\gamma}(-\omega;\omega) = +\Im\langle\langle \mu_\alpha; \Theta_{\beta\gamma} \rangle\rangle_\omega = 0. \tag{42}$$

The second equality holds for real wave functions. Third order quantities are related to the quadratic response functions by, for example,

$$G^{\text{para}}_{\alpha,\beta\gamma}(-\omega;\omega,0) = \Re\langle\langle \mu_\alpha; m_\beta, m_\gamma \rangle\rangle_{\omega,0}. \tag{43}$$

The fourth-order properties are related to cubic response functions, for instance,

$$G^{\text{para}}_{\alpha,\beta\gamma,\delta}(-\omega;\omega,0,0) = -\Re\langle\langle \mu_\alpha; m_\beta, m_\gamma, \mu_\delta \rangle\rangle_{\omega,0,0} \tag{44}$$

and so on. Birefringences are thus amenable to calculations via their link to general response theory, which is nowadays implemented for several approximate wave function models, see next section.

3. GENERAL REMARKS ON COMPUTATION

The identification of the tensor properties entering the quantities A_j $(j = 0, 1, 2, \ldots)$ in equation (8) with response functions has been instrumental in recent years in favoring the development of a computational literature on the subject. In general, to predict the strength of a birefringence by computational approaches we must be able to determine *ab initio* values of first order properties as well as response functions of various order, here up to cubic. Various issues enter the accurate *ab initio* determination of these properties, which in general poses many challenges. We briefly analyze these issues in the following. A broader discussion can be found in the original literature and in Refs. [22] (CME) and [25] (Buckingham birefringence).

3.1. Wave function models, electron correlation and basis set effects

An important recipe in calculations of the optical properties is to employ a computational procedure allowing one to assess the quality of the numerical result and to estimate the absolute error associated with it.

It is well known that the two major sources of errors in *ab initio* electronic-structure calculations stem from the approximations introduced in the one-electron space and in the N-electron space in solving the many-body Schrödinger equation [51]. The use of a hierarchical approach where the description of the one- and N-electron spaces is systematically improved at each "step"—often in conjunction with the determination of vibrational effects—has proven very successful for the accurate determination of many molecular properties [51–55,28,56,26,24,57–59]. The goal of such an approach is to reach the "exact limit"—that is, the result for the exact N-electron wave-function in a complete one-electron basis—in a controlled way, by employing a series of basis sets and wave-function approximations which have the exact solution as limit. Also, a hierarchy of approximations of increasing complexity and reliability allows for the identification of "balanced" levels of theory [51,58], such that the solution to a particular problem of sufficient accuracy for the given purposes is reached without unnecessary computational effort.

As far as the one-electron space is concerned, the correlation-consistent basis sets of Dunning and coworkers [60–67] constitute a good paradigmatic family of hierarchical basis sets—that is, sequences of basis sets that allow one to approach the basis-set limit result by going to higher levels in the hierarchy. As the determination of given molecular or atomic properties often requires a special, flexible description of specific regions of the charge distribution, like the outer regions for dipole and quadrupole moments or the inner region for nuclei-related properties (NMR shieldings, electric field gradients at the nuclei, *etc*.), both diffusely augmented aug-cc-pVXZ [61] and core-valence (aug-)cc-pCVXZ [64, 67] sets have been developed. Further augmentation has been found to be very important for the determination of electric quadrupole moments, due to the quadratic dependence of the quadrupole moment operator on the electronic coordinate [28,56,57,26], and in general of high order response functions.

For single configuration dominated systems, a standard hierarchy of wave-function models for the calculation of energies and other static molecular properties (*i.e.*, multipoles) is represented by the following sequence of models: Hartree–Fock self-consistent field (HF or SCF), second-order Møller–Plesset (MP2) [68], coupled cluster singles and doubles (CCSD) [69] and CSD with a perturbational correction for connected triples, CCSD(T) [70]. All methods are well established and they are exhaustively described, for instance, in Refs. [51,71]. In particular, the CCSD(T) model gives results close to the full configuration interaction (FCI) limit with an accuracy comparable to that of experiment when sufficiently large basis sets are used. Recently further elements have been included to the sequence, with the development of analytic derivative approaches to coupled cluster singles, doubles and triples (CCSDT) [72–76] and in general to arbitrary order CC expansions [77,78]. They have been employed for some benchmark studies of CME of neon and argon in the gas phase [21].

Within the specific case of the birefringences, the application of the above mentioned hierarchies of basis sets and wave-function models allowed us to determine very accurate values for molecular electric quadrupole moments, see Refs. [28,56,26,24,57,30,29].

Concerning frequency-dependent properties, whereas basis set demands are basically the same as for static properties (*e.g.*, the same families of basis sets can be used), an additional problem in the definition of a hierarchy of models is the behavior of the wave function model at the poles. Both MP2 and CCSD(T)—two members of the standard hierarchy for static properties—exhibit in fact the incorrect pole-structure, not consistent with exact theory, due to the orbital relaxation terms (see the discussion in Ref. [79]). A hierarchy of coupled cluster methods particularly suited for the calculation of dynamic properties of single configuration dominated systems is represented by the models CCS, CC2 [80], CCSD, and CC3 [81–84,59]. The advantage of this hierarchy is that within each member of the set, frequency dependent properties can be formulated without an explicit relaxation of the orbitals to the frequency dependent perturbation. This guarantees the correct pole structure. The dependence on the frequency of the properties discussed here can be arranged in power series [85–87], which makes the description of frequency dispersion of optical properties easier and more efficient.

As mentioned above, the hierarchies are designed for single configuration based systems. In specific cases multiconfigurational approaches, such as multiconfigurational SCF (MCSCF) response [50], have been also been used. MCSCF has been seldom used in recent years, due to the very fast increase in the size of the active spaces needed in calculations as the size of the system increases. On the other hand, there has been a fast development of

Density Functional Theory response (see for instance [88,89]), which has been extended and coded to allow computations of up to fourth order properties (cubic response) [90]. DFT response has been employed already with good success in studies of birefringences [91,92,39], and it appears at this stage to provide a valid, cost effective and promising alternative to the *ab initio* hierarchies discussed above when the size of the system increases, or its symmetry lowers. Examples will be given below.

The studies of birefringences using the wave function models, basis sets and techniques discussed in this section have been made possible by the constant development and improvement made within a large community of quantum chemists in computer codes, now widely diffuse, as DALTON [93] and ACES2 [94].

3.2. Vibrational contributions and conformational effects

Vibrational effects in the context of *ab initio* studies of birefringences have been in general discussed in terms of zero-point vibrational average (ZPVA) and pure vibrational contributions (PV). The zero-point vibrational average is the average of the electronic property as a function of the nuclear coordinates over the vibrational ground state. The pure-vibrational contribution arises from the distortion of the electronic potential surface induced by an external perturbing field, which has the effect of modifying the nuclear motion. As a result there is a "purely nuclear" contribution to the property. An exhaustive discussion on this subject can be found, for instance, in Refs. [95–97]. See also Ref. [98] and the very recent work of Ref. [99].

The effect of molecular vibration on the observable and its role in condensed phases may be strong. The contribution of molecular vibrations was found to be significant in natural optical activity [100], and also in recent studies of CME in polyatomic molecules [101, 102,91], electric field gradient induced birefringence [24,26] and other cases. For instance, a study of zero-point vibrational corrections on the optical rotation in methyloxirane [100] shows that they can contribute as much as 20–30% of the electronic counterpart. Effects of similar magnitude are also possible for the magnetochiral birefringence. ZPVA and PV contributions to Buckingham birefringence were determined also for diatomic molecules, as CO [26,25] and Cl_2 [30], and found to be relatively contained. Similar studied have been carried out for the CME, see Ref. [103] but also the work by Bishop and co-workers [104–106].

Another important aspect that needs to be considered when analyzing optical properties of large (especially if chiral) molecules is their conformational flexibility. For instance, in the study of magnetochiral birefringence in Ref. [34] the specific optical rotation calculated at the SCF level for the conformers of carvone, limonene and proline for which we also determined the magnetochiral birefringence shows substantial conformational effects, affecting both the sign and the absolute values. Even larger conformational effects are observed for the magnetochiral birefringence. Large changes in the optical rotation and magnetochiral birefringence occur upon rotation around a single bond (cf. carvone) or modifications in the ring conformation (cf. proline). These effects were confirmed also by the recent study on conformational effects on the optical rotation of alanine and proline made in Ref. [35].

3.3. Condensed phase studies

Very often birefringence experiments are performed in solution or on liquid substances. The comparison should then be made on consistent data. For this reason we have in some cases employed continuum models to describe the specific interactions occurring in condensed phase. The dielectric continuum model [107–109] and subsequently a semi-continuum model [110] have been employed to study the CME of liquid water [109,111]. Evidence showed that this linear birefringence involving mixed magnetic and electric fields can be extremely sensitive to the description of these interactions. Solvent effects are likely to be particularly significant for carvone, limonene, and proline, where the liquid-phase conformation may differ from the gas-phase state one. The probable consequences concerning magnetochiral birefringence have been discussed in Ref. [34].

More recently studies of CME of furan and its homologues, thiophene and selenophene, in the gas phase, for the pure liquids and in solutions [92] were undertaken by resorting to the polarizable continuum model (PCM) [112,113]. The latter, in its integral equation formalism [114–116], has been widely employed, for studies of frequency dependent properties. The use of a suitable continuum model was instrumental in yielding remarkable agreement between theory and experiment in the study of Ref. [92].

3.4. Relativistic effects

With accuracy on the electronic estimates of molecular properties approaching the limit, additional sources of approximation, and thus of possible error, need to be analyzed. Relativistic effects for instance, as well as non-adiabatic effects, can become important especially as we move to systems including heavier atoms.

Estimates of the relativistic effects on the quadrupole moments of N_2, C_2H_2, CO and Cl_2 were included in Refs. [28,56,26,30]. In the study of the molecular quadrupole moment and Buckingham birefringence of molecular chlorine [30] we have also carried out an analysis of the effect of relativity on the response quantities, by employing a Dirac–Hartree–Fock (DHF) wave function model, and exploiting the development and coding of linear and quadratic responses in the relativistic *ab initio* electronic structure program DIRAC [117]. The quadrupole moment of Cl_2 changes by $\approx$1% upon inclusion of the effect of relativity going from an Hartree–Fock wave function model to DHF. A similar, though a bit smaller, effect can be seen for the anisotropy of the electric dipole polarizability. The hyperpolarizability contribution (see Section 4.2) changes by 2–3%. On the other hand, again when the accuracy of the *ab initio* approach is as high as that achieved recently in a study of the CME of neon and argon [21], it makes the need for an accounting for relativistic effects mandatory even for systems involving nuclei usually not considered "heavy".

In this respect, the very recent development of a direct perturbation theory of relativistic effects within closed-shell coupled cluster theory, and its implementation in the DALTON platform are extremely promising [118,119]. This has made possible the computation of first-order relativistic correction to the static and frequency dependent electric dipole polarizability and second hyperpolarizability of neon [119]. The extension to the response functions of relevance for other birefringences should be feasible.

3.5. Interaction properties, effects of the density

Comparison of *ab initio* results for gas phase optical properties with experimental data is often made difficult by the fact that the theoretical model involves isolated species, and the effect of many-body collision—and in macroscopic terms of density—should be taken into account. The effect of two-body and higher order collisions on optical properties is often expressed in virial expansions, where the dependence of the property P of a real gas on the density ρ is written as

$$P = A_P + B_P\rho + C_P\rho^2 + \cdots \tag{45}$$

with the coefficients A_P, B_P, ... defining the first, second ... virial coefficients. See also Refs. [120–124]. In general the study of the effect of density is limited to the determination of the first-order and the second virial coefficients, as it is reasonable to assume that three-body and higher collisions terms would play a minor role. For a mole of an ideal molecular gas—that is, for a system of N_A non-interacting particles

$$P = A_P = N_A\bar{p} \tag{46}$$

where N_A is Avogadro's number and $\bar{p}$ denotes the mean contribution of an individual molecule to the property P. In a semiclassical approach, the second virial coefficient B_P for spherical particles 1 and 2 can be associated with the following quantity [125,126]

$$B_P = 4\pi N_A^2 \int \left[\frac{1}{2}p_{12}(R) - \frac{\bar{p}_1 + \bar{p}_2}{2}\right] \exp\left(-\frac{V(R)}{kT}\right) R^2\,\mathrm{d}R \tag{47}$$

where $R = R_{12}$ is the distance between the two particles, $V(R)$ their interaction potential and p_{12} is the property p of the couple formed by the two particles. p is in principle any property, and in fact virial-type expansions can be written for the "constants" defined, for a given birefringence, in equation (7). They involve integrations, over the whole range of interparticle distances, of so-called "interaction" properties—that is, the fraction $\Delta p = p_{12} - p_1 - p_2$ of p_{12} arising directly from the two-body interaction. The full quantum mechanical analogs of equation (47) involve the complete solution of the two particle Schrödinger equation for the two particle system, to obtain both the discrete and the entire continuum spectrum, and an in-principle infinite sum over the whole energy spectrum.

In the last few years we have performed studies of the effect of density, both at semiclassical and full quantum mechanical levels, for Kerr [127–130], Cotton–Mouton [131] and Buckingham [126] birefringence in rare gases (helium, neon and argon). In some cases, see, *e.g.*, the temperature dependence of the second Kerr virial coefficient of argon [128], we were able to challenge experiment [132], and suggest its revision.

3.6. Gauge-origin dependence of magnetic properties

All magnetic properties calculated within approximate models suffer in principle from a gauge-origin dependence problem. It is for instance well known that magnetizabilities computed with standard basis sets in approximate calculations depend on the choice of the origin of the vector potential [133]. The non-physical dependence on the details of the

calculation thus introduced in every approximate computational study of most magnetic properties can often be circumvented using for instance Perturbation Dependent Basis Sets (PDBS), also known as London Atomic Orbitals (LAO's) or Gauge Including Atomic Orbitals (GIAO's) [134–138]—that is, basis sets which explicitly include the dependence on the strength of the external magnetic induction field in a phase factor. Magnetizabilities computed with LAO's are gauge-origin independent. They are available at the Hartree–Fock, MCSCF and DFT levels within DALTON, and also at the DFT level within the GAUSSIAN suite [139]. Still in the context of birefringences, LAO's can also be employed for linear response properties involving magnetic interactions to obtain gauge-origin independence of the natural optical rotation at the Hartree–Fock, MCSCF and DFT levels. At the CCSD level they ensure gauge-origin independence of the Verdet constant (and the so-called B term) of the Faraday effect [140]. For the examples discussed here the benefits of a gauge-origin independent approach are felt in studies performed at the Hartree–Fock and MCSCF level of CME [141–143] and at the Hartree–Fock level of NOA of chiral systems [34]. LAO's are still unavailable, to the best of our knowledge, for frequency dependent third order properties (or higher).

An alternative way to circumvent the gauge-origin dependence of magnetic properties which has been exploited in the field of birefringences is the use of the continuum set of gauge transformation (CSGT) approach [144,145], which yields an approximate solution to the problem. CSGT magnetizabilities are available for instance within the GAUSSIAN suite [139], and we have resorted to the CSGT approach for our studies of CME in gas phase [91], and in condensed phase [92] where a DFT model was adopted.

When the gauge problem could not be "theoretically" resolved via a special technique (either LAO's or CSGT) the degree of gauge dependence has been explicitly analyzed, see, for instance, Refs. [34,38] for magnetochiral and Jones/magneto-electric birefringences, respectively.

4. REVIEW OF RESULTS: EXAMPLES

The main scope of this review is to analyze the phenomenon of birefringences in as much as it proves to be challenging both for theory and for experiment. In the following a few examples will be given to show where this happens to be the case. We will briefly review some specific cases where either theory or experiment, or both, find a hard match describing the process. Often, a synergy between the two approaches (computational and experimental) can be established, where one comes to the rescue of the other. On the other hand, there is the case of Buckingham's birefringence, where for quite some time two different theories have been in disagreement in the prediction of the observable, and only recently, also thanks to the important clues yielded by accurate computations, the dilemma has been solved. Or the case of magnetochiral birefringence, see also below, where apparently different experiments are in large disagreement on the interpretation of the experiment, and our computational study is in disaccord with all of them. The matter is thus complicated and fascinating, a test bed for advanced molecular properties models and for modern experimental, optical apparata designers.

4.1. Cotton–Mouton linear birefringence

In the general expression of magnetic field induced birefringence, widely known as Cotton–Mouton effect (CME) [9,10],

$$\Delta n = A_0 + \frac{A_1}{T} + \frac{A_2}{T^2}, \tag{48}$$

the quantities A_0, A_1 and A_2 involve the properties shown in Table 2 [22,146]. In Table 2 (and in Tables 8, 12 and 14 below, for other birefringences) we indicate for each of the parameters the molecular quantities they involve, and their expression in terms of first order properties (for which we use the notation $\langle\cdots\rangle = \langle n|\cdots|n\rangle$), linear, quadratic and cubic response functions. In particular, for the CME, the parameter A_0 is proportional to the anisotropy of the hypermagnetizability $\Delta\eta(\omega)$, a combination of components of the (second) hypermagnetizability tensor $\eta_{\alpha\beta,\gamma\delta} = \eta^{\text{dia}}_{\alpha\beta,\gamma\delta}(-\omega;\omega,0) + \eta^{\text{para}}_{\alpha\beta,\gamma\delta}(-\omega;\omega,0,0)$

$$\Delta\eta(\omega) = \frac{1}{5}\left(\eta_{\alpha\beta,\alpha\beta} - \frac{1}{3}\eta_{\alpha\alpha,\beta\beta}\right). \tag{49}$$

Also, A_1 is proportional to the quantity

$$[\alpha\xi] = \left(\alpha_{\alpha\beta}\xi_{\alpha\beta} - \frac{1}{3}\alpha_{\alpha\alpha}\xi_{\beta\beta}\right). \tag{50}$$

For axial systems (z along the principal axis) $[\alpha\xi]$ simplifies to $\alpha_{\text{ani}}(\omega) \times \xi_{\text{ani}}$, the product of the anisotropies $\alpha_{\text{ani}}(\omega) = \alpha_{zz}(-\omega;\omega) - \alpha_{xx}(-\omega;\omega)$ and $\xi_{\text{ani}} = \xi_{zz} - \xi_{xx}$, of the frequency dependent electric dipole polarizability and of the magnetizability, respectively. Note that for systems with a permanent magnetic moment $\boldsymbol{m}$ a contribution to A_1 also arises from the term

$$[\zeta m] = \left(\zeta_{\alpha\beta,\alpha}m_\beta - \frac{1}{3}\zeta_{\alpha\alpha,\beta}m_\beta\right) \tag{51}$$

Table 2. The molecular properties entering the expression of the Cotton–Mouton effect (equation (48))

A_0	$\eta^{\text{para}}_{\alpha\beta,\gamma\delta}(-\omega;\omega,0,0)$	$\propto \Re\langle\langle\mu_\alpha;\mu_\beta,m_\gamma,m_\delta\rangle\rangle_{\omega,0,0}$
	$\eta^{\text{dia}}_{\alpha\beta,\gamma\delta}(-\omega;\omega,0)$	$\propto \Re\langle\langle\mu_\alpha;\mu_\beta,\xi^{\text{dia}}_{\gamma\delta}\rangle\rangle_{\omega,0}$
	$\varsigma^{\text{para}}_{\alpha\beta\gamma\delta}(-\omega;\omega,0,0)$	$\propto \Re\langle\langle m_\alpha;m_\beta,m_\gamma,m_\delta\rangle\rangle_{\omega,0,0}$
	$\varsigma^{\text{dia}}_{\alpha\beta,\gamma\delta}(-\omega;\omega,0)$	$\propto \Re\langle\langle m_\alpha;m_\beta,\xi^{\text{dia}}_{\gamma\delta}\rangle\rangle_{\omega,0}$
A_1	$\alpha_{\alpha\beta}(-\omega;\omega)$	$\propto \Re\langle\langle\mu_\alpha;\mu_\beta\rangle\rangle_\omega$
	$\xi_{\alpha\beta}$	$\propto \Re\langle\langle m_\alpha;m_\beta\rangle\rangle_0 + \langle\xi^{\text{dia}}_{\alpha\beta}\rangle$
	m_α	$\langle m_\alpha\rangle$
	$\zeta_{\alpha\beta,\gamma}(-\omega;\omega,0)$	$\propto \Im\langle\langle\mu_\alpha;\mu_\beta,m_\gamma\rangle\rangle_{\omega,0}$
	$\zeta_{\alpha\beta\gamma}(-\omega;\omega,0)$	$\propto \Im\langle\langle m_\alpha;m_\beta,m_\gamma\rangle\rangle_{\omega,0}$
A_2	m_α	$\langle m_\alpha\rangle$
	$\alpha_{\alpha\beta}(-\omega;\omega)$	$\propto \Re\langle\langle\mu_\alpha;\mu_\beta\rangle\rangle_\omega$
	$\xi_{\alpha\beta}$	$\propto \Re\langle\langle m_\alpha;m_\beta\rangle\rangle_0 + \langle\xi^{\text{dia}}_{\alpha\beta}\rangle$

involving the first hypermagnetizability tensor $\zeta_{\alpha\beta,\gamma}(-\omega;\omega,0)$. Finally A_2 is proportional to the quantity

$$[m^2\alpha] = \left(\alpha_{\alpha\beta}m_\alpha m_\beta - \frac{1}{3}\alpha_{\alpha\alpha}m_\beta m_\beta\right) \tag{52}$$

which for axial systems reduces to $\Delta m^2 \times \alpha_{\text{ani}}(\omega)$, with $\Delta m^2 = m_z^2 - m_x^2$. It is clear that A_2 vanishes, as does the term in equation (51), for systems where the magnetic moment is quenched. For spherical systems (atoms and molecules of cubic or icosahedral symmetry), the anisotropies of the electric dipole polarizability and of the magnetizability also vanish and the only non-zero contribution to the CME comes from the A_0 term.

Other quantities included in the table yield contributions—weighted by a factor c_0^{-2}, c_0 being the speed of light in vacuum—to all three parameters:

$$\Delta\varsigma(\omega) = \frac{1}{5}\left(\varsigma_{\alpha\beta\alpha\beta} - \frac{1}{3}\varsigma_{\alpha\alpha\beta\beta}\right) \tag{53}$$

to A_0, with $\varsigma_{\alpha\beta\gamma\delta} = \varsigma^{\text{dia}}_{\alpha\beta,\gamma\delta}(-\omega;\omega,0) + \varsigma^{\text{para}}_{\alpha\beta\gamma\delta}(-\omega;\omega,0,0)$,

$$\left[\xi^2\right] = \left(\xi_{\alpha\beta}\xi_{\alpha\beta} - \frac{1}{3}\xi_{\alpha\alpha}\xi_{\beta\beta}\right) \tag{54}$$

and

$$[\zeta m] = \left(\zeta_{\alpha\beta\alpha}m_\beta - \frac{1}{3}\zeta_{\alpha\alpha\beta}m_\beta\right) \tag{55}$$

to A_1, and

$$[m^2\xi] = \left(\xi_{\alpha\beta}m_\alpha m_\beta - \frac{1}{3}\xi_{\alpha\alpha}m_\beta m_\beta\right) \tag{56}$$

to A_2. These contributions were proven to be on the order of parts per million compared to the main terms in Ref. [146], and their effect could probably be detected by future generation experimental setups, as they lead to changes in retardances comparable with or slightly below the current limits of detectability. Still their magnitude is far lower than the accuracy which can be achieved in computations, and, with the exception of the study of Ref. [146], they have been neglected to-date in studies of the CME.

4.1.1. The hypermagnetizability anisotropy in molecules

One of the challenges faced by experiment in CME measurements is the determination of the second hypermagnetizability anisotropy $\Delta\eta(\omega)$ from measurements of the temperature dependence of the effect. From equation (48) it can be seen that by extrapolating to infinite temperature a curve of the measured birefringence as a function of T, it should be possible to estimate A_0, and hence $\Delta\eta(\omega)$. This procedure has been applied in several circumstances, and a number of experimental values of hypermagnetizability anisotropy is found in the literature, see, for instance, Ref. [22]. On the other hand, the combination of quadratic and cubic response functions entering the definition of $\Delta\eta(\omega)$ is among the properties which we can evaluate using analytic response theory at several level of approximation, employing Hartree–Fock, MCSCF, CC and DFT wave function models. The anisotropy of the hypermagnetizability computed in approximate calculations exhibits a

dependence on the choice of the magnetic gauge, as the use of PDBS is not yet possible (see Section 3.6). Alternatively, the static limit $\Delta\eta(0)$ can and has been determined in several instances employing a finite (electric) field approach in which analytically determined magnetizabilities $\xi_{\alpha\beta}$ are computed at finite electric field strengths and appropriate numerical derivatives are computed, according to the approximation [141,22]

$$\eta_{\alpha\beta,\gamma\delta} = \left(\frac{\partial^2 \xi_{\gamma\delta}}{\partial E_\alpha \partial E_\beta} \right)_{\boldsymbol{E}\to 0}. \tag{57}$$

Static hypermagnetizability anisotropies obtained using this technique at Hartree–Fock, MCSCF or DFT level can benefit by the use of PDBS's and are thus magnetic gauge-origin independent. Also, a finite (magnetic induction) field has been applied in some selected cases by Bishop and co-workers [105], where the frequency dependent polarizability has been computed at different field strengths, and numerical derivatives have been taken. The technique, which involves complex algebra, yields in principle the hypermagnetizability anisotropy at a finite wavelength directly, but it has only found a limited use to date in calculations of CME.

In Table 3 a comparison is made between experimental and computational estimates of $\Delta\eta(\omega)$ for some selected gases. Experimental conditions and setups vary in the list, and likewise the computational approaches span a wide range. The label B3LYP used in the table is the usually accepted acronym for the Becke-3 parameter-Lee–Yang and Parr (B3LYP) [154–156] hybrid density functional. The details are unimportant here, and for them the interested reader should refer to the original references. The comparison aims at showing how delicate the infinite–temperature extrapolation can be, and how large the error bar of the experimental hypermagnetizability anisotropies are compared to the level of accuracy theory can reach nowadays in their calculation. To give an example, in Table 4 the specific case of $\Delta\eta(\omega)$ of molecular oxygen in its $X^3\Sigma_g^-$ ground state is analyzed in detail [103].

At the end of an accurate analysis, where the major contributions to the property are explicitly accounted for and the remaining causes of uncertainty (possibly with the exception of relativistic effects) are carefully estimated, we end up with a value, $\Delta\eta(\omega) = 2.65$ au, with an absolute error of ± 1.00 au, which is far less indeterminate than the two existing experiments.

4.1.2. The hypermagnetizability anisotropy in atoms

In most cases the A_0 term in equation (48) yields a small if not negligible contribution to the magnetic field induced birefringence, which is then dominated by the A_1 term in diamagnetic systems, or by the A_2 term for paramagnetic systems. As mentioned above, on the other hand, for atoms and for spherical molecules the only non vanishing term in equation (48) is A_0, and the anisotropy of the hypermagnetizability $\Delta\eta(\omega)$ alone determines the magnitude of the birefringence. This is true for instance for the noble gases, which have been the subject of both experimental and computational studies. For the lowest members of the group, helium, neon and to a large extent argon, theory provides nowadays estimates of the observable which can be considered of benchmark value. Table 5 collects both the experimental data and the most reliable and accurate computational results to-date for these three gases.

Table 3. Comparison of experiment and theory for the second hypermagnetizability anisotropy $\Delta\eta$

System	Experiment	Theory	Theoretical approach
N_2	96.9 ± 74.6[a]	27.94[b]	MCSCF
		34.56[c]	B3LYP
O_2	-740 ± 400[d]	2.65(1.00)[e]	MCSCF
	-600 ± 470[f]		
CO	7.5 ± 59.7[a]	35.41[b]	MCSCF
		45.67[c]	B3LYP
C_2H_2	20 ± 60[g]	64.34[h]	MCSCF
	455 ± 34[i]		
CO_2	-110 ± 60[a]	4.66[j]	MCSCF
		6.0[c]	B3LYP
N_2O	-180 ± 130[a]	-7.91[j]	MCSCF
		-9.83[c]	B3LYP
OCS	-860 ± 110[a]	26.26[j]	MCSCF
		22.78[c]	B3LYP
CS_2	-1800 ± 1100[a]	73.95[j]	MCSCF
		-71.13[c]	B3LYP
Benzene	-2700 ± 2000[k]	1026.0[l]	B3LYP
		931.7[l]	CCSD
C_6F_6	-100 ± 880[m]	395.7[l]	B3LYP
Furan	3400 ± 1000[n]	-18.14[o]	B3LYP
Thiophene	6000 ± 8400[n]	82.32[o]	B3LYP

Gas phase. The wavelength is $\lambda = 632.8$ nm unless specified otherwise. Atomic units.

[a] Ref. [147]. [b] Ref. [101]. [c] Ref. [91]. [d] Ref. [148]. [e] Ref. [103]. In parenthesis the estimated absolute error. [f] Ref. [149]. [g] Ref. [150]. [h] Ref. [146]. [i] Ref. [151]. [j] Ref. [101]. These values include an estimate of vibrational contributions. [k] $\lambda = 441.6$ nm, measurements made in the temperature range 300.1–455.5 K, Ref. [152]. [l] Ref. [39]. [m] $\lambda = 441.6$ nm, measurements in the temperature range 304.1–453.5 K, Ref. [152]. [n] Ref. [153]. [o] Ref. [92].

For these rare gases, theory has reached a level of accuracy far exceeding that of experiment. For helium Bishop and Pipin [157,158] employed explicitly correlated wave functions

to obtain an estimate of the hypermagnetizability anisotropy which could be given with five decimal digits. For neon and argon, Rizzo and co-workers [21] have exploited a CCSDT wave function model to obtain the static value, and a CC3 iterative approach to ascertain the effect of frequency dispersion. For neon the authors of Ref. [21] estimated the absolute error (once again with the possible exception of relativistic contribution). On the basis of these results it is possible for example to state with reasonable confidence and in a conclusive way that the measurement of the CME of neon made in Ref. [161] was indeed affected by an undetected source of systematic error.

Table 4. The contributions to $\Delta\eta(\omega)$ of molecular oxygen in its ground ($X^3\Sigma_g^-$) state [103]

$\Delta\eta(0)$ (CASSCF)	6.38
Add dispersion, $\Delta\eta$(632.8 nm)	6.23
Add ZPVA	6.63
Add PV	2.65
Estimated basis set, electron correlation and magnetic gauge dependence	$\pm$1.00

The first row reports the static value obtained in the Complete Active Space SCF—CASSCF—analytic response approximation. The following rows show how this value changes as frequency dispersion, zero point vibrational average (ZPVA) and pure vibrational contributions (PV) are added to the static electronic value. Finally, an estimate of the effects of basis set and electron correlation incompleteness and of the correction due to magnetic gauge dependence is given. The corresponding experimental estimates are, see Table 3, $\Delta\eta(\omega) = (-740\pm400)$ au [148] and $\Delta\eta(\omega) = (-600 \pm 470)$ au [149]. Atomic units.

Table 5. Comparison of experimental and computational results for the hypermagnetizability anisotropy $\Delta\eta(\omega)$ of helium, neon and argon

	λ	Theory	Experiment
Helium	∞	1.06061[a]	
	790 nm		1.7 ± 0.6[b]
	632.8 nm	1.05791[c]	
	514.5 nm		0.80 ± 0.16[d]
Neon	∞	2.89(10)[e,f]	
	790 nm		3.2 ± 1.2[b]
	514.5 nm		1.4 ± 0.1[g]
Argon	∞	24.7[f]	
	790 nm		27 ± 5[b]
	514.5 nm		30.0 ± 4.5[h]

Atomic units.

[a] Refs. [157] and [158]. Explicitly correlated wave function. [b] Ref. [159], pressure of 1.52×10^5 Pa, temperatures in the range 285–293 K. The value is estimated for an average of 289 K. [c] Refs. [22]. Explicitly correlated wave function. [d] From data in Ref. [160]. Measured at 273.15 K. [e] The number in parenthesis indicates the estimated absolute error on the last digit. [f] Ref. [21]. Static value estimated at CCSDT level; frequency dependence estimated using CC3 analytic response (and found to be negligible). [g] Ref. [161], temperature of 298.15 K and extrapolated at a pressure of 1 atm. [h] Ref. [162].

The above discussion is by no means aimed at criticizing the quality and relevance of the CME experiments, which nowadays involve sophisticate optical apparata and state-of-the-art detection devices. As a matter of fact, with only very few exceptions, the huge error bars associated with the experimental estimates in Tables 3 and 5 leave ample space for agreement between theory and experiment.

In some instances measurements of the effect are done via a procedure involving a second gas, used to calibrate the apparatus [22]. The gas used for the purpose must be such that its CME can be easily measured and its value must be know with precision. In the cases where this procedure has been applied to date, the chosen system has been nitrogen, and the reference value has been taken from experiment. We are nowadays in the position to suggest as the reference for the calibration in experiments—parallel to what is widely accepted in electrical nonlinear optical processes—the theoretical values given in Table 5. The CME of helium is too small to be easily measured, and, in spite of the excellent precision yielded by theory, cannot reasonably be employed as reference. Neon yields an anisotropy only marginally larger than that of helium, in the same experimental conditions, and it has proven to be a difficult system for the CME measurements made to-date [161,159]. The CME of argon is, on the other hand, ≈34 times larger than that measured in helium (and still ≈40 times smaller than the effect on nitrogen). It is probably worth considering using argon, and specifically the computed anisotropy corresponding to the hypermagnetizability anisotropy given in Table 5, as a possible candidate when a calibration gas is needed in CME measurements.

4.1.3. The anisotropy of the magnetizability

Often experiment still remains the reference when it comes to the accuracy of the A_1 term, which is obtained in experiment by the linear regression of the data measured at different temperatures. In a study of the CME of ethylene [163], Coonan and Ritchie could show that the orientational term in equation (50), which, see above, is proportional to $\alpha_{\text{ani}}(\omega) \times \xi_{\text{ani}}$ in axial systems, depends quite sensitively on the anisotropies of the electric dipole polarizability and of the magnetizability, and that "small changes or errors in the directional components of either or both of these properties can lead to much larger changes in the computed value" of the A_1 term. They argued convincingly that the temperature dependence estimated *ab initio* in Ref. [143] by means of a CASSCF wave function approximation was inaccurate. It is a fact that the inaccuracy of the orientational parameter of ethylene computed in Ref. [143] is due to an inadequate determination of the magnetizability anisotropy rather than to the anisotropy of the electric dipole polarizability [101]. In this respect quite promising results could be obtained rather recently by employing Density Functional Theory. For a few selected, relatively simple, molecular gases we compare in Table 6 experiment with results, extracted from the studies of Refs. [91] and [101], of magnetizability anisotropies computed with either a DFT/B3LYP approach where the magnetic gauge-origin dependence is dealt with using the CSGT approximation or the Hartree–Fock and CASSCF wave function models exploiting LAO's. It appears that DFT performs reasonably well in most cases, and on the average better than CASSCF in our selection of molecules. It should be noted, on the other hand that, as well understood nowadays, Hartree–Fock can be in most cases a better approximation than MCSCF in the calculation of magnetizabilities and it is in some cases even more satisfactory than DFT.

Analytical second derivatives for the coupled cluster models up to the full CCSDT model [75,76] are nowadays available. Extension to general coupled cluster schemes [77,78] is very recent. Magnetizabilities can thus already be computed, with high accuracy, in systems where magnetic gauge is not an issue, as for atoms or spherical systems [21], using these sophisticated schemes. In this area great advances can be easily foreseen by the possible future developments of gauge invariant approaches within the coupled cluster scheme.

Table 6. Comparison of experimental and computational results for the magnetizability anisotropy ξ_{ani} of some selected molecular species in the gas phase

System	HF-SCF GIAO	DFT CSGT	CASSCF GIAO	Experiment	Ref.
N_2	−1.92	−1.91	−1.71	-1.850 ± 0.076	[147]
CO	−1.79	−1.80	−1.67	-1.739 ± 0.003	[147]
CO_2	−1.15	−1.36	−1.17	-1.32 ± 0.06	[164,165]
				-1.33 ± 0.04	[147,166]
N_2O	−2.08	−2.22	−1.86	-2.195 ± 0.013	[167–169]
OCS	−1.79	−1.97	−1.71	-1.972 ± 0.003	[167–169]
				-1.991 ± 0.003	[169]
				−2.0	[166]
CS_2	−3.53	−3.73	−3.15	-3.61 ± 0.05	[164,165]
				-3.89 ± 0.16	[147]

Theoretical results from Refs. [91,101]. Atomic units.

4.1.4. The CME of furan, thiophene and selenophene: experimentalists and computational chemists working together

To end this section, we mention the recent important mixed theoretical and experimental study in which the anisotropy of the electric dipole polarizability $\alpha_{ani}(\omega)$ at a wavelength of 632.8 nm, anisotropy of the magnetizability ξ_{ani} and the anisotropy of the static hypermagnetizability $\Delta\eta(0)$ of furan, thiophene and selenophene were computed in condensed phase (pure liquids, solutions) by resorting to a PCM/DFT approach and at the same time the Cotton–Mouton constant was measured using a 17 Tesla radial access Bitter magnet at the Grenoble High Magnetic Field Laboratory (GHMFL) [92]. A summary of the results is given in Table 7. Agreement of theory and experiment is good, and experimental trends are quite well reproduced by the computational models. This example should prove the importance of the synergetic interaction between two worlds, theory and experiment, which in the field of birefringences can find the way to complement each other with success.

4.2. Buckingham effect, a linear birefringence

The phenomenological equation of the Buckingham effect [11,12] of closed shell systems can be written as

$$\Delta n = A_0 + \frac{A_1}{T} \tag{58}$$

where the A_0, A_1 terms involve the properties shown in Table 8 [12,23,25].

The temperature independent term A_0 is related to a specific combination—the same for all systems—of components of the dipole–dipole–quadrupole ($B_{\alpha\beta,\gamma\delta}$ and $\mathcal{B}_{\alpha,\beta\gamma,\delta}$) and dipole – magnetic dipole – dipole ($J'_{\alpha,\beta,\gamma}$) hyperpolarizabilities. It is usually indicated

Table 7. DFT/B3LYP and experimental magnetic field induced birefringence $\Delta n_l(T, \lambda)$ of furan, thiophene and selenophene in different solvents

	Furan		Thiophene		Selenophene	
	ab initio	exp.	*ab initio*	exp.	*ab initio*	exp.
pure liquids	1.53	1.42	2.59	1.93	2.38	1.97
acetonitrile	2.11	2.38	4.12	3.67	4.48	
acetone	1.5	1.41	2.92	2.63	3.19	2.81
THF	1.34	1.26	2.62	2.31	2.85	
cyclohexane	1.02	0.98	1.99	1.92	2.18	2.02
CCl_4	1.13	1.1	2.19		2.39	

$\lambda = 632.8$ nm, $T = 293.15$ K. $\Delta n_l(T, \lambda)$ is the anisotropy seen for the solute at infinite dilution in a magnetic field induction field of 1 T and it is given in parts per billion.

Table 8. The molecular properties entering the expressions of the Buckingham birefringence (equation (58))

A_0	$B_{\alpha\beta,\gamma\delta}(-\omega;\omega,0)$	$\propto \Re\langle\langle \mu_\alpha;\mu_\beta,\Theta_{\gamma\delta}\rangle\rangle_{\omega,0}$
(all systems)	$\mathcal{B}_{\alpha,\beta\gamma,\delta}(-\omega;\omega,0)$	$\propto \Re\langle\langle \mu_\alpha;\mu_\delta,\Theta_{\beta\gamma}\rangle\rangle_{0,\omega}$
	$J'_{\alpha,\beta,\gamma}(-\omega;\omega,0)$	$\propto \Im\langle\langle \mu_\alpha;m_\beta,\mu_\gamma\rangle\rangle_{\omega,0}$
A_1	$\alpha_{\alpha\beta}(-\omega;\omega)$	$\propto \Re\langle\langle \mu_\alpha;\mu_\beta\rangle\rangle_\omega$
(quadrupolar)	$\Theta_{\alpha\beta}$	$\langle\Theta_{\alpha\beta}\rangle$
A_1	$\alpha_{\alpha\beta}(-\omega;\omega)$	$\propto \Re\langle\langle \mu_\alpha;\mu_\beta\rangle\rangle_\omega$
(dipolar)	$\Theta_{\alpha\beta}$	$\langle\Theta_{\alpha\beta}\rangle$
	$A_{\alpha,\beta\gamma}(-\omega;\omega)$	$\propto \Re\langle\langle \mu_\alpha;\Theta_{\beta\gamma}\rangle\rangle_\omega$
	$G'_{\alpha,\beta}(-\omega;\omega)$	$\propto \Im\langle\langle \mu_\alpha;m_\beta\rangle\rangle_\omega$
	μ_α	$\langle\mu_\alpha\rangle$

as $b(\omega)$

$$b(\omega) = \frac{1}{15}\{B_{\alpha\beta,\alpha\beta} - \mathcal{B}_{\alpha,\alpha\beta,\beta}\} - \frac{5}{\omega}\varepsilon_{\alpha\beta\gamma}J'_{\alpha,\beta,\gamma}. \tag{59}$$

The expression for A_1 differs for non-dipolar and dipolar systems. In the first case it only involves the permanent (traceless) quadrupole moment $\Theta_{\alpha\beta}$ and the dipole–dipole polarizability $\alpha_{\alpha\beta}$, in the combination

$$[\Theta\alpha] = \Theta_{\alpha\beta}\alpha_{\alpha\beta}. \tag{60}$$

For systems with a n-fold symmetry rotation axis, $n \geqslant 3$, this equation further reduces to $\Theta \times \alpha_{\text{ani}}$, where $\Theta = \Theta_{zz}$. For dipolar systems an additional term appears which involves the permanent electric dipole moment (μ_α) and the dipole–quadrupole ($A_{\alpha,\beta\gamma}$) and dipole – magnetic dipole ($G'_{\alpha,\beta}$) polarizabilities

$$\left[\mu(A + G')\right] = -\mu_\alpha\left(A_{\beta,\alpha\beta} + \frac{5}{\omega}\varepsilon_{\alpha\beta\gamma}G'_{\beta,\gamma}\right). \tag{61}$$

The above combinations are those defined within Buckingham and Longuet-Higgins [12] (BLH) molecular theory of the birefringence induced by the electric field gradient, a theory which was based on forward scattering of a light beam incident on a thin lamina of gas molecules and which is given in terms of the traceless quadrupole moment operator $\Theta_{\alpha\beta}$. An alternative molecular theory of the Buckingham effect derived within wave theory (*i.e.*, solving Maxwell's equations for the refractive indices), was proposed in 1991 by Imrie and Raab [23] (IR) and is expressed in terms of the traced quadrupole moment operator $q_{\alpha\beta}$. The differences between the two theories and their consequences are discussed in the following. Above we only referred to BLH equations for reasons that will become clear later. In the literature, on the other hand, the analogs of the responses B, $\mathcal{B}$ and A involving the traced quadrupole operator are often employed

$$a_{\alpha,\beta\gamma}(-\omega;\omega) \propto \Re\langle\langle \mu_\alpha; q_{\beta\gamma}\rangle\rangle_\omega, \tag{62}$$

$$b_{\alpha\beta,\gamma\delta}(-\omega;\omega,0) \propto \Re\langle\langle \mu_\alpha; \mu_\beta, q_{\gamma\delta}\rangle\rangle_{\omega,0}, \tag{63}$$

$$ß_{\alpha,\beta\gamma,\delta}(-\omega;\omega,0) \propto \Re\langle\langle \mu_\alpha; \mu_\delta, q_{\beta\gamma}\rangle\rangle_{0,\omega}. \tag{64}$$

The relationships between capital and small responses can be easily obtained from the equation linking traceless and traced quadrupole moments

$$\Theta_{\alpha\beta} = \frac{1}{2}(3q_{\alpha\beta} - q_{\gamma\gamma}\delta_{\alpha\beta}). \tag{65}$$

The importance of the Buckingham effect is mainly related to the fact that it is used to determine experimentally molecular quadrupole moments [11]. The interplay between theory and experiment is also in this case strong as for instance computed values of the hyperpolarizability terms A_0 have sometimes been used to correct experiment; the implications are discussed in Ref. [170].

For linear dipolar molecules the comparison between theoretical and experimental quadrupole moments requires the theoretical determination of the reference origin, called effective quadrupole center. It is in particular the computational studies on these systems and comparison with experimental values that have brought to attention a discrepancy between the two above mentioned semiclassical molecular theories of the effect. In view of these results, a revision of both theories has been recently undertaken, the origin of the discrepancy identified and the erroneous theory corrected (*vide infra*) [171,172].

4.2.1. Quadrupolar molecules

It is clear from equations (58)–(60) that, together with knowledge of the polarizability anisotropy, the (accurate) determination of the quadrupole moment from the Buckingham effect requires that measurements are made over an appropriate range of temperatures, so that the A_0 contribution can be separated from A_1, a procedure equivalent to that seen in Section 4.1 for the CME.

Especially in past years, however, the measurements of Buckingham effect were often performed at fixed temperatures due to experimental difficulties. Problems in handling compressed acetylene over a wide range of temperatures prevented for instance an analysis of the T-dependence of the Buckingham birefringence in Ref. [173].

One possible way to circumvent the problem is to neglect A_0. Obviously this procedure is only good if it can be assumed that A_0 is much smaller than A_1/T. In any case a systematic error is introduced in this way in the experimentally derived quadrupole moment.

Many experimental determinations of quadrupole moments exploited this approximation, see, for instance, [174,175,173]. Whether A_0 is indeed negligible in all cases may be debatable and depends on the limits of detectability of the effect attainable with the experimental apparatus.

Another possible solution is to resort to theoretical results for A_0, which leads to the question of availability as well as accuracy and reliability of the computed values. The relatively smaller number of cases in which this solution has been adopted [176,175] compared to the previous one reflects the lack in the literature of reliable values of the properties entering $b(\omega)$ until 1998.

Starting as an attempt to supply experimentalists with accurate values of the A_0 correction term to be used in the determination of quadrupole moments, we carried out in Ref. [170] a systematic Hartree–Fock and CCSD investigation of the Buckingham effect of three quadrupolar molecules—H_2, N_2 and C_2H_2—plus the spherical system CH_4. We tried to assess the importance of the hyperpolarizability term, equation (59), versus the orientational one, equation (60), via calculation of both the quadrupole moment and polarizability anisotropy, thus estimating the error associated with the neglect of the A_0 term.

We also showed that in some cases an incorrect use of *ab initio* data for the $b(\omega)$ correction in the process of extracting the molecular quadrupole moment from measurements of Buckingham birefringence can lead to severe loss of accuracy. Admittedly, there has been a certain degree of confusion in the earlier literature on the subject concerning the hyperpolarizability correction term $b(\omega)$. In the original papers by Buckingham and coworkers [11,174] the hyperpolarizability term was called B and it was referred to as a quadrupole hyperpolarizability. This is probably at the origin of the misunderstanding that led to a misuse of theoretical values of an average static dipole–dipole–quadrupole hyperpolarizability $\frac{2}{15}B_{\alpha\beta\alpha\beta}$ as correction term $b(\omega)$ in the derivation of the quadrupole moment from measurements of Buckingham effect in some experimental work [176,175].

The most striking example of the consequences in terms of accuracy of the experimental results is the N_2 case. In 1998 Graham and co-workers [175] published an experimental result for the quadrupole moment of N_2 based on a single temperature measurement of the birefringence. The measured apparent quadrupole moment (obtained neglecting the A_0 term) was found to be $(-5.25 \pm 0.08) \times 10^{-40}$ C m^2. After correction with an incorrect value of the A_0 term taken from the literature, the quadrupole moment of N_2 was $(-4.65 \pm 0.08) \times 10^{-40}$ C m^2, noticeably lower than previous experimental and theoretical estimates.

Using our CCSD results [170] for $b(\omega)$ we recalculated the experimental moment to be $(-5.01 \pm 0.08) \times 10^{-40}$ C m^2. From a theoretical analysis employing hierarchies of basis sets and wave function models [28] we also calculated the non-relativistic CCSD(T) basis set limit value of the quadrupole moment of N_2. By including vibrational corrections, and estimates of the effects of relativity and of correlation beyond CCSD(T) we derived the reference theoretical result for the quadrupole moment of N_2 to be $(-4.93 \pm 0.03) \times 10^{-40}$ C m^2 [28].

Very recently Ritchie, Watson and Keir [177] carried out new observations of the Buckingham effect of N_2 over a range of temperatures, thus separating the temperature independent contribution from the orientational term. They also performed a new measurement of the polarizability anisotropy and extracted a new value of $(-4.97 \pm 0.16) \times 10^{-40}$ C m^2 for the experimental quadrupole moment of N_2. This means there is no remaining doubt on the experimental value of the quadrupole moment of N_2.

Ritchie's group has been very active during the last few years in measuring the Buckingham effect and its temperature dependence in various systems [173,177–179]. Other relatively recent experimental results (at fixed T) are those obtained by Graham and coworkers [175]. We have carried out parallel computational studies on many of the systems they analyzed, including benzene and hexafluorobenzene [170,28,56,24,26,29,30,39,180]. A comparison of theoretical and experimental data for all quadrupolar systems we have studied so far is given in Table 9. The table includes values for the quadrupole moment Θ, the whole orientational term F/T, where $F = 2\Theta\alpha_{\text{ani}}(\omega)/15k$ (k stands for Boltzmann constant), and the hyperpolarizability correction $b(\omega)$. In the footnotes of Table 9 (and again later in this work) where needed the correlation-consistent basis sets employed in the calculations are indicated with the acronym xYZ as a shorthand notation for the usual x-aug-cc-pVYZ sequence. The results for C_6H_6 [39] and C_6F_6 [180] represent the first study of the Buckingham effect carried out at the DFT level. For Cl_2 [30] relativistic corrections were included in the calculated $b(\omega)$, which was obtained to revise the experimental measure of the quadrupole moment [175], performed at fixed T. Another computational study of the quadrupole moment of Cl_2 was recently carried out by Junquera-Hernández and co-workers [181].

4.2.2. Atoms and spherical systems

For both atomic and spherical systems the birefringence is entirely due to the hyperpolarizability term A_0. From a theoretical point of view rare gas atoms are ideal test systems, since the major sources of possible errors are only related to insufficient treatment of electron correlation and/or basis set saturation, as no vibrational corrections exist. Theoretical results are thus in our view of great value to direct revised experimental determinations. Moreover, for helium, a two electron system, nearly exact results can be obtained.

Table 10 collects our "best results" for the hyperpolarizability term $b(\omega)$ of all atomic and spherical systems we have investigated, together with experimental data in the literature. The table also includes estimates of the anisotropy Δn and of the retardation ϕ calculated at the hypothetical experimental conditions $P = 10^3$ kPa, $T = 298.15$ K, $l = 1.8$ m and $\nabla E = -1 \times 10^9$ V m^{-2} [184].

Both helium and neon appear to be below the threshold of detection of current experimental devices. The latter is, as discussed in Ref. [184], of the order of ± 2 nrad on the retardation.

For krypton, CH_4 and SF_6 theory predicts birefringences of approximatively the same intensity and twice as large as the one predicted for argon.

Experiment [182] is basically unable to determine the effect for argon and SF_6. For CH_4 theory and experiment agree on the sign of the effect, but the theoretical value is much smaller and falls outside three standard deviations of experiment. The experimental result carries a quite large error bar, whereas evidence of a large zero-point vibrational correction for the second dipole hyperpolarizability of CH_4 [185] warns of the possibility of strong vibrational effects, unaccounted for in our case. No experimental values are available, to our knowledge, for krypton.

The quality of the computational results for CH_4 and SF_6 can undoubtedly be improved, in terms of both correlation, basis set and vibrational corrections. On the other hand all experimental data in Table 10, dating back to 1968, are affected by large uncertainties. Theory predicts that the systems in Table 10 should yield measurable birefringences, with krypton, CH_4 and SF_6 having similar estimates for the rotation.

Table 9. Buckingham effect of quadrupolar systems

System	Property	Theory	Experiment
H_2	Θ	0.4561[a]	0.484[a′]
	F/T	130.6[a]	145[a′]
	$b(\omega)$	−36.75[a]	−46 ± 15[a′]
N_2	Θ	−1.098 ± 0.007[b]	−1.11 ± 0.04[b′] ; −1.12 ± 0.02[c′]
	F/T	−785.1[a]	
	$b(\omega)$	−36.13[a]	−76.62 ± 23.57[b′]
C_2H_2	Θ	4.79 ± 0.03[c]	4.66 ± 0.19[d′]
	F/T	9257[a]	
	$b(\omega)$	−193.3[a]	
Cl_2	Θ	2.327 ± 0.010[d]	2.31/2.36 ± 0.04[e′]
	F/T	−6479.9[e]	
	$b(\omega)$	−213.6[e]	
CO_2	Θ	−3.185 ± 0.020[f]	−3.187 ± 0.13[f′] ;−3.18 ± 0.14[g′]
	F/T	−7536.7[g]	
	$b(\omega)$	−54.46[g]	−159 ± 77[f′] ; −118 ± 178[h′]
CS_2	Θ	2.338[h]	2.56 ± 0.11[f′]
	F/T	25500[i]	
	$b(\omega)$	−410[i]	−1179 ± 766[f′]
C_6H_6	Θ	−6.0199;−5.6439[j]	−6.68 ± 0.27[i′]
	F/T	35504, 34351[j]	
	$b(\omega)$	−557;−604.7[j]	−3000 ± 410[i′]
C_6F_6	Θ	−6.3063[k]	−7.95 ± 0.29[i′]
	F/T	−47114[k]	
	$b(\omega)$	−368.4[k]	−2900 ± 2000[i′]

Theoretical estimates and experimental values of the quadrupole moment Θ, the orientational term F/T, with $F = \frac{2\Theta\alpha_{\text{ani}}(\omega)}{15k}$, and temperature independent correction $b(\omega)$. Atomic units. $T = 273.15$ K.

[a] From Ref. [170]. FCI/d5Z (H_2) and CCSD/dQZ/frozen-core (N_2,C_2H_2,CH_4) equilibrium results. [b] From Ref. [28]. ZPVA-CCSD(T) basis set limit including estimates of correlation beyond CCSD(T) and relativistic effects. [c] From Ref. [56]. ZPVA-CCSD(T) basis set limit including estimates of correlation beyond CCSD(T) and relativistic effects. [d] From Ref. [30]. ZPVA-CCSD(T) basis set limit including estimates of correlation beyond CCSD(T) and relativistic contributions. [e] From Ref. [30]. CCSD/dQZ result including relativistic, ZPVA and PV corrections. [f] From Ref. [24]. ZPVA-CCSD(T) basis set limit including estimates of correlation beyond CCSD(T) and relativistic effects. [g] From Ref. [24]. CCSD/dQZ/frozen-core equilibrium results. [h] From Ref. [24]. CCSD(T)/dVQZ/frozen-core equilibrium value. [i] From Ref. [24]. CCSD/aQZ/frozen-core equilibrium value. [j] From Ref. [39]. CCSD/aTZ (first value) and B3LYP/aTZ (second value) results. [k] From Ref. [180]. B3LYP/aDZ results. [a′] From Ref. [182]. [b′] From Ref. [177]. [c′] From the apparent moment $\Theta^{\text{eff}} = -1.170$ in Ref. [175] after revision with b from Ref. [170]. [d′] From the apparent moment $\Theta^{\text{eff}} = -4.55 \pm 0.22$ in Ref. [173] after revision with b from Ref. [170]. [e′] From Ref. [30]. Revision of the apparent quadrupole moment (2.23 ± 0.04) in [175] with the calculated $b(\omega)$. [f′] From Ref. [178]. [g′] From Ref. [175]. [h′] From Ref. [183]. [i′] From Ref. [179].

Table 10. Buckingham effect in spherical systems

System	Property	Theory	Experiment
Helium	$b(\omega)$/au	−3.15[a]	
	$\Delta n \times 10^{17}$	7.33	
	ϕ/nrad	1.31	
Neon	$b(\omega)$/au	−5.89[b]	
	$\Delta n \times 10^{17}$	13.7	
	ϕ/nrad	2.45	
Argon	$b(\omega)$/au	−58.0[b]	0 ± 109[c]
	$\Delta n \times 10^{17}$	135	
	ϕ/nrad	24.1	
Krypton	$b(\omega)$/au	−117.90[d]	
	$\Delta n \times 10^{17}$	274	
	ϕ/nrad	49.0	
CH_4	$b(\omega)$/au	−97.3[e]	-262 ± 66[c]
	$\Delta n \times 10^{17}$	226	
	ϕ/nrad	40.5	
SF_6	$b(\omega)$/au	−95[f]	0 ± 109[c]
	$\Delta n \times 10^{17}$	221	
	ϕ/nrad	39.5	

Best theoretical estimates and experimental values of the hyperpolarizability contribution at 632.8 nm, the anisotropy of the refractive index Δn and the retardance ϕ. The theoretical results for the anisotropy and the retardance are derived from the calculated $b(\omega)$, under the hypothetical experimental conditions $P = 10^3$ kPa, $T = 298.15$ K, $l = 1.8$ m and $\nabla E = -1 \times 10^9$ V m^{-2} [184].

[a] From Ref. [186]. FCI/d-aug-cc-pV6Z results. [b] From Ref. [186]. CCSD/d-aug-cc-pV5Z results. [c] From Ref. [182]. [d] This work. CCSD/d-aug-cc-pV5Z results. [e] From Ref. [170]. CCSD/d-aug-cc-pVQZ results. [f] From Ref. [186]. CCSD/d-aug-cc-pVDZ results.

4.2.3. Dipolar molecules

As any physical observable the anisotropy (or retardance) measured in the Buckingham effect is independent on the choice of the origin of the coordinate system. The quadrupole moment of a dipolar system is, on the other hand, origin dependent. In spite of this dependence, one can still "measure" the quadrupole moment of a dipolar system once the origin with respect to which the quadrupole moment is defined is specified. As an example, molecular-beam electron-resonance (MBER) spectroscopy allows for the determination of the molecular quadrupole moment of dipolar systems with respect to the center of the nuclear masses, see for instance Ref. [167]. Experimental measurements of the Buckingham effect can also be used to obtain an experimental quadrupole moment for dipolar systems, where the appropriate reference origin is identified with the so-called effective quadrupole center (EQC) [12]. This is defined as the point in space at which the combination of dipole–quadrupole and dipole – magnetic dipole polarizabilities scalar-multiplied with the dipole moment (equation (61)) vanishes, such that, for that particular choice of reference origin, an expression for the birefringence similar to the one for quadrupolar

molecules is recovered. The measured Δn yields the quadrupole moment relative to this origin.

The position of the effective quadrupole center, R_z, is thus not determined directly from the Buckingham birefringence experiment, but it is theoretically identified via the origin shift that makes the dipolar contribution in the A_1 term vanish. According to BLH theory the shift with respect to a given reference origin (labelled "(or)" below)—for a linear molecule along the z axis—is given by [26,25]

$$R_z^{\mathrm{BLH}} = \frac{a_{z,zz}^{(or)} + 3a_{x,xz}^{(or)} - a_{z,xx}^{(or)} + 10\omega^{-1}G_{x,y}^{\prime(or)}}{2\alpha_{zz} + 3\alpha_{xx} - 5\alpha_{xx}^{LV}} \tag{66}$$

where the response functions have been defined above, and the superscript on those involving the quadrupole moment operator indicates that they are computed at the reference origin. In IR theory [23] the same shift is given instead by the expression

$$R_z^{\mathrm{IR}} = \frac{2a_{z,zz}^{(or)} + a_{x,xz}^{(or)} + 3a_{z,xx}^{(or)} + 10\omega^{-1}G_{x,y}^{\prime(or)}}{4\alpha_{zz} + \alpha_{xx} - 5\alpha_{xx}^{LV}}. \tag{67}$$

If we indicate with $\Theta^{(R_z)}$ the molecular quadrupole moment referring to the EQC (R_z), we have

$$\Theta^{(R_z)} = \Theta^{(or)} - 2R_z\mu. \tag{68}$$

Above $\alpha_{\alpha\beta}^{LV} = \frac{\mathrm{i}}{\omega}\langle\langle \mu_\alpha; \mu_\beta^p \rangle\rangle$ is the electric polarizability in the mixed length-velocity form. It should be added that differences between the two theories also exist in the expression for the $b(\omega)$ contribution for any system, including atoms and quadrupolar molecules.

We showed in Refs. [26,24,25,30,29] via quantum chemical calculations on the Buckingham effect that the two semiclassical theories led to substantially different numerical results for the induced anisotropy in a variety of cases. In our opinion the differences could not be ascribed to deficiencies in the computational approach, since they persisted even for two-electron systems as helium and H_2 [25], where results practically "exact" can be obtained.

The most striking disagreement was observed for the EQC and the resulting quadrupole moment of CO [26,29]. In the first study [26] we carried out both a CCSD(T) analysis of the quadrupole moment at the center of mass and a CCSD study of the EQC. We derived thus the quadrupole moment referring to the EQC within both theories. The results, once compared to an experimentally derived estimate of R_z, slightly favored the BLH theory, but to a measure that it was impossible to sort out indubitably which of the two theories could be correct.

In Ref. [29] we undertook therefore a second analysis, where we tried to minimize as much as possible the causes of deficiency in the computational approach. In particular, we improved on the description of electron correlation in the calculation of the response properties by resorting to the CC3 approach, a cost-effective approximation to CCSDT. The results for the EQC are given in Table 11. Two other linear dipolar molecules, N_2O and OCS, were also considered in Ref. [29], but we do not discuss them here for sake of brevity.

The comparison of the experimental and theoretical values of the EQC (and the quadrupole moments referring to it) shows that BLH results are well within one standard deviation of the (revised) experimental results, whereas the IR results are still outside three standard

Table 11. Buckingham birefringence of CO

Property	BLH		IR
R_z^{CCSD}	4.52 ± 0.5		2.50 ± 0.5
R_z^{CC3}	5.96 ± 0.5		3.06 ± 0.5
$R_z^{\mathrm{exp,app}}$[a]		7.7 ± 0.5	
$R_z^{\mathrm{exp,CCSD}}$[b]	6.25 ± 0.51		5.78 ± 0.51
$R_z^{\mathrm{exp,CC3}}$[c]	6.16 ± 0.51		5.69 ± 0.51

Computed and experimentally derived shifts with respect to the center of nuclear masses determining the EQC (R_z, in au) for CO at 632.8 nm. The molecule is oriented along the z axis with positive direction pointing from C to O, so that the dipole moment is positive. CCSD/d-aug-cc-pVQZ results are from Ref. [26]. CC3/d-aug-cc-pVQZ results are from Ref. [29]. The computed shifts are rovibrationally corrected.

[a] "Apparent" experimentally derived shift obtained from equation (68) combining the experimental values for the dipole moment μ, the apparent quadrupole moment Θ^{eff} from Buckingham birefringence and the quadrupole moment at the center of mass Θ^{CM} from MBER.

[b] The experimentally derived value where Θ^{eff} from Buckingham birefringence has been corrected for $b(\omega)$ computed at the CCSD level. See Refs. [26,29] for details.

[c] The experimentally derived value where Θ^{eff} from Buckingham birefringence has been corrected for $b(\omega)$ computed at the CC3 level. See Refs. [26,29] for details.

deviations. We could not provide an explanation of the origin of the discrepancy, but our work was instrumental in stimulating a decisive revision of the existing theories.

The revision was made by Raab and de Lange [171,172]. The authors first carried out a completely new calculation of the effect based on forward scattering of a light beam incident on a thin lamina of gas molecules in order to avoid a divergent quantity occurring in BLH theory. In this way they re-obtained exactly BLH formulas [171]. They then revisited IR formulation, based on wave theory, and found that the difference between BLH and IR expressions originated from the assumption, in IR approach, that the light wave propagating in the gas is a plane-wave [172]. By taking into account distortion of the incident wave by the field gradient in the wave theory treatment of the effect the results of the two approaches became identical. The problem of the discrepancy was thus finally resolved and there is now consensus on Buckingham–Longuet Higgins molecular expression for the birefringence induced by the electric field gradient.

4.3. Magnetochiral axial birefringence

The magnetochiral axial birefringence for an isotropic closed-shell system in the transparent region is temperature independent [18]

$$\Delta n = A_0 \tag{69}$$

where

$$A_0 = \frac{\omega}{5} A'_{\alpha,\alpha\beta,\beta} + \varepsilon_{\alpha\beta\gamma} G^{\mathrm{para}}_{\alpha,\beta\gamma} \tag{70}$$

Table 12. The molecular properties entering the expressions for the magnetochiral birefringence (equations (69) and (70))

A_0	$A'_{\alpha,\beta\gamma,\delta}(-\omega;\omega,0)$	$\propto \Im\langle\langle \mu_\alpha; \Theta_{\beta\gamma}, m_\delta \rangle\rangle_{\omega,0}$
	$G^{\text{para}}_{\alpha,\beta\gamma}(-\omega;\omega,0)$	$\propto \Re\langle\langle \mu_\alpha; m_\beta, m_\gamma \rangle\rangle_{\omega,0}$

and the relationship between the above tensor properties and the response functions is shown in Table 12.

Magnetochiral birefringence has been known for a few decades [17,18,3,19,20] and it has recently been observed experimentally [31,32,187,33].

In 2001 Vallet *et al.* [33], in view of a remarkable disagreement on the magnitude of the effect for liquid proline between their results and those obtained by Wagniere and coworkers using a slightly different experimental methodology [32], called for "(. . .) theoretical calculations of magnetochiral anisotropies", which "(. . .) would allow an exact quantitative comparison with the molecular model", a model which was developed by Barron and Vrbancich in their 1984 paper [18].

Prompted by this call, we made an attempt to provide theoretical estimates and carried out an investigation of the magnetochiral birefringence of methyloxirane, C_3H_6O, fluoro- and methyl-cyclopropanone, C_3H_3OF and C_4H_6O, carvone, $C_{10}H_{14}O$, limonene, $C_{10}H_{16}$, and proline, $C_5H_9NO_2$, at the Hartree–Fock level of theory [34] and for isolated molecules.

The effect had not previously been the subject of rigorous quantum chemical calculations, and, from the computational point of view, it posed several challenges. The three systems for which the experimental data were available are large and chiral, *i.e.*, non-symmetric, which somewhat limited the size of the basis sets and the choice of the wave function model one could use. They are characterized by a certain degree of flexibility, so that one could expect that more than one conformer would make a significant contribution to the net effect. For proline the experimental measurements were carried out in solution, whereas those on both carvone and limonene were made for pure liquids. We are yet unable to introduce in our calculations involving high order electric and magnetic optical response functions a satisfactory model accounting for the interactions in condensed phase. As an additional test of the ability of our approach to provide reliable estimates for the magnetochiral birefringence we also carried out calculations of natural optical rotation, the lower order phenomenon to which magneto-chiral birefringence is related, for which many experimental results have been reported [188,189].

The resulting magnetochiral birefringence is given in Table 13 for the conformer corresponding to the global minimum of each molecule in the aug-cc-pVDZ basis, and it is compared with the experimental results [31,33,32]. The density values for the liquid state under standard conditions used are specified in the notes. Wavelengths and field inductions were chosen for each molecules according to experiment and are also given in notes.

From the inspection of the results collected in Table 13 it can be seen that

(i) For proline—having properly taken into account the differences in magnetic field intensity and concentration—the axial anisotropy induced by the magnetic field observed by Vallet *et al.* [33] is ≈20 times weaker than that seen by Kalugin, Kleindienst and Wagnière [32]. This factor increases to almost forty if the effect of frequency dispersion is treated as we discussed in Ref. [34].

Table 13. Comparison of theoretical estimates and experimental values for the magnetochiral birefringence of carvone, limonene and proline

Molecule	$(n^{\uparrow\uparrow} - n^{\uparrow\downarrow}) \times 10^{11}$	
	Theory	Experiment
Carvone	(-2.86×10^{-1})[a]	$(+2.5 \pm 0.6) \times 10^{3}$[e]
Limonene	(1.85×10^{-1})[b]	(5.0 ± 0.8)[f]
Proline	(-5.86×10^{-1})[c]	$(+2.1 \pm 0.3) \times 10^{3}$[g]
	(-4.16×10^{-2})[d]	(3.3 ± 0.7)[h]

The calculated results (HF/aug-cc-pVDZ) refer only to the conformational structures corresponding to the global minima.

[a] Estimate at $B_z = 5$ T and density at normal conditions of 0.9608 g·cm^{-3}. $\lambda = 632.8$ nm.

[b] Estimate at $B_z = 0.13$ T and density at normal conditions of 0.8411 g·cm^{-3}. $\lambda = 488.0$ nm.

[c] Estimate at $B_z = 4.6$ T and molar concentration of 4 M. $\lambda = 632.8$ nm.

[d] Estimate at $B_z = 0.13$ T and molar concentration of 5.4 M. $\lambda = 488.0$ nm.

[e] (S)-carvone (*l*-carvone) at $\lambda = 632.8$ nm and a field of 5 T. Ref. [31].

[f] $\lambda = 488$ nm and a 0.13 T field. The mean value of the modulus of the induced anisotropy, taken for both the (R)- and (S)-enantiomers, is given and the sign of the effect is thus unspecified. Ref. [33].

[g] 5.4 M aqueous solution, $\lambda = 488$ nm, and $B_z = 0.13$ T field. The mean value of the modulus of the induced anisotropy, taken for both the (R)- and (S)-enantiomers, is given and the sign of the effect is thus unspecified. Ref. [33].

[h] (S)-proline (*l*-proline) in a 4 M aqueous solution at $\lambda = 632.8$ nm, 4.6 T field. Ref. [32].

(ii) For limonene, Vallet *et al.* [33] report a much smaller anisotropy than the one measured for carvone in Ref. [31], even though these two molecules are structurally similar.

(iii) We cannot reproduce the sign of the axial birefringence measured experimentally for carvone and proline [31,32].

(iv) Apart from the sign, the birefringence predicted for carvone is almost four orders of magnitude smaller than the experimental value.

(v) For proline our result is more than three orders of magnitude smaller than the value [32] measured by the same group which reported the value for carvone, and almost two orders of magnitude smaller that the one obtained by Vallet *et al.* [33].

(vi) For limonene our result is 15 to 30 times smaller than the experimental value by Vallet *et al.* [33].

(vii) Our calculations predict a magnetochiral axial birefringence of about the same order of magnitude for all three molecules and much weaker than observed experimentally.

The reasons for the large discrepancy between the calculated magnetochiral birefringence and that observed experimentally may be numerous, and are extensively discussed in Ref. [34]. Considering the approximations and limitation of the theory, we cannot claim high accuracy of our results. For this reason we cannot rule out that the factors of $\approx$15 to 30 that are needed to bring our computed anisotropies in agreement with those measured by Vallet *et al.* [33] for limonene and proline, respectively, might be eventually recovered. On the other hand it seems that the magnetochiral birefringence effect for carvone and proline is probably weaker than reported by Wagniére's group [31,32], as discrepancies of

three–four orders of magnitude between theory and experiment remain in our view hard to reconcile.

The wide disagreement between our estimates for the magnetochiral birefringence and experiment calls for further investigation both from the experimental and the theoretical point of view. For the latter, it would be worthwhile to try and include correlation effects, for example at the DFT level, and further analyze the conformational dependence of the property, along the line of the study of Ref. [35], as well as the importance of solvent effects.

4.4. Jones and magneto-electric linear birefringences

Polarized monochromatic light interacting with matter in the presence of external uniform electric and magnetic induction fields applied parallel to each other and perpendicular to the direction of propagation of the beam exhibits a linear birefringence, called Jones birefringence [13–16], which superimposes to the Kerr and Cotton–Mouton birefringences. Jones birefringence is characterized, see Section 2, by a pair of axes bisecting those of the two traditional birefringences.

When the three directions (propagation, electric field and magnetic induction field) are mutually orthogonal, a different (from the experimental point of view) type of birefringence bilinear in the strength of the electric and magnetic induction fields appears, called "magneto-electric birefringence" [15,44,190,16,191]. The optical axes of magneto-electric birefringence coincide with those of the Kerr and Cotton–Mouton effects. The molecular expression for the anisotropy in fluids is identical for Jones and magneto-electric birefringences [16]. One has [38]

$$\Delta n = A_0 + \frac{A_1}{T}, \tag{71}$$

where the response properties involved are shown in Table 14. In particular, the combination of components involved in A_0 is

$$3G_{\alpha,\beta\alpha,\beta} + 3G_{\alpha,\beta\beta,\alpha} - 2G_{\alpha,\alpha\beta,\beta} - \frac{\omega}{2}\varepsilon_{\alpha\beta\gamma}(a'_{\alpha,\beta\delta,\delta,\gamma} + a'_{\alpha,\beta\delta,\gamma,\delta}) \tag{72}$$

Table 14. The molecular properties entering the expressions for the Jones and magneto-electric birefringences (equations (71)–(73))

A_0	$a'_{\alpha,\beta\gamma,\delta,\varepsilon}(-\omega;\omega,0,0)$	$\propto \Im\langle\langle \mu_\alpha; q_{\beta\gamma}, m_\delta, \mu_\varepsilon\rangle\rangle_{\omega,0,0}$
	$G^{\text{para}}_{\alpha,\beta\gamma,\delta}(-\omega;\omega,0,0)$	$\propto \Re\langle\langle \mu_\alpha; m_\beta, m_\gamma, \mu_\delta\rangle\rangle_{\omega,0,0}$
	$G^{\text{dia}}_{\alpha,\beta\gamma,\delta}(-\omega;\omega,0)$	$\propto \Re\langle\langle \mu_\alpha; \xi^{\text{dia}}_{\beta\gamma}, \mu_\delta\rangle\rangle_{\omega,0}$
A_1	$a'_{\alpha,\beta\gamma,\delta}(-\omega;\omega,0)$	$\propto \Im\langle\langle \mu_\alpha; q_{\beta\gamma}, m_\delta\rangle\rangle_{\omega,0}$
(polar)	$G^{\text{para}}_{\alpha,\beta\gamma}(-\omega;\omega,0)$	$\propto \Re\langle\langle \mu_\alpha; m_\beta, m_\gamma\rangle\rangle_{\omega,0}$
	$G^{\text{dia}}_{\alpha,\beta\gamma}(-\omega;\omega)$	$\propto \Re\langle\langle \mu_\alpha; \xi_{\beta\gamma}\rangle\rangle_{\omega}$
	μ_α	$\langle\mu_\alpha\rangle$

where

$$G_{\alpha,\beta\gamma,\delta}(\omega) = G^{\text{para}}_{\alpha,\beta\gamma,\delta}(\omega) + G^{\text{dia}}_{\alpha,\beta\gamma,\delta}(\omega). \tag{73}$$

Note that the contribution of $G^{\text{dia}}_{\alpha,\beta\gamma,\delta}(\omega)$, which should be in principle included also in the expression of magnetochiral birefringence, equation (70), in that case disappears due to rotational averaging.

A_1 vanishes for non dipolar systems. It involves the following combination of response functions

$$\mu_\alpha(3G_{\alpha,\beta\beta} + 3G_{\beta,\alpha\beta} - 2G_{\beta,\beta\alpha}) - \frac{\omega}{2}\varepsilon_{\alpha\beta\gamma}(\mu_\gamma a'_{\alpha,\beta\delta,\delta} + \mu_\delta a'_{\alpha,\beta\delta,\gamma}) \tag{74}$$

and again

$$G_{\alpha,\beta\gamma}(\omega) = G^{\text{para}}_{\alpha,\beta\gamma}(\omega) + G^{\text{dia}}_{\alpha,\beta\gamma}(\omega). \tag{75}$$

Jones (and magneto-electric) birefringences are relatively young phenomena, at least as far as their experimental detection is concerned. In recent years, measurements have been made in liquid samples [36,37,192,193]. In Refs. [38,39] we have carried out *ab initio* studies of these birefringences in the gas phase, and we have compared their strength with those of the birefringences they superimpose to (Kerr and Cotton–Mouton) and of the other linear birefringence we have been studying at length, Buckingham's. In Table 15 we report a summary of the results, namely the anisotropies computed in the gas phase for a few reference systems, including rare gases, linear non-dipolar molecules, a dipolar system (CO) and two aromatic molecules. The results, mostly taken from our previous work on the subject, were obtained employing quite large correlation consistent basis sets and different wave function models. In some cases (most of the Kerr results, and the CME and Buckingham birefringence results for krypton) calculations were carried out expressly for this review. In the case of the CME of helium we have included in the table the benchmark results obtained by Bishop and Pipin [157] employing an explicitly correlated wave function. The same applies to hydrogen, where the reference is to Bishop, Cybulski and Pipin [104] and to the work of Rychlewski and Raynes [194,195]. For a detailed discussion of the literature, comparison with experiment where available, analysis of the assumptions and approximations made, the interested reader should refer to the original references, as once again the scope of Table 15 is only to allow for a reasonable comparison of the strengths of the different birefringences and not to discuss computational strategies in detail.

To estimate directly the birefringence we made some assumptions on plausible experimental conditions, and chose a wavelength of 632.8 nm, pressure of 1 bar, temperature of 273.15 K and field strengths as follows: $E = 2.6 \times 10^6\ \text{V m}^{-1}$, $B = 3\ \text{T}$ and $\nabla E = 1 \times 10^9\ \text{V m}^{-2}$. These values correspond to usual averages employed in experimental work in the field of birefringences. Moreover, we assume a path length l of 1 meter when computing the retardance [38].

Given these hypothetical experimental conditions, Jones and magneto-electric birefringences yield retardances which are comparable to those observed in Buckingham birefringence at least for rare gases and molecular hydrogen. The current detection limit for retardances of ≈2 nrad [184] makes their observation in these systems then extremely challenging. Note once again that Buckingham birefringence has been measured in argon by Buckingham, Disch and Dunmur already in 1968 [182], see Section 4.2.2 above, but that measurement could only establish upper limits for the effect. For the other molecules in

Table 15. Comparison of estimated Jones and magneto-electric birefringences with the values computed for the Kerr, CME and Buckingham's effects for a few atoms and molecules

System	Jones				Kerr			
	Δn	Basis/Wf	Ref.	ϕ/nrad	Δn	Basis/Wf	Ref.	ϕ/nrad
He	-1.3×10^{-17}	t6Z/CCSD	[38]	-1.3×10^{-1}	9.31×10^{-15}	d6Z/CCSD		9.2×10^{1}
Ne	-3.5×10^{-17}	t5Z/CCSD	[38]	-3.5×10^{-1}	2.25×10^{-14}	d5Z/CCSD		2.2×10^{2}
Ar	-3.0×10^{-16}	t5Z/CCSD	[38]	-3.0	2.58×10^{-13}	d5Z/CCSD		2.6×10^{3}
Kr	-6.5×10^{-16}	t5Z/CCSD	[38]	-6.5	5.88×10^{-13}	d5Z/CCSD		5.8×10^{3}
H_2	-4.0×10^{-16}	d5Z/FCI	[38]	-4.0	3.06×10^{-13}	t5Z/FCI		3.0×10^{3}
N_2	-7.5×10^{-16}	dQZ/CCSD	[38]	-7.4	1.19×10^{-12}	dQZ/CCSD		1.2×10^{4}
C_2H_2	-3.0×10^{-15}	aQZ/CCSD	[38]	-3.0×10^{1}	8.15×10^{-12}	dQZ/CCSD	[196]	8.1×10^{4}
CO	-1.2×10^{-15}	dQZ/CCSD	[38]	-1.2×10^{1}	1.36×10^{-12}	dQZ/CCSD		1.4×10^{4}
C_6H_6	2.4×10^{-15}	aTZ/B3LYP	[39]	2.4×10^{1}	7.54×10^{-11}	aTZ/B3LYP	[39]	7.5×10^{5}
C_6F_6	3.9×10^{-15}	aDZ/B3LYP	[39]	3.9×10^{1}	1.09×10^{-10}	aDZ/B3LYP	[39]	1.1×10^{6}
System	CME				Buckingham			
	Δn	Basis/Wf	Ref.	ϕ/nrad	Δn	Basis/Wf	Ref.	ϕ/nrad
He	2.13×10^{-15}	ECW	[22]	2.1×10^{1}	-8.00×10^{-18}	d6Z/CCSD	[186,25]	-7.9×10^{-2}
Ne	5.81×10^{-15}	t5Z/CCSDT	[21]	5.8×10^{1}	-1.50×10^{-17}	d5Z/CCSD	[186,25]	-1.5×10^{-1}
Ar	4.97×10^{-14}	d5Z/CC3	[21]	4.9×10^{2}	-1.47×10^{-16}	d5Z/CCSD	[186,25]	-1.5
Kr	1.03×10^{-13}	d5Z/CCSD		1.0×10^{3}	-3.00×10^{-16}	d5Z/CCSD		-3.0
H_2	9.17×10^{-14}	ECW	[22]	9.1×10^{2}	1.60×10^{-16}	d5Z/FCI	[170]	1.6
N_2	-2.84×10^{-12}	tTZ/B3LYP	[91]	-2.8×10^{4}	-2.09×10^{-15}	dQZ/CCSD	[170,25]	-2.1×10^{1}
C_2H_2	-1.50×10^{-12}	aTZ/MCSCF	[146]	-1.5×10^{4}	2.27×10^{-14}	dQZ/CCSD	[170,25]	2.3×10^{2}
CO	-1.80×10^{-12}	tTZ/B3LYP	[91]	-1.8×10^{4}	-3.10×10^{-15}	dQZ/CC3	[26,29,25]	-3.1×10^{1}
C_6H_6	1.67×10^{-10}	aTZ/B3LYP	[39]	1.7×10^{6}	-8.57×10^{-14}	aTZ/B3LYP	[39]	-8.5×10^{2}
C_6F_6	1.26×10^{-10}	aDZ/B3LYP	[39]	1.3×10^{6}	-1.21×10^{-13}	aDZ/B3LYP	[39]	-1.2×10^{3}

Results for $\lambda = 632.8$ nm, path length $l = 1$ m, pressure $P = 1$ bar, temperature $T = 273.15$ K, electric field strength $E = 2.6 \times 10^6$ V m^{-1}, magnetic induction field $B = 3$ T, electric field gradient strength ∇E of 1×10^9 V m^{-2}. The basis set is indicated with the acronym xYZ as a shorthand notation for the correlation consistent x-aug-cc-pVYZ basis set. "Wf" is the wave function model employed, with "ECW" standing for "explicitly correlated wave function". Where reference is not given to previous work, it is implied that the values were computed expressly for this paper (details available from the authors).

Table 15, Jones and magneto-electric birefringences remain weaker than Buckingham's by a factor of almost one order of magnitude on the average, due to the absence of an orientational term which represents the dominant contribution for all the other three birefringences. They are still in principle measurable. Kerr birefringence appears to be approximately three orders of magnitude stronger for rare gases and H_2, whereas CME is slightly more than two orders of magnitude more intense. For the remaining systems, Kerr and CME are of comparable size and they can be up to almost five orders of magnitude stronger than Jones or magneto-electric birefringences.

As mentioned above, measurements of these optical anisotropies observed in mixed electric and magnetic induction fields has been limited to date to liquid samples, where the enhancement of the effect due to the condensed phase is considerable, making detection far easier. It is thus rather evident the challenge that this field poses to both computational chemists and experimentalists if they want to be able to exchange reliable and useful information on Jones and magneto-electric birefringence as it has been possible in recent years for the other birefringences. Efforts must be made to strengthen the theoretical approach to frequency dependent electric and magnetic high order response properties in condensed phases, and the corresponding computational tools need to be developed. On the other hand, experimentalists are faced with the challenge of further improving the efficiency of their optical apparata, to be able to perform reliable measurements of tiny retardances in the gas phase. The rapid advancement in technology (faster computers but also stronger magnets, better optical instrumentation and more efficient detection devices) should encourage those willing to take up this challenge.

ACKNOWLEDGEMENTS

This review is dedicated to Jan Linderberg and Poul Jørgensen, whose influence on our scientific story and on our lives has been notable. The yellow, the green and the blue books which friends, colleagues and students of Jan and Poul know well are leaving behind a great legacy. The area of molecular properties and their *ab initio* accurate determination has gone through a huge development in the last decades, and the contribution of the Theoretical Chemistry group located at fifth floor in the Chemistry building in Århus, and of their "colored" masterpieces, is invaluable. The fifth floor has also been the place where the authors of this review have spent a now non negligible amount of their life, finding always the right friendly atmosphere, countless occasions for sharing good stories and memories in front of coffee and cake.

Many thanks are due to all the people involved in the work we reviewed here, who have shared over the years our interest and enthusiasm for studies of such a subject as birefringences. We have counted almost forty names of co-authors in several years, a list probably too long to be reproduced here. Without the collaboration of so many people, we would have not been able to gather the information and experience we think we have gained on the subject.

Finally, support from the European Union Marie Curie RTN Network "NANOQUANT, Understanding nano-materials from a quantum perspective", contract no. MRTN-CT-2003-506842, is gratefully acknowledged.

REFERENCES

[1] C.J.F. Böttcher, P. Bordewijk, *Theory of Electric Polarization, vol. II. Dielectric in Time-Dependent Fields*, Elsevier, Amsterdam, 1978.
[2] L.D. Barron, *Molecular Light Scattering and Optical Activity*, second ed., revised and expanded, Cambridge Univ. Press, Cambridge, 2004.
[3] G.H. Wagnière, *Linear and Nonlinear Optical Properties of Molecules*, Verlag Helvetica Chimica Acta, Basel, 1993.
[4] J. Kerr, *Phil. Mag.* **4** (50) (1875) 337.
[5] J. Kerr, *Phil. Mag.* **4** (50) (1875) 416.
[6] A.D. Buckingham, J.A. Pople, *Proc. Phys. Soc. A* **68** (1955) 905.
[7] D.J. Cadwell, H. Eyring, *The Theory of Optical Activity*, Wiley–Interscience, New York, 1971.
[8] A.D. Buckingham, P.J. Stephens, *Annu. Rev. Phys. Chem.* **17** (1966) 399.
[9] A. Cotton, M. Mouton, *Compt. Rend.* **141** (1905) 317.
[10] A.D. Buckingham, J.A. Pople, *Proc. Phys. Soc. B* **69** (1956) 1133.
[11] A.D. Buckingham, *J. Chem. Phys.* **30** (1959) 1580.
[12] A.D. Buckingham, H.C. Longuet-Higgins, *Mol. Phys.* **14** (1968) 63.
[13] R.C. Jones, *J. Opt. Soc. Am.* **38** (1948) 671.
[14] E.B. Graham, R.E. Raab, *Proc. R. Soc. Lond. A* **390** (1983) 73.
[15] F. Pockels, *Radium* **10** (1913) 152.
[16] E.B. Graham, R.E. Raab, *Mol. Phys.* **52** (1984) 1241.
[17] M.P. Groenewege, *Mol. Phys.* **5** (1962) 541.
[18] L.D. Barron, J. Vrbancich, *Mol. Phys.* **51** (1984) 715.
[19] S. Woźniak, R. Zadowny, *Acta Phys. Polonica A* **61** (1985) 175.
[20] G. Wagnière, A. Meier, *Chem. Phys. Lett.* **93** (1982) 78.
[21] A. Rizzo, M. Kállay, J. Gauss, F. Pawłowski, P. Jørgensen, C. Hättig, *J. Chem. Phys.* **121** (2004) 9461.
[22] C. Rizzo, A. Rizzo, D.M. Bishop, *Int. Rev. Phys. Chem.* **16** (1997) 81.
[23] D.A. Imrie, R.E. Raab, *Mol. Phys.* **74** (1991) 833.
[24] S. Coriani, A. Halkier, A. Rizzo, K. Ruud, *Chem. Phys. Lett.* **326** (2000) 269.
[25] S. Coriani, A. Halkier, A. Rizzo, The electric-field-gradient-induced birefringence and the determination of molecular quadrupole moments, in: G. Pandalai (Ed.), *Recent Research Developments in Chemical Physics, vol. 2*, Transworld Scientific, Kerala, India, 2001, p. 1.
[26] A. Rizzo, S. Coriani, A. Halkier, C. Hättig, *J. Chem. Phys.* **113** (2000) 3077.
[27] S. Coriani, *Ab initio* determination of molecular properties, PhD thesis, Aarhus University, Århus, Denmark, July 2000.
[28] A. Halkier, S. Coriani, P. Jørgensen, *Chem. Phys. Lett.* **294** (1998) 292.
[29] S. Coriani, A. Halkier, D. Jonsson, J. Gauss, A. Rizzo, O. Christiansen, *J. Chem. Phys.* **118** (2003) 7329.
[30] C. Cappelli, U. Ekström, A. Rizzo, S. Coriani, *J. Comp. Meth. Sci. Eng. (JCMSE)* **4** (2004) 365.
[31] P. Kleindienst, G.H. Wagnière, *Chem. Phys. Lett.* **288** (1998) 89.
[32] N.K. Kalugin, P. Kleindienst, G.H. Wagnière, *Chem. Phys.* **248** (1999) 105.
[33] M. Vallet, R. Ghosh, A.L. Floch, T. Ruchon, F. Bretenaker, J.-Y. Thépot, *Phys. Rev. Lett.* **87** (2001) 183003.
[34] S. Coriani, M. Pecul, A. Rizzo, P. Jørgensen, M. Jaszuński, *J. Chem. Phys.* **117** (2002) 6417.
[35] M. Pecul, K. Ruud, A. Rizzo, T. Helgaker, *J. Phys. Chem. A* **108** (2004) 4269.
[36] G.L.J.A. Rikken, E. Raupach, T. Roth, *Physica A* **294–295** (2001) 1.
[37] T. Roth, G.L.J.A. Rikken, *Phys. Rev. Lett.* **85** (2000) 4478.
[38] A. Rizzo, S. Coriani, *J. Chem. Phys.* **119** (2003) 11064.
[39] A. Rizzo, C. Cappelli, B. Jansík, D. Jonsson, P. Saíek, S. Coriani, H. Ågren, *J. Chem. Phys.* **121** (2004) 8814.
[40] A.D. Buckingham, *Proc. Phys. Soc. B* **69** (1956) 344.
[41] A.D. Buckingham, M.B. Dunn, *J. Chem. Soc. A* (1971) 1988.
[42] M. Faraday, *Philos. Mag.* **29** (1846) 153.
[43] M. Faraday, *Philos. Mag.* **28** (1846) 294.
[44] N.B. Baranova, Y.V. Bogdanov, B.Y. Zel'dovich, *Optics Comm.* **22** (1977) 243.
[45] A.D. Buckingham, R.A. Shatwell, *Chem. Phys.* **35** (1978) 353.
[46] P.W. Atkins, M.H. Miller, *Mol. Phys.* **15** (1968) 503.
[47] S. Woźniak, *Mol. Phys.* **80** (1993) 355.

[48] A.D. Buckingham, Permanent and induced molecular moments and long-range intermolecular forces, in: J.O. Hirschfelder (Ed.), *Intermolecular Forces*, in: *Adv. Chem. Phys.*, vol. 12, Wiley, New York, 1967, p. 107.
[49] J. Olsen, P. Jørgensen, Time-dependent response theory with applications to self-consistent field and multiconfigurational self-consistent field wave functions, in: D.R. Yarkony (Ed.), *Modern Electronic Structure Theory, part II*, World Scientific, Singapore, 1995, p. 857.
[50] J. Olsen, P. Jørgensen, *J. Chem. Phys.* **82** (1985) 3235.
[51] T. Helgaker, P. Jørgensen, J. Olsen, *Molecular Electronic-Structure Theory*, Wiley, Chichester, 1999.
[52] J. Gauss, J.F. Stanton, *J. Chem. Phys.* **104** (1996) 2574.
[53] T. Helgaker, J. Gauss, P. Jørgensen, J. Olsen, *J. Chem. Phys.* **106** (1997) 6430.
[54] A. Halkier, P. Jørgensen, J. Gauss, T. Helgaker, *Chem. Phys. Lett.* **274** (1997) 235.
[55] K.L. Bak, J. Gauss, T. Helgaker, P. Jørgensen, J. Olsen, *Chem. Phys. Lett.* **319** (2000) 563.
[56] A. Halkier, S. Coriani, *Chem. Phys. Lett.* **303** (1999) 408.
[57] A. Halkier, S. Coriani, *Chem. Phys. Lett.* **346** (2001) 329.
[58] A. Halkier, Accurate static molecular properties from calculations in hierarchical series of basis sets and wavefunction models, PhD thesis, Aarhus University, Århus, Denmark, July 1999.
[59] F. Pawłowski, Development and implementation of CC3 response theory for calculation of frequency-dependent molecular properties. Benchmarking of static molecular properties, PhD thesis, Aarhus University, Århus, Denmark, February 2004.
[60] T.H. Dunning Jr., *J. Chem. Phys.* **90** (1989) 1007.
[61] R.A. Kendall, T.H. Dunning Jr., R.J. Harrison, *J. Chem. Phys.* **96** (1992) 6796.
[62] D.E. Woon, T.H. Dunning Jr., *J. Chem. Phys.* **98** (1993) 1358.
[63] D.E. Woon, T.H. Dunning Jr., *J. Chem. Phys.* **100** (1994) 2975.
[64] D.E. Woon, T.H. Dunning Jr., *J. Chem. Phys.* **103** (1995) 4572.
[65] A.K. Wilson, D.E. Woon, K.A. Peterson, T.H. Dunning Jr., *J. Chem. Phys.* **110** (1999) 7667.
[66] T.H. Dunning Jr., K.A. Peterson, A.K. Wilson, *J. Chem. Phys.* **114** (2001) 9244.
[67] K.A. Peterson, T.H. Dunning Jr., *J. Chem. Phys.* **117** (2002) 10548.
[68] C. Møller, M.S. Plesset, *Phys. Rev.* **46** (1934) 618.
[69] G.D. Purvis, R.J. Bartlett, *J. Chem. Phys.* **76** (1982) 1910.
[70] K. Raghavachari, G.W. Trucks, J.A. Pople, M. Head-Gordon, *Chem. Phys. Lett.* **157** (1989) 479.
[71] F. Jensen, *Introduction to Computational Chemistry*, Wiley, Chichester, 1999.
[72] J. Noga, R.J. Bartlett, *J. Chem. Phys.* **86** (1987) 7041;
J. Noga, R.J. Bartlett, *J. Chem. Phys.* **89** (1988) 3401 (Erratum).
[73] G.E. Scuseria, H.F. Schaefer, *Chem. Phys. Lett.* **152** (1988) 382.
[74] J.D. Watts, R.J. Bartlett, *J. Chem. Phys.* **93** (1990) 6104.
[75] J. Gauss, J.F. Stanton, *J. Chem. Phys.* **116** (2002) 1773.
[76] J. Gauss, *J. Chem. Phys.* **116** (2002) 4773.
[77] M. Kállay, J. Gauss, P.G. Szalay, *J. Chem. Phys.* **119** (2003) 2991.
[78] M. Kállay, P.R. Surján, *J. Chem. Phys.* **115** (2001) 2945.
[79] O. Christiansen, C. Hättig, P. Jørgensen, *Int. J. Quantum Chem.* **68** (1998) 1.
[80] O. Christiansen, H. Koch, P. Jørgensen, *Chem. Phys. Lett.* **243** (1995) 409.
[81] H. Koch, O. Christiansen, P. Jørgensen, A. Sánchez de Merás, T. Helgaker, *J. Chem. Phys.* **106** (1997) 1808.
[82] O. Christiansen, H. Koch, P. Jørgensen, *J. Chem. Phys.* **103** (1995) 7429.
[83] J. Gauss, O. Christiansen, J.F. Stanton, *Chem. Phys. Lett.* **296** (1998) 117.
[84] F. Pawłowski, P. Jørgensen, C. Hättig, *Chem. Phys. Lett.* **391** (2004) 27.
[85] C. Hättig, O. Christiansen, P. Jørgensen, *J. Chem. Phys.* **107** (1997) 10592.
[86] C. Hättig, P. Jørgensen, *Theor. Chim. Acta* **100** (1998) 230.
[87] C. Hättig, P. Jørgensen, *Adv. Quantum Chem.* **35** (1999) 111.
[88] T. Helgaker, P.J. Wilson, R.D. Amos, N.C. Handy, *J. Chem. Phys.* **113** (2000) 2088.
[89] P. Sałek, O. Vahtras, T. Helgaker, H. Ågren, *J. Chem. Phys.* **117** (2002) 9630.
[90] B. Jansík, Density Functional Theory for molecular properties, PhD thesis, KTH Biotechnology, Stockholm, Sweden, May 2004.
[91] C. Cappelli, B. Mennucci, J. Tomasi, R. Cammi, A. Rizzo, *Chem. Phys. Lett.* **346** (2001) 251.
[92] C. Cappelli, B. Mennucci, J. Tomasi, R. Cammi, A. Rizzo, G. Rikken, R. Mathevet, C. Rizzo, *J. Chem. Phys.* **118** (2003) 10712.

[93] T. Helgaker, H.J.A. Jensen, P. Jørgensen, J. Olsen, K. Ruud, H. Ågren, A.A. Auer, K.L. Bak, V. Bakken, O. Christiansen, S. Coriani, P. Dahle, E.K. Dalskov, T. Enevoldsen, B. Fernández, C. Hättig, K. Hald, A. Halkier, H. Heiberg, H. Hettema, D. Jonsson, S. Kirpekar, R. Kobayashi, H. Koch, K.V. Mikkelsen, P. Norman, M.J. Packer, T.B. Pedersen, T.A. Ruden, A. Sánchez de Merás, T. Saue, S.P.A. Sauer, B. Schimmelpfennig, K.O. Sylvester-Hvid, P.R. Taylor, O. Vahtras, DALTON, an *ab initio* electronic structure program, Release 1.2, 2001. See http://www.kjemi.uio.no/software/dalton/dalton.html.
[94] J.F. Stanton, J. Gauss, J.D. Watts, W.J. Lauderdale, R.J. Bartlett, *Int. J. Quantum Chem. Symp.* **26** (1992) 879.
[95] D.M. Bishop, *Rev. Mod. Phys.* **62** (1990) 343.
[96] D.M. Bishop, P. Norman, Calculation of dynamic hyperpolarizabilities for small and medium sized molecules, in: H.S. Nalwa (Ed.), *Nonlinear Optical Materials*, in: *Handbook of Advanced Electric and Photonic Materials and Devices*, vol. 9, Academic Press, San Diego CA, 2000 (Chapter 1).
[97] D.M. Bishop, *Molecular Vibrations and Nonlinear Optics*, *Adv. Chem. Phys.*, vol. 104, Wiley, New York, 1998, p. 1.
[98] P.-O. Åstrand, K. Ruud, P.R. Taylor, *J. Chem. Phys.* **112** (2000) 1655.
[99] O. Christiansen, *J. Chem. Phys.* **120** (2004) 2149.
[100] K. Ruud, P.R. Taylor, P.-O. Åstrand, *Chem. Phys. Lett.* **337** (2001) 217.
[101] D. Jonsson, P. Norman, H. Ågren, A. Rizzo, S. Coriani, K. Ruud, *J. Chem. Phys.* **114** (2001) 8372.
[102] K. Ruud, D. Jonsson, P.R. Taylor, *Phys. Chem. Chem. Phys.* **2** (2000) 2161.
[103] D. Jonsson, P. Norman, O. Vahtras, H. Ågren, A. Rizzo, *J. Chem. Phys.* **106** (1997) 8552.
[104] D.M. Bishop, S.M. Cybulski, J. Pipin, *J. Chem. Phys.* **94** (1991) 6686.
[105] S.M. Cybulski, D.M. Bishop, *J. Chem. Phys.* **101** (1994) 424.
[106] D.M. Bishop, S.M. Cybulski, *J. Chem. Phys.* **101** (1994) 2180.
[107] K.V. Mikkelsen, P. Jørgensen, K. Ruud, T. Helgaker, *J. Chem. Phys.* **106** (1997) 1070.
[108] K.V. Mikkelsen, K. Ruud, T. Helgaker, *Chem. Phys. Lett.* **253** (1996) 443.
[109] K. Ruud, T. Helgaker, A. Rizzo, S. Coriani, K.V. Mikkelsen, *J. Chem. Phys.* **106** (1997) 894.
[110] K.V. Mikkelsen, K.O. Sylvester-Hvid, *J. Phys. Chem.* **100** (1996) 9116.
[111] K. Ruud, H. Ågren, P. Dahle, T. Helgaker, A. Rizzo, S. Coriani, H. Koch, K.O. Sylvester-Hvid, K.V. Mikkelsen, *J. Chem. Phys.* **108** (1998) 599.
[112] S. Miertuš, E. Scrocco, J. Tomasi, *J. Chem. Phys.* **55** (1981) 117.
[113] R. Cammi, J. Tomasi, *J. Comp. Chem.* **16** (1995) 1449.
[114] E. Cancés, B. Mennucci, *J. Math. Chem.* **23** (1998) 309.
[115] E. Cancés, B. Mennucci, J. Tomasi, *J. Chem. Phys.* **107** (1997) 3032.
[116] B. Mennucci, E. Cancés, J. Tomasi, *J. Phys. Chem. B* **101** (1997) 10506.
[117] T. Saue, V. Bakken, T. Enevoldsen, T. Helgaker, H.J.A. Jensen, J.K. Laerdahl, K. Ruud, J. Thyssen, L. Visscher, DIRAC, a relativistic *ab initio* electronic structure program, Release 3.2, 2000. See http://dirac.chem.sdu.dk.
[118] S. Coriani, T. Helgaker, P. Jørgensen, W. Klopper, *J. Chem. Phys.* **121** (2004) 6591.
[119] W. Klopper, S. Coriani, T. Helgaker, P. Jørgensen, *J. Phys. B: At. Mol. Opt. Phys.* **37** (2004) 3753.
[120] A. Buckingham, J. Pople, *Trans. Faraday Soc.* **51** (1955) 1029.
[121] A.D. Buckingham, J.A. Pople, *Trans. Faraday Soc.* **51** (1955) 1173.
[122] A.D. Buckingham, J.A. Pople, *Trans. Faraday Soc.* **51** (1955) 1179.
[123] A.D. Buckingham, *Trans. Faraday Soc.* **52** (1956) 747.
[124] A.D. Buckingham, R.E. Raab, *Trans. Faraday Soc.* **54** (1958) 623.
[125] A. Buckingham, J. Pople, *Faraday Soc. Disc.* **22** (1956) 17.
[126] D. Marchesan, S. Coriani, A. Rizzo, *Mol. Phys.* **101** (2003) 1851.
[127] B. Fernández, C. Hättig, H. Koch, A. Rizzo, *J. Chem. Phys.* **110** (1999) 2872.
[128] H. Koch, C. Hättig, H. Larsen, J. Olsen, P. Jørgensen, B. Fernández, A. Rizzo, *J. Chem. Phys.* **111** (1999) 10108.
[129] A. Rizzo, C. Hättig, B. Fernández, H. Koch, *J. Chem. Phys.* **117** (2002) 2609.
[130] C. Hättig, J. López Cacheiro, B. Fernández, A. Rizzo, *Mol. Phys.* **101** (2003) 1983.
[131] A. Rizzo, K. Ruud, D.M. Bishop, *Mol. Phys.* **100** (2002) 799.
[132] D.A. Dunmur, D.C. Hunt, N.E. Jessup, *Mol. Phys.* **37** (1979) 713.
[133] J.H.V. Vleck, *The Theory of Electric and Magnetic Susceptibilities*, Oxford Univ. Press, Oxford, 1932.
[134] F. London, *J. Phys. Radium* **8** (1937) 397.
[135] R. Ditchfield, *J. Chem. Phys.* **56** (1972) 5688.

[136] H.F. Hameka, *Mol. Phys.* **1** (1958) 203.
[137] H.F. Hameka, *Z. Naturf. A* **14** (1959) 599.
[138] H.F. Hameka, *Rev. Mod. Phys.* **34** (1962) 87.
[139] M.J. Frisch, G.W. Trucks, H.B. Schlegel, G.E. Scuseria, M.A. Robb, J.R. Cheeseman, J.A. Montgomery Jr., T. Vreven, K.N. Kudin, J.C. Burant, J.M. Millam, S.S. Iyengar, J. Tomasi, V. Barone, B. Mennucci, M. Cossi, G. Scalmani, N. Rega, G.A. Petersson, H. Nakatsuji, M. Hada, M. Ehara, K. Toyota, R. Fukuda, J. Hasegawa, M. Ishida, T. Nakajima, Y. Honda, O. Kitao, H. Nakai, M. Klene, X. Li, J.E. Knox, H.P. Hratchian, J.B. Cross, C. Adamo, J. Jaramillo, R. Gomperts, R.E. Stratmann, O. Yazyev, A.J. Austin, R. Cammi, C. Pomelli, J.W. Ochterski, P.Y. Ayala, K. Morokuma, G.A. Voth, P. Salvador, J.J. Dannenberg, V.G. Zakrzewski, S. Dapprich, A.D. Daniels, M.C. Strain, O. Farkas, D.K. Malick, A.D. Rabuck, K. Raghavachari, J.B. Foresman, J.V. Ortiz, Q. Cui, A.G. Baboul, S. Clifford, J. Cioslowski, B.B. Stefanov, G. Liu, A. Liashenko, P. Piskorz, I. Komaromi, R.L. Martin, D.J. Fox, T. Keith, M.A. Al-Laham, C.Y. Peng, A. Nanayakkara, M. Challacombe, P.M.W. Gill, B. Johnson, W. Chen, M.W. Wong, C. Gonzalez, J.A. Pople, GAUSSIAN 03, Revision A.1, Gaussian, Inc., Pittsburgh, PA, 2003.
[140] S. Coriani, C. Hättig, P. Jørgensen, T. Helgaker, *J. Chem. Phys.* **113** (2000) 3561.
[141] A. Rizzo, T. Helgaker, K. Ruud, A. Barszczewicz, M. Jaszuński, P. Jørgensen, *J. Chem. Phys.* **102** (1995) 8953.
[142] S. Coriani, A. Rizzo, K. Ruud, T. Helgaker, *Mol. Phys.* **88** (1996) 931.
[143] S. Coriani, A. Rizzo, K. Ruud, T. Helgaker, *Chem. Phys.* **216** (1997) 53.
[144] T.A. Keith, R.F.W. Bader, *Chem. Phys. Lett.* **194** (1992) 1.
[145] T.A. Keith, R.F.W. Bader, *Chem. Phys. Lett.* **210** (1993) 223.
[146] A. Rizzo, C. Rizzo, *Mol. Phys.* **96** (1999) 973.
[147] H. Kling, W. Hüttner, *Chem. Phys.* **90** (1984) 207.
[148] H. Kling, E. Dreier, W. Hüttner, *J. Chem. Phys.* **78** (1983) 4309.
[149] P.B. Lukins, G.L.D. Ritchie, *Chem. Phys. Lett.* **180** (1991) 551.
[150] M.H. Coonan, G.L.D. Ritchie, *Chem. Phys. Lett.* **202** (1993) 237.
[151] H. Kling, H. Geschka, W. Hüttner, *Chem. Phys. Lett.* **96** (1983) 631.
[152] P.B. Lukins, A.D. Buckingham, G.L.D. Ritchie, *J. Phys. Chem.* **88** (1984) 2414.
[153] M.H. Coonan, I.E. Craven, M.R. Hesling, G.L.D. Ritchie, M.A. Spackman, *J. Phys. Chem.* **96** (1992) 7301.
[154] A.D. Becke, *J. Chem. Phys.* **98** (1993) 5648.
[155] A.D. Becke, *Phys. Rev. A* **38** (1988) 3098.
[156] C. Lee, W. Yang, R.G. Parr, *Phys. Rev. B* **37** (1988) 785.
[157] D.M. Bishop, J. Pipin, *Chem. Phys. Lett.* **186** (1991) 195.
[158] D.M. Bishop, J. Pipin, *Chem. Phys. Lett.* **241** (1995) 484.
[159] K. Muroo, N. Ninomiya, M. Yoshino, Y. Takubo, *J. Opt. Soc. Am. B* **20** (2003) 2249.
[160] R. Cameron, G. Cantatore, A.C. Melissinos, Y. Semertzidis, H. Halama, D. Lazarus, A. Prodell, F. Nezrick, P. Micossi, C. Rizzo, G. Ruoso, E. Zavattini, *Phys. Lett. A* **157** (1991) 125.
[161] R. Cameron, G. Cantatore, A.C. Melissinos, J. Rogers, Y. Semertzidis, H. Halama, A. Prodell, F.A. Nezrick, C. Rizzo, E. Zavattini, *J. Opt. Soc. Am. B* **8** (1991) 520.
[162] S. Carusotto, E. Iacopini, E. Polacco, F. Scuri, G. Stefanini, E. Zavattini, *J. Opt. Soc. Am. B* **1** (1984) 635.
[163] M.H. Coonan, G.L.D. Ritchie, *Chem. Phys. Lett.* **293** (1998) 197.
[164] A.D. Buckingham, R.L. Disch, M.P. Bogaard, Unpublished data.
[165] A.D. Buckingham, W.H. Pritchard, D.H. Whiffen, *Trans. Faraday Soc.* **63** (1967) 1057.
[166] W.H. Flygare, W. Hüttner, R.L. Shoemaker, P.D. Foster, *J. Chem. Phys.* **50** (1969) 1714.
[167] W.L. Meerts, F.H. de Leeuw, A. Dymanus, *Chem. Phys.* **22** (1977) 319.
[168] J.M.L.J. Reinartz, W.L. Meerts, A. Dymanus, *Chem. Phys.* **31** (1978) 19.
[169] F.D. deLeeuw, A. Dymanus, *Chem. Phys. Lett.* **7** (1970) 288.
[170] S. Coriani, C. Hättig, P. Jørgensen, A. Rizzo, K. Ruud, *J. Chem. Phys.* **109** (1998) 7176.
[171] R.E. Raab, O.L. de Lange, *Mol. Phys.* **101** (2003) 3467.
[172] O.L. de Lange, R.E. Raab, *Mol. Phys.* **102** (2004) 125.
[173] R.I. Keir, D.W. Lamb, G.L.D. Ritchie, J.N. Watson, *Chem. Phys. Lett.* **279** (1997) 22.
[174] A.D. Buckingham, R.L. Disch, *Proc. Roy. Soc. A* **273** (1963) 275.
[175] C. Graham, D.A. Imrie, R.E. Raab, *Mol. Phys.* **93** (1998) 49.
[176] A.J. Russell, M.A. Spackman, *Mol. Phys.* **88** (1996) 1109.
[177] G.L.D. Ritchie, J.N. Watson, R.I. Keir, *Chem. Phys. Lett.* **370** (2003) 376.
[178] J.N. Watson, I.E. Craven, G.L.D. Ritchie, *Chem. Phys. Lett.* **274** (1997) 1.

[179] G.L.D. Ritchie, J.N. Watson, *Chem. Phys. Lett.* **322** (2000) 143.
[180] A. Rizzo, C. Cappelli, B. Jansík, D. Jonsson, P. Sałek, S. Coriani, D.J.D. Wilson, T. Helgaker, H. Ågren, *J. Chem. Phys.* **122** (2005) 234314.
[181] J.M. Junquera-Hernández, J. Sánchez-Marín, V. Pérez-Mondéjar, A. Sánchez de Merás, *Chem. Phys. Lett.* **378** (2003) 211.
[182] A.D. Buckingham, R.L. Disch, D.A. Dunmur, *J. Am. Chem. Soc.* **90** (1968) 3104.
[183] M.R. Battaglia, A.D. Buckingham, D. Neumark, R.K. Pierens, J.H. Williams, *Mol. Phys.* **43** (1981) 1015.
[184] G.L.D. Ritchie, Field-gradient induced birefringence: a direct route to molecular quadrupole moments, in: D.C. Clary, B. Orr (Eds.), *Optical, Electric and Magnetic Properties of Molecules*, Elsevier, Amsterdam, The Netherlands, 1997, p. 67.
[185] D.M. Bishop, S.P.A. Sauer, *J. Chem. Phys.* **107** (1997) 8502.
[186] S. Coriani, C. Hättig, A. Rizzo, *J. Chem. Phys.* **111** (1999) 7828.
[187] G.L.J.A. Rikken, E. Raupach, *Phys. Rev. E* **58** (1998) 5081.
[188] Y. Kumata, J. Furukawa, T. Fueno, *Bull. Chem. Soc. Jpn.* **43** (1970) 3920.
[189] R.C. West (Ed.), *Handbook of Chemistry and Physics*, fifty-seventh ed., CRC Press Inc., Cleveland, OH, 1977.
[190] S. Kielich, in: C.T. O'Konski (Ed.), *Molecular Electro-Optics*, Marcel Dekker, New York, 1976.
[191] H.J. Ross, B.S. Sherborne, G.E. Stedman, *J. Phys. B* **22** (1989) 459.
[192] T. Roth, Experimental verification of the Jones birefringence induced in liquids, Master's thesis, Darmstadt University of Technology and Grenoble High Magnetic Field Laboratory, 2000, Diplomarbeit.
[193] T. Roth, G.L.J.A. Rikken, *Phys. Rev. Lett.* **88** (2002) 063001.
[194] J. Rychlewski, W.T. Raynes, *Mol. Phys.* **41** (1980) 843.
[195] J. Rychlewski, *Mol. Phys.* **41** (1980) 833.
[196] S. Coriani, C. Hättig, P. Jørgensen, Unpublished.

The *Ab Initio* Calculation of Optical Rotation and Electronic Circular Dichroism

Magdalena Pecul* and Kenneth Ruud

Department of Chemistry, University of Tromsø, N-9037 Tromsø, Norway

Abstract

We review the theory of the lowest-order manifestations of natural optical activity: optical rotation (OR) and electronic circular dichroism (ECD), and discuss the applications of modern *ab initio* methods to the calculation of these properties, with particular emphasis put on the challenges facing such calculations, including the gauge origin problem. We review the recent applications of *ab initio* methods to calculations of OR and ECD, giving examples of the kind of molecules and questions that can now be addressed using *ab initio* methodology.

Contents

* Permanent address: Department of Chemistry, University of Warsaw, Pasteura 1, 02-093 Warsaw, Poland.

ADVANCES IN QUANTUM CHEMISTRY, VOLUME 50
ISSN: 0065-3276 DOI: 10.1016/S0065-3276(05)50009-1

1. INTRODUCTION

Natural optical activity, the lowest order optical phenomenon associated with chirality, manifested as electronic circular dichroism (ECD) in absorption spectra of circularly polarized light and as optical rotation (OR) in the transparent region, has been known since the beginning of the XIX century. Since the first works of Arago and Biot in 1811 and 1812 [1,2], much effort has been devoted to understanding the connection between these phenomena and the structure of the chiral system. The theoretical background for quantum mechanical calculations of the optical rotation was given by Rosenfeld in 1928 [3]. However, in part due to the difficulties inherent in the calculation of properties involving the magnetic dipole operator, and partly due to the often large size of chiral molecules, calculations of these properties—and in particular of the optical rotation—using quantum chemical methods emerged relatively late.

An *ab initio* calculation of the molecular tensors contributing to the optical rotation was first carried out by Amos [4] at the Hartree–Fock (HF) level in the so-called static limit (*vide infra*) for a few simple, non-chiral molecules (CO, HF, HCl and CH_3F). An implementation and the first calculations of the frequency-dependent tensors were presented for the water molecule by Lazzeretti and Zanasi in 1986 [5]. The first *ab initio* calculations of the optical rotation of chiral molecules appeared in 1997, in this case employing the static-limit approximation [6]. Incidentally, the frequency-dependent, gauge-origin independent tensors required for optical rotation calculations had been implemented a few years earlier [7].

The optical rotatory strengths characterizing the ECD spectrum have been calculated for a much longer time: *ab initio* calculations of rotatory strengths have been performed for almost 30 years [8]. However, it is only recently that reliable calculations of ECD parameters in systems of chemical interest have become possible.

In this review, we will give a short presentation of the theory of electronic circular dichroism and optical rotation, and of the contemporary *ab initio* methods used for their calculations. For both properties, some typical applications presented in the literature will be reviewed. We focus on theoretical investigations of the problems that affect the comparison of *ab initio* results and experimental data, such as basis set and electron correlation effects, the effects of molecular vibrations, as well as solvent effects. Some more typical applications, such as structural studies (including the assignment of the absolute configuration) will also be discussed. For an earlier review of calculations of the optical rotation, we refer to the work by Polavarapu [9].

2. THEORY OF OPTICAL ACTIVITY

2.1. The physical manifestation of optical activity

Natural optical activity manifests itself in the transparent region as the *optical rotation* of the polarization plane of plane-polarized light after passing through a sample of chiral molecules with an excess of one enantiomer. In the absorbing region, left and right circularly polarized light are absorbed differently, a phenomenon called *circular dichroism*. Indeed, both optical rotation and circular dichroism can be traced back to the same origin: chiral molecules have different index of refraction—both the real (contributing to optical

rotation) and the imaginary (contributing to circular dichroism) parts—for circularly polarized light waves of opposite rotation. Consequently, both phenomena are dependent on the electromagnetic wavelength.

Optical rotation can be rationalized by the fact that plane-polarized light can be decomposed into left- and right-circular polarization states of equal amplitudes, as first noted by Fresnel in 1825 [10,11]. Since the real part of the index of refraction for circular waves of opposite rotation are different in a chiral medium, the two waves propagating through such a medium acquire a relative phase shift that leads to a net rotation of the original plane of polarization.

The imaginary component of the refractive index induces an exponential decay of the amplitude of the circularly polarized light. The rate of decay is in chiral samples different for left- and right-circular polarization states, and the difference in the absorption of left- and right-circularly polarized light, the *circular dichroism*, can be measured. Furthermore, plane-polarized light becomes elliptically polarized after passing through an optically active absorbing sample, which is also a consequence of the difference in the absorption of the two circular components, since elliptically polarized light can be decomposed into coherent left- and right-circularly polarized components of different amplitudes.

At the molecular level, the refractive index is related to the mixed electric dipole – magnetic dipole polarizability $G'_{\alpha\beta}(\omega)$ [12]

$$G'_{\alpha\beta}(\omega) = -2\omega \sum_{n\neq 0} \mathrm{Im} \frac{\langle 0|\hat{\mu}_\alpha|n\rangle\langle n|\widehat{m}_\beta|0\rangle}{\omega_{n0}^2 - \omega^2}, \tag{1}$$

where ω is the frequency of light in atomic units, and $\hat{\mu}_\alpha$ and $\widehat{m}_\beta$ are the electric and magnetic dipole moment operators, respectively. These operators are in second quantization given as

$$\hat{\mu}_\alpha = -\sum_{pq} r_\alpha E_{pq}, \tag{2}$$

$$\widehat{m}_\alpha = -\frac{1}{2} \sum_{pq} l_\alpha^O E_{pq}, \tag{3}$$

where l_α^O is the α component of the orbital angular-momentum operator with respect to the gauge origin **O**. In these equations, the summations run over the orbitals in the basis set, and E_{pq} are the generators of the unitary group [13].

Both the optical rotation and the optical rotatory strength are therefore related to $G'_{\alpha\beta}(\omega)$.

The results of a measurement of the optical rotation are usually reported in terms of the specific optical rotation (specific optical rotatory power) $[\alpha]$

$$[\alpha] = \frac{\alpha V}{ml}, \tag{4}$$

where α is the rotation of the original polarization plane, l is the optical path length, and m and V are the mass and volume of the chiral sample, respectively.

The specific optical rotation is related [3] to the trace of the Rosenfeld tensor $\beta_{\alpha\beta}$ by

$$[\alpha] = 288 \cdot 10^{-30} \frac{\pi^2 N_A a_0^4 \omega^2}{M} \beta, \tag{5}$$

where $\beta = 1/3\,\mathrm{Tr}\,\boldsymbol{\beta}$, and where the Rosenfeld tensor can be written in terms of the mixed electric dipole-magnetic dipole polarizability $G'_{\alpha\beta}$

$$\beta_{\alpha\beta}(\omega) = -\omega^{-1} G'_{\alpha\beta}(\omega). \tag{6}$$

In the above equations, N_A is Avogadro's number, a_0 is the Bohr radius, M is the molar mass of the molecule in g·mol^{-1}, ω the frequency of the light in atomic units, and where β is also given atomic units. The units of $[\alpha]$ are deg·cm^3·g^{-1}·dm^{-1}.

Most measurements of the optical rotation are carried out at a single frequency, usually corresponding to the sodium D-line. However, studies of the variation of the optical rotation with the frequency of the incident light are also known, and are referred to as *optical rotatory dispersion* (ORD) [14]. Natural optical activity of oriented samples includes a contribution from the electric dipole – electric quadrupole polarizability tensor which is traceless and thus vanishes for freely rotating molecules [15].

Circular dichroism is usually expressed as the difference between the molar extinction coefficients for left- and right-circularly polarized light ($\varepsilon_L(\lambda)$ and $\varepsilon_R(\lambda)$):

$$\Delta\varepsilon(\lambda) = \varepsilon_L(\lambda) - \varepsilon_R(\lambda), \tag{7}$$

$\Delta\varepsilon(\lambda)$ is related to the rotatory strength ${}^nR$ of the transition between the ground state 0 and the nth excited state.

The rotatory strength ${}^nR$ was derived from quantum mechanical theory by Rosenfeld [3] as the product of the electric dipole and magnetic dipole transition moments, in atomic units given as

$${}^nR_{\alpha\beta} = \frac{3}{4}\,\mathrm{Im}\left[\sum_\gamma \langle 0|\hat{\mu}_\gamma|n\rangle\langle n|\widehat{m}_\gamma|0\rangle\delta_{\alpha\beta} - \langle 0|\hat{\mu}_\alpha|n\rangle\langle n|\widehat{m}_\beta|0\rangle\right]. \tag{8}$$

Assuming a Gaussian band shape, the observed $\Delta\varepsilon(\lambda)$ can be reproduced from the rotatory strengths through the relation [16]:

$$\Delta\varepsilon(\lambda) = \frac{16\pi^2 N_A a_0 e^2}{3\hbar c \cdot 10^7 \ln 10\, m_e} \frac{1}{\Gamma_n\sqrt{\pi}} \sum_n {}^nR \exp\left[\left(-\frac{\lambda - \lambda_{n0}}{\Gamma_n}\right)^2\right], \tag{9}$$

where λ is the light wavelength, λ_{n0} is the wavelength corresponding to the $n \leftarrow 0$ transition, Γ_n is the width of the band (assuming a Gaussian bandshape) at e^{-1} of its maximum, ${}^nR$ is the trace of tensor in equation (8), and the summation is over the bands. In equation (9), ${}^nR$ is converted from atomic units to cgs units by multiplying ${}^nR$ with a factor $\frac{ea_0c\hbar}{m_e}$, where e is the elementary charge, c the speed of light, and m_e the electron mass.

2.2. The molecular origin of optical rotation and circular dichroism

In the following, an outline of the derivation of the quantum mechanical expression for the optical rotation and the rotatory strength will be presented. In the description of electromagnetic interactions, the magnetic dipole operator always occurs together with a molecular quadrupole operator arising from the electric field gradient of the oscillating electromagnetic field, and it is only the sum of these two operators that give rise to origin independent results. However, for isotropic samples, which constitute the majority of the systems studied by *ab initio* methods, the contribution from the quadrupole operator

will not appear since it is purely anisotropic. For simplicity, it is therefore neglected in the following derivations, but it will be reintroduced later in a phenomenological manner.

Our derivation of the electric and magnetic dipole interactions will follow very closely the presentation in Ref. [17], since this approach will allow us to consider optical rotation both in spectral regions close to and far from resonances, and also allow us to consider the absorptive process taking place in ECD spectroscopy in comparison with the non-absorptive processes dominating in optical rotation measurements.

We will consider periodic perturbations, and in this case we may write the electric and magnetic components of the electromagnetic field as

$$F_\alpha(t) = \sum_{k=-N}^{N} F_\alpha^{\omega_k} \mathrm{e}^{-\mathrm{i}\omega_k t}, \tag{10}$$

$$B_\alpha(t) = \sum_{k=-N}^{N} B_\alpha^{\omega_k} \mathrm{e}^{-\mathrm{i}\omega_k t}, \tag{11}$$

where $\omega_{-k} = -\omega_k$, $F^{-\omega_k} = F^{\omega_k *}$, and $B^{-\omega_k} = B^{\omega_k *}$. If we only consider the lowest-order effects of interactions, we can write the induced molecular polarization due to the electromagnetic field as

$$\mu_\alpha(t) = \mu_\alpha^0 + \sum_{k=-N}^{N} \left[\alpha_{\alpha\beta}(\omega_k) F_\beta^{\omega_k} + \chi_{\alpha\beta}(\omega_k) B_\beta^{\omega_k}\right] \mathrm{e}^{-\mathrm{i}\omega_k t}, \tag{12}$$

where μ^0 is the permanent electronic part of the electric dipole moment

$$\mu_\alpha^0 = -\sum_{i}^{N_e} r_{i,\alpha}, \tag{13}$$

and N_e is the number of electrons in the system. In equation (12) we have also introduced $\alpha(\omega)$, which is the frequency-dependent electric dipole polarizability, and $\chi(\omega)$, which is the linear coupling to the external magnetic field. We note that this expression is slightly different from that often used in other presentations, such as for instance Barron [12], but that we can recover the conventional quantity $G'(\omega)$ through the relation

$$G'(\omega) = -\frac{1}{2\mathrm{i}}\left[\chi(\omega) - \chi(-\omega)\right], \tag{14}$$

where $\chi(-\omega) = \chi(\omega)^*$. As mentioned in the previous section, it is the tensor $G'_{\alpha\beta}(\omega)$ that determines the optical rotation and rotatory strengths, and we will therefore not consider the electric polarizability contribution to the polarization any further here.

When exposed to a time-dependent electromagnetic field, the time-development of the molecular system is described by the time-dependent Schrödinger equation

$$\mathrm{i}\frac{\partial}{\partial t}\left|\psi(t)\right\rangle = \widehat{H}\left|\psi(t)\right\rangle, \tag{15}$$

where the Hamiltonian $\widehat{H}$ can be divided into the unperturbed molecular Hamiltonian $\widehat{H}_0$ and the perturbation $\widehat{V}(t)$. We will only consider closed-shell molecular systems, thus ignoring possible spin interactions, and the magnetic perturbation due to the electromagnetic

field can then be written

$$\widehat{V}(t) = -\widehat{m}_\alpha B_\alpha(t). \tag{16}$$

In these equations and in the rest of the paper, atomic units have been used.

Before the time-dependent perturbation is turned on, we will assume that the system is in some reference state $|0\rangle$, and the time-development of this state can be written (assuming exact states)

$$\big|\psi(t)\big\rangle = \mathrm{e}^{-\widehat{P}(t)}|0\rangle, \tag{17}$$

where $\widehat{P}$ is an anti-Hermitian operator of the form

$$\widehat{P}(t) = \sum_{n\neq 0}\big[P_n|n\rangle\langle 0| - P_n^*|0\rangle\langle n|\big]. \tag{18}$$

The state transfer operators $\widehat{\Omega}_n = |n\rangle\langle 0|$ and $\widehat{\Omega}_n^\dagger = |0\rangle\langle n|$ connect the reference state $|0\rangle$ to the complete set of other eigenstates of the unperturbed Hamiltonian $\widehat{H}_0$. We can determine the time-dependent state-transfer amplitudes from a generalized form of the Ehrenfest theorem [18]

$$\frac{\partial}{\partial t}\big\langle\psi(t)\big|\widehat{\Omega}_n\big|\psi(t)\big\rangle = \frac{1}{\mathrm{i}}\big\langle\psi(t)\big|\big[\widehat{\Omega}_n, H\big]\big|\psi(t)\big\rangle - \gamma_n\big[\big\langle\psi(t)\big|\widehat{\Omega}_n\big|\psi(t)\big\rangle - \langle 0|\widehat{\Omega}_n|0\rangle\big], \tag{19}$$

where we have introduced a damping factor γ_n that accounts for the depopulation of the excited state. When we assume that there is no depopulation of the excited states, *i.e.*, when we adopt the so-called infinite-lifetime approximation in which $\gamma_n = 0$, equation (19) is reduced to the Ehrenfest theorem.

By expanding the set of amplitudes to various orders in the applied perturbation

$$P_n = P_n^{(1)} + P_n^{(2)} + P_n^{(3)} + \cdots, \tag{20}$$

and employing the Baker–Campbell–Hausdorff (BCH) expansion in equation (19) with the representation of the time-development of the state as given in equation (17), we get an equation linear in $\widehat{P}$ and $\widehat{V}(t)$

$$\frac{\partial}{\partial t}\langle 0|\big[\widehat{P}, \widehat{\Omega}_n\big]|0\rangle = \frac{1}{\mathrm{i}}\big[\langle 0|\big[\widehat{P}, \big[\widehat{\Omega}_n, \widehat{H}_0\big]\big]|0\rangle + \langle 0|\big[\widehat{\Omega}_n, \widehat{V}(t)\big]|0\rangle\big] - \gamma_n\langle 0|\big[\widehat{P}, \widehat{\Omega}_n\big]|0\rangle. \tag{21}$$

Solving this equation for $P_n^{(1)}$ for a perturbation along the β axis we get

$$P_{n,\beta}^{(1)} = \sum_{k=-N}^{N}\frac{\langle n|\widehat{m}_\beta|0\rangle B_\beta^{\omega_k}\mathrm{e}^{-\mathrm{i}\omega_k t}}{-\omega_{n0} + \omega_k + \mathrm{i}\gamma_n}, \tag{22}$$

where we have defined the excitation energy $\omega_{n0} = E_n - E_0$. Since the first-order perturbed wave function is given as

$$\big|\psi_\beta^{(1)}\big\rangle = -\sum_{n\neq 0}P_{n,\beta}^{(1)}|n\rangle, \tag{23}$$

we can write the first-order magnetic-field induced polarization as

$$\langle 0|\hat{\mu}_\alpha|\psi_\beta^{(1)}\rangle + \langle\psi_\beta^{(1)}|\hat{\mu}_\alpha|0\rangle = \sum_{k=-N}^{N}\sum_{n\neq 0}\left[\frac{\langle 0|\hat{\mu}_\alpha|n\rangle\langle n|\widehat{m}_\beta|0\rangle B_\beta^{\omega_k}}{\omega_{n0}-\omega_k-\mathrm{i}\gamma_n}\mathrm{e}^{-\mathrm{i}\omega_k t} + \frac{\langle n|\widehat{m}_\beta|0\rangle^*\langle n|\hat{\mu}_\alpha|0\rangle B_\beta^{-\omega_k}}{\omega_{n0}-\omega_k+\mathrm{i}\gamma_n}\mathrm{e}^{\mathrm{i}\omega_k t}\right]. \tag{24}$$

Using the fact that the summation runs over both positive and negative frequencies—that is, that we can write $\omega_k = -\omega_k$ in the second term—a comparison with equation (12) gives

$$\chi_{\alpha\beta}(\omega_k) = \sum_{n\neq 0}\left[\frac{\langle 0|\hat{\mu}_\alpha|n\rangle\langle n|\widehat{m}_\beta|0\rangle}{\omega_{n0}-\omega_k-\mathrm{i}\gamma_n} + \frac{\langle 0|\widehat{m}_\beta|n\rangle\langle n|\hat{\mu}_\alpha|0\rangle}{\omega_{n0}+\omega_k+\mathrm{i}\gamma_n}\right]. \tag{25}$$

It is instructive to consider the infinite lifetime expression for the imaginary part of equation (25)—that is, consider the limit $\gamma_n \to 0$. We can then write

$$\mathrm{Im}\,\chi_{\alpha\beta}(\omega_k) = 2\omega_k\sum_{n\neq 0}\mathrm{Im}\,\frac{\langle 0|\hat{\mu}_\alpha|n\rangle\langle n|\widehat{m}_\beta|0\rangle}{\omega_{n0}^2-\omega_k^2} = -G'_{\alpha\beta}(\omega_k), \tag{26}$$

where we have used the fact that $\langle 0|\widehat{m}_\beta|n\rangle = -\langle n|\widehat{m}_\beta|0\rangle$. The contribution to the optical rotation thus corresponds to a mixed electric dipole–magnetic dipole polarizability. We observe from equation (26) that no optical rotation will be observed in the case of static electric and magnetic fields since $\omega_k = 0$ in this case. From equation (5), we recall that in order to determine the optical rotation we do not need $G'_{\alpha\beta}(\omega_k)$ directly, but rather the Rosenfeld tensor $\beta_{\alpha\beta}(\omega_k) = -\omega_k^{-1}G'_{\alpha\beta}(\omega_k)$. Using this we can define a static limit for $\beta_{\alpha\beta}$ as shown by Amos [4]

$$\beta_{\alpha\beta}(\omega_k = 0) = 2\sum_{n>0}\frac{\langle 0|\hat{\mu}_\alpha|n\rangle\langle n|\widehat{m}_\beta|0\rangle}{\omega_{n0}^2} = \langle\psi_\alpha^{(F)}\mid\psi_\beta^{(B)}\rangle, \tag{27}$$

where we have defined the first-order perturbed wave functions $\psi^{(F)}$ and $\psi^{(B)}$ according to equations (22) and (23), setting both ω_k and γ_n to zero.

Although this static limit was used in the first calculations of optical rotations [6], the approximation is in general found to be too crude [19]. Furthermore, since the static limit approximation is computationally more expensive than the frequency-dependent expression equation (25), requiring the determination of both the magnetic and the electric perturbed wave functions, it is currently not much used.

Let us now return to equation (25), but this time consider the infinite lifetime approximation to the real part of $\chi_{\alpha\beta}(\omega_k)$, which will correspond to the absorption process. Using the relation

$$\lim_{\gamma_n\to 0}\left[\mathrm{Im}\left\{\frac{A}{B-\mathrm{i}\gamma_n}\right\}\right] = A\pi\delta(B), \tag{28}$$

we can write

$$\begin{aligned}\lim_{\gamma_n\to 0}\mathrm{Re}\,\chi_{\alpha\beta}(\omega_k) &= \pi\sum_{n>0}\big[\delta(\omega_{n0}-\omega_k)\,\mathrm{Im}\langle 0|\hat{\mu}_\alpha|n\rangle\langle n|\widehat{m}_\beta|0\rangle \\ &\quad + \delta(\omega_{n0}+\omega_k)\,\mathrm{Im}\langle 0|\widehat{m}_\beta|n\rangle\langle n|\hat{\mu}_\beta|0\rangle\big] \\ &= \pi\,\mathrm{Im}\langle 0|\hat{\mu}_\alpha|n\rangle\langle n|\widehat{m}_\beta|0\rangle \propto {}^nR_{\alpha\beta},\end{aligned} \tag{29}$$

where we in order to arrive at the last expression have considered absorption only—that is, we assume that $\omega_k > 0$ and that ω_k coincides with the excitation energy ω_{n0} of one of the excited states.

In this way, by considering the infinite lifetime approximation to the real part of $\chi_{\alpha\beta}(\omega_k)$, we have arrived at the expression for an absorption cross section which involves the product of the electric dipole and magnetic dipole transition moments to the same excited state. The infinite lifetime approximation thus connects the real part of the $\chi_{\alpha\beta}(\omega_k)$ tensor to the rotatory strength which is observed in electronic circular dichroism spectroscopy, see equation (8).

Whereas the use of the infinite lifetime approximation reduces equation (25) to the well-known equations for the optical rotation (equation (5)) and the rotatory strengths (equation (8)), calculating the full tensor in equation (25)—including both the real and imaginary parts of the tensor—allows us to simultaneously calculate the optical rotatory dispersion and the absorption cross sections of ECD at the frequency of the incident light. Such an approach will avoid the divergences appearing in the sum-over-states expression for the optical rotation appearing for $\omega_k = \omega_{no}$ in equation (26), and by integrating the real part of $\chi_{\alpha\beta}(\omega_k)$ over the entire absorption band, we will get the rotatory strength given by equation (8). A Hartree–Fock and DFT approach for such calculations has been presented in Ref. [17], although that study is restricted to ORD.

Before turning to a brief discussion of the calculation of these properties for approximate wave functions, let us introduce the quadrupole interactions. The magnetic dipole interaction operator appears in general together with a quadrupole interaction in the multipolar expansion of the molecular Hamiltonian [12]. This term will give rise to a contribution to the *optical rotation* of the form (in the infinite-lifetime approximation) [15]

$$-\omega_k A_{\alpha\beta\gamma}(\omega_k) = -\omega_k \sum_{n\neq 0} \varepsilon_{\alpha\gamma\delta}\omega_{n0}\frac{\langle 0|\hat{\mu}_\beta|n\rangle\langle n|\widehat{Q}_{\gamma\beta}|0\rangle}{\omega_{n0}^2 - \omega_k^2}, \tag{30}$$

where $\varepsilon_{\alpha\gamma\delta}$ is the Levi-Civita symbol. We have here introduced the electronic quadrupole moment operator

$$\widehat{Q}_{\beta\gamma} = -\sum_{pq} r_\beta r_\gamma E_{pq}. \tag{31}$$

In a similar manner the contribution from the electronic quadrupole moment interaction to the *rotatory strength* is given as [20]

$${}^nR^Q_{\alpha\beta} = \frac{3}{4}\omega_{n0}\varepsilon_{\alpha\gamma\delta}\langle 0|\hat{\mu}_\gamma|n\rangle\langle n|\widehat{Q}_{\delta\beta}|0\rangle. \tag{32}$$

Both $A_{\alpha\beta\gamma}(\omega_k)$ and ${}^nR^Q_{\alpha\beta}$ are as already noted purely anisotropic, and vanish upon orientational averaging.

2.3. Approximate state theory

The electric and magnetic dipole transition matrix elements needed for the evaluation of equation (26) can in principle be calculated directly using approximate state theories, involving a summation over all excited states. However, this approach suffers from slow

convergence and is seldom used in conjunction with standard *ab initio* electronic structure methods. In practical calculations, we therefore need to evaluate equation (25) without explicit knowledge of the eigenstates of $\widehat{H}_0$. A general framework for such calculations is linear response theory [21]. In this framework, the mixed electric dipole – magnetic dipole polarizability can be evaluated from the linear response function [21,22]

$$G'_{\alpha\beta}(\omega_k) = -\operatorname{Im}\langle\langle \hat{\mu}_\alpha; \widehat{m}_\beta \rangle\rangle_{\omega_k}, \tag{33}$$

where the linear response function reduces to equation (25) for exact wave functions. In a similar manner we can determine the rotatory powers of electronic circular dichroism as a single residue of the linear response function

$${}^{n}R_{\alpha\beta} = \lim_{\omega_k \to \omega_{n0}} (\omega_{n0} - \omega_k) \operatorname{Im}\langle\langle \hat{\mu}_\alpha; \widehat{m}_\beta \rangle\rangle_{\omega_k}. \tag{34}$$

We will not discuss the details of response theory here, referring instead to the original paper [21] as well as an excellent review of the theory [23]. It is sufficient to note that the general strategy is based on an efficient parametrization of the wave function—for instance in terms of orbital rotation parameters in the case of Hartree–Fock wave functions—and then solving the corresponding Ehrenfest equation for the given choice of wave function parameterization. This approach leads in general to a set of linear equations that determine the first-order response of the wave function, which we can schematically write as [17,21]

$$\begin{bmatrix} \kappa^{(1)}(\omega_k) \\ \kappa^{(1)*}(-\omega_k) \end{bmatrix} = \left(E^{[2]} - \omega_k S^{[2]}\right)^{-1} \begin{bmatrix} \langle 0|[-\hat{q}^\dagger, \widehat{m}_\alpha]|0\rangle \\ \langle 0|[\hat{q}, \widehat{m}_\alpha]|0\rangle \end{bmatrix} B_\alpha^{\omega_k}, \tag{35}$$

where the amplitudes of the perturbed wave function $\kappa^{(1)}(\omega_k)$ and the perturbation vectors q have been collected in column vectors. The dimension of this matrix equation is equal to twice the number of parameters describing the perturbed wave functions. In the above equation, $S^{[2]}$ represent a generalized metric, and $E^{[2]}$ an electronic Hessian, see for instance Refs. [21,23].

Using the first-order perturbed wave function determined from equation (35), we can obtain the first-order magnetic-field induced polarization as

$$\chi_{\alpha\beta}(\omega_k) = \begin{bmatrix} \langle 0|[\hat{q}, \hat{\mu}_\alpha]|0\rangle \\ \langle 0|[-\hat{q}^\dagger, \hat{\mu}_\alpha]|0\rangle \end{bmatrix}^\dagger \left(E^{[2]} - \omega_k S^{[2]}\right)^{-1} \begin{bmatrix} \langle 0|[-\hat{q}^\dagger, \widehat{m}_\beta]|0\rangle \\ \langle 0|[\hat{q}, \widehat{m}_\beta]|0\rangle \end{bmatrix}. \tag{36}$$

The general formalism for linear and higher-order response functions for exact states as well as for Hartree–Fock and multiconfigurational self-consistent field (MCSCF) wave functions was presented by Olsen and Jørgensen [21], and an implementation of the singlet linear response functions for Hartree–Fock and MCSCF wave functions was presented in 1988 [24]. The approach was applied to the study of optical rotation in 2000 [25] building on the implementation of vibrational Raman optical activity presented in 1994 [7]. The first calculations of rotatory strengths based on this general linear response formalism appeared in 1994 [26]. All these studies used London orbitals to ensure that the results obtained were gauge origin independent (*vide infra*).

Linear response functions have also recently been implemented for density-functional theory methods based on the fundamental theorem of time-dependent density functional theory (TDDFT) by Runge and Gross [27]. Such TDDFT implementations have been presented by a large number of groups [22,28–32]. The various TDDFT implementations differ primarily in their choice of gauge, using either the length or the velocity gauge, and

in the case of the length gauge, whether or not London Atomic Orbitals (LAOs) have been used. Of the methods that employ the length gauge, only two implementations of optical rotation employ London orbitals to ensure gauge origin independence [22,28], whereas the only implementation of circular dichroism using LAOs at the DFT level are the one by our own group [26,33].

The linear response formalism can also be extended to non-variational wave functions, either by recasting the parameterization of the wave function using Lagrangian multipliers so that the Lagrangian of the wave function is variational [34,35], or through the use of the quasi-energy formalism [36]. These approaches have been used in the implementation of coupled-cluster linear response functions [35] and this formalism has been applied to the calculation of optical rotation [37] and optical rotatory strengths [38]. We note, however, that for non-variational wave functions, the gauge origin problem is particularly difficult to solve.

Various other approaches also exist for the *ab initio* calculation of optical rotation and rotatory strengths and we will refer to these methods in the overview of the different *ab initio* studies that have been done on optical rotation and optical rotatory strengths. Before proceeding to this overview, we will however need to discuss the problem of *gauge origin dependence* in approximate calculations of optical rotation and optical rotatory strengths.

2.4. Gauge origin dependence

As most *ab initio* calculations have been done on isotropic solutions, we will illustrate the origin independence of the trace of the electric dipole–magnetic dipole polarizability $G'_{\alpha\beta}$ for exact states. Considering the change in the electric dipole – magnetic dipole polarizability when the gauge origin is shifted from $\mathbf{O}$ to $\mathbf{O}' = \mathbf{O} + \mathbf{D}$ (using implicit summation over repeated indices)

$$\begin{aligned} G'_{\alpha\beta}(\mathbf{O}') &= -\frac{1}{2}\sum_{\gamma\delta} \langle\langle \hat{\mu}_\alpha ; \varepsilon_{\beta\gamma\delta}(\hat{r}_\gamma - D_\gamma)\hat{p}_\delta \rangle\rangle_\omega \\ &= G'_{\alpha\beta}(\mathbf{O}) + \frac{1}{2}\varepsilon_{\beta\gamma\delta} D_\gamma \,\mathrm{Im}\langle\langle \hat{r}_\alpha ; \hat{p}_\delta \rangle\rangle_\omega . \end{aligned} \tag{37}$$

Using the relation

$$\mathrm{i}\langle 0|\hat{p}_\alpha|n\rangle = \omega_{n0}\langle 0|\hat{r}_\alpha|n\rangle , \tag{38}$$

the origin dependence of the electric dipole – magnetic dipole polarizability can be written as

$$G'_{\alpha\beta}(\mathbf{O}') = G'_{\alpha\beta}(\mathbf{O}) - \frac{1}{2}\mathrm{i}\omega\varepsilon_{\beta\gamma\delta} D_\gamma \alpha_{\alpha\delta} . \tag{39}$$

The individual components of this mixed polarizability are thus origin dependent. However, the trace of the tensor is origin independent since

$$\varepsilon_{\alpha\gamma\delta} D_\gamma \alpha_{\alpha\delta} = 0, \tag{40}$$

because $\varepsilon_{\alpha\gamma\delta} = -\varepsilon_{\delta\gamma\alpha}$ and the polarizability is a symmetric tensor. In case of oriented samples, the contributions from the electric dipole – magnetic dipole polarizability and the electric dipole – electric quadrupole polarizability are origin dependent individually, but

their sum is not. Proofs for this can be found in the excellent book of Barron [12], and the origin independence of the rotatory strength of oriented samples have been discussed for instance by Pedersen and Hansen [20].

Since the hypervirial relation equation (38) is only fulfilled for exact states and for variational wave functions in the limit of a complete basis, the origin independence of the calculated optical rotation—as well as the rotatory strengths—is achieved only in these cases, and the results obtained using for instance non-variational wave functions such as truncated coupled-cluster theory are not origin independent even in the limit of a complete basis set.

The problem of lack of origin independence in *ab initio* calculations of optical rotation and circular dichroism in finite basis sets has so far been dealt with in two ways:

(1) through the introduction of London Atomic Orbitals [39], where each individual basis function is made to depend explicitly on the external magnetic field induction, thus creating a magnetic dipole operator that has the origin dependence of the exact operator even for finite basis sets, or
(2) by using hypervirial relations to convert the electric dipole – magnetic dipole and electric dipole – electric quadrupole polarizabilities to the velocity gauge.

2.5. London atomic orbitals

In 1937 [39], London proposed that the atomic basis functions should be multiplied by a complex phase factor explicitly dependent on the external magnetic field induction

$$\omega_\mu(\mathbf{B}, \mathbf{R}_M) = \exp(-\mathrm{i}\mathbf{A}_{OM} \cdot \mathbf{r})\chi_\mu(\mathbf{R}_M), \tag{41}$$

where χ_μ in most modern applications will be a Gaussian basis function, and where we shall refer to $\omega_\mu(\mathbf{B}, \mathbf{R}_M)$ as a London atomic orbital (LAO).[1] The magnetic vector potential appearing in the complex phase factor is given as

$$\mathbf{A}_{OM} = \frac{1}{2}\mathbf{B} \times \mathbf{R}_{OM} = \frac{1}{2}\mathbf{B} \times (\mathbf{R}_M - \mathbf{O}), \tag{42}$$

and the effect of this phase factor is to move the global gauge origin **O** to the best local gauge origin for each individual basis function, namely the atomic center **M** to which the basis function is attached. It can be shown that this choice of local gauge origin is optimal for a spherical one-electron system in an external magnetic field in the sense that the London orbital is correct to first order in the external magnetic field induction for any choice of gauge origin, whereas the ordinary atomic orbitals are correct only to zeroth order for an arbitrary gauge origin [40].

Although briefly explored in the 1970s by Ditchfield [41,42], the use of LAOs in calculations of magnetic properties did not receive much attention before the first efficient implementation of LAOs for the calculation of nuclear magnetic shielding constants at the Hartree–Fock level by Wolinski, Hinton and Pulay [43]. Following this paper, LAOs were extended to a large number of molecular magnetic properties. We note here that for many time-independent magnetic properties such as for instance nuclear magnetic shieldings [43–46], magnetizabilities [47] and vibrational circular dichroism [40], LAOs improve

[1] These orbitals are also known as GIAOs, Gauge Including Atomic Orbitals.

in many cases also the basis set convergence in addition to providing gauge origin independent results (see for instance Ref. [48]).

In the derivation of the LAO integrals for frequency-independent properties, the global gauge origin disappears [49]. However, in order to ensure the origin independence of the sum of the electric dipole – magnetic dipole polarizability and the electric dipole – electric quadrupole polarizability, we need to define a LAO magnetic dipole operator that has the same origin dependence as the exact operator, also for finite basis sets. This was achieved in 1994 [50] and applied to the calculation of optical rotation tensors (also contributing to vibrational Raman Optical Activity) [7] and electronic circular dichroism [26].

The formal derivation of a LAO magnetic dipole operator that has the correct origin dependence also for finite basis sets is rather lengthy, and we restrict ourselves here to noting that the proper operator can in second quantization be written as [13,51]

$$\hat{l}^{\mathrm{LAO}}(\mathbf{O}) = 2\Bigg[\sum_{mn}\big(\tilde{h}^{B}_{mn}(\mathbf{O})E_{mn} + h_{mn}E^{B}_{mn}(\mathbf{O})\big) + \frac{1}{2}\sum_{mnpq}\big(\tilde{g}^{B}_{mnpq}(\mathbf{O})e_{mnpq} + g_{mnpq}e^{B}_{mnpq}(\mathbf{O})\big)\Bigg]. \tag{43}$$

In this equation, h_{mn} and g_{mnpq} are the ordinary one- and two-electron integrals of the unperturbed molecular Hamiltonian in MO basis, E_{mn} and e_{mnpq} are the one- and two-particle excitation operators, respectively, and the perturbed one- and two-electron integrals are given by

$$\tilde{h}^{B}_{mn}(\mathbf{O}) = h^{B}_{mn} + \sum_{o}\big(T^{B}_{mo}(\mathbf{O})h_{on} + \big(T^{B}\big)^{*}_{no}(\mathbf{O})h_{mo}\big), \tag{44}$$

$$\tilde{g}^{B}_{mnpq}(\mathbf{O}) = g^{B}_{mnpq} + \sum_{o}\big(T^{B}_{mo}(\mathbf{O})g_{onpq} + \big(T^{B}\big)^{*}_{no}(\mathbf{O})g_{mopq} + T^{B}_{po}(\mathbf{O})g_{mnoq} + \big(T^{B}\big)^{*}_{qo}(\mathbf{O})g_{mnpo}\big), \tag{45}$$

where the so-called natural connection matrix [50] is defined as

$$T^{B}_{mn}(\mathbf{O}) = -\sum_{\mu\nu}C^{*}_{\mu m}C_{\nu n}\left\langle\chi_{\mu}\,\middle|\,\frac{\partial\omega_{\nu}}{\partial\mathbf{B}}\right\rangle, \tag{46}$$

where $C_{\mu m}$ are the molecular orbital coefficients. In equation (43), we have also introduced the differentiated excitation operators E^{B}_{mn} and e^{B}_{mnpq}. In the natural connection [50], these operators only involve excitations out of the space spanned by the creation and annihilation operators—that is, out of the space spanned by the basis set. In the limit of a complete basis set, there is no complementary space and these contributions will no longer be present.

The LAO magnetic dipole operator in equation (43) has the following important properties: (1) it has the same origin dependence as the exact operator also for finite basis sets, and (2) it reduces to the conventional magnetic dipole operator in the limit of a complete basis set. The proofs of these properties, which can be found in Ref. [26], involve the use of hypervirial relations fulfilled for any variationally optimized wave function, irrespective of the size of the basis set, namely that

$$\langle j|\big[\widehat{H},\hat{r}\big]|n\rangle = \omega_{jn}\langle j|\hat{r}|n\rangle. \tag{47}$$

We make one important observation at this stage. Whereas the operator in equation (43) displays the correct dependence on the gauge origin, it will also behave very similar to the exact operator with respect to the basis set convergence. Therefore, we should not necessarily expect faster basis set convergence of the optical rotation or the rotatory strengths when LAOs are used. We will return to this point in Section 3.1.

2.6. Velocity gauge

The gauge-origin independence of the LAO magnetic dipole operator is only fulfilled for variational wave functions. Since LAOs do not lead to any significant improvements in the basis set convergence of the optical rotation, there is little to be gained from the use of LAOs in optical rotation and circular dichroism calculations using non-variational methods, and indeed no such calculations have been reported to date. A gauge-origin independent coupled-cluster approach has been presented by Pedersen, Koch and coworkers [52, 53] where origin independence is achieved by introducing a coupled-cluster Lagrangian that includes orbital rotations. However, no implementation of this approach has been presented.

Gauge-origin independent results can be achieved in the velocity gauge. The velocity gauge can be obtained from the expressions in the length gauge by using the identity [21, 13]

$$\omega\langle\langle \hat{r}, \hat{p}\rangle\rangle_\omega = \left\langle\left\langle \left[\hat{r}, \widehat{H}\right], \hat{p}\right\rangle\right\rangle_\omega + \langle[\hat{r}, \hat{p}]\rangle, \tag{48}$$

which allows us to write the electric dipole – magnetic dipole contribution to the rotatory strengths in the velocity gauge as [20,38]

$${}^nR^{\mathrm{mv}}_{\alpha\beta} = \frac{3}{4\omega_{n0}}\left[\sum_\gamma \langle 0|\hat{p}_\gamma|n\rangle \cdot \langle n|\hat{l}_\gamma|0\rangle\delta_{\alpha\beta} - \langle 0|\hat{p}_\alpha|n\rangle\langle n|\hat{l}_\beta|0\rangle\right], \tag{49}$$

and the electric dipole – electric quadrupole contribution as [20,38]

$${}^nR^{\mathrm{Qv}}_{\alpha\beta} = -\frac{3}{4\omega_{n0}}\sum_{\gamma\delta}\varepsilon_{\alpha\gamma\delta}\langle 0|\hat{p}_\gamma|n\rangle\langle n|(\hat{p}_\delta\hat{r}_\beta + \hat{r}_\delta\hat{p}_\beta)|0\rangle. \tag{50}$$

Whereas the use of the velocity gauge leads to significantly poorer results for the rotatory strengths than the length gauge when small basis sets are used, modern polarized double-zeta quality basis sets give in general results that are not much worse than those obtained in the length gauge, with the added advantage that the results are independent of the choice of gauge origin. Several studies of electronic circular dichroism using the velocity gauge have been presented at the coupled cluster level [37,38,54,55].

When attempting to employ the velocity gauge in the calculation of optical rotation at the CCSD level, results that were of significantly poorer quality than the length gauge results were obtained [56]. However, as analyzed by Pedersen *et al.* [56], the reason for this poor performance is due to the fact that whereas the length-gauge expression for the electric dipole – magnetic dipole polarizability vanishes in the limit of a static electromagnetic field (see equation (26)), the velocity-gauge polarizability does not. It was demonstrated in Ref. [56] that after correcting for the static-limit value of this mixed polarizability by using

the replacement

$$\langle\langle p_\alpha; l_\beta \rangle\rangle_\omega \rightarrow \langle\langle p_\alpha; l_\beta \rangle\rangle_\omega - \langle\langle p_\alpha; l_\beta \rangle\rangle_0, \tag{51}$$

good basis set convergence for the optical rotation could be achieved [56].

3. CALCULATIONS OF OPTICAL ROTATION AND ELECTRONIC CIRCULAR DICHROISM

3.1. Basis set dependence

The proper choice of basis set is essential for the *ab initio* calculation of any molecular property, and optical rotation and optical rotatory strengths present some unique challenges in this respect. Investigations of the basis set requirements in optical rotation and circular dichroism calculations are briefly reviewed here.

3.1.1. Optical rotatory strength

The basis set convergence of rotatory strengths has been studied by Pecul, Ruud and Helgaker [33] at the DFT level of theory, in both the velocity and length gauge formulations, with conventional Gaussian atomic orbitals and with LAOs. In order to illustrate the most important findings obtained in that work, we have collected the optical rotatory strengths calculated for methyloxirane using a selection of basis sets in Table 1.We have in this table summed the contributions from the 3A, 4A, and 5A transitions, as these corresponds to the Rydberg $n \rightarrow 3p$ transitions and are very closely spaced. As seen from this table, the optical rotatory strength is very sensitive to the description of the outer region of the electronic density—that is, to the number of diffuse functions in the basis set. As expected, optical rotatory strengths of transitions to states with diffuse character (for example Rydberg states) display the slowest basis set convergence. The rate of basis set convergence is approximately the same for both HF and DFT.

From this study it is clear that large basis sets are needed in order to get reliable ECD results, and a double set of diffuse functions is usually required. Using the length-gauge formulation instead of the velocity gauge gives in general somewhat better basis set convergence. No significant improvement in the basis set convergence is in general observed when employing LAOs for basis sets of reasonable quality (aug-cc-pVDZ or better). However, as discussed in Section 2.4, LAOs should be used whenever the length gauge formulation is employed, in order to ensure that the calculated rotatory strengths are unambiguously defined with respect to changes of the gauge origin.

A limited study of the basis set convergence of the optical rotatory strength was also carried out at the CCSD level for twisted ethylene, chosen as a model for the chromophore of (−)-*trans*-cyclo-octene [38]. For the valence transitions in this system, the role of a second set of diffuse basis set functions is less critical than for transitions to states with diffuse character.

3.1.2. Natural optical rotation

Basis set effects on the natural optical rotation at the HF and B3LYP levels of theory were investigated by Cheeseman *et al.* [28], who used the length-gauge formulation together

Table 1. Excitation energies ΔE (in eV) and optical rotatory strength ${}^{n}R$ (in 10^{-40} esu^2·cm^2) of (S)-methyloxirane, obtained using the B3LYP functional

	ΔE	R_n^v	R_n^r	R_n^r (LAO)
2A				
aug-cc-pVDZ	6.504	19.27	19.53	19.46
daug-cc-pVDZ	6.440	16.53	16.71	16.74
aug-cc-pVTZ	6.526	18.63	18.63	18.62
daug-cc-pVTZ	6.487	16.91	16.94	16.94
aug-cc-pVQZ	6.523	18.26	18.25	18.25
exp.[a]	7.12 (7.07)		11.8 (−12.56)	
3A + 4A + 5A[b]				
aug-cc-pVDZ	6.982	−17.27	−17.74	−17.61
daug-cc-pVDZ	6.867	−11.76	−12.06	−12.10
aug-cc-pVTZ	6.992	−16.09	−16.11	−16.18
daug-cc-pVTZ	6.919	−12.46	−12.50	−12.51
aug-cc-pVQZ	6.981	−15.38	−15.38	−15.41
exp.[a]	7.75 (7.70)		−10.8 (6.98)	
6A				
aug-cc-pVDZ	7.352	−9.21	−8.90	−8.94
daug-cc-pVDZ	7.291	−7.88	−7.56	−7.52
aug-cc-pVTZ	7.345	−8.53	−8.53	−8.54
daug-cc-pVTZ	7.310	−7.86	−7.77	−7.76
aug-cc-pVQZ	7.340	−8.35	−8.39	−8.40
exp.[a]	(8.5)		(−4)	

Reproduced from Ref. [33].

[a] All experimental data taken from Ref. [57]. Results for (R)-methyloxirane in parentheses.

[b] Rydberg transition to the *p* orbital. The theoretical excitation energy is given for the central transition, and the theoretical rotatory strength is summed over all three components.

with LAOs. Selected results for the optical rotation are presented in Table 2. As can be seen from Table 2, it is important to include diffuse functions in the calculations of the optical rotations. However, adding diffuse functions to a small basis set does not necessarily lead to reliable results: the numbers obtained using the 6-311++G basis set are in even worse agreement with the aug-cc-pVQZ result (which is probably close to the basis set limit) than those obtained using the 6-31G* basis set. The aug-cc-pVDZ or (larger) 6-311++G(2d,2p) basis sets appear to offer the best compromise of accuracy and computational cost, although the aug-cc-pVDZ basis seems to be the better of the two. Adding a second or third set of diffuse functions improves the results, but it is not so critical for accuracy as in the case of the rotatory strengths of transitions to diffuse states (see above). We note from the data for methyloxirane in Table 2 that for small optical rotations, the

Table 2. Natural optical rotation of (S)-methyloxirane and (R,R)-dimethyloxirane (in deg·cm^3·g^{-1}·dm^{-1}), obtained using the B3LYP functional

Basis	(S)-methyloxirane		(R,R)-methyloxirane	
	HF	B3LYP	HF	B3LYP
6-31G	−33.92	−41.55	167.16	149.42
6-31G*	−16.49	−24.26	118.39	99.42
6-31G**	−18.45	−26.87	121.76	103.96
6-31+G**	−12.97	−2.59	169.81	213.10
6-311G	−60.32	−86.13	270.83	269.23
6-311G*	−41.09	−63.59	210.90	207.35
6-311G**	−43.81	−68.43	210.81	209.06
6-311++G	−43.96	−56.56	192.98	198.85
6-311++G*	−20.46	−29.36	161.80	169.52
6-311++G**	−19.68	−29.05	164.87	173.93
6-311++G(2d,2p)	−12.27	−17.09	144.33	150.58
cc-pVDZ	−30.21	−49.94	181.94	177.04
cc-pVTZ	−15.56	−26.50	166.70	169.28
cc-pVQZ	−9.78	−16.69	145.10	151.02
aug-cc-pVDZ	−13.14	−20.37	143.73	154.46
aug-cc-pVTZ	−8.00	−13.12	126.70	128.23
aug-cc-pVQZ	−7.46	−12.33	124.43	124.27
d-aug-cc-pVDZ	−11.31	−16.99	125.88	125.93
t-aug-cc-pVDZ	−8.72	−12.08	126.39	123.60

Reproduced from Ref. [28].

aug-cc-pVDZ and 6-311++G(2d,2p) basis sets may still lead to errors of almost a factor of two compared to the larger sets. In Ref. [28], a strong dependence of the optical rotation on the gauge origin was observed for the smaller basis sets.

Apart from the correlation-consistent Dunning basis sets with diffuse functions [58–61], the polarizability-consistent Sadlej basis sets [62] have been shown to give an optical rotation for methyloxirane that is consistent with that obtained using larger basis sets (aug-cc-pVTZ) and with experiment, being at the same time smaller than the aug-cc-pVTZ basis [63].

A basis set convergence study of the optical rotation in the velocity and length gauge formulations using the DFT method with conventional atomic orbitals was presented by Grimme, Furche and Ahlrichs [64] for some rigid chiral organic molecules. A slower basis set convergence of the velocity gauge formulation was observed, but only for the smallest basis sets. The aug-cc-pVDZ basis set was found to yield qualitatively satisfactory results and, according to the authors, is sufficient for routine calculations of the optical rotation of organic molecules. Similar conclusions were drawn in the work of Stephens *et al.* [65] in which optical rotation was calculated for 30 rigid chiral molecules using time-dependent density functional theory (with the B3LYP functional) and the Hartree–Fock method, employing LAOs in the length-gauge formulation.

The optical rotations of the chiral rotamers of 1-butene, butane, propene, propane and ethane have been examined at the HF level using different basis sets by Wiberg *et al.* [66]. The work illustrates the critical importance of having diffuse *p* functions on the hydrogen atoms, clearly rationalizing why the aug-cc-pVDZ basis set is the smallest basis set yielding results for which the sign of the optical rotation is consistent with larger basis sets. Standard Pople basis sets [67], even those containing diffuse functions on the heavy atoms, lead to qualitatively wrong optical rotations, and in particular they cannot reproduce the dependence of the optical rotation on the dihedral angles in these molecules. On the other hand, in another work by Wiberg, Vaccaro and Cheeseman [68], the 6-311++G** basis (without diffuse p functions on the hydrogens) was found to be adequate for calculations of the conformational dependence of the optical rotation in 3-chloro-1-butene.

Basis set effects can also significantly influence the shape of the calculated dispersion curve, as shown for methyloxirane [63].

3.2. Electron correlation effects

3.2.1. Optical rotatory strength

The method used most frequently in the past for the calculation of ECD spectra was the Configuration Interaction (CI) method [57,69–72]. More recently, the Coupled Cluster (CC) method has been used for these calculations [38,55]. The CASSI method has been used to calculate scalar rotatory strengths of the lowest-lying singlet transitions of cyanine dyes [73], with the excitation energies obtained as differences of CASPT2 energies.

Carnell, Grimme and Peyerimhoff calculated the ECD spectrum of trans-2,3-dimethyloxirane, using HF and CI [71]. The inclusion of electron correlation beyond single excitations was found to be crucial for reproducing the experimental spectrum.

The small chiral molecules H_2O_2 and H_2S_2 have been attractive subjects for benchmark calculations not only because of their small size, but also because of their intricate electronic structure, making them challenging for *ab initio* calculations of optical rotation and ECD spectra. H_2S_2 exhibits a degeneracy of excited states of opposite polarization at a dihedral angle of about 90° [70] that almost cancel each other, and this cancellation is difficult to reproduce with for instance a HF wave function.

CI calculations of both optical rotatory strengths and optical rotatory power was performed for H_2S_2 [70], and their dependence on the dihedral angle was studied. The optical rotatory power was calculated using the sum-over-states method. The results indicate that the optical rotatory power for H_2S_2 is determined mostly by the four lowest spectroscopic states. The dependence of the optical rotatory power in H_2S_2 on the dihedral angle has also been studied at the multi-reference configuration-interaction (MRCI) level by Ha and Cencek [69]. A similar MRCI study was performed for H_2O_2 by Hutter, Lüthi and Ha [72]. MRCI was also used by Camell *et al.* to calculate the ECD spectrum of methyloxirane [57].

CCSD calculations of the full rotatory strength tensor have been carried out for the ethylene chromophore of (−)-*trans*-cyclo-octene [38]. The results obtained there, even with the largest basis set, show gauge origin dependence in the length gauge formulation. The length and velocity gauge do not lead to the same basis set limit, neither for the individual components of the rotatory strength tensor, nor for the scalar rotatory strength.

3.2.2. Natural optical rotation

Calculations of optical rotation accounting for electron correlation using other methods than density functional theory are relatively scarce [22,25,37]. In the work of Polavarapu, Chakraborty and Ruud [25], HF and CASSCF calculations have been performed to investigate the dependence of the specific optical rotation of H_2O_2, H_2S_2 and allene on the dihedral angle, and to examine the applicability of semi-empirical models for the problem. The results obtained using Kirkwood's polarizability model were found to be in good agreement with the CASSCF prediction, and HF and CASSCF results were found to differ significantly.

The CC2 and CCSD methods were used by Ruud *et al.* [37] to calculate the optical rotation of 14 organic molecules. For all of them, except for norbornenone, agreement of the optical rotation calculated at the CCSD level with experimental values is good, comparable to DFT/B3LYP calculations. This suggests that CCSD, in spite of the lack of gauge origin independence, can be used for benchmarking purposes, at least for molecules of relatively small size. We note, however, that for the only molecule where electron correlation effects were large (norbornenone), the predictions by CC2/CCSD differ significantly from both experiment and DFT/B3LYP results, the DFT/B3LYP results on the other hand being in very good agreement with experiment.

Ruud and Helgaker [22] used CCSD and MCSCF methods to calculate the dependence of the specific optical rotation on the dihedral angle for the same systems as in Ref. [25]. Since the purpose of this work was mainly to use these high-level results to benchmark the DFT numbers, the findings are discussed in the next section.

3.3. Density functional calculations

The most widespread method in use for calculations of optical rotation and ECD spectra is, apart from the Hartree–Fock method, density functional theory, and its applications to the calculation of ECD and OR will be reviewed here.

Grimme developed a formalism in which the density functional calculations are combined with a singles-excitation configuration interaction treatment [29] (later extended to multi-reference configuration interaction [30]), which has been applied for the calculation of optical rotatory strengths in the velocity gauge [74,75].

Gauge-origin independence of the rotatory strength in the length gauge formulation is ensured, for variational methods including Kohn–Sham DFT, by the use of LAOs. Such an implementation was presented by Pecul *et al.* [33]. Expressions for the time-dependent DFT calculations of optical rotation in the length gauge (although without the use of LAOs) was also presented by Autschbach and Ziegler [31]. The same formalism was also proposed for the calculation of optical rotatory strengths [76]. Another implementation of the time-dependent density functional theory (LDA only) for this purpose was presented by Yabana and Bertsch [32]. In this implementation, a grid representation of the wave function is employed instead of atomic orbitals.

There are several works in which the performance of DFT for the calculation of ECD spectra and optical rotation was tested against hierarchical *ab initio* methods and against experiment. We shall first discuss such investigations for ECD, and then for the optical rotation.

3.3.1. Optical rotatory strength

The formalism of Grimme [29] was applied by Pulm *et al.* to model ECD spectra of bicyclic ketones (norcamphor, camphor and fenchone) [74]. The theoretical results were found to be in fair agreement with experiment, and allowed for an interpretation of the experimental spectra, and in particular they helped to differentiate between overlapping Rydberg and valence bands.

The same group presented large-scale TDDFT calculations of the ECD spectra of [*n*]helicenes [77]. The calculations were performed with conventional atomic orbitals, but the differences between the length and velocity gauge formulations were found to be less than 10%. The results obtained allowed for an interpretation of the experimental ECD spectra of [*n*]helicenes, and demonstrated that TDDFT can be used for simulations of ECD spectra in realistic rigid chemical systems. The same formalism was used for the study of the ECD spectrum of a chiral azulenophane [78].

A systematic investigation of the performance of various exchange-correlation functionals (with conventional atomic orbitals) for calculations of optical rotatory strengths was presented by Diedrich and Grimme [75], and the results were compared to two multireference methods (MRMP2 and DFT/MRCI), and to experimental ECD spectra. The molecules investigated were the three model systems H_2S_2, twisted ethylene, and dimethyloxirane, and seven larger molecules, some of them with chiral chromophores (4,5-dimethylphenanthrene) and some with achiral chromophores (camphor, norcamphor). The authors concluded that the TDDFT method should be used with care, especially for systems with important diffuse or charge-transfer states, and that in these cases multireference methods are preferable. Good performance was also observed for the coupled cluster model CC2. It was found that when the TDDFT method is used, the hybrid B3LYP functional is probably the best functional for the calculation of ECD spectra. The relatively good performance of the B3LYP functional was confirmed also in the study by Pecul *et al.* [33]. The study also confirmed that the DFT methods fail to model excited states with a diffuse character such as Rydberg states.

A limited study of the performance of different exchange-correlation functionals for ECD spectra (for methyloxiranes, cyclohexanone derivatives, and aziridines) was also performed by Autschbach and Ziegler [76], who found that none of the functionals tested were entirely satisfactory for the calculation of the optical rotatory strengths, although some functionals with semi-empirical corrections performed better than LDA and GGA (the last in the form of the BP86 functional). However, due to restrictions in their code, no hybrid functional could be tested.

3.3.2. Natural optical rotation

The optical rotations of 30 small organic molecules were calculated at the HF and B3LYP computational levels and compared to experiment by Stephens *et al.* [65]. For the B3LYP calculations, comparison with experimental values of $[\alpha]_D$ for 28 of the 30 molecules yielded an average absolute deviation between calculated and experimental values in the range 20–25 $\mathrm{deg \cdot cm^3 \cdot g^{-1} \cdot dm^{-1}}$ for the three largest basis sets, all of which included diffuse functions. HF/SCF $[\alpha]_D$ values were substantially less accurate; at the aug-cc-pVDZ basis set level, the average deviation from experiment was 63 $\mathrm{deg \cdot cm^3 \cdot g^{-1} \cdot dm^{-1}}$.

The dependence of the specific optical rotation of H_2O_2, H_2S_2 and allene on the dihedral angle has been studied by Ruud and Helgaker [22] using HF, MCSCF, CCSD (for H_2O_2

only) and DFT methods. It was found that whereas DFT tends to overestimate the optical rotation (as a result of a general underestimation of the excitation energies), it gives the correct dependence on the dihedral angle (in contrast to the HF method). The B3LYP functional was found to perform better than BLYP and LDA in comparison with CCSD.

It should be noted that there are systems for which currently available DFT methods fail completely for all optical properties, and therefore also for the optical rotation. An example of such a system is anionic proline [79], where DFT/B3LYP fails to describe the excited states, yielding much too low excitation energies, which propagate into the results for the second-order molecular properties, including the optical rotation. Another example are very diffuse excited states, such as Rydberg states [33].

3.4. Structural dependence

3.4.1. Determination of absolute configurations

For rigid molecules, or flexible molecules with only a few low-lying conformers, *ab initio* calculations of rotatory strengths and optical rotation provide a very valuable tool for determination of the absolute configuration [80], superior to empirical correlations such as the octant rule [14]. A methodology usually employed for determination of absolute configuration is to combine calculations of optical rotation or of rotatory strengths with calculation of other properties associated with chirality, such as vibrational circular dichroism (VCD) or Raman Optical Activity (ROA) intensities in order to have an independent confirmation of the assignment. This approach has been shown to be useful in several cases [80–84], and is becoming a standard in the determination of the absolute conformation for molecules of moderate size.

DFT calculations of the ECD spectrum and optical rotation have been performed by Stephens *et al.* [80] for bicyclo[3.3.1]nonane diones, in order to establish their absolute configuration. The assignment obtained in this study is consistent with previous assignments based on empirical correlations, with the exception of one case in which the empirical octant rule was found to fail. This is encouraging for further applications of calculations at this level of accuracy (B3LYP/aug-cc-pVDZ) as a supplementary tool in organic chemistry. Stephens *et al.* [80] also confirmed the necessity for accounting for all low-lying conformers in such calculations.

A combination of DFT/B3LYP calculations of the optical rotation and calculations of Raman Optical Activity (ROA) spectra was presented in the work of Polavarapu [81] with the purpose of confirming the absolute configuration of bromochlorofluoromethane. The previous [82] assignment of (S)-(+) and (R)-(−) was confirmed by means of calculations with larger basis sets.

The group of Polavarapu combined calculations of the specific optical rotation with calculations of vibrational circular dichroism [83] in order to study the structural dependence of these parameters in substituted butynes. On the basis of these data, the absolute configuration of (+)-3-chloro-1-butyne have been determined.

Another work in which density functional theory has been used to calculate the optical rotation in order to determine the absolute configuration of a molecule is that of Stephens *et al.* [84]. On the basis of the study of several organic molecules, rigid and flexible, the authors concluded that as long as the experimental specific optical rotation of a rigid molecule is larger than 20–30 $\mathrm{deg \cdot cm^3 \cdot g^{-1} \cdot dm^{-1}}$, the sign of the optical rotation can be reliably

predicted by means of DFT/aug-cc-pVDZ calculations and therefore the absolute configuration can be correctly assigned from these calculations. In the case of flexible molecules, the problem is much more intricate, as will be discussed in the next subsection.

3.4.2. Conformational dependence

Both the specific optical rotation [25,79,85–87] and the optical rotatory power [79,88,89] depend strongly on the conformation of the molecule and are therefore in principle sensitive tools for structural investigations. To date, structural investigations based on ECD spectra have relied on experimental correlations only, which in many cases may lead to wrong conclusions [88], so the application of this fast and inexpensive spectroscopy for structural investigation has been limited. *Ab initio* calculations can rectify this, and also enable some structural information to be derived from measurements of the optical rotation, for which empirical correlations seem even less reliable than for the ECD spectra [90].

3.4.2.1. Optical rotatory strength. One of the most important areas of application of ECD spectroscopy is the investigation of the spatial structure of polypeptides and proteins on the basis of transitions in the amide chromophore. Consequently, there have been several papers [91–94] focusing on calculating the electronic spectrum of the model amide *N*-methylacetamide, and using this to model the ECD spectrum of the protein backbone. However, we are not aware of any rigorous *ab initio* calculations of the optical rotatory strength for a model peptide.

The ECD spectrum of several conformers of 1-(1-naphtyl)ethylamine was calculated by means of the CI-singles (CIS) approach using the 6-311+G(d) basis set by Plusquellic *et al.* [89] in order to interpret the experimental ECD spectrum. Theoretical Boltzmann-averaged results obtained at this level of theory are in qualitatively good agreement with the recorded experimental spectrum. The signs of the rotatory strengths calculated for different conformers are in this case in agreement with the so-called sector rule [95] for chirally substituted aromatic rings.

The effect of internal rotations on the rotatory strengths in 1-(R)-phenylethanol have been calculated by Macleod *et al.* [88]. When a chiral side chain is rotated around the bond connecting it to the benzene ring, there is an oscillation in the sign of the rotatory strength. The orientation of the hydroxyl group was also found to significantly influence the rotatory strength.

3.4.2.2. Natural optical rotation. The first *ab initio* study of the conformational dependence of the optical rotation was that of Polavarapu and Chakraborty on H_2O_2, H_2S_2 and 3-butyn-2-ol [96]. In the last molecule, the sign of the optical rotation was found to change with conformation, despite the molecule not changing its enantiomeric state (unlike H_2O_2 and H_2S_2). The large torsional dependence of the optical rotation in H_2O_2 and H_2S_2 have been investigated several times for methodological purposes, as discussed in Section 3.2.

The optical rotations of the large flexible organic molecules indoline, azetidine, menthol and menthone, have been calculated at the HF level by Kondru, Wipf and Beratan [97], where particular attention was paid to taking into account all conformers of the molecule using Monte Carlo sampling. The optical rotation of these molecules showed a strong dependence on the conformation: changing the conformation often changed the sign of the optical rotation. If the prediction of the optical rotation of a flexible molecule is attempted,

all possible conformations therefore need to be accounted for. Moreover, in indoline a correlation between the dihedral angle of the allyl substituent and the atomic contribution to the optical rotation were postulated. It should be noted, however, that the results of Kondru, Wipf and Beratan [97] were obtained using a very small basis set (6-31G*), which might have significantly affected the conclusions (see Section 3.1). The same probably applies to another study of this group [98], in which the optical tensor was explicitly expressed in terms of atomic integrals and molecular orbital coefficients, and atomic contributions to the optical rotation were analyzed for small organic molecules in a manner analogous to Mulliken population analysis [99,100].

The concept of partitioning the optical rotatory power into atomic contribution was also introduced by Ligabue *et al.* [101], who employed it to rationalize the torsional dependence of optical rotatory power in H_2O_2. The same idea was used in the work of Bécar Varela, Ferraro and Rail [102], where the dependence of the optical rotation of N_2H_4 on the dihedral angle was studied. However, since these studies were performed at the HF level, and since the conformational dependence of the optical rotation is significantly affected by electron correlation (see Section 3.2), the conclusions of Refs. [101,103] may not be correct in view of the results in Refs. [22,25].

Another study of the conformational effects on the optical rotation was carried out for two amino acids: proline (neutral, anionic, and cationic forms) and alanine [79]. The optical rotations of both amino acids were found to be very sensitive to the molecular geometry, giving rise to different signs for different conformers. For alanine, the sign of the optical rotation varies with the relative orientation of the amino and carbonyl groups. In proline, the conformation of the ring as well as the orientations of the amino and carboxylic groups influence the optical rotation and the optical rotatory strengths, the *endo* conformers having a more negative specific rotation than the *exo* ones. The increase in the optical rotation of proline with increasing pH, observed experimentally, was reproduced by the calculations.

Polavarapu, Petrovic and Wang [90] investigated the large solvent dependence of the optical rotation of (R)-(−)-epichlorohydrin using DFT calculations, and found that it originates from the existence of two low-lying conformers of epichlorohydrin with nearly the same magnitude of specific rotation, but with opposite sign. They demonstrated that a combination of intrinsic rotation measurements with density functional calculations of the specific optical rotation is a useful method for determining the structures of molecules.

Wiberg, Vaccaro and Cheeseman [68] investigated the conformational dependence of the optical rotation in 3-chloro-1-butene, and found that the changes in the C=C–C–C torsional angle lead to a change of the optical rotation in the range from approximately -530 deg·cm^3·g^{-1}·dm^{-1} to $+370$ deg·cm^3·g^{-1}·dm^{-1}. This large dependence of the optical rotation on the molecular conformation was confirmed by a study of the temperature dependence of the rotation, although the observed rotations were smaller than the calculated values by a factor of 2.6.

3.5. Vibrational effects

Ab initio predictions of the full vibrational structure of an ECD spectrum is undoubtedly a feasible and very interesting undertaking. However, the authors are not aware of any work published so far on this subject.

Investigations of the influence of molecular vibrations of the optical rotation have appeared only recently. The vibrational contributions to the optical rotation calculated by Ruud, Taylor and Åstrand [104] indicate that these effects are substantial, as are the conformational effects (see Section 3.4.2). Zero-point vibrational effects—which were studied for methyloxirane and trans-2,3-dimethylthiirane [104] at the HF level—were found to be as large as 20–30% of the electronic counterpart.

Another problem investigated by Ruud, Taylor and Åstrand [104] is the optical rotation due to isotopic substitution, in which only the vibrational part contributes to the chirality of the molecule, calculated for mono-deuterated oxirane. The vibrationally induced chirality was found to lead to an optical rotation of 1.32 $deg \cdot cm^3 \cdot g^{-1} \cdot dm^{-1}$ at the sodium wavelength, an effect which would certainly be experimentally observable.

3.6. Solvent effects

It is well known from experiment that both optical rotations and ECD spectra are very sensitive to solvent effects [105,106]. In some cases, a change of the solvent can even lead to a change of sign of the optical rotatory strength or of the optical rotation [105,106], even for rigid molecules such as methyloxirane [106].

3.6.1. Optical rotatory strengths

Ab initio calculations of solvent effects on the ECD spectra are few. An *ab initio* study of the solvent effects on the ECD spectra has been carried out by Pecul *et al.* [107] using the PCM method [108–110] at the DFT/B3LYP level using LAOs. The results for S-methyloxirane obtained there are summarized in Table 3. The rotatory strengths are strongly influenced by the change in the solvent, and for certain transitions even the sign

Table 3. Solvent effects excitation energies ΔE (in eV) and optical rotatory strength ${}^{n}R$ (in $10^{-40} esu^2 cm^2$) of (S)-methyloxirane. PCM method at the B3LYP/d-aug-cc-pVDZ computational level

		Gas	C_6H_{12}	CH_3CN	CH_3OH	CF_3CH_2OH	H_2O
2A	ΔE	6.44	6.53	6.67	6.66	6.66	6.67
2A	${}^{n}R$	16.74	16.94	9.74	9.79	9.91	9.34
3A–5A[a]	ΔE	6.87	6.93	7.09	7.08	7.08	7.09
3A–5A[a]	${}^{n}R$	−12.10	−12.28	−5.27	−5.32	−5.43	−4.88
6A	ΔE	7.29	7.36	7.48	7.48	7.48	7.49
6A	${}^{n}R$	−7.52	−6.91	0.69	0.58	0.33	1.17
7A	ΔE	7.39	7.46	7.60	7.60	7.60	7.61
7A	${}^{n}R$	−0.11	−0.48	1.15	1.01	0.63	1.62

Reproduced from Ref. [107].

[a] Rydberg transition to the *p* orbital. The theoretical excitation energy is given for the central transition, and the theoretical rotatory strength is summed over all three components.

is changed. This is in spite of the fact that methyloxirane is rigid, and does not change its conformation upon changing the solvent. On the other hand, such sensitivity of the ECD spectrum of methyloxirane to solvent effects can be expected considering the large solvent effects observed experimentally for the optical rotation [106]. For flexible molecules, even larger solvent effects can be anticipated. In the same work [107], calculations of the ECD spectra of chiral bicycloketones in several organic solvents were performed, and the initial results show promising agreement with experiment.

Another approach based on a dielectric continuum model to calculate solvent effects on ECD spectra was presented by Kongsted *et al.* [55], who used the coupled cluster method in a spherical cavity to model the influence of a solvent on the rotatory strength tensors of formaldehyde (a non-chiral molecule that exhibits optical activity only in oriented samples, see Section 2.2). Both the length and velocity gauge formulations were employed. As in Ref. [107], the presence of the dielectric continuum was found to change the sign of the optical rotatory strengths of some transitions.

Another system investigated using continuum models is 1-(R)-phenylethanol, for which the effect of the aqueous solution has been calculated by Macleod *et al.* [88]. In this case, both the PCM method and a supermolecular model (small singly and doubly hydrated clusters) were used to model the effects of the aqueous environment on the ECD spectrum of 1-(R)-phenylethanol, but the results obtained were still at variance with experiment. The best (although still not perfect) agreement with experiment was obtained when calculations were performed on averaged structures of solvated 1-(R)-phenylethanol obtained from molecular dynamics simulations.

3.6.2. Natural optical rotation

Solvent effects on the optical rotation of several conformationally rigid chiral organic molecules were studied by Mennucci *et al.* [111] using the Polarizable Continuum Model (PCM), and were found to be substantial. For the solvents investigated, the results obtained using the PCM model were found to be in agreement with experiment. The exceptions were the solvents benzene, chloroform and carbon tetrachloride, for which it was concluded that other interactions than the purely electrostatic ones play a more important role. The excellent agreement for the wide range of solvents ranging in polarity from cyclyohexane to acetonitrile confirms the good applicability of the PCM model to solvent effects on optical properties.

Solvent effects on the optical rotation were modeled by means of the PCM method also for 6,8-dioxabicyclo[3.2.1]octanes [112]. When the DFT calculations were combined with the PCM model, the errors in the calculated optical rotations when compared to experiment did not exceed 20 $\mathrm{deg \cdot cm^3 \cdot g^{-1} \cdot dm^{-1}}$. To some extent, this may be fortuitous, since only one conformation was taken into account for each molecule. On the other hand, other conformations were found to lie significantly higher in energy. It was also found that the Lorentz effective field approximation does not properly account for the solvent effects in this case.

Goldsmith *et al.* [113] performed what is probably the first *ab initio* study of the influence of dimer formation on the specific optical rotation, calculating the specific optical rotation of pantolactone in its monomeric and dimeric forms. The results were compared with the experimentally established optical rotation as a function of the concentration of pantolactone in CCl_4. The study confirms that aggregated species can have greatly altered

optical rotation compared to the monomeric component, a conclusion supported by the experimental data.

3.7. Optical activity in oriented phases

In oriented phases, optical activity can be exhibited by molecules which are not chiral in themselves, but have anisotropic mutual orientations [114,115]. The rotatory strength tensor, although experimentally accessible, has been the subject of few *ab initio* investigations. In order to obtain the rotatory strength tensor, the quadrupole term, which vanishes for freely tumbling molecules, has to be calculated, not only because it contributes significantly to the tensor components, but also because it is only the sum of the electric dipole – magnetic dipole and the electric dipole – electric quadrupole polarizabilities, and not the individual contributions, which is gauge origin independent.

The first calculation of the rotatory strength tensor was carried out for ethylene twisted into a D_2 conformation (as a model for the ethylene chromophore of (−)-*trans*-cyclo-octene) by Pedersen and Hansen [20], who used the random phase approximation (time-dependent HF) in the velocity gauge. They found that the electric dipole – electric quadrupole contribution is smaller than the electric dipole – magnetic dipole contribution, but that it is by no means insignificant, and that it is essential to include it to ensure the gauge origin independence of the total tensor. The calculations were repeated afterward using the length gauge formulation with LAOs [26].

The same model system was used for CCSD calculations of the full rotatory strength tensor [38]. In this case, both length and velocity gauges were employed. The CCSD calculations of the ECD spectrum, including all components of the rotatory strength tensor, were subsequently carried out for the full (−)-*trans*-cyclo-octene by Pedersen and Koch [54], for the twenty lowest singlet transitions.

Hansen and Bak [116] calculated the anisotropic rotatory strength for planar and helical *cis*-butadiene and for 1,3-cyclohexadiene and some of its allylic methyl derivatives, using the time-dependent Hartree Fock approach.

4. CONCLUDING REMARKS AND OUTLOOK

Ab initio calculations of natural optical rotation and ECD spectra are becoming more and more widespread and they are being established as a standard tool in the interpretation of experimental spectra (ECD) or to assign the absolute configuration of chiral molecules (both ECD and optical rotation). However, before they will have predictive power, several problems still need to be resolved.

One of the remaining problems in the calculation of ECD spectra is the lack of low-scaling and robust methods capable of yielding reliable results for excited states of diffuse or charge-transfer character, since linear response (or time-dependent) density functional methods often fail in such cases. The other problem in calculations of both optical rotation and ECD spectra is that *ab initio* methods which are hierarchical and allow for a systematic investigation of the effects of electron correlation on these properties do not ensure, in the length gauge formulation which is preferable on account of the faster basis set convergence, origin independent results. For flexible molecules, an additional challenge is to account for

all low-lying conformers in order to extract meaningful information from the calculated properties.

Because of the sensitivity to conformational changes, calculations of optical rotation and in particular of ECD spectra for conformational studies are a promising and growing field. It can be expected that theoretical studies of the correlation between conformational structure and ECD spectra (and also optical rotation) will lead to a better understanding of these effects as well as to a more robust method for extracting structural information from ECD spectra than the empirical rules used so far.

Quantitative comparisons of *ab initio* calculations and experiment are still precluded due to vibrational and solvent effects. The effects of molecular vibrations on the optical rotation are estimated to be substantial, and they should be accounted for in order to allow for a quantitative comparison with experimental results.

Solvent effects present an even larger problem than rovibrational effects, and in many cases preclude applications of theoretical calculations of ECD spectra and optical rotation for structural studies, since the solvent may change the sign of the optical rotation and the rotatory strengths. Some studies have been carried out, employing polarizable continuum or supermolecular models, but the results, although encouraging, do not yet seem to have predictive power. This is another field open for future developments.

ACKNOWLEDGEMENTS

This work has received support from the Norwegian Research Council through a Strategic University Program in Quantum Chemistry (Grant No. 154011/420).

REFERENCES

[1] D.F.J. Arago, *Mém. de l'Inst.* **12** (1811) 93.
[2] J.B. Biot, *Mém. de l'Inst.* **13** (1812) 218.
[3] L. Rosenfeld, *Z. Phys.* **52** (1928) 161.
[4] R.D. Amos, *Chem. Phys. Lett.* **87** (1982) 23.
[5] P. Lazzeretti, R. Zanasi, *Phys. Rev. A* **33** (1986) 3727.
[6] P.L. Polavarapu, *Mol. Phys.* **91** (1997) 551.
[7] T. Helgaker, K. Ruud, K.L. Bak, P. Jørgensen, J. Olsen, *Faraday Discuss.* **99** (1994) 165.
[8] A. Rauk, J.M. Barriel, *Chem. Phys.* **25** (1977) 409.
[9] P.L. Polavarapu, *Chirality* **14** (2002) 768.
[10] A. Fresnel, *Bull. Soc. Philomath.* (1824) 147.
[11] A. Fresnel, *Ann. Chim.* **28** (1825) 147.
[12] L.D. Barron, *Molecular Light Scattering and Optical Activity*, Cambridge Univ. Press, Cambridge, 1982.
[13] J. Linderberg, Y. Öhrn, *Propagators in Quantum Chemistry*, Academic Press, London, 1973.
[14] C. Djerassi, *Optical Rotatory Dispersion. Applications to Organic Chemistry*, McGraw-Hill Book Company, Inc., New York, 1960.
[15] A.D. Buckingham, M.B. Dunn, *J. Chem. Soc. A* (1971) 1988.
[16] A. Koslowski, N. Sreeramana, R.W. Woody, Theoretical approach to electronic optical activity, in: N. Berova, K. Nakanishi, R.W. Woody (Eds.), *Circular Dichroism. Principles and Applications*, Wiley-VCG, New York, 2000, p. 55.
[17] P. Norman, K. Ruud, T. Helgaker, *J. Chem. Phys.* **120** (2004) 5027.
[18] P. Ehrenfest, *Z. Phys.* **45** (1927) 455.
[19] P.J. Stephens, F.J. Devlin, J.R. Cheeseman, M.J. Frisch, *J. Phys. Chem. A* **105** (2001) 5356.
[20] T.B. Pedersen, Aa.E. Hansen, *Chem. Phys. Lett.* **246** (1995) 1.

[21] J. Olsen, P. Jørgensen, *J. Chem. Phys.* **82** (1985) 3235.
[22] K. Ruud, T. Helgaker, *Chem. Phys. Lett.* **352** (2002) 533.
[23] J. Olsen, P. Jørgensen, in: D.R. Yarkony (Ed.), *Modern Electronic Structure Theory*, World Scientific, New York, 1995, p. 857.
[24] P. Jørgensen, H.J.Aa. Jensen, J. Olsen, *J. Chem. Phys.* **89** (1988) 3654.
[25] P.L. Polavarapu, D.K. Chakraborty, K. Ruud, *Chem. Phys. Lett.* **319** (2000) 595.
[26] K.L. Bak, Aa.E. Hansen, K. Ruud, T. Helgaker, J. Olsen, P. Jørgensen, *Theor. Chim. Acta* **90** (1995) 441.
[27] E. Runge, E.K.U. Gross, *Phys. Rev. Lett.* **52** (1984) 997.
[28] J.R. Cheeseman, M.J. Frisch, F.J. Devlin, P.J. Stephens, *J. Phys. Chem. A* **104** (2000) 1039.
[29] S. Grimme, *Chem. Phys. Lett.* **259** (1996) 128.
[30] S. Grimme, M. Waletzke, *J. Chem. Phys.* **111** (1999) 5645.
[31] J. Autschbach, T. Ziegler, *J. Chem. Phys.* **116** (2002) 891.
[32] K. Yabana, G.F. Bertsch, *Phys. Rev. A* **60** (1999) 1271.
[33] M. Pecul, K. Ruud, T. Helgaker, *Chem. Phys. Lett.* **388** (2004) 110.
[34] T. Helgaker, P. Jørgensen, N.C. Handy, *Theor. Chim. Acta* **76** (1989) 227.
[35] H. Koch, P. Jørgensen, *J. Chem. Phys.* **93** (1990) 3333.
[36] O. Christiansen, P. Jørgensen, C. Hättig, *Int. J. Quantum Chem.* **68** (1998) 1.
[37] K. Ruud, P.J. Stephens, F.J. Devlin, P.R. Taylor, J.R. Cheeseman, M.J. Frisch, *Chem. Phys. Lett.* **373** (2003) 606.
[38] T.B. Pedersen, H. Koch, K. Ruud, *J. Chem. Phys.* **110** (1999) 2883.
[39] F. London, *J. Phys. Radium* **8** (1937) 397.
[40] K.L. Bak, P. Jørgensen, T. Helgaker, K. Ruud, H.J.Aa. Jensen, *J. Chem. Phys.* **98** (1993) 8873.
[41] R. Ditchfield, W.J. Hehre, J.A. Pople, *J. Chem. Phys.* **54** (1971) 724.
[42] R. Ditchfield, *Mol. Phys.* **27** (1974) 789.
[43] K. Wolinski, J.F. Hinton, P. Pulay, *J. Am. Chem. Soc.* **112** (1990) 8251.
[44] J. Gauss, *Chem. Phys. Lett.* **191** (1992) 614.
[45] J. Gauss, J.F. Stanton, *J. Chem. Phys.* **103** (1995) 3561.
[46] K. Ruud, T. Helgaker, R. Kobayashi, P. Jørgensen, K.L. Bak, H.J.Aa. Jensen, *J. Chem. Phys.* **100** (1994) 8178.
[47] K. Ruud, T. Helgaker, K.L. Bak, P. Jørgensen, H.J.Aa. Jensen, *J. Chem. Phys.* **99** (1993) 3847.
[48] K. Ruud, T. Helgaker, *Chem. Phys. Lett.* **264** (1997) 17.
[49] T. Helgaker, P. Jørgensen, *J. Chem. Phys.* **95** (1991) 2595.
[50] J. Olsen, K.L. Bak, K. Ruud, T. Helgaker, P. Jørgensen, *Theor. Chim. Acta* **90** (1995) 421.
[51] P. Jørgensen, J. Simons, *Second Quantization-Based Methods in Quantum Chemistry*, Academic Press, New York, 1981.
[52] T.B. Pedersen, H. Koch, C. Hättig, *J. Chem. Phys.* **110** (1999) 8318.
[53] T.B. Pedersen, B. Fernandez, H. Koch, *J. Chem. Phys.* **114** (2001) 6983.
[54] T.B. Pedersen, H. Koch, *J. Chem. Phys.* **112** (2000) 2139.
[55] J. Kongsted, T.B. Pedersen, A. Osted, A.E. Hansen, K.V. Mikkelsen, O. Christiansen, *J. Phys. Chem. A* **108** (2004) 3632.
[56] T.B. Pedersen, H. Koch, L. Boman, A.M.J. de Merás, *Chem. Phys. Lett.* **393** (2004) 319.
[57] M. Carnell, S.D. Peyerimhoff, A. Breest, K.H. Gödderz, P. Ochmann, J. Hormes, *Chem. Phys. Lett.* **180** (1991) 477.
[58] T.H. Dunning, *J. Chem. Phys.* **90** (1989) 1007.
[59] R.A. Kendall, T.H. Dunning, R.J. Harrison, *J. Chem. Phys.* **96** (1992) 6796.
[60] D.E. Woon, T.H. Dunning, *J. Chem. Phys.* **98** (1993) 1358.
[61] D.E. Woon, T.H. Dunning, *J. Chem. Phys.* **100** (1994) 2975.
[62] A.J. Sadlej, *Coll. Czech. Chem. Commun.* **53** (1988) 1995.
[63] E. Giorgio, C. Rosini, R.G. Viglione, R. Zanasi, *Chem. Phys. Lett.* **376** (2003) 452.
[64] S. Grimme, F. Furche, R. Ahlrichs, *Chem. Phys. Lett.* **361** (2002) 321.
[65] P.J. Stephens, F.J. Devlin, J.R. Cheeseman, M.J. Frisch, *J. Phys. Chem. A* **105** (2001) 5356.
[66] K.B. Wiberg, Y. Wang, P. Vaccaro, J.R. Cheeseman, M.J. Frisch, *J. Phys. Chem. A* **108** (2004) 32.
[67] M.M. Francl, W.J. Pietro, W.J. Hehre, J.S. Binkley, M.S. Gordon, D.J. DeFrees, J.A. Pople, *J. Chem. Phys.* **77** (1982) 3654.
[68] K.B. Wiberg, P. Vaccaro, J.R. Cheeseman, *J. Am. Chem. Soc.* **125** (2003) 1888.
[69] T.-K. Ha, W. Cencek, *Chem. Phys. Lett.* **182** (1991) 519.

[70] M. Pericou-Cayere, M. Rerat, A. Dargelos, *Chem. Phys.* **226** (1998) 297.
[71] M. Carnell, S. Grimme, S.D. Peyerimhoff, *Chem. Phys.* **179** (1994) 385.
[72] J. Hutter, H.P. Lüthi, T.-K. Ha, *J. Mol. Struct. (Theochem)* **235** (1991) 515.
[73] M. Schreiber, R. Vahrenhorst, V. Buss, N.P. Fulscher, *Chirality* **13** (2001) 571.
[74] F. Pulm, J. Schramm, J. Hormes, S. Grimme, S.D. Peyerimhoff, *Chem. Phys.* **224** (1997) 143.
[75] C. Diedrich, S. Grimme, *J. Phys. Chem. A* **107** (2003) 2524.
[76] J. Autschbach, T. Ziegler, *J. Chem. Phys.* **116** (2002) 6930.
[77] F. Furche, R. Ahlrichs, C. Wachsmann, E. Weber, A. Sobanski, F. Vogtle, S. Grimme, *J. Am. Chem. Soc.* **122** (2000) 1717.
[78] S. Grimme, W. Mennicke, F. Vogtle, M. Nieger, *J. Chem. Soc., Perkin Trans.* **2** (1999) 521.
[79] M. Pecul, A. Rizzo, K. Ruud, T. Helgaker, *J. Phys. Chem. A* **108** (2004) 4269.
[80] P.J. Stephens, D.M. McCann, E. Butkus, S. Stončius, J.R. Cheeseman, M.J. Frisch, *J. Org. Chem.* **69** (2004) 1948.
[81] P.L. Polavarapu, *Angew. Chem. Int. Ed.* **41** (2002) 4544.
[82] J. Costante, L. Hecht, P.L. Polavarapu, A. Collet, L.D. Barron, *Angew. Chem. Int. Ed.* **36** (1997) 885.
[83] J.T. He, A. Petrovich, P.L. Polavarapu, *J. Phys. Chem. A* **108** (2004) 1671.
[84] P.J. Stephens, F.J. Devlin, J.R. Cheeseman, M.J. Frisch, O. Bortolini, P. Besse, *Chirality* **15** (2003) S57.
[85] S. Coriani, M. Pecul, A. Rizzo, P. Jørgensen, M. Jaszuński, *J. Chem. Phys.* **117** (2002) 6417.
[86] R.K. Kondru, P. Wipf, D.N. Beratan, *J. Phys. Chem. A* **103** (1999) 6603.
[87] S. Grimme, A. Bahlmann, G. Haufe, *Chirality* **14** (2002) 793.
[88] N.A. Macleod, P. Butz, J.P. Simons, G.H. Grant, C.M. Baker, G.E. Tranter, *Isr. J. Chem.* **44** (2004) 27.
[89] D.F. Plusquellic, R.J. Lavrich, T. Petralli-Mallow, S. Davis, T.M. Korter, R.D. Suenram, *Chem. Phys.* **283** (2002) 355.
[90] P.L. Polavarapu, A. Petrovic, F. Wang, *Chirality* **15** (2003) S143.
[91] J.D. Hirst, D.M. Hirst, C.L. Brooks, *J. Phys. Chem. A* **101** (1997) 4821.
[92] N.A. Besley, J.D. Hirst, *J. Phys. Chem. A* **102** (1998) 10791.
[93] N.A. Besley, J.D. Hirst, *J. Am. Chem. Soc.* **121** (1999) 9636.
[94] N.A. Besley, J.D. Hirst, *J. Mol. Struct. (Theochem)* **506** (2000) 161.
[95] D.A. Lightner, J.E. Gurst, *Organic Conformational Analysis and Stereochemistry from Circular Dichroism Spectroscopy*, Wiley, New York, 2000.
[96] P.L. Polavarapu, D.K. Chakraborty, *Chem. Phys.* **240** (1999) 1.
[97] R.K. Kondru, P. Wipf, D.N. Beratan, *J. Am. Chem. Soc.* **120** (1998) 2204.
[98] R.K. Kondru, P. Wipf, D.N. Beratan, *Science* **282** (1998) 2247.
[99] R.S. Mulliken, *J. Chem. Phys.* **23** (1955) 1833.
[100] R.S. Mulliken, *J. Chem. Phys.* **36** (1962) 3428.
[101] A. Ligabue, P. Lazzeretti, M.P.B. Varela, M.B. Ferraro, *J. Chem. Phys.* **116** (2002) 6427.
[102] M.P. Bécar Varela, M.B. Ferraro, D. Rail, *Theor. Chem. Acc.* **110** (2003) 428.
[103] M.F. Ruiz-Lopez, D. Rivaldi, J.L. Rivail, *Chem. Phys.* **110** (1986) 403.
[104] K. Ruud, P.R. Taylor, P.O. Åstrand, *Chem. Phys. Lett.* **337** (2001) 217.
[105] T. Müller, K.B. Wiberg, P.H. Vaccaro, *J. Phys. Chem. A* **104** (2000) 5959.
[106] Y. Kumata, J. Furukawa, T. Fueno, *Bull. Chem. Soc. Jpn.* **43** (1970) 3920.
[107] M. Pecul, D. Marchesan, K. Ruud, S. Coriani, *J. Chem. Phys.* **122** (2005) 024106.
[108] S. Miertuš, E. Scrocco, J. Tomasi, *J. Chem. Phys.* **55** (1981) 117.
[109] R. Cammi, J. Tomasi, *J. Comput. Chem.* **16** (1995) 1449.
[110] B. Mennucci, E. Cancés, J. Tomasi, *J. Phys. Chem. B* **101** (1997) 10506.
[111] B. Mennucci, J. Tomasi, R. Cammi, J.R. Cheeseman, M.J. Frisch, F.J. Devlin, P.J. Stephens, *J. Phys. Chem. A* **106** (2002) 6102.
[112] P.J. Stephens, F.J. Devlin, J.R. Cheeseman, M.J. Frisch, B. Mennucci, J. Tomasi, *Tetrahedron-Asymmetry* **11** (2000) 2443.
[113] M.R. Goldsmith, N. Jayasuriya, D.N. Beratan, P. Wipf, *J. Am. Chem. Soc.* **125** (2003) 15696.
[114] H.-G. Kuball, T. Höfer, Circular dichroism of oriented molecules, in: N. Berova, K. Nakanishi, R.W. Woody (Eds.), *Circular Dichroism. Principles and Applications*, Wiley-VCG, New York, 2000, p. 133.
[115] H.-G. Kuball, T. Karstens, A. Schönhofer, *Chem. Phys.* **12** (1976) 1.
[116] Aa.E. Hansen, K.L. Bak, *J. Phys. Chem. A* **104** (2000) 11362.

Response of a Molecule to Adding or Removing an Electron

Jack Simons

Chemistry Department and Henry Eyring Center for Theoretical Chemistry, University of Utah, Salt Lake City, UT 84112, USA
E-mail: simons@chemistry.utah.edu
URL: http://simons.hec.utah.edu

Abstract

The *ab initio* calculation of molecular electron affinities (EA) and ionization potentials (IP) is a difficult task because the energy of interest is a very small fraction of the total electronic energy of the parent species. For example, EAs typically lie in the 0.01–10 eV range, but the total electronic energy of even a small molecule, radical, or ion is usually several orders of magnitude larger. Moreover, the EA or IP is an intensive quantity but the total energy is an extensive quantity, so the difficulty in evaluating EAs and IPs to within a fixed specified (*e.g.*, ± 0.1 eV) accuracy becomes more and more difficult as the system's size and number of electrons grows. The situation becomes especially problematic when studying extended systems such as solids, polymers, or surfaces for which the EA or IP is an infinitesimal fraction of the total energy. Equations of motion (EOM) methods such as the author developed in the 1970s in collaboration with P. Jørgensen and others offer a route to calculating the intensive EAs and IPs directly as eigenvalues of a set of working equations. A history of the development of EOM theories as applied to EAs and IPs, their numerous practical implementations, and their relations to Greens function or propagator theories are given in this contribution. EOM methods based upon Møller–Plesset, multi-configuration self-consistent field, and coupled-cluster reference wave functions are included in the discussion as is the application of EOM methods to metastable states of anions.

Contents

ADVANCES IN QUANTUM CHEMISTRY, VOLUME 50
ISSN: 0065-3276 DOI: 10.1016/S0065-3276(05)50010-8

1. INTRODUCTION

The vertical electron affinity (EA) of a molecule can be estimated by (approximately) solving the Schrödinger equation for the energy $E(0, N)$ of the N-electron neutral molecule and the Schrödinger equation for the energy $E(K, N+1)$ of the Kth state of the $(N+1)$-electron anion and subtracting the two energies:

$$\mathrm{EA} = E(0, N) - E(K, N+1). \tag{1}$$

The corresponding vertical ionization potential (IP) is given as

$$\mathrm{IP} = E(K, N-1) - E(0, N). \tag{2}$$

Here, we use K to label the electronic state of the anion or cation that one wishes to study, and 0 to label the state of the neutral (usually but not necessarily the ground state) to which the electron is being attached or from which it is removed.

In using such an approach to obtaining the EA or IP, one is faced with a very difficult numerical challenge because $E(0, N)$, $E(K, N-1)$, and $E(K, N+1)$ tend to be extremely large (negative) numbers, whereas EA and IP nearly always lies in the range 0–20 eV. For example, the EA of the $^4S_{3/2}$ state of the carbon atom [1] is 1.262119 ± 0.000020 eV, whereas the total electronic energy of this state of C is -1030.080 eV (relative to a C^{6+} nucleus and six electrons infinitely distant and not moving that defines the zero of energy). Since the EA is *ca.* 0.1% of the total energy of C, one needs to compute the C and C^- electronic energies to accuracies of 0.01% or better to calculate the EA to within 10%.

This observation shows only the "tip of the iceberg", however as the major problem relates to the fact that $E(0, N)$, $E(K, N-1)$, and $E(K, N+1)$ are extensive properties whereas EA and IP are intensive quantities. For example, the EA of C_2 in its $X^2\Sigma_g^+$ ground electronic state is [1] 3.269 ± 0.006 eV near the equilibrium bond length R_e but only 1.2621 eV at $R \to \infty$ (*i.e.*, the same as the EA of a carbon atom). However, the total electronic energy of C_2 is -2060.160 eV at $R \to \infty$ and lower by *ca.* 3.6 eV (the dissociation energy [2] of C_2) at R_e, so again EA is a very small fraction of the total energies. For buckyball C_{60}, the EA is [1] 2.666 ± 0.001 eV, but the total electronic energy is sixty times -1030.080 eV minus the atomization energy (*i.e.*, the energy change for $C_{60} \to 60$ C) of this compound. Clearly, the challenge of evaluating EA (or IP) to within even 50% becomes more and more difficult as the size (*i.e.*, number of electrons) in the molecule grows, and it becomes impossible when the system of interest is an infinite solid, surface, or polymer. This same kind of difficulty (*i.e.*, calculating an intensive quantity as the difference between to extensive energies) plagues the computation of EAs and of ionization potentials (IPs), bond energies, and electronic excitation energies.

The problems discussed in the preceding paragraph do not disappear if one uses a computer with higher numerical precision in its arithmetic (*i.e.*, a longer word length) or algorithms that compute the one- and two-electron integrals needed for any quantum chemistry calculation to more significant figures. No mater how precise the integrals and how long the floating point word length (as long as they are finite), the evaluation of intensive properties such as IPs, EAs, and excitation energies as differences between pairs of extensive total electronic energies is doomed to fail.

Of course, much progress can be made in computing EAs and IPs as differences between anion and neutral or cation and neutral total energies [3] because of large systematic cancellation in energy errors [4]. For example, the pair correlation energies of the two 1s electron

pairs in C_2 is quite large, but is very nearly the same as in C_2^-, so even a large percent error made in computing these contributions to the total energy may not greatly affect the EA computed by subtracting $E(K, N+1)$ from $E(0, N)$. Some of the earliest high quality *ab initio* calculations of EAs were carried out using wave function techniques and calculating separate neutral and anion energies. Nevertheless, in the late 1960s and early 1970s, workers were motivated to develop methods that would allow intensive energy differences such as EAs [5], ionization potentials (IPs) and excitation energies (ΔEs) "directly" rather than as differences in two very large numbers. This point of view is what led to the development of so-called equations of motion (EOM) methods as well as Greens function methods [6] pioneered by the Linderberg and Öhrn groups and, more recently, response function approaches [7] of Jørgensen, Olsen, and co-workers. In all of these theories, one performs a derivation in which the two total energies (*i.e.*, ion and neutral or ground and excited state) are subtracted analytically (rather than numerically) thereby achieving an analytical expression for the desired intensive energy difference. It is by thus dealing with equations that involve only intensive energies that one can overcome the problems detailed earlier.

Among the earliest practitioners of EOM methods in the chemistry community were McKoy [8] and his group at Cal Tech. They imported many ideas and mathematical tools from the nuclear physics literature [9], where EOM theories had been used to study excited states of nuclei, and they focused their efforts on electronic excitation energies ΔE, not IPs or EAs. In 1973, the author used the framework of EOM theory [10] as expressed by the McKoy group to develop a systematic (*i.e.*, order-by-order in the Møller–Plesset perturbation theory sense) approach for directly computing molecular EAs and IPs as eigenvalues of the EOM working equations. It is this development and its subsequent improvement, to several of which Prof. Poul Jørgensen contributed, and extensions [11] by our group and others that we now describe.

2. BASICS OF EOM THEORY

2.1. The EA equations of motion

The fundamental working equations of any EOM theory can be derived by writing the Schrödinger equations for the neutral and anion (or neutral or cation or ground and excited) states of interest and subtracting the two equations as a first step toward obtaining a single equation that will yield the EA or IP or ΔE. That is, the EOM theory produces the intensive energy difference directly as an eigenvalue of the working equation. As above, we use $|0, N\rangle$ to denote the 0th electronic state of the N-electron neutral and $|K, N+1\rangle$ to denote the Kth state of the $(N+1)$-electron anion and write the two Schrödinger equations as

$$H|0, N\rangle = E(0, N)|0, N\rangle, \tag{3}$$

$$H|K, N+1\rangle = E(K, N+1)|K, N+1\rangle. \tag{4}$$

Because $|0, N\rangle$ and $|0, N+1\rangle$ contain different numbers of electrons, it is convenient in developing EOM theories of EAs to express the electronic Hamiltonian H in second-

quantized form [12]:

$$H = \sum_{i,j} h(i,\, j) i^{+} j + \frac{1}{2} \sum_{i,j,k,l} \langle i,\, j|k,\, l\rangle i^{+} j^{+} lk \tag{5}$$

where $h(i,\, j)$ represents a matrix element of the one-electron operators (*i.e.*, kinetic energy, electron-nuclear Coulomb attraction, *etc.*) within the orthonormal molecular spin-orbital basis $\{\phi_j\}$, $\langle i,\, j|k,\, l\rangle$ is a matrix element of the two-electron operators (*i.e.*, electron-electron repulsion), and the set of Fermion creation operators $\{i^{+}\}$ create an electron in the $\{\phi_i\}$ spin-orbitals, whereas the $\{i\}$ operators destroy such an electron. Writing H in such a form allows us to use the same H in equations (3) and (4) even those these two Schrödinger equations relate to N and $N + 1$ electrons, respectively.

The next step in developing an EOM equation is to assume that the anion state $|K,\, N+1\rangle$ can be related to the neutral state $|0,\, N\rangle$ through an operator $Q^{+}(K)$:

$$|K,\, N + 1\rangle = Q^{+}(K)|0,\, N\rangle \tag{6}$$

that maps the neutral molecule wave function into the desired anion wave function.

For the EA case at hand, the operator $Q^{+}(K)$ is usually written in terms of scalar coefficients $t(K, l)$ multiplied by operators $T^{+}(l)$, also expressed in second-quantization language, each of which involves adding an electron

$$Q^{+}(K) = \sum_{l} t(K, l) T^{+}(l). \tag{7}$$

Manne showed [13] that a complete set of such $T^{+}(l)$ operators consists of the union of sets of operators $\{p^{+}\}$ that add an electron to a spin-orbital ϕ_p, operators $\{p^{+}q^{+}a\}$ that add an electron to ϕ_p and excite another electron from ϕ_a to ϕ_q, operators $\{p^{+}q^{+}r^{+}ab\}$ that add an electron to ϕ_p excite an electron from ϕ_a to ϕ_r and excite another electron from ϕ_b to ϕ_q as well as higher-level electron addition and excitation operators up to the highest-level operators that add an electron and induce N excitations. In labeling these operators, the indices a, b, c, d, *etc.*, are used to denote spin-orbitals occupied in a so-called reference Slater determinant within $|0,\, N\rangle$ and p, q, r, s, *etc.*, are used to denote unoccupied (*i.e.*, virtual) spin-orbitals. The reference determinant, which is what defines the concept of occupied and unoccupied spin-orbitals, is usually chosen to be the determinant $|0\rangle$ within the neutral-molecule wave function

$$|0,\, N\rangle = \sum_{J=0,M} C(0,\, J)|J\rangle \tag{8}$$

with the largest amplitude $C(0,\, 0)$, but it has been shown [13] that $|0\rangle$ can actually be taken to be any determinant within $|0,\, N\rangle$ that possesses non-zero amplitude. Later we will deal with how one determines the $C(0,\, J)$ amplitudes in the wave function $|0,\, N\rangle$; for now, suffice it to say these amplitudes can, for example, be taken from Møller–Plesset (MP) perturbation theory, from multiconfiguration self-consistent field (MCSCF) theory, from configuration interaction (CI) theory or from coupled-cluster (CC) theory.

Using equation (6) in equation (4) and subtracting equation (3) from (4) gives a single equation whose eigenvalue gives the desired EA:

$$\big(H Q^{+}(K) - Q^{+}(K) H\big)|0,\, N\rangle = \big(E(K,\, N + 1) - E(0,\, N)\big) Q^{+}(K)|0,\, N\rangle \tag{9}$$

or, in terms of the commutator $[H, Q^+(K)]$

$$\big[H, Q^+(K)\big]|0, N\rangle = EQ^+(K)|0, N\rangle \tag{10}$$

where the eigenvalue E is the negative of the EA. The key point is that one now has a single equation to be solved that produces the intensive EA as its eigenvalue. This equation appears to be of the conventional eigenvalue-eigenfunction form, but it is somewhat different because the operator that acts on the eigenfunction $Q^+(K)|0, N\rangle$ is not the Hamiltonian but a commutator involving the Hamiltonian. The fact that the commutator appears is what causes the eigenvalue to be an intensive energy difference.

To progress further toward practical implementation, specific choices must be made for how one is going to approximate the neutral-molecule wave function $|0, N\rangle$ and at what level one is going to truncate the expansion of the operator $Q^+(K)$ given in equation (7). It is also conventional to reduce equation (10) to a matrix eigenvalue equation by projecting this equation onto an appropriately chosen space of $(N+1)$-electron functions. Let us first deal with the latter issue.

Once the number of $T^+(l)$ operators used to construct $Q^+(K)$ has been chosen (we discuss this choice later), the total number $l^{\max}$ of $t(K, l)$ amplitudes has been determined. Multiplying equation (10) on the left by the adjoint $T(j)$ of any one of the T^+ operators, and then projecting the resultant equation against $\langle 0, N|$ gives one form of the working EOM EA equations:

$$\sum_l \langle 0, N|T(j)\big[H, T^+(l)\big]|0, N\rangle t(K, l) = E\sum_l \langle 0, N|T(j)T^+(l)|0, N\rangle t(K, l). \tag{11}$$

To make use of this equation, the $\langle 0, N|T(j)[H, T^+(l)]|0, N\rangle$ and $\langle 0, N|T(j)T^+(l)|0, N\rangle$ matrices of dimension $l^{\max} \times l^{\max}$ must first be evaluated in terms of one-and two-electron integrals (appearing in H) and one-, two-, and higher-body density matrices (depending upon the level at which the $\{T^+(l)\}$ operator expansion is truncated). Subsequently, the EA values (*i.e.*, EAs for the various anion states, K, relative to the $|0, N\rangle$ state of the neutral) are computed as minus the eigenvalues E of equation (11).

2.2. The analogous equations of motion for ionization potentials

It is useful to explore how this same framework has been used to compute molecular ionization potentials (IPs). It is fairly straightforward to show that an equation analogous to equation (10) but reading

$$\langle 0, N|\big(HQ^+(K) - Q^+(K)H\big) = \big(E(0, N) - E(K, N-1)\big)\langle 0, N|Q^+(K) \tag{12}$$

is valid if the operators $\{Q^+(K)\}$ are as given in equation (7) but with the $\{T^+(l)\}$ defined to include operators of the form $\{a^+, a^+b^+p, a^+b^+c^+qr,\ etc.\}$. Of course, in equation (12), the operators within $Q^+(K)$ act to the left on $\langle 0, N|$ to generate cationic states. As a result, neutral-cation energy differences appear in equation (12) and thus this offers a route to computing IPs. Multiplying this equation on the right by any one of the $T(j)$ operators and then projecting against $|0, N\rangle$ gives

$$\sum_l \langle 0, N|\big[H, T^+(l)\big]T(j)|0, N\rangle t(K, l) = E\sum_l \langle 0, N|T^+(l)T(j)|0, N\rangle t(K, l) \tag{13}$$

but now the eigenvalues E denote values of $(E(0, N) - E(K, N - 1))$, which are the negatives of the IPs.

Thus far, we see that EOMs can be written that allow EAs or IPs to be computed. The fundamental constructs within these equations are as follows:

(i) For the EA case, matrix elements $\langle 0, N|T(j)[H, T^+(l)]|0, N\rangle$ involving the commutator of H with the $T^+(l)$ operators then multiplied on the left by a $T(j)$ operator, as well as an analogous overlap matrix element $\langle 0, N|T(j)T^+(l)|0, N\rangle$;
(ii) for the IP case, matrix elements $\langle 0, N|[H, T^+(l)]T(j)|0, N\rangle$ of the same commutator but with the $T(j)$ operator on the right, as well as the corresponding overlap matrix element $\langle 0, N|T^+(l)T(j)|0, N\rangle$;
(iii) the neutral-molecule wave function $|0, N\rangle$ with respect to which the EA or IP is to be evaluated.

2.3. The rank of the operators

It is now useful to analyze the density matrix elements[1] that enter into these equations. Each of the $T^+(j)$ operators contains an odd number of creation or annihilation operators, and the Hamiltonian H contains two (*i.e.*, i^+j) or four (*i.e.*, i^+j^+lk) such operators. It can be seen that the commutator $[H, T^+(l)]$ does not contain four plus the number of creation or annihilation operators in $T^+(l)$, but two fewer operators. For example, the commutator $[i^+j^+lk, p^+q^+a]$ does not yield any terms with four creation and three annihilation operators but only terms with three creation and two annihilation operators. We say that the act of forming the commutator (which is what causes the higher order operators to cancel) gives rise to a reduction in the rank of the operators. As a result, both the operator products $T(j)[H, T^+(l)]$ and $[H, T^+(l)]T(j)$, which appear in the EA and IP equations of motion, respectively, contain terms only involving both creation and annihilation operators equal to the number of creation operators in $T^+(l)$ plus one plus the number of creation operators in $T(j)$. For example, if $T^+(l) = p^+q^+a$ and $T(j) = b^+rs$, then $T(j)[H, T^+(l)]$ and $[H, T^+(l)]T(j)$ will contain terms with no more than four creation and four annihilation operators. This means that the density matrices needed to from $\langle 0, N|T(j)[H, T^+(l)]|0, N\rangle$ and $\langle 0, N|[H, T^+(l)]T(j)|0, N\rangle$ will be, at most, fourth order density matrices of the $\langle 0, N|\ldots|0, N\rangle$ density.

2.4. Equations of lower rank for both EAs and IPs

Indeed, in the early years of using EOM methods [14] to compute EAs and IPs, operator manifolds of the form $\{T^+(l)\} = \{p^+;\ p^+q^+a,\ p^+q^+r^+ba,\ \textit{etc.}\}$ or $\{T^+(l)\} = \{a^+, a^+b^+p, a^+b^+c^+qr,\ \textit{etc.}\}$ were employed with Møller–Plesset approximations to $|0, N\rangle$ (usually taken through first order) to form the kind of matrix elements appearing in equations (11) and (13) and to then evaluate EAs and IPs from their eigenvalues E. However, it became more common to use a combination of the EA and IP EOMs formed

[1] The first- and second-order density matrices, respectively, have elements given by $\langle 0, N|j^+k|0, N\rangle$ and $\langle 0, N|j^+k^+lh|0, N\rangle$.

by adding equations (11) and (13), while expanding the $\{T^+(l)\}$ operator manifold to include both those needed to evaluate EAs $\{p^+;\ p^+q^+a,\ p^+q^+r^+ba,\ \textit{etc.}\}$ and those needed for the IPs $\{a^+, a^+b^+p, a^+b^+c^+qr,\ \textit{etc.}\}$, to simultaneously compute both such energy differences.

To understand why such a combination has proven beneficial, it suffices to examine the form and rank of the operators whose $\langle 0, N|\ldots|0, N\rangle$ matrix elements must be evaluated

$$\sum_l \langle 0, N|\big[H, T^+(l)\big]T(j) + T(j)\big[H, T^+(l)\big]|0, N\rangle t(K, l)$$
$$= E\sum_l \langle 0, N|T^+(l)T(j) + T(j)T^+(l)|0, N\rangle t(K, l). \tag{14}$$

Recall that the $T^+(j)$ operators contain an odd number of creation or annihilation operators. Each of the products $[H, T^+(l)]T(j)$, $T(j)[H, T^+(l)]$, $T^+(l)T(j)$, and $T(j)T^+(l)$ thus contain an even number of such operators. However, because of the fundamental anticommutation properties of these operators

$$i^+j + ji^+ = \delta_{i,j}, \tag{15}$$
$$ij + ji = 0, \tag{16}$$
$$i^+j^+ + j^+i^+ = 0 \tag{17}$$

it can easily be shown that the *operator combinations* $T^+(l)T(j) + T(j)T^+(l)$ and $[H, T^+(l)]T(j) + T(j)[H, T^+(l)]$ contain one fewer creation and one fewer annihilation operator than does either of the two terms in the sums. So, by combining the EA and IP EOMs, one effects a rank reduction in the operators appearing in the equations although the dimensions of the matrices one needs to construct are doubled (because the $\{T^+(l)\}$ operator manifold was doubled when both EA and IP operators were included. The rank reduction is important because it means that the density matrices that need to be evaluated to compute the $\langle 0, N|\ldots|0, N\rangle$ matrix elements are of lower rank in equation (14) than in either equation (11) or equation (13). As we said, it has become more common to use the combined EA and IP equation (14) because lower-order density matrices are required.

2.5. Summary

Thus far, we have shown how one can obtain eigenvalue equations, in which the energy eigenvalues correspond to the intensive EAs (or IPs), by postulating that the anion (or cation) wave function can be related to the neutral-molecule wave function through an operator. We have also shown how the EA and IP equations of motion can be combined to generate a combined EOM from which both EAs and IPs can be obtained. The advantage to the latter approach is that the operators appearing in the resultant equations are of lower rank and thus lower-order density matrices must be evaluated to carry out the calculations. Let us now move on to address more specific embodiments of such EOM theories that result from different choices of the neutral-molecule wave function and of the operator connecting the neutral and anion wave functions.

3. PRACTICAL IMPLEMENTATIONS OF EOM THEORIES FOR EAS AND IPS

The basic ideas underlying any EOM method for computing EAs or IPs appear above. However, as discussed earlier, in any specific embodiment of such a method, one must commit to

(i) a specific approximation to the neutral-molecule wave function $|0, N\rangle$,
(ii) a specific choice of how large an operator manifold $\{T^+(l)\}$ to employ, and
(iii) how to solve the resultant EOM equations for the eigenvalues E that then produce the EAs or IPs. In the following subsections, we describe the most commonly used choices for these three issues.

3.1. The Møller–Plesset based approximations

In the earliest implementation of EOM approaches to EAs, the author's group [10,14] chose to represent the $|0, N\rangle$ wave function in a Møller–Plesset (MP) expansion

$$|0, N\rangle = \psi^0 + \psi^1 + \psi^2 + \cdots \tag{18}$$

with the single-determinant unrestricted Hartree–Fock (HF) function being ψ^0 and the corresponding neutral-molecule HF Hamiltonian being H^0. This choice was made because there existed substantial evidence that EAs and IPs computed at the Koopmans' theorem level would not meet the desired 0.1 eV accuracy. The evidence on atoms and small molecules also showed that EAs and IPs computed using standard second-order MP theory were much more accurate but not sufficient to approach the 0.1 eV standard. For this reason, the author's group set their sites on the next reasonable level, that of third-order MP theory.

The operator manifold $\{T^+(l)\}$ was taken to consist of $\{p^+;\ p^+q^+a\}$ and $\{a^+,\ a^+b^+p\}$. In a close collaboration with P. Jørgensen, this choice of operator manifold was shown to be capable of producing EAs and IPs that were precise through third order[2] in the MP perturbation, which is why this choice was made.

The resultant variant of equation (14) was not solved by finding the eigenvalues of this matrix eigenvalue equation whose dimension is the sum of the dimensions of the $\{p^+;\ p^+q^+a\}$ and $\{a^+,\ a^+b^+p\}$ operator manifolds. Rather, that large matrix eigenvalue problem was partitioned [10] using a primary subspace defined by the $\{p^+,\ a^+\}$ operators and a secondary subspace defined by the $\{p^+q^+a,\ a^+b^+p\}$ operators. The partitioned eigenvalue problem

$$\sum_{j=a,p} H_{i,j}(E)X_j = EX_i \tag{19}$$

whose dimension was that of the $\{p^+,\ a^+\}$ operator space was used to find the eigenvalues E. Of course, the act of partitioning the higher-dimension matrix eigenvalue problem does not change the values of E that represent solutions to the equations. That is, the same E values that fulfill the original equations are also solutions to the partitioned equations. However, once one introduces approximations designed to evaluate elements of the partitioned $H_{i,j}(E)$ matrix to a chosen order in perturbation theory, this equivalence is lost.

[2] See Ref. [6k].

It is precisely by making such an order analysis (*e.g.*, computing $H_{i,j}(E)$ through second or third order) that EOM theories capable of evaluating EAs or IPs to a given order were obtained.

When the elements of the partitioned matrices were evaluated through second order in the MP series, the following expression was obtained for the matrix elements $H_{i,j}$;

$$H_{i,j}(E) = \varepsilon_i \delta_{i,j} - \sum_{p,q,a} \frac{\langle i,a||p,q\rangle\langle p,q||j,a\rangle}{\varepsilon_p + \varepsilon_q - \varepsilon_a - E} + \sum_{a,b,p} \frac{\langle i,p||a,b\rangle\langle a,b||j,p\rangle}{\varepsilon_a + \varepsilon_b - \varepsilon_p - E}. \quad (20)$$

Here, the ε_j denote the UHF spin-orbital energies of the neutral molecule and the $\langle i,j||k,l\rangle$ denote differences in two-electron integrals ($\langle i,j||k,l\rangle = \langle i,j|k,l\rangle - \langle i,j|l,k\rangle$). Such expressions were also obtained by Reinhardt and Doll [17] within the Greens function framework, but they had not extended their efforts to third or higher orders.

The expression for $H_{i,j}(E)$ valid through third order in the MP series is more complicated and is derived in Refs. [10].[3] The partitioned matrix eigenvalue equation was written in those works as

$$\mathbf{H}(E)\mathbf{X} = E\mathbf{X} \quad (21)$$

where the elements of the **H** matrix were defined as follows:

$$H_{i,j}(E) = A_{i,j} + \sum_{\alpha<\beta,\,m} \frac{B_{i,\alpha m\beta} B^*_{j,\alpha m\beta}}{E^m_{\alpha\beta} + E} - \sum_{N+1<n,\,\alpha} \frac{B_{i,n\alpha N+1g} B^*_{j,n\alpha N+1}}{E^{N+1n}_{\alpha} - E} - \sum_{N+1<m<n,\,\alpha} \frac{B_{i,n\alpha mg} B^*_{j,n\alpha m}}{E^{mn}_{\alpha} - E}. \quad (22)$$

In turn, the elements of the A and B matrices are shown below:

$$B_{i,\alpha m\beta} = -\langle im|\alpha\beta\rangle - \frac{1}{2}\sum_{p,q}\langle im|pq\rangle K^{(pq)}_{\alpha\beta} + \sum_{\gamma,p}\left[\langle i\gamma|p\alpha\rangle K^{(mp)}_{(\beta\gamma)} - \langle i\gamma|p\beta\rangle K^{(mp)}_{(\alpha\gamma)}\right], \quad (23)$$

$$B_{i,n\alpha m} = \langle i\alpha|mn\rangle + \frac{1}{2}\sum_{\gamma,\delta}\langle i\alpha|\gamma\delta\rangle K^{mn}_{(\delta\gamma)} + \sum_{\gamma,p}\left[\langle ip|\gamma n\rangle K^{(mp)}_{(\alpha\gamma)} - \langle ip|\gamma m\rangle K^{(np)}_{(\alpha\gamma)}\right], \quad (24)$$

$$A_{i,j} = \delta_{i,j}\varepsilon_i + \sum_{k,l}\langle ik|jl\rangle F_{kl} \quad (25)$$

to which one adds the following E-independent terms

$$\delta A_{i,j} = \sum_{\delta,\beta,p,m,n} \frac{\langle jp||i\delta\rangle\langle\delta\beta||mn\rangle\langle mn||p\beta\rangle}{(\varepsilon_\delta - \varepsilon_p)(\varepsilon_\delta + \varepsilon_\beta - \varepsilon_m - \varepsilon_n)} + \sum_{\delta,\beta,p,m,n} \frac{\langle j\delta||ip\rangle\langle p\beta||mn\rangle\langle mn||\delta\beta\rangle}{(\varepsilon_\delta - \varepsilon_p)(\varepsilon_\delta + \varepsilon_\beta - \varepsilon_m - \varepsilon_n)}$$

[3] See Ref. [6k].

$$+\sum_{\delta,\alpha,\beta,p,n}\frac{\langle jp||i\delta\rangle\langle\delta n||\beta\alpha\rangle\langle\alpha\beta||pn\rangle}{(\varepsilon_\delta-\varepsilon_p)(\varepsilon_\alpha+\varepsilon_\beta-\varepsilon_p-\varepsilon_n)}$$

$$+\sum_{\delta,\alpha,\beta,p,n}\frac{\langle j\delta||ip\rangle\langle\delta n||\beta\alpha\rangle\langle\alpha\beta||pn\rangle}{(\varepsilon_\delta-\varepsilon_p)(\varepsilon_\alpha+\varepsilon_\beta-\varepsilon_p-\varepsilon_n)}. \tag{26}$$

The energy denominators appearing in the H_{ij} matrix elements are

$$E_\alpha^{mn}=\varepsilon_m+\varepsilon_n-\varepsilon_\alpha-\langle\alpha m|\alpha m\rangle-\langle\alpha n|\alpha n\rangle+\langle mn|mn\rangle, \tag{27}$$

$$E_{\delta\gamma}^{p}=\varepsilon_p-\varepsilon_\delta-\varepsilon_\gamma-\langle\delta p|\delta p\rangle-\langle\gamma p|\gamma p\rangle+\langle\delta\gamma|\delta\gamma\rangle. \tag{28}$$

Finally, the F quantities appearing above are given as

$$F_{kl}=\sum_{\alpha<\beta,\ p}\left[K_{\alpha\beta}^{pk}K_{\alpha\beta}^{pl}+K_{\alpha\beta}^{kp}K_{\alpha\beta}^{lp}\right]-\sum_{p<q,\ \alpha}\left[K_{\alpha l}^{pq}K_{\alpha k}^{pq}+K_{l\alpha}^{pq}K_{k\alpha}^{pq}\right] \tag{29}$$

where

$$K_{\alpha\beta}^{(pq)}=K_{\alpha\beta}^{pq}-K_{\alpha\beta}^{qp}, \tag{30}$$

$$K_{(\alpha\beta)}^{pq}=K_{\alpha\beta}^{pq}-K_{\beta\alpha}^{pq}, \tag{31}$$

$$K_{(\alpha\beta)}^{(pq)}=K_{\alpha\beta}^{pq}-K_{\alpha\beta}^{qp}-K_{\beta\alpha}^{pq}+K_{\beta\alpha}^{qp}, \tag{32}$$

and the latter quantities are the MP expansion coefficients of the first-order wave function:

$$K_{\alpha\beta}^{mn}=\frac{\langle mn|\alpha\beta\rangle}{\varepsilon_\alpha+\varepsilon_\beta-\varepsilon_m-\varepsilon_n}. \tag{33}$$

Although more complicated than their second-order counterparts, the basic structure of the above expressions for $H_{i,j}(E)$ are the same as those shown earlier.

These third-order equations have been used in many applications in which molecular EAs have been computed for a wide variety of species as illustrated in Refs. [14]. Clearly, all of the quantities needed to form the second- or third-order EOM matrix elements $H_{j,k}$ are ultimately expressed in terms of the orbital energies $\{\varepsilon_k\}$ and two-electron integrals $\langle j,k|l,h\rangle$ evaluated in the basis of the neutral molecule's Hartree–Fock orbitals that form the starting point of the Møller–Plesset theory. However, as with most electronic structure theories, much effort has been devoted to recasting the working EOM equations in a manner that involves the atomic-orbital (AO) two-electron integrals rather than the molecular-orbital based integrals. Because such technical matters of direct AO-driven calculations are outside the scope of this work, we will not delve into them further here although we note that J. Oddershede [15] and our group looked into how to express EOM-type calculations in the AO basis.

3.2. Relationship to Greens functions/propagators

It turns out that in the early 1970s when we were developing and implementing the EOM method for treating EAs and IPs, several groups had taken a different approach to the evaluation of atomic and molecular electronic energy differences using what were called Greens

functions (GF) or propagators. Linderberg and Öhrn pioneered[4] the use of such methods in quantum chemistry, while Cederbaum and co-workers [16], Reinhardt and Doll [17], Taylor, Yaris, and co-workers [18] and Pickup and Goscinski [19] were among the first to apply the methods to EAs and IPs using an *ab initio* approach. Purvis and Öhrn [20] soon thereafter expanded the range of the theory to include open-shell systems. These workers as well as Jørgensen and Oddershede [21] and others [22] developed Møller–Plesset based GFs for evaluating electronic excitation energies but we will not discuss these developments further here because our emphasis is on IPs and EAs.

The GF EA and IP theories were derived from consideration of the following time-dependent matrix elements:

$$G_{j,k}(t) = (1/\mathrm{i}\hbar)\Theta(t)\langle 0, N|\exp(\mathrm{i}Ht/\hbar)j^{+}\exp(-\mathrm{i}Ht/\hbar)k|0, N\rangle + (1/\mathrm{i}\hbar)\Theta(-t)\langle 0, N|k\exp(\mathrm{i}Ht/\hbar)j^{+}\exp(-\mathrm{i}Ht/\hbar)|0, N\rangle. \quad (34)$$

Here, $\Theta(t)$ is the Heaviside step function, which equals unity when t is positive and zero when t is negative, j^{+} and k are the same creation and annihilation operators discussed earlier, and $|0, N\rangle$ is the neutral-molecule reference wave function. Introducing complete sets of $N-1$ and $N+1$ electron Hamiltonian eigenfunctions into the first and second terms in equation (34), it is straightforward to see that one observes time dependences varying as $\exp(\mathrm{i}[E(0, N) - E(K, N-1)]t/\hbar)$ and $\exp(\mathrm{i}[E(K, N+1) - E(0, N)]t/\hbar)$, respectively.

Taking the time derivative of equation (34), one obtains expressions involving commutators of the form $[H, j^{+}]k$ and $k[H, j^{+}]$ just as one finds in equation (14). By analyzing the resulting time-derivative equations, workers in this field were able to obtain equations that such $G_{j,k}(t)$ matrix elements obey (n.b., these were called the equations of motion for these quantities). The workers named above were able to express the resulting equations in terms of one-and two-electron integrals and corresponding density matrices much as the author had done within the EOM framework. In fact, it turned out that the final working equations of the so-called one-electron Greens function (GF) or electron propagator defined in equation (34), when Fourier transformed from the time to the energy domain, were exactly the same as the EOM equations given above (*i.e.*, equation (20) and those reproduced from Refs. [10].[5] However, only the Cederbaum group achieved the full third-order expressions within the GF framework analogous to what we reproduced above.

Especially in recent years, much of the work aimed at calculating EAs and IPs using these direct-calculation EOM and GF methods has been performed within the notation of Greens functions and has been carried out by Vince Ortiz's group [23] as well as by the Cederbaum group. The workers who pioneered GF theory have also shown that the residues (or eigenvectors, depending on how one solves the equations) also provide a wealth of information other than energy differences. To further illustrate the impact that such advances have had within the quantum chemistry community, we note that the Ortiz group has implemented various (*i.e.*, Møller–Plesset and other) variants of these theories within the highly successful Gaussian [24] suite of computer codes as a result of which many workers worldwide now employ EOM of GF-type methods to evaluate EAs and IPs.

[4] See Refs. [6l] and [6r].
[5] See Ref. [6k].

3.3. The natural orbital or extended Koopmans' theorem approach

In the mid 1970s, R.G. Parr and co-workers [25] and, independently, D. Smith and co-workers [26] proposed to use an equation such as equation (13) for computing IPs and they referred to these methods as natural orbital or extended Koopmans' theorem theories. Subsequently, E. Andersen and the author analyzed [27] the working equations of this approach through second and third order in the MP series and noted differences between them and the Greens function and equivalent EOM theories computed through these same orders. Of course, based on the discussion of Section 2. D, these differences relate to the ranks of the operators appearing in the working equations and are not surprising. More recently, Cioslowski and co-workers [28] have shown that these extended Koopmans' theorem approaches indeed offer a very efficient and reasonably accurate route to computing IPs or EAs, so it is likely that these methods will continue to develop. One of the more attractive aspects of the extended Koopmans approaches is that they have been shown [29] to be capable, at least in principle, to be able to yield the correct lowest ionization potential of a neutral molecule because they are capable of generating the proper asymptotic form for the density.

3.4. Multi-configuration based approximations

Following on the proof by R. Manne [13] that the operator spaces $\{T^+(l)\} = \{p^+;\ p^+q^+a,\ p^+q^+r^+ba,\ etc.\}$ and $\{T^+(l)\} = \{a^+, a^+b^+p, a^+b^+c^+qr,\ etc.\}$ can be used (*i.e.*, is capable of forming complete sets of ion states) even when no single determinant forms a dominant component of the neutral-molecule wave function $|0, N\rangle$, the author's group extended the combined EA and IP EOM theory to the case in which $|0, N\rangle$ is of an arbitrary multi-configuration self-consistent field (MC-SCF) form [30] and the ionization operator manifold $\{T^+(l)\}$ included operators of the form $\{p^+;\ p^+q^+a\}$ and $\{a^+, a^+b^+p\}$. The resultant working equations were written as in equation (19), with the $H_{j,k}$ matrix elements given in equations (18) of Ref. [30a], which we do not reproduce here because of their complexity. The primary additional difficulty involved in implementing these multi-configuration-based equations is the fact that three-electron density matrices $\langle 0, N|i^+j^+k^+lhn|0, N\rangle$ taken with respect to the MC-SCF wave function $|0, N\rangle$ are involved. These density matrices arise when the commutators $[H,\ p^+q^+a]$ and $[H, a^+b^+p]$ are evaluated.

To date, not much use has been made of the MC-SCF based EOM theories as developed in the author's group. Instead, the framework of time-dependent response theory, which can treat essentially any kind of reference wave function $|0, N\rangle$ including the MC-SCF variety, has superseded the EOM-based developments for such cases. It is important to keep in mind, however, that both the EOM and response function theories involve formulating and solving sets of equations whose solution (*i.e.*, the unknown energy) is an intensive energy.

3.5. Coupled-cluster based EOM

The use of coupled-cluster (CC) wave functions within EOM theory for excitation energies, IPs, and EAs has been developed [31,32] upon slightly different lines than outlined in Section 2. The CC wave function ansatz for $|0, N\rangle$ is written as usual in terms of an exponential

operator acting on a single-determinant (*e.g.*, unrestricted HF) "reference function" $|0\rangle$

$$|0, N\rangle = \exp(T)|0\rangle. \tag{35}$$

The so-called cluster operator T is expressed in terms of spin-orbital excitation operators of the form $\{T_1\} = \{p^+a\}$, $\{T_2\} = \{p^+q^+ba\}$, $\{T_4\} = \{p^+q^+r^+cba\}$, *etc.*, with T_k relating to the excitation of k electrons from occupied spin-orbitals (a, b, c, *etc.*) to virtual spin-orbitals (p, q, r, *etc.*). Prior to forming any EA EOM, the neutral-molecule CC equations need to be solved for the amplitudes $\{t_n\}$ that multiply the $\{T_n\}$ operators to form the CC T operator. For completeness, let us briefly review how the conventional CC wave function evaluation is carried out.

We recall the CC equations are formed by manipulating the Schrödinger equation

$$H\exp(T)|0\rangle = E\exp(T)|0\rangle \tag{36}$$

to read

$$\exp(-T)H\exp(T)|0\rangle = E|0\rangle \tag{37}$$

and subsequently projecting this equation against the set of functions $\{\langle 0|T_n^+\}$. Because the T operator contains only creation operators for unoccupied spin-orbitals and annihilation operators for occupied spin-orbitals, it turns out that the commutator expansion

$$\begin{aligned}\exp(-T)H\exp(T) = H - [T, H] + 1/2\big[T, [T, H]\big] - 1/3!\big[T, \big[T, [T, H]\big]\big] \\ + 1/4!\big[T, \big[T, \big[T, [T, H]\big]\big]\big] + \cdots\end{aligned} \tag{38}$$

exactly truncates at the fourth order term. So, the final working equations of CC theory can be written as

$$\begin{aligned}\langle 0|T_n^+\big\{H - [T, H] + 1/2\big[T, [T, H]\big] - 1/3!\big[T, \big[T, [T, H]\big]\big] \\ + 1/4!\big[T, \big[T, \big[T, [T, H]\big]\big]\big]\big\}|0\rangle = 0.\end{aligned} \tag{39}$$

Once the CC amplitudes $\{t_n\}$ are determined by solving these quartic equations, the CC energy is computed as

$$\begin{aligned}\langle 0|H - [T, H] + 1/2\big[T, [T, H]\big] - 1/3!\big[T, \big[T, [T, H]\big]\big] \\ + 1/4!\big[T, \big[T, \big[T, [T, H]\big]\big]\big]|0\rangle = E.\end{aligned} \tag{40}$$

The operator $Q^+(K)$ that maps the CC wave function $|0, N\rangle$ into an anion or cation state is expressed as in equation (7) with the $\{T^+(l)\}$ operators including, for example, $\{T^+(l)\} = \{p^+;\ p^+q^+a,\ p^+q^+r^+ba,\ etc.\}$ when EAs are to be computed and the adjoints of $\{a^+, a^+b^+p, a^+b^+c^+qr,\ etc.\}$ when IPs are computed. The basic EOM analogous to equation (10) is then written as

$$\big[H, Q^+(K)\big]\exp(T)|0\rangle = EQ^+(K)\exp(T)|0\rangle. \tag{41}$$

Multiplying on the left by $\exp(-T)$ and realizing that T and $Q^+(K)$ commute reduces this equation to

$$\big[H', Q^+(K)\big]|0\rangle = EQ^+(K)|0\rangle \tag{42}$$

where

$$H' = \exp(-T)H\exp(T), \tag{43}$$

which can be expanded as in equation (38) to involve at most quartic terms in the $\{t_n\}$ amplitudes. Then, multiplying on the left by $\langle 0|T(j)$ reduces the EOM equations to their final working form

$$\sum_l \langle 0|T(j)\big\{H - [T,H] + 1/2\big[T,[T,H]\big] - 1/3!\big[T,\big[T,[T,H]\big]\big] + 1/4!\big[T,\big[T,\big[T,[T,H]\big]\big]\big]\big\}, T^+(l)|0\rangle t(K,l) = E\sum_l \langle 0|T(j)T^+(l)|0\rangle t(K,l). \quad (44)$$

This set of matrix eigenvalue equations are then solved to obtain E which gives the EA or the IP (depending on what operator set was used). Such so-called electron-attached and electron-removed equations of motion (EA-EOM and IP-EOM) approaches have proven highly successful [31,32] in computing EAs and IPs of a wide range of atoms and molecules primarily because the coupled-cluster treatment of electron correlation provides such a highly accurate treatment of the dynamical electron correlation. At present there is a great deal of activity within this framework of utilizing EOM theories for computing EAs, IPs, and ΔEs.

4. SOME SPECIAL CASES

4.1. Calculating EAs as IPs

In this discussion, we have focused on computing EAs and IPs by forming a neutral-molecule wave function $|0, N\rangle$ and computing the EA or IP as an eigenvalue of an EOM matrix problem. Consider applying such an approach to evaluate the EA of the $X^2\Pi$ state of the NO molecule. Because the X-state wave function of NO is spatially degenerate (*i.e.*, the π_x and π_y orbitals should be degenerate), one may encounter artifactual symmetry breaking when forming this neutral-molecule wave function. That is, the π_x and π_y orbitals may not turn out to be degenerate; in fact, most commonly employed electronic structure codes are not able to guarantee this degeneracy as they should. It would then be unwise to use this symmetry-broken wave function to compute any property of this state of NO, including the EA. To overcome such difficulties, one could use the $X^3\Sigma^+$ state of NO^- as $|0, N\rangle$ and employ an EOM method to evaluate the IP of NO^- (actually the electron detachment energy of NO). The advantage to this approach is that the open-shell $^3\Sigma^+$ state of NO^- would not be susceptible to symmetry breaking because it is not spatially degenerate and has its π_x and π_y orbitals equivalently occupied. This example shows that it may sometimes be better to compute an EA of a molecule as the IP of the corresponding anion. Likewise, it may be better to compute an IP of a molecule as the EA of the molecule's cation in some cases.

4.2. Metastable anion states

A different kind of problem arises when one attempts to compute the EA of a molecule whose anion is not electronically bound relative to the corresponding neutral. For example,

the $X^1\Sigma_g^+$ state of the N_2 molecule does not bind an electron to form an electronically stable anion. Instead the $X^2\Pi_g$ state of N_2^-, formed by adding an electron to the π_g antibonding orbital of N_2 is a so-called resonance state that lies higher in energy than N_2 and can spontaneously eject its excess electron. One cannot simply employ conventional basis sets and *ab initio* electronic structure methods (including EOM or GF or response-function methods) to correctly determine the energies of such states.

The most common and powerful tool for studying such metastable states theoretically is the so-called stabilization method (SM). This method, pioneered by Professor Howard Taylor's group [33], involves embedding the system of interest (*e.g.*, the N_2^{-1} anion) within a finite "box" in order to convert the continuum of states corresponding, for example, to $N_2 + e^-$, into discrete states that can be handled by conventional square-integrable basis functions using, for example, the EOM method. By varying the size of the box, one can vary the energies of the discrete states that correspond to $N_2 + e^-$ (*i.e.*, one varies the box size to vary the kinetic energy KE of the orbitals containing the excess electron). As the box size is varied, one eventually notices (*e.g.*, by plotting the orbitals) that one of the $N_2 + e^-$ states obtained in the EOM process possesses a significant amount of valence character. That is, one such state has significant amplitude not only at large-r but also in the region of the two nitrogen centers. It is this state that corresponds to the metastable resonance state, and it is the EOM eigenvalue E of this state that provides the stabilization estimate of the resonance state energy relative to that of the neutral N_2.

Let us continue using N_2^{-1} as an example for how one usually varies the box within which the anion is constrained. One uses a conventional atomic orbital basis set that likely includes s and p functions on each N atom, perhaps some polarization d functions and some conventional diffuse s and p orbitals on each N atom. These basis orbitals serve primarily to describe the motions of the electrons within the usual valence regions of space. To this basis, one appends an extra set of diffuse π-symmetry orbitals. These orbitals could be p_π (and maybe d_π) functions centered on each nitrogen atom, or they could be d_π orbitals centered at the midpoint of the N–N bond. Either choice can be used because one only needs a basis capable of describing the large-r $L = 2$ character of the metastable $^2\Pi_g$ state's wave function. One usually would not add just one such function; rather several such functions, each with an orbital exponent α_J that characterizes its radial extent, would be used. Let us assume, for example, that K such additional diffuse π functions have been used.

Next, using the conventional atomic orbital basis as well as the K extra π basis functions, one carries out an EOM calculation for the EA of the N_2 molecule. In this calculation, one tabulates the energies of many (say M) of the EOM EA eigenvalues. One then scales the orbital exponents $\{\alpha_J\}$ of the K extra π basis orbitals by a factor $\eta : \alpha_J \rightarrow \eta\alpha_J$ and repeats the calculation of the energies of the M lowest EOM eigenvalues. This scaling causes the extra π basis orbitals to contract radially (if $\eta > 1$) or to expand radially (if $\eta < 1$). It is this basis orbital expansion and contraction that produces expansion and contraction of the "box" discussed above. That is, one does not employ a box directly; instead, one varies the radial extent of the more diffuse basis orbitals to simulate the box variation.

If the conventional orbital basis is adequate, one finds that the extra π orbitals, whose exponents are being scaled, do not affect appreciably the energy of the neutral N_2 system. This can be probed by plotting the N_2 energy (computed as $\langle 0, N|H|0, N\rangle$) as a function of the scaling parameter η; if the energy varies little with η, the conventional basis is adequate.

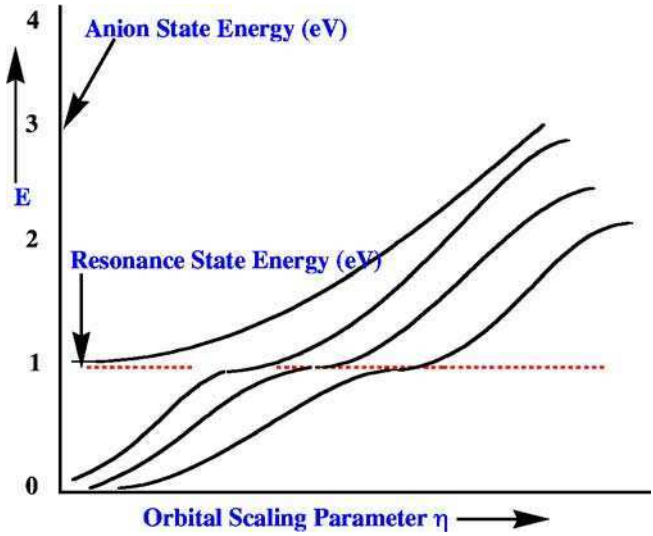

Fig. 1. Plots of the EOM EA eigenvalues for several anion states vs. the orbital scaling parameter η. Note the avoided crossing of state energies near 1 eV.

In contrast to plots of the neutral N_2 energy vs. η, plots of the energies of the MN_2^{-1} anion states relative to the energy of N_2, obtained as EOM eigenvalues, show significant η-dependence as Fig. 1 illustrates.

What does such a stabilization plot tell us and what do the various branches of the plot mean? First, we notice that each of the plots of the energy of an anion state (relative to the neutral molecule's energy, which is independent of η) grows with increasing η. This η-dependence arises from the η-scaling of the extra diffuse π basis orbitals. Because most of the amplitude of such basis orbitals lies outside the valence region, the kinetic energy is the dominant contributor to such states' relative energies. Because η enters into each orbital as $\exp(-\eta\alpha r^2)$, and because the kinetic energy operator involves the second derivative with respect to r, the kinetic energies of orbitals dominated by the diffuse π basis functions vary as η^2. It is this quadratic growth with η that appear as the basic trends in the energies vs. η plots in Fig. 1.

For small η, all of the π diffuse basis functions have their amplitudes concentrated at large r and have low kinetic energy. As η grows, these functions become more radially compact and their kinetic energies grow just as the particle-in-a-box energies grow as the box length decreases. For example, note the three lowest energies shown above in Fig. 1 increasing from near zero as η grows. As η further increases, one reaches a point at which the third and fourth anion-state energies in Fig. 1 undergo an avoided crossing. At higher η values, it is the second and third states and then the first and second states whose energies undergo such avoided crossings. At such η values, if one examines the nature of the two anion wave functions (obtained as in equation (6)) whose energies avoid one another, one finds they contain substantial amounts of both valence and extra diffuse π function character. Just to the left of the avoided crossing, the lower-energy state (the third state in Fig. 1 for the smallest η at which an avoided crossing occurs) contains predominantly extra diffuse π orbital character, while the higher-energy state (the fourth state) contains largely valence π^* orbital character. To the right of the avoided crossing, the situation is

reversed—the lower-energy state (the third state in Fig. 1 for small η) contains predominantly valence orbital character, while the higher-energy state (the fourth state) contains largely diffuse orbital character.

However, at the special values of η where the two states nearly cross, the kinetic energy of the diffuse state (as well as its radial size and de Broglie wavelength) are appropriate to connect properly with the valence state to form a single resonance state. By connect properly we mean that the two states have wave function amplitudes, phases, and slopes that match. It is such boundary condition matching of valence-range and long-range character in the wave function that the stabilization method achieves. So, at such special η values, one can achieve a description of the resonance state that correctly describes this state both in the valence region and in the large-r region. Only by tuning the energy of the large-r states using the η scaling can one obtain this proper boundary condition matching.

Another observation helps to understand the content of such stabilization plots. One considers the density of states (*i.e.*, how many states are there between energy E and $E + \mathrm{d}E$ for a fixed small value of $\mathrm{d}E$?) in a plot such as Fig. 1. Clearly, in the range of energies near the avoided crossings, there is an enhanced density of states, while the state density is lower at "off resonance" energies. When viewed either from the point of view of state densities or avoided crossings, there is something special about the region of energies near such resonances. As noted above, it is the fact that the valence-range and continuum components of the wave function can be properly matched at such energies that is "special".

If one attempts to study metastable anion states without carrying out such a stabilization study, one is doomed to failure, even if one employs an extremely large and flexible set of diffuse basis functions. In such a calculation, one will certainly obtain a large number of anion "states" with energies lying above that of the neutral, but one will not be able to select from these states the one that is the true resonance state because the true state will be buried in the myriad of "states" representing the $N_2 + e^-$ continuum.

In summary, by carrying out a series of anion-state energy calculations for several states and plotting them vs. η, one obtains a stabilization graph. By examining this graph and looking for avoided crossings, one can identify the energies at which metastable resonances occur. It is absolutely critical to identify these resonance energies if one wishes to probe metastable anions. It is also possible [34] to use the shapes (*i.e.*, the magnitude of the energy splitting between the two states and the slopes of the two avoiding curves) of the avoided crossings in a stabilization graph to compute the lifetimes of the metastable states. Basically, the larger the avoided-crossing energy splitting between the two states, the shorter is the lifetime of the resonance state.

5. SUMMARY

We have tried to illustrate how, by focusing on the intensive energies that one wishes to compute when studying EAs, IPs, or electronic excitation energies, one can replace the solution of the Schrödinger equation by the solution of so-called equations of motion. It is the eigenvalues of these EOMs that produce the EAs and IPs directly. We have reviewed some of the history of the development of EOM theory, especially as it applied to EAs and IPs, and we have attempted to show its relationships to Greens functions and extended Koopmans' theorem approaches to these same intensive energies. We have shown that a wide variety of EOM theories can be developed depending on how one chooses to describe

the neutral molecule's wave function (*i.e.*, in MP, MC-SCF, or CC fashion). Finally, we discussed some of the pitfalls that one encounters when applying EOM theory to EAs of molecules whose anion states are not bound but are metastable resonance states. It is our hope and belief that EOM methods have proven useful computationally and for gaining insight and will continue to have a bright future.

Readers who wish to learn more about how molecular EAs (and to a lesser extent, IPs) have been studied theoretically are directed to this author's web site http://simons.hec.utah.edu as well as to a series [35] of his reviews and chapters. The species that this group have examined include dipole-bound anions, zwitterion ions, conventional valence anions, multiply charged anions, as well as a wide variety of metastable anions.

ACKNOWLEDGEMENTS

This work was supported by NSF grants #9982420 and #0240387 and by years of close friendship and collaboration with Poul Jørgensen and Jan Linderberg.

REFERENCES

[1] J.C. Rienstra-Kiracofe, G.S. Tschumper, H.F. Schaefer III, S. Nandi, G.B. Ellison, *Acc. Chem. Res.* **102** (2002) 231–282.

[2] G. Herzberg, *Molecular Spectra and Molecular Structure I*, Van Nostrand, New York, 1950, p. 512.

[3] (a) G.I. Gutsev, A.I. Boldyrev, The theoretical investigation of the electron affinity of chemical compounds, *Adv. Chem. Phys.* **61** (1985) 169–221;
(b) J. Baker, R.H. Nobes, L. Radom, The evaluation of molecular electron affinities, *J. Comp. Chem.* **7** (1986) 349–358;
(c) J. Simons, K.D. Jordan, *Ab initio* electronic structure of anions, *Chem. Rev.* **87** (1987) 535–555;
(d) J. Kalcher, A.F. Sax, Gas phase stabilities of small anions—theory and experiment in cooperation, *Chem. Rev.* **94** (1994) 2291–2318;
J. Kalcher, Gas-phase stabilities of small anions, *J. Ann. Reports, Sec. C, Royal Soc. of Chem.* **93** (1996) 147–186;
(e) R.S. Berry, Small free negative ion, *Chem. Rev.* **69** (1969) 533–542.
The most up to date overview is given in Ref. [1].

[4] See Ref. [3e] and references contained therein. Some of the earlier successes are given in the following:
(a) E. Clementi, A.D. McLean, *Phys. Rev. A* **133** (1964) 419;
E. Clementi, A.D. McLean, D.L. Raimondi, M. Yoshimine, *Phys. Rev. A* **133** (1964) 1274;
E. Clementi, *Phys. Rev. A* **135** (1964) 980;
(b) C.L. Pekeris, *Phys. Rev.* **112** (1958) 1649;
(c) A.W. Weiss, *Phys. Rev.* **166** (1968) 70;
(d) P.E. Cade, *J. Chem. Phys.* **47** (1967) 2390;
P.E. Cade, *Proc. R. Soc. A* **91** (1967) 842;
(e) S. Taylor, F.E. Harris, *J. Chem. Phys.* **39** (1963) 1012;
(f) V. Bondybey, P.K. Pearson, H.F. Schaefer, *J. Chem. Phys.* **S7** (1972) 1123;
(g) D. Feller, E.R. Davidson, The electron affinity of oxygen: A systematic configuration interaction approach, *J. Chem. Phys.* **90** (1989) 1024;
D. Feller, E.R. Davidson, *Ab initio* multireference CI determination of the electron affinity of carbon and oxygen, *J. Chem. Phys.* **82** (1985) 1024;
In addition to Ref. [1], good sources for EA and IP data include:
(h) H. Hotop, W.C. Lineberger, Binding energies in atomic negative ions, *J. Phys. Chem. Ref. Data* **4** (1975) 539–576;
H. Hotop, W.C. Lineberger, Binding energies in atomic negative ions: II, *J. Phys. Chem. Ref. Data* **14** (1985) 731–750;

(i) T. Andersen, H.K. Haugen, H. Hotop, Binding energies in atomic negative ions, *J. Phys. Chem. Ref. Data* **28** (1999) 1511–1533;
(j) B.K. Janousek, J.I. Brauman, in: M.T. Bowers (Ed.), *Electron Affinities in Gas Phase Ion Chemistry*, vol. 2, Academic Press, New York, 1979, pp. 53–86;
(k) T.M. Miller, Electron affinities, in: R.C. West, M.J. Astle, W.H. Beyer (Eds.), *CRC Handbook of Chemistry and Physics*, seventy-fourth ed., CRC Press, Boca Raton, FL, 1993, pp. 10-180–10-191;
(l) J.E. Bartmess, Negative Ion Energetics Data in NIST Chemistry Web-Book, in: W.G. Ballard, P.J. Linstrom (Eds.), *NIST Standard Reference Database Number 69*, National Institute of Standards and Technology, Gaithersburg, MD, February, 2000; http://webbook.nist.gov;
(m) J.L. Franklin, J.G. Dillard, F.H. Field, Ionization potentials, appearance potentials, and heats of formation of gaseous positive ions, *Nat. Stand. Ref. Data Ser. Nat. Bur. Stand. (U.S.)* **26** (1969).

[5] Much of what is presently known about atomic and molecular EAs can be found in Refs. [3] and [4] as well as in the following:
(a) G.I. Gutsev, A.I. Boldyrev, The theoretical investigation of the electron affinity of chemical compounds, *Adv. Chem. Phys.* **61** (1985) 169–221;
(b) J. Baker, R.H. Nobes, L. Radom, The evaluation of molecular electron affinities, *J. Comp. Chem.* **7** (1986) 349–358;
(c) J. Simons, K.D. Jordan, *Ab initio* electronic structure of anions, *Chem. Rev.* **87** (1987) 535–555;
(d) J. Kalcher, A.F. Sax, Gas phase stabilities of small anions—theory and experiment in cooperation, *Chem. Rev.* **94** (1994) 2291–2318;
J. Kalcher, Gas-phase stabilities of small anions, *J. Ann. Reports, Sec. C, Royal Soc. of Chem.* **93** (1996) 147–186;
(e) R.S. Berry, Small free negative ion, *Chem. Rev.* **69** (1969) 533–542;
(f) H. Massey, *Negative Ions*, Cambridge Univ. Press, Cambridge, UK, 1976;
(g) L.M. Branscomb, in: D.R. Bates (Ed.), *Atomic and Molecular Processes*, Academic Press, New York, 1962.

[6] Some of the early chemistry developments of Greens functions include:
(a) O. Goscinski, B. Lukman, *Chem. Phys. Lett.* **6** (1970) 573;
(b) P. Jørgensen, J. Oddershede, *J. Chem. Phys.* **57** (1972) 277;
(c) J. Linderberg, P. Jørgensen, J. Oddershede, M. Ratner, *J. Chem. Phys.* **56** (1972) 6213;
(d) G. Csanak, H.S. Taylor, R. Yaris, *Phys. Rev. A* **3** (1971) 6213;
G. Csanak, H.S. Taylor, R. Yaris, *Adv. At. Mol. Phys.* **7** (1971) 288;
(e) J. Linderberg, Y. Öhrn, *J. Chem. Phys.* **49** (1968) 716;
J. Linderberg, Y. Öhrn, *Chem. Phys. Lett.* **1** (1967) 295;
J. Linderberg, Y. Öhrn, *Proc. R. Soc. A* **185** (1963) 445;
J. Linderberg, Y. Öhrn, *Phys. Rev. A* **139** (1965) 1063;
(f) J. Linderberg, M. Ratner, *Chem. Phys. Lett.* **6** (1970) 37;
(g) J. Linderberg, E.W. Thulstrup, *J. Chem. Phys.* **49** (1968) 710;
(h) W.P. Reinhardt, J.D. Doll, *J. Chem. Phys.* **50** (1969) 2767;
(i) B. Schneider, H.S. Taylor, R. Yaris, *Phys. Rev. A I* (1970) 855;
(j) J.D. Doll, W.P. Reinhardt, *J. Chem. Phys.* **57** (1972) 1169;
(k) P. Jørgensen, J. Simons, A complete treatment of the electron propagator through third order, *J. Chem. Phys.* **63** (1975) 5302;
(l) J. Linderberg, Y. Öhrn, *Propagators in Quantum Chemistry*, Academic Press, London, 1973;
(m) L.S. Cederbaum, G. Holneicher, S. Peyerimhoff, *Chem. Phys. Lett.* **11** (1971) 421;
L.S. Cederbaum, G. Holneicher, W. von Niessen, *Chem. Phys. Lett.* **18** (1973) 503;
L.S. Cederbaum, *Theo. Chim. Acta* **31** (1973) 239;
(n) B.S. Yarlagadda, Gy. Csanak, H.S. Taylor, B. Schneider, R. Yaris, *Phys. Rev. A* **7** (1973) 146;
(o) B.T. Pickup, O. Goscinski, *Mol. Phys.* **36** (1973) 1013;
(p) G.D. Purvis, Y. Öhrn, *J. Chem. Phys.* **60** (1974) 4063;
G.D. Purvis, Y. Öhrn, *J. Chem. Phys.* **62** (1975) 2045;
G.D. Purvis, Y. Öhrn, *Int. J. Quantum Chem. S* **11** (1977) 359;
(q) For a more recent overview, see J.V. Ortiz, J. Leszczynski (Eds.), *Computational Chemistry: Reviews of Current Trends*, vol. 2, World Scientific, Singapore, 1997, pp. 1–61;
(r) G.D. Purvis, Y. Öhrn, *Int. J. Quantum Chem. S* **11** (1977) 359.

[7] A good overview of time-dependent response function theory, including linear and non-linear response functions is offered in: J. Olsen, P. Jørgensen, Time-dependent response theory with applications to self-consistent field and multiconfigurational self-consistent field wave functions, in: D. Yarkony (Ed.), *Modern Electronic Structure Theory*, World Scientific, Singapore, 1995, pp. 857–990.
[8] T.H. Dunning, V. McKoy, *J. Chem. Phys.* **47** (1967) 1735;
T.H. Dunning, V. McKoy, *J. Chem. Phys.* **48** (1968) 5263;
T.I. Shibuya, V. McKoy, *J. Chem. Phys.* **53** (1970) 2208.
[9] D.J. Rowe, *Rev. Mod. Phys.* **40** (1968) 153;
D.J. Rowe, *Nuclear Collective Motion—Models and Theory*, Methuen, and Co., London, 1970.
[10] J. Simons, W.D. Smith, Theory of electron affinities of small molecules, *J. Chem. Phys.* **58** (1973) 4899;
This work exploited developments made earlier in studies of excited electronic states and reduced density matrices:
J. Simons, Direct calculation of first- and second-order density matrices. The higher RPA method, *J. Chem. Phys.* **55** (1971) 1218–1230;
J. Simons, Energy-shift theory of low-lying excited electronic states of molecules, *J. Chem. Phys.* **57** (1972) 3787–3792.
[11] J. Simons, P. Jørgensen, *J. Chem. Phys.* **64** (1976) 1413;
T.-T. Chen, J. Simons, K.D. Jordan, *Chem. Phys.* **14** (1976) 145;
J. Simons, *J. Chem. Phys.* **64** (1976) 4541;
J. Simons, *Int. J. Quantum Chem.* **XII** (1977) 227;
E. Dalgaard, J. Simons, *J. Phys. B: Atom. Molec. Phys.* **10** (1977) 2767;
J. Simons, *Ann. Rev. Phys. Chem.* **28** (1977) 15;
A. Banerjee, R. Shepard, J. Simons, *Int. J. Quantum Chem.: Quantum Chemistry Symposium* **12** (1978) 389;
R.A. Donnelly, J. Simons, *J. Chem. Phys.* **73** (1980) 2858.
[12] See, for example, P. Jørgensen, J. Simons, *Second Quantization-Based Methods in Quantum Chemistry*, Academic Press, San Diego, CA, 1981, or
T. Helgaker, P. Jørgensen, J. Olsen, *Modern Electronic Structure Theory*, Wiley, New York, 2000.
[13] R. Manne, *Chem. Phys. Lett.* **45** (1977) 470.
[14] J. Simons, T.-T. Chen, W.D. Smith, *Chem. Phys. Lett.* **26** (1974) 296;
W.D. Smith, T.-T. Chen, J. Simons, *Chem. Phys. Lett.* **27** (1974) 499;
K.M. Griffing, J. Simons, *J. Chem. Phys.* **62** (1975) 535;
J. Kenney, J. Simons, *J. Chem. Phys.* **62** (1975) 592;
K. Griffing, J. Kenney, J. Simons, K. Jordan, *J. Chem. Phys.* **63** (1975) 4073;
K. Griffing, J. Simons, *J. Chem. Phys.* **64** (1976) 3610;
K.D. Jordan, K.M. Griffing, J. Kenney, E.L. Andersen, J. Simons, *J. Chem. Phys.* **64** (1976) 4730;
E. Andersen, J. Simons, *J. Chem. Phys.* **64** (1976) 4548;
K.D. Jordan, J. Simons, *J. Chem. Phys.* **65** (1976) 1601;
E. Andersen, J. Simons, *J. Chem. Phys.* **65** (1976) 5393;
E. Andersen, J. Simons, *J. Chem. Phys.* **66** (1977) 2427;
J. Simons, *Ann. Rev. Phys. Chem.* **28** (1977) 15.
[15] M. Feyereisen, J. Nichols, J. Oddershede, J. Simons, *J. Chem. Phys.* **96** (1992) 2978–2987.
[16] L.S. Cederbaum, G. Holneicher, S. Peyerimhoff, *Chem. Phys. Lett.* **11** (1971) 421;
L.S. Cederbaum, G. Holneicher, W. von Niessen, *Chem. Phys. Lett.* **18** (1973) 503;
L.S. Cederbaum, *Theo. Chim. Acta* **31** (1973) 239.
[17] J.D. Doll, W.P. Reinhardt, *J. Chem. Phys.* **67** (1972) 1169.
[18] B.S. Yarlagadda, Gy. Csanak, H.S. Taylor, B. Schneider, R. Yaris, *Phys. Rev. A* **7** (1973) 146.
[19] B.T. Pickup, O. Goscinski, *Mol. Phys.* **36** (1973) 1013.
[20] G.D. Purvis, Y. Öhrn, *J. Chem. Phys.* **60** (1974) 4063;
G.D. Purvis, Y. Öhrn, *J. Chem. Phys.* **62** (1975) 2045.
[21] P. Jorgensen, J. Oddershede, *J. Chem. Phys.* **57** (1972) 277.
[22] J. Linderberg, P. Jørgensen, J. Oddershede, M. Ratner, *J. Chem. Phys.* **56** (1972) 6213;
J. Linderberg, Y. Öhrn, *J. Chem. Phys.* **49** (1968) 716;
J. Linderberg, Y. Öhrn, *Chem. Phys. Lett.* **1** (1967) 295;
J. Linderberg, Y. Öhrn, *Proc. R. Soc. A* **185** (1963) 445;
J. Linderberg, Y. Öhrn, *Phys. Rev. A* **139** (1965) 1063;
J. Linderberg, M. Ratner, *Chem. Phys. Lett.* **6** (1970) 37;
J. Linderberg, E.W. Thulstrup, *J. Chem. Phys.* **49** (1968) 710.

[23] See, for example, J.V. Ortiz, J. Leszczynski (Eds.), *Computational Chemistry: Reviews of Current Trends*, vol. 2, Singapore, World Scientific, 1997, pp. 1–61.

[24] M.J. Frisch, G.W. Trucks, H.B. Schlegel, G.E. Scuseria, M.A. Robb, J.R. Cheeseman, J.A. Montgomery Jr., T. Vreven, K.N. Kudin, J.C. Burant, J.M. Millam, S.S. Iyengar, J. Tomasi, V. Barone, B. Mennucci, M. Cossi, G. Scalmani, N. Rega, G.A. Petersson, H. Nakatsuji, M. Hada, M. Ehara, K. Toyota, R. Fukuda, J. Hasegawa, M. Ishida, T. Nakajima, Y. Honda, O. Kitao, H. Nakai, M. Klene, X. Li, J.E. Knox, H.P. Hratchian, J.B. Cross, C. Adamo, J. Jaramillo, R. Gomperts, R.E. Stratmann, O. Yazyev, A.J. Austin, R. Cammi, C. Pomelli, J.W. Ochterski, P.Y. Ayala, K. Morokuma, G.A. Voth, P. Salvador, J.J. Dannenberg, V.G. Zakrzewski, S. Dapprich, A.D. Daniels, M.C. Strain, O. Farkas, D.K. Malick, A.D. Rabuck, K. Raghavachari, J.B. Foresman, J.V. Ortiz, Q. Cui, A.G. Baboul, S. Clifford, J. Cioslowski, B.B. Stefanov, G. Liu, A. Liashenko, P. Piskorz, I. Komaromi, R.L. Martin, D.J. Fox, T. Keith, M.A. Al-Laham, C.Y. Peng, A. Nanayakkara, M. Challacombe, P.M.W. Gill, B. Johnson, W. Chen, M.W. Wong, C. Gonzalez, J.A. Pople, *Gaussian 03, Revision C.02*, Gaussian Inc., Wallingford, CT, 2004;
J.V. Ortiz, Toward an exact one-electron picture of chemical bonding, in: *Advances in Quantum Chemistry*, vol. 35, Academic Press, New York, 1999, pp. 33–52;
J.V. Ortiz, H.A. Kurtz (Eds.), *Propagating Insight: A Tribute to the Works of Yngve Öhrn*, *Advances in Quantum Chemistry*, vol. 35, Academic Press, New York, 1999.

[25] M.M. Morrel, R.G. Parr, M. Levy, *J. Chem. Phys.* **62** (1975) 549.

[26] O.W. Day, D.W. Smith, C. Garrod, *Int. J. Quantum Chem.* **S8** (1974) 501;
D.W. Smith, O.W. Day, *J. Chem. Phys.* **62** (1975) 113.

[27] E. Andersen, J. Simons, *J. Chem. Phys.* **66** (1977) 1067.

[28] J. Cioslowski, P. Piskorz, G. Liu, *J. Chem. Phys.* **107** (1997) 6804.

[29] J. Katriel, E.R. Davidson, Asymptotic behavior of atomic and molecular wave functions, *Proc. Natl. Acad. Sci.* **77** (1980) 4403.

[30] (a) A. Banerjee, R. Shepard, J. Simons, One-particle Green's function with multiconfiguration reference states, *Int. J. Quantum Chem.: Quantum Chemistry Symposium* **12** (1978) 389;
(b) D. Heryadi, D.L. Yeager, *J. Chem. Phys.* **114** (2001) 5124.

[31] Among the first workers to develop the requisite EOM machinery for a CC reference wave function was the following:
(a) H.J. Monkhorst, *Int. J. Quantum Chem. Symp.* **11** (1977) 421;
(b) The framework for applying EOM-CC theory to EAs was developed in: M. Nooijen, R.J. Bartlett, Equation-of-motion coupled-cluster method for electron attachment, *J. Chem. Phys.* **102** (1995) 3629;
The use of CC wave functions and EOM-type theories to compute excitation energies was advanced by:
(c) D. Mukhopadhyay, S. Mukhopadhyay, R. Chaudhuri, D. Mukherjee, Aspects of separability in the coupled cluster based direct method for energy differences, *Theor. Chim. Acta* **80** (1991) 441;
as well as:
(d) J.F. Stanton, R.J. Bartlett, The equation of motion coupled-cluster method. A systematic biorthogonal approach to molecular excitation energies, transition probabilities, and excited state properties, *J. Chem. Phys.* **98** (1993) 7029.

[32] A good overview is given in: R.J. Bartlett, J.F. Stanton, in: K.B. Lipkowitz, D.B. Boyd (Eds.), *Reviews in Computational Chemistry*, vol. 5, VCH, New York, 1994.

[33] A.U. Hazi, H.S. Taylor, *Phys. Rev. A* **1** (1970) 1109.

[34] J. Simons, *J. Chem. Phys.* **75** (1981) 2465;
R.F. Frey, J. Simons, *J. Chem. Phys.* **84** (1986) 4462.

[35] (a) J. Simons, P. Skurski, The roles of electrostatics in forming molecular anions and dianions, in: J. Kalcher (Ed.), *Recent Res. Devel. Phys. Chem., Theoretical Prospect of Negative Ions*, 2002, pp. 117–138;
(b) J. Simons, Encyclopedia of mass spectrometry: vol. 5. Theory and ion chemistry 2. Theory (energies and potential energy surfaces). Anions, 2002, pp. 55–68;
(c) M. Gutowski, P. Skurski, K.D. Jordan, J. Simons, Energies of dipole-bound anionic states, *Int. J. Quantum Chem.* **64** (1997) 183–191;
(d) J. Simons, Electron propagator studies of molecular anions, *Int. J. Quantum Chem. Symp.* **16** (1982) 575–581;
(e) J. Simons, Theoretical studies of negative molecular ions, in: *Theoretical Chemistry: Advances and Perspectives*, vol. 3, Academic Press, San Diego, CA, 1978;
(f) J. Simons, Theoretical studies of negative molecular ions, *Ann. Rev. Phys. Chem.* **28** (1977) 15–45;
(g) J. Simons, K.D. Jordan, *Ab initio* electronic structure of anions, *Chem. Rev.* **87** (1987) 535–555.

This page intentionally left blank

A Non-Iterative Numerical Solver of Poisson and Helmholtz Equations Using High-Order Finite-Element Functions

Raphael J.F. Berger and Dage Sundholm

Department of Chemistry, University of Helsinki, P.O. Box 55 (A.I. Virtanens Plats 1), FIN-00014 University of Helsinki, Finland

Abstract

A non-iterative finite-element solver for n-dimensional Poisson and Helmholtz equations has been developed. The electrostatic potential and the charge-density distributions are expanded in finite-element functions consisting of up to sixth-order Lagrange interpolation functions. The method can also be applied to differential equations in more than three-dimensional spaces. It is efficient and well suited for parallel computers, since the innermost loops constitute matrix multiplications and the outer ones can be used as parallelizing index on a parallel computer. The solution of the n-dimensional Poisson and Helmholtz equations scales as $N^{(\frac{n+1}{n})}$, where $N = N_i^n$ denotes the grid size and N_i is the number of element functions, *i.e.*, the number grid points, in each dimension.

Contents

1. INTRODUCTION

The electrostatic potential plays a fundamental role in many chemical, biological, and physical processes. It can be obtained analytically only for some simple model systems, and therefore its determination relies on numerical methods. The calculation of the electrostatic potential is formally straightforward, since the potential is generated as the integral

ADVANCES IN QUANTUM CHEMISTRY, VOLUME 50
ISSN: 0065-3276 DOI: 10.1016/S0065-3276(05)50011-X

of the reciprocal inter-particle distance, $|\mathbf{r}_1 - \mathbf{r}_2|^{-1}$, times a charge distribution. However, that approach is rarely used since it would involve a six-dimensional (6D) space with singularities at $\mathbf{r}_1 = \mathbf{r}_2$.

The preferred route to the electrostatic potentials is to solve the n-dimensional Poisson equation which is a second-order elliptical partial differential equation describing the electrostatic potential caused by a charge distribution [1,2]. Most relevant and challenging is the $n = 3$ case yielding the three-dimensional (3D) Poisson equation. The solution of the Poisson equation is a nontrivial task, since it involves large linear matrix equations with crucial system-specific boundary conditions. Owing to its scientific importance and challenge, lots of efforts have been put on the development of efficient methods to solve the Poisson equation [1–8]; hundreds of articles involving the solution of the Poisson equation appear every year, but also other approaches have been used for obtaining the electrostatic potential [8–14]. Many of these methods provide potentials of qualitative rather than quantitative accuracy. Efficient numerical methods to determine the electrostatic potential in chemical and biological systems have been developed and implemented in computer programs such as APBS [7,15], DelPhi [16], ITPACT [17], and Mainfold Code [18], to mention a few.

An equal important application of Poisson solvers is real-space computational methods for electronic structure calculations, the success of which completely relies on accurate solutions to the Poisson equation [1,19–23]. In each cycle of the self-consistent field optimization of the electronic structure, the electrostatic potentials caused by the electrons have to be determined with high accuracy. This is one of the most time-consuming steps in real-space computations especially when the Hartree–Fock exchange interaction is explicitly considered [19,24]. Accurate electrostatic potentials are also of importance in studies of semiconductor devices. For example, solutions to the Poisson equation are needed in real-space calculations on semiconductor structures and quantum dots. The electrostatic potentials can provide information about electron-transportation properties of quantum-dot systems, and physical insights into the single-electron charging processes are also obtained in this way [25,26].

In this work, a non-iterative approach to the solution of the Poisson equations in high-order finite-element bases is presented. The charge density and the potential are approximated by tensor-product finite-element functions which separates the equation. The solution to the 3D Poisson equation can be constructed from the solutions of three one-dimensional (1D) eigenvalue problems. Similar approaches have previously been used for solving two-dimensional (2D) and 3D elliptical differential equations using B-splines [6,27]. The first papers presenting direct numerical solutions of differential equations employing tensorial basis sets appeared about forty years ago [28–31]. Numerical approaches based on tensorial basis sets have more recently been employed in solution of Navier–Stokes equation [32] and they have proven to be very useful in the calculation of multi-dimensional integrals [33]. The tensor-product finite-element approach used for solving the Poisson equation can with tiny modifications be used for solving the Helmholtz equation, which is structurally reminiscent of the Poisson equation. It is appropriate to mention that the tensor-product approach has also been used to formulating efficient expressions to calculate second-order Møller–Plesset perturbation energy corrections using atomic orbital basis sets [34].

2. THEORY

2.1. The Poisson equation

The electrostatic potential for a given charge density $\rho(x, y, z)$ can be obtained by solving the Poisson equation. The 3D Poisson equation in Cartesian coordinates reads

$$\left(\frac{\partial^2}{\partial x^2} + \frac{\partial^2}{\partial x^2} + \frac{\partial^2}{\partial x^2}\right) V(x, y, z) = -4\pi\rho(x, y, z) \tag{1}$$

where $V(x, y, z)$ is the electrostatic potential created by the given charge-density distribution. Instead of solving the differential equation in equation (1), a corresponding equation yielding variational solutions to the Poisson equation can be obtained by constructing a functional F

$$F = \frac{1}{2}\int_{-\infty}^{\infty}\int_{-\infty}^{\infty}\int_{-\infty}^{\infty}\left(\frac{\partial V(x, y, z)}{\partial x}\right)^2 + \left(\frac{\partial V(x, y, z)}{\partial y}\right)^2 + \left(\frac{\partial V(x, y, z)}{\partial z}\right)^2 \mathrm{d}x\,\mathrm{d}y\,\mathrm{d}z$$
$$- 4\pi\int_{-\infty}^{\infty}\int_{-\infty}^{\infty}\int_{-\infty}^{\infty} V(x, y, z)\rho(x, y, z)\,\mathrm{d}x\,\mathrm{d}y\,\mathrm{d}z \tag{2}$$

the minimum of which yields an expression for the electrostatic potential involving symmetric matrices. The potential and the charge density in equation (2) are first expanded in a finite basis and then F is minimized with respect to the expansion coefficients of the potential. Here, it is assumed that the boundary terms, appearing due to the integration by parts, vanish. The electrostatic potential and the charge density are expanded in a finite-element tensorial basis set

$$V(x, y, z) = \sum_{\alpha\beta\gamma} v_{\alpha\beta\gamma}\chi_\alpha(x)\chi_\beta(y)\chi_\gamma(z) \tag{3}$$

and

$$\rho(x, y, z) = \sum_{\alpha\beta\gamma} r_{\alpha\beta\gamma}\chi_\alpha(x)\chi_\beta(y)\chi_\gamma(z) \tag{4}$$

where $\chi_\alpha(x)\chi_\beta(y)\chi_\gamma(z)$ are some locally defined basis functions. $v_{\alpha\beta\gamma}$ and $r_{\alpha\beta\gamma}$ are the expansion coefficients of the electrostatic potential and the charge density, respectively. The equation yielding the potential is obtained by minimizing F with respect to the expansion coefficients, $v_{\alpha\beta\gamma}$

$$\frac{\partial F}{\partial v_{\alpha\beta\gamma}} = 0. \tag{5}$$

2.2. The Helmholtz equation

The Helmholtz equation is structurally very similar to the Poisson equation. Compared to the Poisson equation an additional term proportional to k^2 appears in the Helmholtz equation, where k is a wave number. The solution of the Helmholtz equation, $\phi(x, y, z)$,

represents the spatial part of the solutions of the wave equation. Thus the right-hand side of the equation, $g(x, y, z)$ can be thought as a wave source. The 3D Helmholtz equation in Cartesian coordinates reads

$$-\left(\frac{\partial^2}{\partial x^2}+\frac{\partial^2}{\partial x^2}+\frac{\partial^2}{\partial x^2}\right)\phi(x, y, z)+k^2\phi(x, y, z)=g(x, y, z). \tag{6}$$

For real k values, the solutions are "bound", whereas imaginary k values correspond to plane waves when the source term in equation (6) is set to zero. For real k values, the Helmholtz operator is positively definite, whereas in the case of imaginary k it has both positive and negative eigenvalues which are often causing additional complications. A symmetric matrix expression for the Helmholtz equation can be obtained by applying the same variational approach as used in the case of the Poisson equation. Helmholtz equation has proven to be even more difficult to solve than the Poisson equation [35] and lots of effort has therefore been put on the development of efficient numerical methods to solve it [36,37].

2.3. The local basis functions

The use of a tensorial basis set reduces the complexity of the algorithm since it introduces a partial separation of the equations. This property of the present finite-element functions is explored in the computational algorithm and it is actually the key to the success of this approach. The computational method can be applied on equations with general source distributions, since the finite-element functions in each element are defined as a tensor product of the 1D components and element functions of different elements do not overlap.

The 1D components of the local tensorial basis set can consist of all kinds of basis functions. They can be different representations of polynomial functions, splines, wavelets, *etc*. In this work, the element functions in each element are constructed as an outer (tensor) product of Lagrange interpolation functions (LIF). In the LIF basis, the expansion coefficients are simply the amplitude of the potential and the charge density in the given grid points.

For simplicity, the space is in the present applications divided into a isotropic grid meaning that the same distribution of grid points is used in all dimensions. However, this is not necessary; different grids in all dimensions result in only a slight modification of the algorithm at almost no additional computational costs.

The expressions can be written in a more compact form by introducing vector and matrix notations. The expansion coefficients are collected in vectors such as $\mathbf{v}$ and $\mathbf{r}$ of the length $N = N_x \times N_y \times N_z$, where N_x, N_y and N_z are the number of grid points in the x, y, and z direction, respectively. Matrices of dimension $N \times N$ are denoted by bold capital letters ($\mathbf{S}$ and $\mathbf{A}$) and matrices with subscripts such as $\mathbf{S}_x$ ($\mathbf{A}_x$), $\mathbf{S}_y$ ($\mathbf{A}_y$), and $\mathbf{S}_z$ ($\mathbf{A}_z$) are of the size $N_x \times N_x$, $N_y \times N_y$, and $N_z \times N_z$, respectively.

2.4. The finite-element equations

The choice of a tensorial finite-element basis results in a separation of the overlap and Laplacian integrals. In this basis, the overlap matrix can be written as

$$\mathbf{S} = \mathbf{S}_x \otimes \mathbf{S}_y \otimes \mathbf{S}_z \tag{7}$$

where the matrix elements of the $\mathbf{S}_x$, $\mathbf{S}_y$, and $\mathbf{S}_z$ matrices are the overlap integrals of the element functions in each direction

$$S_x(\alpha,\alpha') = \int_{\Omega} \chi_\alpha(x)\chi_{\alpha'}(x)\,\mathrm{d}x,$$
$$S_y(\alpha,\alpha') = \int_{\Omega} \chi_\alpha(y)\chi_{\alpha'}(y)\,\mathrm{d}y,$$
$$S_z(\alpha,\alpha') = \int_{\Omega} \chi_\alpha(z)\chi_{\alpha'}(z)\,\mathrm{d}z. \tag{8}$$

Since element functions from different elements do not overlap, the $\mathbf{S}_i$ ($i = x, y, z$) matrices are sparse connected block-diagonal matrices. For an isotropic grid, the $\mathbf{S}_i$ matrices are identical.

The matrix elements of the 1D second-derivative matrices, $\mathbf{A}_x$, $\mathbf{A}_y$, and $\mathbf{A}_z$, needed for the construction of the 3D Laplacian can be obtained analogously

$$A_x(\alpha,\alpha') = \int_{\Omega} \frac{\partial\chi_\alpha(x)}{\partial x}\frac{\partial\chi_{\alpha'}(x)}{\partial x}\,\mathrm{d}x,$$
$$A_y(\alpha,\alpha') = \int_{\Omega} \frac{\partial\chi_\alpha(y)}{\partial y}\frac{\partial\chi_{\alpha'}(y)}{\partial y}\,\mathrm{d}y,$$
$$A_z(\alpha,\alpha') = \int_{\Omega} \frac{\partial\chi_\alpha(z)}{\partial z}\frac{\partial\chi_{\alpha'}(z)}{\partial z}\,\mathrm{d}z. \tag{9}$$

The element functions are defined only in one element, therefore the integration of the overlap and Laplacian integrals are performed only in the element domain Ω to which it belongs. Continuity conditions connect the functions in neighbor elements. The full 3D Laplacian can then be expressed using the three $\mathbf{S}_i$ and $\mathbf{A}_i$ matrices as

$$\mathbf{A} = \mathbf{A}_x \otimes \mathbf{S}_y \otimes \mathbf{S}_z + \mathbf{S}_x \otimes \mathbf{A}_y \otimes \mathbf{S}_z + \mathbf{S}_x \otimes \mathbf{S}_y \otimes \mathbf{A}_z \tag{10}$$

where $\otimes$ denotes the tensor (outer) product of the matrices. Analogously, the overlap matrix in 3D can be written as

$$\mathbf{S} = \mathbf{S}_x \otimes \mathbf{S}_y \otimes \mathbf{S}_z. \tag{11}$$

In the tensorial finite-element basis, the Poisson functional the minimum of which yields the equation for the potential is

$$F = \frac{1}{2}\mathbf{v}^T\mathbf{A}\mathbf{v} - \mathbf{v}^T\mathbf{S}\mathbf{r} \tag{12}$$

where the factor 4π has been incorporated into $\mathbf{r}$. Minimization of F yields the matrix equation

$$\mathbf{A}\mathbf{v} = \mathbf{S}\mathbf{r} \tag{13}$$

or

$$(\mathbf{A}_x \otimes \mathbf{S}_y \otimes \mathbf{S}_z + \mathbf{S}_x \otimes \mathbf{A}_y \otimes \mathbf{S}_z + \mathbf{S}_x \otimes \mathbf{S}_y \otimes \mathbf{A}_z)\mathbf{v} = (\mathbf{S}_x \otimes \mathbf{S}_y \otimes \mathbf{S}_z)\mathbf{r}. \tag{14}$$

The corresponding expression for the Helmholtz equation is

$$(\mathbf{A} + k^2\mathbf{S})\mathbf{f} = \mathbf{S}\mathbf{g} \tag{15}$$

or

$$\begin{aligned}(\mathbf{A}_x \otimes \mathbf{S}_y \otimes \mathbf{S}_z + \mathbf{S}_x \otimes \mathbf{A}_y \otimes \mathbf{S}_z + \mathbf{S}_x \otimes \mathbf{S}_y \otimes \mathbf{A}_z + k^2\mathbf{S}_x \otimes \mathbf{S}_y \otimes \mathbf{S}_z)\mathbf{f} \\ = (\mathbf{S}_x \otimes \mathbf{S}_y \otimes \mathbf{S}_z)\mathbf{g}.\end{aligned} \tag{16}$$

In the Poisson and Helmholtz equations, the matrix on the left-hand side, which is to be inverted, can thus be expressed as a sum of tensor products of the 1D $\mathbf{S}_i$ and $\mathbf{A}_i$ matrices. This implies that the spectral representation of the 3D matrices can be obtained by construction.

2.5. Construction of the spectral representation

The first step in the construction of the spectral representation of the $\mathbf{A}$ and $\mathbf{A} + k^2\mathbf{S}$ matrices is to solve the three generalized eigenvalue equations

$$\mathbf{A}_i\mathbf{q}_i = \mathbf{S}_i\mathbf{q}_i\mathbf{E}_i, \quad i = x, y, z. \tag{17}$$

The $\mathbf{A}_i$ and $\mathbf{S}_i$ matrices can then be expressed using the eigenvalues and the eigenvectors obtained by the diagonalization of equation (17) as

$$\mathbf{A}_i = \mathbf{w}_i\mathbf{E}_i\mathbf{w}_i^T, \quad \mathbf{S}_i = \mathbf{w}_i\mathbf{w}_i^T, \quad i = x, y, z, \tag{18}$$

where $\mathbf{w}_i^T$ denotes the inverse of the eigenvector matrices

$$\mathbf{w}_i^T = \mathbf{q}_i^{-1}, \quad i = x, y, z. \tag{19}$$

The inverse $\mathbf{A}_i$ matrices can analogously be written as

$$\mathbf{A}_i^{-1} = \mathbf{w}_i^{T^{-1}}\mathbf{E}_i^{-1}\mathbf{w}_i^{-1} = \mathbf{q}_i\mathbf{E}_i^{-1}\mathbf{q}_i^T, \quad i = x, y, z. \tag{20}$$

The eigenvalues, the eigenvector matrix, and the inverse of the eigenvector matrix for the 3D equation can be constructed as a tensor product of the 1D components as

$$\begin{aligned}\mathbf{E}_P &= \mathbf{E}_x \otimes \mathbf{I}_y \otimes \mathbf{I}_z + \mathbf{I}_x \otimes \mathbf{E}_y \otimes \mathbf{I}_z + \mathbf{I}_x \otimes \mathbf{I}_y \otimes \mathbf{E}_z, \\ \mathbf{Q} &= \mathbf{q}_x \otimes \mathbf{q}_y \otimes \mathbf{q}_z, \\ \mathbf{W} &= \mathbf{w}_x \otimes \mathbf{w}_y \otimes \mathbf{w}_z\end{aligned} \tag{21}$$

where $\mathbf{I}_x$ $\mathbf{I}_y$, and $\mathbf{I}_z$ are the 1D unit matrices for the x, y, and z directions, respectively. In the case of the Helmholtz equation, the $\mathbf{E}_H$ matrix will also contain contributions from the wave number term yielding

$$\mathbf{E}_H = \mathbf{E}_x \otimes \mathbf{I}_y \otimes \mathbf{I}_z + \mathbf{I}_x \otimes \mathbf{E}_y \otimes \mathbf{I}_z + \mathbf{I}_x \otimes \mathbf{I}_y \otimes \mathbf{E}_z + k^2\mathbf{I}_x \otimes \mathbf{I}_y \otimes \mathbf{I}_z, \tag{22}$$

$\mathbf{E}_P$ and $\mathbf{E}_H$ are the eigenvalues of the Poisson and Helmholtz operators in the spectral representation. The spectral representation of the 3D Poisson and Helmholtz matrices and

their inverses can now be written as

$$\mathbf{A}_P = \mathbf{W}\mathbf{E}_P\mathbf{W}^T, \qquad \mathbf{A}_P^{-1} = \mathbf{Q}\mathbf{E}_P^{-1}\mathbf{Q}^T,$$
$$\mathbf{A}_H = \mathbf{W}\mathbf{E}_H\mathbf{W}^T, \qquad \mathbf{A}_H^{-1} = \mathbf{Q}\mathbf{E}_H^{-1}\mathbf{Q}^T. \tag{23}$$

The inverse of the Laplacian and the Helmholtz matrices can thus be constructed from the eigenvalues and eigenvectors obtained by the diagonalization of the 1D generalized eigenvalue equations for each dimension. This implies that Poisson and Helmholtz equations in more than three dimensions can also be analogously solved by construction. The expansion parameters of the electrostatic potential are obtained as

$$\mathbf{v} = \mathbf{A}_P^{-1}\mathbf{S}\mathbf{r} \tag{24}$$

yielding

$$\mathbf{v} = \mathbf{Q}\mathbf{E}_P^{-1}\mathbf{Q}^T\mathbf{W}\mathbf{W}^T\mathbf{r}. \tag{25}$$

As seen in equations (19) and (21), the 3D matrix $\mathbf{Q}^T$ is the inverse of $\mathbf{W}$

$$\mathbf{Q}^T\mathbf{W} = \mathbf{I}. \tag{26}$$

Thus, two slightly different strategies to calculate the potentials can be used. In Algorithm 1, the expansion coefficients of the charge distribution are first multiplied by the overlap matrix. This operation can be made to scale linearly with the number of grid points since the overlap matrices in each dimension are band-diagonal matrices consisting of connected block matrices. The next step in the solution of the Poisson equation then includes a linear transformation with the $\mathbf{Q}^T$ matrix, multiplication with the inverse diagonal matrix $\mathbf{E}_P^{-1}$, and finally the back transformation with the $\mathbf{Q}$ matrix.

In Algorithm 2, we explore the identity in equation (26). This algorithm involves a linear transformation with the $\mathbf{W}^T$ matrix, multiplication with the inverse diagonal matrix $\mathbf{E}_P^{-1}$, and finally a back transformation with the $\mathbf{Q}$ matrix. The $\mathbf{W}^T$ matrix is constructed from the inverse of the eigenvectors $\mathbf{w}_i$; this strategy will also involve the calculation of the inverse of the eigenvectors of the 1D generalized eigenvalue problems.

The complete matrices in the 3D space are never constructed. The linear transformations are instead performed using a direct matrix-times-vector multiplication approach. Since the Laplacian is a semi-definite operator, the solution of the Poisson equation in a finite basis involves a singular matrix. However, in this direct approach the spectral representation is explicitly constructed and the zero eigenvalue is easily identified and can be removed.

3. BOUNDARY CONDITIONS

For a localized charge-density distribution, the electrostatic potential at the boundaries can be obtained using a multipole expansion. When the boundaries are far away from the charge-density distribution the first few terms in the multipole expansion is enough to give accurate potential values at the boundaries. Dirichlet boundary conditions can easily be incorporated in this approach by deleting the first and last column of either the $\mathbf{S}_i$ or the $\mathbf{A}_i$ matrices along with modifications of the right-hand side [6,27]. However, in the application examples of this work the right-hand side has been chosen such that the appropriate boundary conditions at large distances are automatically fulfilled due to symmetry reasons.

4. THE ALGORITHMS

4.1. The right-hand side

In finite-element approaches, the right-hand-side vector is constructed by multiplying the source term, *e.g.*, the charge-density distribution with the overlap matrix ($\mathbf{S} = \mathbf{S}_x \otimes \mathbf{S}_y \otimes \mathbf{S}_z$). The 1D $\mathbf{S}_i$ matrices are connected block diagonal matrices which means that the innermost loops can be rewritten as matrix multiplications of matrices the size of which is equal to the number of Lagrange interpolation functions of the 1D elements. Typical sizes for the diagonal block matrices are 5 or 7. Such an approach to construct the right-hand side scales linearly with the number of grid points. However, in the present implementation, it is assumed that the $\mathbf{S}_i$ matrices are dense. Then, the construction of the right-hand side consists of N_i sets of matrix multiplications whose size is N_i thus it scales as $N^{4/3}$, where N is the total number of grid points. The outermost index is not involved in the matrix multiplications and can be used as parallelization index on a parallel computer. The computational time needed for the construction of the right-hand-side vector is shown in Fig. 1.

In the test applications the source term has been taken to be

$$\rho(x, y, z) = xyz\left(6 + 4r^2\right)\mathrm{e}^{-r^2}, \quad r^2 = x^2 + y^2 + z^2. \tag{27}$$

In the Poisson case, we have assumed that the factor of 4π is incorporated in the charge density, since it does not appear in the Helmholtz equation. The equations are approximated in a cubic domain with boundaries at ± 10. The domain is in each dimension divided isotropically into a number of elements, and each 1D element contains 7 element functions; sixth-order LIF are used. A non-equidistant grid has been used. Each element is taken to be a factor of 1.3 longer that the previous one starting from the center of the box, whereas in each element the grid points are equidistant.

The precision of the method was checked by calculating the self-interaction integral as a function of the grid size for the charge density given in equation (27). The self-interaction

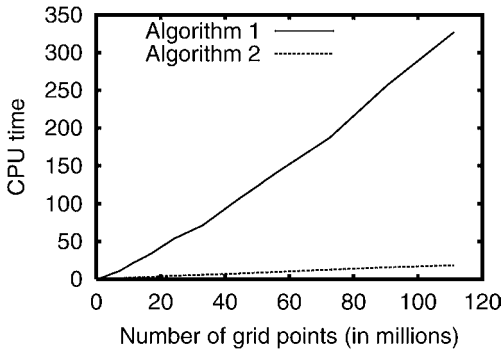

Fig. 1. The CPU time (in seconds) for constructing the right-hand side of the Poisson equation. The calculations have been performed using a DEC Alpha workstation equipped with a 600 MHz EV6 processor.

Table 1. The self-interaction integral, $(\rho|\rho)$ as a function of the grid size obtained by solving the Poisson equation ($k^2 = 0$) equation as well as the Helmholtz equation with $k^2 = \pm 1$

Grid	$k^2 = 0$	$k^2 = 1$	$k^2 = -1$
$25 \times 25 \times 25$	1.4374409362	1.1784597644	2.0889675911
$37 \times 37 \times 37$	1.3287968899	1.0842696689	1.9652547531
$49 \times 49 \times 49$	1.3315672651	1.0868529977	1.9676160263
$61 \times 61 \times 61$	1.3317110807	1.0869883397	1.9676210396
$73 \times 73 \times 73$	1.3314981186	1.0868078129	1.9673633520
$85 \times 85 \times 85$	1.3315254242	1.0868316094	1.9673914024
$97 \times 97 \times 97$	1.3315234616	1.0868293521	1.9673920879
$109 \times 109 \times 109$	1.3315223680	1.0868284706	1.9673907180
$121 \times 121 \times 121$	1.3315223246	1.0868284564	1.9673905408
$133 \times 133 \times 133$	1.3315223421	1.0868284711	1.9673905285
$145 \times 145 \times 145$	1.3315223475	1.0868284726	1.9673905301

integral is obtained as:

$$(\rho|\rho) = \int_{-\infty}^{\infty} \int_{-\infty}^{\infty} \int_{-\infty}^{\infty} \rho(x, y, z)\phi(x, y, z)\, \mathrm{d}x\, \mathrm{d}y\, \mathrm{d}z \tag{28}$$

where $\phi(x, y, z)$ is the solution of the Poisson equation for the source $\rho(x, y, z)$ given in equation (27). The same integral was calculated using the solutions of the Helmholtz equation with $k^2 = 1$ and $k^2 = -1$, respectively. As seen in Table 1, the integrals converge smoothly with increasing size of the grid. The difference between the integrals calculated using the 133^3 and 145^3 grids is a few part per billion (ppb).

4.2. The generalized eigenvalue problems

The initialization of the Poisson solver algorithms involves in the general case the solution of three generalized eigenvalue problems, whereas for an isotropic grid the eigenvalue equations are identical and only one of them has to be solved. The obtained eigenvectors $\mathbf{q}_i$ and eigenvalues $\mathbf{E}_i$ are used for the construction of the 3D spectral representation of the differential operators. The CPU time for the diagonalization of the generalized eigenvalue problem and the inversion of the eigenvector matrices scale as N_i^3, *i.e.*, linearly with the grid size. As seen in Fig. 2, for the largest grids less than 1% of CPU time is spent on the solution of the eigenvalue problem and the inversion of the eigenvector matrix is even faster. The multiplication with the 3D eigenvalue matrix scales also linearly with the grid size. These steps are not the rate-determining steps; only a few percent of the total CPU time is used in these parts of the algorithms.

4.3. Transformations using the 3D eigenvectors

The most time-consuming steps of both algorithms are the linear transformation and corresponding back transformation with the 3D eigenvectors constructed from the eigenvectors

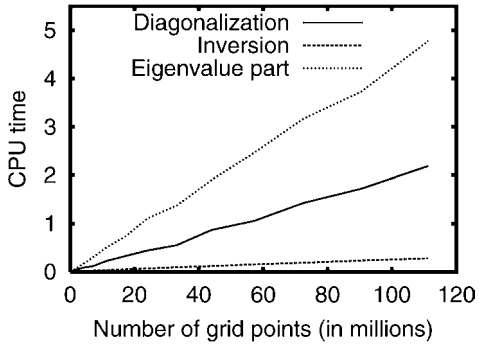

Fig. 2. The CPU time (in seconds) used for solving one generalized eigenvalue problem, for calculating the inverse of the eigenvector matrix, and for multiplying with the inverse of the diagonal 3D eigenvalue matrix.

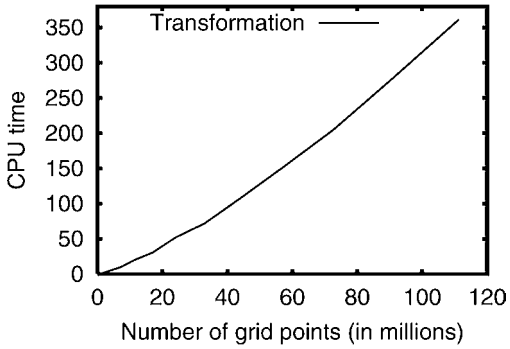

Fig. 3. The CPU time (in seconds) used for one linear transformation with the 3D (inverse) eigenvectors.

of the 1D eigenvalue problems. See Fig. 3. These transformations has to be repeated for each charge-density distribution. They scale as $N^{4/3}$ and become the bottleneck of the computation.

The linear transformation steps consist of three matrix multiplications of matrices the size of which is N_i. In the 3D case, the third index can be considered as an external index and used for distribution of the tasks over a number of parallel processors. The number of matrix multiplications is proportional to N_i which results in a scaling of $N^{4/3}$ for the CPU time.

5. SUMMARY

Depending on the strategy, two slightly different algorithms to solve the Poisson equation can be derived. By introducing some tiny modifications, they can also be applied on the Helmholtz equation. In the Helmholtz case, the wave number k^2 is added to the eigenvalues in the construction of the 3D eigenvalue matrix.

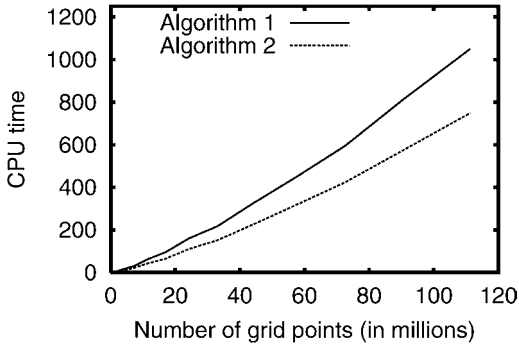

Fig. 4. The total CPU time (in seconds) for solving the Poisson equation in a cubic domain as a function of the number of grid points.

The diagonalization of the generalized eigenvalue problems in step 1 is done only once. Furthermore, for isotropic grids the three eigenvalue equations are identical. Only a few percent of the computational time is spent in this step. The calculation of the inverse eigenvectors in step 2 of Algorithm 2 is computationally fast in comparison with the linear transformations in steps 3 and 5.

In the present applications, Algorithm 2 is slightly faster than Algorithm 1 since the multiplication of the overlap matrix on the right-hand side vector is avoided. However, the comparison is not quite fair, since the computation of the overlap matrix times a vector can be made more efficient, scaling linearly with the grid size. The CPU time needed for solving the Poisson equation with the present implementation of the algorithms is compared in Fig. 4.

ALGORITHM 1.

1. Solve $\mathbf{A}_i\mathbf{q}_i = \mathbf{S}_i\mathbf{q}_i\mathbf{E}_i$, $i = x, y, z$.
2. Calculate right-hand side as $\mathbf{b} = \mathbf{S}\mathbf{r}$.
3. Perform the linear transformation $\mathbf{a} = \mathbf{Q}^T\mathbf{b}$.
4. Multiply with the inverse of the eigenvalue part $\mathbf{c} = \mathbf{E}_P^{-1}\mathbf{a}$.
5. Perform the back transformation $\mathbf{v} = \mathbf{Q}\mathbf{c}$.

ALGORITHM 2.

1. Solve $\mathbf{A}_i\mathbf{q}_i = \mathbf{S}_i\mathbf{q}_i\mathbf{E}_i$, $i = x, y, z$.
2. Calculate the inverse of the eigenvectors $\mathbf{w}_i^T = \mathbf{q}_i^{-1}$.
3. Perform the linear transformation $\mathbf{b} = \mathbf{W}^T\mathbf{r}$.
4. Multiply with the inverse of the eigenvalue part $\mathbf{c} = \mathbf{E}_P^{-1}\mathbf{b}$.
5. Perform the back transformation $\mathbf{v} = \mathbf{Q}\mathbf{c}$.

6. DISCUSSION

The present numerical method to solve the Poisson equation is efficient and scales almost linearly with increasing grid size. The tensorial basis-set method is also well suited for

solving differential equations in four and higher dimensional spaces. Multi-dimensional Poisson equations result in algorithms that are structurally similar to the 3D case, the main difference is that one in the linear transformation steps has to loop over indices representing all dimensions. The main bottleneck in the solution high-dimensional Poisson and Helmholtz equations is of course the amount of data; a six-dimensional (6D) space with 33 grid points in each direction corresponds to 20 GB data, whereas one linear transformation step would take about 15 minutes on the DEC Alpha workstation. Recent applications of the tensorial finite-element approach show that it is an efficient method to calculate multi-dimensional integrals [33,14].

ACKNOWLEDGEMENTS

We acknowledge support from the European research training network on "Molecular Properties and Molecular Materials" (MOLPROP), contract No. HPRN-2000-00013, and from The Academy of Finland, grants 53915, 200903, and 206102. We would also like to thank Magnus Ehrnrooths Foundation for their generous support.

REFERENCES

[1] T.L. Beck, *Rev. Mod. Phys.* **72** (2000) 1041.
[2] A. Castro, A. Rubio, M.J. Stott, *Can. J. Phys.* **81** (2003) 1151.
[3] A.A. Coelho, R.W. Cheary, *Comp. Phys. Commun.* **104** (1997) 15.
[4] S. Goedecker, O.V. Ivanov, *Solid State Commun.* **105** (1998) 665.
[5] R.D. Coalson, T.L. Beck, in: P. von Ragué Schleyer, *et al.* (Eds.), *Encyclopedia of Computational Chemistry*, vol. 3, Wiley, New York, 1998, p. 2086.
[6] L. Plagne, J.Y. Berthou, *J. Comput. Phys.* **157** (2000) 419.
[7] N.A. Baker, D. Sept, M.J. Holst, J.A. McCammon, *IBM J. Res. Dev.* **45** (2001) 427.
[8] W. Rocchia, E. Alexov, B. Honig, *J. Phys. Chem. B* **105** (2001) 6507.
[9] J.S. Murray, P. Politzer, in: P. von Ragué Schleyer, *et al.* (Eds.), *Encyclopedia of Computational Chemistry*, vol. 2, Wiley, New York, 1998, p. 912.
[10] M.E. Davis, J.A. McCammon, *Chem. Rev.* **90** (1990) 509.
[11] O. Engkvist, P.O. Åstrand, G. Karlström, *Chem. Rev.* **100** (2000) 4087.
[12] A. Gavezzotti, *J. Phys. Chem. B* **106** (2002) 4145.
[13] Y. Ma, P. Politzer, *J. Chem. Phys.* **120** (2004) 3152.
[14] D. Sundholm, *J. Chem. Phys.* **122** (2005) 194107.
[15] M.E. Davis, J.A. McCammon, *J. Comput. Chem.* **10** (1989) 386.
[16] A. Nicholls, B. Honig, *J. Comput. Chem.* **12** (1991) 435.
[17] C. Cortis, R. Friesner, *J. Comput. Chem.* **18** (1997) 1591.
[18] M. Holst, N. Baker, F. Wang, *J. Comput. Chem.* **21** (2000) 1319.
[19] J. Kobus, L. Laaksonen, D. Sundholm, *Comput. Phys. Commun.* **98** (1996) 346, http://scarecrow.1g.fi/num2d.html.
[20] S. Goedecker, *Rev. Mod. Phys.* **71** (1999) 1085.
[21] J.R. Chelikowsky, Y. Saad, S. Ogut, I. Vasiliev, A. Stathopoulos, *Phys. Status Solidi A* **217** (2000) 173.
[22] M. Heiskanen, T. Torsti, M.J. Puska, R.M. Nieminen, *Phys. Rev. B* **63** (2001) 245106.
[23] U.V. Wagmare, *et al.*, *Comput. Phys. Commun.* **137** (2001) 341.
[24] L. Laaksonen, P. Pyykkö, D. Sundholm, *Chem. Phys. Lett.* **96** (1983) 1.
[25] P. Matagne, J.P. Leburton, *Phys. Rev. B* **65** (2002) 235323.
[26] S. Bednarek, B. Szafran, K. Lis, J. Adamowski, *Phys. Rev. B* **68** (2003) 155303.
[27] L. Kaufman, D.D. Warner, *SIAM J. Numer. Anal.* **21** (1984) 672.
[28] R.E. Lynch, J.R. Rice, D.H. Thomas, *Numer. Math.* **6** (1964) 185.

[29] B.L. Buzbee, G.H. Golub, C.W. Nielson, *SIAM Numer. Anal.* **7** (1970) 627.
[30] R.E. Bank, *Numer. Math.* **31** (1978) 49.
[31] F.W. Dorr, *SIAM Rev.* **12** (1970) 315.
[32] G.H. Golub, L.C. Huang, H. Sinom, W.-P. Tang, *SIAM J. Sci. Comput.* **19** (1998) 1606.
[33] T. Gerstner, M. Griebel, *Computing* **71** (2003) 65.
[34] P.E. Maslen, M. Head-Gordon, *Chem. Phys. Lett.* **283** (1998) 102.
[35] O.C. Zienkiewicz, *Int. J. Num. Meth. Eng.* **47** (2000) 9.
[36] H.C. Elman, D.P. O'Leary, *J. Comput. Phys.* **142** (1998) 163.
[37] R. Kechroud, A. Soulaimani, Y. Saad, in: *Lecture Notes in Comput. Sci.*, Springer-Verlag, Heidelberg, 2003, pp. 847–858.

This page intentionally left blank

Some Trends in Relativistic and Electron Correlation Effects in Electric Properties of Small Molecules

M. Urban and V. Kellö

Department of Physical and Theoretical Chemistry, Faculty of Natural Sciences, Comenius University, Mlynská dolina, SK-842 15 Bratislava, Slovakia

Dedicated to Professor Jan Linderberg and to Professor Poul Jørgensen on the occasion of their birthday.

Abstract

Trends in the relativistic and electron correlation effects in properties of molecules containing a heavy metal element are discussed. Numerical results analyzed in this paper have been mostly obtained by the Douglas–Kroll–Hess quasi-relativistic approach combined with the Coupled Cluster method. We discuss dipole moments and static electric dipole polarizabilities of diatomic molecules, like fluorides of the Ia and Ib group elements (RbF, CsF, and FrF; CuF, AgF, and AuF), coinage–aluminium intermetallic molecules (CuAl, AgAl, and AuAl) and group IVa elements oxides (GeO, SnO, and PbO). Trends in each group of molecules were related to relativistic effects in the heavy metal element ionization potential, electron affinity and the dipole polarizability. The relativistic shrinking of the electron density is also considered. Related topics are the bond dissociation energies of selected diatomic molecules and interaction energies in $CuOH_2$, $AgOH_2$, $AuOH_2$, in $CuSH_2$, $AgSH_2$, $AuSH_2$ and in $CuNH_3$, $AgNH_3$ and $AuNH_3$. Interaction energies are interpreted in terms of the charge transfer mediated by the lone pair of the ligand. It is linked with relativistic increase of electron affinities of the coinage metal elements. Long-range terms are affected by relativistic changes of their polarizabilities and ionization potentials.

Contents

1. INTRODUCTION

It took nearly half a century to accept the fact, that the consequences of the relativistic theory are important in the physical and chemical behavior of atoms and molecules. Returning

ADVANCES IN QUANTUM CHEMISTRY, VOLUME 50
ISSN: 0065-3276 DOI: 10.1016/S0065-3276(05)50012-1

back to the history, one observes that Mendeleev did not succeed in placing a few elements on their proper positions in his original Periodic Table. Mendeleev's achievement was great in his ability to systematize and to generalize the accumulated knowledge and even to make predictions based on his periodic law. Using the present measures and terminology one would say that this was one of most spectacular achievements of the theory as we understand its mission now. Yet he has failed in some particular cases and it is not surprising that it concerns mostly heavy elements, like gold, thallium, mercury, lead. Really, the physical and chemical behavior of these and some other elements and their compounds are affected by relativistic effects to such extent that they show well-known irregularities within the series of elements belonging to the same group. Among those who were able to point out the importance of relativistic effects in molecular properties and in their chemical behavior is P. Pyykkö [1], and K. Pitzer [2]. Presently we know that essentially all elements and their compounds throughout the Periodic Table, starting from the hydrogen up to artificial superheavy elements are affected by relativistic contributions, depending on the particular molecular property and the accuracy needed for its description. Several excellent review articles describing the physical background, basic theoretical principles and most spectacular chemical consequences of relativistic effects have appeared [3–11]. Knowledge accumulated in atomic relativistic effects includes properties like ionization potentials, electron affinities, electric field gradients, static dipole polarizabilities, magnetic properties, *etc.*, and concern a variety of elements up to superheavy elements [8], see, *e.g.*, [12–16]. Irregularities of these properties within the group with the same valence electronic structure are attributed to relativistic effects. They are frequently large enough to change the monotonic trend at high atomic number Z. Relativistic effects reflect themselves in metal macroscopic properties like melting points, specific resistivity, thermal conductivity, electric resistance, *etc.*, and of course, in molecular properties.

Review articles on relativistic effects in molecular properties were primarily focused on equilibrium geometries, spectroscopic properties of molecules, dissociation and reaction energies. Much less attention was paid so far to the understanding of the general trends in molecular electric properties throughout the series of molecules that contain elements extending from the light up to heavy or even superheavy elements. Thus, the aim of this contribution is to summarize selected electric properties, mostly electric dipole moments and static dipole polarizabilities for the series of molecules. Our goal is the comparison of trends in molecular electric properties with trends observed before for properties of participating heavy elements and the understanding of these trends. Obviously, any peculiarities of the properties within the series of molecules are difficult to deduce just from the valence electronic structure. The understanding of relativistic effects in the series of molecules containing heavy elements thus gives more detailed and qualitatively more correct insight into their behavior in relation to their position in the Mendeleev Periodic Table [5]. We will also try to show that to relate the knowledge of relativistic changes of electric properties to the chemical reactivity and intermolecular interactions is a viable approach.

Another aim of the present work is to demonstrate the usefulness of theoretical methods as a tool for obtaining dipole moments, atomic and molecular polarizabilities and higher order properties, like hyperpolarizabilities. The importance of theoretical methods is continuously increasing and they serve presently as a real partner to experiment. We also note that experimental measurements occasionally face unexpected problems. This includes, for example, optical properties of inorganic molecules important in material chemistry which are often difficult to obtain experimentally [17].

Obviously, accurate description of molecular properties is inconceivable without considering the electron correlation effects [18]. This fact is generally better understood by the chemical audience than was the acceptance of the relativistic effects, even if the route to this cognition was not quite straightforward either. The Hartree–Fock (HF) orbital one electron picture has remained to be quite attractive for a long time, and, in fact, it may still be qualitatively useful in some simple cases. However, the HF orbital picture is not capable to provide results, which are accurate enough for analyzing even trends in molecular properties. Correspondingly we will pay attention to the simultaneous treatment of the electron correlation and relativistic effects.

2. BASIC METHODS FOR CORRELATED SCALAR RELATIVISTIC CALCULATIONS

Numerical results analyzed in this paper have been mostly obtained by the Douglas–Kroll–Hess (DK) [19] approach. DK method is a one-component quasi-relativistic approach and appears to be the most frequently used method for estimating the scalar relativistic effects. When combined with a suitable method for considering electron correlation effects it represents a very pragmatic and efficient tool for obtaining reliable results for properties of atoms and molecules containing heavy elements [13,20–22]. In the context of its application to molecular properties it deserves two notes. First, one has to keep in mind the change of picture effect [23,24], see also Refs. [25–27] in relation to calculations of electric properties. Fortunately enough, the picture change has negligible effect in calculations of the valence-determined properties, as it was demonstrated, *e.g.*, for dipole moments of the PbO molecule [28]. Second, the DK method appears to be extremely useful when spin-orbit (SO) effects play a limited role. This usually holds for closed shell molecules and some specific states, like, *e.g.*, $^2\Sigma$ molecular states. Using, again, the PbO molecule as an example the spin-orbit effects appear to be significant in its dipole moment at the orbital level. However, Dolg, Nicklass and Stoll [29] have found that the SO coupling is to the large extend quenched when the electron correlation is included. Only relatively small SO effect was observed by Mayer, Krüger and Rösch [30] in some other molecular properties, like the bond length and the harmonic frequency of PbO. Small effect of the SO coupling (SOC) was convincingly confirmed by Roos and Malmqvist [31]. Their Complete Active Space second-order perturbation calculations (CASPT2) with and without SOC have shown that the dipole moment of PbO is lowered by SOC by only 0.025 a.u. (1.14%) and the dipole polarizability by 0.16 a.u., *i.e.*, by 0.26%. Such SOC contributions can not affect our considerations about trends within selected atoms and molecules.

Results discussed in this paper follow from the DK approach in its standard second-order form. Extensions of the Foldy–Wouthuysen transformation on which the DK method is based are focused to the third order [32] and higher order DK approaches [33]. These efforts, pioneered by Hess, Hirao, Nakajima, Barysz, Sadlej, and their coworkers, also extend the one component DK approach to its two-component generalizations [34,35]. Applications to, *e.g.*, spectroscopic properties of SnO have shown [36] that higher order corrections to the second order Douglas–Kroll–Hess transformation has negligible effect.

The treatment of the electron correlation was in most cases performed by the single determinant reference Coupled Cluster CCSD and CCSD(T) methods. Single and double excitation amplitudes in CCSD are obtained iteratively, while triples in CCSD(T) are

obtained in a perturbative-like way using the converged single and double excitation amplitudes from CCSD [37,38]. When combined with the DK approach we use the notation DK–CCSD and DK–CCSD(T), respectively. Some caution in using CCSD(T) is needed when the system under investigation is not well represented by a single determinant reference [39,40]. The capability of CCSD(T) in calculations of electric properties of atoms and molecules was demonstrated in many previous papers and reviews [41–44]. We note that the full four-component CCSD(T) approach has been implemented by Visscher *et al.* [45].

An important step toward the accurate correlated description of electric and magnetic properties of molecules using the CC methods represents the implementation of the analytic derivative and response techniques [18,46–50]. These techniques appear to be preferable to the more straightforward finite field techniques. The finite field approaches [51–54] that rely on the numerical energy derivatives still remain very useful in some cases since they are applicable any time when the energy for the molecule under investigation is available for a series of external homogeneous electric or magnetic fields along with the field-free energy. This is topical, *e.g.*, when combining electron correlation method with the relativistic treatment and was actually used in most results discussed in this paper. We note, however, that the implementation of response theory within a 4-component relativistic approach has been reported recently [55].

Another point is a careful selection of the basis sets. Results used in this paper mostly refer to the family of Gaussian basis sets, called polarized basis sets, invented for electric properties [56–61], or their extensions. Standard Pol (intended for calculations of dipole moments and polarizabilities) and HyPol (for hyperpolarizabilities) can be used for nonrelativistic as well as for the DK one component relativistic calculation. The difference is only in obtaining the contraction coefficients. Basis sets used in DK calculations are denoted as Pol_dk. The details concerning orbital exponents and contraction coefficients can be found on the web page [62]. Pol and HyPol basis sets and their relativistically contracted counterparts are reasonably small basis sets still performing very well in predictions of molecular properties. They allow some insight into the basis set dependence of calculated properties, even if these bases are not best suited for using extrapolation techniques toward the Complete Basis Set (CBS) limit, which is another prerequisite for obtaining accurate results [63–65]. Relativistic ANO type (atomic natural orbital) basis sets for a wide spectrum of elements were developed by Roos *et al.* [66]. These basis sets allow including the spin-orbit effects via the RASSI (restricted active space SCF state interaction) method. RASSI [67] is based on the so-called Atomic Mean Field approach (AMFI) [68,69] which is a suitable approximation to the true solution of the SO Hamiltonian.

3. EXAMPLES OF TRENDS FOR SELECTED ATOMIC AND MOLECULAR PROPERTIES

3.1. An illustration of trends in properties of selected heavy elements

Let us first discuss some trends in the behavior of the coinage metal elements Cu, Ag, and Au, all having the same valence electronic structure, $\ldots (n-1)s^2(n-1)p^6(n-1)d^{10}ns^1$. Yet their physical properties and chemical behavior shows many differences. It is well known, that the pattern of, *e.g.*, valence ionization potentials (IP), electron affinities (EA), and the electric dipole polarizabilities within the Ib group elements is a consequence of relativistic

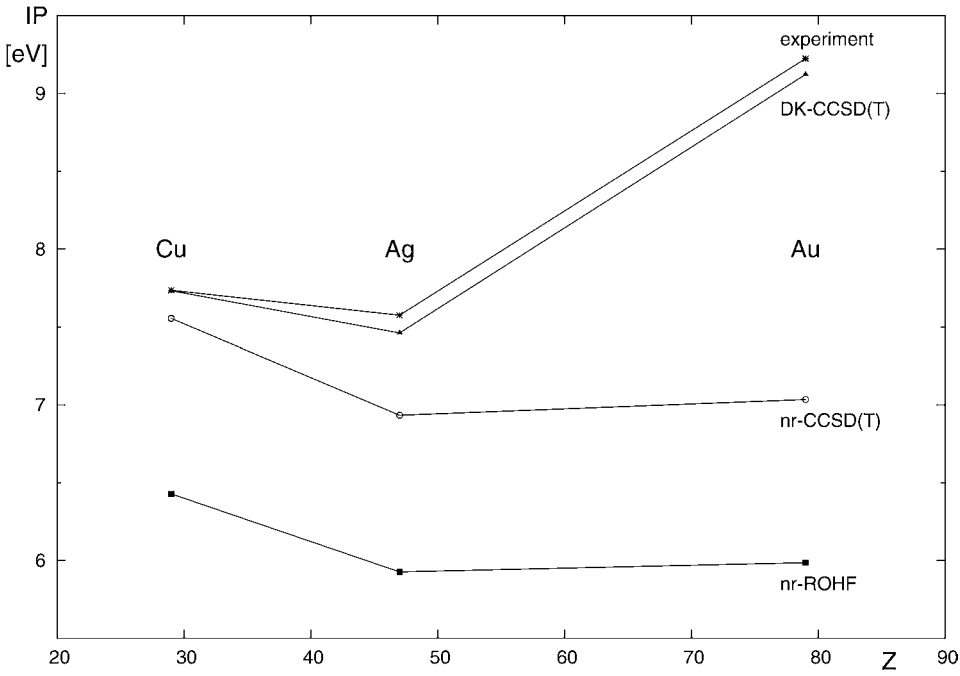

Fig. 1. Comparison of ionization potentials of coinage metal atoms calculated in Pol+3s3p1d1f basis set and experimental data. Ref. [13].

effects. The physical background for relativistic changes in these properties is essentially the same. Valence s- and p-electrons are relativistically stabilized and their radial distribution is relativistically shrinked. On the contrary, valence d-electrons are relativistically destabilized and their radial distribution is expanded. Of course, this effect is most significant in the heaviest element, *i.e.*, gold. Thus, the relativistic stabilization and shrinking of the valence s-electron leads to large relativistic increase of IP and EA of gold leading to the irregularity within the group of Ib elements. At the same time, the stabilization and shrinking of the valence s-electrons leads to the lowering of the polarizability. All these trends are demonstrated [13,70] by the comparison of DK–CCSD(T) and nonrelativistic nr–CCSD(T) results in Figs. 1–3. The agreement with experiment is only possible when both electron correlation and relativistic effects are properly considered. DK–CCSD(T) calculations with the Pol basis set give reasonable agreement of theoretical values with experiment. Further improvement is possible primarily by increasing the basis set and by improving the relativistic treatment. SO effects would split semivalence orbitals with the nonzero angular momentum but seem to be relatively unimportant in these elements.

Electron correlation at the CCSD(T) level should be very reliable within the accuracy which can be expected with methods and basis sets used in calculations presented in Figs. 1–3. Small CCSD excitation amplitudes and other diagnostics show no multireference character of the wave function and problems due to the eventual quasidegeneracy. Possible changes of calculated properties due to higher excitations are not expected to affect by no means our analysis of trends within the group of elements. We note that the electron correlation shows more-or-less the same pattern within the group of the Ib elements reflecting

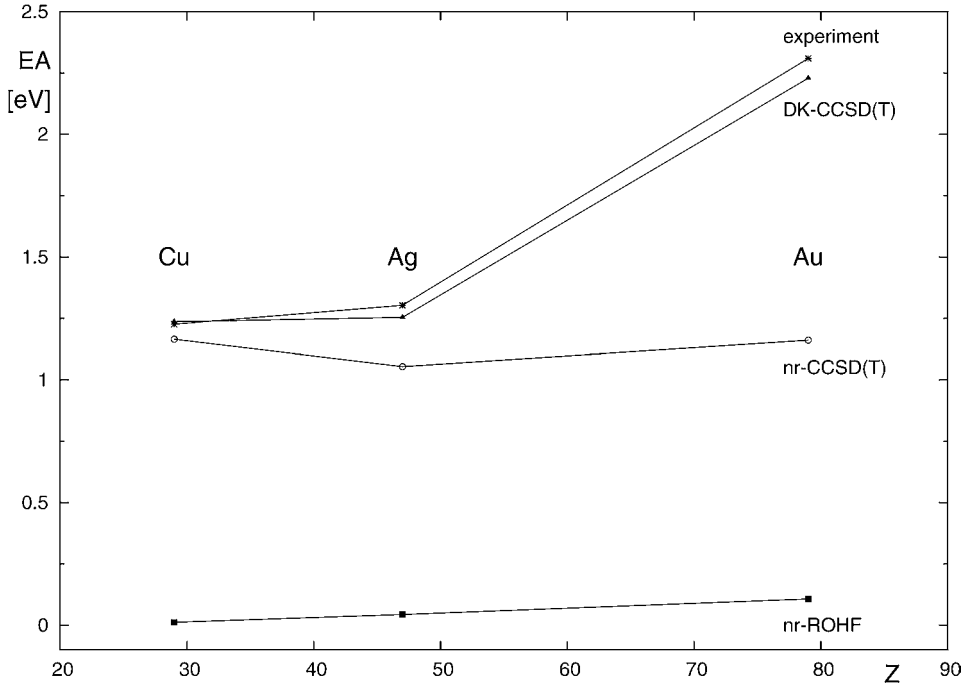

Fig. 2. Comparison of electron affinities of coinage metal atoms calculated in Pol+3s3p1d1f basis set and experimental data. Ref. [13].

thus their similar electronic structure. This is demonstrated by the comparison of nonrelativistic Hartree–Fock (nr–ROHF) and nr–CCSD(T) results. The largest contribution of the electron correlation to IP and EA is found for Cu, reflecting the smaller energy gap between the valence d- and s-electrons and the transition-metal character of this element. We stress that the HF orbital picture completely fails in predicting IP, EA, and dipole polarizabilities of Cu, Ag, and Au. Electron affinities of these elements at the nr–ROHF level are close to zero, completely off the experimental values.

The appearance of the non monotonic pattern of, *e.g.*, atomic dipole polarizabilities, is quite general. Figure 4 shows polarizabilities for the Group Ia, Ib, IIb, and IVa elements (we restrict ourselves to the three heaviest elements in each group). We note that the pattern of polarizabilities is the same for all four groups. Since all elements in the Zn, Cd, and Hg group and in the Rb, Cs, and Fr groups have similar valence electronic structure (valence s-electrons) as Ib group elements, the interpretation of the pattern remains the same. IVa elements are characterized by the valence np^2 electronic structure. For these elements, especially for properties of Pb, the spin-orbit interaction can not be ignored. Polarizabilities of Ge, Sn, and Pb were taken from the review of Schwerdtfeger [12]. In this review the discussion on polarizabilities in the spin-orbit split states can be found. SO contribution to the dipole polarizability is known also for the Ia elements, even if estimated at the uncorrelated level [14]. Dirac–Hartree–Fock calculations revealed that the SO contribution to the polarizability of Rb is negligible. SO coupling lowers the polarizability of Cs very slightly, by 2.7 a.u., while for Fr its magnitude is 13.0 a.u. It further supports the tendency to the

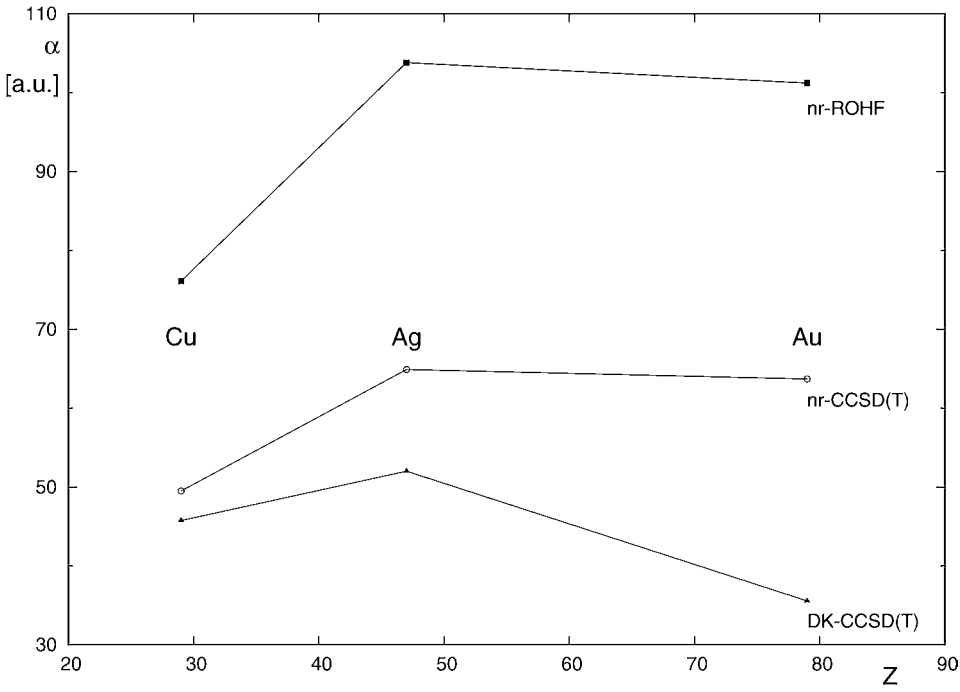

Fig. 3. Atomic dipole polarizabilities of coinage metal atoms calculated in Pol basis set. Refs. [13,70].

non monotonic pattern. In any case these values are too small to affect our discussion of the general trends within the group Ib elements. To proceed further, Lim *et al.* [14] calculated the polarizability of the superheavy element 119. It is as low (185 a.u.) as the polarizability of the Na atom (165 a.u.). The SO contribution is not negligible but still no larger than 16 a.u. Electric dipole polarizabilities of the halogen atom in the $^2P_{1/2}$ and $^2P_{3/2}$ spin-orbit split states have been investigated by Fleig and Sadlej [71]. They used the two-component variational treatment and showed that for heaviest homologs it is necessary to replace averaged values by individual component polarizabilities. Difficult calculations of electric properties for separated atomic SO states are rather unique. Full account of atomic polarizabilities throughout the Periodic Table was reviewed by Schwerdtfeger [12]. His analysis shows that Ia elements have the largest polarizabilities, followed by IIa elements polarizabilities. The polarizability then decreases within one period of the Periodic Table.

3.2. Trends in molecular dipole moments

It would be a bit naive to expect such uniform pattern in electric properties of molecules as it holds for atoms having analogous valence electronic structure. To make our discussion more transparent we have selected a series of diatomic molecules which all have an element discussed in Section 3.1. We have tried to analyze some trends in molecular dipole moments and dipole polarizabilities, [72,73], dissociation energies [72] and intermolecular interactions [74] in relation to electric properties of participating heavy metal elements

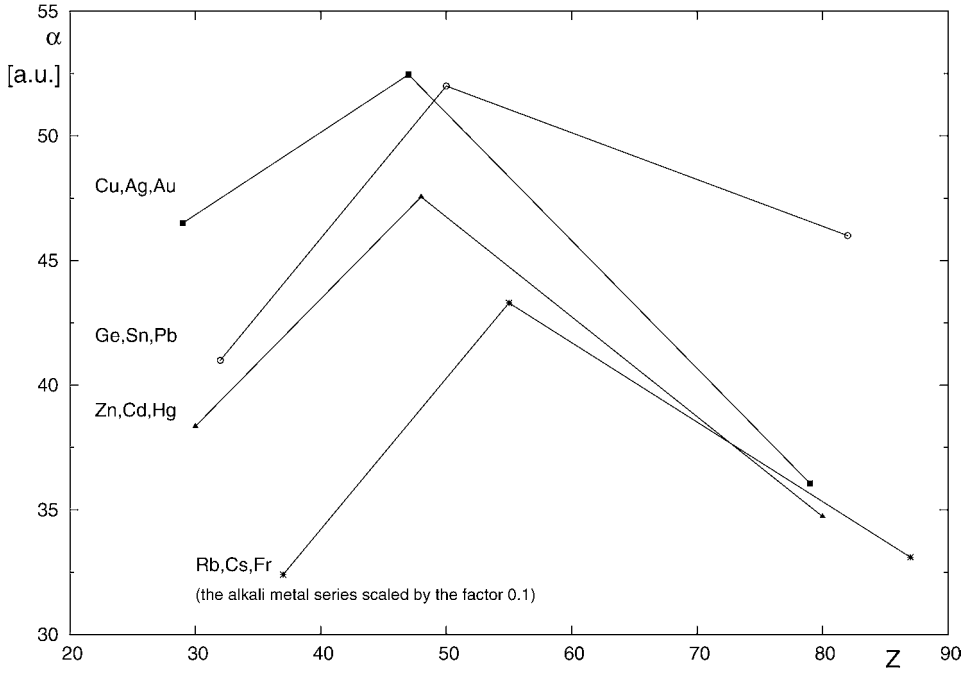

Fig. 4. Theoretical atomic dipole polarizabilities, relativistic effects included. Refs. [12–14,80,84].

Table 1. Dipole moments of GeO, SnO, and PbO (all values in a.u.)

Method/Basis[a]	μ_z		
	GeO	SnO	PbO
nr–CCSD(T)			
HyPolf	1.263	1.565	1.669
DK–SCF			
HyPolf	1.681	2.114	2.374
DK–CCSD(T)			
Pol	1.275	1.563	1.729
HyPolf	1.280	1.598	1.764
Experiment	1.291	1.70	1.83

[a] In DK calculations Pol family bases with the DK contractions were used. HyPolf is the HyPol basis set extended by two f functions, see Ref. [73].

some time ago. Miadoková *et al.* [75] have analyzed the trends of polarizabilities of alkali metal fluorides using the polarization model [76]. Recently calculated data on dipole moments and the dipole polarizabilities in the series of oxides of the IVa elements [73] allow to extend previous analysis. Numerical results are collected in Tables 1 and 2. Before

Table 2. Dipole polarizabilities of GeO, SnO, and PbO (all values in a.u.)

Method/Basis[a]	α_{zz}			α_{xx}		
	GeO	SnO	PbO	GeO	SnO	PbO
nr–CCSD(T)						
HyPolf	40.52	57.18	65.76	28.23	40.34	45.85
DK–SCF						
HyPolf	35.02	47.89	53.39	28.19	37.19	34.97
DK–CCSD(T)						
Pol	40.04	56.05	61.67	27.46	37.94	36.97
HyPolf	40.33	56.29	62.55	27.62	37.75	37.46

[a] See footnote in Table 1.

we will concentrate to relativistic effects throughout the group we note that the lowering of dipole moments of GeO, SnO, and PbO due to electron correlation is more important than are relativistic effects. Quite small relativistic change of the dipole moment of PbO is particularly surprising. As is usually the case, the electron correlation and the relativistic effects are not additive [73].

In general, the agreement of theoretical and experimental results is good, especially for GeO. Dipole moments for SnO and PbO are systematically lower than experimental ones by about 5.9 and 3.8%, respectively. The SO effect is rather small even for PbO, as it follows from results obtained recently by Roos and Malmqvist [31], see also discussion in Section 3.1. Theoretical values presented in Table 1 are uncorrected for vibrational effects, but their accuracy is still sufficient for discussion of trends within the group of molecules.

Good agreement of theoretical dipole moments with experiment gives some confidence to theoretical polarizabilities presented in Table 2. For GeO and SnO experimental data are missing. The only experimental values are available for PbO from the optical measurements for the solid state [77]. As with dipole moments of all IVa oxide molecules, parallel component of the polarizability is less affected by relativistic effects than by the electron correlation. The electron correlation for α_{zz} of PbO (9.16 a.u. or 14% of the final DK–CCSD(T) value with the HyPolf basis set) is almost three times larger than is the scalar relativistic effect for α_{zz} of PbO (3.21 a.u. or 5.1% of the final DK–CCSD(T) value). Again, as with dipole moments, the signs of electron correlation and relativistic effects, respectively, are opposite. Similar compensation of relativistic and electron correlation effects is observed in calculations of α_{xx}. This time, however, the α_{xx} component of the PbO polarizability is more affected by scalar relativistic effects than by the electron correlation. Indeed, results in Table 2 show, that relativistic effects lower α_{xx} of PbO by 8.39 a.u. (22.3% of the final value) with the HyPolf basis at the CCSD(T) level. With the electron correlation α_{xx} increases by 2.49 a.u. Both relativistic and electron correlation effects in α_{xx} of GeO and SnO are much smaller than in PbO but relativistic effects remain more important than are correlation effects even for the molecules containing relatively lighter atoms.

Dipole moments for the series of the alkali metal fluorides, coinage metal fluorides, the IVa elements oxides and the coinage–aluminium intermetallic molecules are presented in

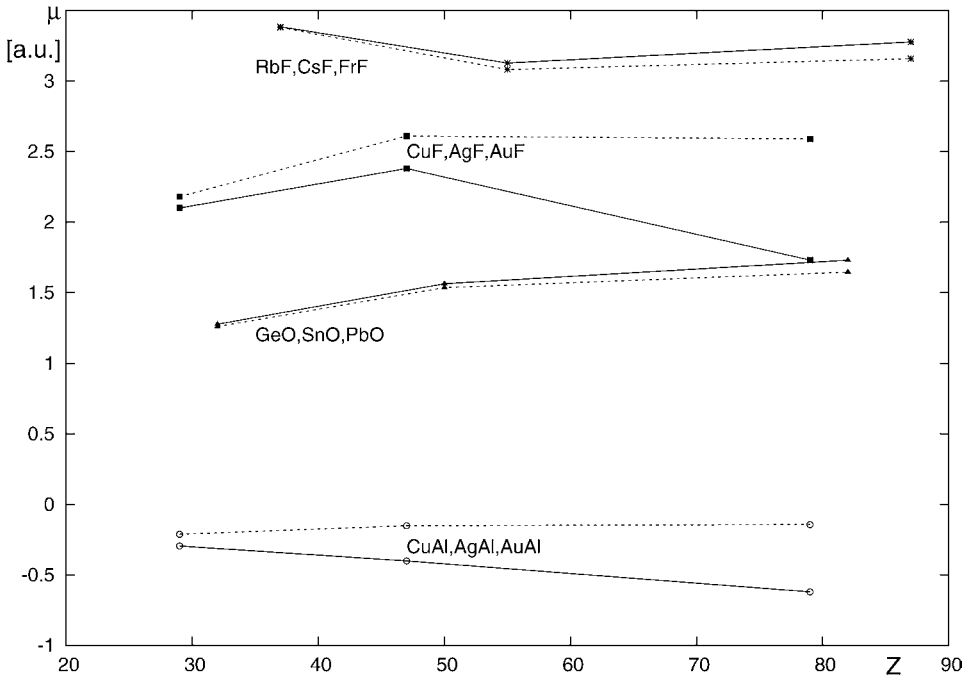

Fig. 5. Non-relativistic (dashed lines) and DK (full lines) dipole moments calculated in CCSD(T) approximation using the Pol family bases. Refs. [72,73,75,78].

Fig. 5. With the exception of GeO, SnO, and PbO group all molecules are characterized by the valence σ bonds. GeO, SnO, and PbO molecules have valence triple bonds. Dipole moments of the three series increase by relativistic effects. Relativistic changes of dipole moments of Ia fluorides and IVa oxides are very small. On the contrary, dipole moments of CuF, AgF, and AuF decrease very significantly. The dependence of dipole moments on the heavy atom atomic number Z for four series of diatomic molecules selected in Fig. 5 seems to be completely non-transparent. It by no means resembles the uniform picture valid for atomic polarizabilities as collected in Fig. 4. When going from the lowest Z to the highest Z within each group, we observe the non monotonic pattern for dipole moments of molecules in both fluorine series. However, the direction of the relativistic change in the coinage metal fluorides and in the alkali metal fluorides is opposite.

If taken separately, the trends for dipole moments and dipole polarizabilities of the coinage metal fluorides [72] and the coinage metal–aluminium diatomics [78], respectively, seem to be understandable (see also [73]). First, dipole moments of CuF, AgF, and AuF molecules are very high and the polarity is Me^+F^-. This is in accord with high EA of the fluorine atom (3.40 eV) [79]. The relativistic increase of IP of the coinage metal elements hinders the charge transfer from the coinage metal element to the fluorine atom and leads to the relativistic decrease of the dipole moment of CuF, AgF, and especially AuF.

Electron affinity of the aluminium elements is quite low (0.441 eV). CuAl, AgAl, and AuAl molecules have polarity Me^-Al^+ and the dipole moment is low. Actually, nonrelativistic CCSD(T) dipole moments of these molecules are almost zero and the Me^-Al^+ polarity is only obtained at the correlated level [78]. This can be understood easily, since

Table 3. Ionization potentials of selected atoms (all values in eV)

Atom	nr–CCSD(T)	DK–CCSD(T)	experiment[a]
Rb[b]	4.068	4.137	4.1771
Cs[b]	3.681	3.821	3.8939
Fr[b]	3.542	3.977	4.0727
Cu[c]	7.555	7.733	7.7264
Ag[c]	6.934	7.461	7.5762
Au[c]	7.035	9.123	9.2255
Ge			7.8994
Sn			7.3439
Pb			7.4167

[a] All experimental data from Ref. [81]. [b] Ref. [14]. [c] Ref. [13].

the ROHF electron affinity is unrealistically low (Fig. 2) and thus considerations at the HF orbital level are completely useless. Electron correlation and relativistic contributions support the charge transfer from aluminium to the coinage metal element. In accord with relativistic changes of EA, Fig. 2, the (negative) dipole moment of AuAl, Fig. 5, relativistically increased by 0.48 a.u., *i.e.*, four times.

To explain trends in dipole moments for remaining two groups of molecules is more difficult. The polarity of RbF, CsF, and FrF is very high [75], which can by attributed to the magnitude of the fluorine EA and relatively small IPs of the Ia elements [14]. DK–CCSD(T) IPs are 4.137, 3.821, and 3.977 eV for Rb, Cs, and Fr atoms, respectively. IPs of the two heaviest members of the group differ very little and all IPs in this group are much smaller than are IPs of the coinage elements [13] (7.733, 7.461, and 9.123 eV, respectively). Relativistic effects in IPs of Ia elements, Table 3, are also much smaller than those in coinage elements. Small relativistic changes of dipole moments in RbF, CsF, and FrF correspond to these facts.

The physically sounded rationalization of trends of dipole moments of highly ionic molecules, like RbF, CsF, and FrF, was proposed by Miadoková *et al.* [75]. The so called polarization model [76] was used to explain different relativistic effects in the alkali metal fluorides and the coinage metal hydrides, respectively [80]. The difference between the relativistic and nonrelativistic dipole moment μ for a molecule with the bond distance R can be related to the difference between the relativistic $\alpha(Me^n, rel)$ and the nonrelativistic $\alpha(Me^n, n.r)$ polarizability of the metal ion (Me^n). Neglecting relativistic effects in the F^- anion,

$$\mu(rel) - \mu(n.r) = -\frac{1}{R^2}\left[\alpha(Me^n, rel) - \alpha(Me^n, n.r)\right]. \quad (1)$$

Relativistic and nonrelativistic polarizabilities of the heaviest element are $\alpha(Fr^+, rel) = 19.2$ a.u. and $\alpha(Fr^+, n.r.) = 20.5$ a.u., respectively. For FrF with $R_e = 4.65$ a.u. the polarization model leads to the relativistic increase by about 0.06 a.u. This agrees fairly well with the DK–CCSD(T) result. The polarization model is less applicable to relativistic effects in dipole moments of *Me*Al molecules (*Me* = Cu, Ag, and Au) since *Me*Al bonds

are to large extend covalent. The polarity of *Me*Al molecules is $Me^{-}Al^{+}$. Polarizability of the Au anion decreases by relativistic effects enormously, by 157 a.u. $\alpha(Au-, n.r.) = 249$ and $\alpha(Au-, rel) = 92$ a.u. [82]. This would lead to much larger increase of the *negative* dipole moment of AuAl due to relativity than is actually calculated, see Fig. 5.

Another point, not discussed so far, is the change of the interatomic distance, which is related to the relativistic shrinking of a heavy atom. This, in turn, affects the dipole moment. No unique source of bond distances is available for all molecules discussed in this part. Nonrelativistic and DK–CCSD(T) optimized bond distances corresponding to calculated dipole moments are known for CuF, AgF, and AuF [72]. Relativistic effect reduces R_e of AuF by 0.162 Å and makes its DK–CCSD(T) value (1.947 Å) shorter than is R_e of AgF (2.004 Å). This further supports lowering of the dipole moment of AuF, along with large relativistic increase of IP of the gold element. Bond distance in FrF at which the dipole moment was calculated (2.46 Å) [75] is by 0.11 Å longer than that of CsF. Relative bond distances of these two molecules support the increase of the dipole moment of FrF in comparison to CsF. This is partly quenched by the relativistic increase of IP of the Fr element. These considerations may explain small relativistic change of the FrF dipole moment. Interplay of different factors makes the detailed explanation of the "Z behavior" more difficult, especially when relativistic changes of underlying physical quantities are subtle, as is the case of RbF, CsF, and FrF.

Discussion of trends for dipole moments of GeO, SnO, and PbO can be directed in a similar way as for RbF, CsF, and FrF. GeO, SnO, and PbO molecules have large dipole moments, the polarity is $Me^{+}O^{-}$. Experimental bond lengths [83] which were used in DK–CCSD(T) calculations of the dipole moment for these molecules monotonically increase within the group. The bond length of PbO (1.922 Å) is by 0.09 Å longer than that of SnO. Information about relativistic effects of IPs for Ge, Sn, and Pb elements is not available due to the necessity of considering SO effects. We know from experimental data [79] that the first IP of the Pb atom (7.416 eV) is only slightly higher than is IP of the Sn atom (7.344 eV). Relative magnitude of IPs for these two elements would support slight lowering of the dipole moment, *i.e.*, it acts opposite to the effects arising from relative bond lengths of SnO and PbO. The result is very small change of relativistic effects in dipole moment of these molecules. Finally, oxygen has much smaller electron affinity (1.461 eV) than has fluorine, 3.401 eV [79]. This explains lower dipole moments of GeO and SnO than CuF and AgF. Molecules with the heaviest elements, AuF and PbO have dipole moments about the same at the relativistic level. This is rationalized by large relativistic increase (2.088 eV) of IP of gold. Note that the nonrelativistic dipole moment of AuF is much larger that is the dipole moment of PbO.

We conclude that relativistic effects, which affect the magnitude of IP and EA of the heavy metal elements, play a decisive role in understanding the trends in dipole moments within the group of diatomic molecules. Relativistic shrinking of the size of these elements needs to be considered along with changes of IPs and EAs for more detailed insight.

3.3. Trends in parallel dipole polarizabilities

The pattern for relativistic and nonrelativistic CCSD(T) calculations of parallel dipole polarizabilities of the twelve molecules, Fig. 6, seems to be equally non-transparent as was the pattern for dipole moments. However, we are able to show that the trends within the

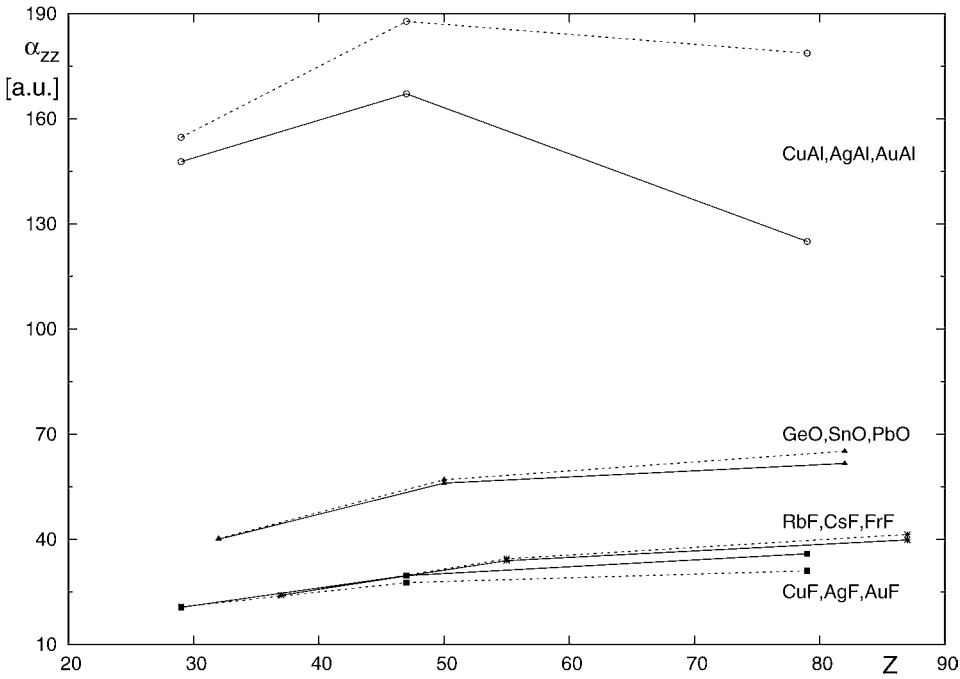

Fig. 6. Non-relativistic (dashed lines) and DK (full lines) dipole parallel polarizabilities calculated in CCSD(T) approximation using the Pol family bases. Refs. [72,73,75,78].

group of molecules can be explained in a relatively simple way. Before proceeding further, let us remind that the three series of molecules are highly ionic. Only CuAl, AgAl, and AuAl are primarily covalent, with the σ(s–p) valence bond, and have small dipole moments. These molecules all have large polarizabilities, show the non monotonous pattern and are characterized by very large relativistic effects. All highly polar ionic molecules behave differently. Their polarizabilities are relatively small, increase monotonically within the group, the relativistic effect being positive or negative. It is very small, even for AuF, although its dipole moment decreased due to relativity enormously, by 0.86 a.u., *i.e.*, by 50% of the final DK–CCSD(T) value, 1.73 a.u. [72].

Let us start with the group of CuF, AgF, and AuF molecules. Their dipole polarizabilities were essentially interpreted [72] in terms of the additivity of the Me^+ and F^- ionic polarizabilities. Me^+ ions have much lower polarizabilities than their neutral atoms [70] and increase monotonically. The trend for polarizabilities of the group of the coinage metal cations is shown in Fig. 7. After ionization, the valence electronic structure in all these cations is $(n-1)d^{10}$. Valence d-electrons are relativistically destabilized and, consequently, their polarizabilities increase [70,80]. The same trend is observed in the group of CuF, AgF and AuF molecules. Analogous arguments are used in the explanation of trends in the group RbF, CsF, and FrF. However, the valence electronic structure of their metal element cations corresponds to the noble gas element and is $(n-1)p^6$. Valence p-electrons are relativistically stabilized, and the polarizability of Rb^+, Cs^+, and Fr^+ ions relativistically decreases. The same trend is, again, observed in polarizabilities of RbF, CsF, and FrF molecules. Analogous interpretation, with some reservation, is also valid for GeO, SnO,

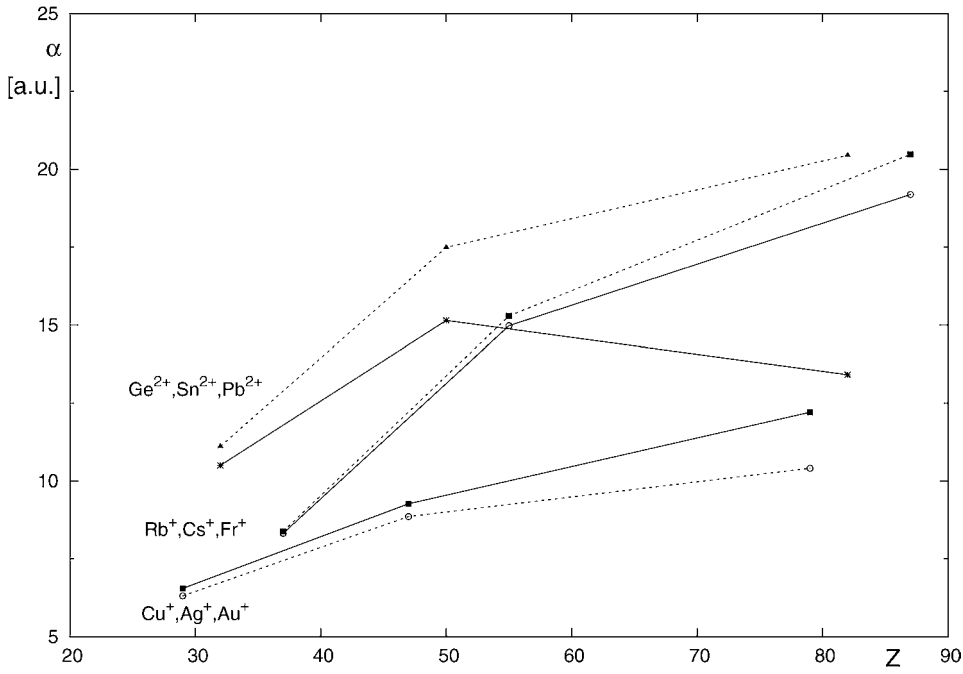

Fig. 7. Non-relativistic (dashed lines) and DK (full lines) dipole polarizabilities of ions calculated in CCSD(T) approximation using the Pol family bases. Refs. [73,80,84].

and PbO molecules. Polarizabilities of these molecules also increase monotonically with increasing atomic number of the metal element. If we could interpret these molecules as ionic species with the charge of the metal Me^{2+}, the polarizability of PbO should decrease by relativistic effects much more than it is observed in Fig. 6. Valence electronic structure of the Ge^{2+}, Sn^{2+}, and Pb^{2+} ions is ns^2np^0. These electrons are relativistically stabilized and their polarizabilities relativistically decrease [73] (like in isoelectronic elements Zn, Cd, and Hg, Fig. 4). This is qualitatively in line with relativistic effects in GeO, SnO, and PbO, but the effect in ions is larger and the "Z" dependence is not monotonic. The change of the polarizability due to relativistic effects in PbO is 3.21 a.u., while in Pb^{2+} it is 7 a.u. This quantitative discrepancy is explained by the fact, that PbO can not be completely represented as $Pb^{2+}O^{2-}$; the charge on participating atoms is actually lower. This can be supported by the Mulliken population analysis (with all the reservation to any interpretation based on the HF orbital picture) which shows that there is the charge transfer of about 1.5 electrons from the metal atom to the oxygen atom. We note that the polarizability of the O^{2-} anion is estimated by DK–CCSD(T) as 75.3 a.u.

Large polarizabilities of CuAl, AgAl, and AuAl [78] are partly attributed to the bond polarizability and partly to some charge transfer from Al to the coinage metal. Relativistic effect lowers the polarizability of AuAl by 54 a.u., which is much less than in the Au^- anion, 157 a.u. [82].

There is less information on α_{xx} polarizabilities for the series of molecules than for their parallel components. For that reason we will not analyze the trends in perpendicular

polarizabilities. Less detailed discussion on parallel polarizabilities can be found in our recent paper [73].

3.4. Trends in bond dissociation energies in heteronuclear molecules

Relativistic effects in the bond dissociation energies, equilibrium bond distances, force constants, vibrational frequencies, were discussed in many papers and reviews, see, *e.g.*, [3,11,85,86] and references therein. There are also some generalizations. For example, Schwarz *et al.* [86] present relativistic corrections to the bond energy for a series of molecules including IVa monoxides GeO, SnO, and PbO. Theoretical considerations and the empirical experience about the Z-dependence of the valence electron densities lead to the expected Z-dependence for a homologous series of molecules as roughly proportional to Z^2. Regarding the availability of excellent review articles about relativistic effects in bond dissociation energies, our discussion will be rather short. We will concentrate ourselves to the relation of the bond dissociation energies with electric properties of participating heavy metal elements.

We can follow essentially the same physical arguing as was used in our discussion on dipole moments and dipole polarizabilities. Here we will illustrate the relation between the dipole moment and the relativistic change of the bond energy in heteronuclear diatomic molecules. Let us consider dissociation energies D_e for the two groups of molecules discussed above, CuF, AgF, and AuF [72], and another group, CuAl, AgAl, and AuAl [78]. Both share the same metal element and differ by the ligand. CuF, AgF, and AuF molecules have large dipole moment and the polarity is Me^+F^-. CuAl, AgAl, and AuAl have small dipole moments and the polarity is opposite, Me^-Al^+. The charge transfer between the metal and the ligand, like the polarity, is mainly determined by the electronegativity of participating elements. Some other aspects, particularly relativistic effects in the bond length should be considered as well. Using simple arguments, relativistic changes in D_e, Table 4, can be understood easily. Ionization potential of the coinage element, which determines the charge transfer to the fluorine relativistically increases, especially in gold, and hinders the charge transfer to the ligand. The charge transfer from aluminium to the coinage element in *Me*Al molecules is supported by the relativistically increased electron affinity of *Me*, especially gold. Thus, relativistic effects act in the two groups differently, destabilizing *Me*F

Table 4. Dissociation energies D_e (all values in eV)

Molecule	nr–RHF	nr–CCSD(T)	DK–CCSD(T)	experiment
CuF[a]	2.53	4.08	4.04	4.4(2)
AgF[a]	2.17	3.55	3.32	3.6(4)
AuF[a]	2.04	3.39	2.93	3.01[c]
CuAl[b]	0.59	2.08	2.25	2.315
AgAl[b]	0.41	1.58	1.95	∼2.22
AuAl[b]	0.51	1.68	3.41	3.34

[a] Data from Ref. [72]. [b] Data from Ref. [78]. [c] Ref. [87].

bonds and stabilizing *Me*Al bonds. The relativistic destabilization of the AuF bond is very large, 0.46 eV. Enormous, however, is the relativistic stabilization in AuAl, 1.7 eV. This means that D_e is twice as large at the relativistic level in comparison to the nonrelativistic CCSD(T) result. Due to relativity, D_e of AuAl is even larger than that of AuF. Without considering relativistic effects, the AuAl bond D_e would be about half of D_e for AuF.

Up to now we were discussing only relativistic effects in this chapter. Obviously, electron correlation must not be forgotten in the discussion of bond energies. Like as relativistic effects are unavoidable in understanding the underlying coinage metal properties, the HF one electron picture is completely useless in interpreting EAs and IPs of these species. Thus, it is not surprising that electron correlation plays so important role in bonding dissociation energies in *Me*F and *Me*Al molecules. Electron correlation is essentially equally important in all molecules presented in Table 4. It behaves monotonically, always increasing the bond dissociation energy by about 1.35–1.55 eV in *Me*F molecules and by 1.2–1.5 eV in *Me*Al molecules. In the gold compounds it makes no sense to discuss the relative importance of the electron correlation and relativistic effects. It is imperative that both must be considered at highly sophisticated level together, to avoid inaccuracies caused by the nonadditivity of both contributions.

It is, of course, impossible to explain relativistic changes quantitatively with arguments used so far. Other effects, including exchange repulsion which is connected with the relativistic shrinking of valence orbitals plays a role as well. Also, there is the difference in the bonding character in *Me*F and *Me*Al molecules. All are characterized by the bonding valence σ(s–p) orbital. *Me*F bonds are more ionic, which is demonstrated not only by larger dipole moments, but also by the dipole moment curves, which are almost perfectly linear [72] and correspond to what can be expected from the Coulomb law. The *Me*Al bonds are more covalent. Due to the stabilization of the metal valence s-electrons, the *Me*Al σ orbital can be relativistically stabilized as well. This can further contribute to the increase of D_e of *Me*Al molecules.

The overall pattern for D_e of all molecules presented in Table 4 corresponds to available experimental data only when relativistic effects are considered. In general, the agreement between theory and experiment is very good even for heaviest members of both groups. The thermodynamic stability of AuF, Au_2F_2 and related compounds has been subjected to many discussions [11,88].

3.5. Weak intermolecular interactions

We will try to show in this part that ideas which lead to the understanding of trends in the molecular properties are useful also in the interpretation of some trends in the intermolecular interaction energies. Schwerdtfeger and Bowmaker [89] have studied interactions of coinage metals with CO. They concluded that the metal–carbonyl interactions may be best described as a combination of dispersion, donor–acceptor (charge-transfer) and repulsive interactions. Obviously, these terms can be related to the relativistic effect in electric properties of atoms and molecules, their ionization potentials, electron affinities as well as to the size of the electron distribution in a heavy metal element.

To proceed in a more systematic way we present in Table 5 interaction energies of a group of the coinage metal elements, Cu, Ag, and Au (*Me*), interacting with H_2O, NH_3 [74] and SH_2 [90] as ligands (L). The weakest interactions are calculated for the

Table 5. Nonrelativistic and relativistic CCSD(T) interaction energies (all values in kJ/mol)

Molecule	nr-ΔE	DK-ΔE
$CuNH_3$[a]	−39.0	−43.8
$AgNH_3$[a]	−17.1	−18.0
$AuNH_3$[a]	−13.7	−38.4
$CuOH_2$[a]	−9.95	−9.93
$AgOH_2$[a]	−5.59	−4.75
$AuOH_2$[a]	−4.25	−4.63
$CuSH_2$[b]		−15.71
$AgSH_2$[b]		−5.22
$AuSH_2$[b]		−23.83

[a] Data from Ref. [74]. [b] Data from Ref. [90].

$MeOH_2$ complexes, even though the water dipole moment is 1.26 times larger than dipole moment of NH_3 and two times larger than dipole moment of SH_2. The leading long-range dipole–induced-dipole induction term is not sufficient for explaining the calculated order of stabilities. Theoretical data support available experimental evidence. First, they allow to explain the problems with identifying $AgOH_2$ (the weakest complex) experimentally, while $AgNH_3$ [91] could be observed [92] in the REMPI (Resonantly Enhanced Multiphonon Ionization) spectrum. Available are recent ZEKE (Zero Kinetic Energy) spectroscopic measurements [93] which lead to binding energies 47 ± 15 kJ/mol for $CuNH_3$ and 8 ± 13 kJ/mol for $AgNH_3$. Theoretical data agree with these measurements fairly well. Thus, data in Table 5 seem to be sufficiently reliable to serve as a basis for a deeper analysis.

All MeL species in Table 5 are van der Waals complexes. Electron correlation is essential in the description of the geometry and the interaction energy in all complexes. Only $MeNH_3$ exhibit a shallow minimum on the potential energy curve calculated at the ROHF level. All other complexes are repulsive when electron correlation is omitted. $MeNH_3$ complexes preserve the C_{3v} symmetry of the ligand. $MeOH_2$ and $MeSH_2$ complexes are nonplanar, with the metal directed roughly to the lone electron pair of the ligand. This suggests a possibility of a charge transfer mediated through the lone pair. Such charge transfer is related to the IP of the ligand. IP of H_2O, 12.6 eV, is significantly larger than are IPs of NH_3 and SH_2, 10.2 and 10.5 eV, respectively [79]. Consequently, admitting that the charge transfer plays an important role in the bonding mechanism in MeL complexes, SH_2 should resemble NH_3 rather than OH_2 as a ligand, which is really the case. Due to large IP of the water molecule the charge transfer in $MeOH_2$ is less favorable than with other two ligands. Finally, EA of the metal should be considered. It increases due to the relativity, especially in Au, see Fig. 2, which explains large relativistic contribution to the stabilization energy in $AuNH_3$. Relativistic effects in $MeSH_2$ are, unfortunately, not yet available. However, relatively large DK–CCSD(T) interaction energy in $AuSH_2$, supports suggested mechanism. We also note that interactions of Cu and Au with ligands, particularly with NH_3, are frequently accompanied with the rehybridization of the metal element valence orbitals [94].

This effect is linked with significant increase of the magnitude of the CCSD excitation amplitudes [95]. For Au complexes this effect is significant at the relativistic level.

Relativistic effects play only marginal role in all $MeOH_2$ complexes. Accepting the expectation that the charge transfer is not dominating in this case, long-range induction interaction and the dispersion interaction should be considered. Around the minima the induction interaction was shown [74] to be unimportant. The dispersion interaction energy (E^{D}) is expressed as

$$E^{\mathrm{D}} = -\frac{3}{2}\frac{I_{\mathrm{A}} I_{\mathrm{B}}}{I_{\mathrm{A}} + I_{\mathrm{B}}}\left[\alpha_{\mathrm{A}}\alpha_{\mathrm{B}} + \frac{1}{3}\alpha_{\mathrm{A}}\left(\alpha_{\parallel}^{\mathrm{B}} - \alpha_{\perp}^{\mathrm{B}}\right)\left(\frac{3}{2}\cos^2\theta - \frac{1}{2}\right)\right]R^{-6} \tag{2}$$

where α_{A}, α_{B} are mean polarizabilities of the subsystems A and B, respectively, and $\alpha_{\parallel}^{\mathrm{B}}$, $\alpha_{\perp}^{\mathrm{B}}$ are parallel and perpendicular components of the polarizability tensor with respect to the dipole moment direction of compound B. R is the intermolecular distance and θ is the angle between the dipole moment direction and the position vector of interacting compound A. In this formulation are both compounds treated as being composed of point charge distributions, but at least for large R this is a reasonable approximation [96]. IPs of the coinage metals relativistically increase, dipole polarizabilities decrease. Neglecting the polarizability anisotropy and the geometry considerations, the two important relativistic effects cancel each other in the dispersion energy term. Due to large relativistic increase of EA of gold, the charge transfer may still to some extend contribute to the interaction energy of $AuOH_2$, in spite of large IP of the water molecule. Also, the relativistic shrinking of the Au atom reduces the bond distance and thus contributes to the increase of E^{D}. This means that relativistic effects in the $AuOH_2$ complex result from the interference of a few contributions. In any case, however, relativistic effects in $AuOH_2$ remain very small in comparison with NH_3 as a ligand for all metal elements.

Relativistic and electron correlation effects in $AuOH_2$ were considered by Lambropoulos *et al.* [97]. Akinaga, Nakajima and Hirao studied the adsorption of SCH_3 on Cu, Ag, and Au surfaces using DFT with nonrelativistic and quasirelativistic pseudopotentials [98]. Their aim was to elucidate some problems related to the construction of the Self Assembled Monolayers (SAM). Relativistic effects in $MeSCH_3$ were similar to what can be expected from the analysis presented above, *i.e.*, the binding energy of the $AuSCH_3$ complex increased by relativity. However, the relativistic effects decrease the adsorption energy of SCH_3 on the Au(111) surface. The explanation of these differences is not straightforward [98].

4. SUMMARY

This review has attempted to demonstrate that phenomena, which follow from the one-component Douglas–Kroll–Hess quasi-relativistic approach are useful in interpreting some trends in dipole moments, static electric dipole polarizabilities, bond dissociation energies, and selected intermolecular interactions. Only molecules and interacting complexes in which spin-orbit coupling was unimportant were treated. The starting point for the discussion were the well known relativistic effects in heavy elements, namely relativistic changes of ionization potentials, electron affinities, polarizabilities, and the relativistic shrinking (expanding) of the atomic electron distributions. We have mentioned repeatedly that the Hartree–Fock orbital picture fails in understanding basic trends discussed in this paper. It

is fair to note that in the Density Functional Theory one may, however, fruitfully use an orbital picture depending on the quality of the exchange-correlation potential [99]. It is shown that learning from the relativistic effects in participating elements has improved our understanding of the pattern of dipole moments and dipole polarizabilities of molecules containing atoms from the same group of the Periodic Table. The understanding of the apparently diverse behavior of different groups of molecules is also attainable with this approach. The knowledge, which was useful in generalizations concerning electric properties of molecules is also useful in understanding positive or negative changes and trends in the bond dissociation energies. The understanding of the pattern of interactions between a heavy metal element and lone-pair ligands was also facilitated by learning from relativistic effects, which affect properties of participating elements with the same valence electronic structure. We also would like to stress the increasing usefulness of theoretical methods as a tool for obtaining dipole moments, atomic and molecular polarizabilities and higher order properties, which are frequently not amenable to experiment. Theoretical methods capable to treat atomic and molecular properties for the spin-orbit split states have already emerged, but these methods are not yet routine.

ACKNOWLEDGEMENTS

The support of the Slovak Grant Agency (Contract No. 1/0115/03) is gratefully acknowledged. Many results discussed in this paper have been obtained within the European program COST-D26/007/02.

REFERENCES

[1] P. Pyykkö, J.P. Desclaus, *Acc. Chem. Res.* **12** (1979) 276.
[2] K.S. Pitzer, *Acc. Chem. Res.* **12** (1979) 271.
[3] P. Pyykkö, *Chem. Rev.* **88** (1988) 563.
[4] P. Pyykkö, *Chem. Rev.* **97** (1997) 597.
[5] P. Pyykkö, *Int. J. Quantum Chem.* **85** (2001) 18.
[6] P. Pyykkö, *Angew. Chem. Int. Ed.* **41** (2002) 3573.
[7] W. Kutzelnigg, *Phys. Rev. A* **54** (1996) 1183.
[8] P. Schwerdtfeger, M. Seth, in: P. Von Ragué Schleyer (Ed.), *Encyclopedia of Computational Chemistry*, John Wiley & Sons, Chichester, 1998, p. 2480.
[9] B.A. Hess, in: P. von Ragué Schleyer (Ed.), *Encyclopedia of Computational Chemistry*, John Wiley & Sons, Chichester, 1998, pp. 2499–2508.
[10] J. Almlöf, O. Gropen, in: K.B. Lipkovitz, D.B. Boyd (Eds.), *Reviews in Computational Chemistry*, vol. 8, VCH Publishers, New York, 1996.
[11] H. Schwarz, *Angew. Chem. Int. Ed.* **42** (2003) 4442.
[12] P. Schwerdtfeger, in: G. Maroulis (Ed.), *Atoms, Molecules and Clusters in Electric Fields: Theoretical Approaches to the Calculation of Electric Polarizability*, Imperial College Press, in press.
[13] P. Neogrády, V. Kellö, M. Urban, A.J. Sadlej, *Int. J. Quantum Chem.* **63** (1997) 557.
[14] I.S. Lim, M. Pernpointner, M. Seth, J.K. Laerdahl, P. Schwerdtfeger, P. Neogrády, M. Urban, *Phys. Rev. A* **60** (1999) 2808.
[15] M. Iliaš, P. Neogrády, *Chem. Phys. Lett.* **309** (1999) 441.
[16] V. Kellö, A.J. Sadlej, *Phys. Rev. A* **60** (1999) 3575.
[17] K.D. Bonin, V.V. Kresin, *Electric-Dipole Polarizabilities of Atoms, Molecules and Clusters*, World Scientific, Singapore, 1997.

[18] T. Helgaker, Jørgensen, J. Olsen, *Molecular Electronic-Structure Theory*, John Wiley & Sons, Chichester, 2000.
[19] M. Douglas, N.M. Kroll, *Ann. Phys.* **82** (1974) 89;
B.A. Hess, *Phys. Rev. A* **33** (1986) 3742;
G. Jansen, B.A. Hess, *Phys. Rev. A* **39** (1989) 6016.
[20] M. Iliaš, V. Kellö, T. Fleig, M. Urban, *Theoret. Chem. Acc.* **110** (2003) 176.
[21] J. Bieroń, P. Pyykkö, D. Sundholm, V. Kellö, A.J. Sadlej, *Phys. Rev. A* **64** (2001) 052507.
[22] J.N.P. van Stralen, L. Visscher, *J. Chem. Phys.* **117** (2002) 3103.
[23] A. Messiah, *Quantum Mechanics, vol. II*, North-Holland, Amsterdam, 1969, p. 943.
[24] R.E. Moss, *Advanced Molecular Quantum Mechanics*, Chapman and Hall, London, 1973.
[25] V. Kellö, A.J. Sadlej, B.A. Hess, *J. Chem. Phys.* **105** (1996) 1995.
[26] M. Barysz, A.J. Sadlej, *Theor. Chim. Acta* **97** (1997) 260.
[27] V. Kellö, A.J. Sadlej, *Int. J. Quantum Chem.* **68** (1998) 159.
[28] V. Kellö, A.J. Sadlej, K. Faegri Jr., *J. Chem. Phys.* **108** (1998) 2056.
[29] M. Dolg, A. Nicklass, H. Stoll, *J. Chem. Phys.* **99** (1993) 3614.
[30] M. Mayer, S. Krüger, N. Rösch, *J. Chem. Phys.* **115** (2001) 4411.
[31] B.O. Roos, P.-Å. Malmqvist, *Adv. Quantum Chem.* **47** (2004) 37.
[32] T. Nakajima, K. Hirao, *J. Chem. Phys.* **113** (2000) 7786.
[33] A. Wolf, M. Reiher, B.A. Hess, *J. Chem. Phys.* **117** (2002) 9215.
[34] M. Barysz, A.J. Sadlej, *J. Mol. Struct. (Theochem)* **573** (2001) 181;
M. Barysz, A.J. Sadlej, *J. Chem. Phys.* **116** (2002) 2696.
[35] M. Barysz, *J. Chem. Phys.* **114** (2001) 9315, *Acta Phys. Pol. A* **101** (2002) 815.
[36] A. Wolf, M. Reiher, B.A. Hess, *J. Chem. Phys.* **120** (2004) 8624.
[37] M. Urban, J. Noga, S.J. Cole, R.J. Bartlett, *J. Chem. Phys.* **83** (1985) 4041.
[38] K. Raghavachari, G.W. Trucks, J.A. Pople, M. Head-Gordon, *Chem. Phys. Lett.* **157** (1989) 479.
[39] J.D. Watts, M. Urban, R.J. Bartlett, *Theoret. Chim. Acta* **90** (1995) 341.
[40] V. Parasuk, P. Neogrády, H. Lischka, M. Urban, *J. Phys. Chem.* **100** (1996) 6325.
[41] R.J. Bartlett, in: D.R. Yarkony (Ed.), *Modern Electronic Structure Theory, part II*, World Scientific, Singapore, 1995, p. 1047.
[42] J. Paldus, X. Li, *Adv. Chem. Phys.* **110** (1999) 1.
[43] M. Urban, I. Černušák, V. Kellö, J. Noga, in: S. Wilson (Ed.), *Methods in Computational Chemistry*, Plenum Press, New York, 1987, p. 117.
[44] T.J. Lee, G. Scuseria, in: S.R. Langhoff (Ed.), *Quantum Mechanical Electronic Structure Calculations with Chemical Accuracy*, Kluwer Academic Publishers, Dordrecht, 1995, p. 47.
[45] L. Visscher, T.J. Lee, K.G. Dyall, *J. Chem. Phys.* **105** (1996) 8769.
[46] P. von Ragué Schleyer (Ed.), *Encyclopedia of Computational Chemistry*, John Wiley & Sons, Chichester, 1998, pp. 615–636.
[47] L. Adamowicz, W.D. Laidig, R.J. Bartlett, *Int. J. Quantum Chem.* **18** (1994) 245;
N.C. Handy, H.F. Schaefer, *J. Chem. Phys.* **81** (1984) 5031.
[48] P. Jørgensen, T. Helgaker, *J. Chem. Phys.* **89** (1988) 1560.
[49] R. Kobayashi, H. Koch, P. Jørgensen, *Chem. Phys. Lett.* **219** (1994) 30;
O. Christiansen, A. Halkier, H. Koch, P. Jørgensen, T. Helgaker, *J. Chem. Phys.* **108** (1998) 2801.
[50] O. Christiansen, P. Jørgensen, C. Hattig, *Int. J. Quantum Chem.* **68** (1998) 1.
[51] H.D. Cohen, C.C.J. Roothaan, *J. Chem. Phys.* **43** (1965) 534.
[52] A.D. McLean, M. Yoshimine, *J. Chem. Phys.* **46** (1967) 3682.
[53] I. Černušák, G.H.F. Diercksen, A.J. Sadlej, *Phys. Rev. A* **33** (1986) 814.
[54] G. Maroulis, *J. Chem. Phys.* **108** (1998) 5432.
[55] T. Saue, H.J.Aa. Jensen, *J. Chem. Phys.* **118** (2002) 522.
[56] A.J. Sadlej, *Collect. Czech. Chem. Commun.* **53** (1988) 1995.
[57] A.J. Sadlej, *Theor. Chim. Acta* **81** (1991) 45.
[58] A.J. Sadlej, *Theor. Chim. Acta* **81** (1992) 339.
[59] V. Kellö, A.J. Sadlej, *Theor. Chim. Acta* **83** (1992) 351.
[60] T. Pluta, A.J. Sadlej, *Chem. Phys. Lett.* **297** (1998) 391.
[61] I. Černušák, V. Kellö, A.J. Sadlej, *Collect. Czech. Chem. Commun.* **68** (2003) 211.
[62] All available Pol family bases sets can be found on the web page http://www.qch.fns.uniba.sk/Baslib.
[63] P. Neogrády, M. Medveď, I. Černušák, M. Urban, *Mol. Phys.* **100** (2002) 541.

[64] A. Halkier, W. Klopper, T. Helgaker, P. Jørgensen, *J. Chem. Phys.* **111** (1999) 4424.
[65] A. Halkier, T. Helgaker, P. Jørgensen, W. Klopper, H. Koch, J. Olsen, A.K. Wilson, *Chem. Phys. Lett.* **286** (1998) 243.
[66] B.O. Roos, V. Veryazov, P.O. Widmark, *Theoret. Chem. Acc.* **111** (2004) 345.
[67] P.A. Malmqvist, B.O. Roos, B. Schimmelpfennig, *Chem. Phys. Lett.* **357** (2002) 230.
[68] B.A. Hess, C.M. Marian, U. Wahlgren, O. Gropen, *Chem. Phys. Lett.* **251** (1996) 365.
[69] O. Christiansen, J. Gauss, B. Schimmelpfennig, *Phys. Chem. Chem. Phys.* **2** (2000) 965.
[70] P. Neogrády, V. Kellö, M. Urban, A.J. Sadlej, *Theor. Chim. Acta* **93** (1996) 101.
[71] T. Fleig, A.J. Sadlej, *Phys. Rev. A* **65** (2002) 032506.
[72] M. Iliaš, P. Furdík, M. Urban, *J. Phys. Chem.* **102** (1998) 5263.
[73] V. Kellö, A. Antušek, M. Urban, *J. Comput. Methods Sci. Eng.* **4** (2004) 753.
[74] A. Antušek, M. Urban, A.J. Sadlej, *J. Chem. Phys.* **119** (2003) 7247.
[75] I. Miadoková, V. Kellö, A.J. Sadlej, *Mol. Phys.* **96** (1999) 179.
[76] A.D. Buckingham, *Adv. Chem. Phys.* **9** (1967) 107.
[77] R.R. Reddy, Y. Nazeer Ahammed, K. Rama Gopal, P. Abdul Azeem, B. Sasikala Devi, T.V.R. Rao, S.H. Behere, *Opt. Mater.* **22** (2003) 7.
[78] M. Urban, A.J. Sadlej, *Mol. Phys.* **92** (1997) 587.
[79] D.R. Lide (Ed.), *CRC Handbook of Chemistry and Physics*, seventy-fourth ed., CRC Press, Boca Raton, FL, 1993.
[80] V. Kellö, A.J. Sadlej, *Theoret. Chim. Acta* **94** (1996) 93.
[81] NIST Ground Levels and Ionization Energies, http://physics.nist.gov/PhysRefData/IonEnergy/tblNew.html.
[82] V. Kellö, M. Urban, A.J. Sadlej, *Chem. Phys. Lett.* **253** (1996) 383.
[83] K.P. Huber, G. Herzberg, *Molecular Spectra and Molecular Structure, vol. 4*, Van Nostrand, New York, 1979.
[84] I. Miadoková, V. Kellö, A.J. Sadlej, *Theoret. Chem. Acc.* **96** (1997) 166.
[85] P. Schwerdtfeger, M. Dolg, W.H.E. Schwarz, G.A. Bowmaker, P.D.W. Boyd, *J. Chem. Phys.* **91** (1989) 1762.
[86] W.H.E. Schwarz, A. Rutkowski, S.G. Wang, *Int. J. Quantum Chem.* **57** (1996) 641.
[87] T. Okabayashi, Y. Nakaoka, E. Yamazaki, M. Tanimoto, *Chem. Phys. Lett.* **366** (2002) 406.
[88] P. Schwerdtfeger, J.S. McFeaters, M.J. Liddell, J. Hrušák, H. Schwarz, *J. Chem. Phys.* **103** (1995) 245.
[89] P. Schwerdtfeger, G.A. Bowmaker, *J. Chem. Phys.* **100** (1994) 4487.
[90] J. Granatier, M. Urban, in press.
[91] V. Dubois, P. Archirel, P. Maitre, *Chem. Phys. Lett.* **323** (2000) 1.
[92] J. Miyawaki, K. Sugawara, H. Takeo, C. Dedonder-Lardeux, S. Martnenchard-Barra, C. Jouvet, D. Solgadi, *Chem. Phys. Lett.* **302** (1999) 354.
[93] J. Miyawaki, K. Sugawara, *J. Chem. Phys.* **119** (2003) 6539.
[94] D.Y. Wu, M. Hayashi, C.H. Chang, K.K. Liang, S.H. Lin, *J. Chem. Phys.* **118** (2003) 4073.
[95] M. Urban, A.J. Sadlej, *J. Chem. Phys.* **112** (2000) 5.
[96] P. Hobza, R. Zahradník, *Intermolecular Complexes (The Role of van der Waals Systems in Physical Chemistry and in Biodisciplines)*, Elsevier, Amsterdam, 1988.
[97] N.A. Lambropoulos, J.R. Reimers, N.S. Hush, *J. Chem. Phys.* **116** (2002) 10277.
[98] Y. Akinaga, T. Nakajima, K. Hirao, *J. Chem. Phys.* **114** (2001) 8555.
[99] E.J. Baerends, *Theoret. Chem. Acc.* **103** (2000) 265.

This page intentionally left blank

Restricted Density Functional Response Theory for Open-Shell Systems

Zilvinas Rinkevicius, Lyudmyla Telyatnyk and Olav Vahtras

Royal Institute of Technology, Department of Biotechnology, SE-10691 Stockholm, Sweden

Abstract

This work presents development, implementation and applications of density functional theory (DFT) methods for calculation molecular properties of open-shell molecules. The theory of restricted open-shell density functional response theory is briefly summarized and the advantages and disadvantages of a spin-restricted formulation is discussed. Sample calculations are presented and discussed for excitation energies, polarizabilities and ESR spectral parameters: g-tensors and A-tensors (hyperfine coupling constants). For the A-tensors a recent generalization of the restricted-unrestricted approach [Fernandez, *et al., J. Chem. Phys.* **97** (1992) 3412] has been used. It is found that the additional complexity of spin-restricted methods is motivated by the quality of our results.

Contents

1. INTRODUCTION

Density functional theory (DFT) relies on two basic theorems by Hohenberg and Kohn [1] and an ingenious computational scheme known as Kohn–Sham equations [2]. The basic quantity is the one-electron density; the ground-state energy of an interacting system of electrons is in the absence of degeneracies a unique functional of the density, and its one-to-one relation to the external potential suggests the existence of a non-interacting system with the same density.

The most common approach to density functional theory for closed as well as open-shell systems is in the form of spin-density functional theory (SDFT), where particle and

ADVANCES IN QUANTUM CHEMISTRY, VOLUME 50
ISSN: 0065-3276 DOI: 10.1016/S0065-3276(05)50013-3

spin density (or equivalently α- and β-density) are optimized separately. Besides the vast body of computational experience, the theoretical foundations for SDFT is still not clear which is illustrated by specific examples on non-unique density-potential mappings [3,4]. However, the tradition of DFT is to let the results judge the merits of a method, and we submit to this tradition. On the other hand, we do not follow the most common path for solving open-shell problems—the spin-unrestricted optimization method. We will in this communication motivate the use of the spin-restricted method.

1.1. Spin contamination in DFT

It is a fundamental fact of quantum mechanics, that a spin-independent Hamiltonian will have pure spin eigenstates. There are classes of approximate wave functions that are not spin eigenstates, *e.g.*, those obtained with various unrestricted methods. These wave functions give increased flexibility at the cost of spin contamination which is not present in the exact state. For many molecular properties, such as equilibrium geometries, this disadvantage is of minor importance. However, when it comes to ESR spectral parameters which are directly related to the spin state of the molecule there is need for caution. The expectation value of the square of the total spin angular momentum operator, $\langle S^2 \rangle$, has been used as a measure of the degree of spin contamination. Wang *et al.* [5] used various approximations for the two-electron density required for evaluating $\langle S^2 \rangle$ in DFT. They expressed the two-electron density matrix in terms of one-electron density matrices, using Löwdin's relation [6]. The one-electron density matrix was further written in terms of the density and a correlation hole function, of which the latter was estimated within two simple approximations: a Gaussian function and a homogeneous electron gas approximation. It was shown that for the electron gas approximation the exact value $S(S+1)$ was a lower bound for the calculated value of $\langle S^2 \rangle$ and that spin contamination was absent whenever $\rho^{\alpha}(\vec{r}) > \rho^{\beta}(\vec{r})$ in all space. This obviously holds for a spin-restricted density functional method where the non-interacting wave-function is a high-spin determinant. A compelling argument for using such a method is thus that the underlying wave function of the interacting system is a spin eigenfunction.

One of our main motivations for pursuing the development of a density functional response theory for open-shell systems has been to calculate spin-Hamiltonian parameters which are fundamental to experimental magnetic resonance spectroscopy. In most cases the effective spin operator of the spin Hamiltonian coincide with the total electronic spin of the molecule. Then, it is only within the context of a state with well-defined spin that theory can make predictions about the parameters. The relationship between microscopic and effective Hamiltonians rely on the Wigner–Eckart theorem for tensor operators of a specific rank and states which transform according to their irreducible representations [7].

Below we briefly repeat the theory for open-shell density functional KS and response theory. In the applications section we have collected applications to excitation energies, dynamic polarizabilities, electronic g-tensors (in vacuum and solution) and paramagnetic nuclear magnetic shieldings. In many cases we observe for restricted calculations an improved agreement with available experimental data, over similar unrestricted calculations. When there is lack of agreement between theory and experiment for both restricted and unrestricted calculations we are in a position to dismiss explanations that the disagreement in the unrestricted case is due to spin contamination. Our restricted method thus complements the unrestricted methods.

2. THEORY

2.1. Restricted open-shell Kohn–Sham theory

In Kohn–Sham theory [2] the ground state energy of an interacting system of N electrons in an external potential $v(\vec{r})$ is obtained from

$$E[\rho] = -\frac{1}{2}\int \mathrm{d}\vec{r}\,\langle\Psi|\hat{\psi}(\vec{r})^{\dagger}\nabla^2\hat{\psi}(\vec{r})|\Psi\rangle + \frac{1}{2}\iint \mathrm{d}\vec{r}_1\,\mathrm{d}\vec{r}_2\frac{\rho(\vec{r}_1)\rho(\vec{r}_2)}{|\vec{r}_1-\vec{r}_2|} + E_{xc}[\rho] + \int \mathrm{d}\vec{r}\,\rho(\vec{r})v(\vec{r}) \tag{1}$$

where the use of Kohn–Sham (KS) spin-orbitals $\{\phi_i\}$ is implied;

$$\rho(\vec{r}) = \sum_i^N \phi_i^*\phi_i \equiv \langle\Psi|\hat{\psi}(\vec{r})^{\dagger}\hat{\psi}(\vec{r})\Psi\rangle \equiv \langle\Psi|\hat{\rho}(\vec{r})\Psi\rangle, \tag{2}$$

$$\hat{\psi}(\vec{r}) = \sum_i \phi_i(\vec{r})a_i \tag{3}$$

which diagonalize the effective one-electron Hamiltonian

$$F(\vec{r}) = -\frac{1}{2}\nabla^2 + \int \mathrm{d}\vec{r}'\frac{\rho(\vec{r}')}{|\vec{r}-\vec{r}'|} + \frac{\delta E_{xc}}{\delta\rho(\vec{r})} + v(\vec{r}). \tag{4}$$

The expectation values in (1) and (2) are with respect to the KS determinant which represents the state of the non-interacting reference system

$$|\Psi\rangle = \left(\prod_{i=1}^N a_i^{\dagger}\right)|\mathrm{vac}\rangle. \tag{5}$$

The exact energy functional (and the exchange correlation functional) are indeed functionals of the total density, even for open-shell systems [8]. However, for the construction of approximate functionals of open-shell systems, it has been advantageous to consider functionals with more flexibility, where the α- and β-densities can be varied separately, *i.e.*, $E[\rho_\alpha, \rho_\beta]$. The variational search for a minimum of the $E[\rho_\alpha, \rho_\beta]$ functional can be carried out by unrestricted and spin-restricted approaches. The two methods differ only by the conditions of constraint imposed in minimization and leads to different sets of Kohn–Sham equations for the spin orbitals. The unrestricted Kohn–Sham approach is the one most commonly used and is implemented in various standard quantum chemistry software packages. However, this method has a major disadvantage, namely a spin contamination problem, and in recent years the alternative spin-restricted Kohn–Sham approach has become a popular contester [9–11].

Consider a trial KS determinant which is parameterized by a real unitary exponential operator

$$|\widetilde{\Psi}\rangle = \mathrm{e}^{-\hat{\kappa}}|\Psi\rangle. \tag{6}$$

If the α and β orbitals are constructed from the same set and the transformation is of the form

$$\hat{\kappa} = \sum_{rs}\kappa_{rs}(a_{r\alpha}^{\dagger}a_{s\alpha} + a_{r\beta}^{\dagger}a_{s\beta}) \tag{7}$$

we have a spin-restricted optimization. Thus a variation of the energy then gives

$$\delta E[\rho_\alpha, \rho_\beta] = \sum_\sigma \int \mathrm{d}\vec{r} \frac{\delta E}{\delta \rho_\sigma(\vec{r})} \delta\rho_\sigma(\vec{r}) = \sum_\sigma \int \mathrm{d}\vec{r} \frac{\delta E}{\delta \rho_\sigma(\vec{r})} \langle [\delta\hat{\kappa}, \hat{\rho}_\sigma(\vec{r})\rangle$$
$$= \langle [\delta\hat{\kappa}, \widehat{F}\,]\rangle \tag{8}$$

where we have introduced the Fock operator

$$\widehat{F} = \sum_\sigma \int \mathrm{d}\vec{r} \hat{\psi}^\dagger_\sigma(\vec{r}) \frac{\delta E}{\delta \rho_\sigma(\vec{r})} \hat{\psi}_\sigma(\vec{r}) = \sum_{rs\sigma} F^\sigma_{rs} a^\dagger_{r\sigma} a_{s\sigma} \tag{9}$$

of which the α- and β-parts have matrix representations corresponding to the KS Fock matrices. A restricted open-shell Roothan optimization which is based on the diagonalization of an effective Fock matrix can be designed in different ways—the main criterion is that the off-diagonal blocks (closed-open, open-virtual, closed-virtual) are zero for a converged state. If we translate $\langle [\hat{\kappa}, \widehat{F}]\rangle$ to a matrix formulation in an atomic orbital basis and we use the overlap S, the closed (c) and open-shell (o) Fock matrices

$$F^c = \frac{F^\alpha + F^\beta}{2}, \tag{10}$$
$$F^o = F^\alpha \tag{11}$$

and density matrices

$$D^c = 2D^\beta, \tag{12}$$
$$D^o = D^\alpha - D^\beta \tag{13}$$

we obtain a gradient of the form

$$S(D^c F^c + D^o F^o) - (F^c D^c + F^o D^o) S. \tag{14}$$

Similarly, a specific choice of an adequate effective Fock matrix is the closed shell Fock matrix with a correction such that the off-diagonal blocks associated with the open-shell orbitals are adjusted to be proportional to the orbital gradient [12]

$$F = F^c + F^v + (F^v)^T,$$
$$F^v = SD^o(F^c - F^o)\big((D^c + D^o)S - 1\big). \tag{15}$$

The effective Fock matrix (15) is in our implementation [13] the quantity which is averaged in the optimization based on the direct inversion in the iterative subspace (DIIS) method [14]. This formulation applies equally to doublet states ($S = 1/2$) and high-spin states ($S > 1/2$).

2.2. Restricted open-shell density functional response theory

When a molecular system is subject to a time-dependent perturbation V, a property A has a time evolution which can be expressed in terms of response functions

$$\langle \tilde{0}|\hat{A}|\tilde{0}\rangle = \langle 0|\hat{A}|0\rangle + \int \langle\!\langle \hat{A}; \widehat{V}^{\omega_1} \rangle\!\rangle_{\omega_1} \mathrm{e}^{-\mathrm{i}\omega_1 t} d\omega_1 + \cdots, \tag{16}$$

where the perturbation is assumed to have a Fourier representation

$$\widehat{V}(t) = \int_{-\infty}^{\infty} \widehat{V}^{\omega} \mathrm{e}^{-\mathrm{i}\omega t}\, \mathrm{d}\omega. \tag{17}$$

The response of a property that is a simple functional of the density can be determined within the non-interacting system if we can solve the time-dependent Kohn–Sham equations [15]

$$\left(\widehat{F}(t) + \widehat{V}(t)\right)\left|\widetilde{\Psi}\right\rangle = \mathrm{i}\frac{\mathrm{d}}{\mathrm{d}t}\left|\widetilde{\Psi}\right\rangle. \tag{18}$$

This can be done for standard model functionals within the adiabatic approximation; the time-dependence of the exchange-correlation potential is implicit and the functional dependence on the density is assumed to be the same as in the time-independent case.

In the previous section we used an exponential operator as a tool for optimizing the Kohn–Sham orbitals. Here we use an exponential operator of the same form, but now the interpretation is an explicit parameterized time-evolution operator. Following Olsen and Jørgensen [16] we can then formulate a time-dependent variational principle based on the Ehrenfest principle

$$\langle\Psi|\left[\mathbf{q}^{\dagger}, \mathrm{e}^{\kappa}\left(\widehat{F} + \widehat{V} - \mathrm{i}\frac{\mathrm{d}}{\mathrm{d}t}\right)\mathrm{e}^{-\kappa}\right]|\Psi\rangle = 0 \tag{19}$$

where $\mathbf{q}$ is arbitrary, but chosen as a column vector of the non-redundant excitation operators. This gives systems of equations for solving the parameters, *i.e.*, the matrix elements of the operator κ. Expanding the parameter matrix in powers of the perturbation

$$\kappa = \kappa^{(1)} + \kappa^{(2)} + \cdots \tag{20}$$

we require that (19) be satisfied in all orders. The first-order change in A with an exponential evolution operator is

$$A^{(1)} = \left\langle\left[\kappa^{(1)}, \hat{A}\right]\right\rangle = \int \mathrm{d}\omega\left\langle\left[\kappa^{\omega}, \hat{A}\right]\right\rangle \mathrm{e}^{-\mathrm{i}\omega t} \equiv \int \mathrm{d}\omega\left\langle\!\left\langle \hat{A}; \widehat{V}^{\omega_1}\right\rangle\!\right\rangle_{\omega} \mathrm{e}^{-\mathrm{i}\omega t} \tag{21}$$

and the first-order parameters are solved from the first-order expansion of (19)

$$\langle\Psi|\left[\mathbf{q}, \left[\kappa^{\omega}, \widehat{F}\right] + \widehat{F}^{\omega} + \widehat{V}^{\omega} + \omega\kappa^{\omega}\right]|\Psi\rangle = 0 \tag{22}$$

where $\widehat{F}^{\omega}$ is the first-order Fock-matrix containing the exchange-correlation kernel. For details we refer to Refs. [17,18].

2.3. Excitations in open-shell systems

A few remarks are in place on the excitations in open-shell system. Maurice and Head-Gordon [19] proposed a generalization of a single-excitation configuration interaction (CIS) for open-shell molecules. They made it clear that in standard CIS scheme, some configurations are missing that may be important for the description of excited states. In Fig. 1 we have a graphical presentation of the excitations in open-shell systems; open-virtual (I), closed-open (II), closed-virtual and the double excitations closed-open and open-virtual

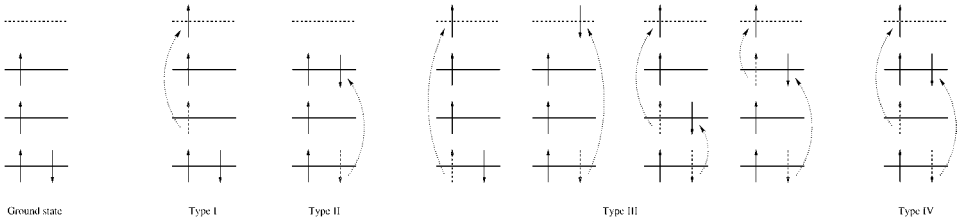

Fig. 1. Classification of excitation schemes in open-shell molecules with high spin ground state.

involving the same open-shell orbitals (III), and finally similar double excitations which involve two different open-shell orbitals (IV).

Most TD-DFT implementations are based on single excitations that are adequate for closed-shell systems. The generalizations to open-shell systems are obtained by including excitations of type I and II. In other aspects the RPA equations (22) are similar in structure. If the off-diagonal blocks (excitation, de-excitation) are omitted in the RPA matrix we have a Tamm–Dancoff approximation which is equivalent to CIS. Although the off-diagonal blocks couple the reference determinant with doubly excited configurations it is clear that the double excitations of type III are not represented. They can be perceived as combinations of closed-virtual triplet excitations and a spin-flip of the open-shell orbital. It can therefore be expected that the quality of Hartree–Fock RPA calculations of open-shell molecules will deteriorate when there are low-lying excited state of double excitation character, and that these problems will carry over to DFT.

2.4. Spin polarization in evaluation of molecular properties: the restricted–unrestricted approach

Hyperfine couplings, in particular the isotropic part which measures the spin density at the nuclei, puts special demands on spin-restricted wave-functions. For example, complete active space (CAS) approaches are designed for a correlated treatment of the valence orbitals, while the core orbitals are doubly occupied. This leaves little flexibility in the wave function for calculating properties of this kind that depend on the spin polarization near the nucleus. This is equally true for self-consistent field methods, like restricted open-shell Hartree–Fock (ROHF) or Kohn–Sham (ROKS) methods. On the other hand, unrestricted methods introduce spin contamination in the reference (ground) state resulting in overestimation of the spin-polarization.

The philosophy of the restricted–unrestricted (RU) approach is a physically motivated compromise between the restricted and unrestricted methods; to optimize the wave function with a spin-restricted approach and to account for perturbations with an unrestricted approach. That is, a ground state constructed from α and β spin-orbitals with common orbital parts is used with satisfies the variational condition

$$\frac{\mathrm{d}E}{\mathrm{d}\kappa} = 0 \tag{23}$$

where E is the electronic energy and κ is a molecular (spatial) orbital parameter (*i.e.*, the parameters of equation (7) collected in a vector). Next, the properties are calculated

with a set of parameters that allow the α- and β-orbitals respond independently to the perturbation. This can be done by considering parameters for α and β-orbitals separately, or as in the work of Fernandez *et al.* [20] in terms of singlet and triplet rotations of the ground state orbitals $\kappa = (\kappa_s, \kappa_t)$.

Next we outline the derivations of Fernandez *et al.* [20] and the generalization for DFT. The hyperfine coupling (HFC) Hamiltonian is scaled with a perturbation strength and a energy a perturbation strength x is used

$$\widehat{H}(x) = \widehat{H}_0 + x\widehat{H}_{\text{hfc}} \tag{24}$$

such that energy and the parameters are functions of x

$$E(x, \kappa) = \langle \kappa(x) | \widehat{H}(x) | \kappa(x) \rangle. \tag{25}$$

This gives a first-order change in the total electronic energy as

$$\begin{aligned} E_{\text{hfc}} = \frac{\mathrm{d}E}{\mathrm{d}x}\bigg|_{x=0} &= \frac{\partial E}{\partial x} + \sum_{\sigma=s,t} \frac{\partial E}{\partial \kappa_\sigma} \frac{\mathrm{d}\kappa_\sigma}{\mathrm{d}x}\bigg|_{x=0} \\ &= \langle \kappa(0) | \widehat{H}_{\text{hfc}} | \kappa(0) \rangle + \frac{\partial E}{\partial \kappa_t} \frac{\mathrm{d}\kappa_t}{\mathrm{d}x}\bigg|_{x=0} \end{aligned} \tag{26}$$

where we used equation (23), the variational condition for the singlet parameters; if the wave function is assumed to be optimized for finite x, the first-order response of the singlet-parameters is by definition zero.

In order to determine the response of the triplet parameters Fernandez *et al.* [20] assume that the change in the non-zero energy gradient is negligible when the perturbation is turned on ($x \neq 0$); this gives a logical connection between perturbed and un-perturbed systems and ensures a continuous energy. We need then to solve the coupled equations

$$0 = \frac{\mathrm{d}}{\mathrm{d}x} \frac{\partial E}{\partial \kappa_\sigma} = \frac{\partial^2 E}{\partial x \partial \kappa_\sigma} + \sum_{\tau=s}^{t} \frac{\partial^2 E}{\partial \kappa_\sigma \partial \kappa_\tau} \frac{\partial \kappa_\tau}{\mathrm{d}x}\bigg|_{x=0}, \quad \sigma = s, t. \tag{27}$$

A second approximation involves neglecting the singlet contributions in the calculations of the polarization effects. This is the same as to neglect the singlet-triplet coupling in the second derivative of the energy. It simplifies equation (27) considerably and the problem is reduced to solving conventional RPA-type equations

$$E_{\text{hfc}} = \langle \kappa | \widehat{H}_{\text{hfc}} | \kappa \rangle - \frac{\partial^2 E}{\partial x \partial \kappa_t} \left(\frac{\partial^2 E}{\partial \kappa_t^2} \right)^{-1} \frac{\partial E}{\partial \kappa_t}\bigg|_{x=0} \tag{28}$$

which using the notation for response functions is equivalent to

$$E_{\text{hfc}} = \langle \widehat{H}_{\text{hfc}} \rangle + \langle\langle \widehat{H}_{\text{hfc}}; \widehat{H}_0 \rangle\rangle_0. \tag{29}$$

In DFT the energy is not the expectation value of a Hamiltonian, but rather a functional of the form

$$E[\rho_x, x] = E[\rho_x] + x\langle \widehat{H}_{\text{hfc}} \rangle. \tag{30}$$

The ground state density will depend on the field strength parameter x, which is denoted by a subscript. The functional has both an explicit and an implicit dependence on x and the first-order energy correction, the total derivative is formed by a partial derivative and a

functional derivative

$$\left.\frac{\mathrm{d}E}{\mathrm{d}x}\right|_{x=0} = \frac{\partial E}{\partial x} + \int \mathrm{d}\vec{r}\,\frac{\delta E}{\delta \rho_x(\vec{r})}\left.\frac{\partial \rho_x(\vec{r})}{\partial x}\right|_{x=0}. \tag{31}$$

The first term is the expectation value and from the fact that the density change is the static linear response function

$$\left.\frac{\partial \rho_x}{\partial x}\right|_{x=0} = \left\langle\!\left\langle \hat{\rho}(\vec{r});\, \widehat{H}_{\mathrm{hfc}} \right\rangle\!\right\rangle \tag{32}$$

and identifying the Fock operator of equation (9) we have that the second part of (31) is the linear response function for the Fock operator and the perturbation giving

$$\left.\frac{\mathrm{d}E}{\mathrm{d}x}\right|_{x=0} = \left\langle \widehat{H}_{\mathrm{hfc}} \right\rangle + \left\langle\!\left\langle \widehat{F};\, \widehat{H}_{\mathrm{hfc}} \right\rangle\!\right\rangle \tag{33}$$

For the special case that the exchange-correlation potential is the Hartree–Fock exchange, equations (29) and (33) are identical.

3. SAMPLE APPLICATIONS

In this section we review some of our recent applications of restricted density functional response theory. The calculations below are subsets of larger investigations, some of which have been published elsewhere. We find it valuable to summarize these results to illustrate the range of properties that our methods apply to. For a detailed account of these calculations we refer to the original articles, where referenced.

3.1. Excitation energies: the naphthalene cation

The spin-restricted DFT linear response method was first applied to the excitation spectrum of the naphthalene cation radical [18]. This radical which has a ^2A_u ground state is a good test case as there is plenty of experimental [21,22] as well as computational data, with *ab initio* (MRSDCI [23], CASPT2 [21]) as well as DFT [24] methods. In Table 1 we have collected the excitation spectrum for the ten lowest states. The most interesting excitations where the spin-restricted method seems to fail concern the 6^2B_{3g}, 7^2B_{2g}, 9^2B_{1u} and 10^2B_{2g} states for which our formalism overestimates the excitation energies considerably. However, a singles-doubles configuration interaction (SDCI) analysis shows that the reason for this is that these states have a high degree of double excitation character—in particular the 10^2B_{2g} state for which a double excitation of type III (a triplet excitation singlet coupled with a spin-flip in the open-shell orbital) has a 81% weight. An RPA-like method where higher-order excitations have been neglected is then bound to fail. The reason why the unrestricted methods are more reliable in these situations could be that the combination of singlet and triplet excitations (which is effectively an unrestricted approach) generate a part of the configuration having a triplet character (see Section 2.3)—the double excitations are lacking here as well. However, similar comparison of restricted and unrestricted Hartree–Fock methods does not show the same improvement [25] so we are inclined to believe that there is some other cancellation of errors.

Table 1. Lowest vertical excitation energies[a] of naphthalene cation radical calculated with RDFT-LR approach

State	LDA	BLYP	B3LYP	ULDA[b]	UBLYP[b]	UBLYP[b,c]	UB3LYP[b]	MRSDCI[d]	CASPT2[e]	Exp.[f]
$1\ ^2B_{1u}$	0.99	1.02	1.07	1.01	1.05	1.11	1.13	1.13	0.99	0.73[g]
$2\ ^2B_{2g}$	2.21	2.17	2.16	2.21	2.16	2.35	2.15	2.16	1.89	1.84
$3\ ^2B_{3g}$	2.83	2.78	2.97	2.83	2.78	2.85	2.99	2.94	2.70	2.69
$4\ ^2A_g$	2.57	2.88	3.36	2.60	2.92	2.92	3.43	...	...	...
$5\ ^2B_{1g}$	2.66	2.94	3.44	2.68	2.97	2.97	3.49	...	...	...
$6\ ^2B_{3g}$	3.65	3.61	3.87	3.62	3.53	3.73	3.61	3.51	3.24	3.25
$7\ ^2B_{2g}$	4.30	4.29	4.55	3.81	3.75	3.78	3.92	4.38	3.98	4.02
$8\ ^2B_{2u}$	3.54	3.83	4.45	3.56	3.87	3.87	4.50	...	...	...
$9\ ^2B_{1u}$	4.43	4.39	4.77	4.32	4.19	4.26	4.23	4.25	4.03	...
$10\ ^2B_{2g}$	5.63	5.61	5.83	4.32	4.33	4.35	4.65	5.14	4.44	4.55

Reproduced from *J. Chem. Phys.* 119 (2003) 34.

[a] Calculations performed for naphthalene cation radical ^2A_u ground state using B3LYP/6-31G* optimized geometries from Ref. [21] in 6-31G** basis set.

[b] Ref. [24]. Unrestricted TD-DFT calculations in 6-31G** basis set.

[c] Tamm–Dancoff approximation.

[d] Ref. [23]. Multireference single and double excitation configuration interaction.

[e] Ref. [21]. CASPT2 calculation with nine active electrons in five occupied and five virtual π molecular orbitals.

[f] Ref. [21]. Peak positions of electronic absorption spectra.

[g] Ref. [21]. Peak positions of photoelectron spectra.

A comparison of exchange-correlation functionals shows that the LDA functional gives an incorrect ordering of the 3^2B_{3g}, 4^2A_g and 5^2B_{1g} for both restricted and unrestricted methods so the gradient corrections of GGA type functionals seem to be important for the description of excited states. The B3LYP functional systematically overestimates the excitation energies and is in fact the most sensitive functional regarding excited states of double excitation character. For both unrestricted and restricted methods the BLYP functional give results that are closest to experiment.

To summarize, excluding the excited states with substantial double excitation character, the restricted calculations closely reproduce the unrestricted results, with an agreement with available experimental data within 0.4 eV for the BLYP exchange–correlation functional.

3.2. Dynamic polarizabilities: the CN radical

The dynamic polarizability tensor were calculated for a set of functionals (LDA, BLYP, B3LYP) for the CN radical, [18] using the augmented correlation consistent valence quintuple zeta (aug-cc-pV5Z) basis set [26]. From the apparent lack of correlated calculations of this property we used the TDROHF-MP2 method as a Ref. [27].

In Fig. 2 we show the frequency dependence of the averaged polarizabilities. We observe that the reference TDROHF-MP2 calculation show an unusual increase in the higher frequency range. This is attributed to a poor pole structure in the corresponding response function. The B3LYP results show a similar increase - the overestimation of the polarizability is coupled with an underestimation of the first excitation energy by as much as 0.3 eV. The LDA and BLYP functionals on the other hand reproduce the experimental excitation energy within 0.06 eV [28] and show a consistent increase with respect to frequency. These functionals were most accurate for the static polarizabilities where spin-adapted coupled cluster calculations where used as reference [18] and it is natural to believe that the same applies to the static polarizabilities as well.

3.3. *g*-tensors of transition metal radicals

The electronic g-tensor has first- and second-order contributions in a perturbation theory that is based on the partitioning of the electronic Hamiltonian into a non-relativistic and a relativistic part. The first-order contributions are the relativistic mass corrections in the Zeeman effect and the field-dependent part of the spin-orbit operator (diamagnetic or gauge-correction terms). The second-order contribution (paramagnetic), which is often dominating, is the cross term between the orbital Zeeman operator and the field-free (canonical) part of the spin-orbit operator.

As the spin-orbit operator contains two-electron terms a density functional application is not straightforward. For correlated methods it is well known that the mean-field approximation [29] of the spin-orbit operator is an excellent approximation for molecules containing heavy atoms. The diamagnetic two-electron is further negligible in most cases and is not expected to have an effect here. With these approximations we have thus solved the two-electron dilemma.

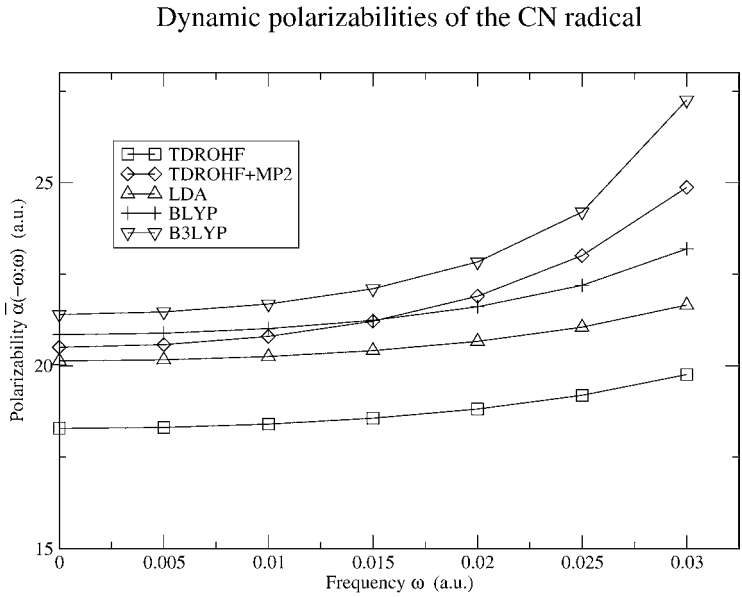

Fig. 2. Frequency dependence of the averaged dynamic polarizability of the CN radical.

Another dilemma is that the paramagnetic contribution is a combination of two differential operators and that density functional theory only asks questions which can be answered by the density, not the density matrix. All is well though, if we consider a perturbation theory which starts out with relativistic Kohn–Sham equations and that we have knowledge about relativistic functionals. This is of course not the case, but as many others we take a practical approach to relativistic functionals and use what we have—the standard non-relativistic functionals.

In Ref. [30], the restricted density functional linear response method was used to calculate g-tensors for a series of transition metal compounds: TiF_3, VOF_4^{2-}, $VOCl_4^{2-}$, CrO_4^- and $Cu(NO_3)_2$. These had been studied before by Neese [31] with unrestricted methods and were thus suitable test cases.

The results are reported in Table 2. It can be concluded the g-shifts are underestimated for both restricted and unrestricted methods. A conclusion that can be drawn is that spin contamination is not the source of error in these cases. We believe that the functionals are not just capable of describing properties of this kind and that it is natural to expect that magnetic properties requires functionals that include current densities.

3.4. *g*-tensors in solution using the polarizable continuum model

In Ref. [33] we applied the polarizable continuum model (PCM) in the integral equation formalism [34] to calculate the g-tensor of di-*t*-butyl nitric oxide (N-I) (Fig. 3, right), and diphenyl nitric oxide (left), using the B3LYP and BP86 exchange-correlation functionals and IGLO-II basis sets [35,36]. As solvents we used both protic (methanol, water) and aprotic solvents (carbon tetrachloride, toluene, acetone, acetonitrile).

Table 2. Electronic g-tensors of transition metals compounds evaluated with various exchange–correlation functionals[a,b]

Molecule	Δg_{ii}	LDA	BLYP	B3LYP	UBP[c]	UB3LYP[d]	Exp[e]
TiF_3	$\Delta g_{\parallel}$	0.3	0.3	0.2	−1.7	−1.1	−11.1
	$\Delta g_{\perp}$	−47.0	−32.9	−49.1	−42.8	−41.8	−111.9
VOF_4^{2-}	$\Delta g_{\parallel}$	−37.0	−30.3	−39.5	−36.0	−34.1	−58.8
	$\Delta g_{\perp}$	−29.6	−21.8	−24.2	−28.0	−25.0	−51.1
$VOCl_4^{2-}$	$\Delta g_{\parallel}$	−20.6	−16.0	−28.3	−18.0	−20.5	−51.1
	$\Delta g_{\perp}$	−17.9	−14.4	−16.9	−20.0	−20.6	−32.2
$CrOF_4^{-}$	$\Delta g_{\parallel}$	−15.9	−12.4	−17.5	−19.0	−18.1	−33.5
	$\Delta g_{\perp}$	−27.9	−21.4	−21.9	−29.0	−27.0	−50.7
$Cu(NO_3)_2$	Δg_{11}	126.5	120.0	173.3	...	171.2	246.6
	Δg_{22}	31.6	30.9	44.4	...	46.0	49.9
	Δg_{33}	29.0	28.9	43.9	...	44.6	49.9

Reproduced from *J. Chem. Phys.* 119 (2003) 10489.

[a] Calculation performed at the geometries taken from Ref. [31].

[b] Electronic g-tensor shifts are given in the principle axis system. Values are in ppt.

[c] Ref. [32]. Unrestricted coupled perturbed Kohn–Sham calculations in gauge invariant atomic orbitals.

[d] Ref. [31]. Unrestricted coupled perturbed Kohn–Sham calculations.

[e] Experimental data taken form Ref. [31].

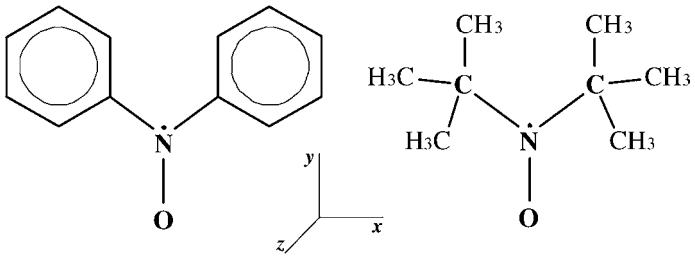

Fig. 3. The diphenyl nitric oxide (left) and the di-*t*-butyl nitric oxide (right) geometries and orientation of principal axes for electronic g-tensor.

It was found that in the case aprotic solvents, the model was capable of qualitative predictions of the solvent effects on the g-tensor. In Fig. 4 we see that with the solvents arranged with increasing dielectric constant the calculated isotropic g-shifts decrease and thus follow the experimental trends. The dominating solvent effect on the g-shift is due to a blue-shift of the $n - \pi^*$ which has consequences for the paramagnetic contribution to the g-tensor.

However, in the case of protic solvents hydrogen bonding is responsible for the major change in the electronic structure of the solute which influences the g-tensor. In these cases the PCM model fails which is only designed to handle long-range electrostatic effects. In Table 3 we show the hydrogen bonding effects on the calculated g-tensors. The results

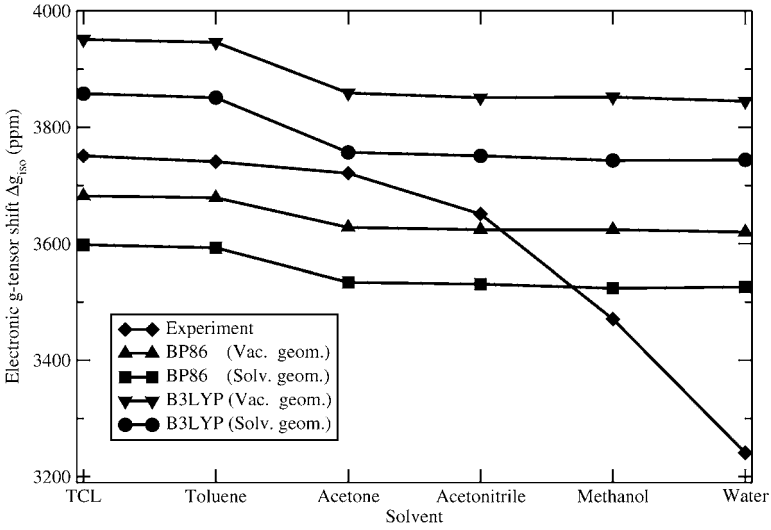

Fig. 4. The experimentally determined isotropic g-tensor shift and corresponding theoretically evaluated isotropic g-tensor shift dependence on the employed solvent.

suggest that in these cases it is necessary to include explicit solvent molecules and calculate the g-tensor for the whole complex. On top of that one can apply the PCM model to the hydrogen bonded complex to account for long-range solvent effects.

3.5. Hyperfine-coupling in transition metal radicals

The restricted-unrestricted (RU) approach (Section 2.4) have been applied to calculate the isotropic hyperfine coupling constants of a sequence of transition metal compounds: TiO($X^3\Delta$), VN($X^3\Delta$), VO($X^4\Sigma^-$), MnO($X^6\Sigma^-$), MnH($X^7\Sigma^+$), $TiF_3(^2A_1')$ and $MnO_3(^2A_1')$, which have been investigated previously by Kaupp [38] with an unrestricted Kohn–Sham method. In Table 4 it can be seen that the overall quality of the RU results is slightly better than the corresponding unrestricted results, independent of functional. The isotropic constants obtained with the BHPW91 functional are the most problematic ones, and the reason is the failure to reproduce the excitation energies which are necessary to get the response term accurately. In Table 5 we have displayed the individual average and response contributions to the metal hyperfine couplings.

In the first group of radicals (TiO, VN, VO) the average term is the dominating part. These molecules have a singly occupied molecular orbital (SOMO) with a 4s character and the direct contribution from the electron density is more important.

The MnO and MnH are high spin systems with additional SOMOs; of 3d and 4p character and the spin-polarization is expected to be more important. These cases put a higher demand on the calculations as it is important have accurate excitation energies in order to have an accurate response term. Our calculations do not quite meet these requirements as the calculated response terms are smaller in absolute value than in the first group, which we believe to be the reason why the experimental agreement is worse.

Table 3. Electronic g-tensor of N-I in protic solvents[a]

Environment[b] Complex	B3LYP							
	Vacuum				Solvent			
	Δg_{xx}	Δg_{yy}	Δg_{zz}	Δg_{iso}	Δg_{xx}	Δg_{yy}	Δg_{zz}	Δg_{iso}
Methanol:								
N-I	−7	4135	7909	4012	−8	4044	7520	3852
N-I · CH_3OH	−86	3737	6963	3538	−87	3668	6696	3426
N-I · $(CH_3OH)_2$	−94	3662	6877	3482	−93	3611	6685	3401
N-I · $(CH_3OH)_3$	−108	1174	1014	693	−109	1216	1023	710
Water:								
N-I	−7	4135	7909	4012	−8	4040	7505	3845
N-I · H_2O	−77	3780	7034	3579	−77	3705	6772	3466
N-I · $(H_2O)_2$	−79	3667	6658	3415	−78	3624	6487	3344
N-I · $(H_2O)_3$	−94	3568	6531	3335	−96	3528	6390	3274

Environment[b] Complex	BP86								Exp.[c]
	Vacuum				Solvent				
	Δg_{xx}	Δg_{yy}	Δg_{zz}	Δg_{iso}	Δg_{xx}	Δg_{yy}	Δg_{zz}	Δg_{iso}	Δg_{iso}
Methanol:									
N-I	11	3907	7233	3717	12	3848	7013	3624	
N-I · CH_3OH	−71	3544	6477	3317	−71	3495	6318	3247	
N-I · $(CH_3OH)_2$	−70	3492	6483	3302	−70	3455	6372	3252	
N-I · $(CH_3OH)_3$	−88	1124	951	662	−90	1168	958	678	3471 ± 20
Water:									
N-I	11	3907	7233	3717	12	3846	7003	3620	
N-I · H_2O	−63	3587	6555	3360	−65	3534	6401	3290	
N-I · $(H_2O)_2$	−55	3485	6278	3236	−58	3458	6176	3192	
N-I · $(H_2O)_3$	−69	3400	6202	3178	−75	3371	6125	3140	3241 ± 10

[a] Electronic g-tensor shift values are in ppm.

[b] Geometry used in calculations is optimized in vacuum using B3LYP exchange-correlation functional. The calculations of g-tensor are carried out in vacuum (Environment–Vacuum) and in protic solvents (Environment–Solvent).

[c] Experimental data taken from Ref. [37].

Finally we have the MnO_3 and TiF_3 radicals which have SOMOs dominated by a $3d_{z^2}$ orbital which indicate a higher contribution from the direct term. However there are also substantial response terms. We have observed that the response term has different signs for different functionals. This inconsistency is attributed to the description of the excited states. In these cases the unrestricted results are closer to experiment.

A conclusion is that the RU approach often give better results than for the unrestricted approach. The exceptions are cases when the response terms are large and the excitation

Table 4. Calculated isotropic HFC constants, in MHz, of transition metal compounds and their dependence on the exchange-correlation functionals[a]

Molecule	Isotope	LDA	BP86	BLYP	B3LYP	BHPW91	UBP86	UBLYP	UB3LYP	UBHPW91	Exp.
TiO	^{47}Ti	−259.0	−245.0	−252.7	−248.6	−211.1	−251.0	−257.5	−252.8	−227.0	−241.0(60)
	^{17}O	−11.6	−11.5	−11.3	−7.9	3.7	−8.2	−8.2	−4.9	1.6	...
VN	^{51}V	1400.9	1321.8	1367.5	1317.4	1764.9	1393.5	1432.6	1388.9	1081.7	1311.8
	^{14}N	9.1	8.7	8.2	4.7	35.7	6.2	6.0	3.2	−7.2	...
VO	^{51}V	815.8	780.2	808.4	791.2	784.5	821.0	847.8	829.5	753.4	778.0(2)
	^{17}O	−6.9	−6.9	−6.0	−2.5	1.8	−3.1	−2.7	1.1	8.0	0(4)
MnO	^{55}Mn	512.7	507.8	527.9	508.6	904.5	526.8	543.1	521.8	504.7	479.9(100)
	^{17}O	−3.4	−5.6	−7.0	−9.4	−24.2	−5.4	−6.6	−8.0	−8.8	...
MnH	^{55}Mn	353.3	355.8	360.7	309.7	242.9	380.0	380.0	331.8	276.3	279.4(12)
	^{1}H	25.6	24.7	34.3	28.1	7.1	25.8	35.6	28.0	10.1	20.7(39)
TiF_3	^{47}Ti	−132.9	−127.5	−131.4	−158.2	−175.2	−216.6	−218.0	−192.2	−149.4	−184.8(4), −177.1(4)
	^{19}F	9.7	17.1	18.8	1.6	−13.8	5.0	8.7	−5.6	−24.3	8.3(4), 8.0(4)
$^{2}MnO_3$	^{55}Mn	1284.9	1262.2	1267.6	1476.2	1900.8	2009.3	2042.4	1735.5	1111.7	1613(6)
	^{17}O	−3.2	−3.9	−6.2	−6.4	8.4	−4.1	−5.1	2.6	19.0	...

[a] The geometry of radicals and experimental data are taken from Ref. [38].

Table 5. R-U contributions to isotropic HFC, in MHz, of transition metal compounds and their dependence on the exchange-correlation functionals

Molecule	Contr.	LDA	BP86	BLYP	B3LYP	BHPW91
^{47}TiO	Average	−284.58	−270.88	−274.54	−267.25	−238.21
	Response	25.61	25.84	21.82	18.66	27.06
^{51}VN	Average	1558.61	1483.36	1503.84	1474.55	1344.30
	Response	−157.68	−161.56	−136.37	−157.16	420.61
^{51}VO	Average	955.12	918.91	925.13	907.04	934.67
	Response	−139.29	−138.72	−116.69	−115.82	−150.21
^{55}MnO	Average	621.30	621.27	619.75	569.89	474.94
	Response	−108.64	−113.49	−91.83	−61.27	429.55
^{55}MnH	Average	493.92	496.00	479.32	430.91	399.18
	Response	−140.66	−140.16	−118.58	−121.20	−156.30
$^{47}TiF_3$	Average	−151.32	−146.47	−146.64	−166.89	−189.62
	Response	18.41	18.95	15.27	8.69	14.44
$^{55}MnO_3$	Average	1357.80	1327.72	1323.84	1215.64	936.37
	Response	−72.92	−65.54	−56.24	260.58	964.46

energies are not accurate. These cases can easily be identified however, and the RU method gives a higher degree of control over the calculational process and its analysis.

4. SUMMARY

We have presented a summary of recent theoretical developments and applications of spin-restricted density functional response theory to open-shell systems. We use a formalism that is free from spin contamination; to determine the ground state density the variational principle was applied to a trial Kohn–Sham determinant constructed from α- and β-orbitals of a common set. The response to a perturbation is parameterized in terms of an exponential unitary operator and the parameters are determined by a time-dependent variational principle.

In the restricted–unrestricted approach spin-polarization of the system is accounted for in the form a perturbation. This has the effect of increasing the computational complexity—a linear response function is required where expectation values suffices for unrestricted methods—but has the advantage of removing spin-contamination in the unperturbed system.

We have reported calculations on excitation energies of the naphthalene cation which essentially reproduce previously published unrestricted calculations. There are exceptions, when the excited states are predominantly of double excitation character, the excitation energies are overestimated. The best overall results were obtained for the BLYP functional.

The calculated dynamic polarizability of the CN radical show an anomalous increase with frequency for the B3LYP functional, which is related to an underestimation of the first excitation energy. The LDA and BLYP functionals are more reliable and in reproducing the experimental excitation energy and also show a more consistent increase.

From our calculations of g-tensors we selected a set of transition metal compounds. As was the case for the unrestricted calculations by Neese [31] our calculations underestimated the experimental g-tensors considerably. As our method is free from spin contamination we could rule out this as a possible source error.

Our calculations of g-tensors for molecules in solution was done within the PCM model. For diphenyl nitroxide and di-t-butyl nitric oxide we could reproduce the general trends of solvent effects on the g-tensor. For protic solvents the model fails because hydrogen bonding effects become important. In these cases it was necessary to include explicit solvent molecules in the model.

Finally we demonstrated applications of the RU method for hyperfine couplings. The examples that were problematic with our method where characterized by large cancellation effects between direct and response terms and incorrect excitation energies which determine the response part. In most cases however, our calculations show an improved experimental agreement over corresponding unrestricted calculations and demonstrate that the RU method is a useful complement to the unrestricted methods.

ACKNOWLEDGEMENTS

ZR acknowledges the support from the EU network “Molecular Properties and Molecular Materials” (MOLPROP, contract HPRN-CN-2000-0013). OV acknowledges support from the Swedish Research Council (VR) and the Carl Trygger Foundation (CTS).

Computational resources were provided by National Supercomputing Center, Linköping, the Center for Parallel Computers, Stockholm, and The High Performance Computing Program of the University of Tromsø.

REFERENCES

[1] P. Hohenberg, W. Kohn, *Phys. Rev.* **136** (1964) B864.
[2] W. Kohn, L.J. Sham, *Phys. Rev.* **140** (1965) A1133.
[3] U. von Barth, L. Hedin, *J. Phys. C* **5** (1972) 1629.
[4] K. Capelle, G. Vignale, *Phys. Rev. Lett.* **86** (2001) 5546.
[5] J. Wang, A.D. Becke, J. Vedene, H. Smith, *J. Chem. Phys.* **102** (1995) 3477.
[6] P.-O. Löwdin, *Phys. Rev.* **97** (1955) 1490.
[7] J.E. Harriman, *Theoretical Foundations of Electron Spin Resonance*, Academic Press, New York, 1978.
[8] R.G. Parr, W. Yang, *Density-Functional Theory of Atoms and Molecules*, Clarendon Press, Oxford, 1989.
[9] I. Okazaki, F. Sato, T. Yoshihiro, T. Ueno, H. Kashiwagi, *J. Mol. Struct.* **451** (1998) 109.
[10] M. Filatov, S. Shaik, *Chem. Phys. Lett.* **288** (1998) 689.
[11] T.V. Russo, R.L. Martin, P.J. Hay, *J. Chem. Phys.* **101** (1994) 7729.
[12] H.J.A. Jensen, Private communication (see also Ref. [13]).
[13] Dalton, A molecular electronic structure program, Release 2.0, 2004.
[14] T.P. Hamilton, P. Pulay, *J. Chem. Phys.* **84** (1986) 5728.
[15] E. Runge, E.K.U. Gross, *Phys. Rev. Lett.* **52** (1983) 997.
[16] J. Olsen, P. Jørgensen, *J. Chem. Phys.* **82** (1985) 3235.
[17] P. Salek, O. Vahtras, T. Helgaker, H. Ågren, *J. Chem. Phys.* **117** (2002) 9630.
[18] Z. Rinkevicius, I. Tunell, P. Sałek, O. Vahtras, H. Ågren, *J. Chem. Phys.* **119** (2003) 34.
[19] D. Maurice, M. Head-Gordon, *J. Phys. Chem.* **100** (1996) 6131.
[20] Fernandez, *et al.*, *J. Chem. Phys.* **97** (1992) 3412.
[21] T. Bally, C. Carra, M.P. Fulscher, Z. Zhu, *J. Chem. Soc. Perkin Trans. 2* **8** (1998) 1759.
[22] B.J. Kelsal, L. Andrews, *J. Chem. Phys.* **76** (1982) 5005.

[23] C. Niederalt, S. Grimme, S.D. Peyerimhoff, *Chem. Phys. Lett.* **245** (1995) 455.
[24] S. Hirata, T.J. Lee, M. Head-Gordon, *J. Chem. Phys.* **111** (1999) 8904.
[25] S. Hirata, M. Head-Gordon, *Chem. Phys. Lett.* **302** (1999) 375.
[26] J.T.H. Dunning, *J. Chem. Phys.* **90** (1989) 1007.
[27] T. Kobayashi, K. Sasagane, K. Yamaguchi, *Int. J. Quantum Chem.* **65** (1997) 665.
[28] J. Guan, M.E. Casida, D.R. Salahub, *J. Mol. Struct. (Theochem)* **527** (2000) 229.
[29] B.A. Hess, C.M. Marian, U. Wahlgren, O. Gropen, *Chem. Phys. Lett.* **251** (1996) 365.
[30] Z. Rinkevicius, L. Telyatnyk, P. Sałek, O. Vahtras, H. Ågren, *J. Chem. Phys.* **119** (2003) 10489.
[31] F. Neese, *J. Chem. Phys.* **115** (2001) 11080.
[32] S. Patchkovskii, T. Ziegler, *J. Phys. Chem. A* **105** (2001) 5490.
[33] Z. Rinkevicius, L. Telyatnyk, O. Vahtras, K. Ruud, *J. Chem. Phys.* **121** (2004) 5051.
[34] E. Cancés, B. Mennucci, J. Tomasi, *J. Chem. Phys.* **107** (1997) 3032.
[35] W. Kutzelnigg, U. Fleischer, M. Schindler, Dummy, in: P. Diehl, E. Fluck, H. Günther, R. Kosfeld, J. Seelig (Eds.) *NMR Basic Principles and Progress*, vol. 23, Springer-Verlag, Heidelberg, 1990, p. 165.
[36] S. Huzinaga, *Approximate Atomic Functions*, Univ. of Alberta, Edmonton, 1971.
[37] T. Kawamura, S. Matsunami, T. Yonezawa, K. Fukui, *Bull. Chem. Soc. Jpn.* **38** (1965) 1935.
[38] M.L. Munzarova, M. Kaupp, *J. Phys. Chem. A* **103** (1999) 9966.

The Multiconfigurational Spin-Tensor Electron Propagator Method (MCSTEP)

Danny L. Yeager

Chemistry Department, Texas A&M University, P.O. Box 300012, College Station, TX 77842-3012, USA

Abstract

With electron propagator (also known as single particle Green's function) techniques vertical electron removal and attachment energies are calculated directly. This avoids the sometimes inaccurate process of separately determining the total electronic energies of the neutral and an ionic state and then subtracting one large number from another to obtain a relatively small value, *i.e.*, the ionization potential (IP) or electron affinity (EA) of a molecule. Traditionally these electron propagator/Green's function (GF) methods used a single determinant wavefunction as the "zero order" initial state which was improved with Møller–Plesset perturbation theory often obtained via diagrammatic techniques. Although these usual perturbative electron propagator/GF methods have been very successful, they are limited in applicability. Usual perturbative approaches usually cannot handle reliably (or at all) systems with initial states that are open shell and/or highly correlated (non-dynamical correlation) for either IPs or EAs.

We specifically designed the multiconfigurational spin tensor electron propagator method (MCSTEP) and its predecessor the multiconfigurational electron propagator method (MCEP) to provide accurate IPs and EAs for systems that cannot be accurately handled by usual perturbational approaches to electron propagator/single particle Green's function methods, namely, when the initial state is open shell and/or has non-dynamical correlation that must be accounted for. In addition, of course, the goal is to also be able to provide accurate IPs and EAs for systems with closed shell initial states without non-dynamical correlation, *i.e.*, those systems that could be handled as well by usual perturbational electron propagator/GF methods.

In this article I will first review the theory behind the multiconfigurational spin-tensor electron propagator method. Since the introduction of MCSTEP over fifteen years ago, several accurate MCSTEP atomic and molecular IPs and EAs have been determined. I will summarize some of the more significant calculations to date.

An electron propagator method using a multiconfigurational second-order perturbation theory wavefunction as the initial state in the fermion operator block (block 1) in the MCSTEP matrix equations was initially developed by Heryadi and Yeager. In the other blocks an MCSCF wavefunction is the initial state. This new method is called EPCASPT2 and should be viewed as an extension of MCSTEP. In this article I will review the theory behind EPCASPT2 and some of the recent calculations done using a CASPT2 wavefunction as the initial state in the electron propagator. We compare our results with the results of the calculations using MCSTEP, full configuration interaction, and the multireference configuration interaction method with the same geometries and basis sets.

Contents

ADVANCES IN QUANTUM CHEMISTRY, VOLUME 50
ISSN: 0065-3276 DOI: 10.1016/S0065-3276(05)50014-5

1. INTRODUCTION

With electron propagator (also known as single particle Green's function) methods, vertical ionization potentials (IPs) and electron affinities (EAs) are determined directly [1,2]. This avoids the oftentimes tedious and sometimes inaccurate more traditional techniques where separate wavefunctions and total electronic energies are determined for the initial (neutral) state and final (ionic) states of interest and individual IPs and EAs are determined by subtracting one fairly large total electronic energy from another to obtain a relatively small energy difference. While non-electron propagator techniques can be very accurate, it is also sometimes especially difficult to properly balance correlation effects in the initial versus the final state.

The usual approach to using electron propagator methods for IPs and EAs is to solve the equations consistently through a certain order in the electron–electron interaction [3–11]. The initial state is chosen to be a single determinant closed shell Hartree–Fock state corrected using Møller–Plesset perturbation theory. Operators are included which allow for both simple electron removal and addition as well as more complicated processes such as simple removal + single excitation, electron addition + simple single excitation, ... The simple removal + single excitation, electron addition + simple single excitation, ... processes are usually included in a secondary space which is coupled to the primary space of simple electron removal and electron addition [5].

These usual perturbational electron propagator approaches have been highly successful for low-lying principal IPs and EAs of atoms and molecules where the initial state is closed shell with no non-dynamical correlation [3–22]. For these kinds of systems perturbational approaches solved through at least third order in the electron–electron interaction have provided accurate results. Typically, IPs and EAs can be determined with these usual perturbative methods for low-lying principal vertical IPs and EAs for closed shell initial state systems with no non-dynamical correlation to within 0.3 eV or sometimes better provided terms are kept to at least third order (and sometimes higher) in the electron–electron interaction. The well-developed computer codes for these perturbational electron propagator methods are now usually very rapid.

Usual perturbational electron propagator approaches have not been successful, in general, for open shell molecules. This is because open shell molecules often have orbital energies that are close-lying, giving small denominators in certain terms. Sometimes with perturbational approaches for open shell initial states, IPs and EAs are not from and/or to states of pure spin symmetry.

Since these perturbational methods have traditionally been based on a single determinant initial state corrected by perturbation theory they have not been successful, in general, either for systems where several determinants (non-dynamical correlation) are necessary

to provide a good "zero order" description of the initial state. Simple examples of where a at least two determinants are necessary include the Be atom and the ozone molecule.

The multiconfigurational spin tensor electron propagator method (MCSTEP) [23] and its predecessor the multiconfigurational electron propagator method (MCEP) [24] were specifically designed to provide accurate low-lying IPs and EAs for systems that can not be accurately handled by usual perturbational approaches to electron propagator methods, namely when the initial state is open shell and/or has non-dynamical correlation that must be accounted for. In addition, of course, the goal is to also be able to provide accurate IPs and EAs for systems with closed shell initial states without non-dynamical correlation, *i.e.*, those systems that could be handled as well by usual perturbational Green's function methods. Several calculations have demonstrated the accuracy and reliability of MCSTEP for both closed and open shell initial state molecules even when non-dynamical correlation is important [19,23,25–44].

Heryadi and Yeager [43] developed an electron propagator method using a multiconfigurational second-order perturbation theory (CASPT2) wavefunction as the reference state. With this new method a better initial state than an MCSCF state is used in the electron propagator calculations. CASPT2 is specifically designed to handle both dynamical and non-dynamical electron correlation effects [45,46]. Of the five blocks in the MCSTEP matrices, the initial MCSCF state is replaced with a CASPT2 state in only block 1. This is the block that involves only simple electron removal and addition operators. It is the most important part of the MCSTEP matrices for calculating low-lying principal IPs. The remaining MCSTEP blocks are not changed.

We have applied the newly developed method, the electron propagator method with a CASPT2 wave function as the initial state (EPCASPT2) to calculate the IPs of several systems [43,44].

In Section 2, we briefly present the theory behind MCSTEP and EPCASPT2. In Section 3, the results of some of our recent calculations are reviewed. Finally, we summarize and conclude in Section 4.

2. THEORY

2.1. The spectral resolution of electron propagator/single particle Green's function

The single particle Green's function for an exact N-electron state of total spin S_0 and spin projection M_0 is defined as [1,2,47]

$$\begin{aligned} G_{r\sigma,p\sigma'} = \lim_{\eta\to 0^+} \Big[&\big\langle \psi_0^{NS_0M_0} \big| \mathrm{a}_{r\sigma}^\dagger \big(E + E_0^{NS_0} - H + \mathrm{i}\eta\big)^{-1} \mathrm{a}_{p\sigma'} \big| \psi_0^{NS_0M_0} \big\rangle \\ &+ \big\langle \psi_0^{NS_0M_0} \big| \mathrm{a}_{p\sigma'} \big(E - E_0^{NS_0} + H - \mathrm{i}\eta\big)^{-1} \mathrm{a}_{r\sigma}^\dagger \big| \psi_0^{NS_0M_0} \big\rangle \Big] \end{aligned} \tag{1}$$

where

$$H\big|\psi_0^{NS_0M_0}\big\rangle = E_0^{NS_0}\big|\psi_0^{NS_0M_0}\big\rangle, \tag{2}$$

$$S^2\big|\psi_0^{NS_0M_0}\big\rangle = S_0(S_0+1)\big|\psi_0^{NS_0M_0}\big\rangle, \tag{3}$$

$$S_z\big|\psi_0^{NS_0M_0}\big\rangle = M_0\big|\psi_0^{NS_0M_0}\big\rangle. \tag{4}$$

H is the nonrelativistic electronic Hamiltonian in the Born–Oppenheimer approximation

$$H = \sum_{ij\sigma} \mathrm{h}_{ij} \mathrm{a}^{\dagger}_{i\sigma} \mathrm{a}_{j\sigma} + \frac{1}{2} \sum_{ijkl\sigma\sigma'} \langle ij|kl\rangle \mathrm{a}^{\dagger}_{i\sigma} \mathrm{a}^{\dagger}_{j\sigma'} \mathrm{a}_{l\sigma'} \mathrm{a}_{k\sigma}. \tag{5}$$

The creation and the annihilation operators in H are summed over a formally complete orthonormal basis of spatial orbitals $\{\phi_i\}$ and the spin indices, σ and σ' can have the value of α or β spin.

The spectral resolution of equation (1) is

$$\begin{aligned} G_{r\sigma,p\sigma'} = \lim_{\eta\to 0^+} \sum_{\mathrm{f}} \Big[& \big\langle \psi_0^{NS_0M_0} \big| \mathrm{a}^{\dagger}_{r\sigma} \big| \psi_{\mathrm{f}}^{(N-1)S_{\mathrm{f}}M_{\mathrm{f}}} \big\rangle \big(E + E_0^{NS_0} - E_{\mathrm{f}}^{(N-1)S_{\mathrm{f}}} + \mathrm{i}\eta \big)^{-1} \\ & \times \big\langle \psi_{\mathrm{f}}^{(N-1)S_{\mathrm{f}}M_{\mathrm{f}}} \big| \mathrm{a}_{p\sigma'} \big| \psi_0^{NS_0M_0} \big\rangle + \big\langle \psi_0^{NS_0M_0} \big| \mathrm{a}_{p\sigma'} \big| \psi_{\mathrm{f}}^{(N+1)S_{\mathrm{f}}M_{\mathrm{f}}} \big\rangle \\ & \times \big(E - E_0^{NS_0} + E_{\mathrm{f}}^{(N+1)S_{\mathrm{f}}} - \mathrm{i}\eta \big)^{-1} \big\langle \psi_{\mathrm{f}}^{(N+1)S_{\mathrm{f}}M_{\mathrm{f}}} \big| \mathrm{a}^{\dagger}_{r\sigma} \big| \psi_0^{NS_0M_0} \big\rangle \Big] \end{aligned} \tag{6}$$

where the summations in the first and second terms contain a complete set of exact $N-1$ and $N+1$ electronic eigenstates, respectively, and

$$H \big| \psi_{\mathrm{f}}^{(N\pm1)S_{\mathrm{f}}M_{\mathrm{f}}} \big\rangle = E_{\mathrm{f}}^{(N\pm1)S_{\mathrm{f}}} \big| \psi_{\mathrm{f}}^{(N\pm1)S_{\mathrm{f}}M_{\mathrm{f}}} \big\rangle, \tag{7}$$

$$S^2 \big| \psi_{\mathrm{f}}^{(N\pm1)S_{\mathrm{f}}M_{\mathrm{f}}} \big\rangle = S_{\mathrm{f}}(S_{\mathrm{f}}+1) \big| \psi_{\mathrm{f}}^{(N\pm1)S_{\mathrm{f}}M_{\mathrm{f}}} \big\rangle, \tag{8}$$

$$S_z \big| \psi_{\mathrm{f}}^{(N\pm1)S_{\mathrm{f}}M_{\mathrm{f}}} \big\rangle = M_{\mathrm{f}} \big| \psi_{\mathrm{f}}^{(N\pm1)S_{\mathrm{f}}M_{\mathrm{f}}} \big\rangle. \tag{9}$$

It can easily be seen from equation (6) that the exact ionization potentials and electron affinities are the poles of the Green's function.

2.2. The eigenvalue equation

The single particle Green's function can be written in a form more convenient for calculations. Arranging the set of annihilation operators $\mathbf{a}_i$ as a super-row vector, $\mathbf{a}$, equation (1) can be rewritten as [2,48,49]

$$G(E) = (\mathbf{a}| \big(E\hat{I} - \widehat{H} \big)^{-1} |\mathbf{a}). \tag{10}$$

In equation (10), the superoperators $\hat{I}$ and $\widehat{H}$ are characterized by their effect on an arbitrary operator Ω:

$$\hat{I}\Omega = \Omega, \tag{11}$$

$$\widehat{H}\Omega = [H, \Omega] \tag{12}$$

and the binary product is defined as

$$(\Omega_i|\Omega_j) = \big\langle \psi_0^{NS_0M_0} \big| \{\Omega_i, \Omega_j\} \big| \psi_0^{NS_0M_0} \big\rangle. \tag{13}$$

In equation (13), $\{\,,\}$ denotes the anticommutator, $\{A, B\} = AB + BA$. Taking the inner projection [50] gives

$$G(E) = (\mathbf{a}|\mathbf{h})(\mathbf{h}|E\hat{I} - \widehat{H}|\mathbf{h})^{-1}(\mathbf{h}|\mathbf{a}). \tag{14}$$

Equation (14) can easily be verified by inserting unity in equation (10) [51]:

$$\hat{I} = |\mathbf{h})(\mathbf{h}|\mathbf{h})^{-1}(\mathbf{h}| \tag{15}$$

and utilizing the identity

$$(\mathbf{h}|\mathbf{h}) = (\mathbf{h}|E\hat{I} - \widehat{H}|\mathbf{h})(\mathbf{h}|\mathbf{h})^{-1}(\mathbf{h}|\left(E\hat{I} - \widehat{H}\right)^{-1}|\mathbf{h}). \tag{16}$$

If the operator manifold **h** is complete equations (10) and (14) are identical.

Since the IPs and EAs occur at the poles of the Green's function, equation (14) shows that the IPs and EAs can be determined as an eigenvalue problem

$$(\mathbf{h}|E\hat{I} - \widehat{H}|\mathbf{h}) = 0. \tag{17}$$

Approximations that are introduced into the one-electron propagator bring equation (17) into a computationally tractable form.

Equation (17) is the same as the equations-of-motion for ionization potentials and electron affinities [6,8,52]

$$\left\langle \psi_0^{NS_0M_0} \middle| \left\{ \delta O_\mathrm{f}, \left[H, O_\mathrm{f}^\dagger \right] \right\} \middle| \psi_0^{NS_0M_0} \right\rangle = \omega_\mathrm{f} \left\langle \psi_0^{NS_0M_0} \middle| \left\{ \delta O_\mathrm{f}, O_\mathrm{f}^\dagger \right\} \middle| \psi_0^{NS_0M_0} \right\rangle \tag{18}$$

when the electron affinity/ionization potential operator $O_\mathrm{f}^\dagger$ which is identified with the ionic state $|\psi_\mathrm{f}^{(N\pm1)S_\mathrm{f}M_\mathrm{f}}\rangle$ is expanded using the operator manifold **f** and each δO_f is one member of that manifold. ω_f is the electron affinity or ionization potential. In practical calculations the symmetric double anticommutator is usually used:

$$\{A, B, C\} = \frac{1}{2}\left(\left\{A, [B, C]\right\} + \left\{[A, B], C\right\}\right) \tag{19}$$

instead of $\{A, [B, C]\}$.

2.3. Approximate electron propagator calculations and MCSTEP

In all practical electron propagator or Green's function calculations, the exact initial state is approximated and the operator manifold is truncated.

With MCSTEP (and also with an earlier version of the theory called the multiconfigurational electron propagator MCEP) the initial state is chosen to be an MCSCF state $|0\rangle$. With MCSTEP (but not with MCEP) the reference state is a tensor state (see below) which contains all M_S components for a given S.

In equations (17) and (18) the operator manifold is complete. Of course, in practical calculations a truncated operator manifold is used. Dalgaard [53] and Manne [54] give one choice for a complete operator manifold which includes singles electron removal with all possible excitations of the remaining electrons and single electron addition with all possible excitations from a specified single determinant. The operators in this manifold will act on a state $|0\rangle$ which is not orthogonal to the specified single determinant to give a complete $N \pm 1$ basis of states.

While the operator manifold of Dalgaard and Maane is formally complete, it is not the most convenient for calculations where the initial state (also called the "reference state") is open shell. This can be easily seen by examining the effect of simple electron removal,

$a_{i\sigma}$, from an open shell state with for example $S = 1$. From the simple rules for angular momentum coupling, the resulting $N - 1$ states for this example will generally be a mixture of a doublet and a quartet since no explicit coupling has been introduced. That is, for open shell reference state ionization potentials and electron affinities, pure ion spin states will not be obtained in general with a method which utilizes a truncated operator manifold.

In addition, the Dalgaard–Manne manifold is not optimal in cases where two or more determinants are important for a good "zero order" description of the initial state. This is because an operator manifold chosen for one determinant and then truncated may not be the optimal choice for other necessary "zero order" determinants.

The operator manifold for MCEP and MCSTEP, is $\{a_i, a_i|\Gamma\rangle\langle 0|, |0\rangle\langle\Gamma|a_i\}$ (with appropriate modifications with both methods as explained below to assure that the final states are eigenfunctions of S^2 and S_z). The index i in this operator manifold refers to all spin orbitals present (occupied, partially occupied, and unoccupied). The states $\{|\Gamma\rangle\}$ are all states in the MCSCF orthogonal complement space to the initial state $|0\rangle$. For example, if the complete active space for Be atom was chosen to be two electrons in the 2s and 2p orbital, The optimized MCSCF ground state $|0\rangle$ is primarily $1s^2 2s^2$ with about 10% (C^2) $1s^2 2p^2$. All possible other orthonormal states of all possible spin and spatial symmetries involving two electrons in the 1s orbital and two electrons in the (2s,2p) orbitals compose the MCSCF orthogonal complement states. For both the reference and orthogonal complement states the orbitals that are used are those from the MCSCF calculation for $|0\rangle$.

$O_{\mathrm{f}}^{\dagger}$ is expanded in terms of the operator manifold $\{a_i, a_i|\Gamma\rangle\langle 0|, |0\rangle\langle\Gamma|a_i\}$:

$$O_{\mathrm{f}}^{\dagger} = \sum_i X_i^{\mathrm{F,f}} a_i + \sum_{i,\Gamma} X_{i,\Gamma}^{\mathrm{TIP,f}} a_i|\Gamma\rangle\langle 0| + \sum_{i,\Gamma} X_{i,\Gamma}^{\mathrm{TEA,f}} |0\rangle\langle\Gamma|a_i \tag{20}$$

$$= \sum_j X_j^{\mathrm{f}} O_j^{\dagger}. \tag{21}$$

In equation (20) the superscript F refers to the fermion operators $\{a_i\}$, the superscript TIP refers to the transfer ionization potential operators $\{a_i|\Gamma\rangle\langle 0|\}$ and the superscript TEA refers to the transfer electron affinity operators $\{|0\rangle\langle\Gamma|a_i\}$. The sum in equation (21) is over all non-zero members of the operator manifold $\{a_i, a_i|\Gamma\rangle\langle 0|, |0\rangle\langle\Gamma|a_i\}$. The operators a_i are involved both for electron attachment and removal since they occur in $O_{\mathrm{f}}^{\dagger}$ and as hermitian conjugate operators in δO_{f} in equation (18). IPs and EAs may have non-zero X_j^{f} amplitudes for all F, TIP, and TEA $O_{\mathrm{j}}^{\dagger}$ operators since all operators are coupled together in equation (18).

The IP and EA transfer operators, $\{a_i|\Gamma\rangle\langle 0|\}$ and $\{|0\rangle\langle\Gamma|a_i\}$, respectively, are analogous to the N-electron transfer operators $|0\rangle\langle\Gamma|$ and $|\Gamma\rangle\langle 0|$ that occur naturally in multiconfigurational linear response [55,56] and MCSCF optimization [57–59]. The EA and IP transfer operators are necessary to obtain good ionization potentials and electron affinities even for low-lyings IPs and EAs. The operator manifold of Dalgaard and Manne is not particularly convenient or useful for a multiconfigurational reference state even if the initial state is closed shell since a large number of operators would typically be necessary to duplicate the important effects of the IP and EA transfer operators.

The use of equation (21) in equation (18) gives the matrix eigenvalue equation

$$\mathbf{M}X_{\mathrm{f}} = \omega_{\mathrm{f}}\mathbf{N}X_{\mathrm{f}} \tag{22}$$

where

$$\mathrm{M}_{ij} = \langle 0|\left\{O_i, H, O_j^\dagger\right\}|0\rangle,$$
$$\mathrm{N}_{ij} = \langle 0|\left\{O_i, O_j^\dagger\right\}|0\rangle \tag{23}$$

and ω_f is an ionization potential or electron affinity.

With MCSTEP we use tensor states and tensor operators in order to assure that the final state is an eigenfunction of S^2 and S_z [60]. With MCSCF typically convergence is to one N-electron state with spin S_0 and spin projection M_0. The MCSCF state $|0\rangle$ ($\equiv |0^{NS_0M_0}\rangle$) is one component of an N-electron tensor state $|0^{NS_0}\rangle\!\rangle$. The MCSCF reference tensor state with $2S_0 + 1$ components is composed of the individual states that are connected by S_+ and S_-.

The operator manifold for MCSTEP consists of tensor operators. In order to ensure that $N \pm 1$ electron states of pure spin symmetry are obtained even for open shell reference states for which the initial spin is non-zero these operators are angular momentum coupled to the components of $|0^{NS_0}\rangle\!\rangle$. The operator manifold is

$$\mathbf{h} = \left\{\mathrm{a}_i(1/2), T_{i\Gamma}(N-1,k), T_{i\Gamma}(N+1,k)\right\} \tag{24}$$

where $\{\mathrm{a}_i(1/2)\}$ are the spin tensor operators of spin rank $1/2$ for an electron in orbital i and $\{T_{i\Gamma}(N \mp 1, k)\}$ are $N \mp 1$ tensor operators of rank k that can be formed from the action of $\mathrm{a}_i(1/2)$ on the ket part of $|\Gamma^{NS_\Gamma}\rangle\!\rangle \times \langle\!\langle 0^{NS_0}|$ and $\mathrm{a}_i(1/2)$ on the bra part of $|0^{NS_0}\rangle\!\rangle \times \langle\!\langle \Gamma^{NS_\Gamma}|$. The MCSCF orthogonal complement space $|\Gamma\rangle$ ($\equiv |\Gamma^{NS_\Gamma M_\Gamma}\rangle$) is one component of an N-electron tensor state $|\Gamma^{NS_\Gamma}\rangle\!\rangle$. The MCSCF orthogonal complement tensor state with $2S_\Gamma + 1$ components is composed of the individual states that are connected by S_+ and S_-.

The operator manifold in equation (24) is over complete. Linear dependencies are removed via a modified Schmidt procedure [23,24]. In addition, an energy criterion is usually used to further limit the number of operators included.

In MCSTEP we actually use a modified version of equation (17) where the operator manifold of equation (24) is explicitly vector coupled to the different spin components in an MCSCF reference tensor state with spin S_0 to form a new $N \mp 1$ electron state with spin S_f. Subsequent Racah recoupling results in the generalized matrix eigenvalue equation [23,61]

$$\mathbf{M}X_\mathrm{f} = \omega_\mathrm{f}\mathbf{N}X_\mathrm{f} \tag{25}$$

where

$$\mathrm{M}_{rp} = \sum_\Lambda (-1)^{S_0-\Lambda-S_\mathrm{f}-\gamma_r} W(\gamma_r\gamma_p S_0 S_0; \Lambda S_\mathrm{f})(2\Lambda+1)^{1/2} \times \left\langle 0^{NS_0}\middle\|\left\{h_r^\dagger(\overline{\gamma}_r), H, h_p(\gamma_p)\right\}^\Lambda\middle\|0^{NS_0}\right\rangle \tag{26}$$

and

$$\mathrm{N}_{rp} = \sum_\Lambda (-1)^{S_0-\Lambda-S_\mathrm{f}-\gamma_r} W(\gamma_r\gamma_p S_0 S_0; \Lambda S_\mathrm{f})(2\Lambda+1)^{1/2} \times \left\langle 0^{NS_0}\middle\|\left\{h_r^\dagger(\overline{\gamma}_r), h_p(\gamma_p)\right\}^\Lambda\middle\|0^{NS_0}\right\rangle \tag{27}$$

and ω_f is an IP or an EA to the final state $|\mathrm{f}^{(N\pm1)S_0}\rangle\!\rangle$ which has spin S_f. W is the usual Racah coefficient, and $h_p(\gamma_p)$ and $h_r^\dagger(\overline{\gamma}_r)$ are tensor operator members of the operator manifold in equation (24) with ranks γ_p and γ_r respectively.

2.4. Characterization

In this section, for the sake of clarity all reference to tensor coupling in MCSTEP is ignored. Of course, in practical calculations tensor coupling is included and the MCSTEP equations are blocked according to spatial symmetry as well.

In performing an MCSTEP calculation we first may set up equation (25) using only the simple electron destruction tensor operators $\{a_r(1/2)\}$ and no transfer operators. The three subblocks of this matrix for which the indices r and p both represent inactive (*i.e.*, doubly occupied), both active (*i.e.*, partially occupied) and secondary (*i.e.*, unoccupied) orbitals are then separately diagonalized. A unitary transformation within each of these three orbital sets is thus obtained. This transformation does not allow the inactive, active, or secondary orbitals to mix with each other but, of course, does allow mixing of the orbitals within each set. CAS MCSCF orbitals can be arbitrarily rotated (or mixed) with their own kind (inactive with inactive, active with active, and secondary with secondary) without moving to another point on the MCSCF energy surface [23]. Hence, the MCSCF reference state energy is unchanged. These transformed orbitals are the same as those latter proposed and used by Anderson, Malmqvist, Roos, Sadlej, and Wolinski [45].

The state formed with these transformed orbitals and the same MCSCF configuration state functions (with new state expansion coefficients which diagonalize the CAS MCSCF CI using the new orbitals) has the same electronic energy and properties as the original MCSCF state; however, these new MCSCF orbitals better describe simple electron addition and removal. This rotation of the MCSCF orbitals is analogous to the rotations which can be used in closed shell SCF calculations among doubly occupied orbitals and also separately among the virtual orbitals to obtain canonical Hartree–Fock orbitals which have Koopmans' theorem orbital energies. In fact, in the limit of a single determinant initial state for a closed shell system, the orbitals obtained from our rotation procedure are the canonical Hartree–Fock orbitals and virtual orbitals.

This orbital transformation procedure is useful in obtaining MCSTEP contributions from primarily only one operator rather than several operators when the IP is a low-lying principal IP and thus, serves as an aid in characterization. (A principal IP is one that can be described as primarily removal of an electron from a single orbital without additional excitation of the remaining electrons. A shake-up IP is one that can be described as primarily removal of a single electron from an orbital with some additional excitation of the remaining electrons.)

The exact final $N \pm 1$ electron states $|\psi_f^{(N\pm1)S_fM_f}\rangle$ are given by

$$O_f^\dagger \left|\psi_0^{NS_0M_0}\right\rangle = \left|\psi_f^{(N-1)S_fM_f}\right\rangle \quad \text{for IPs} \quad \text{and} \tag{28}$$

$$O_f \left|\psi_0^{NS_0M_0}\right\rangle = \left|\psi_f^{(N+1)S_fM_f}\right\rangle \quad \text{for EAs.} \tag{29}$$

The MCSTEP generalized eigenvalue equation (equation (18)) may also be derived making use of equations (28) and (29) and the "killer" conditions [5,8,52]

$$O_{\mathrm{f}}\left|\psi_0^{N S_0 M_0}\right\rangle = 0 \quad \text{for IPs,} \tag{30}$$

$$O_{\mathrm{f}}^{\dagger}\left|\psi_0^{N S_0 M_0}\right\rangle = 0 \quad \text{for EAs.} \tag{31}$$

The commutator norm (*i.e.*, superoperator binary product) of the $O_{\mathrm{f}}^{\dagger}$ operator with respect to the initial state is

$$\langle 0|\left\{O_{\mathrm{f}}, O_{\mathrm{f}}^{\dagger}\right\}|0\rangle = \langle 0|O_{\mathrm{f}}O_{\mathrm{f}}^{\dagger}|0\rangle + \langle 0|O_{\mathrm{f}}^{\dagger}O_{\mathrm{f}}|0\rangle = 1. \tag{32}$$

Using equation (30) the second term is approximately zero for an MCSTEP IP vector (in the limit of a complete operator manifold and the exact initial state it is exactly zero) and the first term is approximately zero for an MCSTEP EA vector. This may be used to help determine whether the obtained MCSTEP eigenvector corresponds to an IP or an EA.

2.5. EPCASPT2

The equations to be solved in EPCASPT2 is of the form of equations (25)–(27) with CASPT2 wavefunction as the reference state:

$$|\psi\rangle = X\big(|0\rangle + |\psi_1\rangle\big) = X\left(|0\rangle + \sum_{j=1}^{R} C_j|j\rangle\right) \tag{33}$$

where X is the normalization constant, $|0\rangle$ is the zeroth-order MCSCF wavefunction, $|\psi_1\rangle$ is the first-order wavefunction as defined in equation (4) of Andersson, Malquist, and Roos [46] (hereafter referred to as Andersson *et al.*), R states $\{|i\rangle\}$ are generated according to equation (1) of Andersson *et al.*, and $\{C_i\}$ are expansion coefficients solved in equation (3) of Andersson *et al.* In this initial implementation, the correction is made only to the first block of the MCSTEP **M** and **N** matrices in which the operator manifold consists of electron removal and creation operators, $\mathrm{a}_{p\sigma'}$ and $\mathrm{a}_{r\sigma}^{\dagger}$. The rest of the blocks are evaluated using an MCSCF wavefunction as the initial state exactly as in MCSTEP. The explicit formulas of matrix elements $\mathrm{M}_{r,p}$ and $\mathrm{N}_{r,p}$ (shown below without including the tensor couplings for clarity) in the first block are

$$\begin{aligned}\mathrm{M}_{rp} &= \langle\psi|\{\mathrm{a}_{r\sigma}^{\dagger}, H, \mathrm{a}_{p\sigma'}\}|\psi\rangle \\ &= \delta_{\sigma\sigma'}\Bigg(-h_{pr}\langle\psi|\psi\rangle + \sum_{q,s} V_{qprs}\langle\psi|\mathrm{a}_{q\sigma}^{\dagger}\mathrm{a}_{s\sigma}|\psi\rangle \\ &\quad - \sum_{q,s} V_{qprs}\langle\psi|(\mathrm{a}_{q\alpha}^{\dagger}\mathrm{a}_{s\alpha} + \mathrm{a}_{q\beta}^{\dagger}\mathrm{a}_{s\beta})|\psi\rangle\Bigg),\end{aligned} \tag{34}$$

$$\mathrm{N}_{rp} = \langle\psi|\{\mathrm{a}_{r\sigma}^{\dagger}, \mathrm{a}_{p\sigma'}\}|\psi\rangle = \delta_{rp}\delta_{\sigma\sigma'}\langle\psi|\psi\rangle. \tag{35}$$

The overlap matrix $\langle\psi|\psi\rangle$ and one-body spin density matrix elements $\langle\psi|\mathrm{a}_{q\sigma}^{\dagger}\mathrm{a}_{s\sigma}|\psi\rangle$ are needed. Using the orthonormality conditions in the zeroth-order MCSCF wavefunction, the value of the overlap matrix is

$$\langle\psi|\psi\rangle = 1 + \sum_{i,j=1}^{R} C_j^{\dagger}C_i\langle j|i\rangle. \tag{36}$$

where the normalization constant is dropped in this and subsequent equations since X^2 appears in both equations (34) and (35).

The expansion vector **C** is obtained from a CASPT2 calculation. Andersson and Roos [62] described the computer implementation of CASPT2 in MOLCAS quantum chemistry software [63]. This information was provided for the users who would modify the codes. We extract **C** from MOLCAS codes and use it in the calculation of CASPT2 spin density matrix elements. The spin density matrix elements, $\langle\psi|a^\dagger_{q\sigma}a_{s\sigma}|\psi\rangle$, can then easily be evaluated

$$\langle\psi|a^\dagger_{q\sigma}a_{s\sigma}|\psi\rangle=\langle 0|a^\dagger_{q\sigma}a_{s\sigma}|0\rangle+\langle 0|a^\dagger_{q\sigma}a_{s\sigma}\psi_1+\langle\psi_1|a^\dagger_{q\sigma}a_{s\sigma}|0\rangle + \langle\psi_1|a^\dagger_{q\sigma}a_{s\sigma}|\psi_1\rangle. \tag{37}$$

The first term in the equation above is an MCSCF spin density matrix element. The other terms are transition spin density matrix elements that can be evaluated once the expansion coefficient vector **C** is obtained. The last terms, for example, may be evaluated as follows:

$$\langle\psi_1|a^\dagger_{q\sigma}a_{s\sigma}|\psi_1\rangle=\sum_{i,j=1}^{R}C^\dagger_j C_i\langle j|a^\dagger_{q\sigma}a_{s\sigma}|i\rangle. \tag{38}$$

By writing the equation above in a matrix form, removing the linear dependencies in states $\{|i\rangle\}$, and using the othogonalized states, the following formula is obtained

$$\boldsymbol{\rho}^{(2)}=\tilde{\tilde{\mathbf{C}}}^\dagger\mathbf{T}^\dagger\mathbf{A}\mathbf{T}\tilde{\tilde{\mathbf{C}}} \tag{39}$$

where $A_{pq}=\langle j|a^\dagger_{q\sigma}a_{s\sigma}|i\rangle$ and $\rho^{(2)}_{pq}=\langle\psi_1|a^\dagger_{q\sigma}a_{s\sigma}|\psi_1\rangle$. The vector $\tilde{\tilde{\mathbf{C}}}$ and matrix **T** are described in equations (15)–(17) of Anderson *et al.* and can be extracted from CASPT2 codes.

In this initial implementation of EPCASPT2 the remaining blocks of the MCSTEP matrices are not corrected by perturbation theory. In addition, the operator manifold we use in EPCASPT2 is the same as that in MCSTEP. Hence, because block one is the most important block for low-lying principal IPs, we expect that the lowest few principal ionization potentials that are usually well-determined with MCSTEP will be slightly improved and, in the very few cases where MCSTEP does not do that well for an IP usually because of a too small CAS choice, the use of a CASPT2 initial state should significantly improve the value of this IP.

3. SOME RECENT CALCULATIONAL EXAMPLES WITH MCSTEP AND EPCASPT2

Since 1983 there have been several calculations reported with MCEP and MCSTEP [19,23–44,64]. These have demonstrated the reliability and accuracy of MCEP and MCSTEP. Typically, for low-lying principal IPs (under 20 eV) and EAs with reasonable choices of a complete active space (CAS) accuracy is about ±0.2 eV when compared with Δ full configuration interaction (FCI) or experiment. Initial calculations show that accuracy is significantly improved with EPCASPT2.

For most of the calculations reported below Dunning cc-pVXZ (X = D, T, Q) basis sets are used [65]. For convenience these basis sets will typically simply be labeled pVXZ, *i.e.*, without the "cc".

3.1. O_2 [32,33]

The O_2 $X^2\Sigma_g^-$ ground state principal configuration is $1\sigma_g^2\ 1\sigma_u^2\ 2\sigma_g^2\ 2\sigma_u^2\ 3\sigma_g^2\ 1\pi_u^4\ 1\pi_g^2$. In order to demonstrate the accuracy of MCSTEP for vertical IPs we report these IPs at 2.282 a.u. (1.208 Å), the neutral O_2 $X^2\Sigma_g^-$ equilibrium experimental geometry and compare our results with experiment [66–69] and some other recent methods [17,70].

In Table 1 we compare the vertical MCSTEP IPs using the pVTZ and pVTZ++ basis sets with IPs calculated using the techniques coupled-cluster electron propagator theory (CC-EPT) [17] and the Fock space multireference coupled-cluster method (FSMRCC) [70] using the same basis sets and at the same geometry [33]. Experimental vertical IPs are also listed [66].

The IPs to the same states obtained with both MCSTEP and CC-EPT are fairly close to each other and also to experiment. The MCSTEP IPs are, however, very slightly less sensitive to details of the basis set. The IPs differ by only 0.08–0.09 eV in going from the pVTZ to the pVTZ++ bases for the $X^2\Pi_g$, $a^4\Pi_u$, $b^4\Sigma_g^-$ and $c^4\Sigma_u^-$ states, while the CC-EPT differ by 0.09–0.10 eV for these states. CC-EPT results were not reported for the other cation states listed in Table 1.

In Table 2 we present comparison calculations between MCSTEP and FSMRCC using pVQZ and pVQZ++ basis sets in addition to the pVTZ and pVTZ++ basis sets reported

Table 1. Vertical principal ionization potentials of O_2 at $R = 2.282$ a.u.: Comparison among the forefront methods MCSTEP,[a] CC-EPT(R)[b] and FSMRCCSD[c] using pVTZ and pVTZ++ basis sets[d]

Ion state	MCSTEP pVTZ	CC-EPT(R) pVTZ	FSMR-CCSD pVTZ	MCSTEP pVTZ++	CC-EPT(R) pVTZ++	FSMR-CCSD pVTZ++	Expt. PES[e]
$X^2\Pi_g$	12.12	12.34	12.16	12.21	12.43	12.24	12.3
$a^4\Pi_u$	16.72	16.55	16.74	16.80	16.64	16.80	16.8
$A^2\Pi_u$	17.76			17.84			17.7
$b^4\Sigma_g^-$	18.47	18.13	18.12	18.55	18.23	18.21	18.4
$B^2\Sigma_g^-$	20.68			20.75			20.7
$^2\Pi_u$	24.21			24.29			24.0
$c^4\Sigma_u^-$	24.94	24.86	24.55	25.03		24.63	24.6

[a] Ref. [33].

[b] Coupled-Cluster Electron Propagator Theory (CC-EPT) [17].

[c] Fock Space Multireference Coupled-Cluster Method (FSMRCCSD) [70].

[d] All results are in eV. For basis sets see Ref. [65].

[e] Ref. [66].

Table 2. Vertical principal ionization potentials of O_2 at $R = 2.282$ a.u.: Comparison among MCSTEP,[a] FSMRCCSD[b] and ΔCCSD(T) using pVQZ and pVQZ++ basis sets[c]

Ion state	MCSTEP pVQZ	FSMR CCSD pVQZ	MCSTEP pVQZ++	FSMR CCSD pVQZ++	ΔCCSD(T) pVQZ++	Expt. PES[d]
$X^2\Pi_g$	12.16	12.34	12.19	12.37	12.39	12.3
$a^4\Pi_u$	16.76	16.90	16.79	16.93	16.76	16.8
$A^2\Pi_u$	17.80		17.83			17.7
$b^4\Sigma_g^-$	18.51	18.31	18.54	18.34	18.26	18.4
$B^2\Sigma_g^-$	20.72		20.74			20.7
$^2\Pi_u$	24.25		24.28			24.0
$c^4\Sigma_u^-$	24.97	24.71	24.99	24.74	24.82	24.6

[a] Ref. [33].

[b] Fock Space Multireference Coupled-Cluster Method (FSMRCCSD) [70].

[c] All results are in eV. For basis sets see Ref. [65].

[d] Ref. [66].

in Table 1. (Note that no CC-EPT results have been reported using pVQZ and pVQZ++ basis sets.) The same features are apparent when comparing MCSTEP with FSMRCC in Tables 1 and 2 as with the comparison of MCSTEP with CC-EPT in Table 1, namely that both methods give accurate vertical ionization potentials compared to experiment, that MCSTEP appears to be less sensitive to basis set choice than the FSMRCC approach (*i.e.*, the MCSTEP IPs differ by 0.07, 0.07, 0.07 and 0.05 eV while the FSMRSDCC IPs differ by 0.21, 0.19, 0.22, and 0.19 eV comparing the largest (pVQZ++) with the smallest basis (pVTZ) listed for the $X^2\Pi_g$, $a^4\Pi_u$, $b^4\Sigma_g^-$ and $c^4\Sigma_u^-$ states, respectively) and that for the FSMRCC approach IPs to certain cation states were not reported.

Also given in Table 2 are reported coupled cluster singles + doubles with perturbative triples (ΔCCSD(T)) IPs using the pVTZ++ basis set [70]. These results appear to be about as accurate compared to experiment as the other results reported in Tables 1, 2.

We would like to point out that all of these methods (MCSTEP, CC-EPT, FSMRCC, and CCSD(T)) are apparently very accurate and reliable for determining vertical ionization potentials. MCSTEP may have some advantages in being slightly less sensitive to basis set variations (provided, of course, that the basis sets are of at least of double-zeta with polarization quality) and in being capable of determining accurate IPs for more states when the initial state is open shell.

3.2. Electron affinity of CH_2 [29]

The core-valence parts of the basis sets we have chosen for CH_2 were obtained from the standard Dunning pVTZ sets [65]. We designate that part of our basis sets inside $\langle \ldots \rangle$. The pVTZ bases are $\langle$4s3p2d1f$\rangle$ on C and $\langle$3s2p1d$\rangle$ on the H's. For CH_2 the basis is listed as $\langle$4s3p2d1f/3s2p1d$\rangle$. For several calculations on both systems we modified the pVTZ bases

by deleting the f function on C, *i.e.*, ⟨4s3p2d⟩, and the d function as well on the H's in CH_2, *i.e.*, ⟨4s3p2d/3s2p⟩.

For some basis sets we also included one g function on C for CH_2. Our initial choice for this exponent was the pVQZ exponent, 1.011 [65].

In order to properly account for the more diffuse anion charge clouds we added sets of diffuse functions to the core-valence (pVTZ and modified pVTZ) basis sets. These are indicated by + (...). The additional diffuse functions were chosen by adding functions with exponents determined from the geometric ratio of the two smallest pVTZ exponents of functions of the same symmetry that were on the same center. If there were not two pVTZ functions of the same symmetry on the same center then the geometric ratio was obtained from the exponents of the next lower "angular momentum" functions where there were at least two sets of pVTZ functions.

All six d function components, ten f function components, and fifteen g function components were included in our basis sets.

The geometries we used for CH_2 were the same as were used by Noro and Yoshimine [71] for their EA calculations. They obtained these optimized second order configuration interaction (SOCI) geometries using a contracted Cartesian Gaussian basis set (CGTO) supplemented with extra diffuse functions to [6s4p2d/3s1p]. They call this their TZP basis. Noro and Yoshimine also performed larger total electronic energy calculations at the TZP SOCI geometries using the TZP basis, a [13s10p5d3f/5s2p1d] basis which they call EXTF and a [13s10p5d3f2g/5s2p1d] basis which they call EXTG. Noro and Yoshimine do not include an estimate zero point vibrational corrections in their reported EAs. We also do not include an estimate of zero point vibrational corrections in any of our results.

Even though single particle Green's function techniques give both IPs and EAs directly, for calculational simplicity in determining EAs the MCSTEP initial state should be the $N + 1$ electron system. That is, an electron affinity should be calculated as the lowest ionization energy of the ground state of the negative ions. This is because the charge cloud in a neutral reference state is not sufficiently diffuse to properly also describe an anion. Hence, Green's function methods must incorporate considerably more operators to properly describe electron attachment to a neutral rather than to describe ionization from the anion. For all the MCSTEP EA calculations we report here [29], the electron affinities were determined as the lowest ionization potentials of the ground states of the anions.

For calculational convenience we chose an MCSCF initial state with a complete active space (CAS) set of configurations. That is, all configurations were included that could be obtained from all possible arrangements of a certain number of electrons in a chosen set of orbitals. CAS choices for MCSTEP are discussed extensively in Refs. [19,27,31,34–38].

A full valence MCSCF CAS was used for the CH_2^- X^2B_1 reference state, *i.e.*, seven electrons in the $(2a_1 1b_2 3a_1 1b_1 2b_2 4a_1)$ orbitals.

Since single particle Green's function methods determine only vertical IPs and EAs, adiabatic corrections must be included in order to obtain the adiabatic EAs for CH_2. For the adiabatic EAs reported here, the MCSTEP vertical EAs were determined as the lowest IP from the anion ground state at the geometry of the neutral X^3B_1 ground state. The adiabatic EAs were then calculated by adding to the vertical EAs the energy differences between the anionic X^2B_1 total electronic energy at the neutral ground state X^3B_1 geometry and the X^2B_1 total electronic energy at the X^2B_1 anionic ground state geometry. The total electronic energies we used for the adiabatic corrections were determined by either

MCSCF or by multireference singles + doubles CI [72–75] with quadruples estimated by a Davidson correction [76].

We also make several difference (Δ) calculations using multireference singles and doubles configuration interaction (MRSDCI) and multireference singles and doubles configuration interaction with quadruples estimated using a DV3 Davidson correction (MRSDCI + Q) for both the neutral and cation states. In order to have a direct calculational comparisons, all of our ΔMRCI calculations reported here are at the same CH_2 geometries and using the same C and CH_2 basis sets as the corresponding MCSTEP calculations. As was previously noted above, the CH_2 geometries we used are the same as were used by Noro and Yoshimine.

The multireference CAS used for the CH_2 and CH_2^- MRCI calculations was the full valence CAS, *i.e.*, $(2a_1 1b_2 3a_1 1b_1 2b_2 4a_1)$. MCSCF orbitals were generated for each state of interest at each geometry of interest using these CASs. These orbitals were subsequently used for their respective MRCIs. For the MRSDCI and MRSDCI + Q calculations, in addition to the CAS configurations all configurations of the desired symmetry were included that involved single and double excitations from the CAS reference configurations. No configurations were included that involved excitations from the core orbital, *i.e.*, the $1a_1$ in CH_2 or CH_2^-.

Our CH_2 ΔMRSDCI, ΔMRSDCI + Q and MCSTEP adiabatic EAs are listed in Table 3. Table 3 MCSTEP EAs are the MCSTEP vertical EAs at the $^3B_1$ geometry corrected with ΔMRSDCI + Q adiabatic corrections. The "best basis" adiabatic EA is 0.6306 eV using MRSDCI + Q and 0.6356 eV using MCSTEP (with ΔMRSDCI + Q adiabatic corrections). Experiment is 0.628 ± 0.031 eV [77].

Even with a basis as small as ⟨4s3p2d/3s2p⟩ + (2s2p1d/1s), the adiabatic ΔMRSDCI + Q EA agrees closely with experiment almost to within experimental error. The ⟨4s3p2d1f1g/3s2p1d⟩ + (2s2p2d1f/1s1p1d) ΔMRSDCI + Q EA agrees with experiment to within experimental error. MCSTEP (with ΔMRSDCI + Q adiabatic corrections) agrees with experiment to within experimental error with bases as small as ⟨4s3p2d/3s2p⟩ + (2s2p2d/1s1p) and ⟨4s3p2d1f/3s2p1d⟩ + (2s2p1d/1s). None of our ΔMRSDCI results agrees with experiment.

Also given in Table 3 are some adiabatic EAs calculated by others. From this table it is obvious that in order to obtain very accurate EAs for CH_2 ΔCI calculations at the ΔMRSDCI + Q level or MCSTEP (with ΔMRSDCI + Q adiabatic corrections) should be done in general. ΔSDCI+Q and ΔMRSDCI are not adequate for very accurate CH_2 EAs. It is also obvious from our EAs ("This work") that basis sets with large numbers of additional diffuse s, p, d, and f functions in addition to a good core-valence basis are not necessary and also that relatively few functions with angular momentum higher than d are needed. However, a few additional diffuse functions are necessary, *e.g.*, +(2s2p2d1f/1s1p1d).

3.3. IPs of O_3 [36,38]

We use pVXZ basis sets where X = D, T, Q (*i.e.*, double, triple, quadruple) [65]. For all basis sets used for the calculations reported here we retained only the spherical components, *i.e.*, five d-components, seven f-components, and nine g-components. In O_3 the pVDZ (⟨3s2p1d⟩ on each nucleus) contains 42 basis functions, the pVTZ (⟨4s3p2d1f⟩ on

Table 3. Summary of the best results for the adiabatic EAs of CH_2

Basis[a]	Method	EA (eV)	Reference
[6s5p2d/4s2p]	MRSDCI	0.2519	This work [29]
[6s5p2d/4s2p]	MRSDCI + Q	0.4416	This work [29]
[6s5p2d/4s2p]	MCSTEP	0.5872[b]	This work [29]
[6s5p4d/4s3p]	MRSDCI	0.3190	This work [29]
[6s5p4d/4s3p]	MRSDCI + Q	0.5295	This work [29]
[6s5p4d/4s3p]	MCSTEP	0.6114[b]	This work [29]
[6s5p3d1f/4s2p1d]	MRSDCI	0.3549	This work [29]
[6s5p3d1f/4s2p1d]	MRSDCI + Q	0.5702	This work [29]
[6s5p3d1f/4s2p1d]	MCSTEP	0.6239[b]	This work [29]
[6s5p4d1f/4s3p1d]	MRSDCI	0.3615	This work [29]
[6s5p4d1f/4s3p1d]	MRSDCI + Q	0.5792	This work [29]
[6s5p4d1f/4s3p1d]	MCSTEP	0.6270[b]	This work [29]
[6s5p4d2f1g/4s3p2d]	MRSDCI	0.4067	This work [29]
[6s5p4d2f1g/4s3p2d]	MRSDCI + Q	0.6306	This work [29]
[6s5p4d2f1g/4s3p2d]	MCSTEP	0.6356[b]	This work [29]
[5s3p2d/2s1p] + b.f.	MRDCI + Q	0.32	Shih *et al.* [78]
[9s7p2d/6s2p]	SDCI + Q	0.30	Feller *et al.* [79]
[6s4p2d/3s1p]	MRSDCI	0.227	Noro and Yoshimine [71]
[6s4p2d/3s1p]	MRSDCI + Q	0.266	Noro and Yoshimine [71]
[13s10p5d3f/5s2p1d]	SDCI + Q	0.454	Noro and Yoshimine [71]
[13s10p5d3f/5s2p1d]	MRSDCI	0.544	Noro and Yoshimine [71]
[13s10p5d3f/5s2p1d]	MRSDCI + Q	0.577	Noro and Yoshimine [71]
[13s10p5d3f2g/5s2p1d]	SDCI + Q	0.472	Noro and Yoshimine [71]
[13s10p5d3f2g/5s2p1d]	MRSDCI	0.559	Noro and Yoshimine [71]
[13s10p5d3f2g/5s2p1d]	MRSDCI + Q	0.604	Noro and Yoshimine [71]
Experiment		0.628 ± 0.031	Leopold *et al.* [77]

[a] The CGTO basis sets in this column are listed in square brackets to indicate the total number of (contracted) functions regardless of whether or not they are core-valence or added diffuse functions. Thus, our ⟨4s3p2d/3s2p⟩ + (2s2p/1s) basis is listed as [6s5p2d/4s2p], our ⟨4s3p2d/3s2p⟩ + (2s2p2d/1s1p) as [6s5p4d/4s3p], our ⟨4s3p2d1f/3s2p1d⟩ + (2s2p1d/1s) as [6s5p3d1f/4s2p1d], our ⟨4s3p2d1f/3s2p1d⟩ + (2s2p2d/1s1p) as [6s5p4d1f/4s3p1d], and our ⟨4s3p2d1f1g/3s2p1d⟩ + (2s2p2d1f/1s1p1d) as [6s5p4d2f1g/4s3p2d]. Our basis sets are listed this way in order to more clearly indicate the total number of functions present for comparison with the work of others. For details see the text.

[b] The added adiabatic correction is ΔMRSDCI + Q. See the text.

each nucleus) contains 90 basis functions, and the pVQZ (⟨5s4p3d2f1g⟩ on each nucleus) contains 165 basis functions.

We apply a 3-parameter exponential fitting function first described in Ref. [80] to estimate values at the complete basis set (CBS) limit:

$$\mathrm{A}(x) = \mathrm{A}_{\mathrm{CBS}} + \mathrm{B}e^{-\mathrm{C}x} \tag{40}$$

where $x = 2$, 3, and 4 for DZ, TZ, and QZ basis sets. In our case, the A(x) values are the MCSTEP IPs obtained using pVDZ, pVTZ and pVQZ basis sets.

The geometry we used in this calculation is the same as that used by Barysz, Rittby, and Bartlett [81], *i.e.*, C_{2V} geometry with bond angle 117.4° and bond length 2.387 a.u. This is the experimental geometry. The ground state principal configuration of O_3 is $1a_1^2 1b_2^2 2a_1^2 3a_1^2 2b_2^2 4a_1^2 5a_1^2 1b_1^2 3b_2^2 4b_2^2 6a_1^2 1a_2^2$. Inclusion of the configuration $1a_1^2 1b_2^2 2a_1^2 3a_1^2 2b_2^2 4a_1^2 5a_1^2 1b_1^2 3b_2^2 4b_2^2 6a_1^2 2b_1^2$ is also needed for adequately describing the neutral $^1A_1$ ground state since it is necessary to properly describe the important contribution of biradical structure to the ground state [82–86]. Thus, perturbative Green's function approaches (which are based on a single determinant ground state corrected by perturbation theory) should not be adequate for describing the IPs of O_3 [12,87]. However, since MCSTEP uses a multiconfigurational initial state, MCSTEP IPs should be accurate and reliable.

The complete active space (CAS) we used for these MCSTEP calculations was chosen by a method described previously in detail [31,35,37]—it is composed of the highest three (in energy) occupied orbitals from the SCF calculation and the next three (in energy) unoccupied orbitals regardless of symmetry. This CAS has been previously demonstrated to give accurate and reliable MCSTEP IPs for several systems tested to date. Thus the CAS for these MCSTEP calculations is composed of all possible configurations of six electrons in the ($4b_2 6a_1 1a_2 2b_1 7a_1 5b_2$) orbitals. For the neutral $^1A_1$ ground state there are only 104 determinants. Note that this CAS choice along with the $5a_1$, $1b_1$, and $3b_2$ orbitals represents all the orbitals that can be obtained from the 2p atomic orbitals and that the CAS includes both the $1a_1^2 1b_2^2 2a_1^2 3a_1^2 2b_2^2 4a_1^2 5a_1^2 1b_1^2 3b_2^2 4b_2^2 6a_1^2 1a_2^2$ and the $1a_1^2 1b_2^2 2a_1^2 3a_1^2 2b_2^2 4a_1^2 5a_1^2 1b_1^2 3b_2^2 4b_2^2 6a_1^2 2b_1^2$ configurations (as well as others) in the $^1A_1$ ground state.

We report in this subsection MCSTEP IPs to hundredths of eV in order to compare with experimental results for the vertical IPs which are reported to this accuracy [87]. From the observed photoelectron spectroscopy peaks it is somewhat unclear, however, where the exact position of the maxima occur since the three lowest IPs are fairly close in energy and these peaks overlap. There has also been some controversy about their assignment [12,87].

In Table 4 we report the lowest three MCSTEP IPs using the pVDZ, pVTZ, and pVQZ basis sets as well as the complete basis set limit (CBS) IPs. With all of the basis sets used in Table 4, MCSTEP gives IPs in very good to excellent agreement with experiment. The pVDZ MCSTEP IPs in Table 4 differ from the vertical IPs reported experimentally by −0.02, −0.16, and −0.24 eV and the pVTZ MCSTEP IPs differ from experiment by 0.12, −0.08, and −0.19 eV for the $^2A_1$ $(6a_1)^{-1}$, $^2B_2$ $(4b_2)^{-1}$, and $^2A_2$ $(1a_2)^{-1}$ states respectively. The pVQZ MCSTEP IPs in Table 1 differ from experiment by 0.14, −0.02, and −0.12 eV for the $^2A_1$ $(6a_1)^{-1}$, $^2B_2$ $(4b_2)^{-1}$, and $^2A_2$ $(1a_2)^{-1}$ states respectively. The CBS limit MCSTEP IPs differ from experiment by 0.14, 0.16, and −0.01 eV for the $^2A_1$ $(6a_1)^{-1}$, $^2B_2$ $(4b_2)^{-1}$, and $^2A_2$ $(1a_2)^{-1}$ states respectively.

Other low-lying principal IPs for O_3 include the $^2A_1$ $(5a_1)^{-1}$, the $^2B_2$ $(3b_2)^{-1}$, and the $^2B_2$ $(1b_1)^{-1}$. Since the $5a_1$, $3b_2$, and $1b_1$ orbitals are outside of the CAS, these principal IPs calculated with MCSTEP are not expected to be as accurate as those for the three lowest IPs and so they are not listed in the tables or reported in this paper.

Using a single-reference state perturbational electron propagator theory method known

Table 4. O_3 MCSTEP vertical IPs using several different standard basis sets[a]

Ion state	pVDZ[b]	pVTZ[b]	pVQZ[b]	CBS[c]	Experiment[d]
$^2A_1\ (6a_1)^{-1}$	12.71	12.85	12.87	12.87	12.73
$^2B_2\ (4b_2)^{-1}$	12.84	12.92	12.98	13.16	13.00
$^2A_2\ (1a_2)^{-1}$	13.30	13.35	13.42	13.53	13.54

[a] All results in eV. The MCSTEP IPs are reported to hundredths of an eV for comparison with experimentally reported vertical IPs.

[b] Basis sets from Ref. [65].

[c] Complete basis set limit from equation (40).

[d] Ref. [87]. The authors report experimental photoelectron spectroscopy (PES) values for vertical IPs to 0.01 eV.

as T1, Ortiz [88] obtained 12.54, 12.67, and 13.19 eV for IPs to the $^2A_1$, $^2B_2$, $^2A_2$ states respectively with the pVDZ basis set and 12.98, 13.10, and 13.52 eV with the pVTZ basis set. When an approximate Brueckner doubles reference state (BD-T1) was used instead, thus incorporating some non-dynamical correlation, the results were 12.10, 12.29, and 13.27 eV with the pVDZ basis set and 12.51, 12.68, and 13.53 eV with the pVTZ basis set [88].

3.4. MCSTEP and EPCASPT2 calculations on NH_2 and CH_3

We have applied MCSTEP and EPCASPT2 to evaluate the low-lying principal IPs of Be and several small molecules [44,89]. In this review, we present and discuss the low-lying MCSTEP and EPCASPT2 principal IPs of NH_2 and CH_3 using correlation consistent (cc-) pVDZ, pVTZ, and pVQZ Gaussian basis sets [65] with the only spherical components (e.g., 1s, 3p′s, 5d′s, 7f′s, *etc.*) retained. In addition we estimate the complete basis set limit using equation (40).

We compared EPCASPT2 results to the results of the Δ full configuration interaction (FCI) calculations if the FCI calculations were possible with our computational resources, as well as to multireference configuration interaction calculations with single excitations, double excitations, and Davidson's correction as an approximation for the quadruple excitations (ΔMRSDCI + Q) calculations. (A ΔFCI (ΔMRSDCI + Q) IP is obtained by subtracting the FCI (MRSDCI + Q) energy of the ground state neutral from the FCI (MRSDCI + Q) energy of the cation state of interest.) We note that MRCI calculations are not size consistent, in general. The FCI and MRSDCI + Q calculations were performed using the MOLPRO 2000 program package [90–92]. The FCI method provides the exact solution to the Schrödinger equation for the chosen basis sets and geometry, and, hence, may be used as a benchmark for the calculations using a newly-developed method, such as EPCASPT2. In cases where ΔFCI IPs could not be obtained with cc-pVTZ and cc-pVQZ basis sets due to the limitations in our computational resources, we have shown that our ΔMRSDCI + Q IPs are good approximations to ΔFCI IPs using smaller basis sets. We then use ΔMRSDCI + Q IPs for comparison with MCSTEP and EPCASPT2 with the larger basis sets.

3.4.1. Ionization potentials of NH_2 [43]

The principal electron configuration of the X^2B_1 ground state of NH_2 is $1a_1^2\ 2a_1^2\ 1b_2^2\ 3a_1^2\ 1b_1^2$.

Previously we reported MCSTEP calculations using a full valence CAS, *i.e.*, all possible arrangements of seven electrons in the ($2a_1\ 1b_2\ 3a_1\ 1b_1\ 2b_2\ 4a_1$) orbitals, as well as an optimal balanced CAS, *i.e.*, all possible arrangements of five electrons in the ($1b_2\ 3a_1\ 1b_1\ 2b_2\ 4a_1\ 3b_2$) orbitals [31,37]. The calculations were performed at the experimental geometry (*i.e.*, the HNH angle is 103.30° and the bond length is 1.93508 a.u.) [93–96] and employed several different basis sets.

Recently, Stephens, Yamaguchi and Schaefer [97] have calculated NH_2 vertical ionization potentials to the lowest three ion states. Using a TZ3P(2f,2d) + two sets of diffuse functions basis set, they reported IPs of 11.96, 12.40 and 14.09 eV using CASSCF-SOCI for IPs to the $^3B_1\ (3a_1)^{-1}$, $^1A_1\ (1b_1)^{-1}$, and $^1B_1\ (3a_1)^{-1}$ states respectively. Using the same basis set and CCSD(T) their vertical IPs to the $^3B_1\ (3a_1)^{-1}$ and $^1A_1\ (1b_1)^{-1}$ states were 12.01 and 12.46 eV. (They did not report the vertical IP to the $^1B_1\ (3a_1)^{-1}$ state using CCSD(T).) Experimental vertical IPs are 12.00, 12.45 and 14.27 eV to the $^3B_1\ (3a_1)^{-1}$, $^1A_1\ (1b_1)^{-1}$, and $^1B_1\ (3a_1)^{-1}$ states respectively [98,99].

We used two CAS choices—one was our usual choice for MCSTEP which almost gives excellent MCSTEP low-lying IPs and another CAS that should be inadequate for some of the low-lying MCSTEP IPs. By comparing EPCASPT2 IPs with MCSTEP IPs, we demonstrated the effects of adding more dynamical correlation in the initial state on the ionization potentials with our single particle Green's function method MCSTEP, *i.e.*, EPCASPT2.

MCSTEP and EPCASPT2 calculations were performed at the experimental geometry. We report here only the optimal balanced CAS as explained above, *i.e.*, our usual and better of our two CASs. For convenience this CAS will be called the (5,6) CAS. All calculations are done with the cc-pVDZ, cc-pVTZ, and cc- pVQZ basis sets where the spherical components (1s, 3p′s, 5d′s, 7f′s, *etc.*) are retained.

We also performed full configuration interaction (FCI) calculations on the ground state and the first five ion states of NH_2 to determine the first five low-lying vertical ΔFCI IPs of NH_2. The calculations were performed using the same cc-pVDZ basis set at the same (experimental) geometry as the MCSTEP and EPCASPT2 calculations. Since ΔFCI calculations using cc-pVTZ and cc-pVQZ basis sets were not possible with our computational resources, we performed ΔMRSDCI + Q calculations to approximate ΔFCI IPs with these basis sets. The MCSCF initial states for the MRSDCI + Q calculations have the (5,6) CAS explained above for the neutral. For the cation states the CAS for the MRSDCI + Q calculations is four electrons in the same six orbitals.

With the (5,6) CAS, three strongly occupied and three weakly occupied orbitals are included. There are 76 $M_S = 0.5$ determinants generated for the ground state. This CAS is an "optimal" MCSTEP CAS for the low-lying valence principal IPs. Since the strongly occupied $1b_2$, $3a_1$, $1b_1$ are in this CAS, we expect very good principal MCSTEP IPs involving primarily electron removal from these orbitals.

EPCASPT2 IPs are compared with MCSTEP, MRSDCI + Q, and FCI IPs in Table 5.

Using cc-pVDZ basis set at the experimental geometry, MCSTEP and EPCASPT2 IPs are in very good to excellent agreement compared to ΔFCI IPs. MCSTEP IPs differ from ΔFCI IPs by −0.05, 0.09, 0.08, 0.20, and 0.25 eV for ionization to the $^3B_1\ (3a_1)^{-1}$, $^1A_1\ (1b_1)^{-1}$, $^1B_1\ (3a_1)^{-1}$, $^3B_2\ (1b_2)^{-1}$, and $^1B_2\ (1b_2)^{-1}$ states respectively. For the same ion

Table 5. Vertical ionization potentials of NH_2 (in eV) determined using MCSTEP and EPCASPT2 with the (5,6) CAS[a,b]

Basis set[c]	Ion states	MCSTEP	EPCASPT2	ΔMRSDCI + Q[a,b]	ΔFCI[b]
cc-pVDZ	$^3B_1\ (3a_1)^{-1}$	11.40	11.46	11.44	11.45
	$^1A_1\ (1b_1)^{-1}$	12.09	12.10	11.99	12.00
	$^1B_1\ (3a_1)^{-1}$	13.82	13.80	13.73	13.74
	$^3A_2\ (1b_2)^{-1}$	16.48	16.40	16.28	16.28
	$^1A_2\ (1b_2)^{-1}$	17.87	17.77	17.59	17.62
cc-pVTZ	$^3B_1\ (3a_1)^{-1}$	11.67	11.71	11.86	
	$^1A_1\ (1b_1)^{-1}$	12.30	12.31	12.31	
	$^1B_1\ (3a_1)^{-1}$	14.03	14.07	13.99	
	$^3A_2\ (1b_2)^{-1}$	16.68	16.70	16.55	
	$^1A_2\ (1b_2)^{-1}$	18.08	17.98	17.81	
cc-pVQZ	$^3B_1\ (3a_1)^{-1}$	11.74	11.89	11.98	
	$^1A_1\ (1b_1)^{-1}$	12.34	12.36	12.40	
	$^1B_1\ (3a_1)^{-1}$	14.07	14.07	14.07	
	$^3A_2\ (1b_2)^{-1}$	16.73	16.71	16.65	
	$^1A_2\ (1b_2)^{-1}$	18.13	18.00	17.87	
CBS limit[d]	$^3B_1\ (3a_1)^{-1}$	11.77	11.91	12.03	
	$^1A_1\ (1b_1)^{-1}$	12.36	12.38	12.44	
	$^1B_1\ (3a_1)^{-1}$	14.09	14.07	14.11	
	$^3B_2\ (1b_2)^{-1}$	16.75	16.71	16.71	
	$^1A_2\ (1b_2)^{-1}$	18.15	18.00	17.91	

[a] The CAS for the (neutral) initial state and transfer operators consists of all possible arrangements of five electrons in the ($3a_1$ $4a_1$ $1b_1$ $1b_2$ $2b_2$ $3b_2$) orbitals. For the cation states the CAS for the MRSDCI + Q calculations is four electrons in the same six orbitals.
[b] The geometry is explained in the text.
[c] The cc-pVDZ, cc-pVTZ, and cc-pVQZ basis sets are from Dunning [65] with only the spherical components retained.
[d] The complete basis set limit formula is equation (40) in the text.

states and using the same basis set and geometry the differences between EPCASPT2 IPs and ΔFCI IPs are 0.01, 0.10, 0.06, 0.12, and 0.15 eV.

Using the cc-pVDZ basis set, ΔMRSDCI + Q IPs are essentially the same as ΔFCI IPs, differing by −0.01, −0.01, −0.01, 0.00 eV, and −0.03 eV for ionization to the first five ion states. Therefore, the results of our ΔMRSDCI + Q calculations are expected to be excellent approximations to ΔFCI calculations in determining the low-lying IPs of NH_2 for basis sets larger than cc-pVDZ.

The first five MCSTEP and EPCASPT2 IPs in other basis sets are also in very good to excellent agreement compared to ΔMRSDCI+Q IPs. Using the cc-pVTZ basis set, the first five MCSTEP IPs reported in Table 5 differ from ΔMRSDCI + Q IPs by −0.19, −0.01, 0.04, 0.13, and 0.27 eV. For the same ion states and basis set, the differences between EPCASPT2 IPs and ΔMRSDCI + Q IPs are −0.15, 0.00, 0.08, 0.15, and 0.17 eV. The first

five IPs obtained using MCSTEP with the cc-pVQZ basis set differ from ΔMRSDCI + Q IPs by −0.24, −0.06, 0.00, 0.08, and 0.25 eV. For the same ion states and basis set, EPCASPT2 IPs differ from ΔMRSDCI + Q IPs by −0.09, −0.04, 0.00, 0.06, and 0.12 eV.

In Table 5 we also report the first five IPs at the CBS limit determined using EPCASPT2, MCSTEP, and ΔMRSDCI + Q. The MCSTEP IPs to these five low-lying states are 11.77, 12.36, 14.09, 16.75, and 18.15 eV respectively; EPCASPT2 IPs are 11.91, 12.38, 14.07, 16.71, and 18.00 eV respectively; and the ΔMRSDCI + Q IPs are 12.03, 12.44, 14.11, 16.71, and 17.91 eV respectively.

3.4.2. Ionization potentials of CH_3 [44]

The principal ground state configuration of CH_3 is $X^2A_2''\ (1a_1')^2\ (2a_1')^2\ (1e')^4\ (1a_2'')^1$. The first adiabatic IP has been determined experimentally at 9.843 ± 0.001 eV [100,101]. The equilibrium ground state geometries of the cation and the neutral are about the same so the vertical and the adiabatic IPs are nearly equal. This IP is the $CH_3^+(^1A_1') \leftarrow CH_3(^2A_2'')$ transition. Dixon and co-workers [102] recently reported the results of calculations to determine the first vertical and adiabatic IP of CH_3 using the coupled cluster method with single and double excitations and with non-iterative correction to the triple excitation (CCSD(T)). The result of their calculations at the CBS limit was 9.78 eV for the vertical IP.

We have used MCSTEP to calculate the lowest two IPs of CH_3. Calculations were done at the experimental geometry (*i.e.*, planar D_{3h} with a bond length of 1.079 Å) using spherical correlation consistent pVDZ, pVTZ, and pVQZ basis sets. The optimal MCSTEP CAS used in all calculations includes all possible arrangement of 5 electrons in the $(1e'1a_2''3a_1'2e')$ orbitals.

We have also performed full configuration interaction calculations on the ground state and the first two ion states of CH_3. The calculations employ the cc-pVDZ basis set at the experimental geometry. Due to the limitations in our computational resources, FCI calculations using cc-pVTZ and cc-pVQZ basis sets were not possible.

To approximate ΔFCI IPs at the cc-pVTZ and cc-pVQZ basis sets we have performed ΔMRSDCI + Q calculations using cc-pVTZ and cc-pVQZ basis sets in addition to the cc-pVDZ basis set. Our ΔMRSDCI + Q calculations were also at the experimental geometry of the neutral. The reference CAS used was the same as that used for MCSTEP and EPCASPT2. For the cation states only four electrons were present in the $(1e'1a_2''3a_1'2e')$ orbitals.

The first two IPs of CH_3 obtained using different methods are reported in Table 6.

With the cc-pVDZ basis set, ΔMRSDCI + Q IPs differ from ΔFCI IPs by −0.01 and −0.02 eV for the first two ion states respectively. Therefore, as with NH_2, we expect the results of the ΔMRSDCI + Q calculations to be in excellent agreement compared to ΔFCI results with cc-pVTZ and cc-pVQZ basis sets.

Using the cc-pVDZ basis set the MCSTEP IP for the first ionic state is lower by 0.39 eV compared to the ΔFCI IP. Using the cc-pVTZ and cc-pVQZ basis sets respectively, MCSTEP IPs for the first ion state differ from ΔMRSDCI + Q IPs by −0.50 and −0.54 eV respectively.

We have also performed MCSTEP calculations using a larger CAS, *i.e.*, all possible configurations of seven electrons in the $(2a_1'1e'1a_2''3a_1'2e')$ orbitals. Our MCSTEP IP for the lowest ion state with this large CAS still differs by as much as −0.51 eV compared to ΔFCI or ΔMRSDCI + Q IPs.

Table 6. Vertical ionization potentials of CH_3 (in eV) determined using MCSTEP and EPCASPT2 compared with other methods[a]

Basis set	Ion states	MCSTEP[b]	EPCAS-PT2[b]	ΔMRSDCI + Q[b,c]	ΔFCI	ΔMC-SCF[b,c]	ΔCAS-PT2[b,c]
pVDZ	$^1A_1'$	9.13	9.44	9.51	9.52	8.76	9.57
	^3E	14.73	14.72	14.72	14.74	14.32	14.63
pVTZ	$^1A_1'$	9.20	9.54	9.70		8.77	9.78
	^3E	14.82	14.83	14.91		14.34	14.79
pVQZ	$^1A_1'$	9.21	9.60	9.75		8.78	9.84
	^3E	14.86	14.88	14.97		14.39	14.85
CBS limit[d]	$^1A_1'$	9.21	9.69	9.77		8.81	9.86
	^3E	14.89	14.92	15.00		14.31	14.90

[a] Geometries are explained in the text. With the cc-pVDZ, cc-pVTZ, and cc-pVQZ basis sets [65] only spherical components are retained.

[b] Neutral state CAS consists of all possible arrangements of 5 electrons the ($1e'1a_2''3a_1'2e'$) orbitals.

[c] Cation state CAS consists of all possible arrangements of 5 electrons the ($1e'1a_2''3a_1'2e'$) orbitals.

[d] Complete basis set limit (CBS) formula is given in the text (equation (40)).

The low values of MCSTEP IPs are due to the fact that some important dynamical correlation effects are neglected in the initial MCSCF state. For all previous cases, MCSTEP with our choice of an optimal CAS for the initial state provided IPs with better agreement compared to ΔFCI, ΔMRSDCI + Q, and experimental low-lying vertical IPs. A reason for this can be seen by realizing that the orbitals in simple valence MO theory result with no orbitals to provide any in-out correlation for the out of plane singly occupied $3a_1'$ orbital. This is also exhibited by the standard CAS choices we use for MCSTEP (3 highest HOMOs and 3 lowest SCF LUMOs are used as initial guesses and symmetries for the CAS MCSCF orbitals). Hence, the neutral's energy is too high. This effect is corrected by "dynamical" correlation. For example, with the pVTZ basis set there are several more than typical unoccupied orbitals with fairly low-lying eigenvalues of the Lagrangian for the CH_3 neutral ground state (e.g., <0.4 a.u.). It is these that will contribute significantly to the dynamical correlation effects that are neglected in MCSTEP.

Using a CASPT2 wavefunction as the initial state in block 1, that is, using EPCASPT2, significant improvements to the first IP are obtained. For the cc-pVDZ basis set, the EPCASPT2 IP to the first ion state differs from the ΔFCI IP to the same ion state by -0.08 eV. Using two other basis sets, EPCASPT2 IPs for the first ion state are in very good agreement compared to ΔMRSDCI + Q IPs. EPCASPT2 IPs for the ionization from the neutral $^2A_2''$ state to the $^1A_1'$ ion state differ from ΔMRSDCI + Q IPs by -0.16 and -0.15 eV for the calculations employing cc-pVTZ and cc-pVQZ basis set respectively. At the CBS limit the first EPCASPT2 IP differs by -0.08 eV from the ΔMRSDCI + Q IP.

For all the correlation consistent basis sets, the second IPs predicted using both MCSTEP and EPCASPT2 are in excellent agreement compared to the ΔFCI and ΔMRSDCI + Q IPs.

In Table 6 we have also reported MCSCF and CASPT2 IPs. As is well-known, MCSCF IPs are generally unreliable [64]. Both EPCASPT2 and CASPT2 IPs are in excellent agreement with the ΔFCI and ΔMRSDCI + Q IPs.

4. SUMMARY AND CONCLUSIONS

Different forms of the wavefunction have been used as the initial state in Green's function/electron propagator methods. Our previous method for the single particle Green's function (or electron propagator), the multiconfigurational spin tensor electron propagator method (MCSTEP), used a small CAS MCSCF state as the initial state. We have developed an electron propagator method that uses a multiconfigurational-based second order perturbation theory (CASPT2) wavefunction as the initial state. With this new method a better initial state is used in the electron propagator calculations. CASPT2 is specifically designed to handle both dynamical and non-dynamical electron correlation effects. In this first implementation a CASPT2 initial state is used only in the most important part of the MCSTEP matrices for low-lying principal IPs (block 1) with the usual MCSCF state used for the other blocks.

MCSTEP calculations are reported here for the vertical IPs of O_2, the adiabatic EA of CH_2, and the vertical IPs of O_3. The results are in general in very good to excellent agreement with experiment or other accurate large scale *ab initio* calculations.

MCSTEP and EPCASPT2 results are presented here for the IPs of NH_2 and CH_3 [43, 44]. ΔFCI IPs are used as the benchmark for EPCASPT2 and MCSTEP IPs with the same basis set and at the same geometry if FCI calculations were possible with our computational resources since FCI is the exact result for a given basis set. We have demonstrated that our ΔMRSDCI + Q calculations effectively mimic ΔFCI IPs. When FCI calculations cannot be performed for these systems because of the limitations in our computational resources, we compare EPCASPT2 results to ΔMRSDCI + Q results.

It appears that the use of a CASPT2 wavefunction in block 1 of the MCSTEP matrices (EPCASPT2 versus MCSTEP) does not significantly alter the MCSTEP IPs when the MCSTEP CAS choice is very good-to-excellent for low-lying MCSTEP IPs; however, the IPs usually become closer, in general, to ΔFCI and ΔMRSDCI+Q for EPCASPT2. When the CAS choices are inadequate for low-lying MCSTEP IPs, it appears that EPCASPT2 significantly improves the IPs compared to MCSTEP IPs giving very good-to-excellent agreement with ΔFCI and ΔMRSDCI + Q IPs.

ACKNOWLEDGEMENTS

I would like to acknowledge support for this research from The Robert A. Welch Foundation Grant No. A-770. In addition, I would like to thank my former students Jeffrey Nichols, Joseph Golab, Dodi Heryadi, Rajiv Saha (deceased) and Alexander McKellar and my former post-docs N.O.J. Malcolm and S. Mahalakshmi for contributing to the research reported here and also to my current graduate student Kousik Samanta for his help in preparing this article.

I also especially thank both Poul Jørgensen and Jan Linderberg for being good friends for 30 and 25 years respectively and to Poul for being a fine collaborator. We have published 28 papers together since 1979.

REFERENCES

[1] J. Linderberg, Y. Öhrn, *Propagators in Quantum Chemistry*, Academic Press, London, 1973; second ed., John Wiley, Hoboken, NJ, 2004.
[2] P. Jørgensen, J. Simons, *Second Quantization-Based Methods in Quantum Chemistry*, Academic Press, New York, 1981.
[3] L.S. Cederbaum, G. Hohlneicher, W. von Niessen, *Chem. Phys. Lett.* **18** (1973) 503.
[4] L.T. Redmon, G. Purvis, Y. Öhrn, *J. Chem. Phys.* **63** (1975) 5011.
[5] C.W. McCurdy, T. Rescigno, D.L. Yeager, V. McKoy, in: H.F. Schaefer III (Ed.), *Methods of Electronic Structure*, vol. 3, Wiley, New York, 1977, p. 339.
[6] J. Simons, *Annu. Rev. Phys. Chem.* **28** (1977) 15.
[7] J.V. Ortiz, Y. Öhrn, *J. Chem. Phys.* **72** (1980) 5744.
[8] M.F. Herman, K.F. Freed, D.L. Yeager, *Adv. Chem. Phys.* **48** (1981) 1.
[9] Y. Öhrn, G. Born, *Adv. Quantum Chem.* **13** (1981) 1.
[10] J. Schirmer, L.S. Cederbaum, W. von Niessen, *Chem. Phys.* **56** (1981) 285.
[11] W. von Niessen, L.S. Cederbaum, J. Schirmer, G.H.F. Diercksen, W.P. Kraemer, *J. Electron Spectrosc. Relat. Phenom.* **28** (1982) 45.
[12] L.S. Cederbaum, W. Domcke, W. von Niessen, *Mol. Phys.* **34** (1977) 381.
[13] L.S. Cederbaum, W. Domcke, J. Schirmer, W. von Niessen, *Adv. Chem. Phys.* **65** (1986) 115.
[14] J.V. Ortiz, Y. Öhrn, *Chem. Phys. Lett.* **77** (1981) 548.
[15] J.V. Ortiz, R. Basu, Y. Öhrn, *Chem. Phys. Lett.* **103** (1983) 29.
[16] J.V. Ortiz, *Int. J. Quantum Chem. Symp.* **23** (1989) 321.
[17] J.V. Ortiz, *Chem. Phys. Lett.* **199** (1992) 530.
[18] M.S. Deleuze, L.S. Cederbaum, *J. Chem. Phys.* **105** (1996) 7583.
[19] V.G. Zakrzewski, J.V. Ortiz, J.A. Nichols, D. Heryadi, D.L. Yeager, J.T. Golab, *Int. J. Quantum Chem.* **60** (1996) 29.
[20] V.G. Zakrzewski, O. Dolgounitcheva, J.V. Ortiz, *J. Chem. Phys.* **105** (1996) 8748.
[21] O. Dolgounitcheva, V.G. Zakrzewski, J.V. Ortiz, *Int. J. Quantum Chem.* **65** (1997) 463.
[22] J.V. Ortiz, *J. Chem. Phys.* **109** (1998) 5741.
[23] J.T. Golab, D.L. Yeager, *J. Chem. Phys.* **87** (1987) 2925.
[24] J.A. Nichols, D.L. Yeager, P. Jørgensen, *J. Chem. Phys.* **80** (1984) 293.
[25] R.L. Graham, J.T. Golab, D.L. Yeager, *J. Chem. Phys.* **88** (1988) 2572.
[26] R.L. Graham, D.L. Yeager, A. Rizzo, *J. Chem. Phys.* **91** (1989) 5451.
[27] D.L. Yeager, J.A. Nichols, J.T. Golab, *J. Chem. Phys.* **97** (1992) 8841.
[28] D.L. Yeager, in: D. Mukherjee (Ed.), *Applied Many-Body Methods in Spectroscopy and Electronic Structure*, Plenum, New York, 1992.
[29] D.L. Yeager, J.A. Nichols, J.T. Golab, *J. Chem. Phys.* **98** (1993) 8790.
[30] J.A. Nichols, D. Heryadi, D.L. Yeager, J.T. Golab, *J. Chem. Phys.* **100** (1994) 2947.
[31] D.L. Yeager, *J. Chem. Phys.* **105** (1996) 8170.
[32] D.L. Yeager, J.A. Nichols, J.T. Golab, *J. Chem. Phys.* **100** (1994) 6514.
[33] D. Heryadi, D.L. Yeager, J.T. Golab, J.A. Nichols, *J. Chem. Phys.* **102** (1995) 9444.
[34] D. Heryadi, D.L. Yeager, J.T. Golab, J.A. Nichols, *Theor. Chim. Acta* **90** (1995) 273.
[35] D. Heryadi, C.T. Jones, D.L. Yeager, *J. Chem. Phys.* **107** (1997) 5088.
[36] A.J. McKellar, D.L. Yeager, J.A. Nichols, J.T. Golab, *J. Chem. Phys.* **105** (1996) 9927.
[37] A. McKellar, D. Heryadi, D. Yeager, *Int. J. Quantum Chem.* **70** (1998) 729.
[38] A. McKellar, D. Heryadi, D.L. Yeager, J. Nichols, *Chem. Phys.* **238** (1998) 1.
[39] A.J. McKellar, D. Heryadi, D.L. Yeager, *Int. J. Quantum Chem.* **70** (1998) 729.
[40] D.L. Yeager, *Trends Chem. Phys.* **7** (1999) 65.
[41] D. Heryadi, D.L. Yeager, *J. Chem. Phys.* **112** (2000) 4572.
[42] N.O.J. Malcolm, D.L. Yeager, *J. Chem. Phys.* **113** (2000) 8.
[43] D. Heryadi, D.L. Yeager, *J. Chem. Phys.* **114** (2001) 5124.
[44] D. Heryadi, S. Mahalakshmi, D.L. Yeager, *Chem. Phys. Lett.* **351** (2002) 92.
[45] K. Andersson, P.-Å. Malmqvist, B.O. Roos, A.J. Sadlej, K. Wolinski, *J. Phys. Chem.* **94** (1990) 5483.
[46] K. Andersson, P.-Å. Malmqvist, B.O. Roos, *J. Chem. Phys.* **96** (1992) 1218.
[47] D.N. Zubarev, *Nonequilibrium Statistical Mechanics*, Consultants Bureau, New York, 1974.
[48] O. Goscinski, B. Lukman, *Chem. Phys. Lett.* **7** (1970) 573.

[49] B.T. Pickup, O. Goscinski, *Mol. Phys.* **26** (1973) 1013.
[50] P.-O. Löwdin, *Phys. Rev.* **139** (1965) 357.
[51] J. Simons, *J. Chem. Phys.* **64** (1976) 4541.
[52] D.J. Rowe, *Nuclear Collective Motion*, Methuen, London, 1970.
[53] E. Dalgaard, *Int. J. Quantum Chem.* **15** (1979) 169.
[54] R. Manne, *Chem. Phys. Lett.* **45** (1977) 470.
[55] D.L. Yeager, P. Jørgensen, *Chem. Phys. Lett.* **65** (1979) 77.
[56] E. Dalgaard, *J. Chem. Phys.* **72** (1980) 816.
[57] D.L. Yeager, P. Jørgensen, *J. Chem. Phys.* **71** (1979) 755.
[58] D.L. Yeager, P. Jørgensen, *Mol. Phys.* **39** (1980) 587.
[59] J. Olsen, D.L. Yeager, P. Jørgensen, *Adv. Chem. Phys.* **54** (1983) 1.
[60] M.E. Rose, *Elementary Theory of Angular Momentum*, John Wiley, New York, 1957.
[61] D.J. Rowe, C. Ngo-Trong, *Rev. Mod. Phys.* **47** (1975) 471.
[62] K. Andersson, B.O. Roos, in: D.R. Yarkony (Ed.), *Modern Electronic Structure Theory, part I*, World Scientific Publishing Co., Singapore, 1995, p. 55.
[63] K. Andersson, M.R.A. Blomberg, M.P. Fülscher, G. Karlstrm, R. Lindh, P.-Å. Malmqvist, P. Neogrády, J. Olsen, B.O. Roos, A.J. Sadlej, M. Schütz, L. Seijo, L. Serrano-Andrés, P.E.M. Siegbahn, P.-O. Widmark, *MOLCAS4*, Lund University, Lund, Sweden, 1997.
[64] J.T. Golab, B.S. Thies, D.L. Yeager, *J. Chem. Phys.* **84** (1985) 284.
[65] T.H. Dunning Jr., *J. Chem. Phys.* **90** (1989) 1007.
[66] J.A.R. Samson, J.L. Gardner, G.N. Haddad, *J. Electron Spectrosc. Relat. Phenom.* **12** (1977) 281.
[67] R.M. Holmes, G.V. Marr, *J. Phys. B* **13** (1980) 945.
[68] E. Nishitani, I. Tanaka, K. Tanaka, T. Kato, I. Koyano, *J. Chem. Phys.* **81** (1984) 3429.
[69] R.G. Tonkyn, J.W. Winniczek, M.G. White, *J. Chem. Phys.* **91** (1989) 6632.
[70] J.F. Stanton, R.J. Bartlett, C.M.L. Rittby, *J. Chem. Phys.* **97** (1992) 5560.
[71] T. Noro, Y. Yoshimine, *J. Chem. Phys.* **91** (1989) 3012.
[72] H. Lischka, R. Shepard, F.B. Brown, I. Shavitt, *Int. J. Quantum Chem. Symp.* **S15** (1981) 91.
[73] R. Shepard, R.A. Bair, R.A. Eades, A.F. Wagner, M.J. Davis, L.B. Harding, T.H. Dunning Jr., *Int. J. Quantum Chem. Symp.* **S17** (1983) 613.
[74] R. Ahlrichs, H.-J. Böhm, C. Ehrhardt, P. Scharf, H. Schiffer, H. Lischka, M. Schindler, *J. Comput. Chem.* **6** (1985) 200.
[75] R. Shepard, I. Shavitt, R.M. Pitzer, D.C. Comeau, M. Pepper, H. Lischka, P.G. Szalay, R. Ahlrichs, F.B. Brown, J.-G. Zhao, *Int. J. Quantum Chem. Symp.* **S22** (1988) 149.
[76] S.R. Langhoff, E.R. Davidson, *Int. J. Quantum Chem.* **8** (1974) 61.
[77] D.G. Leopold, K.K. Murray, A.E.S. Miller, W.C. Lineberger, *J. Chem. Phys.* **83** (1985) 4849.
[78] S. Shih, S. Peyerimhoff, R. Buenker, M. Peric, *Chem. Phys. Lett.* **55** (1978) 206.
[79] D. Feller, L. McMurchie, W. Borden, E. Davidson, *J. Chem. Phys.* **77** (1982) 6134.
[80] K.A. Peterson, T.H. Dunning, *J. Chem. Phys.* **102** (1995) 2032.
[81] M. Barysz, M. Rittby, R.J. Bartlett, *Chem. Phys. Lett.* **193** (1992) 373.
[82] P.J. Hay, T.H. Dunning Jr., W.A. Goddard III, *J. Chem. Phys.* **62** (1975) 3912.
[83] K.-H. Thunemann, S.D. Peyerimhoff, R.J. Buenker, *J. Mol. Spectr.* **70** (1978) 432.
[84] W.D. Laidig, H.F. Schaefer III, *J. Chem. Phys.* **74** (1981) 3411.
[85] N. Kosugi, H. Kuroda, S. Iwata, *Chem. Phys.* **58** (1981) 267.
[86] M.V.R.K. Krishna, K.D. Jordan, *Chem. Phys.* **115** (1987) 423.
[87] P. Decleva, G. De Alti, A. Lisini, *J. Chem. Phys.* **89** (1988) 367.
[88] J.V. Ortiz, *Chem. Phys. Lett.* **297** (1998) 193.
[89] D.L. Yeager, D. Heryadi, S. Mahalakshmi, *Recent Research Developments in Chemical Physics* **3** (2002) 119.
[90] P.J. Knowles, N.C. Handy, *Chem. Phys. Lett.* **111** (1984) 315.
[91] P.J. Knowles, N.C. Handy, *Comp. Phys. Commun.* **54** (1989) 75.
[92] P.J. Knowles, H.-J. Werner, MOLPRO is a package of *ab initio* programs written by H.-J. Werner and P.J. Knowles, with contributions from J. Almlöf *et al*.
[93] K. Dressler, D.A. Ramsay, *J. Chem. Phys.* **27** (1957) 971.
[94] G. Herzberg, D.A. Ramsey, *J. Chem. Phys.* **20** (1952) 347.
[95] G. Herzberg, D.A. Ramsey, *Discuss. Faraday Soc.* **14** (1953) 11.
[96] G. Herzberg, *Electronic Spectra of Polyatomic Molecules*, Van Nostrand, Princeton, NJ, 1967.

[97] J.C. Stephens, Y. Yamaguchi, H.F. Schaefer III, *J. Molecular Structure (Theochem)* **461–462** (1999) 41.
[98] S.J. Dunlavey, J.M. Dyke, N. Jonathan, A. Morris, *Mol. Phys.* **39** (1980) 1121.
[99] J.M. Dyke, N. Jonathan, A. Morris, *Int. Rev. Phys. Chem.* **2** (1982) 3.
[100] G. Herzberg, J. Shoosmith, *Can. J. Phys.* **34** (1956) 523;
G. Herzberg, *Proc. R. Soc. London Ser. A* **262** (1961) 291.
[101] S.G. Lias, J.E. Bartmess, J.F. Liebman, J.L. Holmes, R.D. Levin, W.G. Mallard, *J. Phys. Chem. Ref. Dat. Suppl.* **1** (1988) 17.
[102] D.A. Dixon, D. Feller, K.A. Peterson, *J. Phys. Chem. A* **101** (1997) 9405.

This page intentionally left blank

Subject Index

D

E

F

G

H

I

J

K

This page intentionally left blank